NOTE: This report has been made available for use by ORNL and the AEC and is not to be transmitted to other organizations or to private individuals.

71:02

Technical Report of the

Molten - Salt Group

Part I

MOLTEN - SALT REACTOR TECHNOLOGY

EBASCO SERVICES INCORPORATED
TWO RECTOR STREET
NEW YORK
DECEMBER 1971

71:022

Technical Report of the
Molten-Salt Group

Part I

EVALUATION OF A 1000 MWe MOLTEN-SALT BREEDER REACTOR

Edited by

J. R. Trinko

D R de Boisblanc

D. R. deBoisblanc
Technical Director

PREFACE

Ebasco Services Incorporated has followed the research and development of molten-salt reactor technology at ORNL for many years. As early as 1968, it became evident that the technology was sufficiently advanced to warrant the serious attention of utilities and nuclear industries. Accordingly, L F C Reichle, Vice President, Nuclear Department of Ebasco Services Incorporated, proposed the formation of the Molten-Salt Group (MSG) and organized the combination of utilities and industries for the purpose of undertaking an independent, in-depth study of this technology with the utilities supplying financial support and the industries senior level technical participants (Table 1). This study was performed in New York as a group effort under the technical direction of Ebasco Services Incorporated. The principal participants, their titles, and companies are presented in Table 2.

The study aims:

1 - To evaluate the state of molten reactor technology,

2 - To develop a critique of a 1000 MWe MSBR concept,

3 - To identify technological uncertainties and necessary research and development,

4 - To generate alternate MSR concepts based on the experienced engineering of industries well established in the field of nuclear power.

This report, Part I, is concerned with the first objective. Part II is concerned primarily with a critique of a particular molten-salt breeder reactor concept.

The conduct of this study depended upon the availability of technical information from ORNL. The interest demonstrated by the laboratory and the many private communications with laboratory scientists were an indispensable part of this effort.

Table 1

MOLTEN SALT GROUP PARTICIPANTS

Industries:

Babcock & Wilcox Company

Byron Jackson Pump Division,
Borg-Warner Corporation

Stellite Division, Cabot Corporation

Continental Oil Company, Inc

Ebasco Services Incorporated,
A Boise Cascade Company

Union Carbide Corporation,
Carbon Products Division

Utilities:

Dallas Power & Light Company

Houston Lighting & Power Company

Kansas Gas and Electric Company

Middle South Services, Incorporated representing -

- Arkansas Power & Light Company
- Louisiana Power & Light Company
- Mississippi Power & Light Company
- New Orleans Public Service, Incorporated

Minnesota Power & Light Company

Northeast Utilities Service Company representing -

- Connecticut Light and Power Company
- Hartford Electric Light Company
- Holyoke Water Power Company
- Western Massachusetts Electric Company

Texas Electric Service Company

Texas Power & Light Company

Union Electric Company

Table 2

Principal Contributors

Dr Jerry A Acciarri, Fuels Technology Development, Research & Engineering Department, Continental Oil Company.

Mr R M Bushong, Assistant to Director of Advanced Technology Projects, Carbon Products Division, Union Carbide Corporation.

Mr Gary C Clasby, Senior Project Engineer, Byron Jackson Pump Division, Borg-Warner Corporation.

Dr D R deBoisblanc, Chief Consulting Nuclear Engineer and Manager of R&D, Ebasco Services Incorporated.

Mr. B J Goulding, Supervisor of Mechanical Design in Nuclear Power Generation Department, Babcock & Wilcox Company.

Dr H C Ott, Manager Nuclear Technology, Ebasco Services Incorporated.

Mr T K Roche, Senior Metallurgical Engineer, Cabot Corporation.

Mr H K Smith, Senior Mechanical Engineer, Babcock & Wilcox Company.

Dr J R Trinko, Senior R&D Scientist, Ebasco Services Incorporated.

TABLE OF CONTENTS

	Page No.
1.0 INTRODUCTION	1
2.0 SUMMARY AND CONCLUSIONS	6
2.1 Introduction	6
2.2 General Conclusions	6
2.3 Specific Conclusions	7
2.3.1 Hastelloy N (Modified)	10
2.3.2 Chemical Processing	10
2.3.3 Coolant Medium	15
2.3.4 Tritium	18
2.3.5 Graphite	20
2.3.6 Reactor Physics	23
2.3.7 Components	24
2.3.8 Maintenance and Repair	28
2.3.9 Safety	29
3.0 BRIEF DESCRIPTIONS OF SEVERAL CREDIBLE MSBR CONCEPTS	32
3.1 Common Features	32
3.1.1 Fuel Sale	32
3.1.2 Reactor Internals	32
3.1.3 Primary System	32
3.1.4 Secondary System	33
3.1.5 Steam System	33
3.1.6 Chemical Process System	34
3.1.7 Drain Systems	35
3.1.8 Off-Gas System	36
3.2 Reference Concept	37
3.3 Single-Fluid, Nonreplaceable Core	38
3.4 Single-Fluid, Replaceable Core With Separate Blanket	39
3.5 Two-Fluid Replaceable Core With Separate Blanket	40
4.0 REACTOR INTERNALS	41
4.1 Core Graphite Moderator Elements	41
4.1.1 Influence on Nuclear Performance	41
4.1.2 Thermal-Hydraulic Characteristics	42
4.1.3 Fabrication	43
4.2 Blanket Regions	44
4.3 Reflector Regions	44
4.4 Salt Inlet and Outlet Plena	45

TABLE OF CONTENTS (Cont'd)

	Page No.
4.5 Reactor Hydraulics	45
4.5.1 Total Mass Flow Rate	46
4.5.2 Salt Velocity in Core	46
4.5.3 Pressure Considerations	47
5.0 COMPONENT TECHNOLOGY	48
5.1 Introduction	48
5.2 Intermediate Heat Exchangers	50
5.3 Steam Generator	53
5.4 Reactor Vessel	55
5.5 Control Rod Drives	56
5.6 Molten Salt Valves	56
5.7 Pump Technology	57
5.7.1 Factors Influencing Design	57
5.7.2 Definition of Current Technology	58
5.7.3 Adaptation of Current Technology	77
6.0 SPECIAL MATERIALS TECHNOLOGY	95
6.1 Fuel and Fertile Salts	95
6.1.1 Criteria	95
6.1.2 Attractive Salts	95
6.1.3 Salts Examined by Laboratories	98
6.2 Coolant Salt	109
6.2.1 Criteria	109
6.2.2 Attractive Molten Coolant Salts	111
6.2.3 Invariant Equilibria Data and Phase Diagrams	114
6.3 Compatability With Reactor Materials	114
6.3.1 Compatability With Graphite	114
6.3.2 Compatability With Containment Materials	115
6.4 Graphite Technology	117
6.4.1 Radiation Damage	117
6.4.2 Molten Salt Compatability	132
6.4.3 Fission Product Retention	140
6.4.4 Manufacturing Technology	153

TABLE OF CONTENTS (Cont'd)

		Page No.
6.5	Hastelloy Alloy N	159
6.5.1	Composition	160
6.5.2	Melting and Casting	160
6.5.3	Fabrication	162
6.5.4	Welding	163
6.5.5	Oxidation Resistance	164
6.5.6	Corrosion Resistance to Fuel Salts	165
6.5.7	Corrosion Resistance to Coolant Salts	172
6.5.8	Corrosion Resistance to Steam	173
6.5.9	Mechanical Properties	174
6.5.10	Irradiation Damage	177
6.5.11	Modified Hastelloy Alloy N	179
7.0	MSR NUCLEAR CHARACTERISTICS	183
7.1	Unique Features of MSR's	183
7.2	Figures-of-Merit	183
7.3	Calculational Models	184
7.3.1	Geometry	184
7.3.2	Approach to Equilibrium	186
7.3.3	Calculation of Equilibrium Salt Composition	190
7.3.4	Comparison of ROD With CITATION	191
7.4	Comparison of MSRE Calculations With Experimental Data	193
7.5	Comparison of MSRE and MSBR Calculations	194
7.5.1	Neutron Leakage	195
7.5.2	Effect of ^{232}Th	195
7.5.3	Fission Product Distribution	195
7.6	Steady State Physics Characteristics	196
7.6.1	Neutron Balance for a Typical MSBR	196
7.6.2	Effect of Chemical Processing	197
7.6.3	Effect of Fission Gas Removal	198
7.6.4	Effect of Reactor Size	199
7.7	Rationale for Choice of Design Parameters	199
7.7.1	Th Concentration	199
7.7.2	Graphite Lifetime	201
7.7.3	Salt Fraction	201
7.7.4	Region Dimensions	202
7.8	Uncertainties in Physics Calculations	202

TABLE OF CONTENTS (Cont'd)

		Page No.
8.0	FLUORINATION IN MOLTEN SALTS	205
8.1	Summary	205
8.1.1	Fluorination System	206
8.1.2	UF_6 Decontamination System	209
8.1.3	Cold Trap System	212
8.1.4	Purge Gas System	213
8.2	Processing of the Aircraft Reactor Experiment (ARE) Fuel	213
8.2.1	Pilot Plant Description	213
8.2.2	Processing	215
8.3	Laboratory Fluorination Tests	224
8.4	Protactinium Fluoride Volatility Test	224
8.5	Continuous Fluorination Tests	226
8.6	Fluorine Disposal Experiments	228
8.6.1	Charcoal	228
8.6.2	SO_2 Process	230
8.6.3	Caustic Process	231
8.7	Chromium Fluoride Trapping	232
8.8	Frozen Wall Experiment	233
8.9	Fluorination-Corrosion Study	235
8.10	Fission Product Behavior	237
8.11	Processing of MSRE Salt	242
8.11.1	Pilot Plant Process Description	242
8.11.2	Equipment Description	246
8.11.3	Fluorination of Flush Salt	253
8.11.4	Fluorination of Fuel Salt	254
8.11.5	Fluorine Utilization	255
8.11.6	Corrosion	259
8.11.7	Molybdenum	260
8.11.8	Plutonium	263
8.11.9	Niobium	263
8.11.10	Iodine and Tellurium	265
8.11.11	Uranium Adsorption	266
8.11.12	Uranium Product Purity	267
8.12	Fluorination-Valence State Study	269
8.13	UF_6-NaF Adsorption Equilibria	271
8.14	Temperature Effect on UF_6 Adsorption	273
8.15	Axial Mixing	276
8.16	Corrosion Rates in Continuous Fluorinators	278

TABLE OF CONTENTS (Cont'd)

		Page No.
9.0	REDUCTIVE EXTRACTION	281
9.1	Introduction	281
9.1.1	Protactinium Isolation	282
9.1.2	Rare-Earth Removal	282
9.1.3	Data Presentation	283
9.2	Protactinium Isolation and Rare-Earth Removal	286
9.2.1	Reductive Extraction of Uranium, Sodium, Europium, Lanthanum From Fuel Salts	286
9.2.2	Reductive Extraction of Uranium, Thorium, and Europium From MSBR Fuel Salt	289
9.2.3	Extraction of Thorium and Rare Earths Europium, Lanthanum, and Neodymium	291
9.2.4	Reductive Extraction of Uranium, Protactinium, and Thorium From Fuel Salts	292
9.2.5	Reductive Extraction of Uranium, Protactinium, and Thorium From Fuel Salts - Further Studies	294
9.2.6	Reductive Extraction of Europium From Fuel Salt	296
9.2.7	Reductive Extraction of Cerium by Thorium From Fuel Salt Mixtures	298
9.2.8	Reductive Extraction of Cerium, Neodymium, and Samarium From Fuel Salt Mixtures	300
9.2.9	Separation Factors for Uranium, Protactinium, and Thorium From Fuel Salt Mixtures	302
9.2.10	Extraction of Uranium, Protactinium, Zirconium, and Plutonium From Fuel Salts	303
9.2.11	Extraction of Rare Earths Europium, Lanthanum, Neodymium and Samarium From Fuel Salts	307
9.2.12	Reductive Extraction of Transuranium Elements Neptunium, Plutonium, Americium, Curium, and Californium From Fuel Salts	309
9.2.13	Rare-Earth Separation of Promethium, Europium, Lanthanum, Samarium, and Thorium From Fuel Salts	309
9.2.14	Extraction of Cerium and Thorium From Fuel Salt Mixtures	313
9.2.15	Extraction of Barium and Thorium From Fuel Salts	314
9.2.16	Thorium, Lithium Distribution From Fuel Salts in the Presence of Nickel	314
9.2.17	Extraction of Sodium From Fuel Salts	316
9.2.18	Extraction of Strontium From Fuel Salts	317
9.2.19	Extraction of Rubidium From Fuel Salts	317
9.2.20	Extraction of Cesium From Fuel Salts	318

TABLE OF CONTENTS (Cont'd)

		Page No.
9.3	Metal Transfer Process	318
9.3.1	Distribution of Cerium, Strontium, and Europium	318
9.3.2	Extraction of Cesium From LiCl into Bismuth	319
9.3.3	Distribution Data for Uranium, Protactinium, Thorium, and Various Rare Earths in Metal Transfer Systems	320
9.3.4	Distribution of Sodium and Potassium in Metal Transfer Salts	322
9.3.5	Measurement of Distribution Coefficients in Molten Salt-Metal Systems	324
9.3.6	Extraction of Cesium From Lithium Chloride	326
9.3.7	Distribution of Barium, Lanthanum, Neodymium, and Thorium in Lithium Bromide	327
9.3.8	Extraction of Europium and Strontium From Lithium Chloride	328
9.3.9	Extraction of Protactinium From Lithium Chloride	328
9.3.10	Distribution of Transuranium Elements in Lithium Chloride	328
9.3.11	Distribution of Europium in Lithium Chloride	329
9.3.12	Distribution of Europium in Lithium Chloride-Fluoride Salts	331
9.3.13	Extraction of Uranium From Lithium Chloride	331
9.3.14	Distribution Coefficients in Metal Transfer Systems	333
9.3.15	Engineering Metal Transfer Experiments	337
9.4	Reductive Extraction Engineering Studies	346
9.4.1	Uranium Mass Transfer Studies	346
9.4.2	Flooding and Pressure Drop Studies in Packed Columns	352
9.5	Axial Mixing in Columns	362
9.5.1	Packed Columns	362
9.5.2	Open Columns	369
9.6	Solubilities in Reductive Extraction	373
9.6.1	Thorium in Bismuth	373
9.6.2	Protactinium and Thorium in Bismuth	373
9.6.3	Effect of Nickel on Thorium in Bismuth	376
9.6.4	Bismuth in Fuel Salt	377
9.6.5	Neodymium in Lithium-Bismuth-Thorium Solutions	379
9.6.6	Thorium and Neodymium in Lithium-Bismuth Solutions	380
9.6.7	Lithium and Bismuch in Lithium Chloride	382

TABLE OF CONTENTS (Cont'd)

		Page No.
9.7	Removal of Chloride From Fuel Salt	383
9.8	Removal of Fluoride From Molten Lithium Chloride	385
9.9	Iron Fluoride Reduction	387
10.0	OFF-GAS SYSTEM TECHNOLOGY	389
10.1	Purge Gas System	389
10.1.1	Bubble Injection and Extraction	389
10.1.2	Spray Chambers	393
10.2	Purge Gas Cleanup System	393
10.2.1	^{135}Xe Backpressure	393
10.2.2	Holdup Tank	394
10.2.3	Charcoal Sorption	395
10.3	Removal of Other Contaminants	396
10.4	Provisions for a Clean Gas Stream	397
11.0	FUEL SALT DRAIN TANK TECHNOLOGY	398
11.1	Design Criteria	399
11.2	Design Philosophy	399
11.2.1	Subcriticality	399
11.2.2	Probability of Unsafe Failure	399
11.2.3	Contamination Prevention	401
11.2.4	State of Readiness	402
11.2.5	Cooling Capacity	402
11.2.6	Salt Transfer	402
11.2.7	Instrumentation	403
11.3	Choice of Coolants	403
12.0	INSTRUMENTATION, CONTROL, AND PROTECTIVE SYSTEMS	407
12.1	Philosophy	407
12.2	Steam Temperature and Flow Control	408
12.3	Secondary System Flow Control	408
12.4	Primary System Power Control	408
12.5	Short-Term Reactivity Control	410
12.6	Long-Term Reactivity Control	411
12.7	Xenon Transients	411
12.8	Measurements	413

TABLE OF CONTENTS (Cont'd)

		Page No.
13.0	RADWASTE	415
13.1	Fuel Salt	415
13.1.1	Rate of Salt Discard	415
13.1.2	Heat Production in Discard Salt	416
13.1.3	Salt Disposal	416
13.2	Graphite	417
13.3	Effluent From Charcoal Bed Regeneration	418
14.0	TRITIUM PROBLEM	419
14.1	Consequences of Tritium Release	420
14.2	Measurements of Tritium Releases From MSRE	420
14.3	Possible Solutions to the Tritium Problem	421
15.0	MOLTEN SALT REACTOR SAFETY	428
15.1	Summary	428
15.2	Safety Analysis by Systems	430
15.2.1	Reactor System	432
15.2.2	Steam System	434
15.2.3	Fuel Reprocessing System	435
15.2.4	Off-Gas System	435
15.3	Operating Reactor Safety Aspects	436
15.3.1	Reactivity Coefficients and Kinetics Parameters	437
15.3.2	Control-Rod Function	439
15.3.3	Reactor Incidents	440
15.3.4	Reactivity Additions	441
15.3.5	Mechanical and Physical Integrity - Containment	448
15.3.6	Miscellaneous Incidents	450
16.0	MAINTENANCE AND REPAIR	452
16.1	Semidirect	453
16.2	Remote	453
16.3	Graphite Replacement	453
16.3.1	Unit Core Replacement	454
16.3.2	Assembly Replacement	457
16.4	Component Replacement	458
16.5	Decontamination	459
17.0	ACKNOWLEDGMENTS	460

1.0 INTRODUCTION

Over 12 years ago the Fluid Fuel Reactors Task Force of the Atomic Energy Commission evaluated the technology and potential of three reactor concepts: Acqueous homogenous (AHR), Molten Salt (MSR), and Liquid Metal Fuel (LMFR). This task force concluded:

1 - MSR's had the highest probability of achieving technical feasibility.

2 - MSR's had potential as breeder reactors.

3 - MSR's had the potential for producing low cost power.

Based on these conclusions, MSRE (Molten Salt Reactor Experiment), an 8 MWt reactor, was built and operated at Oak Ridge National Laboratory. Using a molten salt of $LiF-BeF_2-ZrF_4-UF_4$ (65.0-29.1-5.0-0.9 mole percent) and fueled with ^{235}U, it operated successfully from June 1965 to March 1968. At that time all uranium was recovered from the salt via on-site fluorination. It was then fueled with ^{233}U, and it continued to operate successfully from October 1968 to December 1969. MSRE demonstrated the following:

1 - High reliability. It was critical 80 percent of the time over a 15 month interval.

2 - Uranium recovery via batch fluorination. Virtually all uranium was recovered from the salt.

3 - Operation with a small delayed neutron fraction. ^{233}U together with circulating fuel resulted in a much smaller delayed neutron fraction than fixed-fuel reactors. No operational or safety problems occurred.

4 - Predictable nuclear characteristics. The critical fuel concentration, the fissile concentration coefficient, the temperature coefficient of reactivity, and the reactivity loss due to circulating fuel were predicted extremely well prior to operation.

5 - Excellent salt stability and chemical behavior. Core graphite showed no sign of attack. Hastelloy N showed some pitting (5-10 mils deep) which is attributed to oxidizing contamination.

1.0 INTRODUCTION (Cont'd)

6 - Dynamic stability. The entire system was stable. Results of kinetics experiments were in general agreement with predictions.

7 - Excellent containment of fission products.

8 - Maintainability. Maintenance of contaminated components was accomplished without unreasonable delay and with very little radiation exposure to personnel. Because of its high reliability, however, little maintenance was required.

9 - Efficient separation of fission gases from fuel salt. ^{135}Xe poisoning was consistently less than anticipated.

All objectives of MSRE were attained; technical feasibility was largely demonstrated; and a great deal of information pertinent to MSBR's was obtained.

As a result of MSRE experience the molten salt reactor concept now appears attractive and promising as a commercial power source. The attractive features characteristic of MSBR's are as follows:

1 - Fuel element fabrication, transportation, and reprocessing is eliminated.

2 - Continuous processing of the salt is possible. This results in:

a - A very low inventory of volatile fission products. Volatile fission products having half-lives greater than 10 minutes are reduced to less than 1/10 of the inventory in solid fueled reactors.

b - Very little excess reactivity. Because the salt is kept well-mixed, local fuel depletion does not occur. Fuel can be added (or removed) from the salt continuously for coarse reactivity control.

3 - MSR's have inherent safety characteristics. In addition to having little excess reactivity and a relatively small volatile fission product inventory, MSR's have a large prompt negative reactivity coefficient due to thermal expansion of the salt. Being graphite-moderated, they have a very large heat capacity. In general, reactivity accidents which could threaten the integrity of the primary

1.0 INTRODUCTION (Cont'd)

3 - (Cont'd)

system are hardly credible.

4 - MSBR's will be able to utilize thorium resources and realize breeding ratios up to 1.08 and doubling times as low as 10 years.

5 - New MSBR's can be started up on any fissionable material (or mixture) and gradually converted to ^{233}U operation as it is bred.

6 - After several MSR's are built, the plant capital cost is expected to be comparable to that for LWR's. The fuel cycle cost for MSR's, however, should be substantially lower.

7 - MSR's are largely independent of support industries. They require only:

a - A continuous supply of small amounts of ^{7}Li, F, Be, and Th (about 0.1 ft^3-salt/day).

b - A supply of fabricated graphite moderator elements. In high power density cores the graphite will require replacing every 4-6 years. (Low power density reactors require no graphite replacement.)

c - A radwaste industry to dispose of contaminated graphite and fuel salt.

8 - Except for the steam system, all systems in an MSR plant are low pressure - at most about 300 psi.

MSR's also have some inherent unattractive features:

1 - Four major systems are highly contaminated: The primary system, chemical process system, off-gas system, and drain system.

2 - The salts have high melting temperatures and, therefore, require heated cells on trace heating.

3 - Relatively large amounts of tritium are produced.

In addition, there are several technology uncertainties and/or design problems which could add to this list. After completing this study, it appears that existing technology will support MSBR designs which attain

many of the attractive features. MSR technology is, therefore, sufficiently advanced to warrant serious consideration by industries. Paradoxically nuclear industries have shown little interest in the molten salt concept. Two reasons are evident:

1 - Most nuclear industries depend on fuel fabrication as a continuing money-making activity. Since MSR's require no fuel fabrication, there is no incentive for these industries to invest in MSR R & D.

2 - Until the postmortem inspection of MSRE, there remained many technical uncertainties which made the molten-salt a high risk concept.

The formation of the MSG constitutes a demonstration of industrial interest in the MSR concept. Represented in this group are all the industries (Table 1) required to span the technology. Goals of this group were to:

1 - Acquire a broad understanding of the technology.

2 - Generate a document presenting the technology applicable to MSBR's in general.

3 - Generate a document describing an evaluation of a Reference Concept[1/].

4 - Identify technical uncertainties and assess their impact on MSR potential.

5 - Determine the potential attractive and unattractive features of MSR's.

This document, Part I, attempts to state what is known about MSR technology. Where possible, we have appraised the information in terms of its significance to MSBR design and feasibility. Since, by far, most of the pertinent information was generated by ORNL, we relied heavily upon ORNL reports and personnel for information. In some instances we found that ORNL documents stated the technology sufficiently well. Thus, portions of this report (particularly the sections on graphite technology, fluorination, and reductive-extraction) were taken directly from ORNL reports.

1/ Technical Report of the Molten Salt Group - Part II, "Evaluation of a 1000 MWe Molten Salt Breeder Reactor", October 1971.

1.0 INTRODUCTION (Cont'd)

The second report[1/] of the MSG presents our evaluation of the best MSBR concept documented. This concept was appraised in terms of the existing technology. Throughout this portion of the study every effort was made to remain independent of ORNL and to evaluate the concept objectively.

In that report it was concluded that several attractive MSBR concepts were possible within existing technology. The particular concept evaluated, however, was an advanced concept designed to guide R&D efforts and to illustrate the potential of MSBR's. Although it is based on reasonable extensions of technology and expected R&D progress, it has a great deal of merit.

2.0 SUMMARY AND CONCLUSIONS

2.1 Introduction

One purpose of the Molten-Salt Group (MSG) was to define, appraise, and document that body of technology applicable to MSBR's. The purpose of this document is to present in one place the applicable technology as it is now known. Nearly all of the technology was generated by ORNL. Thus, the MSG relied on ORNL documents and on ORNL personnel for much of the information. Portions of this report were taken directly from ORNL documents, particularly the sections on graphite, fluorination, and reductive extraction.

In addition to stating the technology, this document attempts to identify technology uncertainties and to assess the significance of these uncertainties on the general feasibility of MSBR's. Thus, much of this document dwells on uncertainties and their implications. It is not our intent, however, to detract in any way from the excellent work done by ORNL; we wish only to clarify objectively the state of technology to the sponsors (Table 2) of this study. We do wish to acknowledge and emphasize our conclusion that ORNL has done a great deal of outstanding and brilliant work in developing MSR technology. As will become apparent to the reader, the body of technology is extensive and largely complete. Many of the technology gaps will be closed and uncertainties will be resolved only by operation of an MSR demonstration plant.

2.2 General Conclusions

Existing technology is sufficient to justify the construction of a complete demonstration plant including a supercritical steam system and a chemical process plant. Because of uncertainties, however, it is not possible to state with confidence what the performance characteristics will be. It can be stated confidently that a complete plant can be made to work and it will have a breeding ratio greater than unity, provided the chemical process plant works. Maintainability, reliability, costs, and plant life cannot be predicted reliably from the existing technology. These uncertainties will be elucidated somewhat with additional design

2.2 General Conclusions (Cont'd)

work and a great deal more with the construction and operation of a demonstration plant.

2.3 Specific Conclusions

2.3.1 Hastelloy N (Modified)

Corrosion

Hastelloy N (modified or standard) is thermodynamically stable toward a wide range of fluoride salts including the proposed MSBR fuel salt. Experiments have demonstrated that it is sufficiently resistant to corrosion and erosion when exposed to uncontaminated fuel salt.

Post-operation examination of MSRE revealed, however, that all Hastelloy N surfaces in contact with fuel salt contain cracks 5-10 mils deep. The mechanism is believed to be corrosion caused by impurities in the salt. Fission products and oxidizing salt conditions are suspect. The uniform depth of penetration suggests that it is not stress dependent.

While not completely discounted, ORNL believes that fission products are not likely the cause of this attack because similar cracking has been found on test samples exposed to fuel salt uncontaminated with fission products.

Oxidizing salt conditions are believed more likely because oxygen, water vapor, or HF contamination give rise to such a condition. During its four year life MSRE was drained, flushed, and opened 14 times. It is likely that some air entered the primary system each time. To reduce oxidizing conditions beryllium was dissolved into the salt, but this was done infrequently and irregularly. Hence, some oxygen and water vapor contamination was quite possible.

When ^{235}U was recovered from the fuel salt by fluorination, some HF was introduced into the system. Either HF or

2.3.1 Hastelloy N (Modified) (Cont'd)

Corrosion (Cont'd)

oxygen contamination, or both, could be the cause of the observed cracking.

A commercial MSBR will be opened much less frequently reducing the opportunity for introducing oxygen. Furthermore, MSBR fuel salt, which differs from MSRE fuel salt primarily by the addition of ThF_4 and the elimination of ZrF_4 (~5 mole % in MSRE), is less tolerant of oxygen. MSBR's will, therefore, require greater care in preventing oxygen contamination. The chemical process plant will extract such contamination and reestablish the desired oxidation potential of the salt after exposure to contamination such as that anticipated during graphite replacement.

Several MSBR concepts were advanced by ORNL prior to the observation of cracking in MSRE Hastelloy. The validity of these concepts now rests on the assumption that the cracking in MSRE is a form of corrosion which can be eliminated by maintaining the oxidizing potential of the salt sufficiently low. This assumption is inescapable because there is no other known material more resistant to corrosion which could be considered a feasible substitute for heat exchanger tubes. Based on the large quantity of corrosion data available, we agree with ORNL that cracking can be prevented in MSBR's. Thus we regard this phenomenon as a potential problem which could, if neglected, limit the useful life of an MSBR; we do not regard it as a technology barrier which must be resolved prior to the successful operation of an MSBR.

Neutron Irradiation Embrittlement

Standard and, to a lesser extent, modified alloys embrittle under thermal neutron irradiation because of the production of helium in the grain boundaries. Boron, always present

2.3.1 Hastelloy N (Modified) (Cont'd)

Neutron Irradiation Embrittlement (Cont'd)

in Hastelloy N as an impurity, precipitates at the grain boundaries and gives rise to the production of helium via the $^{10}B(n, \alpha)^{7}Li$ reaction.

To reduce the damage at the grain boundaries, modified alloys contain small amounts ($\leq$ 2.4 wt percent) of Ti and/or Hf. These elements combine with carbon to form a fine, uniformly dispersed particulate which provides nucleation sites for boron other than grain boundaries. By distributing the boron uniformly, the radiation damage will also be distributed uniformly rather than being concentrated at the grain boundaries.

Many small heats of modified alloy have demonstrated satisfactory physical and mechanical properties including ductility after neutron irradiation at temperatures up to 1400°F. Larger heats (100 lb) containing Hf, however, have not been so successful. It is believed that the slower cooling rates of the larger heats permit some of the carbides, as well as the boron, to migrate to the grain boundaries.

Heats containing only Ti have been scaled-up successfully. A few 100 lb heats containing up to 2 wt percent Ti retain sufficient ductility (4 percent minimum strain to rupture) after neutron irradiation at 1400°F. It is likely that this alloy will be reproducible in larger heats of commercial size. As yet, however, proof is not available. Much scale-up work remains before any of these modified alloys could be qualified for reactor vessels.

Many other less attractive modified alloys have been made in heats up to 5000 lb which demonstrate adequate ductility when irradiated at 1200°F or less. These alloys, also uncoded, have demonstrated reproducibility,

2.3.1 Hastelloy N (Modified) (Cont'd)

Neutron Irradiation Embrittlement (Cont'd)

and it is believed several could be coded relatively easily. These alloys are satisfactory for MSR design if the design assures that the metal temperature remains safely below 1200°F during all normal modes of operation. Of course, a better alloy is highly desirable, but several are adequate if cooled.

In sum, current concepts are based on the assumption that the Hastelloy N will retain adequate ductility when irradiated at temperatures greater than 1300°F. This, in turn, is based on the assumption that small experimental heats having this capability will have reproducible and predictable properties when scaled-up. As previously stated, successful scale-up is likely but, as yet, undemonstrated.

A more conservative approach to MSBR design would be to adopt the limitations of the 5000 lb heats. The primary limitation is that the metal temperature during irradiation must be safely below 1200°F. It is entirely possible to design a high performance MSBR within this limitation.

2.3.2 Chemical Processing

General Conclusions

The chemistry upon which the chemical process plant is based is well established and documented.

The important equilibrium constants and distribution coefficients are large enough that the desired chemical reactions and ion exchanges can be made to occur with reasonably sized components and flow rates.

2.3.2 Chemical Processing (Cont'd)

General Conclusions (Cont'd)

The primary uncertainties pertain to engineering and economics. Of particular importance is the design of a continuous fluorinator having a protective frozen salt film and the design of the liquid bismuth loops. Although these systems can be designed with existing data, additional experimentation and engineering data are required before the useful life or performance of these systems can be predicted.

Graphite and molybdenum are the only known materials suitable for containing liquid bismuth. Whereas ORNL considers molybdenum the better choice, it is our conclusion that graphite is more promising because of its ease of fabrication and lower cost. It is easily fabricated into simple shapes and carbon based cements or packing appear suitable for joints and seals.

Design of components such as fluorinators, extraction columns, pumps, piping, and valves has received very little consideration as yet. There appear to be no engineering or design problems which cannot be resolved.

Instrumentation and control criteria are not yet established. On-line sampling analyses will undoubtedly be necessary. Methods of analysis remain to be developed.

Little consideration has been given to safety or waste disposal. It appears that the process plant presents no potential safety hazards which cannot be protected against by proper engineering safeguards and containment. Waste treatment and disposal methods must be engineered. This is, however, well within existing technology.

2.3.2 Chemical Processing (Cont'd)

General Conclusions (Cont'd)

It is our conclusion that sufficient data exists to permit design and construction of a demonstration chemical process plant. The data are insufficient to insure an optimum or reliable plant to predict or warrant its performance. It is doubtful if such data will become available without the construction of a demonstration plant.

Description Summary

The function of the chemical process plant is to maintain sufficiently low concentrations of ^{233}Pa and rare earths in the fuel salt. ^{233}Pa and rare earths are therefore removed from the fuel salt by chemical processes.

The reductive extraction method of separating Pa from the rare earths has the disadvantage that it also removes uranium (U). Thus to achieve efficient removal of Pa without requiring a large feedrate of reductant, the UF_4 is first removed as UF_6 from the salt by fluorination. Next the salt stream is contacted with a bismuth stream containing 0.2 mole percent metallic ^{7}Li as the reductant. Because Pa has a high distribution coefficient for bismuth relative to salt (221 at 600 C), about 93 percent of the Pa transfers to the bismuth stream. Any U which survived the fluorination process also transfers to the bismuth stream. Some of the rare earths also transfer to this bismuth stream; however, the rare earths have much smaller distribution coefficients and most remain in the salt stream until they enter the next extraction column having a much higher bismuth/salt flow rate ratio. This second contactor extracts the remaining Pa and a sufficient fraction of the rare earths. The salt is then reconstituted by contacting it with UF_6 and H_2 resulting in UF_4

2.3.2 Chemical Processing (Cont'd)

Description Summary (Cont'd)

going into solution. It is then purified and returned to the primary system.

Fluorination

Fluorination is required at three different places in the process: The fuel salt stream is fluorinated; ^{233}U produced by decay of ^{233}Pa in the Pa decay tank is recovered by fluorination; and U is recovered from the waste storage tank by fluorination.

Although fluorinators have received little design work as yet, they probably will be vertical columns about 5 in. ID by 10-12 ft long. They will contain fuel salt and free fluorine at 1000-1100°F. No known structural material is compatible with this mixture, thus ORNL proposes a protective frozen salt film to prevent corrosion. With a protective film, Hastelloy N or stainless steel probably will be suitable.

Continuous removal of U from fluoride salts has been demonstrated but with salt feed rates more than 100 times smaller than proposed in the Reference Concept. Over 99 percent of the UF_4 was removed from the salt with salt residence times as low as 28 minutes.

Ability to maintain a frozen salt film while fluorinating salt has been demonstrated. Detection of film loss has not yet been demonstrated. It appears, however, that film loss could be detected by monitoring the external wall temperature.

Remote fluorination of contaminated fuel salt has been demonstrated by the successful recovery of U from MSRE fuel salt.

It is concluded that continuous fluorination of fuel salt

2.3.2 Chemical Processing (Cont'd)

Fluorination (Cont'd)

is technically feasible. There are no apparent reasons why continuous remote fluorination of fuel salt cannot be done by scaling up the demonstrated methods. Uncertainties exist, of course, but they pertain to the ability to predict, with confidence, the performance of a particular design. These uncertainties will be resolved with additional experimentation. In the event that unforeseen difficulties arise, batch fluorination is a proven alternative.

Extractor Columns

The reductive extraction process in the salt-bismuth contactors has been demonstrated. The reported distribution coefficients are based on small scale experiments at the chemical equilibrium. Although reaction rate data are sparse, it is expected that at 600 C the rates are fast enough that equilibrium data are applicable. If this proves to be true, the reaction rates will be limited by the mass transfer rates of Pa and Li between the salt and bismuth phases. Thus dispersion of the two phases is important to get sufficient contact.

To get good dispersion ORNL proposes to use columns with various packings such as Raschig rings. Using mercury (dispersed phase) and water (continuous phase) to simulate bismuth and salt, column dynamics have been studied. Enough of the data has been substantiated from actual bismuth-salt data to lend confidence to the mercury-water experiments.

The data obtained suggest that only six theoretical stages are required for a Pa removal efficiency of 93 percent. The column would be about 6 in. ID by about 10 ft long. Either graphite or molybdenum would be suitable materials

2.3.2 Chemical Processing (Cont'd)

Extractor Columns (Cont'd)

of construction. Whereas ORNL considers molybdenum the better choice, we have tentatively concluded that graphite is more promising because of its ease of fabrication and lower cost.

Because of the high distribution coefficient of Pa, there is little doubt that the reductive extraction column can be made to work. As with the fluorinator, the primary uncertainty is in ability to design a column with existing data which will perform to specifications.

In general, it appears that most liquid transfers can be accomplished by pressurized gas; hence, few pumps are necessary. For reasons of safety and maintenance the process plant will contain several dump tanks with walk-away cooling systems. The plant will probably be arranged for vertical (remote) access and designed for easy removal and replacement of failed parts.

The total heat production rate in the process plant due to decay of fission products and Pa amounts to roughly 7 Mw of which 6 Mw appears in the Pa decay tank.

It is concluded that sufficient data to build a demonstration chemical process plant exists. There are not sufficient data to build an optimum or reliable process plant or to predict or guarantee its performance.

2.3.3 Coolant Medium

The fuel salt cannot transfer heat directly to steam because of:

1 - The adverse consequences of a tube failure causing a large amount of high temperature, high pressure steam to enter the primary system, and

2.3.3 Coolant Medium (Cont'd)

2 - The unreasonably high feedwater temperature required to prevent salt freezing.

Thus, the primary system and steam system must be separated by some intermediary coolant.

Sodium fluoroborate has received much attention as a coolant salt. It is known to be compatible with Hastelloy N when essentially no water is present. The tolerable water content is not yet established but is known to be very low - less than 10 ppm. This means the steam generators must be essentially free of leaks and, should a leak occur, that loop must be shut down, drained and repaired.

The consequences of mixing the fuel and coolant salts as a result of a failed heat exchanger tube are not well known. Although some data are available, it is not yet known how the sodium would be removed from the fuel salt or how fuel would be recovered from the coolant salt. The reductive extraction process does not remove sodium from fuel salt.

The salt cleanup problem is greatly simplified if leakage can be assured to be in one direction only. By pressurizing the secondary loop contamination of the coolant can in principle, be avoided. Provisions should exist for cleanup of either salt.

Ideally, the coolant salt should be chemically compatible with fuel salt and steam. Leaks should cause no adverse consequences. In addition it should have good heat transfer properties, be chemically stable up to about 1300°F, be noncorrosive, and have a sufficiently low liquidus temperature that a low feedwater temperature is possible. It should also be a material which would getter tritium and prevent its leakage into the steam system. No ideal coolant exists.

2.3.3 Coolant Medium (Cont'd)

The liquid metals generally suffer from compatibility problems: NaK and sodium precipitate UF_3 from fuel salt; the others are agressive toward or dissolve most structural materials.

Many molten salts appear suitable. The choice of sodium fluoroborate is based upon its physical properties and cost. It has three disadvantages, however: Sustained leaks cannot be tolerated; it does not getter tritium; and it requires a high feedwater temperature because of its high melting temperature. As an alternative $^7LiF\text{-}BeF_2$ salts are chemically compatible with the fuel salt. Such salts would be permitted to leak slowly into the fuel salt. A sustained steam leak, however, still could not be tolerated because precipitation of BeO would occur. It would not help prevent tritium leakage. The liquidus of the eutectic (48 mole percent LiF) is 752°F, about 27°F higher than that of sodium fluoroborate, but its viscosity is much higher. Nevertheless, these properties are satisfactory as proved by MSRE which used this salt as its coolant. ORNL rejected this salt as a coolant for the MSBR, however, because its cost.

An inert gas (He or A) coolant satisfies all requirements except one: It has poor heat transfer properties and thus requires large amounts of pumping power. It is nevertheless feasible. As a result of its low film coefficient, it will require a greater heat transfer area and thus, a larger salt volume in the heat exchanger.

A fluidized bed for transferring heat from fuel salt to steam has potential and should be developed for MSBR's. The state of technology of fluidized beds, however, is in its infancy. As yet, no fluidized bed has been built to transfer heat from one liquid to another. Correlations for heat transfer from tubes to the bed have been developed

2.3.3 Coolant Medium (Cont'd)

from experimental data. Preliminary calculations suggest that heat transfer coefficients will be adequate. It is clear that a fluidized bed heat exchanger offers the following potential advantages: A small gas leak into the fuel salt could be tolerated indefinitely; tritium can be trapped; freeze-up problems vanish; and the feedwater temperature can be lowered and the feedwater pressure-booster pumps eliminated. A fluidized bed heat exchanger would greatly simplify the MSBR concept and improve its reliability, availability and salability.

2.3.4 Tritium

The ORNL Reference Concept produces tritium in the amount of 2420 curies/day. Fifty percent is produced from the ^{6}Li (n,α) T reaction, 48 percent from the ^{7}L(n,α) T reaction, and the balance by ternary fission and the ^{19}F (n, $^{17}0$) T reaction. The behavior of tritium in this environment is not well understood. Because of the high temperatures, however, it is believed that a large fraction dissolves into the Hastelloy and diffuses into the coolant salt and on to the steam system. ORNL calculations indicate that about 69 percent of the tritium produced will enter the steam system in the Reference Concept and, subsequently, be released to the environment.

It is desirable to establish an acceptable release rate for MSBR's as a design objective. This release rate should be competitive with other reactor concepts. An advanced 1000 MWe PWR having zircaloy cladding will put only about 2 curies/day into the primary coolant water. It is intended, however, that the coolant be held indefinitely so that even this relatively small amount of tritium probably will not be released to the environment at the reactor site. The tritium retained by the element will eventually be released to the environment at the fuel

2.3.4 Tritium (Cont'd)

processing plant. This release rate for one 1000 MWe PWR amounts to about 350 curies/day.

An advanced 1000 MWe BWR having zircaloy cladding will produce tritium in the fuel at a similar rate (350 curies/day) and, hence, the release rate at the process plant will be roughly the same as a PWR. Because BWR's will not have borated water, the accumulation rate of tritium in the water is only about 0.5 curies/day based on one percent release from zircaloy cladding. (The fraction of tritium released from zircaloy cladding can vary by a factor of three for various zircaloy material.) Very little of this tritium is released to the environment from an advanced BWR, however. Blowdowns are prevented and leaks are collected, scrubbed and recycled into the primary system.

Thus in order for MSR's to be competitive with BWR's, more than 99.98 percent of the tritium produced must be trapped. Since substantial fractions of the tritium enter reactor and steam cell atmospheres, it is clear that these atmospheres must be processed for tritium recovery.

Two reliable methods for preventing tritium from entering the steam system have been advanced:

1 - ORNL has proposed that a third salt loop containing "Hitec" (53 wt % KNO_3, 40 wt % $NaNO_2$, and 7 wt % $NaNO_3$) be inserted between the coolant salt and the steam system.

2 - The Molten Salt Group has proposed use of a fluidized bed for transferring heat from the fuel salt to the steam system.

The "Hitec" loop cannot replace the sodium fluoroborate loop because hitec must be isolated from fuel salt. Tritium entering the hitec loop will form OT^- which is not soluble in Hastelloy N and, hence, will not leak out.

2.3.4 Tritium (Cont'd)

This method has the disadvantages of added cost, and a reduction in steam temperature since hitec is chemically stable up to only about 1000°F.

Of course, it is desired to drive the tritium into the off-gas system directly from the fuel salt. As yet, there is no evidence which suggests that this can be accomplished.

We do not consider the tritium problem to be a technological barrier to MSR's because two solutions to the problem exist.

Whereas the third salt loop has the two inherent disadvantages mentioned above, the fluidized bed has several inherent advantages which are not compromised by using it as a tritium trap.

2.3.5 Graphite

Fabrication

Graphite moderator elements can be fabricated in a wide variety of sizes and shapes. The technology for fabricating nuclear grade graphite elements having predictable and dependable characteristics (e.g.,density, grain size distribution, porosity, strength, and behavior under neutron irradiation) is well established. Since nuclear performance depends primarily upon salt fraction rather than element geometry, the element geometry should be chosen for easy fabrication, assembly and handling.

Reflector blocks, because of their larger size, require a modest scale-up over past experience but no extension of technology.

Dimensional Stability

Graphite having a maximum linear contraction of about 2 percent at a neutron fluence of 1.5×10^{22} nvt. is commercially available. Additional exposure causes it to swell.

2.3.5 Graphite (Cont'd)

Dimensional Stability (Cont'd)

In MSR's the graphite lifetime is approximately the time at which it returns to its original volume. In the Reference Concept this occurs after a neutron fluence of 3×10^{22} nvt ($E > 50$ kev), or four years of operation at a plant factor of 80 percent.

It is clear that only that graphite near core center is fully exposed. If the criteria were adopted that end of life occur when the entire graphite matrix returns to its original dimensions, the graphite would last at least five years. Substantial improvements over this, however, are not likely.

The possibility of allowing the graphite to expand beyond its original dimensions is probably limited by its porosity. In additional to being impermeable to fuel salt, it should also be impermeable to xenon.

Surface Seals

ORNL assumed that the graphite would have to be sealed to maintain a low ^{135}Xe poison fraction (0.5 percent or 0.005 neutrons absorbed in ^{135}Xe per neutron absorbed in fissile isotopes). It was proposed that the graphite be sealed by a pyrolytic coating. Although such coatings can be applied to graphite, experimental results thus far indicate that it deteriorates under neutron irradiation and will not survive an exposure of 3×10^{22} nvt ($E < 50$ kev). As yet, there is little or no experimental evidence which suggests that a pyrolytic coating will last the desired exposure.

MSRE Experience

MSRE experience strongly suggests that the xenon poison fraction will be acceptably low without a surface seal. MSRE operated with a poison fraction between 0.2-0.3 percent without sealed graphite and with poorly controlled

2.3.5 Graphite (Cont'd)

MSRE Experience (Cont'd)

conditions of void fraction, bubble size, and bubble stripping. Evidence which suggests that the graphite must be sealed in the Reference Concept is founded on analyses based on a speculative model and constants (e.g., mass transfer coefficients and solubility constants) which have large uncertainties. It is entirely possible and likely that MSBR graphite will not require sealing or perhaps very little sealing.

If the ^{135}Xe poisoning in an MSBR proves to be substantial, several alternate possibilities exist:

1 - The efficiency of ^{135}Xe stripping could be improved by increasing the gas purge rate or by increasing the bubble surface area via smaller bubbles.

2 - The graphite pores could be sealed by impregnation of a salt, such as ^{7}LiF.

3 - A pyrolytic seal could be used and the graphite replaced more frequently.

4 - A spray chamber for stripping xenon could be used.

Although we have not explored these alternates in detail, we have examined them sufficiently to determine that each has potential for reducing the poison fraction.

Our conclusion is that the graphite limitations do not constitute a technological barrier to successful MSBR's. The worst possibility is that the allowable neutron fluence might be about 1.5×10^{22} nvt ($E > 50$ kev) - about half of what is assumed in the Reference Concept. In this case the graphite would be replaced every two years instead of every four years. The fuel cycle cost would suffer but not seriously.

2.3.6 Reactor Physics

The models and methods for estimating MSBR nuclear performance are quite adequate for conceptual design. This conclusion is based upon extensive examination of ORNL computer codes, input data, and calculated results.

Breeding ratios up to 1.08 are possible. This value can be achieved by a) making the single fluid reactor so large that neutron leakage becomes negligible (~4000 MWe), or b) by the two-fluid concept (single fluid core surrounded by a fertile blanket). Doubling times as low as 10 years appear possible. In smaller sizes (~1000 MWe) the two-fluid concept, having little or no fuel in the blanket salt, has a substantially lower fissile inventory than the single fluid concept, and thus, a much shorter doubling time.

Single fluid MSBR's producing about 1000 MWe can achieve nominal breeding ratios between 1.06-1.07 and a doubling time of roughly 20 years - provided the salt inventory outside the core is reduced to an absolute minimum.

The total uncertainty in breeding ratio is reported[1/] to be 0.016. Eta for ^{233}U is, by far, the most significant contributor to this uncertainty. It alone contributes an uncertainty of 0.012 to the breeding ratio. Uncertainties in η, α, and μ for ^{233}U and ^{235}U yield an overall uncertainty of 0.014 in breeding ratio. Including uncertainties in cross sections of salt constituents, graphite, and fission products, the overall uncertainty was calculated to be 0.016. The uncertainties assigned to the data are, in our opinion, conservative. Thus, we consider it very unlikely that the actual breeding ratio would be outside of this range. Although these uncertainty calculations were performed for a specific MSBR concept, the neutron spectrum and neutron balance for that concept are very similar to a large class of MSBR's. Thus, the results are applicable to the entire class.

1/ USAEC Report ORNL-TM-2157, March 8, 1968, A M Perry

2.3.6 Reactor Physics (Cont'd)

MSBR's can be started up on ^{235}U or Pu. Cores having moderately low fissile inventories (i.e., those having a doubling time of about 20 years) will produce enough ^{233}U in four years to sustain operation thereafter on the Th-^{233}U cycle. At that time the nuclear performance is very nearly equilibrium, although other heavy isotopes are far from equilibrium.

Because the fuel is in liquid form isotope depletion (and buildup) occurs homogeneously. Without local depletion of fuel and with fuel concentration controlled by chemical processing (for breeders) or fuel addition (for converters), very little excess reactivity is required. The excess reactivity requirements, therefore, are simply to provide ample shutdown margin (0.25-0.50 dollars) and to override the power reactivity decrement. The power reactivity decrement is difficult to estimate and reliable values are not available. However, based on ORNL calculations of reactivity temperature coefficients and a xenon poison fraction of 0.5 percent (i.e., 0.005 neutrons absorbed in ^{135}Xe per neutron absorbed in fissile) a nominal value of $3 or roughly 0.3 percent $\Delta k/k$ appears reasonable.

2.3.7 Components

Hastelloy N

Hastelloy N has not been fabricated by suppliers of nuclear components; thus they will have to learn how to work with it.

MSRE components were fabricated almost entirely at ORNL with little difficulty. Those components performed satisfactorily. With the exception of a poorly designed freeze valve, no components failed and no leaks occurred.

Hastelloy type alloys are widely used by the chemical industry. Many large vessels have been fabricated from formed plate.

Hastelloy N is much more difficult to machine than mild steel. Nevertheless, common tools, machinery, and procedures are

2.3.7 Components (Cont'd)

Hastelloy N (Cont'd)

widely used for machining and forming it. It welds and forms easily.

Vessels

MSBR reactor vessels will probably be larger than any ever fabricated from Hastelloy. Because of its size, it will require field fabrication. The method of construction will probably be no different from that used by the chemical industry. The reactor vessel will be large and thin-walled (nominally 22 ft diameter, 2 in. thick), it will be flimsy and difficult to keep round.

After loading the graphite, raising the temperature to over 1000°F, and loading the fuel salt, warpage of as much as 2 in. on the diameter can be expected. The internals must therefore, be designed to accommodate this dimensional change, otherwise some of the stand-off ridges will be crushed causing some flow restriction.

The outlet nozzles and hot leg piping are subjected to a high temperature (roughly 1300°F) and will suffer thermal shock many times throughout the 30-year plant life. (A sudden reactor shutdown will cause the outlet salt temperature to drop by about 250°F in a few seconds.) Such severe conditions should be avoided by cooling and insulating the nozzles from the outlet salt.

We believe that a current Reference Concept should be based on the properties of Hastelloy N which are demonstrated to be reproducible in production heats. Since 1200°F is the temperature above which proven alloys lose much of their resistance to neutron irradiation, the vessel and nozzles should be cooled to some temperature safely below 1200°F.

Models will be required to demonstrate satisfactory flow distributions not only in the cooling channels next to the vessel, but in the plena as well.

2.3.7 Components (Cont'd)

Primary Piping

The delayed neutron flux in the hot leg piping is low enough and the spectrum hard enough that embrittlement is unlikely even at a metal temperature of 1300°F.

In addition to carrying normal pressure and moment loads, it must have enough flexibility to accommodate thermal expansion and survive thermal shock. It should also survive seismic forces. But piping failure does not precipitate the adverse consequences which ensue in LWR's.

It seems reasonable that pumps be mounted to comply with hot leg piping flexures. The heat exchangers can be mounted so that the bottom ends flex to accommodate thermal expansion in the cold leg piping. The vessel diameter increases by about 2-1/2 in. when heated from room to operating temperature. Vertically the vessel grows by about 3 in.

Due to large thermal growth and low strength of Hastelloy N at high temperature, adequate cooling and flexibility are serious design considerations.

Salt Circulating Pumps

Whereas ORNL believes that MSBR pumps could be a scaled-up, improved version of the MSRE pumps, the molten salt group does not consider this a feasible approach. Instead, it is our belief that submerged, hydrostatic bearings pressurized by the pump discharge are more attractive and more likely to succeed.

The pump should be located at the highest point in the system so that a free surface can be maintained. This permits the pump seal to be located above the salt.

It appears that the purge glands proposed by ORNL to prevent leakage of fission gas are not necessary. Instead, oil seals, cooled by forced oil circulation, can be made to work. There is much motivation for eliminating purge

2.3.7 Components (Cont'd)

Salt Circulating Pumps (Cont'd)

glands to eliminate the need for a clean gas stream and, hence, an elaborate gas cleanup system. Oil seals require that the primary system tolerate oil leakage at the rate of a few cc's/day. This requirement will probably apply even without oil seals.

The pump and motor should be mounted rigid with respect to one another. The entire pump-motor unit should be gimbaled to accommodate pipe flexures.

To avoid high pressure in the reactor vessel the primary pumps must be located in the hot leg. Thus, thermal shock is a problem. Although the pump housing could be cooled and insulated from high temperature salt, the impeller cannot. It must, like bearings and seals, be accessible for replacement.

A great deal of LMFBR pump development is directly applicable to the MSBR. Many large (up to 1000 horsepower) LMFBR-type pumps have operated successfully with pressurized hydrostatic bearings and oil lubricated seals.

Primary Heat Exchangers

To prevent excessive fuel salt inventory, the intermediate heat exchanger (IHX) must have very small tubes - probably about 3/8 in. OD. No manufacturer of components for nuclear systems has ever built an IHX with such small tubes and is not now tooled-up to do so. There is no technical reason, however, why this capability cannot be developed within a reasonable period of time.

The smaller, lighter tubes are more likely to vibrate. Although analytical methods for vibration analysis are available, only a demonstration plant (with full-length tubes and the actual salts at operating temperature) will prove a design.

2.3.7 Components (Cont'd)

Primary Heat Exchangers (Cont'd)

The delayed neutron flux is low enough that embrittlement of Hastelloy N (Modified) is unlikely even at temperatures over 1200°F. The hot tubesheet must be designed to withstand severe thermal shock and high thermal stress.

Heat transfer correlations are based on the analytical model by Dittus-Boelter and MSRE data. Because the viscosity of sodium fluoroborate and fuel salt is a sensitive function of temperature, entrance effects persist throughout the tube length. Hence heat transfer calculations are more uncertain than with conventional fluids. The smaller tubes and use of sodium fluoroborate are significant departures from the MSRE design. Since MSRE calculations erred by about 20 percent and the MSBR design introduces new uncertainties, we somewhat arbitrarily assume that the uncertainty in heat transfer coefficient of the MSBR is about 20 percent.

2.3.8 Maintenance and Repair

Maintenance and repair are two of the principal uncertainties in MSR technology. To insure successful maintenance and repair, it is necessary to design contaminated systems for remote access, to identify all such operations deemed conceivable, and to delineate the necessary tools and procedures. The plant design must be compatible with these tools and procedures.

MSRE was successfully maintained, although very little maintenance was required. It was arranged for vertical access to the entire primary system. Access was gained by removing portable concrete shielding blocks and cutting through an air-tight liner enclosing the primary system. Piping was sloped for complete drainage. A portable work shield with windows together with long-handled tools provided adequate shielding and permitted visual inspection as well as mechanical access.

2.3.8 Maintenance and Repair (Cont'd)

This arrangement worked satisfactorily for MSRE and a similar arrangement is proposed for the MSBR Reference Concept. The primary differences between MSRE and MSBR are the radiation levels and the physical size of piping and components.

Radiation levels at pipe surfaces will be at least ten times larger. It appears that the additional shielding requirements can be built into the work shield.

The larger pipes and components will require powered tools for manipulation of equipment. Remote cutting, welding, and inspection devices will be required if work is done on piping.

The design philosophy is to build contaminated systems conservatively with sufficient quality control that the need for repair or replacement of permanent items (e.g., reactor vessel, piping, pump housing, IHX shells, etc.) is very unlikely. Such repair, however, should be possible. Items such as graphite, IHX tube bundles, pump impellers, seals, and bearings should be easily accessible for replacement.

It is our opinion that a good design which is compatible with maintenance and repair procedures can be maintained and repaired without undue risk of prolonged outage or expense. Of course, earthquakes and accidents can be postulated which constitute economic calamity. We believe the probability of such events can be made acceptably low.

2.3.9 Safety

Analyses of the kinetic response of the Reference Concept to reactivity insertions show that it is difficult if not impossible to cause a nuclear excursion which constitutes a threat to the public or plant personnel. The reasons for this result are as follows:

1 - Large sources of excess reactivity are not available.
2 - The large prompt negative temperature reactivity coefficient of the fuel salt quickly terminates a prompt excursion.

2.3.9 Safety (Cont'd)

3 - The large heat capacity of the graphite absorbs the energy released.

4 - The physical properties of the salt and graphite remain approximately constant over a wide temperature range. Thus pressure surges, chemical reactions, or phase changes are not credible even with extreme temperature excursions.

Generally, MSR safety questions are based on postulated mechanisms which could cause loss of control of fuel salt and/or fission products. Because of the continuous processing, the fission product inventory in the fuel salt is at least an order of magnitude smaller than in LWR's. Although separated from the fuel, these fission products are still on site. Most of the short-lived fission products reside in the fuel salt or in the purge gas. Most of the long-lived fission products reside in the charcoal decay beds (fission gases) in the off-gas system, or in the chemical process plant (fission products with volatile fluorides or those soluble in bismuth), or deposited on surfaces (noble metal fission products or those with insoluble stable fluorides).

A fuel salt spill will cause no safety problem provided a catch pan and drain tank with adequate cooling is operable and the containment is not breached. Most of the fission products will remain in the salt. Those that do not will be in an inert atmosphere which can be purged or on surfaces which could be cleaned, if necessary. The same can be said for a spill in the chemical process plant. Walk-away cooling systems with redundant circulating loops will assure that the salt is maintained safely in the drain tanks.

It is probable that the purge gas emerging from the salt will be held up in a tank two or more hours before returning to the salt or entering a cleanup system. Such a tank

2.3.9 Safety (Cont'd)

will contain several hundred million curies of activity, although most of it is short-lived. The decay heat from the fission gases alone will amount to 10-12 Mw. If noble metals are carried into this tank by the gas stream, the heat load could double. Thus, this tank must assure the safe confinement of this activity and assure reliable heat rejection capability. High activity levels of gases and liquids is a unique but inherent characteristic of fluid fueled reactors. It appears that all contaminated systems can be made sufficiently safe, and the successful operation of MSRE supports this position. However, a 1000 MWe MSBR will produce more fission products in a few days than MSRE did in its entire life. Thus, activity levels and decay heat loads will be orders of magnitude greater in a 1000 MWe MSBR.

As yet, there are no official guidelines or safety criteria applicable to these unique aspects of MSBR safety. Therefore, safety considerations must be based on engineering judgement. Although we have not investigated all of the hypothetical safety problems, nor have we identified the maximum credible accident, it is our judgement that MSBR's can be made sufficiently safe.

3.0 BRIEF DESCRIPTIONS OF SEVERAL CREDIBLE MSBR CONCEPTS

This section presents brief descriptions of four MSBR concepts. The purpose of these descriptions is to illustrate the range of concepts supported, at least in part, by the technology presented in this report. It is intended to illustrate the flexibility of design and the options open to the designer. Each of these concepts was advanced and analyzed by ORNL.

3.1 Common Features

The concepts described in the following sections have many common features.

3.1.1 Fuel Salt

All use a carrier salt of $LiF-BeF_2-ThF_4$ (approximately 72-16-12 mole percent) in which small amounts of UF_4 and/or PuF_3 are dissolved.

3.1.2 Reactor Internals

All reactors are graphite-moderated. Each has long slender graphite moderator elements which determine the salt-to-graphite ratio and, thus, the neutron energy spectrum. They also define vertical flow channels. For optimum neutron economy a core salt fraction of 13 volume percent was chosen. Blanket regions can be formed by increasing the salt fraction to 30-60 volume percent. This produces a harder neutron energy spectrum which accentuates captures in Th resonances and reduces the fission rate. Reflector regions are over 98 percent graphite. Some salt flow is required to cool the graphite since it is heated by neutron and gamma scattering.

3.1.3 Primary System

The fuel salt enters the reactor at the bottom at about $1050^{\circ}F$, flows upwards through the core, and exits at about $1300^{\circ}F$. The salt then flows through a circulation pump, a heat exchanger, and returns to the reactor. Although the number is somewhat arbitrary, each concept has four parallel circuits (pumps and heat exchangers). The pumps are in the

3.1.3 Primary System (Cont'd)

hot leg to avoid high pressure in the reactor vessel (about 22 ft diameter by 20 ft high). The heat exchangers have small tubes (about 3/8 in. OD) to provide adequate heat transfer area without excessive salt inventory. The material of construction in the primary system is Hastelloy N (modified).

3.1.4 Secondary System

The fuel salt cannot transfer heat directly to steam for three reasons:

1 - A steam generator tube failure would cause pressurization and possible rupture of the primary system.

2 - A steam leak into fuel salt would cause a chemical reaction resulting in precipitation of UO_2 and BeO_2.

3 - Because the fuel salt has a very high melting temperature (930°F) the feedwater temperature would have to be very high to avoid salt freezing.

To circumvent these difficulties a secondary system transfers the heat from the fuel salt to the steam. This coolant circuit contains another salt, sodium fluoroborate ($NaBF_4$-NaF, 92-8 mole percent), which melts at 725°F and does not react with fuel salt or water. This salt circulates through a heat exchanger, a pump, and a steam generator or steam reheater. The proposed hot leg temperature is 1150°F and the cold leg 850°F.

3.1.5 Steam System

Since the coolant salt freezes at 725°F, the feedwater must enter the steam generator at about 700°F to avoid coolant salt freezing. Thus, a supercritical feedwater pressure is required, and the steam cycle must be supercritical. Feedwater pressure booster pumps which develop about 3800 psi are required. Except for these pressure booster pumps and steam temperature control by attemperation, the steam cycle is a conventional supercritical cycle.

3.1.6 Chemical Process System

Many parasitic neutron absorbers which form stable, soluble fluorides are produced by nuclear transmutation and as fission products. These isotopes will build up in concentration until the total production rate equals the total removal rate. The removal mechanisms are burnup, decay, and chemical removal.

It is desired that neutron losses to these isotopes be insignificant compared to neutron losses to the major parasitic constituents (Li, Be, F, and graphite). It appears feasible that all parasitic neutron losses can be less than 10 percent and losses to Pa and fission products can be less than 1 percent. This means the breeding ratio will be within 1 percent of its maximum theoretical value (i.e., the breeding ratio predicted if all neutron absorptions by Pa and fission products were eliminated). For an MSBR having a breeding ratio of 1.06 the breeding gain and, hence, fissile yield will be within 18 percent (0.01 x 1.06/0.06) of the maximum theoretically possible value.

It appears that this level of neutron economy can be achieved in many MSR concepts if the fuel salt is processed at the rate of about 1 gpm, providing the stripping efficiency of Pa from this stream is very high (about 98 percent) and the stripping efficiency of the most important rare earth, Sm, is 40 percent or greater.

Pa and rare earths can be removed from the salt stream by contacting it with liquid bismuth containing a reductant, either ^{7}Li or Th. Pa has a relatively high distribution coefficient (mole fraction of Pa in bismuth/mole fraction of PaF_4 in salt at equilibrium); therefore, it readily transfers from the salt into a small Bi stream containing only 0.2 percent Li. Rare earths, however, have a much smaller distribution coefficient. Thus, the flow rate ratio of Bi-to-salt must be much greater. Pa is first extracted in one contactor and rare earths are extracted in a second contactor having a greater Bi/salt flow ratio.

3.1.6 Chemical Process System (Cont'd)

Unfortunately, U also transfers to Bi via ion exchange with ^{7}Li. Although U could be recovered and returned to the salt, the rate of reductant (^{7}Li) transfer to the salt would be much greater than if it were absent, and the salt discard rate would be much greater. To avoid a large feed rate of reductant, U is removed from the salt by fluorination before the salt stream enters the Bi contactors. U is removed as UF_6 (gas) by injecting F_2 gas into the salt. Since the salt-fluorine mixture is highly corrosive and no known material of construction is inert towards this mixture, a frozen salt film is proposed. The fluorinators, as well as the Bi contactors, have received little conceptual design or engineering as yet.

UF_6 gas flows with the F_2 stream through NaF adsorbers where UF_6 is adsorbed onto NaF. This uranium is returned to the processed salt stream by heating the NaF adsorbers to drive off UF_6. The UF_6 is contacted with the salt in the presence of H_2. UF_6 is thereby reduced to UF_4 which dissolves in the salt.

^{233}Pa is transferred from the Bi to an isolated salt stream via hydrofluorination and held up for decay to ^{233}U. ^{233}U is then recovered via fluorination and returned to the fuel salt or sold.

3.1.7 Drain Systems

To assure personnel and plant safety there must be backup systems capable of receiving the highly contaminated liquids and containing them indefinitely. Aside from safety considerations it will be necessary to have storage tanks for use during normal maintenance. Safety considerations, however, require that these storage tanks have highly reliable cooling systems since decay heat will amount to many megawatts long after shutdown.

3.1.7 Drain Systems (Cont'd)

In case of a primary system rupture, the salt will spill into a catch pan, and after opening freeze valves, will drain into the tank. The heat rejection capacity of the drain tank cooling system was sized for 50 MW to accomodate the maximum credible heat load. Because of its size and heat rejection capability, it is a convenient place to hold up fission gases before they enter the off-gas system (discussed below).

For reliability, it is desired that this cooling system be independent of external power. This is achieved by many independent, natural convection cooling circuits. The drain tank contains many (about 1000) bayonet tubes inside thimbles. This arrangement provides a double barrier between the coolant and the fuel salt. Thus, heat transfer occurs by radiation across the gap. If the coolant is compatible with the fuel salt (i.e., if the coolant is $^{7}LiF\text{-}BeF_2$) only a single barrier is necessary. However, radiant heat transfer has the advantage that it varies as $(\text{temperature})^4$. Thus, the salt temperature can be maintained within a narrow temperature range in spite of a wide range of heat loads. With a double barrier, coolants such as Na and NaK are possible.

To assure that the cooling system functions properly and the tank is near operating temperature and ready to receive salt, it is desired to keep the cooling system in continuous operation. This is accomplished by using the tank for purge gas holdup. Fission gas decay heat drives the natural convection circuits and, thereby provides measureable flow rates and ΔT's.

3.1.8 Off-Gas System

Fission gases, primarily ^{135}Xe, are removed from the fuel salt by injecting helium bubbles. The bubbles will be chopped into very fine bubbles (0.001-0.005 in. diameter) by

3.1.8 Off-Gas System (Cont'd)

the primary pumps. A very large mass transfer surface is provided which enables the bubbles to absorb a large fraction of the fission gases. These bubbles circulate with the salt, on the average, 10 times before entering a side stream where they are separated from the salt. The purge gas flow amounts to about 10 scfm.

This highly contaminated gas stream is mixed with a small gas stream which purges the pump seals and provides cover gas over the salt in the control rod thimble and in the pump bowl. The combined stream then flows to the drain tank where it is held up before entering charcoal beds. Most of the decay heat appears in the tank. The off-gas system consists of charcoal-filled tubes submerged in water. Boiling or forced convection cools the charcoal and enables it to adsorb fission gases from the helium stream. Although not difficult to design, the charcoal beds are massive (about 27 miles of tubing) and thus, expensive.

As an alternate method of gas disposal, the purge gas could simply be diluted in a tank somewhat larger than the drain tank and recycled directly to the bubble generator. In this concept the concentration of ^{135}Xe would build up until the decay rate equalled the transfer rate to bubbles. This concentration would be acceptably low insofar as xenon poisoning is concerned.

3.2 Reference Concept

This concept is characterized by its high power density, good neutron economy and four-year graphite lifetime. A four-year replacement interval appears attractive because it gives near optimum nuclear performance for a single-fluid, 1000 Mw(e) MSBR, and it coincides with high-pressure turbine maintenance schedules anticipated in the future.

The graphite replacement interval determines the peak fast neutron

3.2 Reference Concept (Cont'd)

flux (E > 50 kev) and hence, the peak power density. Optimizing the reactor design subject to the constraints on peak fast flux and total power (2250 MWt) lead to the following:

Core salt fraction	13 vol %
Core diameter	14.4 ft
Core height	13.0 ft
Breeding ratio	1.07
Fissile yield	3.6%/yr
Fissile doubling time	19 years
Fissile inventory	1500 kg
Conservation coefficient	14.1 $(MWt/kg)^2$
Blanket salt fraction	37 vol %
Radial blanket thickness	1.25 ft
Axial blanket thickness (including plenum)	1.00 ft
Reflector thickness	2.5 ft

3.3 Single-Fluid, Non-Replaceable Core

This concept has a sufficiently low power density that the graphite will last the entire 30-year plant life. Its physical features have not yet been defined, but nuclear calculations indicate that a cylindrical core will have a diameter of about 26 ft and a height of 20 ft. The core would have a 2-1/2 ft thick reflector resulting in a vessel about 30 ft in diameter by 30 ft high[1/]. With chemical processing it would have a breeding ratio of 1.07, like the Reference Concept. But the fissile inventory would be larger, 2300 kg compared to 1500 kg, so that the annual yield is lower, only about 2.4 percent compared to 3.6 percent. Because of its lower power density, several favorable features, relative to the Reference Concept, result:

1 - The salt velocity in the core flow channels is lower; hence the Reynold's number and mass transfer rate of ^{135}Xe to the graphite is lower.

2 - The neutron and gamma fluence on the vessel is much lower reducing the cooling requirements and degree of Hastelloy embrittlement.

1/ ORNL-4548

3.3 Single-Fluid, Non-Replaceable Core (Cont'd)

3 - By eliminating the graphite replacement procedure, much maintenance equipment is eliminated and the system is simplified.

4 - Disposal of residual decay heat after a sudden salt drain, a serious problem in the Reference Concept, can be accommodated by radiation.

The primary objection to this concept is its low annual yield compared with other breeder concepts.

3.4 Single-Fluid Replaceable Core with Separate Blanket

The core, blanket, and overall dimensions of this concept are similar to those of the Reference Concept. It differs primarily in that the blanket is separated from the core by a graphite container which keeps the core salt separate from the blanket salt. The core salt is virtually identical to that in the Reference Concept. The blanket salt is like the core salt but without uranium.

Eliminating uranium from the blanket salt offers the following benefits:

1 - It substantially reduces the fissile inventory and, thereby, improves the annual yield.

2 - Neutron leakage is reduced so that the breeding ratio improves.

3 - By eliminating fissions near the vessel, the neutron fluence and neutron and gamma heating are greatly reduced.

4 - It greatly reduces the amount of decay heat produced near the vessel following a sudden drain and thus, reduces the cooling requirements.

The primary disadvantage of this concept is the requirement for a barrier separating the two salts. A 1-2 gpm leak rate of blanket salt into the fuel salt could, however, be tolerated. In principle, this concept offers a breeding ratio of 1.08-1.09, a fissile inventory as low as about 900 kg for an annual yield of 8-9 percent, and a doubling time of about 10 years.

3.5 Two-Fluid Replaceable Core with Separate Blanket

This concept was proposed by ORNL before the chemistry for processing a salt containing both fuel and fertile material was developed. At that time it was believed that one chemical process would be used for processing fuel salt and another for fertile salt. Accordingly, ORNL proposed a core consisting of graphite elements which contained separate fuel and fertile salts. The two salts were kept apart by confining them to separate flow channels throughout the reactor.

This concept had the serious disadvantage that it depended upon the structural integrity of a large number of graphite elements for keeping the salts separate. When a chemical process was developed which would remove Pa and rare earths from a salt containing both uranium and thorium, this concept was abandoned. Performance-wise, this concept had about the same potential as the previous one.

4.0 REACTOR INTERNALS

4.1 Core Graphite Moderator Elements

The core moderator elements are an important aspect of MSR design because they greatly influence the nuclear performance, thermal-hydraulic characteristics, and the fuel cycle cost. As design criteria they must a) set the desired salt fraction, b) define salt flow channels, c) permit orificing, d) be sealable (if sealing proves necessary), and e) be economical.

4.1.1 Influence on Nuclear Performance

The geometry of the moderator element influences nuclear performance in two ways: It determines the neutron energy spectrum via the salt/graphite ratio or salt fraction, and it determines the extent of flux depressions in the salt due to the thickness of the flow channels.

The salt fraction is chosen for optimum neutron economy and, therefore, depends on the figure-of-merit to be optimized. That an optimum salt fraction exists is evident from the following: Too much graphite causes excessive neutron captures in graphite; too little causes a hard neutron spectrum which requires an excessive fissile concentration to achieve criticality. Optimization studies[1/] performed by ORNL, based on the conservation coefficient as a figure-of-merit indicate that a salt fraction in the range 11-15 vol percent is near optimum for the core region of moderately high power density cores. Blanket regions can be made by reducing the graphite fraction thereby hardening the neutron spectrum and increasing absorptions in ^{232}Th resonances. This also reduces the fission rate in the blanket and, thus, reduces neutron leakage.

The effect of flux depression in the flow channels is small.

1/ ORNL-4541, pages 31-35, Sections by H F Bauman

4.1.1 Influence on Nuclear Performance (Cont'd)

Flow channels have substantial flux depressions in the energy range of ^{232}Th resonances. But because the resonances are narrow, the effect on reaction rates at lower energies is small for flow channels less than 1/2 in. thick. Although this effect could be significant for larger flow channels, it does not greatly influence the element design because the flow channels are made sufficiently small for other reasons.

4.1.2 Thermal-Hydraulic Characteristics

Most of the fission energy appears as heat in the flowing salt. A small portion, due to neutron and gamma scattering, appears in the graphite. This heat is removed by conduction through the graphite to the salt. Thus, the graphite will operate at a higher temperature than the salt. The peak temperature is controlled primarily by the geometry and thermal conductivity of the graphite rather than the film coefficient. For this reason the element geometry is chosen such that excessive temperatures are avoided since higher temperatures reduce the useful graphite lifetime (see Section 6.3). In other words, the peak graphite temperature sets an upper limit on the heat rejection path in the element. As a practical consideration, this limits the spacing of flow channels to a maximum of about 1-1/2 in.

For a fixed salt fraction, smaller elements result in more but narrower flow channels. Narrower flow channels require a greater pressure drop across the core for a specific salt velocity because the friction loss is, by far, the dominant mechanism for pressure loss. Since it is desired to avoid excessive pressure in the reactor vessel, it follows that the flow channels should be no smaller than necessary to satisfy graphite temperature requirements.

It turns out that a wide range element design is possible. For example, a plate-type element 1 in. thick will have a peak temperature of about 70°F above the surface temperature (for

4.1.2 Thermal-Hydraulic Characteristics (Cont'd)

a power density of 70 w/cc). For 13 vol percent salt the flow channel will be 0.15 in. wide and give rise to a pressure drop of about 20 psi in a core 13 ft high.

4.1.3 Fabrication

Many element geometries are possible from the standpoint of fabrication. For sealing, however, geometries having unaccessible surfaces, such as the hole in the square elements proposed by ORNL, are undesirable. Not only is the application of a uniform seal over the element length difficult, but inspection is nearly impossible. Hence geometries having only accessible surfaces are much preferred. (The application of seals is discussed elsewhere in this report.)

Plate-type elements appear to be easily fabricated, sealed, and inspected. Stand-off ridges can be machined into one side only to reduce the amount of machining required. Plates can be easily joined into assemblies for handling. Assemblies large enough for core replacement (or partial replacement) without involving an excessive number of assemblies, yet small enough that they are easily handled by machinery of moderate size are easily fabricated.

Elements can be assembled by joining them with glue (in low flux regions) and/or by using graphite boxes which bind them together at top and/or bottom ends. Alternately, the elements can be unassembled but handled in groups by a handling machine which can attach to an entire group.

Plates should be thin enough to prevent an excessive peak temperature. As discussed elsewhere, the graphite lifetime is greater at a lower temperature for a constant neutron fluence. Conversely, thinner plates require thinner flow channels for a constant salt fraction.

Analysis shows that plates 1-1½ in. thick having flow

4.1.3 Fabrication

shows that plates 1-1½ in. thick having flow channels 0.12-0.20 in. wide will have peak temperatures of 1280-1340 F and require pressure drops of 40-20 psi. These values are based on a peak power density of 70 watt/cc of core.

Spheres and cylinders have received consideration. Randomly packed spheres yield a salt volume fraction of 37 percent which is too large for good neutron economy (too many neutrons are absorbed parasitically in the carrier salt). Cylinders, like spheres, are easily fabricated and sealed but have several unattractive features: When packed into a triangular array they produce a salt volume fraction of 9 percent which is too low. For good nuclear performance 12-16 percent is desired. Cylinders could be spaced by a helical ridge but the flow in the cusps is poor resulting in poor heat transfer. Second, orificing of the flow channels is difficult and third, assembly into handling units is more difficult than plates.

4.2 Blanket Regions

Blanket regions differ from core regions only in that they have a larger salt fraction, about 37 percent. This salt fraction produces a hard neutron spectrum, relative to the core, and enhances neutron absorption in ^{232}Th resonance. Graphite elements in this region could be similar to those in the core, but the ridges should be deeper to increase the salt fraction. Generally, the power density is lower which relaxes cooling requirements and permits thicker elements.

4.3 Reflector Regions

Ideally, reflector regions would be 100 percent graphite. Because of neutron and gamma heating, however, some salt flow is required for cooling. The reflector will consist of rectangular or pie-shaped graphite blocks, separated by ridges for salt flow. The amount of neutron and gamma heating together with the maximum allowable temperature determines the size of the blocks and the salt flow for cooling.

4.3 Reflector Regions (Cont'd)

Since this is a low importance region, this graphite does not need to be sealed against ^{135}Xe. Reflector graphite nearest the core will require more cooling and, hence, a larger salt flow than that near the vessel. To reduce the fast fluence on the vessel the salt fraction in that vicinity should be as low as possible.

Axial reflector graphite should be attached to the heads such that salt flows between the metal and the graphite for cooling. The lower reflector graphite should be attached to prevent it from tending to float. The top reflector graphite should be attached so it can be removed with the top head.

Radial reflector graphite should be arranged so that it maintains the desired salt annulus between it and the vessel when the system is heated from room to operating temperature. This is desired for two reasons: To prevent the formation of a nonproductive salt volume and to prevent an unnecessarily high fast flux on the vessel. The salt volume in this annulus could be significant since the vessel diameter increased by about 2.5 in. when heated from room to operating temperature.

4.4 Salt Inlet and Outlet Plena

The primary purpose of the plena is to provide good flow distributions from the nozzles to the flow channels. They also serve as axial blanket regions.

Since graphite floats in the fuel salt, the elements will rise until restrained by the upper reflector. By allowing several inches of rise a lower plenum of 100 percent salt is formed. The upper plenum is formed by reducing the cross-sectional area of the graphite elements so that the salt fraction is 80-90 percent and salt can flow radially around the elements to the nozzles.

4.5 Reactor Hydraulics

Because nearly all of the fission energy appears in the circulating salt, the flow requirements are calculated very easily. This section presents simple expressions for the total mass flow

4.5 Reactor Hydraulics (Cont'd)

required, the salt velocity in the flow channels and a discussion of pressure considerations.

4.5.1 Total Mass Flow Rate

For a reactor producing a thermal power P using a salt with specific heat Cp and an average plenum-to-plenum temperature rise ΔT, the mass flow rate is given by

$$P = mCp\Delta T.$$

For a 2250 MWt MSBR having a temperature rise of $250^{o}F$, the mass flow is about 10^{8} lb/hr.

4.5.2 Salt Velocity in Core

The above expression can be applied to a single flow channel. In this case, P is the total power produced in that channel and m is the mass flow rate through that channel. Since the salt density changes very little from inlet to outlet, it is admissible to write

$$m = \rho A_f v$$

where ρ = average salt density in the channel

A_f = cross-sectional flow area

v = average salt velocity in the channel.

The power generated in a single channel is

$$P = \int_{V_f} P(\bar{r})d\bar{r}$$

where $P(\bar{r})$ = power per unit volume of salt

$d\bar{r}$ = differential volume

V_f = volume of flow channel

Then $P = p(\bar{r})HA$

where $\bar{p}(r)$ = axial-average power density at radius r

H = channel height

4.5.2 Salt Velocity in Core (Cont'd)

$$\text{Thus} \quad \bar{p}(r)\, HA_f = A_f v Cp \Delta T$$

$$\text{and} \quad v(r) = \frac{\bar{p}(r) H}{\rho\, Cp\, \Delta T}.$$

For a constant temperature rise the salt velocity is not dependent upon the cross-sectional area of the flow channel. It is simply proportional to the radial power density distribution and the channel height H, and inversely proportional to the salt heat capacity and temperature rise. Peak velocities of 8-10 ft/sec are likely in MSR's.

4.5.3 Pressure Considerations

As the salt enters the flow channel, there is a pressure drop due to the flow contraction. If the element geometry is such that blanket regions are at the top and bottom ends, there will be another flow contraction when the salt passes from the lower blanket into the core. There will be a pressure rise where the flow channel expands into the upper blanket and another one when the flow channel expands into the upper plenum. There will be friction losses in the core and axial blanket regions. By far, the largest pressure drop results from the friction loss in the core. The pressure changes due to channel contraction and expansion is over an order of magnitude smaller than the core friction loss. Overall pressure drops in the range of 20 psi across the core are likely in MSR's.

5.0 COMPONENT TECHNOLOGY

5.1 Introduction

The development of a MSBR plant must be directed primarily to the understanding and delineation of plant and component engineering considerations. The interplay between these areas is important as an acceptable design can only be achieved in a short time period by parallel work efforts with a full interchange of information.

Successful, economical and safe operation of the large molten salt breeder reactors will depend to a great degree on the reliable performance and the availability of all plant systems. These systems are made up of components and thus the performance and availability of the systems are directly dependent on the functional adequacy of the components, their individual reliability and their requirements for and ease of performing maintenance.

Because of the requirements for minimum fuel inventory and high component reliability, component engineering requires special emphasis on system interaction. The interplay between these areas is accentuated because of the fluid state of the fuel, the coolant's high melting temperature, significant radiation influences on structures, and the quest for good plant economics without compromising the inherent safety of the plant concept.

Component design is affected by many environmental and performance differences between other reactor systems, e.g., LWR, HTGR, LMFBR, GCFBR, and molten salt reactors. In some cases these differences may be resolved analytically but most require development of mathematical models and analytical techniques that are not commonly used commercially. Experimental confirmation of analytical results may be required. In other cases, detailed engineering and design work will clarify the problems and possibly resolve some uncertainties. In still other cases, fabrication of models and nondestructive and even destructive testing will be required before the degree of confidence is raised to a level that will justify construction and operation of the MSBR.

5.1 Introduction (Cont'd)

Of major importance are the components that must function in the molten salt or in the cover gas environment. High temperatures, temperature fluctuations,radiation effects, corrosion, salt deposits and the effects of fission product plateout must all be considered. Availability, reliability of performance, length of life, maintenance and economics are important.

Significant advances have been made in the development of components that are suitable for the high temperature operational environment of the LMFBR's. The molten salt environment is, however, substantially different than for sodium, while, in addition, the operating temperatures are higher. While it is possible to claim certain overlap of component development for both the LMFBR and the MSBR, the development costs for specific designs are likely to be of the same order for both systems, even allowing the LMFBR development to precede the MSBR.

There are other tasks, however, which are common to both plant development areas - for example, the development of high temperature design criteria for code analysis of vessels, development of tube vibration analysis methods (mechanics), and the development of surveillance and remote handling equipment.

The general areas of technology development which are common to all components include:

a - The development and selection of materials.

b - The development of an adequate design criteria for the selected materials which will permit the designer to understand the possible failure mode and use design theories to provide a safe design margin.

c - The development of codes and analytical methods to apply the design criteria to actual production design work.

d - The development of methods to assure freedom from harmful tube vibrations in heat exchange equipment operating in the high temperature molten salt environment.

e - The development of reliable heat transfer correlations for the fuel and coolant salts.

f - The development of design concepts for reactor vessels, intermediate heat exchangers and steam generating equipment.

5.1 Introduction (Cont'd)

g - The development of manufacturing techniques or procedures.

h - The development of methods for remote inspection and repair of components.

In addition, any portion of the system containing fuel salt will become sufficiently radioactive to require that all maintenance operations be accomplished by other than direct methods. The coolant salt pumps, steam generators and reheaters, however, will not become radioactive and after the coolant salt is drained and flushed they could probably be approached for direct maintenance.

Development of large components is probably the most costly of all the technology needs of the MSR. Most of the components built so far have been of MSRE size (8 MWt) or smaller. While the MSRE has demonstrated the workability of some small components, very much larger equipment will be needed for MSBR's.

5.2 Intermediate Heat Exchangers

The core vessel, heat exchangers, piping and indeed all material contacted by the molten salt require the following abilities: (1) resistance to corrosion by fluoride salts; (2) compatibility with the core material; (3) capability of being fabricated into complicated shapes by conventional processes, i.e., rolling, forging and welding; (4) good mechanical strength and ductility from room temperature to 1300°F; and, (5) capability of maintaining reasonable strength and ductility after exposure to a neutron environment.

At present, Hastelloy N appears to be most suited to the requirements. Although the original Hastelloy N developed at ORNL showed an inclination for weld cracking and reduction in high temperature ductility after irradiation in the MSRE, modifications in alloy composition are expected to improve performance. Hastelloy N is not a common material of construction in nuclear industries, and hence they have little experience with it. This material will, therefore, require considerable fabrication experience, exposure and usage before a high level of fabrication confidence and quality control can be assured.

5.2 Intermediate Heat Exchangers (Cont'd)

The development of materials data and design criteria for the material of construction is a major task if the design operating temperature of 1300°F is fixed as a target. The problems of creep, fatigue, interactions of creep and fatigue in the elastic and plastic ranges all require delineation.

Although the materials and design criteria technology is the major development area, additional design technology for a salt-to-salt heat exchanger will require development. The areas of concern are the heat transfer correlations, the requirements for compact design, and the problem of tube vibrations in the high density salt.

The salt-to-salt and sodium-to-sodium heat exchangers have many similarities including the design temperature and pressure range, maintenance and operational requirements, although the MSR conditions will be more severe.

Many sodium heat exchangers have operated reliably, while others have experienced difficulties in attaining design performance (Fermi) and tube vibration failures (Hallum).

Part-load operation has received very little consideration as yet. Any fluid-to-fluid heat exchanger will have lowered performance at part load because of a loss in effectiveness resulting from deviation from pure countercurrent operation. As far as estimating performance is concerned, the major areas of uncertainty are with the heat transfer correlations for the fuel salt and coolant salt. In a sodium heat exchanger, the overall heat transfer coefficient does not vary appreciably because of the large conductivity term in the correlations. The salt heat exchange coefficients developed by ORNL are directly dependent on Reynolds number. Since the salt viscosity is quite sensitive to temperature, the Reynolds number and heat transfer coefficient changes substantially throughout the tube length.

Pressure drop calculations are more of a problem, especially in the area of cross flow, because of the high density of the fluid. The accuracy of pressure drop calculations is of importance in compact

5.2 Intermediate Heat Exchangers (Cont'd)

design systems where the primary coolant salt volume significantly affects the fuel doubling time of the system. Generally, flow distribution devices tend to add to the required driving head.

MSRE experience suggests that salt-to-salt heat transfer coefficients can be predicted from theory to within about 20 percent.

Since ΔP is inversely proportional to (Bundle Diameter)^4, the optimum diameter can be obtained relatively accurately.

The influence of flow distribution devices which increase ΔP (such as baffles) is best observed by a parametric study. B&W has done this in the past where the cost of the pump can be traded off against the unit cost. While the total optimization including costs and pressure drop may give some designers problems, B&W has means of reducing them to a minimum by extending the techniques already developed for LMFBR, to include fuel salt volumes.

The problem areas in manufacturing will be similar to those encountered with PWR steam generators and sodium heat exchangers. Some additional problems may be forecast if very small diameter, thin wall tubing is used to reduce fuel salt inventory or if unusual tube bundle arrangements are found necessary.

One of the traditionally difficult areas to firm up is the design of the tube-to-tube sheet weld. The alternatives in ascending order of manufacturing difficulty are:

1 - Position rolled and welded on the front fore (with or without back brazing).

2 - Explosively expanded and welded on the front face.

3 - Explosively welded.

4 - Internal bore welded (with or without back braze).

5 - Back lip full-penetration weld.

For some designs, e.g., a straight tube bundle, alternates 4 and 5 appears to be out of the question because of the difficulties in assembly caused by weld shrinkage and the use of thicker tubes

5.2 Intermediate Heat Exchangers (Cont'd)

than what would be required, so that the tubes could be welded by these methods without burn through. Many units have performed reliably with the front side welded joint design. This type of weld bar has been used on over 200 steam generators for nuclear service without a single leak. Where there is cause for concern about crevice corrosion, explosive expansion or back brazing can be used. However, both of these techniques require special facilities.

Rapid maintenance without exposure of plant personnel to a radiation hazard is becoming a design objective for many utilities. B&W's sodium heat exchanger design combines the use of a remote orbital pipe cutter developed by ORNL with an explosive tube plugging technique and fixture designed by B&W. Explosive tube plugging techniques have been demonstrated successfully at the Oconee Station of the Duke Power Company on B&W heat exchange equipment.

5.3 Steam Generator

Although a molten salt steam generator has never been operated, a great deal of technology is available from the fossil boiler field and the once-through steam generators built by B&W for nuclear plants. The technology of supercritical operation per se presents no major problems, since it has been developed over the years to a stage where highly reliable units are in operation and have been for almost 20 years. In fact, the lower tube metal temperatures expected in the molten salt unit tend to make it a more conservative design than universal pressure boilers fired by fossil fuels.

Unlike a sodium heated steam generator, the molten salt unit will not experience a violent reaction if a leak should occur. However, there is much concern regarding the possibility of a leak in which high-pressure water and/or steam mixes with the molten coolant salt. The results of such a reaction are difficult to predict in detail. The effects of mixing are probably a function of both salt and water temperature, the flow rate of the water into the salt, and the tube size and ligament spacing.

5.3 Steam Generator (Cont'd)

Small leaks will not generally cause a pressure transient but it will result in contamination of the salt and the accompanying evolution of corrosive gases. Large leaks may produce severe pressure transients which is a function of the inlet water flow rate, the temperature and the time required to actuate the safety rupture discs. The actual kinetics of the saltwater reaction with the steam generators is not well known. Much work remains to be done in determining the effects of the salt-water reactions and in translating these effects into useful design information.

The occurrence of a leak and its accompanying salt-water reaction will necessitate the removal of the intermediate system from service. Assuming that the leak is detected and that the steam generator and associated intermediate system can be isolated and shut down safely, the plant operator still faces the problem of (1) assessing the extent of the damage, (2) locating the damaged areas and making repairs with assurance that all significant damage has been corrected, (3) cleaning up reactor products from the whole coolant system loop and (4) returning the system to operation, safely, and in the shortest possible time. Neither expedient methods for determining the extent of the damage to a steam generator or reheater nor methods for returning the unit to service has been formulated to date.

In consideration of the performance of the steam generator, several investigations of heat transfer to supercritical water have been reported in the literature. The Babcock & Wilcox program was quite extensive and, as a result of this, we believe that extensive work directed toward fundamentally measuring and correlating coefficients is unwarranted at this time. Nevertheless, the technology of supercritical heat transfer using Hastelloy N tubes is relatively new and there are questions of corrosion, fouling and the lower heat flux conditions associated with the molten salt arrangement which have not been evaluated due to the limited nature of this study. A steam generator design study is warranted to determine

5.3 Steam Generator (Cont'd)

the potential development areas. Consideration should be given to alternate materials of construction, cycle conditions and potential design improvements.

5.4 Reactor Vessel

The primary technological problem areas for the reactor vessel are similar to those of the heat exchange equipment; namely, the high temperature environment and the compact nature of the design. The design problems and material requirements become more critical because of the high salt temperatures which aggravate corrosion and neutron induced embrittlement of Hastelloy N.

The design temperature also affects fabrication of the vessel since it will relieve any built-in stresses caused by manufacturing. Some modern methods such as vibratory stress balancing may be applicable to the reactor fabrication to prevent distortion after one cycle to operating temperature.

The solution to flow distribution problems in the reactor vessel (as well as heat exchange equipment) is best carried out by hydraulic models. The size of the model and the fluid to be employed will require study to assure that the dimensionless numbers utilized to design the models will give a good empirical indication of what the actual flow distribution will be, since the scaling parameters may be different for flow and vibration models (which usually require matching densities at test temperature).

The size of the reactor vessel will be similar to or larger than a present-day BWR so that field fabrication will be required in certain cases. The technology for field fabrication will have to be extended to include working with Hastelloy N. Hastelloy N is about a factor of 3 more difficult to machine than carbon steel bar stock. As a rough comparison, type 304 stainless steel is about twice as difficult to work. Consequently, Hastelloy N will require slightly higher fabrication times than standard pressure vessel materials. It has good welding characteristics, but procedures will have to be qualified by all vendors for Section III fabrication.

5.4 Reactor Vessel (Cont'd)

Another field problem may be heat treatment of vessel parts or assemblies. At this time, it appears that the fluoride salts will not cause intergranular corrosion of the Hastelloy N and therefore solution annealing of completed vessels or weldments will not be required. If future findings or the use of alternate coolants necessitates very high-temperature heat treatment (2000°F or higher), advanced field stress relief methods would have to be developed.

Present methods and equipment are adequate for field heat treatment for relief of stresses built up during machining or welding.

5.5 Control Rod Drives

With the existing molten salt reactor concepts reactivity control is achieved by the removal of graphite moderator material from the core. The bouyancy force on the graphite results in an upward expulsion of the graphite control rod enabling the drives to be top mounted and located in the reactor cover gas environment. In this location the mechanism will operate in a similar environment to that of the gas reactors and LMFBR's.

The state of the art, however, has primarily been limited to the mechanical and electromechanical systems that depend on magnetic releases as the prime method of releasing control rods during a reactor scram. The major problem areas for existing LMFBR reactivity control system drives and also MSR's are associated with the deleterious effect that the dry gas environment has caused on materials and mechanisms. As yet there is little applicable data.

5.6 Molten Salt Valves

Experience with medium size or larger molten salt valves is nonexistent. A preliminary conclusion is that MSRE-type designs would not be acceptable and advance designs will be needed. However, the requirement for valves will be dependent upon the concept, the reliability of the major compact items, the engineered safeguards and the desirable plant capacity factor.

5.6 Molten Salt Valves (Cont'd)

Because the steam generator and reheater (if required) will be operated in parallel, a throttling valve may be needed to proportion the salt flow to the reheater for all twelve loads. In addition, a freeze type valve will be needed to isolate the primary salt flow from the fuel drain tank system.

5.7 Pump Technology

5.7.1 Factors Influencing Design

The factors influencing the design of molten salt circulating pumps are (a) functional characteristics, (b) operating environment, (c) weight and space limitations, (d) radiation shielding requirements, (e) containment and isolation requirements, and (f) maintenance considerations.

The functional characteristics include the hydraulic parameters of flow rate, total dynamic head, net positive suction head, efficiency, and operating range, and the service parameters of design life, reliability and availability. A pump will ordinarily be selected for a given set of hydraulic parameters, most often referred to as the rated or design conditions. Generally, the requirements can be satisfied with a single stage centrifugal or axial flow pump if the two expressions, $500 < N_s < 15{,}000$ and $S < 15{,}000$, can be satisfied simultaneously where $N_s = NQ^{0.5}/H^{0.75}$ is the performance specific speed, $S = NQ^{0.5}/H_s^{0.75}$ is the suction specific speed, N = revolutions per minute, Q = rated flow in gallons per minute, H = rated total dynamic head in feet, and H_s = net positive suction head in feet available at rated flow.

Operation of a centrifugal pump at flow conditions differing from the rated condition can be achieved by either throttling the discharge, varying pump speed, or a combination of both. Net positive suction head requirements and efficiency will vary from the values at rated conditions, and must therefore be considered for all possible points of operation.

5.7.1 Factors Influencing Design (Cont'd)

The design life of the pump will ordinarily be equal to the design life of the system it is servicing. Unless the pump is backed up by spare units, the reliability and availability requirements on it will most probably be high.

The operating environment includes the chemical and physical properties of the pumped fluids, the nature and condition of the surrounding atmosphere, temperatures and pressures, static and dynamic loads imposed by the system, and nuclear radiation levels.

Weight and space limitations on pumps are crucial to mission success for aerospace applications but are also of primary concern for earthbound systems, particularly as they are related to the capital cost of large stationary plants.

Radiation shielding requirements influence the pump design if the pump shaft is to penetrate the shielding as is necessary if the motor is to be located in a low radiation area.

Containment and isolation requirements relate to the integrity of system boundaries against egress of salt or cover gas from the pump or ingress of contaminants such as atmospheric air, water vapor, or lubricating oil into the pump.

Maintenance considerations are closely related to the service parameters of reliability and availability and determine in part the degree to which shielding requirements influence pump design. Components requiring periodic maintenance must be accessible for either remote or direct handling to minimize unavailability.

5.7.2 Definition of Current Technology

Beyond small experimental heat transfer and metallurgical test loops, only two working MSR systems have been built and operated to date, the Aircraft Reactor Experiment

5.7.2 Definition of Current Technology (Cont'd)

(ARE) and the Molten Salt Reactor Experiment (MSRE).[1/] After the two major changes in the ARE concept (first, the change from a sodium-cooled, solid-fuel reactor to a sodium-cooled, stagnant liquid-fuel concept, and, second the change to a circulating liquid-fuel, sodium-cooled moderator reactor) the pumping problems grew to include the handling of molten fluoride-salt fuel as well as liquid sodium coolant at temperatures up to 1500°F.[2/]

As a result of a pump development program[3/] a vertical pump shaft orientation was selected which, combined with a pumped-liquid/inert-gas interface, solved two major pump design problems. First, it reduced the pump shaft sealing problem to that of containing inert gas in a low-temperature region removed from the hostile high-temperature liquid environment and secondly, an overhung impeller feature avoided the research and development associated with finding a suitable bearing design for operation in the pumped liquid.

Three different pump sizes were built initially, ranging in capacity from 5 to 150 gpm. More than forty of the smallest of the three models were built and used in forced-circulation metallurgical test loops.[4/] These test loops were operated to investigate the corrosion of reactor structural materials by various molten fluoride salt mixtures, and the pumps performed relatively trouble free in the loops for a total

---

1/ M. W. Rosenthal, P. R. Kasten, and R. B. Briggs, "Molten-Salt Reactors - History, Status, and Potential," Nucl. Appl. Tech., 8, 107-116 (1970).

2/ E. S. Bettis, R. W. Schroeder, G. A. Cristy, H. W. Savage, R. G. Affel, and L. F. Hemphill, "The Aircraft Reactor Experiment - Design and Construction," Nucl. Sci. Eng., 2, 804-825 (1957).

3/ H. W. Savage, G. D. Whitman, W. G. Cobb, and W. B. McDonald, "Components of the Fused-Salt and Sodium Circuits of the Aircraft Reactor Experiment," ORNL-2348, Oak Ridge National Laboratory (February 15, 1958).

4/ A. G. Grindell, W. F. Boudreau, and H. W. Savage, "Development of Centrifugal Pumps for Operation with Liquid Metals Molten Salts at 1100-1500 F," Nucl. Sci. Eng., 7, 83-91 (1960).

5.7.2 Definition of Current Technology (Cont'd)

of several hundred thousand hours.[5/] The two larger models were developed for and used in the ARE. Subsequent to the ARE four additional models were developed and built, ranging in capacity from 500 to 1500 gpm.[4/]

The MSRE was a salt-fueled, graphite-moderated, single-region nuclear reactor designed for a heat generation rate of 10 MWt. The heat was transferred from the fuel salt in the primary circuit to a secondary circuit filled with coolant salt via a fuel-to-coolant salt heat exchanger. Two pumps were required, one in each of the two flow circuits. The two pumps were essentially identical and utilized design features developed for the earlier pumps.[6/] [7/]

The features common to all the successful molten salt centrifugal pumps developed and built to date include vertical orientation, overhung impeller, commercial grade antifriction bearings, and oil-lubricated face-type shaft seals. Table 5.1 summarizes data on the principal molten salt pumps discussed above.

The development of liquid metal pumps for nuclear service over the past 20 years has progressed to a greater extent than that of molten salt pumps because of the larger number of liquid metal systems built in that period and because of the many dissimilarities in those systems and early requirements for relatively high flow rates. Table 5.2 is a

---

5/ W. B. McDonald, J. L. Crowley and D. L. Clark, "Design and Operation of Forced-Circulation Corrosion Loops with Molten Salts," 1959 Annual Meeting, American Nuclear Society, V 15-17, 1959. Gatlinburg, Tennessee. Trans. Am. Nuc. Soc., 8, 174-176 (1959).

6/ P. G. Smith and L. V. Wilson, "Development of an Elevated-Temperature Centrifugal Pump for a Molten-Salt Nuclear Reactor ASME Paper No. 65-WA/FE-27.

7/ P. G. Smith, "Development of Fuel - and Coolant-Salt Centrifugal Pumps for the Molten-Salt Reactor Experiment," ORNL-TM-2987 Oak Ridge National Laboratory (October 1970).

Table 5.1

High-Temperature Molten Salt and Liquid Metal Pumps

Identification	Reference	Capacity (gpm)	Head (ft)	Speed (rpm)	Temperature (°F, max.)	Liquid	Material of Construction	Accumulated Operation at Elevated Temp. (hrs.)
LFB	(4)	5	92	6,000	1,500	Salt Na NaK	316 SS Inconel Hastelloy B Hastelloy N	292,000
DAC	(4)	60	50	1,450	1,500	Salt	Inconel	4,000
DANA	(4)	150	300	3,750	1,500	Salt Na NaK	Inconel	47,000
MN	(4)	500	120	3,600	1,250	Na NaK	-	4,000
MF	(4)	700	50	3,000	1,500	Salt NaK	-	32,000
In-Pile Loop	(12)	1	10	3,000	-	Salt	-	14,000
PKA	(4)	430	360	3,450	1,500	NaK Salt	-	8,000
PKP	(4)	1,200	390	3,500	1,500	NaK Salt	-	20,000
MSRE Fuel	(7)	1,200	50	1,175	1,400	Salt Helium	Hastelloy N	30,000
MSRE Coolant	(7)	800	78	1,775	1,400	Salt Helium	Hastelloy N	30,000
MSRE Fuel Mark-2	(7)	1,200	50	1,175	1,400	Salt	Hastelloy N	14,000

Table 5.2

Liquid Metal Pumps - Nuclear Service

Identification	Number of Units	Temperature of Liquid	Horse-power	Rated Capacity (gpm)	Head (ft)	Speed (rpm)	Type Bearing in Liquid Metal	Type Shaft Seal
Atomics International/ "SRE" Santa Susana Primary Pumps	2	1200°F Sodium	5	1,200	80	1,160	None	Freeze Seal
Atomics International/ "SRE" Santa Susana Secondary Pumps	2	1200°F Sodium	1	50	25	1,160	None	Freeze Seal
Atomic Power Development Assoc./ Enrico Fermi	1	1000°F Sodium	10	300	100	2,300	None	Double Mechanical Seal - Oil Lubricated
California Research Corporation/Brookhaven National Laboratory	1	1000°F Bismuth	10	50	22	1,160	None	Hermetically Sealed Motor
Brookhaven National Laboratory	2	1000°F Bismuth	100	360	64	1,160	Sleeve	Hermetically Sealed Motor
Corps of Engineers Pratt & Whitney/ "CANEL" Project	2	1400°F Sodium	350	2,000	610	3,200	None	Mechanical Seal - Oil Filled Motor
Corps of Engineers Pratt & Whitney/ "CANEL" Project	2	1500°F Sodium	300	2,000	460	3,200	None	Mechanical Seal - Oil Filled Motor
Corps of Engineers Pratt & Whitney/ "CANEL" Project	2	1300°F Sodium	700	4,000	610	2,450	None	Mechanical Seal - Oil Filled Motor

Table 5.2 (Cont'd)

Liquid Metal Pumps - Nuclear Service

Identification	Number of Units	Temperature of Liquid	Horse-power	Rated Capacity (gpm)	Head (ft)	Speed (rpm)	Type Bearing in Liquid Metal	Type Shaft Seal
Brookhaven National Laboratory	3	1000°F Bismuth	5	10	25	1,750	Sleeve	Hermetically Sealed Motor
Los Alamos Scientific Laboratory	1	1100°F Sodium	7.5	230	50	1,750	Sleeve	Double Mechanical Seal - Oil Lubricated
Los Alamos Scientific Laboratory	1	1100°F Sodium	10	230	110	1,700	Sleeve	Double Mechanical Seal - Oil Lubricated
Atomics International/ Hallam Prototype	1	1000°F Sodium	350	7,200	150	830	None	Freeze Seal
Power Reactor Development Associates/Enrico Fermi Overflow Pumps	2	1000°F Sodium	15	100	100	870	Sleeve	Double Mechanical Seal - Oil Lubricated
Argonne National Laboratory/ EBR-II, Idaho Falls	2	800°F Sodium	300	5,500	200	1,075	Pressurized Hydrostatic Bearing	Hermetically Sealed Motor
Power Reactor Development Associates/Enrico Fermi Secondary Pumps	3	950°F Sodium	350	13,000	100	825	Pressurized Hydrostatic Bearing	Double Mechanical Seal - Oil Lubricated
Power Reactor Development Associates/Enrico Fermi Primary Pumps	3	1000°F Sodium	1,000	11,000	310	900	Pressurized Hydrostatic Bearing	Double Mechanical Seal - Oil Lubricated
Atomics International/ Hallam Primary Pumps	3	1000°F Sodium	350	7,200	160	870	Pressurized Hydrostatic Bearing	Double Mechanical Seal - Oil Lubricated

Table 5.2 (Cont'd)

Liquid Metal Pumps - Nuclear Service

Identification	Number of Units	Temperature of Liquid	Horse-power	Rated Capacity (gpm)	Head (ft)	Speed (rpm)	Type Bearing in Liquid Metal	Type Shaft Seal
Atomics International/ Hallam Secondary Pumps	3	1000°F Sodium	350	7,200	160	870	Pressurized Hydrostatic Bearing	Double Mechanical Seal - Oil Lubricated
California Institute of Technology/Jet Propulsion Laboratory	1	300°F Sodium	25	1,000	60	1,160	None	Double Mechanical Seal - Dry Gas Lubricated
Atomics International/ "SCTI" Primary Loop	1	1200°F Sodium	200	4,000	160	1,750	Pressurized Hydrostatic Bearing	Double Mechanical Seal - Oil Lubricated
Pompes Guinard/ "GAAA"	1	1200°F Sodium	300	3,170	302	1,450	Pressurized Hydrostatic Bearing	Double Mechanical Seal - Oil Lubricated
Los Alamos Scientific Laboratory	1	1200°F Sodium	25	500	115	1,710	Sleeve	Double Mechanical Seal - Oil Lubricated
California Institute of Technology/Jet Propulsion Laboratory	1	2200°F Lithium	2	10	100	3,550	Pressurized Hydrostatic Bearing	Single Mechanical Seal - Gas Lubricated
Interatom	1	1040°F Sodium	40	660	164	1,400	Pressurized Hydrostatic Bearing	Double Mechanical Seal - Oil Lubricated
Atomic International/ "SRE" Expansion Primary Pump	1	1200°F Sodium	150	2,700	180	1,075	Pressurized Hydrostatic Bearing	Double Mechanical Seal - Oil Lubricated

Table 5.2 (Cont'd)

Liquid Metal Pumps - Nuclear Service

Identification	Number of Units	Temperature of Liquid	Horse-power	Rated Capacity (gpm)	Head (ft)	Speed (rpm)	Type Bearing in Liquid Metal	Type Shaft Seal
Atomics International/ "SRE" Expansion Secondary Pump	1	616°F Sodium	200	2,500	240	1,680	Pressurized Hydrostatic Bearing	Double Mechanical Seal - Oil Lubricated
Atomics International/ "SRE" Expansion Auxiliary Primary Pump	1	1200°F Sodium	25	102	30	850	Sleeve	Double Mechanical Seal - Oil Lubricated
Atomics International/ "SRE" Expansion Auxiliary Secondary Pump	1	616°F Sodium	30	93	45	980	Sleeve	Double Mechanical Seal - Oil Lubricated
Argonne National Laboratory	1	1200°F Sodium	100	800	320	1,700	Pressurized Hydrostatic Bearing	Double Mechanical Seal - Oil Lubricated
Massachusetts Institute of Technology	1	330°F NaK	30	250	330	3,550	None	Gas Seal - Oil Lubricated
Mine Safety Appliances	3	850°F NaK	25	850	75	1,200	Sleeve	Gas Seal - Oil Lubricated
Atomic Energy of Canada, Limited/ Chalk River	1	800°F Lead Bismuth	30	40	80	1,750	None	Gas Seal - Oil Lubricated
Neratoom	1	1022°F Sodium	880	7,900	410	1,500	Pressurized Hydrostatic Bearing	Double Mechanical Seal - Oil Lubricated

5.7.2 Definition of Current Technology (Cont'd)

chronological listing of the significant liquid metal pumps built to date including their salient features.

The design considerations for the liquid metal pumps have paralleled those for the molten salt pumps. For the most part, the earliest pumps were designed to eliminate the need for bearings in the liquid metal. Liquid metal freeze seals and hermetically-sealed motors were common solutions to the shaft sealing problem. As the pumps increased in size and reliability became essential, the vertical, free surface pump orientation was developed. The features common to the majority of the larger liquid metal pumps listed in Table 5.2 include vertical orientation, hydrostatic bearings pressurized with liquid metal from the pump discharge, and oil-lubricated face-type mechanical shaft seals. The major difference between the majority of the liquid metal pumps in Table 5.2 and the molten salt pumps of Table 5.1 is the use of a bearing wetted by the liquid being pumped.

The technical problems encountered in the development of the current state of the art for molten salt pumps may be categorized in relation to three chronological phases: (1) development, (2) production, and (3) operation.

In the program aimed at developing the pumps for ARE and subsequent applications many concepts were investigated and tested. Some were discarded early in the program and others were successful, became accepted practice, and continue in current routine use.[3/] The two primary areas of concern were bearings and seals for operation in the sodium and salt. Limitations on the space available for pumps in the ARE test facility made horizontal pump orientation preferable to vertical. A horizontal pump shaft requires a seal to operate wetted by the pumped liquid. During the pump development program many different methods of sealing shafts against the pumped liquid were considered and tested.

5.7.2 Definition of Current Technology (Cont'd)

The methods included packing, labyrinths, high-viscosity materials and frozen pumped-liquid seals. Of the methods actually tried, a number of sodium pumps operated satisfactorily with frozen sodium shaft seals, but no acceptable method was found for sealing salt.[8/]

The sealing problem has been defined as critical because of four objectives:[8/]

a - The seal must be virtually leakproof against escape of radioactive liquids or gases.

b - The seal must be virtually leakproof against entrance of oxygen and water vapor to avoid system contamination.

c - The seal must be intimately coupled with the pump rotary components to minimize size and liquid or gas volumes.

d - The seal must be maintained at appropriate temperature to assure dependable performance.

The vertical shaft orientation was selected primarily to reach these objectives, recognizing that it is much easier to seal inert gas in a relatively steady state, low-temperature region than to seal the pumped liquid in a high-temperature region subjected to operating transients.

The most conventional approach to sealing a gas at low temperature is an oil-lubricated face type mechanical seal. The seal must then minimize the leakage of oil into the pump and prevent the escape of cover gas out of the pump. To assure proper lubrication of the faces a slight positive pressure must be provided on the oil side above that on the gas side. Oil leakage rates measured in cc/day are typical for a properly designed face seal, maintained in good condition. The basic problem associated with this type of seal is the

---

8/ H. W. Savage and W. G. Cobb, "High-Temperature Centrifugal Pumps," Chem. Eng. Prog., 50, 445-448 (Sept, 1954).

5.7.2 Definition of Current Technology (Cont'd)

achievement of the optimum oil leak rate. If the faces are not lapped to the proper flatness and the sealing components are not positioned correctly excessive leakage will most probably occur.[4/] To prevent the migration of radioactive gases into a region containing oil which has leaked past the seal where plugging of drain and vent lines can occur as a result of polymerization, purge glands have been provided between the seal and liquid free surface. By providing a continuous flow of clean cover gas through the purge gland, back diffusion of radioactive gas has been shown to be negligible.[6/ 7/]

It has been a common practice to combine the bearing and seal lubrication requirements into one common system to avoid nonredundant duplication of components.[4/] The use of conventional, oil-lubricated antifriction bearings to support the overhung pump impeller eliminates the need for a bearing to operate in the pumped liquid, but does raise the question of the effects of nuclear irradiation on the bearing and seal lubricant. The lower pump bearing must be located as close to the impeller as temperature gradients will allow to minimize shaft deflection and dynamics problems. The area of the lower bearing is typically in a radiation field for nuclear applications. Recognizing the possible deleterious effect of irradiation, the ARE pump bearing housing was tested in a gamma-irradiation facility in the Materials Testing Reactor (MTR). The bearing housing operated in the facility for a total of 6,018 hours, with the total period of gamma irradiation being 5,016 hours, the lower bearing, seal, and oil-leakage reservoir receiving an integrated gamma dose of 10^{10} rads, and the circulating oil receiving approximately 2.4×10^{8} rads. Changes in the lubricant properties were noted, but none of them degraded the bearing housing performance. The test indicated that the bearing housing would operate satisfactorily for

5.7.2 Definition of Current Technology (Cont'd)

extended periods in a reactor if the irradiation dose is limited to 10^{10} rads and the leakage oil is drained away from the high flux region to avoid polymerization and subsequent plugging of lines.[9/] The level of activity to which the ARE pumps were exposed was relatively low because the reactor power was low, and the pumps were located outside of the primary reactor shield.[4/] Modifications were required when the original pump design was adopted for the MSRE where highly radioactive liquids were to be circulated, and the pumps were to be located inside the biological shield and primary containment. The modifications were aimed at minimizing radiation damage to lubricants and elastomers and at providing adequate cooling for removal of heat deposited by nuclear irradiation.[4/] They involved the elimination of elastomers from the shaft seals, the addition of an oil-cooled radiation shield plug between the bearings and the pumped liquid, the addition of a clean cover gas purge down the shaft annulus, and nitrogen cooling of the unwetted portion of the pump tank.

Although the experience represented in Table I indicates that reliable operation of molten salt pumps of the original design concept can be attained for long periods, it was recognized that the development of molten-salt lubricated bearings would be an important step toward reaching the following basic goals: (a) to simplify the auxiliary systems required for each pump, thereby increasing reliability, (b) to ease geometric restrictions and operating limitations inherent in the original bearing and lubrication methods, and (c) to develop designs suitable for operation in high radiation fields.[4/]

9/ D. L. Gray and A. G. Grindell, "Effects of Gamma Irradiation on a Conventional Bearing Housing Utilizing Oil Lubrication" 1959 Annual Meeting, Am. Nuc. Soc., June 1959, Gatlinburg, Tennessee, Trans. Am. Nuc. Soc., 8, 28-29 (1959).

5.7.2 Definition of Current Technology (Cont'd)

A series of tests was performed on a variety of configurations of molten-salt lubricated hydrodynamic journal bearings in a simulated pump environment as well as in an actual pump. The tests included investigation of bearing performance during start-stop and steady-state operating condition, over a Sommerfeld number range of 0.009 to 2.0. The tests also included investigation of the thermal stability of the nickel-molybdenum bearing and journal material common to all configurations tested.[10/]

Preliminary to the testing program a literature search was made to find candidate bearing materials for lubrication with molten salt at temperatures up to 1500 F. The best choice appeared to be the combination of molybdenum and tungsten carbide in a cobalt binder. However, differential thermal expansion would obviously be a serious problem with the coefficient of thermal expansion of molybdenum and tungsten carbide being one-third that of the most likely nickel-molybdenum alloy construction material.[11/]

To avoid developing special bearing mounts to allow for differential thermal expansion the test bearings and journals were fabricated of the nickel-molybdenum alloy, some pieces being case-carburized for wear resistance. The testing program demonstrated the practicability of molten-salt lubricated hydrodynamic bearings for centrifugal pump applications. However, the frequency of bearing seizure and detectable wear occurring during the program was high enough to require more extensive analysis and testing before definite conclusions could be reached. No immediate need was present at the time, therefore the bearing program

---

10/ P. G. Smith, "High-Temperature Molten-Salt Lubricated Hydrodynamic Journal Bearings," ASLE Trans., 4, 263-274 (1961).

11/ P. G. Smith, "Literature Search on Bearing Materials Compatibility with Fused Salts," ORNL CF-58-1-5, Oak Ridge National Laboratory (January 2, 1958).

5.7.2 Definition of Current Technology (Cont'd)

was suspended and no performance testing has been conducted for several years.[13/]

The ORNL MSBR studies brought a renewed interest in molten salt-lubricated bearings when it was realized that the pump shaft lengths required for the two-fluid reactor concept would necessitate a bearing in the salt.[12/] [14/] The switch to a single-fluid concept apparently reduced the pump shaft lengths as a result of the relocation of the pumps near the top of the reactor cell, reviving the possibility of utilizing the MSRE pump features, thus possibly eliminating the need for molten salt-lubricated bearings. However, the need for more definitive information on bearings and similar components wetted by molten salt stimulated a metallurgical study of hard-coated specimens.[14/] [15/] The original materials study program was scaled down to include only determination of composition and thermal stability until such time that an imminent need for additional information develops.[16/]

Production problems encountered with the molten salt pumps built to date have been in the general areas of casting quality and forming techniques. Many futile attempts were made at obtaining Inconel castings with satisfactory defect

---

12/ P. G. Smith, "Experience with High-Temperature Centrifugal Pumps in Nuclear Reactors and Their Application to Molten-Salt Thermal Breeder Reactors," ORNL-TM-1993, Oak Ridge National Laboratory (September 1967).

13/ A. G. Grindell, Oak Ridge National Laboratory, Personal Communication (September 30, 1970).

14/ D. Scott, "Systems and Components Development," Molten-Salt Reactor Program Semiannual Progress Report, ORNL-4191, Oak Ridge National Laboratory (December 1967).

15/ D. Scott, "Systems and Components Development," Molten-Salt Reactor Program Semiannual Progress Report, ORNL-4254, Oak Ridge National Laboratory (August 1968).

16/ D. Scott, "System and Components Development," Molten-Salt Reactor Program Semiannual Progress Report, ORNL-4344, Oak Ridge National Laboratory (February 1969).

5.7.2 Definition of Current Technology (Cont'd)

levels for the ARE pump impellers and volutes. The final solution was to fabricate the parts as weldments, heat-treat, and contour machine for the desired shapes.[3/] Similar problems were encountered in the procurement of the Hastelloy N castings for the MSRE pump impellers and volutes. The MSRE problems were solved by changing sources where closer attention was paid to chemistry and techniques and the performing of acceptable repairs on the castings.[7/] Additional problems were found in the forming of the Hastelloy N dished heads for the MSRE pump tanks. The original heads were hot spun from plate stock and contained defects on the knuckle radius. The final solution to the problem was to hot press the plate stock.[7/]

Difficulties which have become evident during preinstallation testing and during operation in working systems include cover gas purge and outflow problems complicated by oil leakage, problems with liquid level changes, vortexing, and gas entrainment in the pump tank, excessive shaft deflection, vibration, nonuniform preheating, thermal distortion, and failure of conventional auxiliary equipment.

During the testing program for the MSRE salt pumps, purge gas flow through the shaft annulus reversed because of improper pressure differentials and carried droplets of molten salt into the close-running clearance where they solidified and eventually caused friction loading on the shaft. The difficulty was solved by establishing and monitoring the proper gas flow rates in and out of the pump. During a filling operation for a subsequent test of the same pump, the shaft annulus was again plugged with solidified salt as a result of accidental bubbling of gas in the pump tank which splashed molten salt up the shaft.[7/]

The purge gas and fission product gases in the MSRE pumps were removed from the pump tank through an off-gas line which led to charcoal beds prior to release to atmosphere.

5.7.2 Definition of Current Technology (Cont'd)

Salt mist plugging in the off-gas system was observed during both the testing program[7/] and operation in the reactor.[17/] Possible solutions to this nuisance-type problem which have been devised and tested include traps and local heating. A similar problem also developed during operation of the pumps in the MSRE. Lube oil leakage into the pump tank also caused plugging in the off-gas system as decomposition and polymerization products built up at various locations. The solution was to provide added precautions against the entry of the lube oil into the high temperature regions of the pump.[7/ 17/]

As discussed earlier a gas/liquid interface was provided in the majority of the molten-salt pumps built to date to minimize the problems associated with sealing the pump shaft. However, serious difficulties have been encountered in maintaining the liquid free surface at acceptable levels in the pump tanks. A level too high in the tank will create heat transfer problems, flood gas vents, and/or damage low-temperature components. A level too low in the tank will lead to gas entrainment and/or pump starvation.

A common practice has been to place the pumps at the highest point and to provide no other liquid free surface in the system. If additional free surfaces do exist, pressure differentials between all of them must be determined accurately for all possible system flow conditions, transient or steady-state, to avoid unacceptable level changes.[4/]

Level changes will occur in the pump tank due to thermal expansion of the molten salt and variations in the amount of undissolved gas entrained in the liquid. Being a volumetric phenomenon, the expansion must be provided for in vessels containing a liquid free surface. If sufficient volume

---

17/ P. N. Haubenreich and J. R. Engel, "Experience with the Molten-Salt Reactor Experiment," Nucl. Appl. Tech., 8, 118-136 (1970).

5.7.2 Definition of Current Technology (Cont'd)

cannot be provided in the pump tank, a separate expansion tank can be connected to the pump with appropriate piping as was done on the original MSRE fuel salt pump. The separate tank adds a liquid free surface with attendant problems discussed above. The MSRE Mark-2 fuel-salt pump was designed with an enlarged integral tank to eliminate the extra liquid free surface.[7/] Some trouble with low levels in the ARE coolant pump was encountered as a result of leaking valves allowing liquid to drain from the system.[2/]

Vortexing or rotation of the liquid in the pump tank can also lead to heat transfer problems, flooding of low temperature regions, gas entrainment and/or pump starvation. This problem often does not become evident until it is found during a testing program. The primary sodium pumps for Rapsodie, the first French fast reactor, are an example of the vortexing problem found on test and solved with the addition of appropriate baffles within the pump tank.[12/]

Gas entrainment in the system liquid originating in the pump can result from low level and vortexing as discussed above or from severe agitation of the liquid free surface. Although the circulation of a controlled volumetric percentage of gas bubbles is being proposed as a method of stripping dissolved noble gases generated by fission in the MSBR,[16/] the inadvertent entrainment to cover gas in the pump would lead to unpredictable void fractions, accumulation of large pockets of gas in relatively stagnant areas of the system, unacceptable changes in the level of liquid free surfaces, and possible loss of pump prime.

The majority of the molten-salt pumps built to date has contained sources of high velocity leakage into the pump tank volume. Examples of such sources are impeller wear ring labyrinth clearances, stationary fits between mating components, and open vent apertures. It has been observed that if these sources are completely submerged in the

5.7.2 Definition of Current Technology (Cont'd)

free-surface liquid, little or no gas entrainment occurs. If these sources are not submerged, entrainment is likely to occur unless appropriate baffles are provided to channel the leakage into the free-surface at low velocity to minimize agitation.[4/]

The fuel-salt pump for MSRE contained a salt-spraying device designed for removal of dissolved noble gases from the circulating liquid. The device was located in the cover gas space of the pump tank, and the spray jets impinged on the liquid free surface in the tank. An undesirable amount of gas bubbles was carried into the pump suction during certain pump operating conditions which involved severe agitation of the liquid free surface by the impinging salt spray.[7/]

Gas may be introduced to the system liquid by a reversal of leakage through the impeller upper wear ring labyrinth, drawing cover gas from the free surface. The flow reversal will take place whenever the pressure differential across the labyrinth reverses. The pressure may be reversed by operation of the pump at a high flow rate reached by reducing system back pressure on the pump, by operation of the pump in a cavitating condition, or by pumping liquid of less density than that in the pump tank, such as occurs when handling entrained gas. These problems may be eliminated by regulation of system pressures and/or by limiting the operating range of the pump.[4/] If appropriate limitations cannot be placed on the pump, modifications to the design may be warranted as was true for the primary sodium pumps for the Hallam Nuclear Power Facility.[12/]

For pumps with the overhung impeller feature common to the majority of the molten salt pumps built to date, running clearances and allowable operating range must be carefully controlled to eliminate the possibility of excessive shaft deflection resulting in wear on parts not normally contacting, and severe structural damage accompanying shaft seizure.

5.7.2 Definition of Current Technology (Cont'd)

This type of shaft deflection results from a side load on the pump impeller developed by an unsymmetric pressure distribution around its periphery. For most pump case designs the side load is minimum at the pump design conditions, and operation on either side of the design condition at constant speed may result in an increased load. One of the original MSRE prototype pumps suffered a shaft seizure and extensive damage as a result of operation at an off-design condition.[18/] If operation at a condition removed from the pump rating is necessary, the resulting shaft deflection may be accommodated by increasing running clearances if the shaft strength and bearing capacity permit. However, the penalty for increased clearances includes larger gas purge flows through the shaft annulus and decreased pump hydraulic efficiency due to increased wear ring labyrinth leakages. Vibration problems may develop in the system as a result of pump operation at extremely high or low flow conditions.

Rubbing at close-running clearances and general misalignment may result from thermal distortion of high-temperature components. Thermal distortion can be caused by differential thermal expansion of dissimilar materials, uneven heating or cooling, and by lack of proper heat treatment. The pump designer should avoid the use of dissimilar metals or provide designs which will allow differential expansion without sacrificing reliability. Symmetric temperature profiles in a pump established by uniform heat transfer must be achieved to avoid misalignment and binding. The secondary sodium pumps for the Hallam Nuclear Power Facility suffered binding and rubbing of the impeller wear rings, and sodium-pressurized bearing as a result of nonuniform temperatures around the pump tank due to improper external cooling.[12/]

18/ R. B. Briggs, "Molten-Salt Reactor Program Semiannual Progress Report," ORNL - 3708. Oak Ridge National Laboratory (November 1964).

5.7.2 Definition of Current Technology (Cont'd)

Inadequate preheating of components in a molten salt system can be the source of similar problems.[2/] The importance of relieving pump components of residual stress by appropriate stabilization heat treatment is recognized.[4/] The original shaft in the primary sodium pump for EBR-2 was replaced due to permanent distortion attributed to improper heat treatment.[12/]

A common experience has been that following a thorough molten salt pump development program, the significant in-service difficulties with the equipment arise from failures of electrical control systems, electrical insulation, and conventional bearings.[12/]

5.7.3 Adaptation of Current Technology

In an attempt to determine the degree of applicability and possibilities for adaptation of current molten-salt and high-temperature pump technology to satisfy the pump requirements estimated for a 1000 MWe MSBR, the factors influencing the design of such pumps will be considered in light of known levels of achievement. Where the conditions fall into unknown areas, the amount and significance of risk associated with resolving the question will be defined and methods of resolution suggested.

The functional characteristics which influence the design include hydraulic and service parameters. If the hydraulic parameters of flow rate, total dynamic head and net positive suction head satisfy the limits defined by the expressions given earlier, a single-stage pump may be used, and from the standpoint of impeller and case design, maximum simplicity can be achieved. The majority of the pumps discussed earlier are of a single-stage arrangement.

Whenever applicability of previous experience is being considered for a particular set of pumping conditions, questions regarding the validity of scale-up must be answered.

5.7.3 Adaptation of Current Technology (Cont'd)

The pump designer typically works from a smaller hydraulic model which is similar to the larger pump being considered and is related by well-known affinity laws. Often hydraulic performance tests are performed with the smaller model rather than with the full-size pump to ease handling problems, to facilitate design changes, and to minimize the investment in test apparatus. An example of such a model test program was that conducted during the development of the 65,000 horsepower pumps for the pumping plant at the Grand Coulee Dam. These twelve vertical, single-stage, single-suction pumps with 14-ft diameter impellers and 12-ft diameter discharge nozzles were developed with a model scale ratio of 13 to 1, resulting in a very close prediction of full-scale performance.[19/] With due regard for scaling effects, the hydraulic characteristics, including flow rate, total dynamic head, net positive suction head, hydraulic efficiency, and operating range of a large pump can be established and verified by testing a relatively small scale model.

Model testing and/or full scale testing of a large molten salt pump may be conducted in water with good correlation of test results to hydraulic performance in molten salt. The liquid sodium and molten salt pumps for ARE were based on water pump design parameters, tested with water and then with sodium or salt, and found to have no significant disagreements between theory and actual desired performance.[3/] The development programs on molten salt pumps since the ARE project, including the fuel-and-coolant salt pumps for MSRE, have followed the same procedure of water-based design, water test, and salt test, with excellent prediction of hydraulic performance.[4/ 7/] Model testing techniques well established in the centrifugal pump industry,

---

19/ Carl Blom, "Development of the Hydraulic Design for the Grand Coulee Pumps," Transactions of the ASME, 75, 53-70 (1950).

5.7.3 Adaptation of Current Technology (Cont'd)

combined with the predictable correlation of water performance test data, should result in negligible risk in achieving the hydraulic functional characteristics desired for a large molten salt pump.

With sound hydraulic design assured by the proven procedure defined above, the service parameters of life, reliability, and availability will depend primarily on mechanical and electrical considerations. The major areas of concern are materials, structural statics and dynamics, bearings, seals, and electrical drive and control system components. Several of these considerations are interdependent, and all are affected by their respective environments and service conditions. Unlike the factors influencing hydraulic characteristics, the major areas of concern for the service parameters cannot be proven on a small scale model test and factored up to full size by a simple relationship.

A prime example of the difficulty in extrapolating data is the production of wrought and cast raw material in the sizes required for the components of the pumps for a 1000 MWe MSBR. The general topic of materials is treated elsewhere in this report, as it is common to all components wetted by fuel and coolant salt, however it should be noted here that techniques established for small-scale production of the required iron- and nickel-base alloys may not be factored up due to technical or economic problems, resulting in the fabrication of large pumps from a great number of relative small pieces with possible compromises in design. Similar compromises in design may result from the limitation on the size of integral components which can be handled on existing machine tools even if large pieces of raw material should be available. Definite limitations exist on length and diameter of single pieces which are to be machined to close tolerances.

Another aspect of the materials problem is the deterioration of the mechanical properties of iron- and nickel-base alloys

5.7.3 Adaptation of Current Technology (Cont'd)

as a result of exposure at high temperature to thermal-neutron flux. The scale-up difficulty is in this case related to life of components. The deterioration, being partially time dependent, would not be as critical in a short-lived test system as it would be in an MSBR designed for a 30-year life. These two questions on material are of prime concern not only as they may affect the design and life of the pumps but as fundamental to the design and life of all components in similar environments. Therefore resolution of these questions is considered in a general sense of basic importance.

Structural design considerations of a static nature, such as wall thicknesses and geometric configurations for given static loading conditions, are dependent on the high-temperature properties of the materials of construction. Load stresses in the material are usually reduced by increasing section thickness, whereas thermal stresses are generally reduced by decreasing section thickness. These conflicting measures are common in high-temperature design work, but are particularly troublesome when a model is scaled-up to full size. The full-size component may require severe redesign in geometry or rework of existing geometry to include thermal baffles or shields for protection of structural members. These considerations can be resolved by appropriate analytical techniques.

As the weight of pump components increases with the scale-up of dimensions, the stiffness of the structural components must be increased as necessary to control dynamic deflections and vibrations. The achievement of required stiffness may involve an increase in complexity of components rather than a simple scale-up of section thickness for reasons discussed above.

A major consideration included in the topic of structural dynamics is the need for a guide bearing near the pump

5.7.3 Adaptation of Current Technology (Cont'd)

impeller, operating in the pumped liquid. During the design phase of the molten salt pumps built to date it was possible to avoid the requirement for a salt bearing, but this feature limited the geometry and operating range of the pumps and the level of radiation to which the pumps could be subjected. The pump structural components and shafts could be made stiff enough to achieve resonant frequencies or critical speeds well above the highest operating speed. Adjustable speed operation provided variable flow rates without throttle valves, thus minimizing the side load on the pump impeller, a source of shaft deflection and vibration.

As the size of the pumps and length of their shafts are increased, an overhung impeller design becomes impractical from the standpoint of critical speed. Studies have shown that the shaft diameter can become prohibitively large when designing for subcritical operation and too small to transmit the required torque when designing for a supercritical condition.[14/] Further studies have concluded that subcritical design is most desirable to avoid a large number of unknowns associated with supercritical design, and that the most practical way of achieving it, assuming that a bearing is located near the impeller and that the shaft and supporting structure are as stiff as practical, is to reduce shaft length and/or speed.[16/ 20/]

The majority of the larger liquid metal pumps listed in Table 5.2 was designed with at least one guide bearing in the pumped liquid. Both hydrodynamic and pressurized hydrostatic bearings have operated successfully in liquid metal. The portion of this liquid metal bearing technology related to the topic of structural dynamics may be safely applied to molten salt pumps, however the liquid metal

---

20/ Mechanical Technology Incorporated, "Feasibility Study of Rotor-Bearing System Dynamics for a 1250 HP Molten Salt Fuel Pump," MTI-68TR9 (April 12, 1968).

5.7.3 Adaptation of Current Technology (Cont'd)

bearing metallurgy which has been proven by the experience evidenced in Table 5.2 cannot be applied completely. The basic concept of a bearing and journal constructed of the same material as the surrounding components and hard-surfaced with a wear-resistant material is applicable, but the actual metallurgical selections for a molten salt environment will be different from the austenitic stainless steel, nickel- or cobalt-base hard alloy combinations proven for liquid metal service. Final resolution of the metallurgy for bearings in molten salt service may very well depend on the type of bearing selected.

The tilting pad bearing has been selected in design studies for large molten salt pumps because of its inherent stiffness and stability and apparent ability to adapt to conditions which would normally result in bearing damage.[15/ 16/ 20/] However, the most recent design studies and pump specifications for large liquid metal pumps favor the hydrostatic bearing because of its simplicity and history of success.[21/ through 27/] Although the tilting pad bearing concept appears to have advantages in the area of operating

---

21/ Byron Jackson Pump Division, "Large Sodium Pump Design Study, Phase I Report," SAN-681-1, USAEC Contract AT(04-3)-681 (July 1969).

22/ Westinghouse Advanced Reactors Division, "Large Sodium Pump Design Study, Phase I," WARD-3762-1, USAEC Contract AT(30-1) 3762 (March 1968).

23/ Westinghouse Advanced Reactors Division, "Low Capacity Sodium Pump Design Study, Phase II Final Report," WARD-3762-11, USAEC Contract AT(30-1)-3762 (June 1969).

24/ Westinghouse Advanced Reactors Division, "Medium Capacity Sodium Pump Design Study, Phase II Final Report," WARD-3762-12, USAEC Contract AT(30-1)-3762 (July 1970).

25/ Westinghouse Advanced Reactors Division, "FFTF Primary Pump Ordering Data," WARD-BDR-362-19, Fourth Issue (December 1969).

26/ Westinghouse Advanced Reactors Division, "FFTF Secondary Pump Ordering Data, WARD-BDR-362-21, Fourth Issue (December 1969).

27/ Westinghouse Advanced Reactors Division, "LMFBR Low Capacity Prototype Pump Ordering Data," WARD-BDR-362-27, Third Issue (December 1969).

5.7.3 Adaptation of Current Technology (Cont'd)

efficiency and overall simplicity due to its self-acting character, the hydrostatic bearing concept has advantages in ruggedness and simplicity of the critical bearing components, important features in high-temperature design. The tilting pad bearing must be free to adjust for changes in operating speed and loading, requiring joints designed for low relative motion under high unit loading. Whereas the primary bearing surfaces would be protected by a hydrodynamic fluid film, the hinged joints would have to function with minimum boundary lubrication at best. The selection of metallurgy for such joints is limited and may very well compromise bearing design or rule out the tilting pad bearing altogether.

It is recommended that the first generation of large molten salt pumps utilize the hydrostatic bearing concept, pressurized with salt from the pump discharge, to have the greatest probability of success and least chance of complications during development. The design and sizing techniques already established for liquid metal hydrostatic bearings may be applied to molten salt, leaving the question of metallurgy for the hard-surfacing on the bearing journal and bearing bore the primary area of investigation. The studies already begun on this question should be continued until a satisfactory metallurgical combination is found which will assure protection against bearing damage during starting and stopping of the pump.

The import of the structural statics and dynamics considerations is that a small pump may not be scaled up structurally with simple proportionality factors as is the case with the pump hydraulics. Small pumps may avoid the requirement of a guide bearing wetted by the pumped liquid and be constructed of a small number of simple pieces, whereas a larger pump which is similar hydraulically may be very complex in comparison, requiring a proportionately greater amount of analytical verification.

5.7.3 Adaptation of Current Technology (Cont'd)

The vertical, free-surface pump concept was developed to minimize the unknowns and difficulties associated with providing a seal to atmosphere between the rotating and stationary pump components. On small pumps it has been a common practice to design the seal for the dual functions of sealing gas on one side and antifriction bearing lubricant on the other. In some cases the gas side of the seal has been eliminated by utilizing a hermetically-sealed driver with no shaft penetration to atmosphere. The hermetically-sealed driver still requires seals for the single function of preventing contamination by bearing lubricant. The hermetically-sealed driver necessitates complications in peripheral cooling and lubricant systems and complicates maintenance operations. For these reasons the majority of the larger liquid metal pumps listed in Table II were designed to utilize an oil-lubricated, mechanical face type shaft seal, with conventional open driver. This system has also been recommended in the majority of recent design studies and specifications for large liquid metal pumps.[21/ 23/ 25/ 26/ 27/] Because of concern over the possibility of gross seal failure leading to contamination of high-temperature systems with lubricant, gas-lubricated face type seals have been utilized on two liquid metal pumps listed in Table II and have been recommended in several design studies on both molten salt and liquid metal pumps.[16/ 20/ 22/ 24/] However, current state-of-the-art for both hydrodynamic and hydrostatic versions of the gas face seal is in its infancy and very little definitive experience exists. With appropriate design, the probability of contamination by lubricating oil as a result of gross seal failure can be reduced to an acceptable level, hence the proven oil-lubricated version of the mechanical face-type shaft seal is recommended as best meeting the four objectives listed earlier for molten salt pump seals with no significant development required.

5.7.3 Adaptation of Current Technology (Cont'd)

Whereas molten salt pump components are for the most part special designs, the electrical drive and control system components have been of a more commercial variety, if not in fact standard commercial items. The MSRE pump was driven by a squirrel-cage induction motor rated at 75 HP and sealed in a hermetic vessel.[7/] A total of eight pumps listed in Table 5.2 were driven by hermetically-sealed motors of similar conventional design. Where variable speed operation of the squirrel-cage motor has been a requirement, power supply has been from a variable frequency/voltage source. Conventional wound-rotor motors and constant speed squirrel-cage motors, with eddy-current couplings make up the balance of the variable speed drivers for the liquid metal pumps listed in Table 5.2.

It is probable that a variable flow rate will be required in either the primary or secondary loops of a large MSBR as evidenced by recent part-load temperature control studies.[28/] It is unlikely that large control valves will be available to provide throttling or bypassing, leaving adjustable speed pump drive systems the only practical solution. The squirrel-cage induction motor is by far the simplest electrical prime mover. For such a motor, variable speed operation is achieved by providing a variable frequency/voltage power supply. Example sources of such power which may be located remotely from the motor are a-c/d-c/d-c/a-c motor generator sets, a-c/a-c motor generator sets with adjustable speed coupling between motor and generator, and static frequency converters. Variable speed may also be achieved by placing an adjustable speed coupling directly between the induction motor and the pump shaft. Such couplings may be either electrical

---

28/ W. H. Sides, "Two Schemes for Part-Load Temperature Control of the MSBR," MSR-70-56, Intra-Laboratory Correspondence, Oak Ridge National Laboratory (August 21, 1970).

5.7.3 Adaptation of Current Technology (Cont'd)

(eddy-current coupling) or hydraulic (fluid coupling) and provide a controlled slip output from a constant speed input.

A wound-rotor induction motor with remotely located liquid rheostat or power conversion equipment wired into the rotor circuit will provide controlled variable speed down to approximately 50 percent of full speed in driving a centrifugal pump. The liquid rheostat is used to vary the resistance in the rotor circuit, thus varying the slip between the rotor and the stator fields. A direct-current motor with adjustable-voltage power source will provide controlled variable speed down to approximately 10 percent of full speed by adjustment of armature and field voltages.

Recent studies have considered these alternates for large liquid metal pumps and have selected the wound-rotor motor with liquid rheostat because of definite advantages in simplicity of the system and relatively low capital and operating costs.[21/ 22/] To achieve speed ranges greater than 2-to-1, integral tandem wound-rotor motors, brakes, or pony motors may be added to the basic wound-rotor motor. The wound-rotor motor is the simplest overall system in current state-of-the-art for high horsepowers. However, the squirrel-cage motor with static frequency converter, currently limited in horsepower, would be a simpler system if available. The wound-rotor motor requires brush replacement and maintenance on a regular and frequent basis, which would make a hermetically-sealed motor impractical. If for reasons of positive leak-tightness, a hermetic enclosure is deemed necessary, the squirrel-cage motor would be the only practical choice.

For either the wound-rotor or squirrel-cage induction motor, scale-up of horsepower to that estimated for a large MSBR transforms the drive and control system components from a standard commercial nature to a special form, tailor-made

5.7.3 Adaptation of Current Technology (Cont'd)

for each application. Specific power level of the components tends to increase with scale-up, as size or volume does not increase proportionately with power. In addition to size, special inertia requirements to meet spin-down specifications, extra thrust bearing capacity to carry pump shaft loads, and special radiation-resistant electrical insulation and elaborate cooling systems for hermetically-sealed designs all change the drive and control system components from standard to special.

It is recommended that as much of the technology being developed for large liquid metal pump drive systems as possible be utilized in the first generation MSBR, and that smaller molten salt systems should employ the same general type of drive to build up a service history upon which to base improvements. This philosophy would put the greatest concentration on variable speed systems composed of wound-rotor induction motors with liquid rheostat control to achieve the service parameters of life, reliability and availability at the desired levels with the least risk.

The operating environment which influences the design of molten salt pumps consists of the chemical and physical properties of the pumped fluid and of the ambient, and system imposed conditions such as pressure, mechanical, and thermal loading, and nuclear radiation. The fluid properties of interest are density, gas content, vapor pressure, viscosity, surface tension, heat capacity, thermal conductivity, and corrosivity to structural materials, all in terms of temperature in the range from liquidus to maximum.

The general areas of consideration which are affected by these properties are heat transfer (cooling and heating requirements), vapor or mist migration, condensation, and freezing, cavitation and vapor binding, corrosion, and power requirements. The fluoride salts used in the past and currently proposed for fuel circuits have been well documented

5.7.3 Adaptation of Current Technology (Cont'd)

over the past 20 years. Further data measurements are recommended, however, particularly for the sodium fluoride/sodium fluoroborate salt currently proposed for coolant circuits.[1/]

The ambient will undoubtedly be different for components located above and below the crane bay floor (reactor cell roof and radiation shield) of a large MSBR. The components below the floor most likely will be surrounded by a high-temperature nitrogen gas, low in oxygen and water content, and at a pressure somewhat below atmospheric to preclude outleakage in the case of a breach in the containment boundary. The ambient above the floor most likely will be atmospheric air in a closed system with control over temperature and humidity. The decision favoring a totally-enclosed liquid-cooled motor over an open type air-cooled motor will depend not only on the question of absolute containment as discussed earlier, but also on the load imposed on the air-conditioning equipment by the heat dumped from the motor.

Another important consideration involving the ambient is the possibility of unsymmetric heat transfer between the pump components and the nitrogen gas in the reactor cell. An unsymmetric temperature profile around the pump due to uneven convective currents and/or localized heat sources or sinks in close proximity to the pump will result in loss of alignment and possible binding and severe damage.

Closely associated with the ambient nitrogen considerations is the question of auxiliary heating requirements imposed by the molten salt system. The system must be preheated to a temperature above the liquidus temperature of the salt before the salt can be introduced to avoid solidification. The filled system must also be maintained at temperature by the auxiliary heating devices during periods when the reactor is not in operation. There are basically two different philosophies followed on designing the auxiliary heating system. One philosophy is to trace the exterior of each

5.7.3 Adaptation of Current Technology (Cont'd)

component to be heated with electrical resistance elements supported on electrical insulation, and held against the outer surface of the part. An oven is formed around the part with both reflective and mass-type thermal insulation covering but not touching the traced surfaces so as to allow for convective heat transfer within the enclosure.

The other philosophy is to provide electrical space heating of the entire cell within which salt-containing components are located. Thermal insulation is placed on the boundary walls of the cell rather than on the surfaces of the components. This arrangement for auxiliary heating is commonly referred to as the "furnace" concept. Certain advantages and disadvantages become apparent when the "trace" and "space" type auxiliary heating of a large molten salt pump are compared. Advantages in trace heating are found in its rapidity and high degree of control. More symmetric temperature profiles are assured with localized thermal sources and insulation. Space heating is largely dependent on convective heat transfer within the equipment cell. Location of the equipment in relationship to the heater elements and the cell walls will have a significant effect on temperature distributions. Advantages in space heating are found in its simplicity and ease of maintenance. All the fitting and attachment problems associated with the localized heating elements and insulation required for trace heating are eliminated with centralized sources and insulated cell walls. Space-heating elements are easily replaced due to their centralization, and more so if they are made accessible from the crane bay floor. Failure of trace-heating elements would require manual entry into the equipment cell to accomplish repairs or replacement due to the complexity of the heating and insulating system.

The preheating procedure for either the "trace" or the "space" type auxiliary heating system must be planned in

5.7.3 Adaptation of Current Technology (Cont'd)

considerable detail. Components will heat up at different rates depending on their size, shape, and complexity. Therefore heat input must be distributed accurately to avoid building up excessively high thermal stresses within and between components in the system. The circulation of hot gas within the loop during the preheating procedure was accomplished with the MSRE pumps,[7/] and has been suggested for future systems to aid in a more even heating of all components until temperature is high enough to introduce salt. It has also been suggested that the capability of the salt pumps to circulate gas in the loop be utilized to remove afterheat from the reactor core following an emergency salt drain.[29/] It must be recognized, however, that a pump fitted with a molten-salt-lubricated guide bearing could not be converted easily to circulate a gas.

Although some of the smaller and less complex components of a typical molten salt loop may be preheated effectively by the "furnace" concept, it is recommended that at least the critical sections of a large molten salt pump be traced with heating elements to insure control of heatup. Provision could be incorporated for maintenance of the elements from the crane bay floor to gain the advantages of both methods of heating.

As in any high-temperature pump application, the question of fatigue life as related to system imposed thermal transients is of basic concern for a large molten salt pump. Most structural components of a pump can be redesigned or protected with thermal baffles if by analysis thermal stresses are found to be excessive. Pump hydraulic components, in particular the impeller, however, cannot be changed as freely as the structural components because of the geometric restraints

29/ E. S. Bettis and Roy C. Robertson, "The Design and Performance Features of a Single-Fluid Molten-Salt Breeder Reactor," Nucl. Appl. Tech., 8, 190-207 (1970).

5.7.3 Adaptation of Current Technology (Cont'd)

placed on them to insure proper function and efficient operation. Assessment of the severity of the thermal transient question can be made early in the pump design program to reduce the risk of costly redesign after pump and system designs have been developed in detail.

Nuclear radiation and fission products in the pump environment deposit heat in areas not automatically cooled by flowing salt. The largest temperature gradients in the MSRE pumps were attributed to this phenomenon. Because the power rating of a large MSBR would be 50 to 200 times that of the MSRE and the distances between the major components equal to or less than those in the MSRE, diverted-salt cooling of those sections of the pump normally above the free surface has been proposed.[30/] [31/]

With the vapor pressure of the proposed salts at a negligible value throughout the expected temperature range, the only significant pressure loading on a molten salt pump would ordinarily be the pump differential. Cover gas pressure, however, could be increased from slightly above the vapor pressure to provide sufficient pressure at the pump impeller inlet to suppress cavitation. The actual overpressure required would depend on characteristics of the system in which the pump is installed compared with the net positive suction head requirements of the pump.

Additional mechanical loads imposed on the pump by the system would include nozzle loads primarily due to thermal expansion of the loop and seismic loads in the vertical and horizontal directions. The magnitudes of both the thermal expansion and

---

30/ D. Scott and A. G. Grindell, "Components and Systems Development for Molten-Salt Breeder Reactors," ORNL-TM-1855, Oak Ridge National Laboratory (June 30, 1967).

31/ D. Scott, "Systems and Components Development," Molten-Salt Reactor Program Semiannual Progress Report, ORNL-4396, Oak Ridge National Laboratory (August 1969).

5.7.3 Adaptation of Current Technology (Cont'd)

seismic loads depend not only on thermal elongation and seismic accelerations, but on the method of support of the pump in relation to other "fixed" and "floating" points in the molten salt system.

The method of pump support is fundamental to the solution of a number of conflicting physical objectives. The weight of the pump and its contents must be supported with a minimum of static deflection and with due regard for vibratory and seismic action. With the close spacing of components and overall philosophy of space conservation, in a large commercial MSBR thermal expansion of the high-temperature loops must be allowed by "floating" some of the components. The loads generated between the components would be prohibitively high if rigid mounting were utilized at all locations. For practical reasons, it is common practice to "fix" the larger components, whereas the smaller equipment is "floated." The pump, therefore, is customarily free to move as the loop changes temperature. The pump assembly is one of the few pieces of equipment however, that usually penetrates the crane bay floor, which complicates the design of the pump support. Various methods of supporting a large high-temperature free-surface pump have been studied,[21/] but a final decision must be made only after careful study of the synergistic effects of both pump and system objectives. A compromise solution to the pump mounting problem has been proposed in design studies of a large primary-salt pump for a 1000 MWe MSBR,[31/] but the complications associated with the method would warrant further study.

As noted above, it has been a common practice to locate the drive motor and cover gas shaft seals of large high-temperature, free-surface pumps outside the biological shielding to protect motor insulation and lubricants from thermal and radiation damage and to allow for preventative maintenance and servicing procedures on various components. The required

5.7.3 Adaptation of Current Technology (Cont'd)

continuity of both the pump and the biological shield through their mutual intersection necessitates the incorporation of shielding material within the pump structure. Where annular clearances are necessary between pump components which must move relative to each other, the shielding must be stepped to eliminate direct streaming of radiation through the gap. If the pump is mounted flexibly, special attention must be paid to the preservation of shield continuity for all possible orientations of the pump with respect to the stationary shielding.

Of importance equal to that of the radiation shielding requirements is the containment and isolation of fission products, primarily volatile gases. The recommended oil-lubricated, double face type shaft seal would be an effective barrier against the escape of gases to the atmosphere or into the hermetic closure of a totally-enclosed motor. It would be advisable, however, to hold the radioactive gases away from the seal area for two reasons. First, radiation in that area should be minimized to prolong the life of the seal lubricant and to avoid polymerization of the lubricant which has leaked past the lower seal. The other reason would be to have the area as clean as possible if maintenance of the seal should be required. A common method of preventing the contaminated gases from reaching the immediate area of the seal is to provide a purge gland around the shaft somewhat below the lower seal face. By flowing clean cover gas through the gland, contaminated gas is swept back into a lower region of the pump and lubricant vapors are prevented from migrating down the shaft annulus. With appropriate regulation of the purge flow rate, back diffusion of contaminated gas into the seal area can be avoided.

Maintenance of a large, free-surface molten salt pump may be considered under either of two categories: that performed from the crane bay floor with the pump in the loop, or that

5.7.3 Adaptation of Current Technology (Cont'd)

requiring removal of the pump from the loop. The typical arrangement with motor and shaft seal above the crane bay floor allows maintenance of these items without removal of the pump. With appropriate design of the pump-to-motor shaft coupling, the seal may be completely replaced without removing the motor and disturbing its alignment, an important time-saving feature for large pumps. It is common practice to incorporate a secondary pump shaft support and sealing device below the primary seal to function as the coupling is removed and the primary seal opened.

The components of vertical, free-surface pumps which are located below the crane bay floor are typically designed to be removed in one piece without disturbing the integrity of the system. This "pull-out" feature would be accommodated by raising the pump from its usual support into an isolation cask from where it can be decontaminated and repaired. The removal operation could therefore be performed without loss of cover gas from the system and even with the system full of salt if it should be necessary.

6.0 SPECIAL MATERIALS TECHNOLOGY

6.1 Fuel and Fertile Salts

6.1.1 Criteria

The requirements for any fluid reactor fuel are:

a - Adequate solubility of U, Pu and/or Th over the necessary temperature range.

b - Low neutron capture cross section.

c - Thermal stability at temperatures needed for high quality steam.

d - Radiation stability.

e - Low vapor pressure.

f - Low liquidus temperature.

g - Good heat transfer properties (high thermal conductivity and heat capacity).

h - Good hydrodynamic properties, especially viscosity.

i - Low corrosion

i. Towards some suitable container material.
ii. Towards a suitable moderator material.

j - Tolerance for fission products.

k - Low cost.

l - Adaptable to chemical processing.

m - Low chemical reactivity with

i. air

ii. water

6.1.2 Attractive Salts

Based on thermal neutron absorption cross sections, consideration for a thermal spectrum reactor is pretty much limited to the elements tabulated in Table 6.1 except for

6.1.2 Attractive Salts (Cont'd)

the necessary fissile and fertile isotopes. The list may be broken down into

Desirable ($\sigma a < 0.05$ b)

Tolerable as major constituents but with a sacrifice in breeding potential (0.05 b, $< \sigma a <$ 0.35 b)

Tolerable only in limited quantities (0.4 b $< \sigma a <$ 0.7 b)

For epithermal reactors the choice is wider, but from other considerations the list would probably be extended only to include normal lithium and chlorine.

The list of acceptable elements can be narrowed considerably on the basis of thermal stability, volatility and chemical compatibility of available compounds.

Most hydrogen or deuterium compounds are unstable at high temperature. Only alkaline hydroxides and a few hydrides have adequate thermal stability above 1000°F. The hydroxides dissolve very little uranium and are very corrosive to virtually all useful metals, whereas the hydrides are strong reducing agents and not likely to be compatible with uranium compounds.

Uranium and thorium form high-melting binary compounds with O, C, N, S, Si, P.

Oxygenated anions suffer either from thermal or radiation instability or inadequate solubility of uranium and thorium. In general, binary compounds tend to show greater radiation stability than more complex molecules.

As a practical matter, the choice of desirable fluid fuel constituents seems to be limited to fluorides and chlorides. While chlorides tend to have lower melting points than fluorides, the thermal neutron absorption cross section of natural chlorine is undesirably high (32 barns)

Table 6.1

Neutron Absorption Cross Sections of Several Materials
(Barns-2200 M/S)

Material	Absorption Cross Section (Barns)
Nitrogen-15	0.000024
Oxygen	0.0002
Deuterium	0.00057
Carbon	0.0033
Fluorine	0.009
Beryllium	0.010
Bismuth	0.032
Lithium-7	0.033
Boron-11	0.05
Magnesium	0.063
Silicon	0.13
Lead	0.17
Zirconium	0.18
Phosphorus	0.21
Aluminum	0.23
Hydrogen	0.33
Calcium	0.43
Sulfur	0.49
Sodium	0.53
Chlorine-37	0.56
Tin	0.6
Cerium	0.7
Rubidium	0.7

6.1.2 Attractive Salts (Cont'd)

and even separated ^{37}Cl is 0.56 barns. Fluorides also have generally lower vapor pressure than chlorides and a higher heat capacity either by weight or volume. The F^- ion does not provide sufficient moderation for a thermal reactor. On the other hand, it moderates somewhat too well for a really fast reactor for which chlorides would be preferred.

Fluorides (and other salts) of Bi, Pb, Sn are readily reduced by common structural metals and furthermore, these elements as metals tend to dissolve many structural metals.

Hence, the choice of fuel constituents is limited pretty much to fluorides of Be, ^{7}Li, Mg, Zr, Ca, Na and possibly Ce and Rb.

The $LiF-BeF_2$ system almost uniquely meets the requirements for a fluid thermal reactor fuel. Although the eutectic mixture containing 52 percent BeF_2 has the lowest liquidus (360 C), its viscosity is undesirably high and the final choice involves a trade-off between melting point and viscosity.

6.1.3 Salts Examined by Laboratories

a - Invariant equilibria data and phase diagrams

Phase diagrams of attractive systems for molten salt fuel and fertile salts are shown in Figures 6.1 through 6.13 as follows:

Figure 6.1 $LiF-BeF_2-UF_4$

Figure 6.2 $LiF-BeF_2-ThF_4$

Figure 6.3 ThF_4-UF_4

Figure 6.4 $LiF-ThF_4-UF_4$

Figure 6.5 $LiF-PuF_3$.

6.1.3 Salts Examined by Laboratories (Cont'd)

a - Invariant Equilibria Data and Phase Diagrams (Cont'd)

Figure 6.6	$LiF-BeF_2-PuF_3$
Figure 6.7	$LiCl-UCl_3$
Figure 6.8	$LiCl-UCl_4$
Figure 6.9	$NuCl-UCl_3$
Figure 6.10	$NaCl-UCl_4$
Figure 6.11	$KCl-UCl_4$
Figure 6.12	$NaCl-KCl-UCl_3$ (Projected Behavior)
Figure 6.13	$NaCl-KCl-PuCl_3$ (Projected Behavior)

Phase diagrams for less attractive systems are given in ORNL-2548, "Phase Diagrams of Nuclear Reactor Materials," R. E. Thoma, editor, including ternary fluoride systems of UF_4 with various pairs of LiF, NaF, KF, RbF and BeF_2. These are not presented here on the grounds that Na, K and Rb are undesirable in a thermal reactor fuel and F is undesirable in an epithermal reactor. In general, Rb and Cs and K salts show no particular advantage except that the $KCl-UCl_4$ system has a eutectic with a lower liquidus (330 C) than the $NaCl-UCl_4$ system (liquidus 370 C).

The phase diagrams presented do not include the quaternary system $LiF-BeF_2-ThF_4-UF_4$. Most MSR concepts employ salts either with substantial amounts of ThF_4 and a fraction of a percent UF_4 or conversely, with relatively high UF_4

6.1.3 Salts Examined by Laboratories (Cont'd)

a - Invariant Equilibria Data and Phase Diagrams (Cont'd)

concentration and little or no ThF_4. The system UF_4-ThF_4 forms a continuous series of solid solutions without maximum or minimum. The very great similarity in behaviour of ThF_4 and UF_4 permits fractional replacement of ThF_4 by UF_4 with little effect on freezing temperature over the composition range of interest as fuel. In the case of the LiF-ThF_4-UF_4 system substitution of UF_4 for ThF_4 tends to reduce the freezing temperature. The same effect would be expected for the quaternary system.

b - Physical Properties

The physical properties of molten fuel and fertile salts, other than phase transition behavior, which have the greatest influence on the design of molten salt reactors are those related to the thermal-hydraulic characteristics, namely: density, viscosity, heat capacity and thermal conductivity; and the derived combinations of these properties: thermal diffusivity, kinematic viscosity and Prandtl number. Also of interest are the vapor pressure, surface tension and solubility for those gases likely to be present - inert cover gases, fission product gases, hydrogen (tritium) and HF. These and other physical properties of several potential molten salts have been compiled by ORNL in ORNL-TM-2316, "Physical Properties of Molten Salt Reactor Fuel, Coolant and Flush Salts," S. Cantor et al, August 1968. Much of the data of necessity have been estimated because there is a lack of direct measurements for many of the specific compositions of interest. The

The System $LiF-BeF_2-UF_4$

L. V. Jones, D. E. Etter, C. R. Hudgens, A. A. Huffman, T. B. Rhinehammer, N. E. Rogers, P. A. Tucker, and L. J. Wittenberg, "Phase Equilibria in the $LiF-BeF_2-UF_6$ Ternary Fused Salt System", MLM-1080 (Aug. 24, 1959).

L. V. Jones, et al, "Phase Equilibria in the Ternary Fused Salt System $LiF-BeF_2-UF_4$", J. Am. Ceram Soc. 45 (2), 79-83 (1962)

Preliminary diagram.

Invariant Equilibria

Composition of Liquid (mole %)			Temperature (°C)	Type of Equilibrium	Solid Phases Present at Invariant Temperature
LiF	BeF_2	UF_4			
72	6	22	480	Peritectic (decomposition of $4LiF{\cdot}UF_4$ in the ternary system)	$4LiF{\cdot}UF_4$, LiF, and $7LiF{\cdot}6UF_4$
69	23	8	426	Eutectic	LiF, $2LiF{\cdot}BeF_2$, and $7LiF{\cdot}6UF_4$
48	51.5	0.5	350	Eutectic	$7LiF{\cdot}6UF_4$, $2LiF{\cdot}BeF_2$, and BeF_2
45.5	54	0.5	381	Peritectic	$LiF{\cdot}4UF_4$, $7LiF{\cdot}6UF_4$, and BeF_2
29.5	70	0.5	483	Peritectic	UF_4, $LiF{\cdot}4UF_4$, and BeF_2

The minimum temperature in the quasi-binary system $2LiF{\cdot}BeF_2-7LiF{\cdot}6UF_4$ occurs at 65 LiF–29 BeF_2–6 UF_4 (mole %) at 438°C.

Fig. 6.1a Invariant Equilibria Data for $LiF-BeF_2-UF_4$

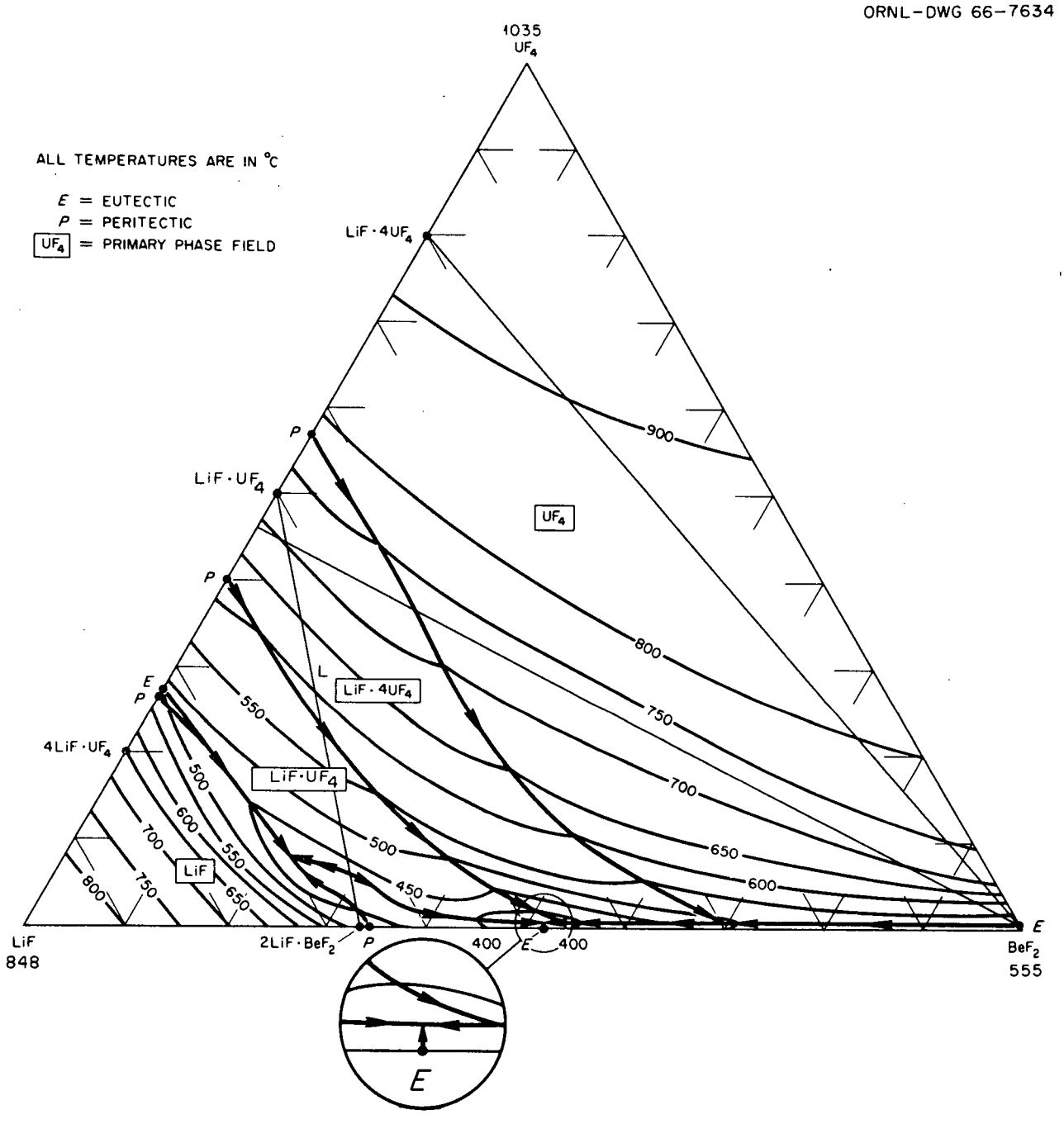

Fig. 6.1b Phase Diagram for $LiF-BeF_2-UF_4$

The System $LiF-BeF_2-ThF_4$

R. E. Thoma, H. Insley, H. A. Friedman, and C. F. Weaver, "Phase Equilibria in the Systems BeF_2-ThF_4 and $LiF-BeF_2-ThF_4$", J. Phys. Chem. 64 865 (1960)

Invariant Equilibria

Composition of Liquid (mole %)			Invariant Temperature (°C)	Type of Invariant	Solids Present at Invariant Point
LiF	BeF_2	ThF_4			
15	83	2	497 ± 4	Peritectic	ThF_4, $LiF{\cdot}4ThF_4$, and BeF_2
33.5	64	2.5	455 ± 4	Peritectic	$LiF{\cdot}4ThF_4$, $LiF{\cdot}2ThF_4$, and BeF_2
47	51.5	1.5	356 ± 6	Eutectic	$2LiF{\cdot}BeF_2$, $LiF{\cdot}2ThF_4$, and BeF_2
60.5	36.5	3	433 ± 5	Peritectic	$LiF{\cdot}2ThF_4$, $3LiF{\cdot}ThF_4ss$, and $2LiF{\cdot}BeF_2$
65.5	30.5	4	444 ± 4	Peritectic	LiF, $2LiF{\cdot}BeF_2$, and $3LiF{\cdot}ThF_4ss$
63	30.5	6.5	448 ± 5	Peritectic	$3LiF{\cdot}ThF_4ss$, $7LiF{\cdot}6ThF_4$, and $LiF{\cdot}2ThF_4$

Fig. 6.2a Invariant Equilibria Data for $LiF-BeF_2-ThF_4$

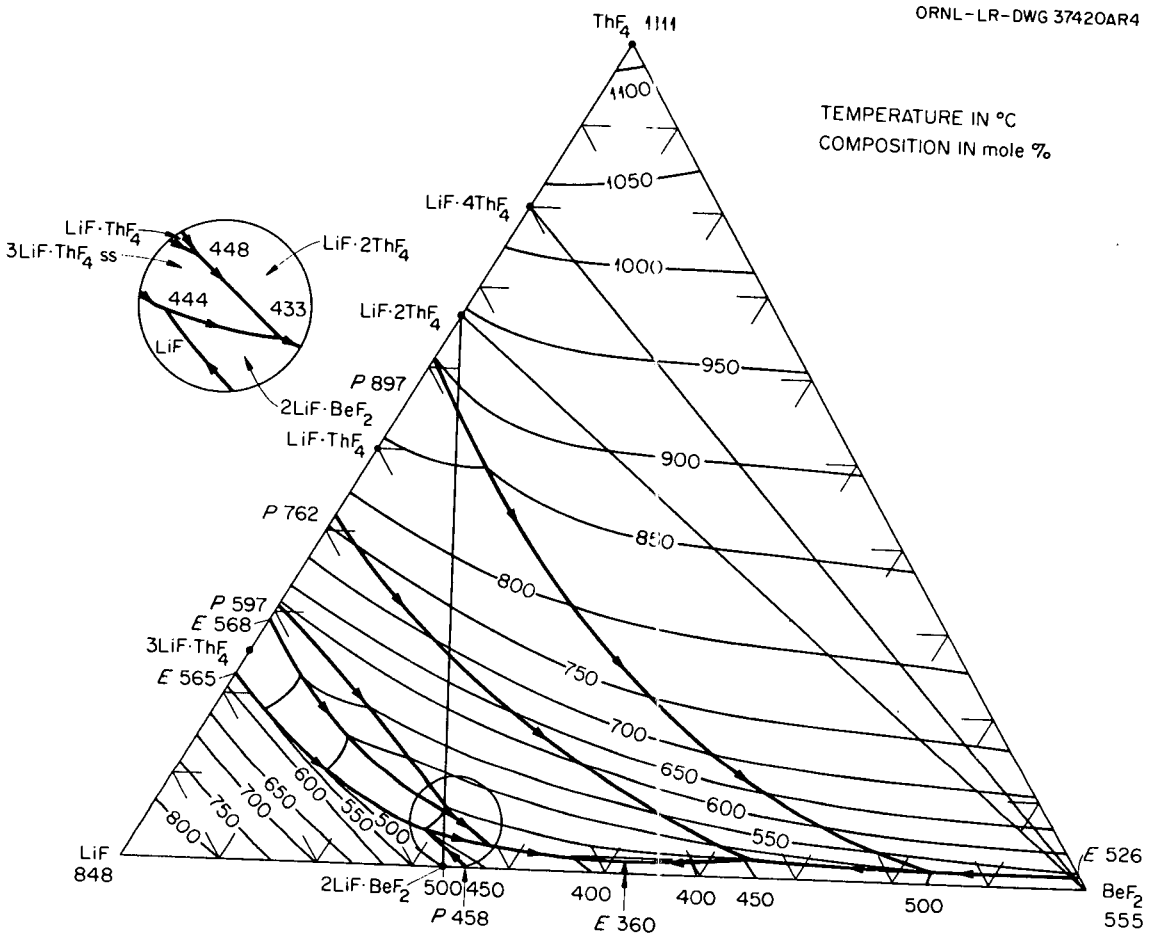

Fig. 6.2b Phase Diagram for $LiF-BeF_2-ThF_4$

The System ThF_4-UF_4

C. F. Weaver, R. E. Thoma, H. Insley and H. A. Friedman, "Phase Equilibria in the Systems UF_4-ThF_4 and LiF-ThF_4-UF_4", J. Am. Ceram Soc. 43 213 (1960)

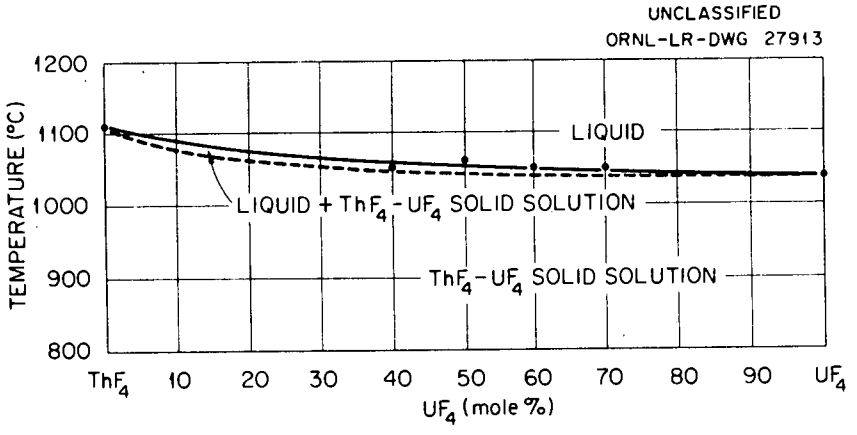

Fig. 6.3 Phase Diagram for ThF_4-UF_4

The System $LiF-ThF_4-UF_4$

C. F. Weaver, R. E. Thoma, H. Insley, and H. A. Friedman, "Phase Equilibria in the Systems UF_4-ThF_4 and $LiF-ThF_4-UF_4$", J. Am. Ceram Soc. 43 213 (1960)

Invariant Equilibria

Composition of Liquid (mole %)			Invariant Temperature (°C)	Type of Equilibrium	Solids Present at Invariant Point
LiF	ThF_4	UF_4			
72.5	7.0	20.5	500	Peritectic	LiF, $3LiF\cdot(Th, U)F_4$, and $7LiF\cdot6(U, Th)F_4$
72.0	1.5	26.5	488	Eutectic	LiF, $4LiF\cdot UF_4$, and $7LiF\cdot6(U, Th)F_4$
53	18	19	609	Peritectic	$7LiF\cdot6(U, Th)F_4$, $LiF\cdot2(Th, U)F_4$, and $LiF\cdot4(U, Th)F_4$

Fig. 6.4a Invariant Equilibria Data for $LiF-ThF_4-UF_4$

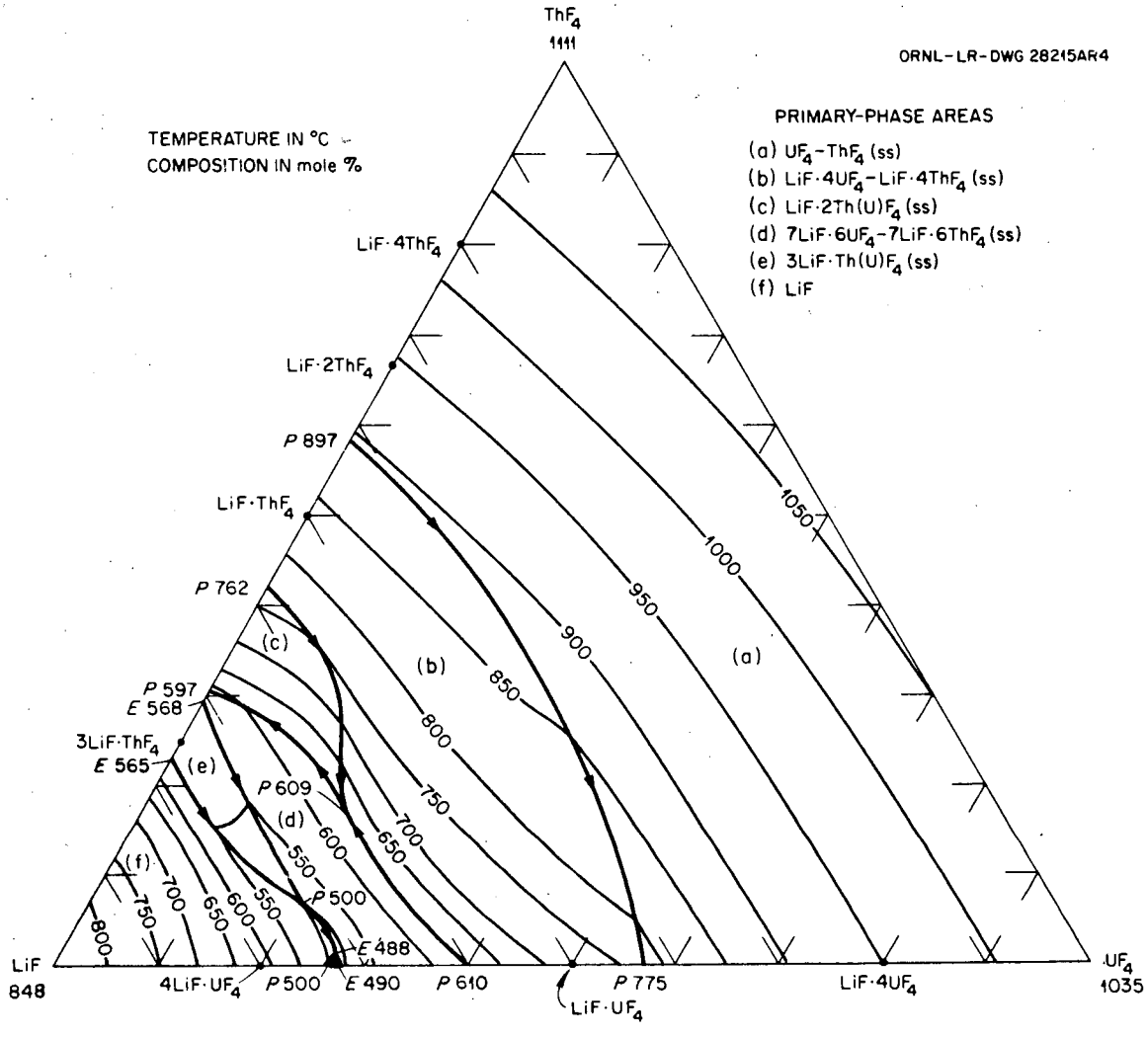

Fig. 6.4b Phase Diagram for $LiF-ThF_4-UF_4$

The System LiF–PuF_3

C. J. Barton and R. A. Strehlow, "Phase Relationships in the System Lithium Fluoride–Plutonium Fluoride," paper presented at the 135th National Meeting of the American Chemical Society, Boston, Mass., Apr. 5–10, 1959.

The system LiF–PuF_3 contains a single eutectic at 80.5 LiF–19.5 PuF_3 (mole %), m.p. 743°C.

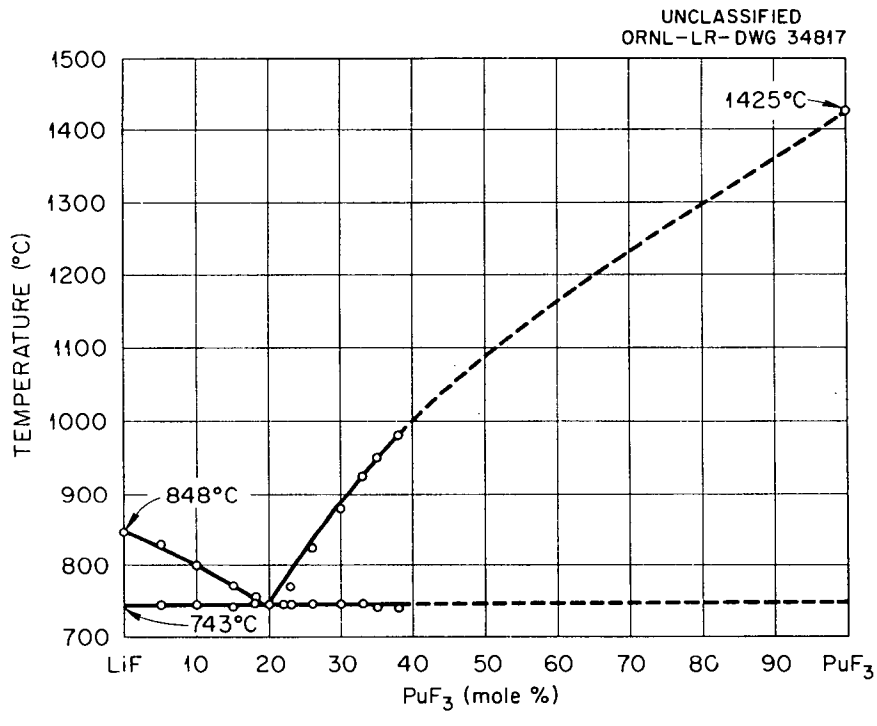

Fig. 6.5 Phase Diagram for LiF-PuF_3

The System $LiF-BeF_2-PuF_3$

C. J. Barton, J. Phys. Chem. 64 306 (1960)

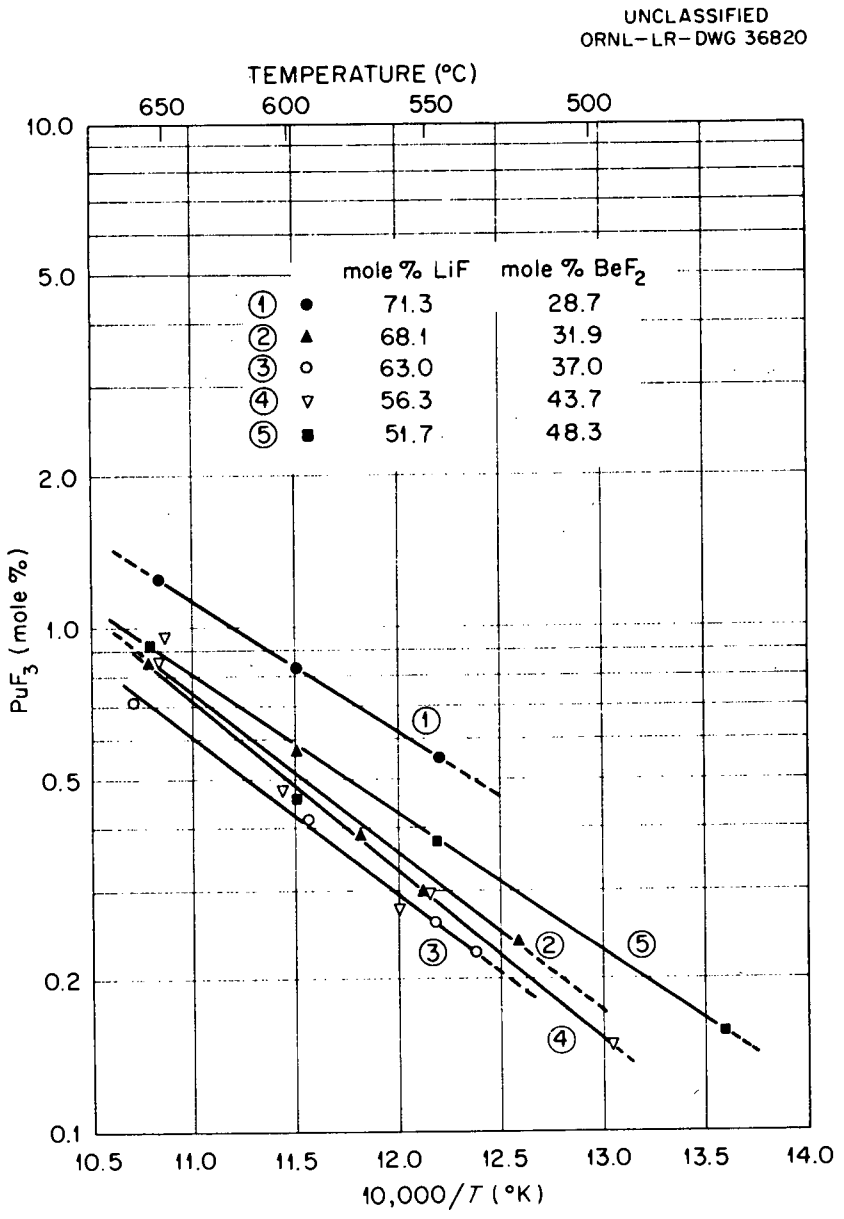

Fig. 6.6 Solubility of PuF_3 as a Function of Temperature for $LiF-BeF_2$ Solvents

The System $LiCl-UCl_3$

C. J. Barton, A. B. Wilkerson, and W. R. Grimes, unpublished work performed at the Oak Ridge National Laboratory, 1953.

Preliminary diagram. The system $LiCl-UCl_3$ contains a single eutectic at 75 LiCl–25 UCl_3 (mole %), m.p. 495 ± 5°C.

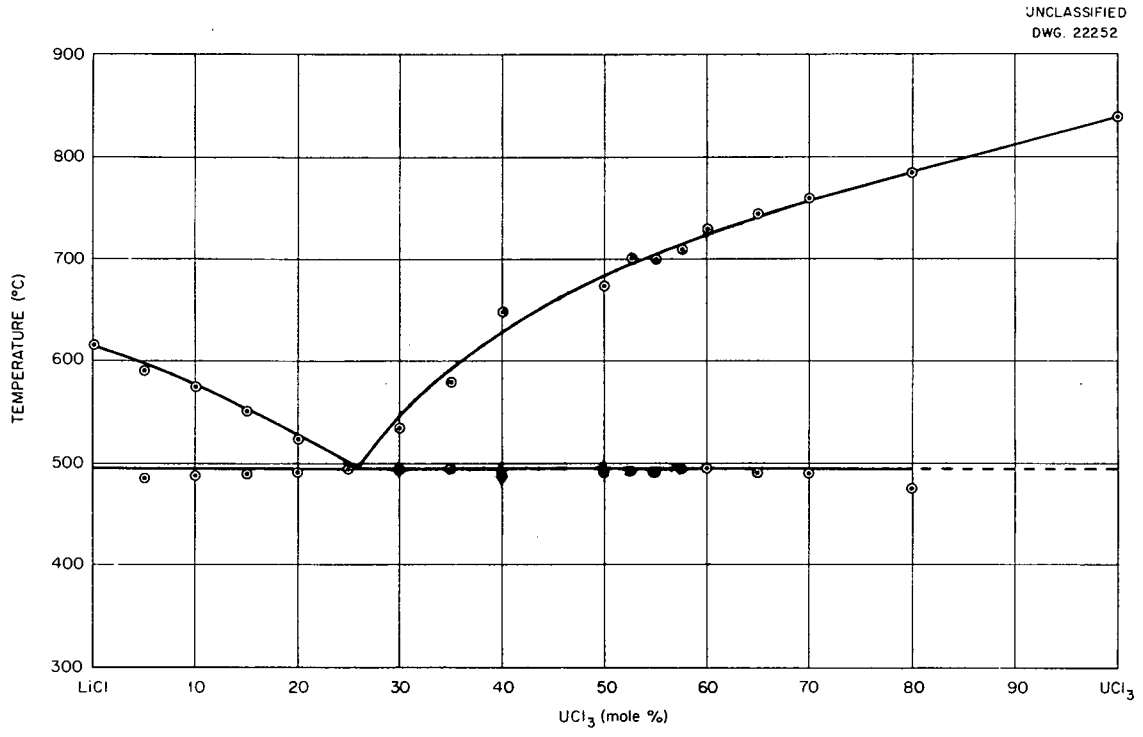

Fig. 6.7 Phase Diagram for $LiCl-UCl_3$

The System $LiCl-UCl_4$

C. J. Barton, R. J. Sheil, and W. R. Grimes, unpublished work performed at the Oak Ridge National Laboratory, 1953.

Preliminary diagram.

Invariant Equilibria

Mole % UCl_4 in Liquid	Invariant Temperature (°C)	Type of Equilibrium	Phase Reaction at Invariant Temperature
29	415	Eutectic	$L \rightleftharpoons 2LiCl{\cdot}UCl_4 + LiCl$
33.3	430 ± 10	Congruent melting point	$L \rightleftharpoons 2LiCl{\cdot}UCl_4$
48	405	Eutectic	$L \rightleftharpoons 2LiCl{\cdot}UCl_4 + UCl_4$

Some data on this system were reported by C. A. Kraus in *Phase Diagrams of Some Complex Salts of Uranium with Halides of the Alkali and Alkaline Earth Metals*, M-251 (July 1, 1943).

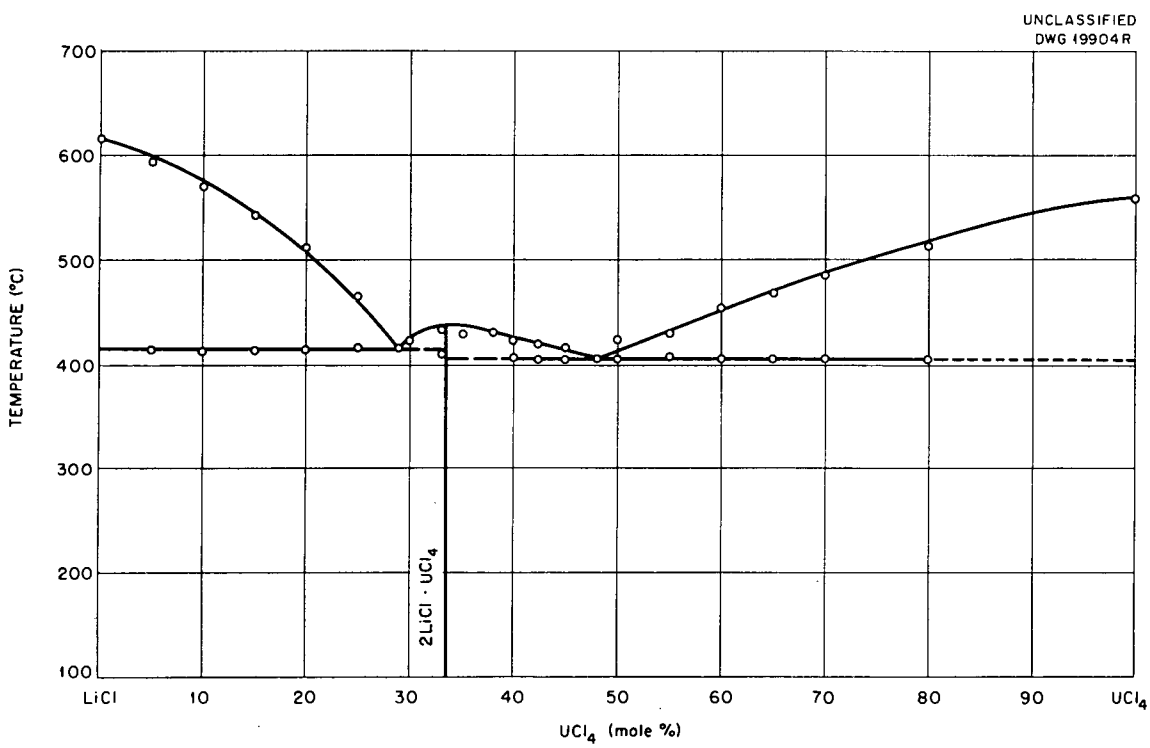

Fig. 6.8 Phase Diagram for $LiCl-UCl_4$

The System $NaCl-UCl_3$

C. A. Kraus, unpublished work.

Preliminary diagram constructed with the author's permission from data reported in *Phase Diagrams of Some Complex Salts of Uranium with Halides of the Alkali and Alkaline Earth Metals*, M-251 (July 1, 1943).

The system $NaCl-UCl_3$ contains a single eutectic at 67 NaCl–33 UCl_3 (mole %), m.p. 525°C.

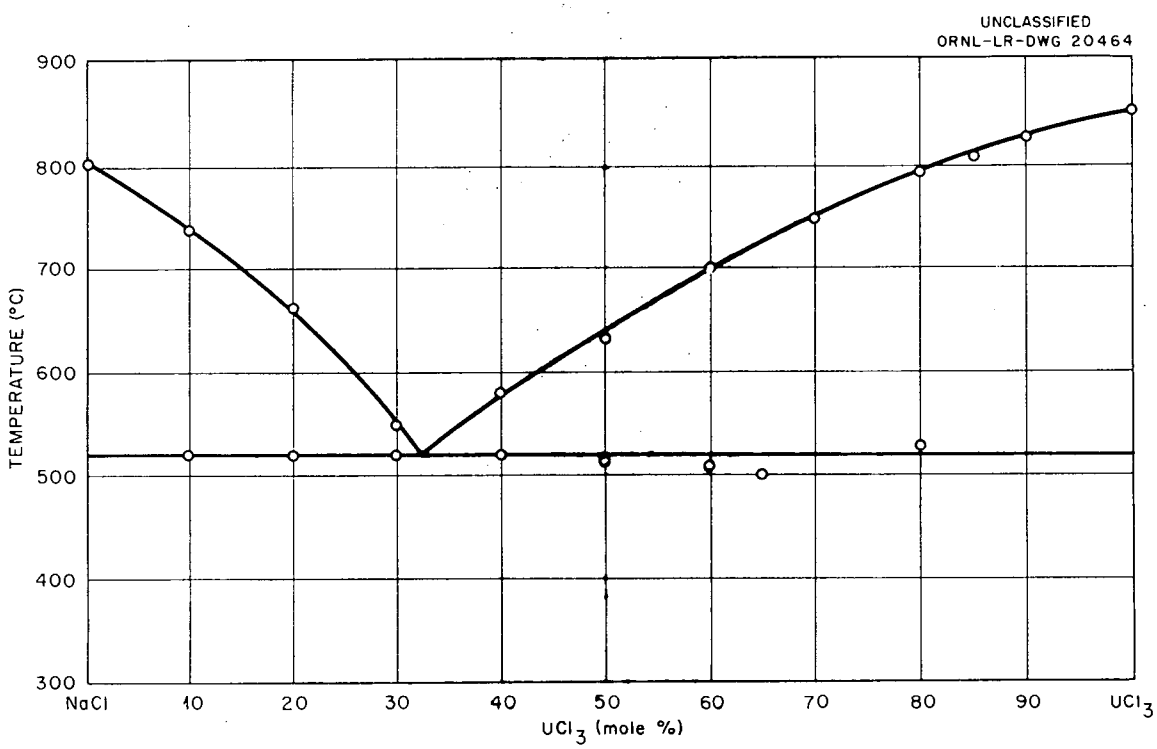

Fig. 6.9 Phase Diagram for $NaCl-UCl_3$

The System $NaCl-UCl_4$

C. J. Barton, R. J. Sheil, A. B. Wilkerson, and W. R. Grimes, unpublished work performed at the Oak Ridge National Laboratory, 1953.

Preliminary diagram.

Invariant Equilibria

Mole % UCl_4 in Liquid	Invariant Temperature (°C)	Type of Equilibrium	Phase Reaction at Invariant Temperature
30	430 ± 5	Eutectic	$L \rightleftharpoons NaCl + 2NaCl{\cdot}UCl_4$
33.3	440 ± 5	Congruent melting point	$L \rightleftharpoons 2NaCl{\cdot}UCl_4$
47	370 ± 5	Eutectic	$L \rightleftharpoons 2NaCl{\cdot}UCl_4$ + unidentified compound
57	415 ± 5	Peritectic	$L + UCl_4 \rightleftharpoons$ unidentified compound

A phase diagram of this system has been reported by C. A. Kraus in *Phase Diagrams of Some Complex Salts of Uranium with Halides of the Alkali and Alkaline Earth Metals*, M-251 (July 1, 1943).

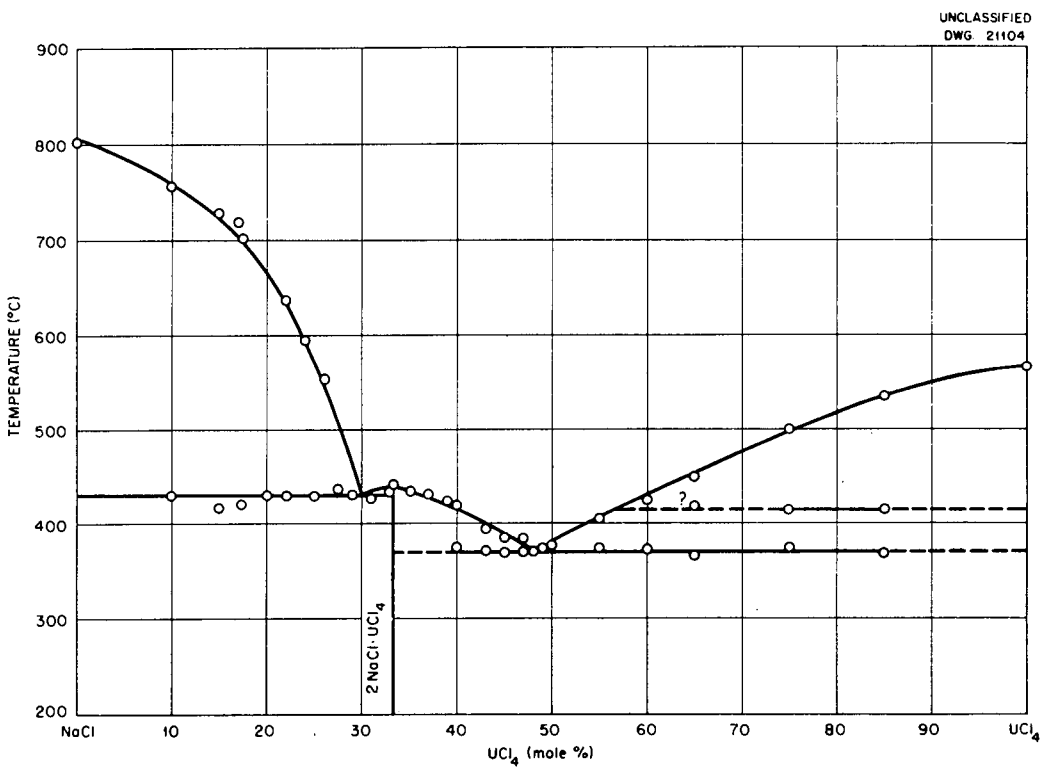

Fig. 6.10 Phase Diagram for $NaCl-UCl_4$

The System $KCl-UCl_4$

C. J. Barton, A. B. Wilkerson, T. N. McVay, R. J. Sheil, and W. R. Grimes, unpublished work performed at the Oak Ridge National Laboratory, 1954.

Preliminary diagram.

Invariant Equilibria

Mole % UCl_4 in Liquid	Invariant Temperature (°C)	Type of Equilibrium	Phase Reaction at Invariant Temperature
25	550	Eutectic	$L \rightleftharpoons KCl + 2KCl{\cdot}UCl_4$
33.3	630	Congruent melting point	$L \rightleftharpoons 2KCl{\cdot}UCl_4$
44	330	Eutectic	$L \rightleftharpoons 2KCl{\cdot}UCl_4 + KCl{\cdot}UCl_4$
49	345	Peritectic	$L + KCl{\cdot}3UCl_4 \rightleftharpoons KCl{\cdot}UCl_4$
61	395	Peritectic	$L + UCl_4 \rightleftharpoons KCl{\cdot}3UCl_4$

A phase diagram of this system has been reported by C. A. Kraus in *Phase Diagrams of Some Complex Salts of Uranium with Halides of the Alkali and Alkaline Earth Metals*, M-251 (July 1, 1943).

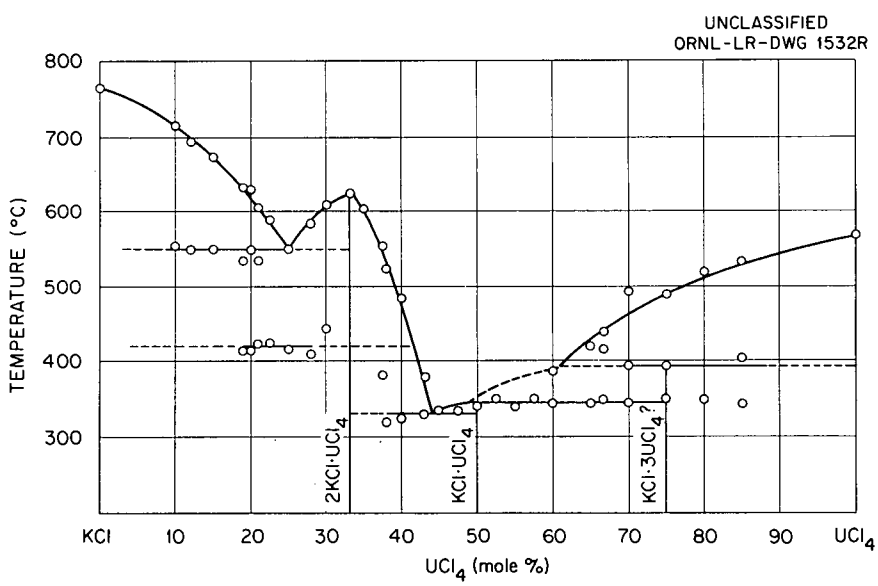

Fig. 6.11 Phase Diagram for $KCl-UCl_4$

The System $NaCl-KCl-UCl_3$

R. E. Thoma, "Predicted Phase Behavior in Ternary Systems of Uranium and Plutonium Chlorides", MSR-63-53 (Oct. 31, 1963)

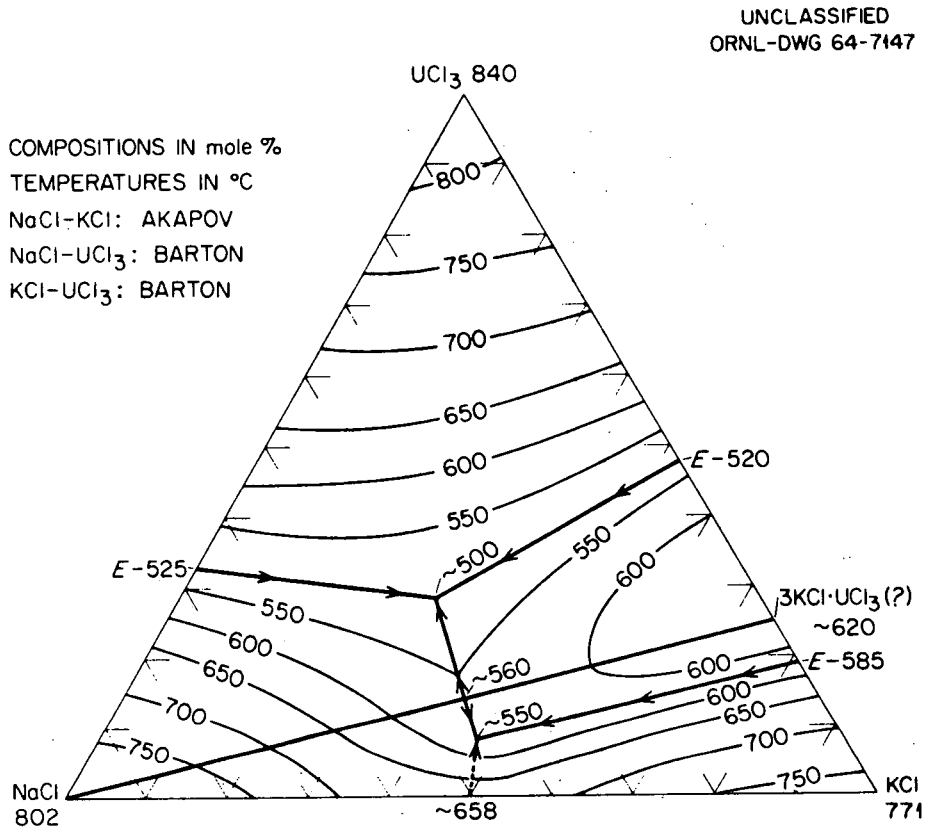

Fig. 6.12 Predicted Phase Diagram for $NaCl-KCl-UCl_3$

The System NaCl-KCl-$PuCl_3$

ORNL-3708, MSRP Semiannual Progress Report, August 31, 1969, p. 317

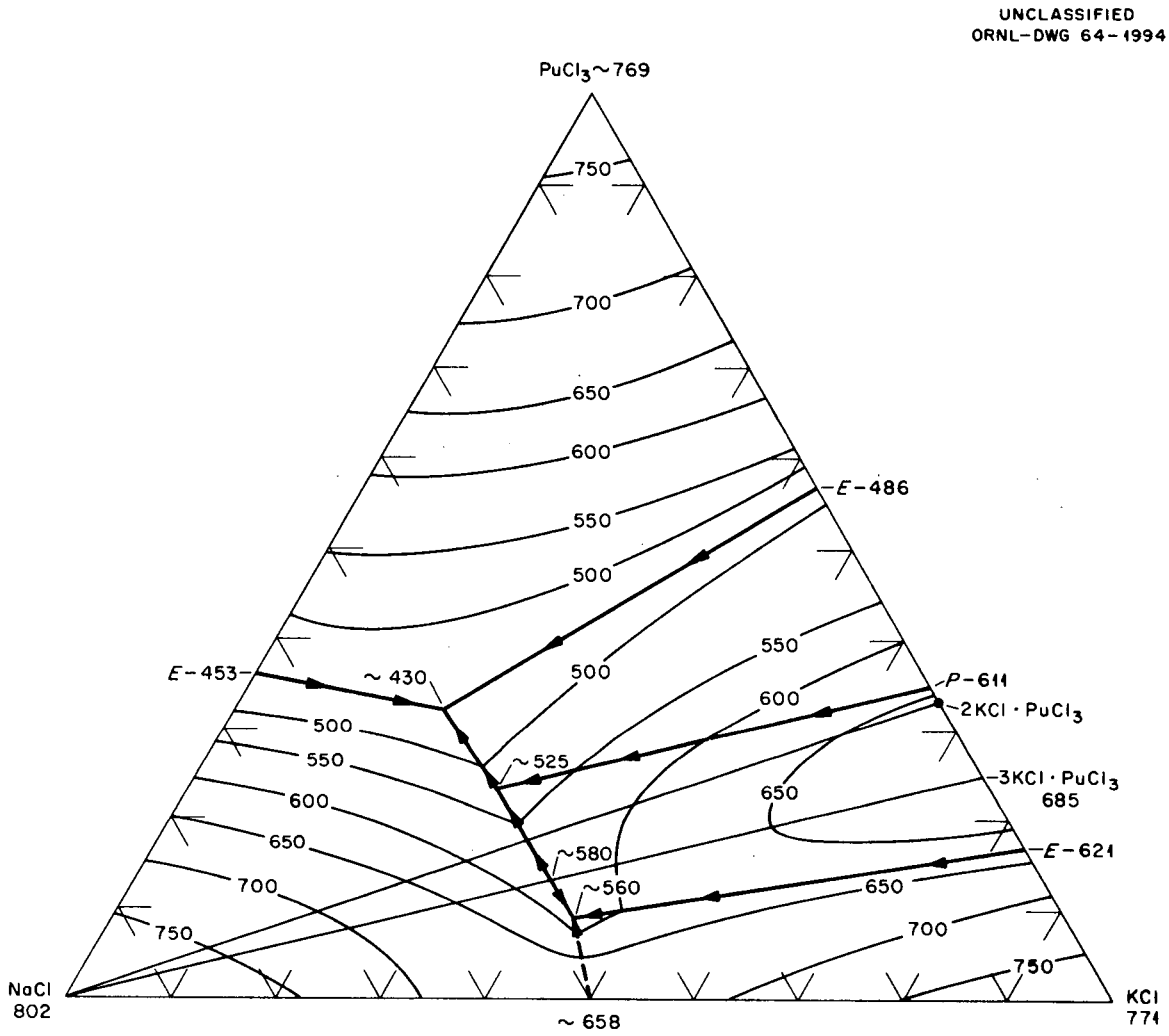

Fig. 6.13 Predicted Phase Behavior for NaCl-KCl-$PuCl_3$

6.1.3 Salts Examined by Laboratories (Cont'd)

b - Physical Properties (Cont'd)

referenced document includes data on such additional physical properties as electrical conductivity, expansivity, compressibility, sonic velocity and heat of fusion which are not reproduced here because they are not deemed to be crucial in the selection of suitable reactor fuels.

(1) Density

ORNL has found that the simple rule of adding empirical values molar volumes for the constituents holds quite well for binary fluoride melts and apparently also for multi-component fluoride melts.

Table 6.2 lists values of empirical molar volumes from several sources. For the most part, estimated densities agree with measured values within 3 percent and sometimes better than 1 percent. For the system $NaF-UF_4$ positive deviations as great as 6 percent were noted.

From the estimated or measured values of densities, the temperature dependence for a specific composition may be expressed in the form:

$$\rho(t) = a - bt$$

Table 6.3 lists values of a and b for several proposed fuel and fertile salts.

(2) Heat Capacity

Heat capacity of molten salt may be estimated assuming mole fraction additivity and assigning 16, 24, and 44 Cal $mole^{-1}$ $^{o}C^{-1}$ for the respective contributions of LiF, BeF_2 and ThF_4 or UF_4. The validity of these assumptions has been checked by

Table 6.2

Emperical Molar Volumes of Several Fluoride Salts

	Molar Volume (cm^3/gm-mole)			
	At 600 C[a/]	At 800 C[a/]	At 600 C[b/]	At 800 C[b/]
LiF	13.46	14.19	13.411	14.142
NaF	19.08	20.20		
KF	28.1	30.0		
RbF	33.9	36.2		
CsF	40.2	43.1		
BeF_2	23.6	24.4	23.6	24.4
MgF_2	22.4	23.3		
CaF_2	27.5	28.3		
ZrF_4	47	50		
ThF_4	46.6	47.7	46.43	47.59
UF_4	45.5	46.7	46.43	47.59

REFERENCES:

a/ ORNL-3913 - Reactor Chem. Div. Ann. Progr. Report, Dec. 31, 1965 (S. Cantor), p. 27-29. (This reference also gives values for ZrF_2, BaF_2, AlF_3,YF_3LaF_3, CeF_3, PrF_3, SmF_3).

b/ ORNL-TM-2316 - Physical Properties of Molten Salt Reactor Fuel, Coolant and Flush Salts (S. Cantor, Ed), Aug. 1968, p. 28.

Table 6.3

Density of Several Fluoride Salts

Density: (gm/cc) = a - b x 10^{-4}t (^{o}C)

Salt Composition (Mole %)								
LiF	BeF_2	ThF_4	UF_4	ZrF_4	a	b	M - Meas. E - Est.	Reference
70.1	23.9	6.0	-	-	3.112	6.71	M	ORNL-4449
70.0	18.0	12.0	-	-	3.824	8.06	M	ORNL-4449
70.0	15.0	15.0	-	-	4.181	9.52	M	ORNL-4449
71.7	16	12	0.3		3.752	6.68	E	ORNL-4541
64.8	30.0	-	0.26	5.0	2.533	5.62	M	ORNL-4449
68.5	31.3		0.2		2.04(@ 1150 F)		E	ORNL-4528
71	2	27			4.44(@ 1200 F)		E	ORNL-4528
66.0	34.0	-	-	-	2.280	4.88	M	ORNL-4449
92 $NaBF_4$	8 NaF				2.252	7.11	M	ORNL-4449
100 $NaBF_4$					2.26	7.4	E	ORNL-2316
57 NaF	43 BeF_2				2.427	5.37	M	ORNL-2316

Table 6.5

Viscosity of Several Fluoride Salts

μ (Centipoise) = A Exp (B/T)

Salt Composition (Mole %)	μ (Centipoise)	Reference
68.5 LiF - 31.3 BeF_2 - 0.2 UF_4	μ = 1.12 (@ 1150°F)	ORNL-4528
71 LiF - 2 BeF_2 - 27 ThF_4	μ = 1.57 (@ 1200°F)	ORNL-4528
71.7 LiF - 16 BeF_2 - 12 ThF_4 - 0.3 UF_4	μ = 0.109 exp (4090/T)	ORNL-4541
72.5 LiF - 15.7 BeF_2 - 11.6 ThF_4	μ = 0.109 exp (4090/T)	ORNL-4449
70.1 LiF - 23.9 BeF_2 - 6.0 ThF_4	μ = 0.660 exp (4380/T)	ORNL-4449
66 LiF - 34 BeF_3	μ = 0.116 exp (3755/T)	ORNL-2316
92 $NaBF_4$ - 8 NaF	μ = 0.0877 exp (2240/T)	ORNL-4449
100 $NaBF_4$	μ = 0.0832 exp (2360/T)	ORNL-4449
100 KBF_4	μ = 0.0946 exp (2280/T)	ORNL-4449

Table 6.4

Specific Heat of Several Fluoride Salts

Salt Composition (Mole %)	Cp(Btu/lb/^{o}F or Cal/gm/C)	Reference
68.5 LiF - 31.3 BeF_2 - 0.2 UF_4	0.55 ± 0.14	ORNL-4528
71 LiF - 2 BeF_2 - 27 ThF_4	0.22 ± 0.06	ORNL-4528
71.7 LiF - 16 BeF_2 - 12 ThF_4 - 0.3 UF_4	0.324 ± 4%	ORNL-4541
66 LiF - 34 BeF_2	0.57 ± 3%	ORNL-TM-2316
92 $NaBF_4$ - 8 NaF	0.36 ± 2%	ORNL-4541 ORNL-TM-2316

6.1.3 Salts Examined by Laboratories (Cont'd)

b - Physical Properties (Cont'd)

(2) Heat Capacity (Cont'd)

comparing with measured values of related salts (66 LiF-34 BeF_2; 72 LiF-16 BeF_2, 12 ThF_4, and 75 LiF 25 ThF_4).[1/]

The specific heat of specific salt compositions are tabulated in Table 6.4.

(3) Viscosity

The viscosity-temperature relationship of several MSR salts is shown in Table 6.5.

(4) Thermal Conductivity

Measured values of thermal conductivity for salts of interest are rather scarce. A theoretical expression derived by Rao[2/] and adapted to molten salts by Turnbull[3/], has been used by ORNL for estimating values of k.

$$k(W\ cm^{-1}\ {}^{o}C^{-1}) = 11.9 \times 10^{-3} \frac{Tm^{\frac{1}{2}}\ \rho m^{2/3}}{(M/n)^{7/6}}$$

where Tm = melting point (^{o}K)

ρm = liquid density at Tm

M = average molar weight

n = average number of discrete ions per molecule

Part of the expression $11.9 \times 10^{-3}\ Tm^{\frac{1}{2}}\ \rho 1/3/(M/n)^{5/6}$ is a good approximation to the average maximum Debye

1/ ORNL-TM-2316

2/ M. Rama Rao, Indian Journal of Physics 16 30 (1942)

3/ A. G. Turnbull, Australian Journal of Applied Science 12 324 (1961)

6.1.3 Salts Examined By Laboratories (Cont'd)

b - Physical Properties (Cont'd)

(4) Thermal Conductivity (Cont'd)

lattice frequency for single ionic salts. It was found that the above expression agreed with experimental results within 15 percent for eleven molten mixtures (nitrates or chlorides) but ORNL found that the theoretical expression yielded values approximately 25 percent less than experiment for 66 LiF-33 BeF_2 and the MSRE fuel salt (71.2 LiF-23 BeF_2-5 ZrF_4-0.8 UF_4).

In applying the theoretical expression ORNL uses the liquidus temperature for Tm and assumes the following ions:

$$Li^+,\ F^-,\ (BeF_4)^{2-},\ (ThF_5)^{-1},\ (UF_5)^{-1}.$$

ORNL claims that assumption of the more plausible ions $(ThF_7)^{-3}$ and $(UF_7)^{-3}$ leads to a lower and less reliable estimated value of k[4/].

The uncertainty in estimated values is at least ± 25 percent. As a first approximation, the temperature dependence of k in the range of interest may be neglected because of the large uncertainty.

Figure 6.14 is a plot of measured values of thermal conductivity for several salt mixtures of interest for MSR[5/]. The variable-gas apparatus at ORNL is currently being used for measurements on LiF-BeF_2-ThF_4 systems. Some additional values are presented in Table 6.6.

4/ ORNL-TM-2316, p. 12

5/ ORNL-4548, p. 102

Table 6.6

Thermal Conductivities of Some Fluoride Salts

Salt Composition (Mole %)		k(watts/ m-C)	k(Btu/ hr-ft-°F)	Reference
68.5 LiF-31.3 BeF_2-0.2 UF_4			0.8	ORNL-4528
71 LiF-2 BeF_2-27 ThF_4			0.6	ORNL-4528
66 LiF-34 BeF_2				ORNL-TM-2316
71.7 LiF-16 BeF_2-12 ThF_4-0.3 UF_4		1.0		ORNL-4541
	at 1300F(977K)	1.19	0.69	
	at 1175F(908K)	1.23	0.71	
	at 1050F(839K)	1.19	0.69	
92 $NaBF_4$-8 NaF				ORNL-4541
	at 1150F(894K)	0.398	0.23	
	at 1000F(811K)	0.398	0.23	
	at 850F(727K)	0.450	0.26	

Conversion factor: Multiply watts/(C) cm by 57.8 to obtain Btu/hr-ft-°F).

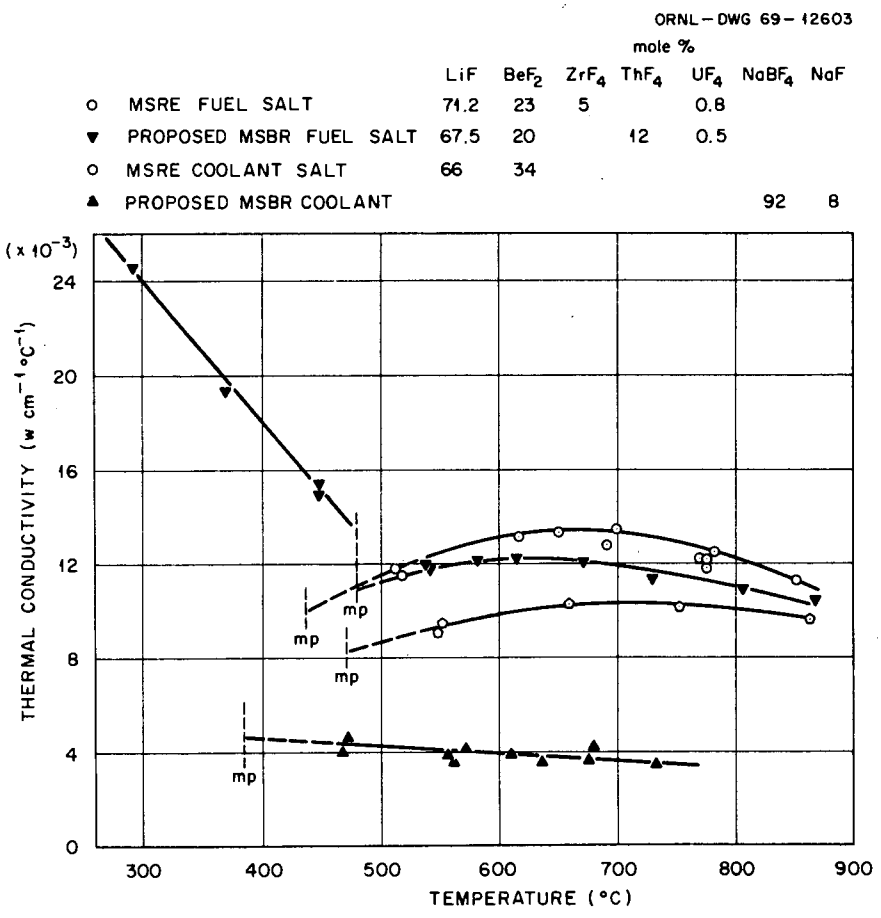

Fig. 6.14 Thermal Conductivity of Several Salt Mixtures of Interest to the MSRE and MSBR Programs

6.1.3 Salts Examined By Laboratories (Cont'd)

b - Physical Properties (Cont'd)

(5) Surface Tension

Recently reported[5/] values of surface tension for MSRE fuel and 66 LiF-34 BeF_2 measured by capillary depression, are:

MSRE fuel γ (dynes/cm) = 237 - 0.08t (^{o}C)

66 LiF-34 BeF_2 γ = 245 - 0.12t

Previously reported estimates[6/] are:

L_2B and other fluoride mixtures = 260 - 0.12t

92 $NaBF_2$ - 8 NaF = 130 - 0.075t

6.2 Coolant Salt

6.2.1 Criteria

The requirements for MSR secondary coolant are much the same as for the primary fuel salt except for solubility of fissile and fertile materials, the requirement for radiation stability and the need for low neutron absorption. Exposure to delayed neutrons and gamma flux from the fuel salt in the IHX is a minor consideration. Low melting point is of greater importance for the coolant than for fuel salt because it may be exposed to lower temperature transients. Compatibility with steam or water assumes greater importance because of the possibility of system leaks, but because of lower radioactivity, the consequences of contacting water and coolant salt are far less than consequences of contacting water and fuel salt. It should also be compatible with the fuel salt.

6/ ORNL-TM-2316, p. 36

6.2.1 Criteria (Cont'd)

Possible secondary coolants include:

a - liquid metals

b - gases

c - molten salts

This report will not attempt to cover the considerable technology of liquid metal and gas coolants which is available as a result of development of SGR, LMFBR, HTGR and GCFR concepts and which would be directly applicable to an MSR. Brief consideration will be given to the most obvious choices, however.

Liquid Metals

Liquid sodium could be considered for the secondary coolant. In this case the problems related to steam generators are virtually identical with those for an LMFBR plant, although the optimum operating conditions might be somewhat different. However, sodium metal is not compatible with fluoride fuel salt, and a leak at the IHX in either direction would result in serious precipitation of UF_3.

Molten lead and bismuth could be considered, but they are generally not compatible with the nickel base alloys considered for containing molten fluorides.

Gases

The objections to use of gas are the high pressure needed for practical heat transport and problems related to assuring emergency cooling in the event of a loss of coolant or loss of flow accident. Also, because of the inherently low heat transfer coefficients for gases, a larger heat transfer surface is required and, hence, the fuel salt inventory would be larger. The problem of emergency cooling may not be serious if

6.2.1 Criteria (Cont'd)

Gases (Cont'd)

multiple isolated cooling loops are provided. On the other hand, a gas coolant loop should permit rather effective trapping of tritium and has no coolant freeze-up problems. Also a gas coolant can be selected which is chemically compatible with the primary fuel and/or blanket salt in the event of a leak, but the primary system would have to be designed to withstand the pressure from a major IHX rupture.

Molten Salts

In the case of molten salt coolants the criteria of major importance are:

a - low liquidus temperature (melting point)

b - good heat transfer and hydraulic properties

c - low vapor pressure

d - thermal stability

e - low corrosion toward suitable construction materials

f - low chemical reactivity toward

  1 - air

  2 - water

  3 - fuel and/or fertile salt

g - low cost

h - relatively low neutron absorption and/or easy removal from fuel and fertile salt (in the event of leakage into the primary system).

6.2.2 Attractive Molten Coolant Salts

As in the case of fuel and fertile salts, primary consideration is given to chlorides and fluorides. While

6.2.2 Attractive Molten Coolant Salts (Cont'd)

chloride mixtures are available with attractively low melting points, they tend to have higher vapor pressure than fluorides and the high neutron absorption of any chlorine leaking into the primary system tends to make chlorides undesirable as coolants for a thermal spectrum reactor. The liquidus of the coolant salt should not be much higher than the critical temperature of water (705.5°F or 374 C) if salt freeze-ups are to be avoided without going to an unduly complicated steam system. For this reason, salt systems which do not have a liquidus below 400 C are not promising.

While several binary chloride eutectics melt below 700°F, they contain high concentrations of such chlorides as TlCl, $ZnCl_2$, $BiCl_3$, $CdCl_2$, or $SnCl_2$, which are easily reduced and, accordingly corrosive; or such chlorides as $AlCl_3$, $ZrCl_4$, $ZrCl_4$, $HfCl_4$, or $BeCl_3$, which are very volatile. The following nonvolatile binary chloride systems containing LiCl have attractively low melting eutectics:

LiCl-45 m/o CsCl 330 C

LiCl-42 m/o KCl 355 C

LiCl-45 m/o RbCl 312 C

Very few fluoride salts are known to melt below 370 C. SnF_2 melts at 212 C. ORNL claims it is probably not stable during long-term irradiation[7/] and that relatively small concentrations of alkali fluorides raise the melting point drastically.

ORNL has shown considerable interest in the eutectic of 92 percent $NaBF_4$-8 percent NaF which has the main attractions of relatively low cost and relatively low

7/ W. R. Grimes, "MSBR Chemistry," Nuclear Applications & Technology 8 142, February 1970.

6.2.2 Attractive Molten Coolant Salts (Cont'd)

liquidus (725°F) and acceptable heat transfer and hydraulic properties, vapor pressure, and corrosion properties toward Hastelloy N. Consideration has also been given to other fluoborate mixtures.

Among oxygenated salts, which might be tolerable as coolant salts, there has been considerable industrial experience with mixed carbonates and nitrite-nitrates as heat transfer or heat-treating fluids. A eutectic of sodium and potassium nitrates and nitrites, available as a proprietary product has a melting point of 288°F. The chemical compatibility with the primary salt in the event of intersystem leakage is probably unacceptable, but this salt would be of interest as a possible third salt loop between coolant salt and steam generator. Both chemical stability and corrosion properties above 1000°F are questionable.

A eutectic of Li_2CO_3-Na_2CO_3-K_2CO_3 (43.5-31.5-25.0 mol percent)[8/] has a melting point of 397°F. This salt is not particularly attractive because its melting point is higher than the NaF-$NaBF_4$ eutectic and because of its relatively high Li content, which would be expensive if ^{7}Li. However, it is known to be noncorrosive to steel at 1400°F and has shown no obvious corrosion of Hastelloy N in 4000 hr at 1200°F. Chemical compatibility with primary salt is unknown but should be better than nitrate salt. Other carbonate mixtures might be more attractive but are not likely to be given serious consideration unless the fluoborate salt proves to be unacceptable.

8/ MSR Semi-Annual Report for Period Ending July 31, 1964 - ORNL-3708

6.2.3 Invariant Equilibria Data and Phase Diagrams

Invariant equilibria data and phase diagrams of attractive systems for coolant salt are shown in Figures 6.15 through 6.21 as follows:

Figure 6.15	$LiF-BeF_2$
Figure 6.16	$NaF-BeF_2$
Figure 6.17	$LiF-NaF-BeF_2$
Figure 6.18	$NaF-KF-ZrF_4$
Figure 6.19	$NaBF_4-KBF_4$
Figure 6.20	$NaF-NaBF_4$
Figure 6.21	$NaF-KF-NaBF_4-KBF_4$

Phase diagrams for less attractive systems are given in ORNL-2548, "Phase Diagrams of Nuclear Reactor Materials," R. E. Thoma, Editor. There is no significant advantage in substituting Rb, Cs or K for Na in the various systems considered, and the higher cost and higher neutron absorption would be objectionable.

6.3 Compatibility With Reactor Materials

6.3.1 Compatibility With Graphite

Graphite does not react chemically with molten fluoride mixtures of the type proposed for MSR's. Available thermodynamic data suggest that the most likely reaction

$$4UF_4 + C \rightleftharpoons CF_4 + 4UF_3$$

should come to equilibrium at CF_4 pressures $\sim 10^{-8}$ atm. CF_4 concentrations over graphite-salt systems maintained for long periods of time at elevated temperatures have been shown to be below the limit of detection ($\sim$1 ppm) by mass spectroscopy[9/].

9/ W. R. Grimes, "Radiation Chemistry of the MSRE System," ORNL-TM-500 (March 31, 1963)

The System $LiF-BeF_2$

This phase diagram is a composite from several published sources[1-3] and from unpublished data derived at the Oak Ridge National Laboratory (R. E. Moore, C. J. Barton, R. E. Thoma, and T. N. McVay) and at the Mound Laboratory (J. F. Eichelberger, C. R. Hudgens, L. V. Jones, and T. B. Rhinehammer). Thermal gradient quenching data (ORNL) and differential thermal analysis data (Mound Laboratory) have served to corroborate this composite diagram.

Invariant Equilibria

Mole % BeF_2 in Liquid	Invariant Temperature (°C)	Type of Equilibrium	Phase Reaction at Invariant Temperature
33.5*	454	Peritectic	$L + LiF \rightleftharpoons 2LiF{\cdot}BeF_2$
52	355	Eutectic	$L \rightleftharpoons 2LiF{\cdot}BeF_2 + BeF_2$
–	280	Upper temperature of stability for $LiF{\cdot}BeF_2$	$2LiF{\cdot}BeF_2 + BeF_2 \rightleftharpoons LiF{\cdot}BeF_2$

*Ref 3.

Roy, Roy, and Osborn have reported the presence of the compound $LiF{\cdot}2BeF_2$ in the system $LiF-BeF_2$ although neither the Mound Laboratory nor the ORNL data have indicated the existence of this compound.

[1] D. M. Roy, R. Roy, and E. F. Osborn, *J. Am. Ceram. Soc.* 37, 300 (1954).

[2] A. V. Novoselova, Yu. P. Simanov, and E. I. Yarembash, *J. Phys. Chem. (U.S.S.R.)* 26, 1244 (1952).

[3] John L. Speirs, *The Binary and Ternary Systems Formed by Calcium Fluoride, Lithium Fluoride, and Beryllium Fluoride: Phase Diagrams and Electrolytic Studies*, Ph.D. thesis, University of Michigan, May 29, 1952.

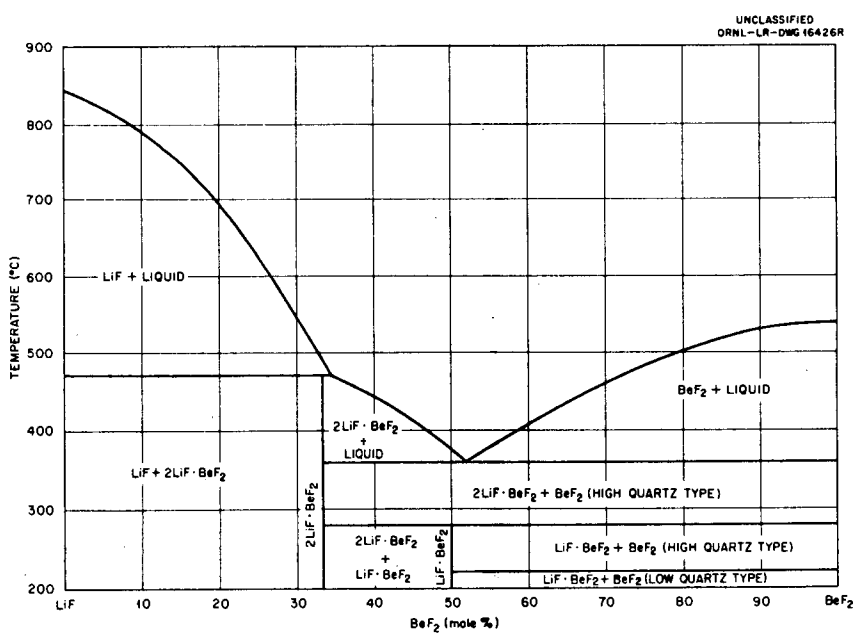

Fig. 6.15 Phase Diagram for $LiF-BeF_2$

The System $NaF-BeF_2$

D. M. Roy, R. Roy, and E. F. Osborn, "Fluoride Model Systems: III. The System $NaF-BeF_2$ and the Polymorphism of Na_2BeF_4 and BeF_2," *J. Am. Ceram. Soc.* **36**, 185 (1953).

Invariant Equilibria*

Mole % BeF_2 in Liquid	Invariant Temperature (°C)	Type of Equilibrium	Phase Reaction at Invariant Temperature
31	570	Eutectic	$L \rightleftharpoons NaF + \alpha\text{-}2NaF\cdot BeF_2$
33.3	600	Congruent melting point	$L \rightleftharpoons \alpha\text{-}2NaF\cdot BeF_2$
–	320	Inversion	$\alpha\text{-}2NaF\cdot BeF_2 \rightleftharpoons \alpha'\text{-}2NaF\cdot BeF_2$
–	225	Inversion	$\alpha'\text{-}2NaF\cdot BeF_2 \rightleftharpoons \gamma\text{-}2NaF\cdot BeF_2$
43	340	Eutectic	$L \rightleftharpoons \alpha\text{-}2NaF\cdot BeF_2 + \beta\text{-}NaF\cdot BeF_2$
50	376 ± 5	Congruent melting point	$L \rightleftharpoons \beta'\text{-}NaF\cdot BeF_2$
55	365	Eutectic	$L \rightleftharpoons \beta'\text{-}NaF\cdot BeF_2 + BeF_2$

*Roy, Roy, and Osborn did not list invariant equilibria; those shown are estimates made from the reportec work and from experiments performed at the Oak Ridge National Laboratory.

Fig. 6.16a Invariant Equilibria Data for $NaF-BeF_2$

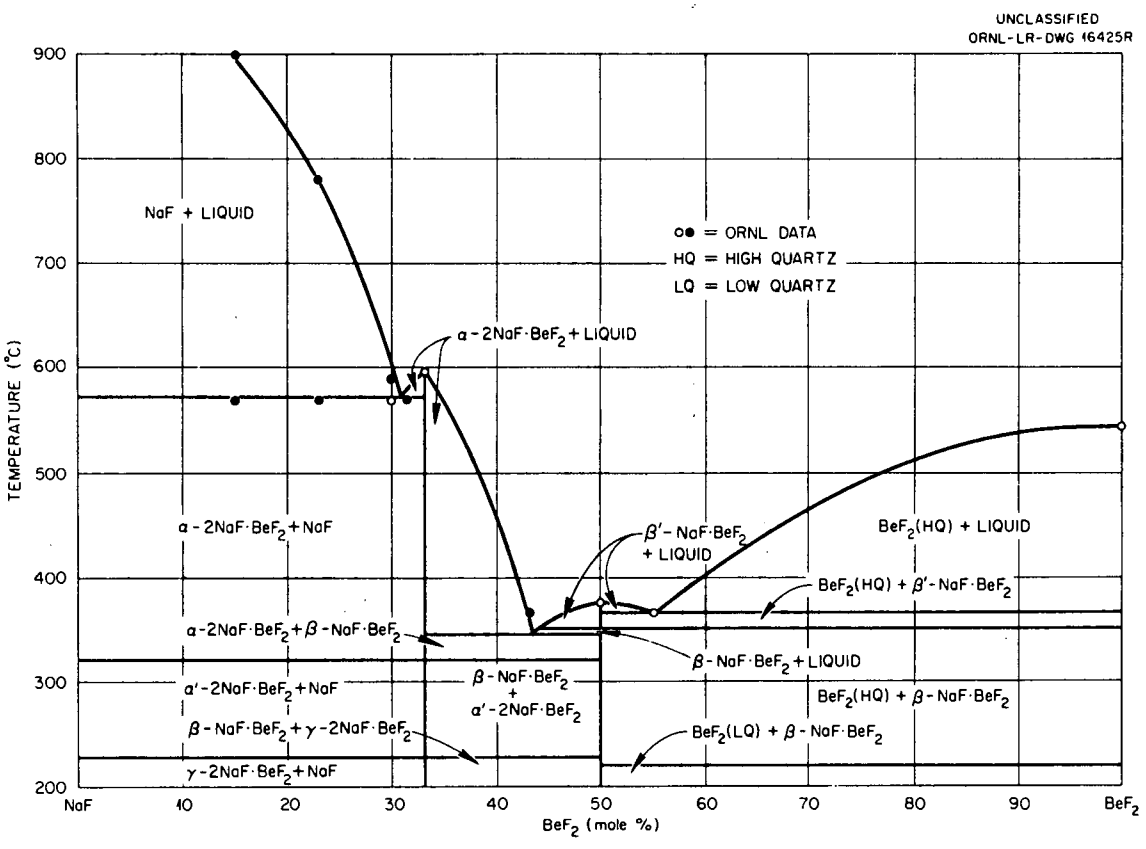

Fig. 6.16b Phase Diagram for $NaF-BeF_2$

The System $LiF-NaF-BeF_2$

R. E. Moore, C. J. Barton, W. R. Grimes, R. E. Meadows, L. M. Bratcher, G. D. White, T. N. McVay, and L. A. Harris, unpublished work performed at the Oak Ridge National Laboratory, 1951–58.

Preliminary diagram.

Invariant Equilibria*

Composition of Liquid (mole %)			Invariant Temperature (°C)	Type of Equilibrium	Solids Present at Invariant Point
LiF	NaF	BeF_2			
15	58	27	480	Eutectic	NaF, LiF, and $2NaF \cdot BeF_2$
23	41	36	328	Eutectic	LiF, $2NaF \cdot BeF_2$, and $2NaF \cdot LiF \cdot 2BeF_2$
20	40	40	355	Congruent melting point	$2NaF \cdot LiF \cdot 2BeF_2$
5	53	42	318	Eutectic	$NaF \cdot BeF_2$, $2NaF \cdot BeF_2$, and $2NaF \cdot LiF \cdot 2BeF_2$
31.5	31	37.5	315	Eutectic	$2LiF \cdot BeF_2$, LiF, and $2NaF \cdot LiF \cdot 2BeF_2$

*Invariant equilibria shown in the phase diagram by the intersections of dotted-line boundary curves have not been determined with sufficient precision to be listed in the table.

Minimum Temperature on Alkemade Lines

Composition of Liquid (mole %)			Temperature (°C)	Alkemade Line
LiF	NaF	BeF_2		
16	56	28	485	$2NaF \cdot BeF_2-LiF$
26	37	37	340	$2NaF \cdot LiF \cdot 2BeF_2-LiF$
11	44	45	332	$NaF \cdot BeF_2-2NaF \cdot LiF \cdot 2BeF_2$
16	45	39	343	$2NaF \cdot BeF_2-2NaF \cdot LiF \cdot 2BeF_2$
30.5	31	38.5	316	$2LiF \cdot BeF_2-2NaF \cdot LiF \cdot 2BeF_2$

Phase relationships of two of the ternary compounds in this system have been reported by W. Jahn ["Silicate Models. V. $NaLi(BeF_4)$, a Model Substance for Monticellite, $CaMg(SiO_4)$," *Z. anorg. u. allgem. Chem.* **276**, 113–27 (1954); "Silicate Models. VI. $Na_3Li(BeF_4)_2$, a New Compound in the Ternary System $NaF-LiF-BeF_2$, and Its Relation to Merwinite, $Ca_3Mg(SiO_4)_2$," *Z. anorg. u. allgem. Chem.* **277**, 274–86 (1954)].

Fig. 6.17a Invariant Equilibria Data for $LiF-NaF-BeF_2$

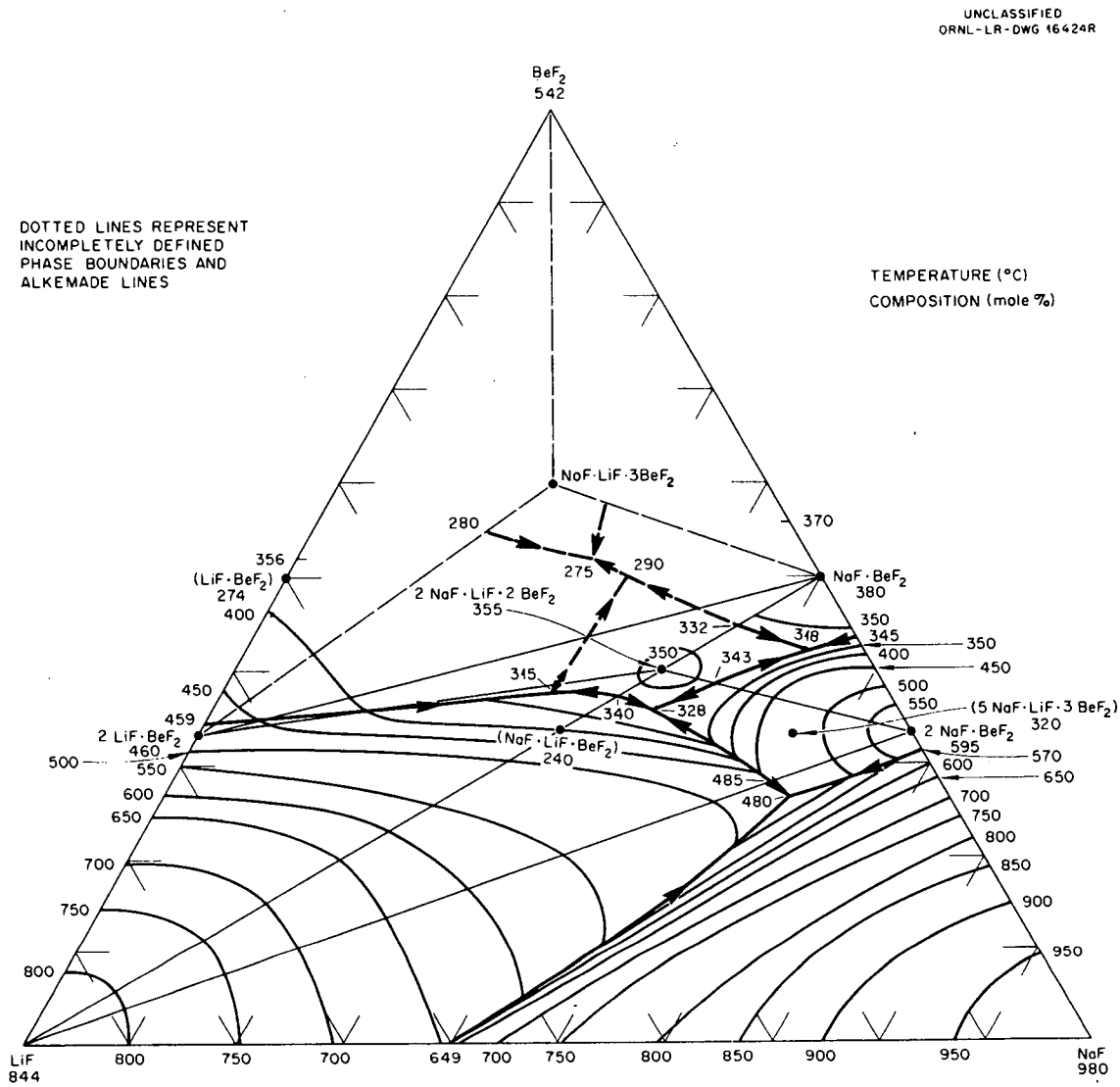

Fig. 6.17b Phase Diagram for LiF-NaF-BeF_2

The System $NaF-KF-ZrF_4$

R. E. Thoma, C. J. Barton, H. Insley, H. A. Friedman, and W. R. Grimes, unpublished work performed at the Oak Ridge National Laboratory, 1951–55.

Preliminary diagram.

Invariant Equilibria*

Composition of Liquid (mole %)**			Invariant Temperature (°C)	Type of Equilibrium	Solids Present at Invariant Point
NaF	KF	ZrF_4			
34	58	8	695	Eutectic	NaF, KF, and $3KF \cdot ZrF_4$
45	38	17	720	Eutectic	NaF, $3KF \cdot ZrF_4$, and $3NaF \cdot 3KF \cdot 2ZrF_4$
61	19	20	710	Eutectic	NaF, $3NaF \cdot ZrF_4$, and $3NaF \cdot 3KF \cdot 2ZrF_4$
52	17	31		Peritectic	$3NaF \cdot ZrF_4$, $3NaF \cdot 3KF \cdot 2ZrF_4$, and $NaF \cdot KF \cdot ZrF_4$
48	18	34		Peritectic	$3NaF \cdot ZrF_4$, $NaF \cdot KF \cdot ZrF_4$, and $5NaF \cdot 2ZrF_4$
33	32	35		Peritectic	$3NaF \cdot 3KF \cdot 2ZrF_4$, $3KF \cdot ZrF_4$, and $NaF \cdot KF \cdot ZrF_4$
12	51	37		Peritectic	$3KF \cdot ZrF_4$, $2KF \cdot ZrF_4$, and $NaF \cdot KF \cdot ZrF_4$
40	21	39		Peritectic	$5NaF \cdot 2ZrF_4$, $2NaF \cdot ZrF_4$, and $NaF \cdot KF \cdot ZrF_4$
39	21	40		Peritectic	$2NaF \cdot ZrF_4$, $7NaF \cdot 6ZrF_4$, and $NaF \cdot KF \cdot ZrF_4$
11	49	40		Peritectic	$2KF \cdot ZrF_4$, $3KF \cdot 2ZrF_4$, and $NaF \cdot KF \cdot ZrF_4$
10	48	42	385	Eutectic	$3KF \cdot 2ZrF_4$, $KF \cdot ZrF_4$, and $NaF \cdot KF \cdot ZrF_4$
15	40	45		Eutectic	$KF \cdot ZrF_4$, $NaF \cdot KF \cdot ZrF_4$, and $2NaF \cdot 3KF \cdot 5ZrF_4$
22	33	45		Peritectic	$NaF \cdot KF \cdot ZrF_4$, $7NaF \cdot 6ZrF_4$, and $2NaF \cdot 3KF \cdot 5ZrF_4$
25	25	50		Eutectic	$7NaF \cdot 6ZrF_4$, $3NaF \cdot 4ZrF_4$, and $2NaF \cdot 3KF \cdot 5ZrF_4$
21	29	51		Eutectic	$3NaF \cdot 4ZrF_4$, ZrF_4, and $2NaF \cdot 3KF \cdot 5ZrF_4$
20	30	50	432	Congruent melting point	$2NaF \cdot 3KF \cdot 5ZrF_4$

*Three solid phases have been observed routinely in the composition region 30–50 mole % ZrF_4 which have not been identified as to composition. Whether these exhibit primary phases at the liquidus surface has not yet been determined.

**Compositions of invariant points shown by the intersection of dotted boundary curves are approximate.

Fig. 6.18a Invariant Equilibria Data for $NaF-KF-ZrF_4$

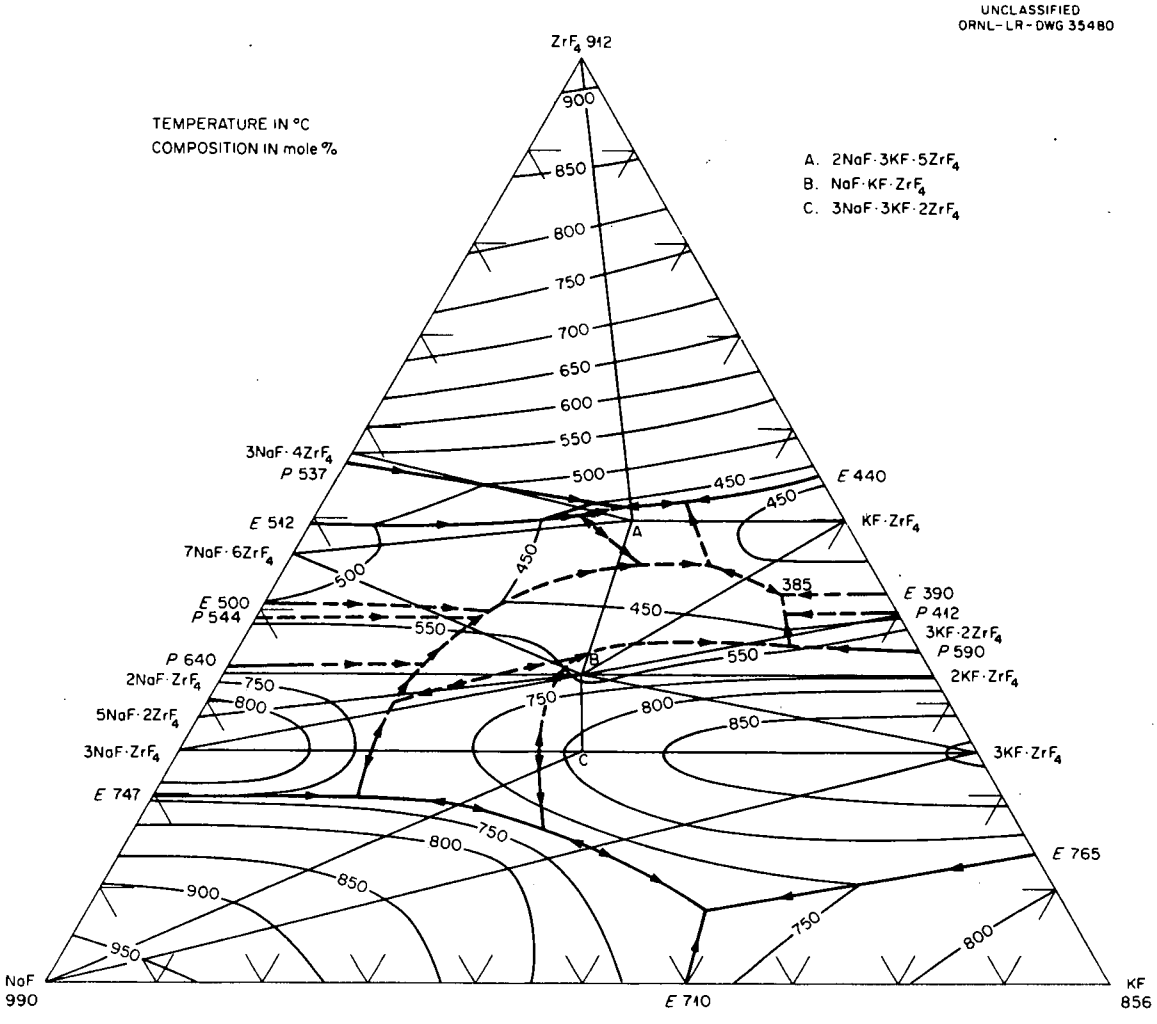

The System NaF–KF–ZrF_4. The isotherms for the temperatures 600, 650, and 700°C between the 30 and 40 mole % ZrF_4 compositions have been omitted in order not to obscure the phase relationships in this polythermal projection.

Fig. 6.18b Phase Diagram for NaF-KF-ZrF_4

The System $NaBF_4$–KBF_4

R. E. Moore, J. G. Surak, and W. R. Grimes, unpublished work performed at the Oak Ridge National Laboratory, 1957.

Preliminary diagram. The system $NaBF_4$–KBF_4 contains a single eutectic at 88 $NaBF_4$–12 KBF_4 (mole %), m.p. 355°C. The dotted line was obtained from thermal effects representing incompletely understood solid-phase transformations of KBF_4 and $NaBF_4$.

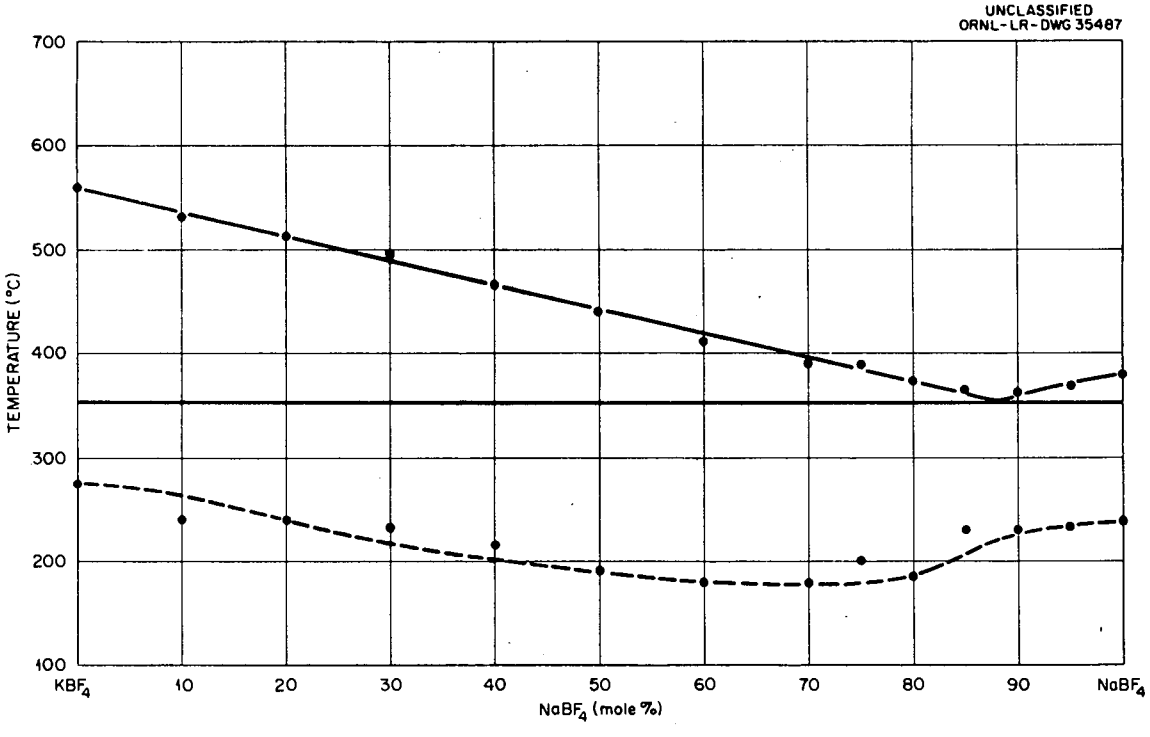

Fig. 6.19 Phase Diagram for KBF_4-$NaBF_4$

The System $NaF-NaBF_4$

E. M. Levin, C. R. Robbins, H. F. McMurdie, "Phase Diagrams for Ceramists", The American Ceramic Society, Inc., Ohio (1964)

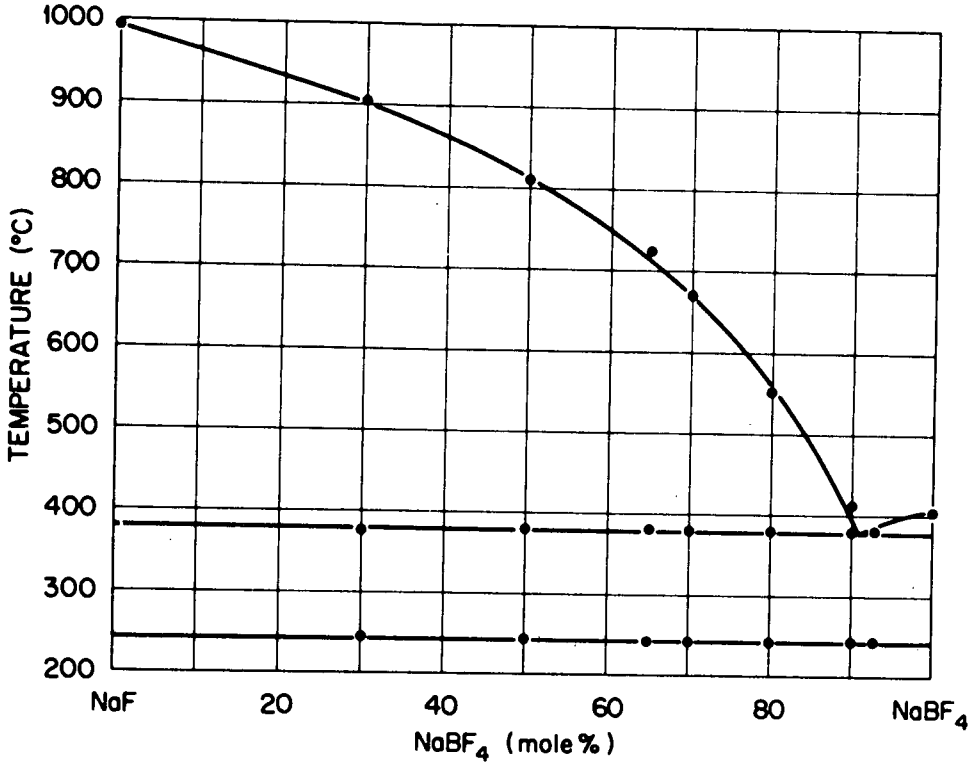

Fig. 6.20 Phase Diagram for $NaF-NaBF_4$

The System $NaF-KF-NaBF_4-KBF_4$

ORNL-4449, p. 129

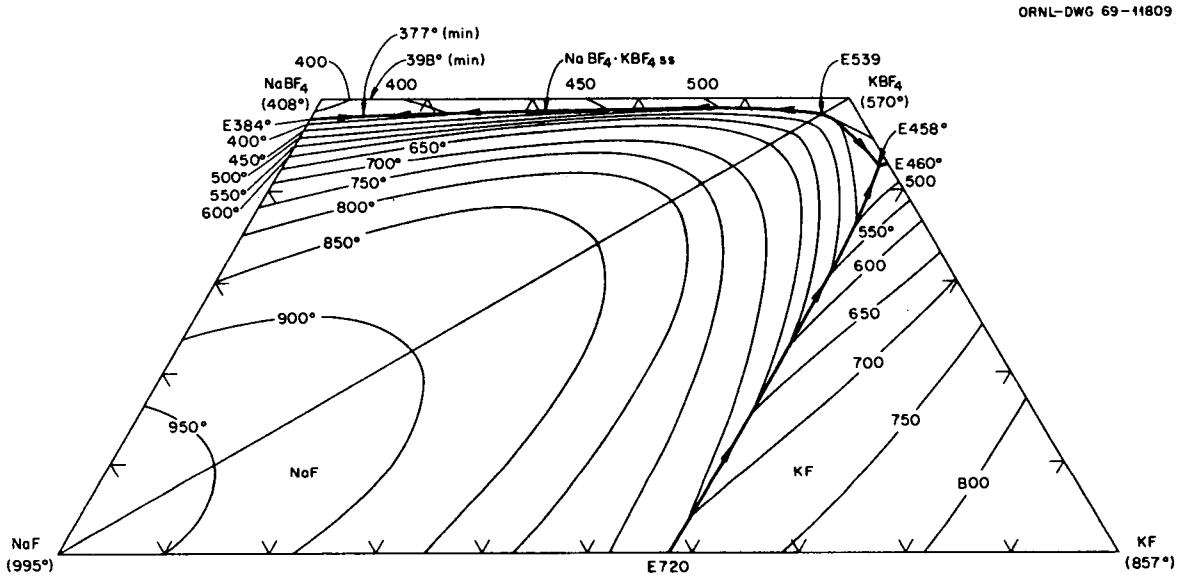

Fig. 6.21 Phase Diagram for $NaF-KF-NaBF_4-KBF_4$

6.3.1 Compatibility With Graphite (Cont'd)

Several potential problems of a chemical nature in addition to chemical stability have been considered. These include (1) possible reaction of fuel material with oxygenated gaseous species desorbed from the graphite and (2) possible carbonization of the container material.

Graphites contain appreciable quantities of gases typically H_2O, CO_2, CO, N_2, H_2 and small quantities of hydrocarbons. The chemical effects of these species are discussed in another section of this report. Operation of MSRE indicates that sorbed gases in the graphite are not a problem.

No significant carbonization of container material (Hastelloy N) was observed during MSRE operation or in capsule tests.

6.3.2 Compatibility With Containment Materials

Most corrosion studies with fluoride salts under consideration for molten salt reactors have been with Hastelloy N which was specifically developed for this application. Corrosion rates of Hastelloy N attributable to the major constituents of the fuel salts have been shown to be extremely low at temperatures considerably above the 1000 to 1300°F range typical of MSR's. Corrosion rates of less than 1 mpy appear to be attainable.

Oxidation of metals by molten fluorides is characterized by the tendency of the corrosion products to be completely soluble in the melt. Thus passivation is precluded and corrosion depends directly on the thermodynamic driving force of the corrosion reactions.

Of the major constituents of Hastelloy N, chromium has the highest solution potential (measured by free

6.3.2 Compatibility With Containment Materials (Cont'd)

energy of formation of CrF_2) under MSR conditions. Thus it tends to dissolve preferentially, but if the oxidation potential of the melt is not too high, the reaction reaches steady state at a relatively low CrF_2 concentration in the melt. Unless the CrF_2 concentration in the melt is disturbed, the corrosion rate tapers off.

The oxidizing potential of the melt, which determines the equilibrium relationship between the many redox couples present is conveniently measured (in the fuel salt) by the concentration ratio of UF_4 to UF_3 so that corrosion can be minimized by reducing the UF_4/UF_3 ratio. As discussed in Section 14 of this report, the tritium problem may be ameliorated by increasing the UF_4/UF_3 ratio so that the optimum adjustment of UF_4/UF_3 ratio may involve a balance between tolerable corrosion and reduction of tritium release.

The CrF_2 concentration may be upset by:

a - mass transfer, i.e., deposition of Cr in cooler surfaces of the fuel salt loop and dissolution from hotter surfaces. The temperature dependence of the CrF_2 solubility constant is not great and, within limits, one would expect that mass transfer effects would tend to build up compensating chromium concentration gradients in the surface layers of the alloy so that the initial mass transfer would tend to be self limiting. The fact that chromium corrosion rates in the MSRE seemed to be lower than anticipated (even with conditions more oxidizing than planned) seems to support this view.

b - depletion of CrF_2 by chemical reprocessing. As far as is known, ORNL has not given serious consideration to this possibility. If it is a problem, one

6.3.2 Compatibility With Containment Materials (Cont'd)

solution may be the deliberate addition of CrF_2 by contacting the salt with a large surface area of Hastelloy N or other chromium alloy in a reconditioning bed.

6.4 Graphite Technology

This report section will review the technology background specific to the graphite requirements for molten salt nuclear power reactors. The primary problem areas of radiation damage, molten salt compatibility, fission product retention, and manufacturing feasibility will be given the major attention in the review.

6.4.1 Radiation Damage

The graphite in the core of molten salt reactors is subjected to a high flux of neutrons at high temperature (650-700 C) for long periods of time (preferably the full life of the reactor). If graphite were available that did not suffer any damage from radiation and an MSBR was designed to optimized nuclear conditions, the reactor would be clearly superior in economical power generation to any other type now known. Unfortunately, graphite is damaged by radiation and MSBR's must be designed to operate within the restraint of the known graphite lifetime at the radiation doses imposed.

a - Dimensional Changes

When graphite is exposed to fast neutron doses, it contracts initially with the rate of contraction decreasing with exposure until a minimum volume is reacted; further exposure causes volume expansion with the rate of expansion increasing rapidly at neutron doses above about 3×10^{22} neutrons/cm^2 ($E > 50$ kev) in all bulk graphite tested to date.

6.4.1 Radiation Damage (Cont'd)

a - Dimensional Changes (Cont'd)

This behavior is due to atomic displacements which take place when graphite is exposed to fast neutrons, resulting in anisotropic crystallite growth rates. The crystal expands in the c-axis direction and contracts in the a-axis directions. The bulk dimensional change depends upon the geometrical summation of the individual crystallite changes and hence is dependent upon the starting materials and the method of fabrication. The extent of the radiation damage is also strongly dependent upon the temperature of the graphite during irradiation. The magnitude of this temperature dependence was not recognized until less than ten years ago and hence the severity of graphite radiation damage at the high temperatures of the MSBR (~ 700 C) was underestimated.

Figure 6.22[10/] shows the volume change in a conventional nuclear graphite (AGOT) during irradiations at various temperatures of relatively high fluences. Figure 6.23[11/] shows the length change in an isotropic nuclear graphite (British Gilsocarbon) during irradiations at various temperatures at relatively high fluences. The actual changes in dimensions are, of course, different from grade to grade and depend largely on the degree of anisotropy present in the graphite. The initial decrease in volume is attributed to the closing of voids

10/ ORNL-TM-2136 Graphite Behavior and its Effects on MSBR Performance, Figure 3.2, page 12.

11/ ORNL-TM-2136 - Figure 3.6, page 19.

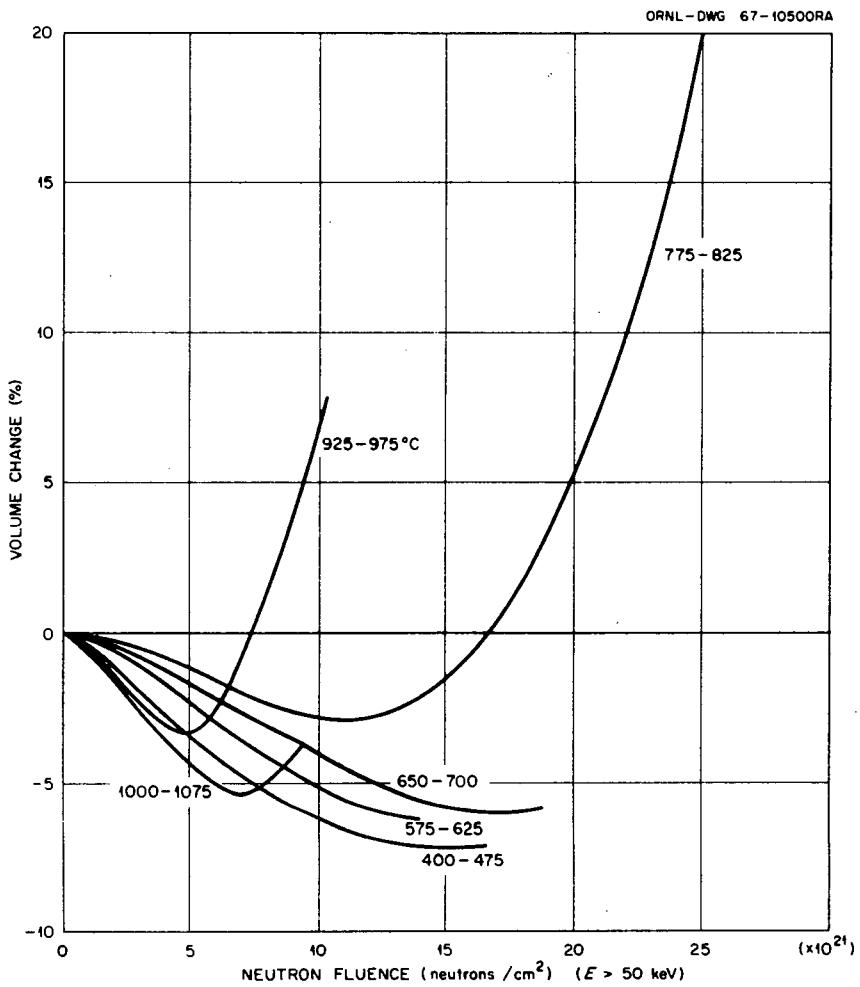

Fig. 6.22 Volume Change in Anisotropic (AGOT) Graphite During GETR Irradiations

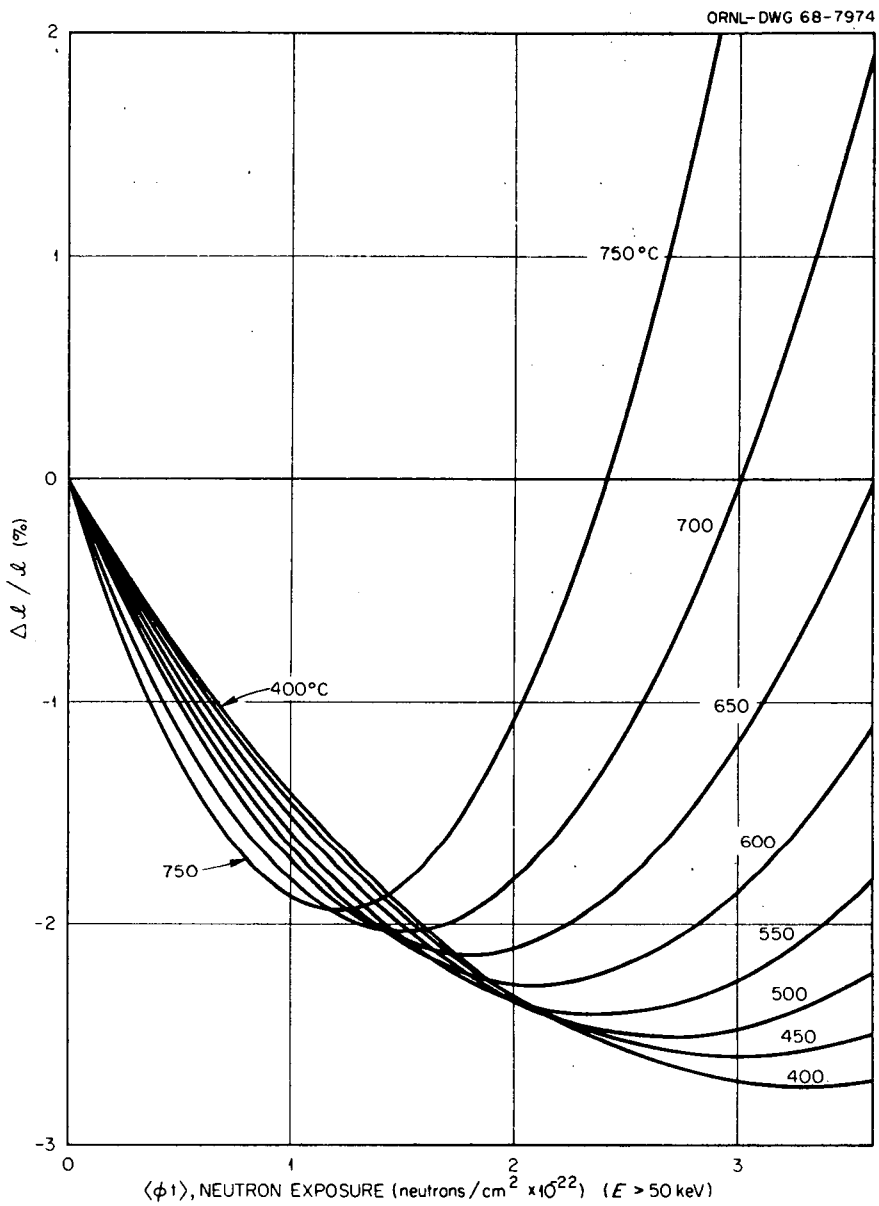

Fig. 6.23 Radiation Induced Dimensional Changes in Gilso Graphite at Various Temperatures

6.4.1 Radiation Damage (Cont'd)

a - Dimensional Changes (Cont'd)

generated by thermal strains during cooling in the fabrication process.

The closing of the void volume is accompanied by c-axis growth, and a-axis shrinkage which allows the c-axis growth to be accommodated internally; the changes in crystallite dimensions do not contribute to the overall changes in macroscopic dimensions until the voids are closed. The magnitude of the temperature effect on the dimensional changes is clearly evident in both the anisotropic (AGOT) and isotropic (Gilsocarbon) graphite grades.

Figure 6.24[12/] shows the volume changes in various commercial and experimental graphites during irradiations at 715 C (maximum operating temperature in MSBR).

It is of interest to note that although the amount of shrinkage varies between grades, all the commercial grades tested and many of the experimental grades regain their original volume at total fluences between ~ 2 to 3×10^{22} neutrons/cm^2. It is reasonably well established that an MSBR design based on graphite dimensional stability at $\sim 3 \times 10^{22}$ neutrons/cm^2 radiation fluence is obtainable.

Recently, considerable study at ORNL has been invested in extremely fine grained isotropic graphites. Figures 6.25[13/] and 6.26[14/] show volume

12/ ORNL-4449 MSR Semi-Annual Report - Aug. 31, 1969, Fig. 17.6, p. 177.

13/ ORNL-4449 MSR Semi-Annual Report - Aug. 31, 1969, Fig. 17.4, p. 176.

14/ ORNL-4449 MSR Semi-Annual Report - Aug. 31, 1969, Fig. 17.5, p. 176.

6.4.1 Radiation Damage (Cont'd)

a - Dimensional Changes (Cont'd)

changes of two different groups of these isotropic graphites, produced by POCO and Great Lakes, respectively. The magnitude of the shrinkage during the earlier stages of radiation has been greatly reduced in these graphites and although the return to original volume still occurs near 3×10^{22} neutrons/cm^2 total fluence, the expansion appears to be somewhat less rapid at this point suggesting that other graphites of this general type may eventually be produced that withstand more radiation without significant damage.

In addition to the variety of bulk graphites tested for radiation stability, several varieties of pyrolytic or vapor deposited graphites have been exposed to significant doses of neutrons. Figure 6.27[15/] shows the effect of fast neutrons at 715 C on dimensional changes of methane-derived pyrolytic carbons. These methane-derived pyrolytic carbons exhibit significant densification at moderate fluences followed by swelling and large dimensional changes at the higher exposures. Figure 6.28[16/] shows the effect of fast neutron exposure at 715 C on dimensional changes of propylene-derived pyrolytic carbons. It is shown that at exposures up to 2×10^{22} neutrons/cm^2, the high density isotropic propylene-derived carbons undergo only small dimensional changes.

15/ ORNL-4548 MSR Semi-Annual, Feb. 28, 1970, Fig. 17.18, p. 217.

16/ "Radiation Induced Dimensional Changes in Large Graphite Bars," R. E. Nightingale and E. N. Woodruff, Nucl. Science Eng. 19, pp. 390-392 (1964).

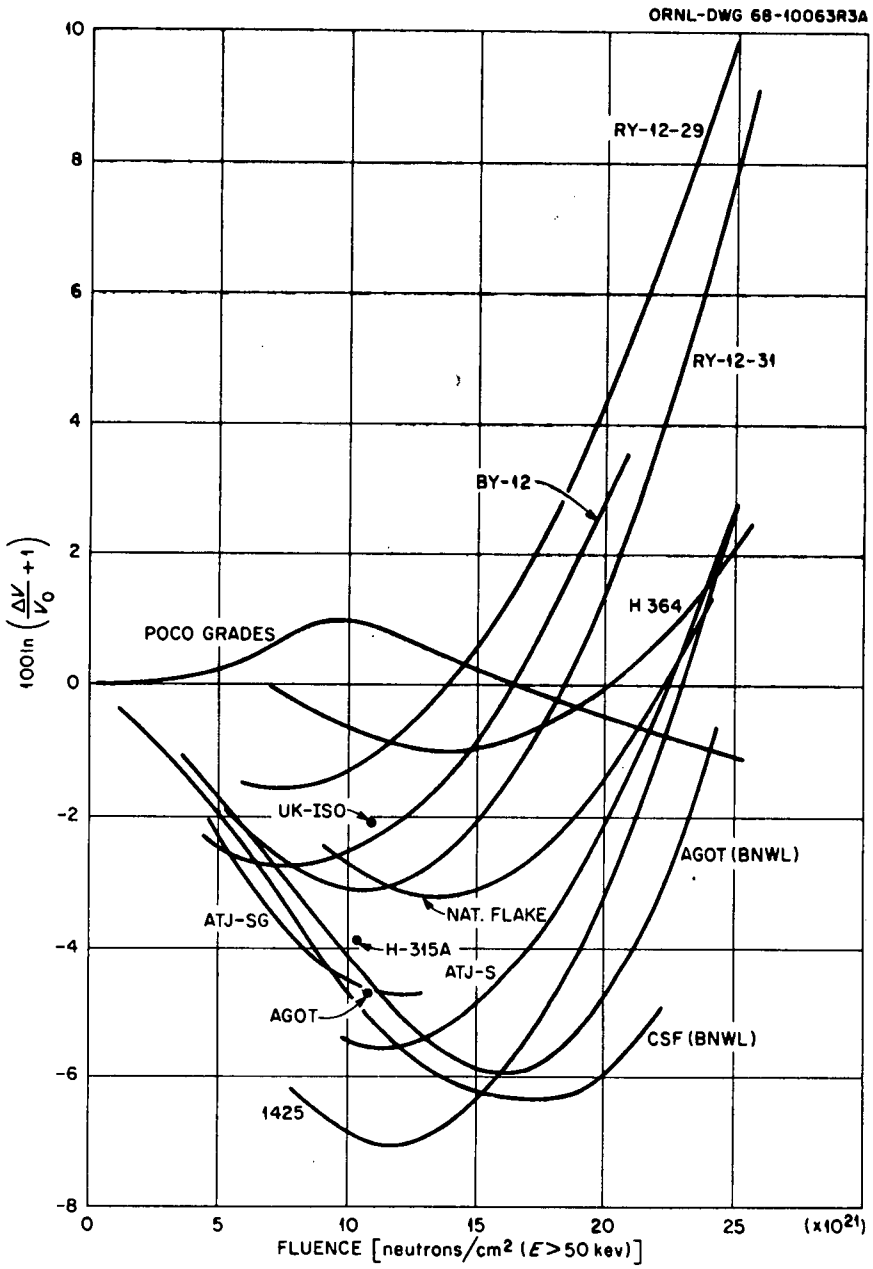

Fig. 6.24 Volume Changes of Several Graphites During Irradiation at 715°C

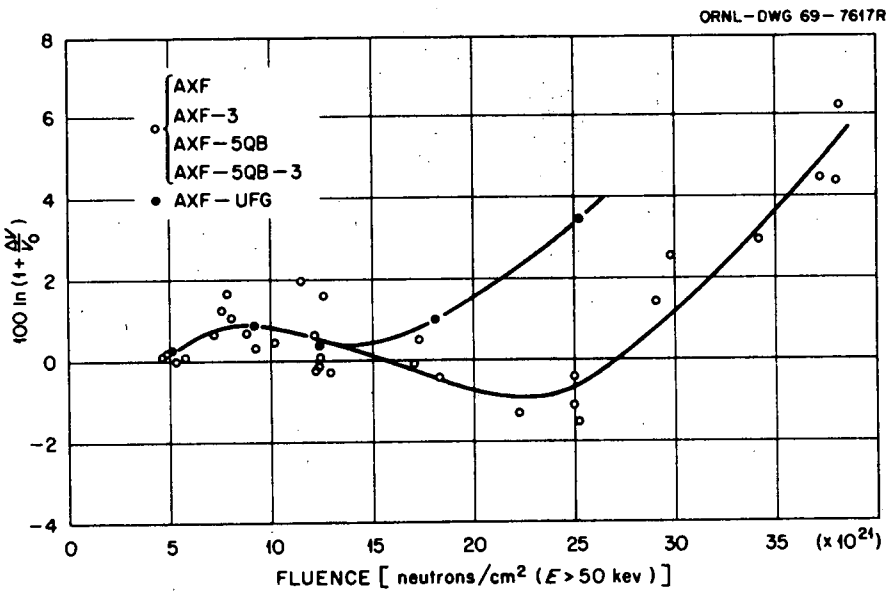

Fig. 6.25 Volume Changes of POCO Graphites at 715°C

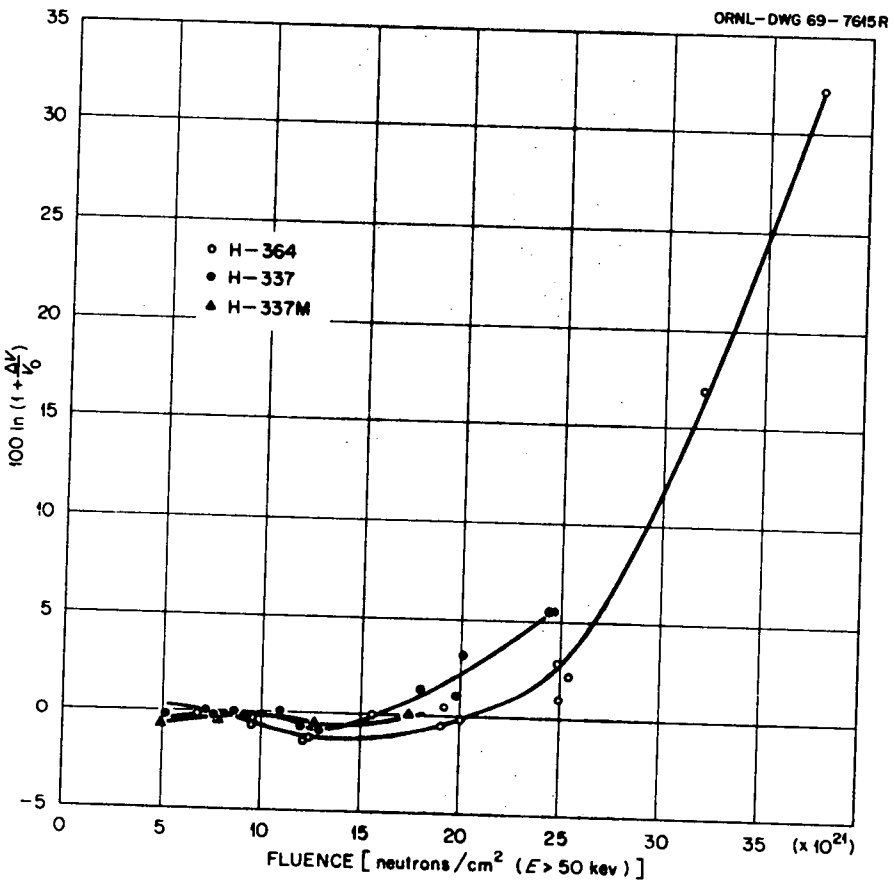

Fig. 6.26 Volume Changes of H364, H337, and H337M at 715°C

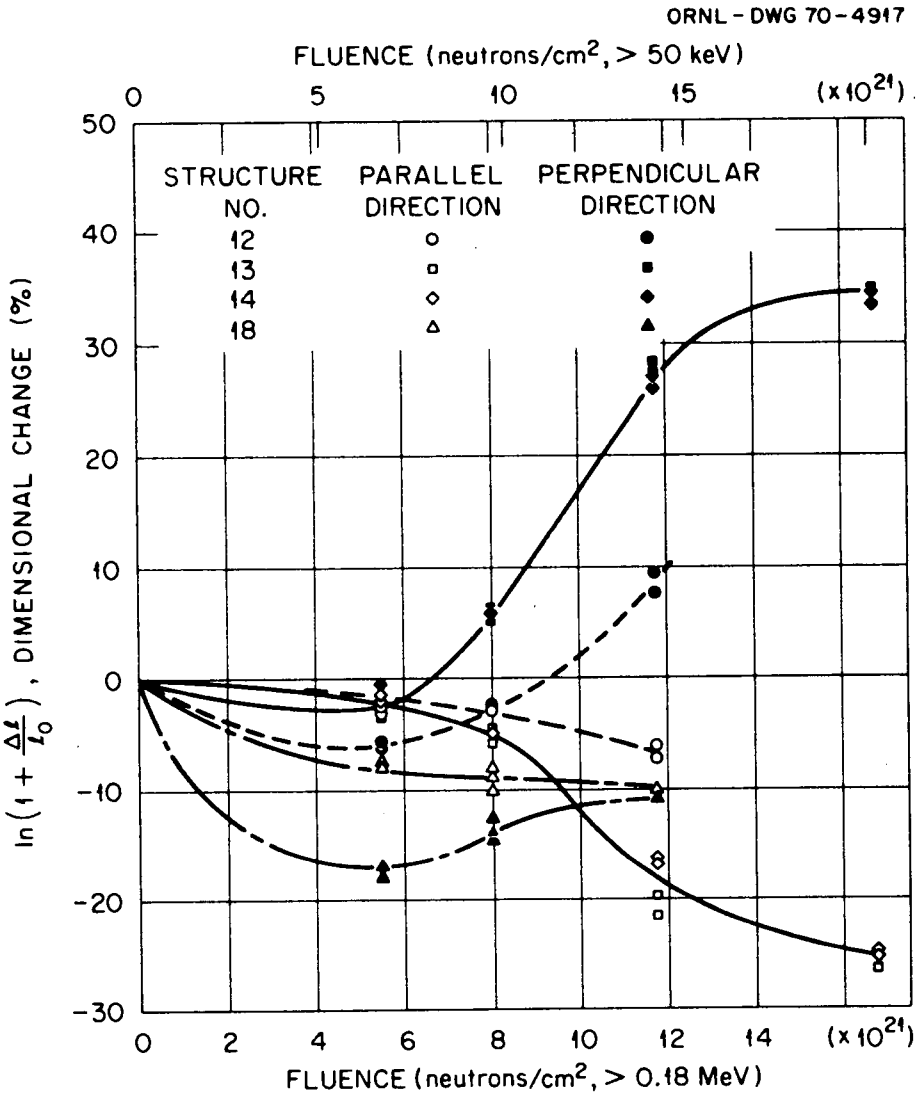

Fig. 6.27 Effect of Fast Neutron Exposure at 715°C on Dimensional Changes of Methane-Derived Pyrolytic Carbons

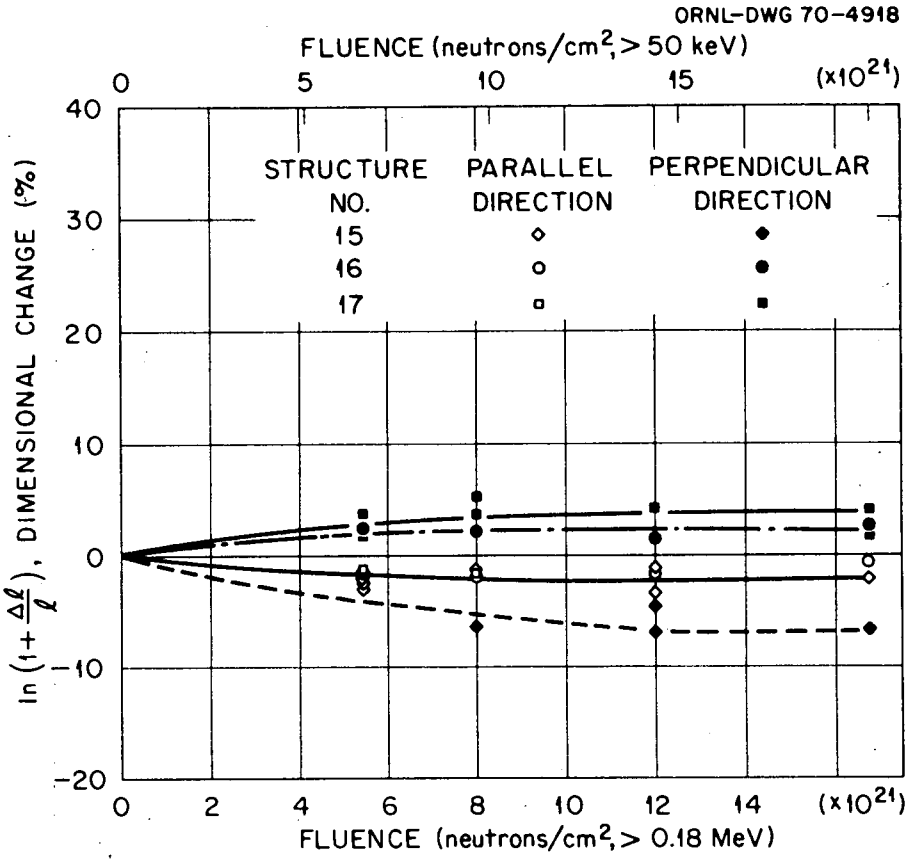

Fig. 6.28 Effect of Fast Neutron Exposure at 715°C on Dimensional Changes of Propylene-Derived Pyrolytic Carbons

6.4.1 Radiation Damage (Cont'd)

a - Dimensional Changes (Cont'd)

These radiation induced dimensional changes are the controlling factors in determining the graphite lifetime in any MSBR. The total background of data on graphite radiation damage at high temperatures is still rather meager, but it appears that several graphites have the capability of surviving about 3×10^{22} n/cm^2 (E > 50 kev) total fluence without serious dimensional changes. It also appears doubtful that new graphites will be forthcoming quickly which are much more resistant to radiation induced dimensional changes. In estimating the useful lifetime of the graphite for the MSBR some speculation is required since there is little information concerning the effects of volume expansion on pore spectrum, gas-penetration characteristics, and strength of the graphite. It appears probable that contraction followed by expansion back to the original graphite volume does not create a structure less sound than the original irradiated material. On this basis, the useful life of the graphite would correspond to the exposure required for the graphite to return to its original volume. Therefore, based upon grades of graphite that have been tested and the results shown, the lifetime expectancy of graphite at 700 C would be about 3×10^{22} neutrons/cm^2 (E > 50 kev).

The graphite temperature in an MSBR varies with core design, power density, and also with spatial position within the reactor. For an MSBR operating at an average power density of 80 kw/liter, peak graphite temperatures would be in excess of 750 C. However, peak temperature is probably not the

6.4.1 Radiation Damage (Cont'd)

a - Dimensional Changes (Cont'd)

proper criterion; rather, the volume-averaged graphite temperature in the vicinity of the highest fast neutron flux would be more appropriate. The peak volume averaged temperature would tend to decrease with increasing number of fuel flow channels and with decreasing power density in a single fluid MSBR. A value of 700 C is representative of the effective volume averaged temperature to be used in estimating permissible graphite exposure for a MSBR such as the reference design, operating at an average core power density of about 40 kw/liter.

The effect of graphite size on dimensional stability during reactor exposure has been reported by Nightingale and Woodruff[16/]. Large blocks have shown a transverse shrinkage rate of up to twice that of subsize specimens. Although the rationale for such behavior is very vague, this "size effect" has occurred. C. R. Kennedy[17/] reports that although the volumetric contraction in the transverse direction with large size graphite specimens is possibly greater by about 1 percent than that obtained with small size samples, the exposure required to obtain minimum volume and reversal in volume growth has not been reduced. The "size effect" would, at the most, only require an allowance in the design for this increase in transverse shrinkage. This would neither increase nor decrease the lifetime expectancy of the graphite.

16/ "Radiation Induced Dimensional Changes in Large Graphite Bars," R. E. Nightingale and E. N. Woodruff, Nucl. Science Eng. 19, pp. 390-392 (1964).

17/ ORNL-TM-2136, p. 17.

6.4.1 Radiation Damage (Cont'd)

b - Stresses Generated in Graphite During Irradiation

The foregoing discussions concerned the limitations on graphite lifetime due to irradiation induced dimensional changes, for the case of graphite in a stress-free condition. In actual fact, temperature and flux gradients in the core will tend to produce differential distortions within the graphite, thus generating internal stresses. These effects have been examined extensively at ORNL and are reported by Chang, Eatherly, and Prados[18/] as follows:

To assess the potential effects of fast-neutron damage in the core graphite of a molten salt reactor, preliminary calculations of induced stress distributions and distortions have been carried out by three different techniques. As a first approximation, the core graphite is assumed to be in the form of long cylindrical tubes, although the actual shape will be more complex.

We start with the basic constitutive equations

$$\dot{\epsilon}_i = \frac{1}{E}[\dot{\sigma}_i - \mu(\dot{\sigma}_j + \dot{\sigma}_k)] + \frac{1}{E}[\dot{\sigma}_i - \mu''(\dot{\sigma}_j + \dot{\sigma}_k)]\, f(\phi, t) + k\phi[\sigma_i - \mu'(\sigma_j + \sigma_k)] + g(\phi, t),$$

in which ϵ and σ are the strain and stress in the ith direction, the first term on the right is the elastic distortion, the second the primary creep, the third the secondary creep and the last the rate

18/ ORNL-4396 MSR Semi-Annual Report - Feb. 28, 1969, Chang, Eatherly, Prados, pp. 229-231.

6.4.1 Radiation Damage (Cont'd)

b - Stresses Generated in Graphite During Irradiation (Cont'd)

of radiation-induced distortion. Since the primary creep is a rapidly saturating function, one may substitute the asymptotic value of the function f, thereby suppressing its time dependence and combining it with the first term. Hence

$$\dot{\epsilon}_i = \frac{1}{\langle E \rangle}\left[\dot{\sigma}_i - \langle\mu\rangle(\dot{\sigma}_j + \dot{\sigma}_k)\right] + k\phi\left[\sigma_i - \mu'(\sigma_j + \sigma_k)\right] + g(\phi, t),$$

where $\langle E \rangle$ and $\langle \mu \rangle$ are the effective Young's modulus and Poisson's ratio, respectively.

A solution to these equations in closed analytic form can be found by using operator algebra. The solution is limited to the requirement that the parameters $\langle E \rangle$, $\langle \mu \rangle$, $k\phi$, and μ' not be functions of radial position in the cylinder. This restriction is not a serious one for the present calculations.

A second solution has been developed by modifying an iterative technique employed in the analysis of stress and distortion in coated particle fuels[19/]. This approach permits $k\phi$ to be a function of radial position, does not require isotropy in the graphite, and permits the secondary creep to be a more general function of the stresses.

The third solution using an impulse-type analysis, has also been derived[20/], which generalizes the

19/ J. W. Prados and T. G. Godfrey, STRETCH, "A Computer Program for Predicting Coated-Particle Irradiation Behavior, Modification IV," ORNL-TM-2127 (April 1968).

20/ S. J. Chang, "Visco-Elastic Analysis of Graphite Under Neutron Irradiation and Temperature Distribution," ORNL-TM-2407, to be published.

6.4.1 Radiation Damage (Cont'd)

b - Stresses Generated in Graphite During Irradiation (Cont'd)

solutions to arbitrary boundary shapes providing only that elastic solutions can be found. It is limited, however, to a linear stress dependence in the secondary creep.

All three solutions have been computer programmed, debugged, and shown to give the same numerical results within their region of overlap. In particular, the stresses and distortions have been calculated for the present reactor parameters aimed at a four-year graphite life.

The material parameters employed are as follows:

Young's modulus: $E = 1.9 \times 10^6$ psi,

Poisson's ratio: $\mu = 0.27$,

thermal expansion coefficient: $\alpha = (5.52 \times 10^{-6} + 1.00 \times 10^{-9} T)(°C)^{-1}$,

thermal conductivity: $K = 37.63\ (T + 273.1)^{0.7}$ wcm^{-1} $(°C)^{-1}$,

secondary "Poisson's ratio": $\mu'' = 0.50$,

creep coefficient: $k = (5.3 - 1.45 \times 10^{-2} T + 1.4 \times 10^{-5} T^2) \times 10^{-27}$ (psi nvt)$^{-1}$

The induced distortion rate $g(\phi, 1)$ was derived primarily from the experimentally determined behavior of British isotropic Gilso graphite:

$$g = \frac{4G_m}{\tau}\left(1 - 2\frac{t}{\tau}\right),$$

where

$G_m = -4.01 + 2.97 \times 10^{-3} T$ percent,

$\phi_\tau = (9.36 - 8.93 \times 10^{-3}\ T) \times 10^{22}$ (nvt),

τ = lifetime, sec.

6.4.1 Radiation Damage (Cont'd)

b - Stresses Generated In Graphite During Irradiation (Cont'd)

In all the above equations T is the graphite temperature in degrees centigrade.

Parameters associated with the reactor were taken as follows:

salt temperature: $T_o = 625 - 75\cos\frac{\pi z}{l} deg\ C$,
flux: $\phi = (3.2 \times 10^{14}) \sin\frac{\pi z}{l}$ neutrons/cm^2 ($E > 50$ kev),
gamma heating: $q = 0.71 + 4.39 \sin\frac{\pi z}{l}$ w/cm^3,
graphite outer radius: $b = 5.39$ cm,
graphite inner radius: $a = 0.762$ cm,

where z/l is the fractional height along the core centerline. The heat transfer coefficient between the salt and graphite was calculated from the Dittus-Boelter equation for turbulent flow with salt properties as follows:

thermal conductivity: 0.75 Btu hr^{-1} ft^{-1} (°F)$^{-1}$,
flow: 6.08×10^6 lb ft^{-2} hr^{-1},
viscosity: 0.193 exp [7816/T(°F)] lb/ft,
specific heat: 0.324 Btu lb^{-1} (°F)$^{-1}$

Over the temperatures of interest this yields a heat transfer coefficient

$$h = 2.012 \times 10^{-3} T - 0.316 \text{ wcm}^{-2} (°C)^{-1}$$

The results of the calculations are as follows: The graphite is under the most severe flux-temperature environment at $z/l = 0.55$ (i.e., slightly over halfway up the core) and at that point has a lifetime[21/] of 4.1 years. The

21/ As the definition of lifetime, we take a period the time at which the most damaged region in the graphite returns to its original volume.

6.4.1 Radiation Damage (Cont'd)

b - Stresses Generated in Graphite During Irradiation (Cont'd)

maximum thermal stresses are tensile and occur at the surfaces of the graphite (see Fig. 6.29). They anneal out due to creep in a few weeks time and do not exceed 560 psi. The maximum radiation-induced stresses are tensile and occur at the end of the of the graphite life (see Fig. 6.30). They do not exceed 500 psi. Since the graphite should have an ultimate tensile strength of about 5000 psi, these stresses are not significant.

The dimensional behaviors are shown in Figures 6.31 and 6.32. These are expressed in terms of the function G_i , representing the percentage distortion of the i th dimension. The cylindrical graphite tubes will show a maximum radial shrinkage of about 2.2 percent and a maximum axial shrinkage of about 1.6 percent. These dimensional changes are significant but can be compensated for in the core design.

Recent data on the irradiation of newer graphites given in Section 17.9 (of ORNL-4396) suggest that materials superior to the British Gilso graphite will be available within the next few years. Hence the above numbers represent an upper limit to the stresses and distortions which can be expected in an actual reactor.

Methods of calculating the lifetime and induced stresses in graphite are reported by Chang[22/] as follows:

22/ ORNL-4548, MSR Semi-Annual Report Feb. 28, 1970, S. J. Chang, pp. 218-221.

6.4.1 Radiation Damage (Cont'd)

b - Stresses Generated in Graphite During Irradiation (Cont'd)

To analyze the effects of fast-neutron damage on the core graphite of a molten salt reactor, three methods have been developed and discussed earlier[23/]. The impulse-type analysis, the most general of the three, has been further developed to lift restrictions on the cross-sectional shape. The method can thus be used to analyze effects of geometrical shape, boundary traction, thermal properties, and neutron-induced dimensional changes provided only that the creep coefficient and the neutron flux not be sensitive to position over a given cross section. The analysis is based on the constitutive equations of the form[24/].

$$\epsilon_x = (1-\mu^2) J * \left(do_x - \frac{\mu}{1-\mu} do_y\right) + (1+\mu)(\alpha T + \psi) - \mu\epsilon_o$$

$$\epsilon_y = (1-\mu^2) J * \left(do_y - \frac{\mu}{1-\mu} do_x\right) + (1+\mu)(\alpha T + \psi) - \mu\epsilon_o$$

$$\gamma_{xy} = 2(1+\mu) J * do_{xy},$$

where $J(D)$ is the uniaxial neutron creep function

$$J(D) = \frac{1}{E} + K(T) \cdot D + \frac{1}{2E}\left(1 - e^{-A_o D}\right)$$

and the symbol * denotes the convolution operation defined by

$$J * do = \int_o^D J(D' - D') \frac{\partial \sigma}{\partial D'} dD'$$

23/ MSR Program Semi-Annual Progress Report February 28, 1969, ORNL-4396, pp. 229-31.

24/ S. J. Chang, C. E. Pugh, and S. E. Moore, "Viscoelastic Analysis of Graphite Under Neutron Irradiation and Temperature Distribution," Fifth Southeastern Conference on Theoretical and Applied Mechanics, Raleigh, N. C., April 1970.

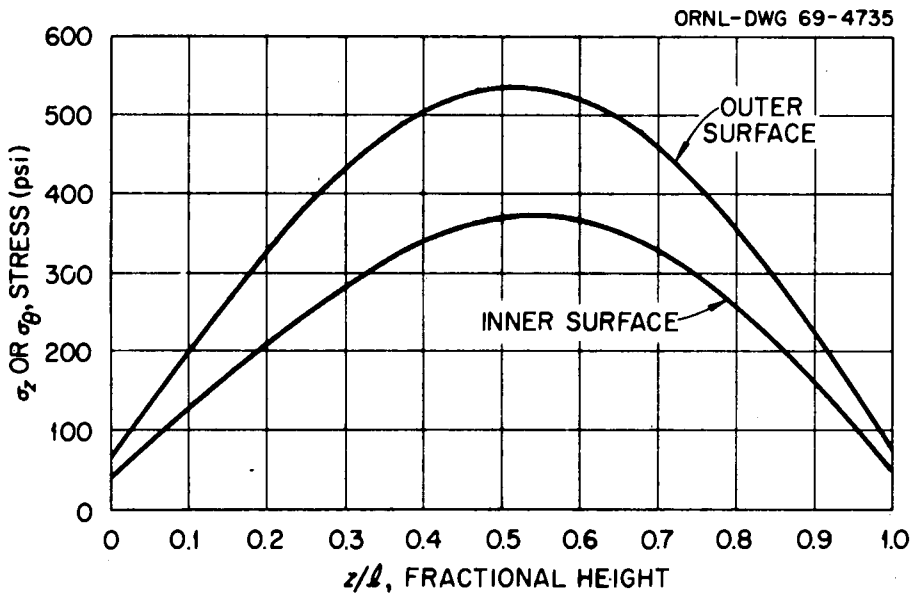

Fig. 6.29 Maximum Thermal Stresses Developed in the Graphite at Reactor Startup

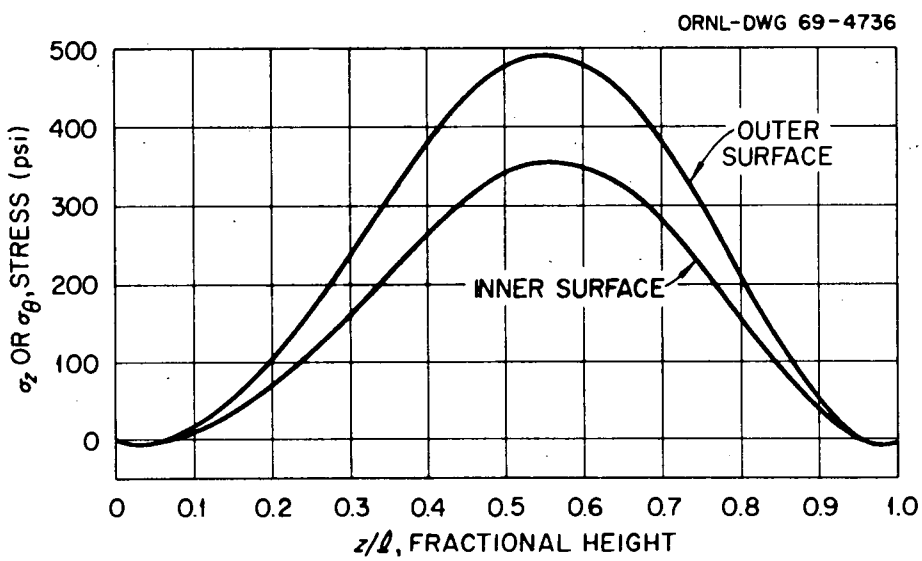

Fig. 6.30 Maximum Radiation-Induced Stresses Developed in the Graphite at the End of Core Life

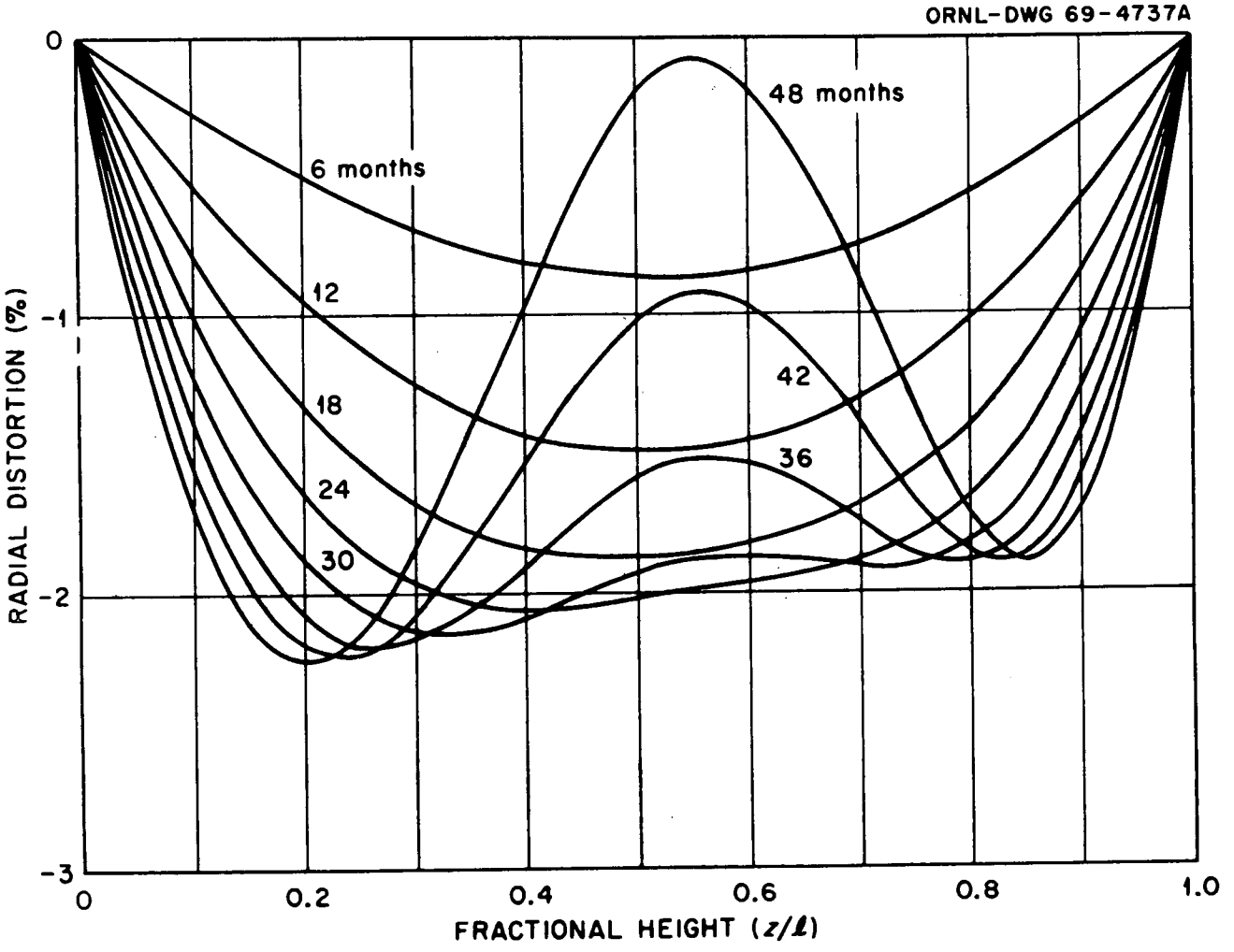

Fig. 6.31 Radially-Induced Distortion of Graphite as a Function of Axial Position on the Reactor Core Centerline as a Function of Time

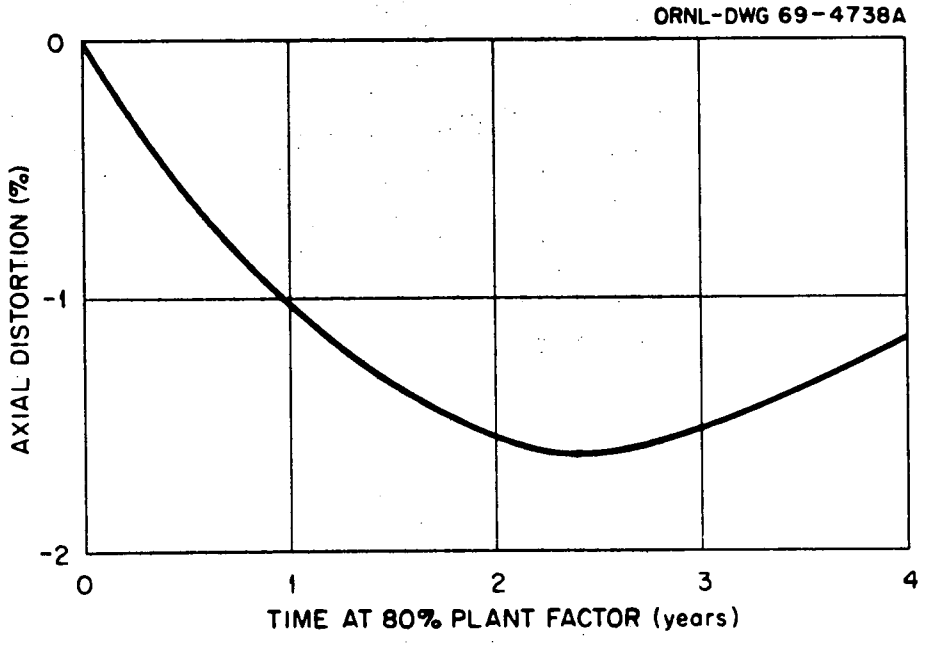

Fig. 6.32 Axially-Induced Distortion of Graphite on Reactor Core Centerline as a Function of Time

6.4.1 Radiation Damage (Cont'd)

b - Stresses Generated in Graphite During Irradiation (Cont'd)

In the above equations ϵ_x and σ_y denote, respectively, the strain and stress in the x direction, μ is Poisson's ratio, E is Young's modulus, ϵ_o and A_o are constants, a is the coefficient of thermal expansion, T is the temperature distribution, ψ is the neutron-induced dimensional change, D is the neutron dose, and $K(T)$ is the creep coefficient from the uniaxial creep test.

If the creep coefficient $K(T)$ is assumed to be a constant, independent of temperature, and the temperature-dependent neutron-induced dimensional change is given by:

$$\psi(D,T) = A_2(T)D^2 + A_1(T)D,$$

then the stress, and therefore the strain, of the two-dimensional problem of arbitrary shape can be expressed as a linear combination of several fictitious elastic solutions with the same cross section. From this result the problem of an arbitrary shape can be solved, provided that solutions of the elastic problems are available.

To apply the method to the preliminary design calculation, numerical results were obtained for the core graphite, which was assumed to be in the form of long cylindrical tubes. Then the design lifetimes of the cylinders were evaluated based on two criteria, one by volumetric distortion and the other by axial strain. The specific problems solved were concentric circular cylinders with inner radius a, outer radius b, length L, and b/a = 6.667. Several values of b ranging from 4

b - Stresses Generated in Graphite During Irradiation (Cont'd)

to 6 cm were used to illustrate the geometric influence.

The material parameters used were:

Young's modulus $E = 1.9 \times 10^6$ psi,

Poisson's ratio $\mu = 0.27$

coefficient of thermal expansion $\alpha = 6.20 \times 10^{-6}\ ^\circ C^{-1}$,

constant $A_o = 2.0 \times 10^{-22}$ neutron^{-1} cm^2,

creep coefficient $K(T) = (5.3 - 1.45 \times 10^{-2} T + 1.4 \times 10^{-5} T^2)\ 10^{-27}\ (\text{psi}\ nvt)^{-1}$,

where T is chosen at the inner radius a, and neutron-induced dimensional change is given by

$$\psi(D,T) = A(T)\,[10^{-22} D)^2 + B(T)\,(10^{-22} D)],$$

where

$$A(T) = \frac{1}{3}\,(0.11 - 7.0 \times 10^{-5} T)/(5.7 - 6.0 \times 10^{-3} T)^2 \text{ per } (10^{22}\ nvt)^{-3}$$

and

$$B(T) = 2 \times (6.0 \times 10^{-3} T - 5.7).$$

In all of the above equations the unit of T was the degree centigrade.

Parameters related to the reactor were:

salt temperature $T_{salt} = 625 - 75 \cos(\pi \frac{Z}{L})\ ^\circ C$,

thermal conductivity of the graphite K_a

$$= 0.358 \left[\frac{T(^\circ K)}{773}\right]^{-0.7} \text{ watts cm}^{-1}\ ^\circ C^{-1}$$

where T at $n = a$ was used,

6.4.1 Radiation Damage (Cont'd)

b - Stresses Generated in Graphite During Irradiation (Cont'd)

heat transfer coefficient $H = a^{-0.2}[1.444 \times 10^{-3} T(°C) - 0.228]$ watts $cm^{-2} °C^{-1}$,

flux θ ($E > 50$ kev) $= 4.5 \times 10^{14} \sin(\pi \frac{Z}{L})$ nvt, and

gamma heating $Q = 1.2 + 9.0 \sin(\pi \frac{Z}{L})$ watts/cm^3

The numerical results are shown in several figures. Figure 6.33 shows a typical temperature distribution at Z/L = 0.6, a crucial section as can be seen from the lifetime curves in the subsequent figures. At this same cross section, the circumferential strain at r = b as a function of neutron dose increases rapidly after $D = 1 \times 10^{22}$ nvt, as shown in Fig. 6.34. The increase of the axial stress σ_z as D increases is seen to approach a straight line for $D > 10^{22}$ nvt in Figure 6.35. In fact, this linear dependence of σ_z on D at high fluence has shown analytically in Reference 2 as a property valid for all stress components. Therefore, above $D > 10^{22}$ nvt, the stress components can be calculated easily if their values at $D = 10^{22}$ nvt are known.

As the definition of graphite life, it has normally been assumed the material will generate macroscopic cracks after it begins to significantly expand beyond its original dimensions. We may define two ad hoc lifetimes, first the fluence at which the material returns to its original volume and second, the fluence at which its axial strain returns to zero. The resulting lifetimes as a function of axial position in the core are shown in Figures 6.36 and 6.37. It is seen the critical

6.411 Radiation Damage (Cont'd)

b - Stresses Generated In Graphite During Irradiation (Cont'd)

section occurs at Z/L = 0.57, approximately, and that the axial strain criterion to define lifetime is slightly more severe.

As mentioned previously, the creep coefficient K(T) was assumed to be constant in this analysis. More realistically, the above method is being generalized to account for a temperature-sensitive K(T). The analytical analysis has been completed, and numerical results are being computed.

6.4.2 Molten-Salt Compatibility

All of the graphite parts in an MSBR reactor will be directly in contact with the molten fuel salt throughout their lifetime in the reactor. All of the graphite parts will, therefore, have to prevent intrusion of the salt at the operating temperatures and pressures of the reactor.

This problem was recognized early in the MSR program and was studied extensively at ORNL prior to the construction of MSRE[25] as is reported by ORNL as follows: a test program was conducted to study the permeation of various potential grades of graphite by molten salt (BULT 14-.5U) at 1300°F and for various times and pressures.

Thirty-one grades of graphite were tested under the conditions described above. Results of the screening tests are summarized in Table 6.7. There were four grades, B-1, S-4-LB, GT-123-82, and CS-112-S, that met

25 ORNL-2973 MSR Quarterly Report for Jan. 31 and April 30, 1960, pp. 53-58.

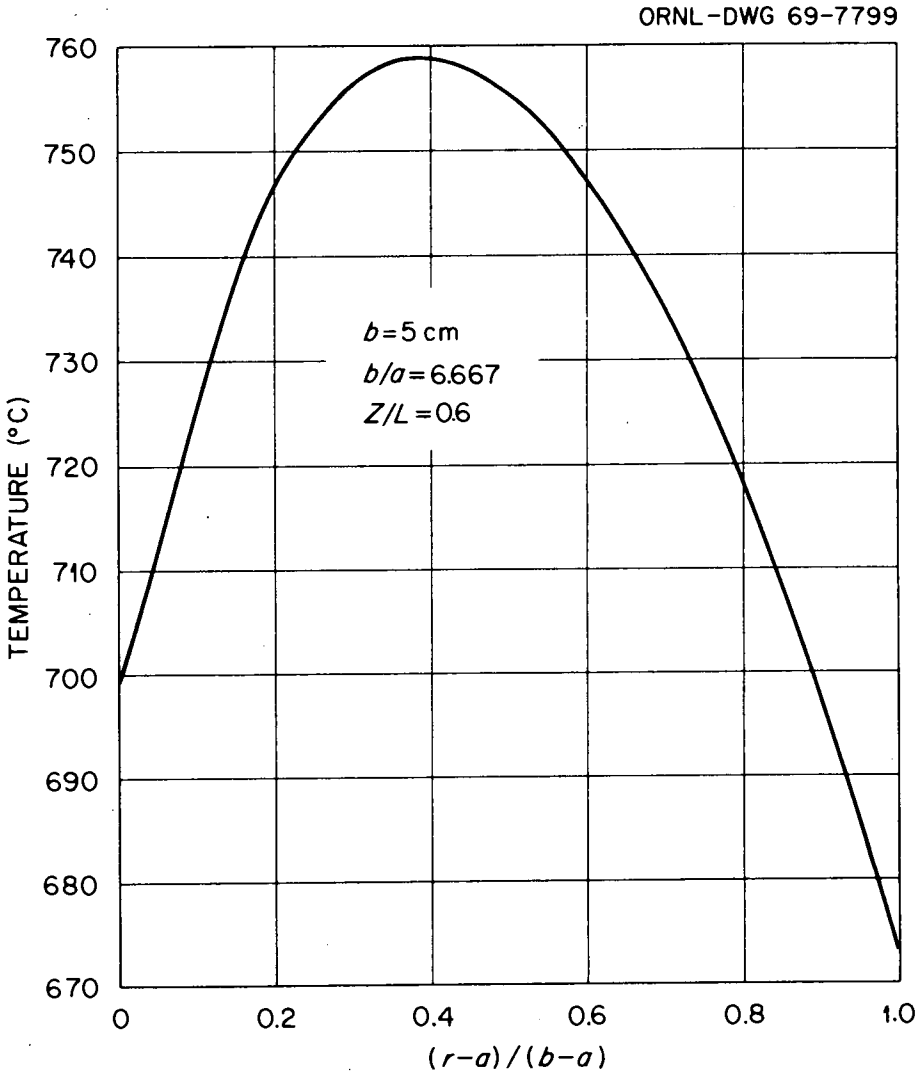

Fig. 6.33 Radial Temperature Profile at the Axial Position Z/L = 0.60

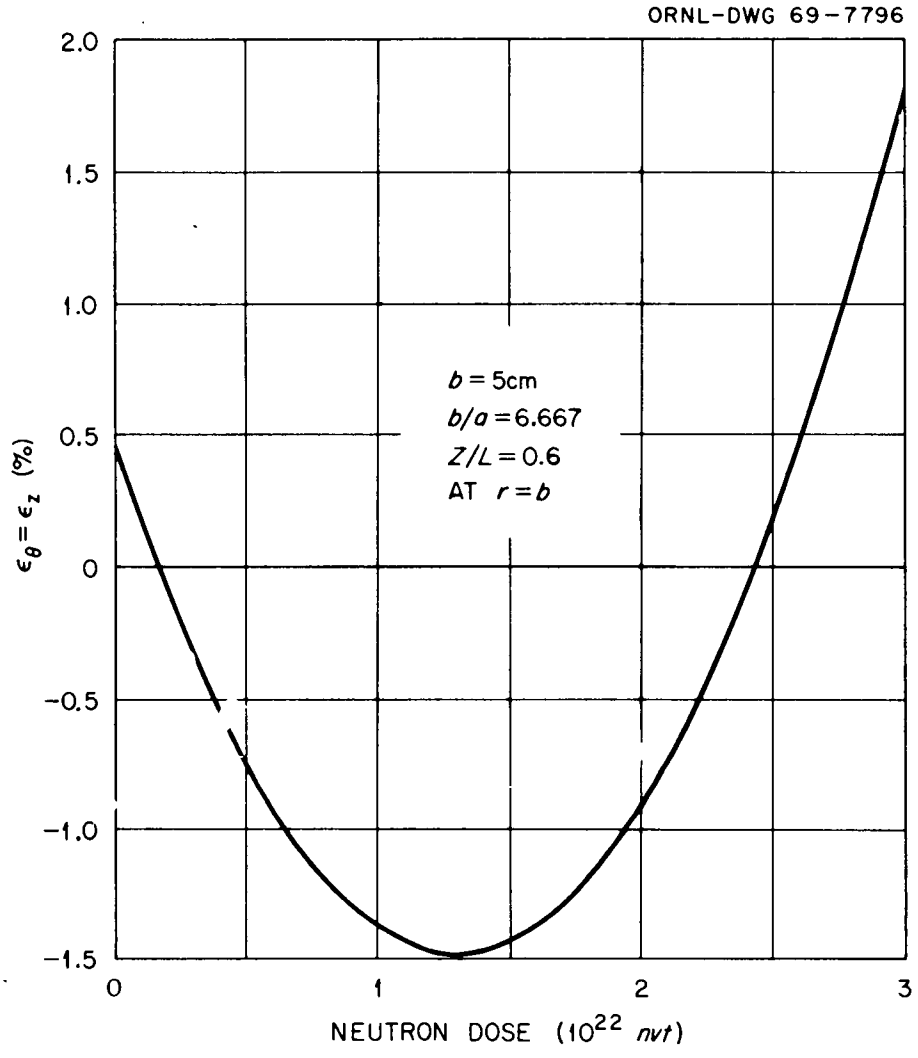

Fig. 6.34 Circumferential Strain at Outside Surface as a Function of Fluence Level at Z/L = 0.60

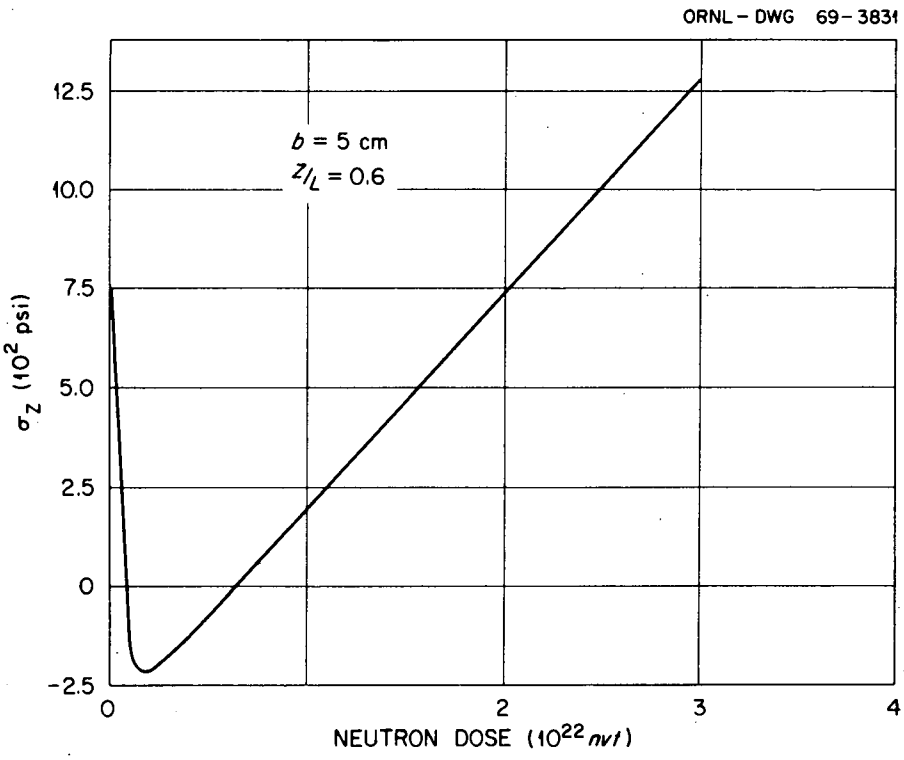

Fig. 6.35 Axial Stress at the Outer Surface as a Function of Fluence Level at Z/L = 0.60

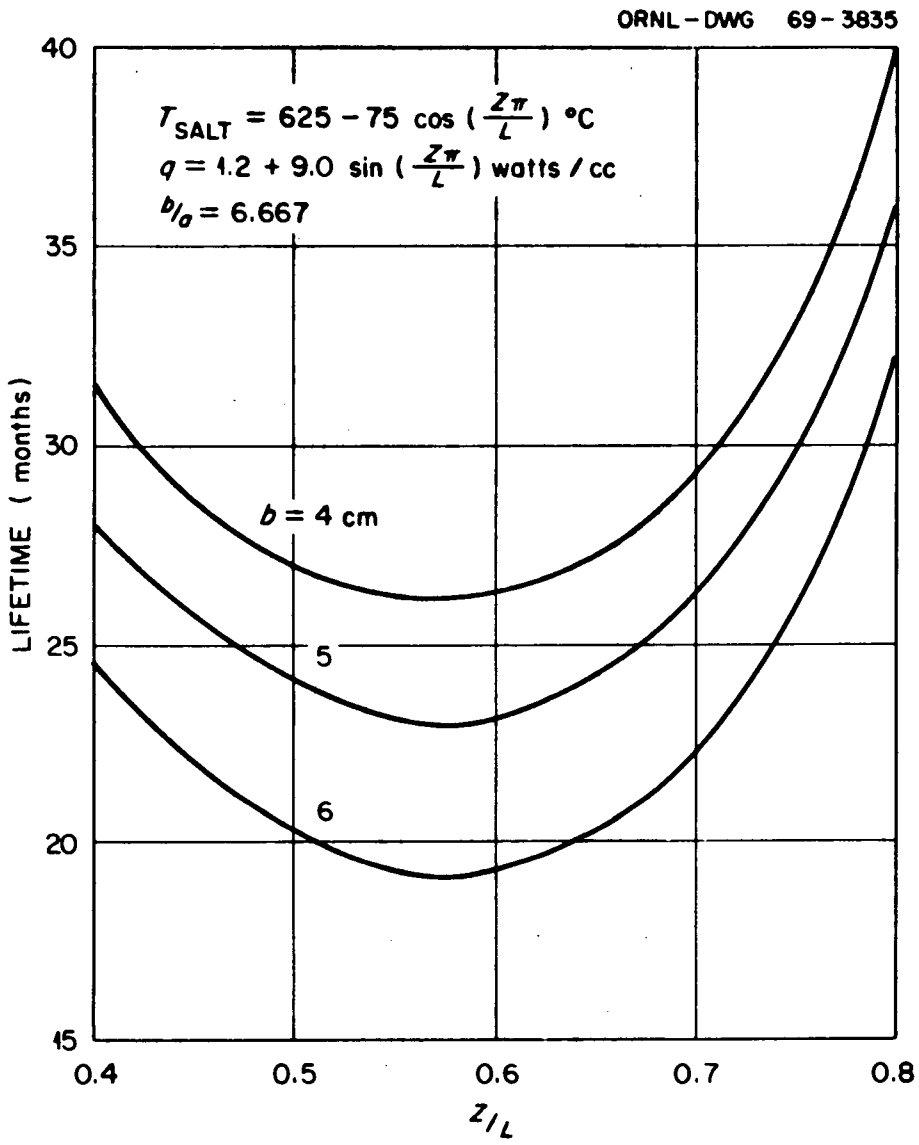

Fig. 6.36 Lifetime of MSBR Graphite Core Cylinders as a Function of Axial Position According to the Volumetric Distortion Criterion

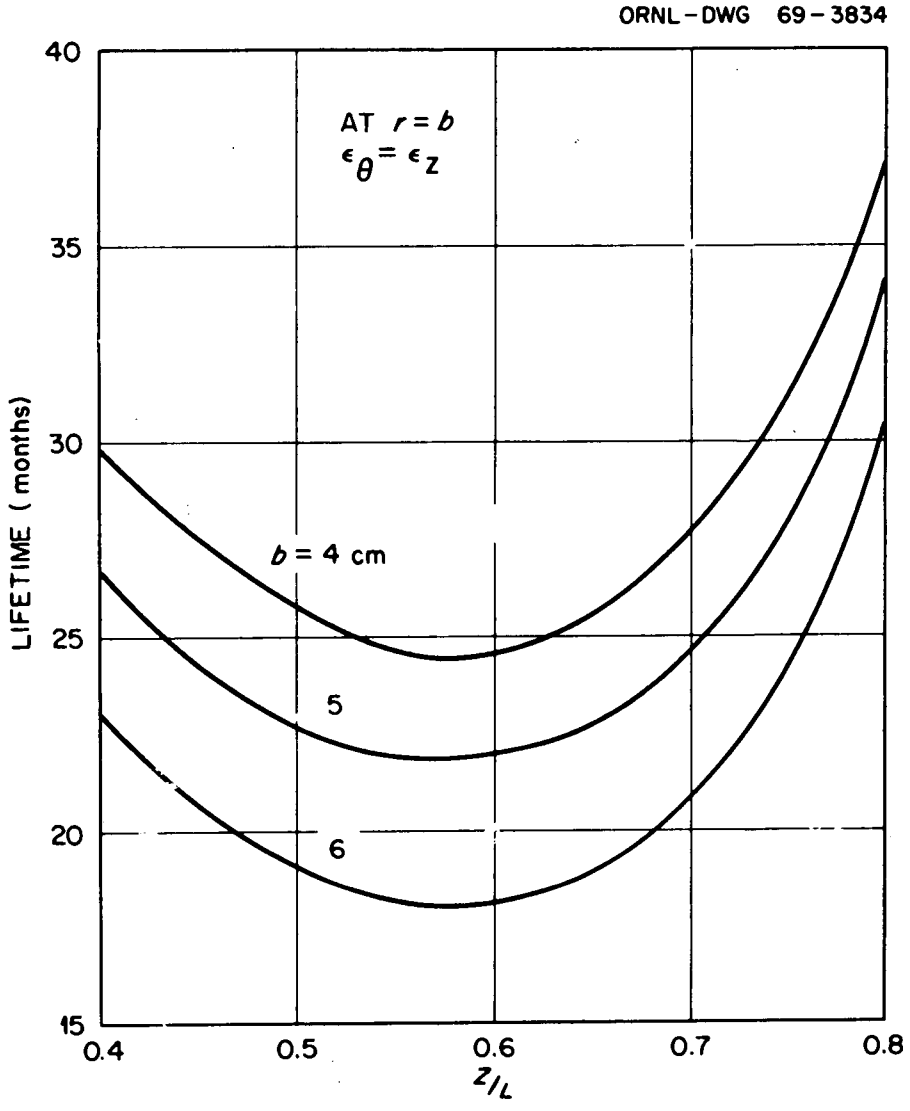

Fig. 6.37 Lifetime of MSBR Graphite Core Cylinders as a Function of Axial Position According to the Axial Strain Criterion

Table 6.7*

Permeation of Various Grades of Graphite
by $LiF-BeF_2-ThF_4-UF_4$
(67-18.5-14-0.5 Mole %, BULT 14-.5U) at 150 Psig

Test Conditions:

Temperature: 1300°F (704 C)
Exposure Period: 100 Hr

All densities and percentages are averages of three with the exception of those with numerical superscripts, which denote the number of values averaged.

Graphite Grade	Graphite Apparent Density (g/cc)	Bulk Volume of Graphite Permeated (%)	Shape	Specimen Dimensions, Nominal (in.) Diameter or OD	ID	Length(s)
B-1	1.91	0.0	Rod	0.90[a]		0.50
S-4-LB	1.90[(4)]	0.2[(4)]	Block	0.50		0.75
GT-123-82[b]	1.91[(6)]	0.3[(6)]	Rod	0.50[a]		1.50
CS-112-S	1.89[(4)]	0.5[(4)]	Rod	0.90[a]		0.50
RH-1	1.89[(6)]	0.6	Rod	0.90[a]		0.50
CEY-1350	1.90	0.7	Pipe	1.24[a]	0.86[a]	0.25
CEY-G	1.88	0.9	Pipe	1.25[a]	0.86[a]	0.50
S-4-LA	1.89[(4)]	1.0[(4)]	Block	0.50		0.75
CEY	1.91[(6)]	1.0[(6)]	Pipe	1.24[a]	0.85[a]	0.50, 0.25
CT-150	1.80	1.8	Pipe	0.53[a]	0.26[a]	1.50
R-0009[b]	1.92[(6)]	1.9[(6)]	Block	0.50		1.50
CEY-82[b]	1.87	1.9	Pipe	1.25[a]	0.86[a]	0.50
R-4[b]	1.92[(13)]	2.0[(13)]	Block	0.50		1.50
R-0009 RG[b]	1.90[(6)]	2.6[(6)]	Block	0.50		1.50
CT-158[b]	1.76[(4)]	3.6[(4)]	Pipe	0.40[a]	0.19[a]	1.50
186[b]	1.86[(6)]	3.8[(6)]	Bar	0.50		1.50
CCN[b]	1.92	4.2	Block	0.50		1.50
CEY-B[b]	1.79	4.3	Pipe	1.25[a]	0.86[a]	0.50

* ORNL-2973. MSR Quarterly Report for January 31 and April 30, 1960, pp. 53-58.

Table 6.7* (Cont'd)

Graphite Grade	Graphite Apparent Density (g/cc)	Bulk Volume of Graphite Permeated (%)	Shape	Specimen Dimensions, Nominal (in.)		
				Diameter or OD	ID	Length(s)
S-4[b]	1.85	4.8	Block	0.50		1.50
R-0025[c]	1.87(24)	5.7(24)	Block	0.50		1.50, 0.50
RLM-24[d]	1.83(6)	5.7(13)	Pipe	0.50		1.50, 0.50
ATJ-82 RG[b]	1.83	6.4	Block	0.50		1.50
R-0013[b]	1.87(6)	6.6(6)	Block	0.50		1.50
MH4LM-82	1.81(24)	8.2(24)	Block	0.50		1.50, 0.50
CS-82 RG[b]	1.80	8.1	Block	0.50		1.50
GT-123	1.79	8.9	Rod	0.50		1.50
ATL-82	1.80	10.8	Block	0.50		1.50
MH4LM	1.76	11.4	Block	0.50		1.50
SM-1	1.72	13.9	Block	0.50		1.50
AGOT[b]	1.68(17)	13.9(17)	Bar	0.50		1.50, 0.50
TSF[b]	1.67	14.4	Bar	0.50		1.50

[a]These are the original dimensions of the graphite as manufactured.

[b]These were previously reported in MSR Quar. Prog. Oct. 31, 1959, ORNL-2890, p 44.

[c]Specimens for R-0025 were taken from a piece 39 in. in diameter and 11 in. long.

[d]Specimens for RLM-24 were taken from the walls of a 5-in.-OD, 3-5/8-in.-ID, 26 in. long pipe.

6.4.2 Molten-Salt Compatibility (Cont'd)

the permeation specification, under the screening-test conditions, that less than 0.5 percent of the bulk volume of graphite be filled with salts. These results were from specimens taken from single pieces of graphite that were relatively small.

In an attempt to determine the effect of pressure on permeation, 20 grades of graphite that were available at the time this test was assembled were screened at a lower pressure. Three or more specimens of each of the 20 grades were exposed simultaneously for 100 hr to $LiF-BeF_2-ThF_4-UF_4$ (67-18.5-14-0.5 mole %, BULT 14-.5U) at 1300°F (704 C) and 95 psig, a potential reactor fluoride-salt pressure. The results of this test are compared in Table 6.8 with those obtained from previous tests in which the pressure was 150 psig. This test suggests that if the reactor pressure were 95 psig, four additional grades, CT-150, CEY-1350, CT-158, and CEY-G, might be brought within the MSRP specification.

The grades of graphite that showed the greatest reductions in quantity of salt permeation as a result of the lower pressure have the highest percentage of small pores comprising their total accessible voids.

Following this work, grade CGB graphite was developed for the molten-salt reactor experiment. McCoy and Weir[26/] described CGB graphite development for MSRE as follows:

> "Grade CGB graphite was designed for use in molten-salt reactors and was first made in commercial quantities for the MSRE. It is

26/ ORNL-TM-1854 Materials Development for Molten-Salt Breeder Reactors.

Table 6.8

Permeation of Various Grades of Graphite by $LiF-BeF_2-ThF_4-UF_4$ (67-18.5-14-0.5 mole %)

Test conditions:
Temperature: 1300°F (704 C)
Exposure Period: 100 hr

Graphite Grade	Bulk Volume of Graphite Permeated (%)[a] At 95 psig	At 150 psig[b]	P95:P150[c]
CT-158	0.04	3.6	0.0_1
CT-150	0.3	1.8	0.2
CEY-1350	0.2	0.7	0.3
CEY-G	0.3	0.9	0.3
CEY-82	1.0	1.9	0.5
CS-82 RG	5.3	8.1	0.6
CEY-B	3.0	4.3	0.7
GT-123	6.6	8.9	0.7
GT-123-82	0.2_5	0.3	0.8
MH4LM	8.9	11.4	0.8
R-0013	5.4	6.6	0.8
SM-1	12.2	13.9	0.9
S-4	4.4	4.8	0.9
ATL-82	10.6	10.8	1.0
ATJ-82 RG	6.3	6.4	1.0
R-0009 RG	2.6	2.5	1.0
R-4	2.3	2.2	1.0
186	4.1	3.8	1.1
AGOT	16.1	14.6	1.1
R-0009	2.2	1.8	1.2

[a]Each value is an average of three or more values.

[b]These data have been reported previously; they are included here for comparison purposes.

[c]The ratio of the percent of the bulk volume of the graphite permeated by BULT 14-.5U at 95 psig to that at 150 psig.

basically a petroleum needle-coke that is bonded with coal-tar pitch, extruded to rough shape, and heated to 5072°F. High density and low permeation are achieved through multiple impregnations and heat treatments. All components are fired to 5072°F or higher. The product is essentially a well-graphitized material and is highly anisotropic. Its properties are tabulated in Table 6.9.

"Grade CGB graphite represents significant progress in development of a low-permeability radiation-resistant graphite. Experiments have demonstrated that the multiple impregnations required to obtain the low permeability and small open-pore size do not appreciably alter the dimensional stability compared to conventional needle-coke graphites.

"In manufacturing the material for the MSRE, experimental equipment and processes were used on a commercial scale for the first time by the Carbon Products Division of Union Carbide Corporation to produce bars 2.50 in. square and 72 in. long which were machined to the shapes required for the MSRE.

Structure

"The MSRE graphite has an accessible void space of only 4.0 percent of its bulk volume. The pore entrance diameters to the accessible voids are small; over 95 percent of the entrances are 0.4 μ in diameter[27/]. The molten salts do not

27/ W. H. Cook, MSRP Semiann. Progr. Rept. July 31, 1964, ORNL-3708, p. 377

Table 6.9*

Properties of MSRE Core Graphite, Grade CGB

Physical properties	
Bulk density,[a] g/cm^3	
Range	1.82-1.89
Average	1.86
Porosity,[b] %	
Accessible	4.0
Inaccessible	13.7
Total	17.7
Thermal conductivity,[a] Btu ft^{-1} hr^{-1} $(^oF)^{-1}$	
With grain	
At 90°F	112
At 1200°F	
Normal to grain	
At 90°F	63
At 1200°F	34
Temperature coefficient of expansion,[c] $(^oF)^{-1}$	
With grain	
At 68°F	0.27×10^{-6}
Normal to grain	
At 68°F	1.6×10^{-6}
Specific heat,[d] Btu lb^{-1} $(^oF)^{-1}$	
At 0°F	0.14
At 200°F	0.22
At 600°F	0.33
At 1000°F	0.39
At 1200°F	0.42
Matrix coefficient of permeability[e] to helium	
At 70°F, cm^2/sec	3×10^{-4}
Salt absorption at 150 psig,[a] vol %	0.20
Mechanical strength[b] at 68°F	
Tensile strength, psi	
With grain	
Range	1500-6200
Average	1900
Normal to grain	
Range	1100-4500
Average	1400
Flexural strength, psi	
With grain	
Range	3000-5000
Average	4300

* ORNL-TM-1854. Materials Development for Molten-Salt Breeder Reactors, H.E McCoy, Jr, and J R Wein, Jr

Table 6.9 (Cont'd)

Mechanical strength[b] at 68°F	
Flexural strength, psi	
Normal to grain	
Range	2200-3650
Average	3400
Modulus of elasticity, psi	
With grain	3.2×10^6
Normal to grain	1.0×10^6
Compressive strength, [d]psi	8600
Chemical purity[f]	
Ash, wt %	0.0041
Boron, wt %	0.00009
Vanadium, wt %	0.0005
Sulfur, wt %	0.0013
Oxygen, cm^3 of CO per 100 cm^3 of graphite	9.0
Irradiation data[a]	
[Exposure: 1.0×10^{20} neutrons/cm^2, (E > 2.9 Mev)	
Shrinkage, % (350-475 C)]	
A_o	0.10
C_o	0.07

a Measurements made by ORNL.

b Based on measurements made by the Carbon Products Division and ORNL.

c Measurements made by the Carbon Products Division.

d Representative data from the Carbon Products Division.

e Based on measurements made by the Carbon Products Division on pilot-production MSRE graphite.

f Data from the Carbon Products Division.

6.4.2 Molten-Salt Compatibility (Cont'd)

wet the graphite, and calculations indicate that pressures in excess of 300 psig would be required to force salt into these accessible voids. The microstructures of a conventional nuclear graphite and the graphite in the MSRE are compared in Figure 6.38."

With the successful operation of MSRE for 2½ years with grade CGB graphite in the reactor the compatibility of graphite with the molten salt is essentially proven. The question remaining to be answered is will any unforeseen problems develop with the higher power densities, and longer times of exposure in MSBR's.

6.4.3 Fission Product Retention

a - ^{135}Xe Poisoning

The large volume of graphite in the reactor and the large ratio of graphite to salt provide a large total potential "sink" for gases even at an available open pore volume of less than 10 percent in the graphite. The problem of keeping the gaseous fission products from entering the graphite is directly related to the breeding ratio of the reactor because of the extremely high capture cross section of ^{135}Xe and the neutron losses that occur if it is allowed to remain in the high flux region of the core. Because of the relatively high xenon partial pressure at very low concentration, it will tend to leave the salt through any free surface available before the concentration becomes high enough to make a significant contribution to the ^{135}Xe poisoning. The problem, therefore, is to quickly and effectively strip the ^{135}Xe from the system by a helium gas sparge, or salt spray into helium; or by effectively sealing all the pore entrances of the

6.4.3 Fission Product Retention (Cont'd)

a - ^{135}Xe Poisoning (Cont'd)

graphite; or by a combination of both methods. A sealed surface will act as an effective barrier to the transfer of xenon into the graphite interior if the value of the diffusivity of the sealed surface can be reduced to $\sim .25 \times 10^{-8}$ cm^2/sec, and the associated void volume is 1 percent.

Considerable attention has been given to the development of very low permeability graphite during the last 15 years. Current state of technology can provide bulk graphite in the size range needed for MSBR reactor cores with permeability of 1×10^{-4} cm^2/sec (such as CGB used in MSRE) and perhaps as low as 1×10^{-5} cm^2/sec. Experience has indicated that serious spalling and microcracking prevents production of large pieces, or good yields of small pieces at lower levels of permeability such as the level of 1×10^{-8} cm^2/sec desired for the MSBR.

The major effort to produce graphite with a surface sealed to 1×10^{8} cm^2/sec for the MSBR has been conducted at ORNL. After consideration of the various alternatives such as liquid impregnation and thin metallic coatings, pyrolytic carbon coatings and infiltrations were selected as most promising. Beatty developed a technique by which graphite can be sealed with pyrolytic carbon to the desired levels[28/]. In an experiment at ORNL[29/], specimens of two different base stock graphites were gas impregnated by the referenced vacuum pulse technique

28/ ORNL-4254 MSR Semi-Annual. Feb. 29, 1968, p.191
29/ ORNL-4548 MSR Semi-Annual. Feb. 28, 1970, p.209

6.4.3 Fission Product Retention (Cont'd)

a - ^{135}Xe Poisoning (Cont'd)

to helium permeabilities ranging from 3.5×10^{-7} to 2×10^{-9} cm^2/sec and were then subjected to irradiation to fast neutron fluences ranging from 5.2 to 13.9×10^{21} neutrons/cm^2 at 715 C in HFIR. The first measurements taken after irradiation were the helium permeabilities. Results were found to range from 4.27×10^{-8} to as great as 10^{-4} cm^2/sec. Helium permeability of the specimens as a function of fluence is plotted in Fig. 6.39. The gas-impregnated H337 graphite had an appreciable change in helium permeability at about 8×10^{21} neutrons/cm^2, while drastic change in the gas-impregnated Poco graphite appeared to occur at about 1.0×10^{22} neutrons/cm^2. Helium permeabilities of the specimen appeared to be leveling off at about 10^{-5} cm^2/sec after irradiation to the higher fluences. No variable other than fluence appeared to exert any appreciable influence on the postirradiation helium permeability values.

Superficially the increases in helium permeability observed in this experiment are somewhat disappointing. However, let us consider how the helium permeability was obtained. The equations used to calculate the helium permeability and the sample geometry are shown in Figure 6.40. We used the entire wall thickness of the specimen to calculate the permeability. If we assumed that the permeability was controlled by a surface layer of perhaps 0.004 to 0.04 cm, then the calculated values for helium permeability of that layer would decrease by one or two orders of magnitude below the values plotted in Figure 6.39. Our preirradiation values for helium permeability would

ORNL-TM-1854, "Materials Development for Molten-Salt Breeder Reactors", H. E. McCoy and J. R. Weir, Jr., p. 50

PHOTO 67670

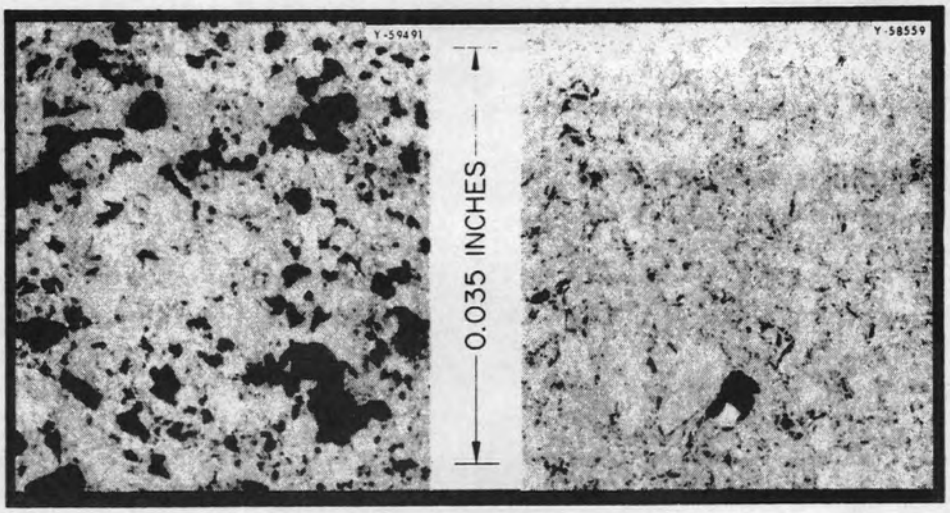

AGOT	CGB
1.68 g/cm^3	1.86 g/cm^3
21.7 % ACCESSIBLE VOID VOL.	4.0 % ACCESSIBLE VOID VOL.
3.7 % INACCESSIBLE VOID VOL.	14.0 % INACCESSIBLE VOID VOL.
25.4 % TOTAL VOID VOL.	18.0 % TOTAL VOID VOL.

Fig. 6.38 The Microstructures of a Conventional Nuclear Graphite Grade AGOT, and of the MSRE Graphite, Grade CGB

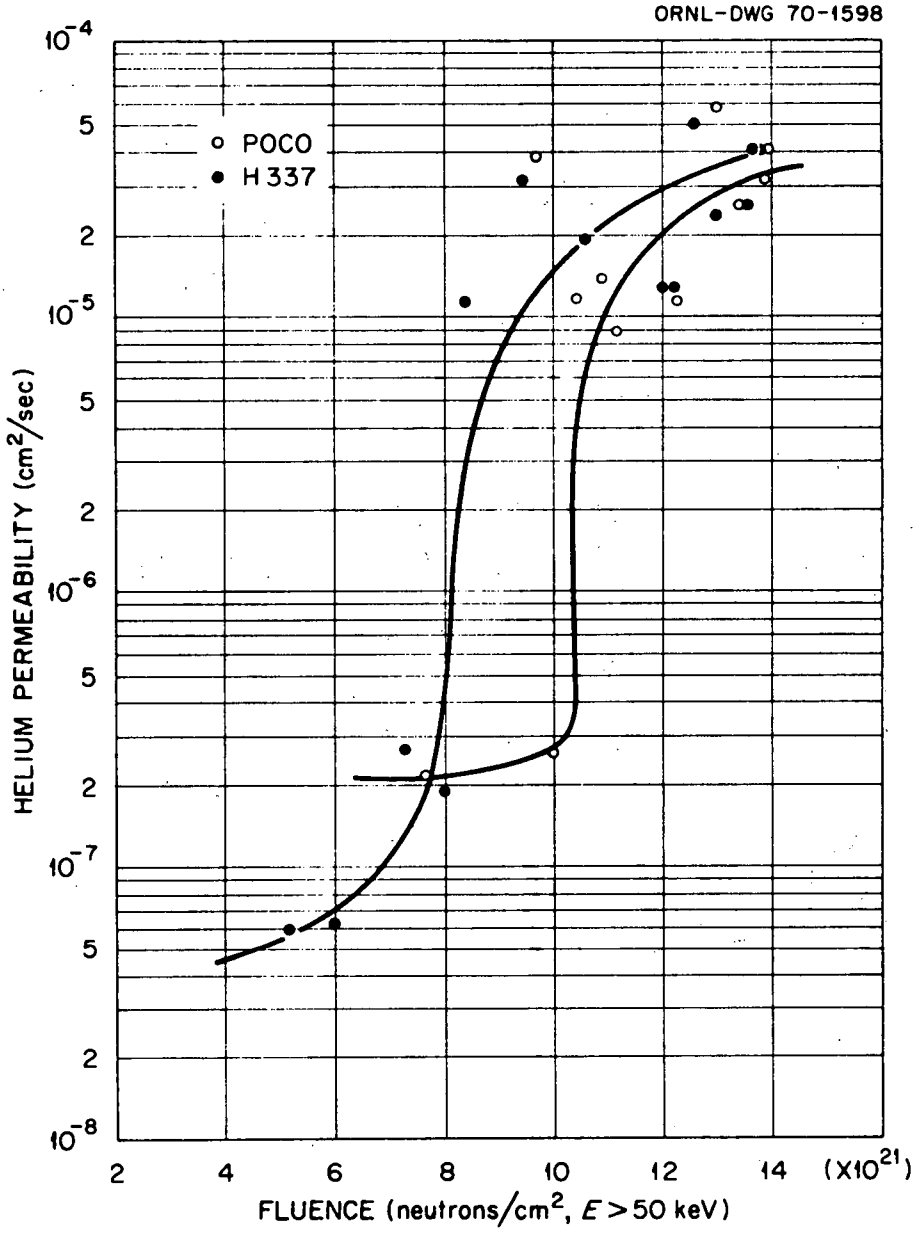

Fig. 6.39 Changes in Helium Permeability with Neutron Irradiation at 715°C. Samples were sealed by gas impregnation with butadiene

ORNL-DWG 70-2274R

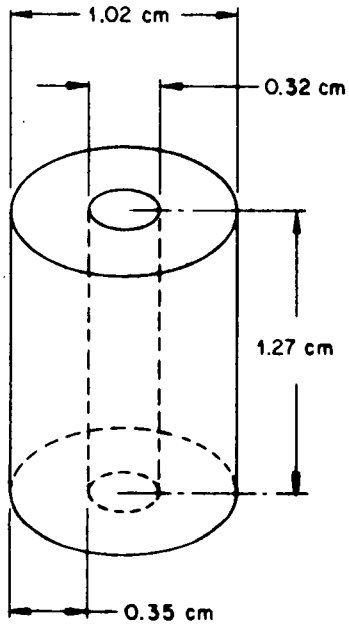

$$P_{He} = \frac{\text{LEAK RATE}}{K}$$

$$K = \frac{\text{SURFACE AREA AT THE MIDSECTION OF SAMPLE}}{\text{THICKNESS OF SAMPLE}}$$

$$P_{He} = \frac{cm^3/sec}{cm^2/cm} = cm^2/sec$$

SURFACE AREA = 2.67 cm^2

THICKNESS = 0.348 cm

K = 7.67 cm

Fig. 6.40 Sample Geometry and Equations Used to Compute the Gas Permeability

ORNL-TM-1853, "Chemical Research and Development for Molten-Salt Breeder Reactors", W. R. Grimes, p. 75

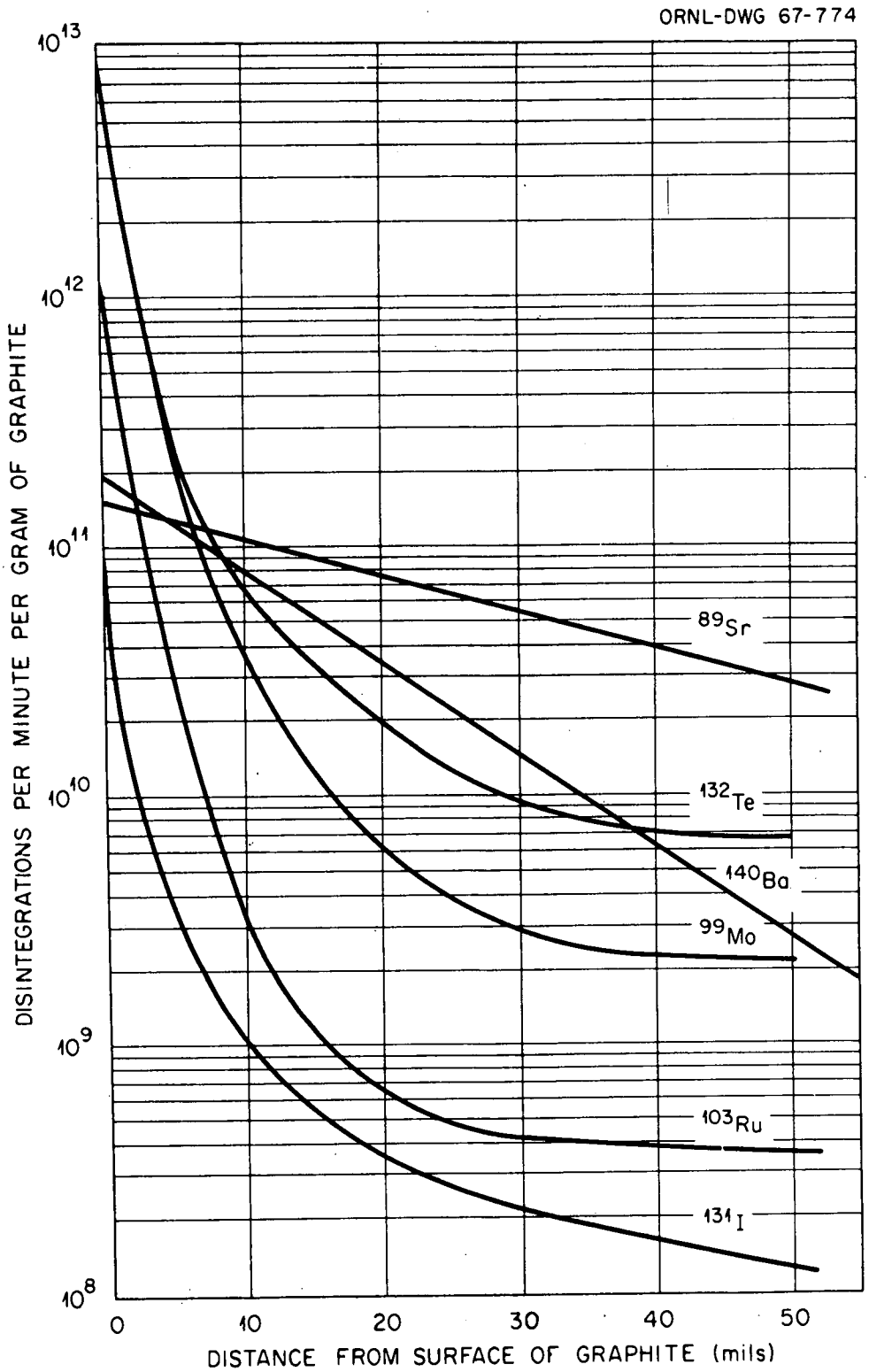

Fig. 6.41 Concentration Profile of Fission Products in MSRE Core Graphite After 8000 MWh

6.4.3 Fission Product Retention (Cont'd)

a - ^{135}Xe Poisoning (Cont'd)

decrease to less than 10^{-9} cm^2/sec, and the post-irradiation values would be less than 10^{-7} cm^2/sec, or very close to the desired levels. Previous radiographic studies of sealed samples indicated that the highest density of deposited carbon is very near the surface. Thus there is strong justification for using the smaller values for the thickness t.

Studies of pyrolytic carbon sealing of graphite are continuing at ORNL and the most recent information is somewhat more encouraging[30/]. Graphite samples coated with pyrolytic carbon derived from propylene were irradiated in HFIR to a total fluence of 1.6 x 10^{22} neutrons/cm^2. These samples irradiated to about half the total lifetime radiation level only increased about one order of magnitude in permeability (from $\sim 10^{-8}$ to $\sim 10^{-7}$ cm^2/sec.

b - Other Fission Product Deposition

Assemblies of surveillance specimens of graphite were exposed as the central stringer within the MSRE core during operation with ^{235}U fuel[31/]. Their removal at reactor shutdowns permitted study of fission product depositions after 8000, 20,000, and 70,000 MWh of operation.

Deposition on the graphite specimens was established as a function of depth of penetration. This was accomplished by careful milling of successive thin

30/ Reported by Eatherly in Semi-Annual MSR Information Meeting - Oct. 1970.

31/ Molten-Salt Reactor Chemistry, W. R. Grimes, Nuclear Applications & Technology, Vol. 8, Feb. 8, 1970, pp. 147-149.

6.4.3 Fission Product Retention (Cont'd)

b - Other Fission Product Deposition (Cont'd)

layers from each surface of the rectangular specimens. The removed layers were separately recovered and analyzed for several fission product isotopes.

The fission gases Kr and Xe form no compounds under conditions existing in a molten-salt reactor, and these elements are only very sparingly soluble in the molten fluoride. The helium purge gas introduced into the MSRE pump bowl serves to strip these gases from the incoming salt to charcoal filled traps downstream in the exit gas system. This stripping ensures that the fission product daughters of these gases will appear within the reactor system at lower than the theoretical concentration. The MSRE graphite is, of course, permeable to Kr and Xe; radioactive daughters of these gases are, accordingly, expected in the graphite specimens.

The fission products Rb, Cs, Sr, Ba, the lanthanides and yttrium, and Zr all form quite stable and well-known fluorides which are soluble in MSRE fuel. These fission products were expected (except to the extent that volatile precursor Kr and Xe had escaped) to be found almost completely in the molten fuel. These expectations have been confirmed. Isotopes such as ^{95}Zr, ^{91}Sr, and ^{143}Ce which have no precursors of consequence are typically found in the salt at 90^{+} percent of the calculated quantity. Isotopes such as ^{89}Sr and ^{140}Ba whose Kr and Xe precursors have appreciable half-lives are found in less than the calculated quantity: these isotopes are, as expected, found in the graphite specimens and the gas samples as well.

6.4.3 Fission Product Retention (Cont'd)

b - Other Fission Product Deposition (Cont'd)

The elements (molybdenum, niobium, ruthenium, and tellurium) whose higher valence fluorides are volatile and relatively unstable toward reduction by UF_3 are virtually absent from the salt. Typical analyses of samples (which have been carefully protected from the pump bowl gas by use of the evacuated bulb samples) show $<$ 2 percent of the calculated concentration of these isotopes.

Deposition of fission products on the ~ 7- to 10-mil outer layers of graphite specimens exposed for 8000 MWh in MSRE is shown in Table 6.10a. It is clear that, with the assumption of uniform deposition in or on the moderator graphite, appreciable fractions of Mo, Te, and Ru and a larger fraction of the Nb are associated with the graphite. Subsequent examinations of graphite after 22,000 and 70,000 MWh have shown somewhat smaller fractions deposited for all these isotopes. The data of Table 6.10 described below show values more typical of the longer exposures.

A careful determination of uranium in or on the graphite specimens led to values $< 1\,\mu g/cm^2$. This quantity of uranium - equivalent to a few grams in the moderator stack - seems completely negligible.

Figure 6.41 shows the change in concentration of the fission product isotopes with depth in the graphite. Those isotopes (such as ^{140}Ba) which penetrated the graphite as noble gases show straight lines on the logarithmic plot; they seem to have remained at the point where the noble gas

Table 6.10a

Fission Product Deposition on Surface[a/] of MSRE Graphite

Isotope	Graphite Location		
	Top Percent of Total[b/]	Top Percent of Total[b/]	Top Percent of Total[b/]
^{99}Mo	13.4	17.2	11.5
^{132}Te	13.8	13.6	12.0
^{103}Ru	11.4	10.3	6.3
^{95}Nb	12	59.2	62.4
^{131}I	0.16	0.33	0.25
^{95}Zr	0.33	0.27	0.15
^{144}Ce	0.052	0.27	0.14
^{89}Sr	3.24	3.30	2.74
^{140}Ba	1.38	1.85	1.14
^{141}Ce	0.19	0.63	0.36
^{137}Cs	0.07	0.25	0.212

a/ Average of values of 7- to 10-mil cuts from each of three exposed graphite faces.

b/ Percent of total in reactor deposited on graphite if each cm^2 of the 2×10^6 cm^2 of moderator had the same concentration as the specimen.

Table 6.10b

Fission Product Distribution for MSRE at End of ^{235}U Operation

Nuclide	Quantity Found (% of Calculated Inventory)				
	In Fuel	On Graphite[a/]	On Hastelloy-N[a/]	In Purge Gas[b/]	Total
^{99}Mo	0.17	9.0	19	50	78
^{132}Te	0.47	5.1	9.5	74	89
^{129}Te	0.40	5.6	11.5	31	48
^{103}Ru	0.033	3.5	2.5	49	55
^{106}Ru	0.10	4.3	3.2	130	138
^{95}Nb	0.001 to 2.2	41	12	11	64
^{95}Zr	94	0.14	0.06	0.43	95
^{89}Sr	83	8.5	0.08	17	109
^{140}Ba	96	1.9	0.05	0.48	98
^{141}Ce		0.33	0.03	0.83	
^{144}Ce		0.92	0.03	2.7	
^{131}I	60	0.11	0.3	19	80

a/ Calculated on assumption that average values for surveillance specimens are representative of all graphite and metal surface in MSRE.

b/ These values are the percentage of production lost assuming mean values found in gas samples apply to the 4-liter/min purge.

6.4.3 Fission Product Retention (Cont'd)

b - Other Fission Product Deposition (Cont'd)

decayed. As expected, the gradient for ^{140}Ba with 16-sec ^{140}Xe precursor is much steeper than that for ^{89}Sr, which has a 3.2-min ^{89}Kr precursor. All the others shown show a much steeper concentration dependence. Generally, the concentration drops a factor of 100 from the top 6 to 10 mils to the second layer. More recent examinations which used cuts as thin as 1 mil show the materials to be concentrated in an extremely thin layer. Typically, 95 percent of the metallic species are within 3 mils of the surface.

Deposition of fission products on or in the graphite is, of course, undesirable since there they serve most efficiently as nuclear poisons. Of the species studied only Nb (whose carbide is stable at MSRE temperatures) seems to prefer the graphite.

It seems likely that in an MSBR the molten fuel will contain virtually all of the zirconium, the lanthanides and yttrium produced, and a large fraction of the iodine, rubidium, cesium, strontium, and barium. These species would, therefore, be available for removal in the processing plant. The salt will contain very little Mo, Nb, Te, Ru, and (presumably) technetium. These will report to the MSBR metal, graphite, and purge gas systems in fractions which are probably not very different from those indicated for MSRE.

Possible Formation of Cesium Carbide in MSBR Graphite

The alkali metals form intersticial carbides with graphite at elevated temperatures, and if sufficient quantities are available, disruptive expansion of

6.4.3 Fission Product Retention (Cont'd)

b - Other Fission Product Deposition (Cont'd)

Possible Formation of Cesium Carbide in MSBR Graphite (Cont'd)

the graphite can result. Consequently, ORNL considered the possibility of formation of cesium carbide from the decay of xenon nuclides in MSBR graphite[32/]. The results were reported by Baes and Evans as follows:

> "Previously, several investigators have considered the neutron poisoning effect caused by diffusion of ^{135}Xe into the graphite moderator of a molten-salt reactor. It is the present purpose to consider as well the effects of the cesium which is born within the graphite by decay of the various fission product xenon nuclides which have diffused there. In particular, it is of interest to estimate whether or not sufficient concentrations of cesium might occur to form (lamellar) cesium carbides, as by:
>
> $$Cs^0(g) + nC(s) \rightleftharpoons CsC_n(s),$$
>
> and whether or not a sufficient amount of CsC_n could be formed to damage the graphite in a full-scale MSBR.
>
> "In an attempt to answer these questions, the partial pressure of cesium within the graphite void spaces was calculated using the following model and assumptions:

32/ ORNL-4037 MSR Semi Annual, Aug. 31, 1966, C. F. Baes, Jr. and R. B. Evans III, pp. 158-162.

6.4.3 Fission Product Retention (Cont'd)

b - Other Fission Product Deposition (Cont'd)

Possible Formation of Cesium Carbide in MSBR Graphite (Cont'd)

1 - Diffusion of gaseous xenon into the graphite void spaces and diffusion of gaseous cesium out of the graphite were approximated as one dimensional; that is, the moderator was represented as a slab of graphite infinite in two dimensions, with a specified thickness (2L), immersed in the fuel salt.

2 - All cesium born in the graphite was assumed to be in the gaseous elemental form. Cesium born in the fuel salt or reaching the fuel salt by diffusion from the graphite was assumed to be oxidized to Cs^+ and to remain in the salt.

3 - Steady-state conditions were assumed.

"The resulting expressions and the parameters employed (which correspond approximately to the present MSBR reference design) are summarized in Table 6.11. The steady-state partial pressure of each cesium nuclide (P_{Cs}) was a function of the depth into the graphite (x), the porosity of the graphite (ϵ), the partial pressure of the parent xenon at the salt-graphite interface (P^0_{Xe}), the diffusion coefficients of cesium and xenon (D, assumed to be the same for both), and the appropriate decay constants (λ) and neutron capture cross sections (σ). The xenon partial pressure at the salt-graphite interface (P^0_{Xe}) was, in turn, a function of several terms: Y corresponds to the xenon production rate; S reflects the xenon loss from the fuel salt by decay, stripping, and burnup; G reflects diffusion of xenon into the graphite; and, finally, F is a factor reflecting the effect of the film

coefficient H at the salt-graphite interface. This film coefficient is defined by the relationship for the flux J_{Xe},

$$J_{Xe} = H(C_{Xe} - C^0_{Xe}),$$

wherein C_{Xe} is the concentration of the nuclide in the bulk of salt and C^0_{Xe} is the concentration in equilibrium with P^0_{Xe} at the interface.) The terms S, F, and G also appear in the ^{135}Xe poison factor, which is the ratio of the ^{135}Xe poison fraction under the conditions specified to the maximum possible poison fraction, approximately 0.005.

"The rather cumbersome expressions in Table 6.11 were evaluated with a computer. The effects of variations in the gas stripping rate (λ_{ST}), the diffusion coefficients (D), and the film coefficient (H) were determined.

"Cesium Carbide Formation. The maximum total pressure of cesium (at the center of the graphite slab) was found to increase as D was decreased (Figure 6.42). This is a paradoxical result since it is usually thought desirable that the graphite possess the lowest possible D values. In the range of D values tested here, however, the rate-controlling step in the diffusion of parent xenon into the graphite appeared to be at the salt-graphite interface (see below) and did not depend significantly upon D.

6.4.3 Fission Product Retention (Cont'd)

b - Other Fission Product Deposition (Cont'd)

Possible Formation of Cesium Carbide in MSBR Graphite (Cont'd)

"As a result, lowering D for xenon and cesium appreciably decreased only the diffusion of cesium out of the graphite, causing the steady-state accumulation of cesium ($\overline{P_{Cs}}$) to be higher.

"Included for comparison in Figure 6.42 is the partial pressure of cesium at which carbide formation might be expected at 600 C, based on an estimate by Manowitz. It appears that in all cases tested the cesium partial pressure in the graphite was high enough to produce carbide formation. As a consequence, it is likely that the actual quantities of cesium which could accumulate within the graphite will be higher than estimated in the present calculations. While no detailed calculation of this effect was attempted, considerable comfort may be found in the following observations.

1 - By the present calculations the amount of cesium accumulation in the graphite is very small; even with a xenon partial pressure as high as 0.01 atm, for example, there would be only 1 atom of cesium present for every 25,000,000 atoms of carbon. At acceptably low ^{135}Xe poisoning levels, the calculated maximum cesium concentration would be approximately 100-fold (10^{-4} atm) lower than this. Thus, although the present estimates of cesium accumulation would probably be increased if carbide formation occurs, an enormous increase (e.g., 10^5-fold) in the accumulation could occur before it would become a matter of concern.

2 - Even if it were assumed that all the cesium born in the graphite were to remain there, the rate of accumulation would be low.

Table 6.11

Analytical Model and Data Used for Estimating Partial Pressure of Cs and Poison Fraction

Parameters[a]		Assigned Values	MSRE Values
ϕ	Average thermal-neutron flux, $cm^{-2}\ sec^{-1}$	7×10^{14}	1.5×10^{13}
C_{25}	^{235}U concentration in fuel, $moles/cm^3$	2×10^{-4}	1.8×10^{-4}
T	Temperature of core, °K	873	873
Q_H	Henry's law distribution coefficient for xenon	6000	6000
V_T/V_c	Ratio of total fuel volume to fuel volume in flux	4.37	4.0
A/V_c	Ratio of graphite area to fuel volume in flux, cm^{-1}	2.0	2.5
L	Half thickness of graphite slab, cm	0.5	2
ϵ	Porosity of graphite	0.05	0.09
λ_{ST}	Fraction of fuel stripped per second, sec^{-1}	0.001–0.1	0.0004–0.002
D	Effective diffusion coefficient for both Xe and Cs, cm^2/sec	10^{-8}–10^{-4}	1.3×10^{-4}
H	Film coefficient at salt-graphite interface, cm/sec	0.002–0.02	0.00045

Partial Pressure of Cs Nuclide in Graphite

$$P_{Cs} = P^0_{Xe}\left[\frac{\epsilon\lambda_{Xe}}{D_{Cs}\,(\beta^2_{Xe} - \beta^2_{Cs})}\right](E_{Cs} - E_{Xe})\begin{cases}\beta_i = \sqrt{\epsilon(\lambda_i + \sigma_i\phi)/D_i} \\ E_i = \left[e^{\beta_i x} + e^{\beta_i(2L-x)}\right] \Big/ \left(e^{2\beta_i L} + 1\right)\end{cases}$$

Partial Pressure of Xe Parent at Salt-Graphite Surface

$$P^0_{Xe} = \frac{Y}{FS + G}$$

^{135}Xe Poison Factor

$$P.F. = \frac{\sigma_{135}\phi}{\sigma_{135}\phi + \lambda_{135}}\left[\frac{\dfrac{(\sigma_{135}\phi + \lambda_{135})}{Q_H} + \dfrac{G}{F}}{S + \dfrac{G}{F}}\right]$$

$$Y = y_{Xe}\sigma_{25}C_{25}\phi RT$$

$$S = \frac{(V_T/V_c)\,(\lambda_{Xe} + \lambda_{ST}) + \sigma_{Xe}\phi}{Q_H}$$

$$F = 1 + \frac{Q_H D_{Xe}\beta_{Xe}}{H}\,\frac{(e^{2\beta_{Xe}L} - 1)}{(e^{2\beta_{Xe}L} + 1)}$$

$$G = \frac{AD_{Xe}\beta_{Xe}}{V_c}\,\frac{(e^{2\beta_{Xe}L} - 1)}{(e^{2\beta_{Xe}L} + 1)}$$

[a] y, σ, and λ denote, as usual, the yield, neutron capture cross section, and decay constant of a given nuclide.

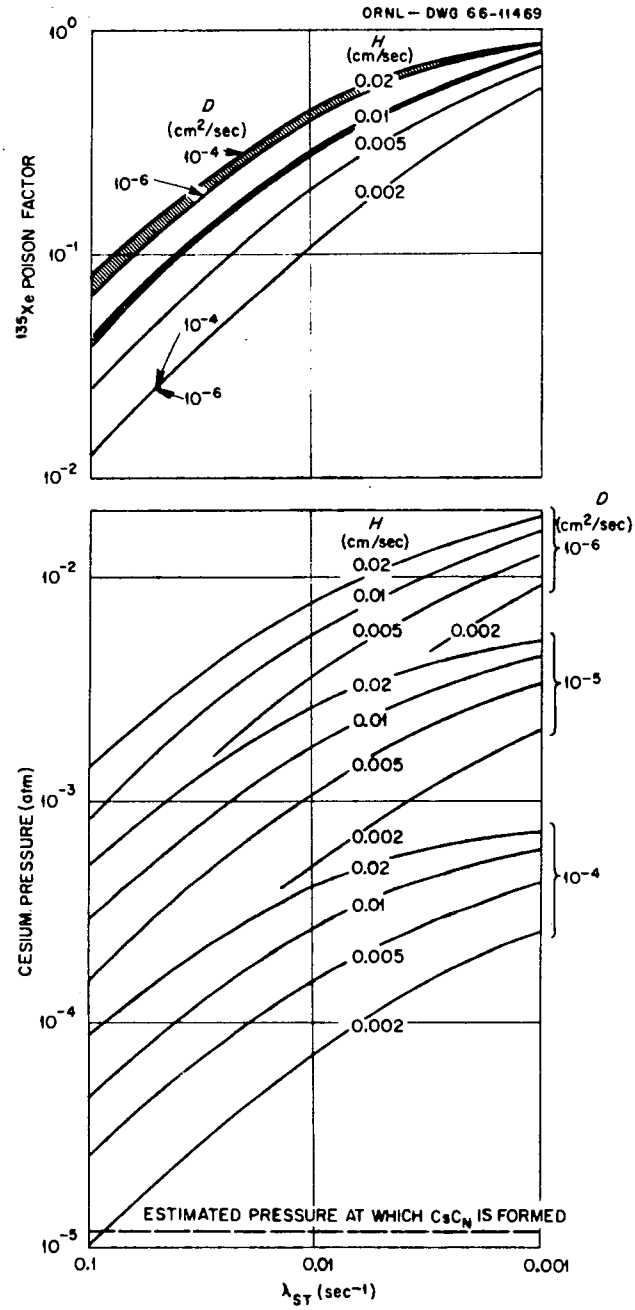

Fig. 6.42 Calculated Steady-State Pressure of Cesium at Center of Graphite Slab as a Function of the Gas Stripping Rate (λ_{ST}), the Diffusion Coefficient (D), and the Film Coefficient (H). Other conditions are specified in Table 5.8. The upper curves show the corresponding variation in the ^{135}Xe poison factor.

6.4.3 Fission Product Retention (Cont'd)

b - Other Fission Product Deposition (Cont'd)

Possible Formation of Cesium Carbide in MSBR Graphite (Cont'd)

Thus, under the most unfavorable conditions tested ($H = 0.02$ cm/sec, $\lambda_{ST} = 0.001$ sec^{-1}, and $D = 10^{-6}$ cm^2/sec, which gave a ^{135}Xe poison factor of 0.9) the total of all xenon nuclides entered the graphite at a rate

$$\Sigma J_{Xe} = \frac{V_c}{RTA} \Sigma GP^0_{Xe}$$

$$= 1.29 \times 10^{-11} \text{ mole cm}^{-2} \text{ sec}^{-1},$$

so low that even if it all were to decay to cesium, 150 days would be required to produce a cesium-to-carbon ratio of 1:1000. With more realistic calculations and a more realistic calculation of the accumulation rate — in particular, a calculation which includes the diffusion of CsC_n as well as gaseous cesium out of the slab — much lower accumulation rates undoubtedly would result."

6.4.4 Manufacturing Technology

a - Background

The commercial production of carbon and graphite is a relatively time-consuming process because carbon cannot be melted and cast or rolled, etc., as is practiced in the metal industries. All carbon and graphite products must be formed by conversion of "carbonaceous" or carbon rich hydrocarbons to carbon by pyrolysis. In conventional manufacture of carbon articles a selected aggregate of nearly 100 percent carbon material such as calcined petroleum coke, anthracite coal, carbon black, natural graphite, etc., is mixed with coal tar pitch (a

6.4.4 Manufacturing Technology (Cont'd)

a - Background (Cont'd)

readily available thermoplastic carbonaceous binding material) and formed by extrusion through a die, or by moldings in a closed cavity mold. The formed article is not all carbon and the pitch must be pyrolyzed or "baked" to convert the majority of the pitch to carbon and expell the remainder as gaseous waste products.

During this pyrolysis step the article must be supported against a sagging or distortion in the early stages and yet must be permitted to shrink or change volume during the latter stages. The heating cycle must be carefully programmed to avoid disruptive gas pressure buildup and heat application must be uniform over all areas of the piece to avoid distortion and strains from nonuniform dimensional changes. Graphite is produced by further heating the pyrolyzed "carbon" article in an electric-fired furnace to a temperature in the range of 2600 C - 3000 C. All of these elevated temperature operations must be carried out in an inert or protective atmosphere to prevent burning of the carbon. The graphite article produced by a conventional process as outlined above will have a density of perhaps 70 - 75 percent of theoretical and nearly all of the porosity will be open to intrusion of gas or liquids. Further densification is achieved conventionally by vacuum pressure impregnation of the graphite or carbon article with a "carbonaceous" liquid (usually coal-tar pitch) followed by further pyrolysis to convert the impregnant material to carbon and gas.

6.4.4 Manufacturing Technology (Cont'd)

a - Background (Cont'd)

The carbon industry has solved these problems for a range of products where there was sufficient commercial incentive to motivate the development of the technology. Today the carbon and graphite industry produces hundreds of millions of pounds of carbon and graphite products per year. Graphite electrodes are commercially available in sizes up to 45" diameter, 110" long. Other graphite shapes have been produced up to 105" diameter, 60" long and slabs 26' long x 2' x 6' have been made. At the other end of the scale spectroscopic electrodes are regularly stocked in 1/8" diameter by 12" long and are available in 1/16" diameter x 12" long.

b - Nuclear Graphite

Graphite has been widely used in nuclear reactors since the beginning of the "nuclear age" with the use of 385 tons of high purity graphite in the world's first reactor. It is a proven material for neutron moderators, reflectors, thermal columns, and exponential piles. Its low neutron capture cross section, high temperature properties, machinability, and low cost make graphite an exceptionally attractive material for these uses.

Most of the nuclear graphite produced has been in the density range of 1.70 gm/cc and the main special manufacturing attention was on the high purity requirement. Special graphitization and gas treatment techniques along with "clean room" handling are requirements.

Extensive experimental work has been performed to produce low permeability graphite capable of

6.4.4 Manufacturing Technology (Cont'd)

b - Nuclear Graphite (Cont'd)

containing high temperature gas at moderate pressure. Most of the effort was on multiple liquid impregnation-carbonization sequences. Problems of spalling and cracking at the lower permeability levels have kept this low permeability graphite from becoming a commercial reality, although helium permeability as low as 10^{-4} - 10^{-5} cm^2/sec have been obtained with reasonable yields. Individual pieces with permeabilities of 10^{-8} - 10^{-9} have been made.

c - Graphite for Molten-Salt Breeder Reactors

The only production of graphite for molten-salt reactors was the production of grade CGB graphite for the MSRE at Oak Ridge.

Grade CGB graphite was produced by Union Carbide Corporation Carbon Products Division about ten years ago. The starting material was a needle coke, believed at that time to be the preferred material for withstanding neutron irradiation. The forming was done by extrusion using a very fine grained flour and a modified pitch binding system in order to obtain high density uniform structure. The graphite was further processed through multiple pitch-furfural impregnations and rebakes to obtain the final 1.86 gms/cc density and low permeability of 10^{-4} cm^2/sec. The main items of production were rectangular bars finishing to dimensions of about 2" x 2" x 60". Several of the operations were carried out in equipment which at that time was developmental in nature.

6.4.4 Manufacturing Technology (Cont'd)

c - Graphite for Molten-Salt Breeder Reactors (Cont'd)

The production was completed and the graphite was delivered, but only after a great deal of difficulty. Most of the problems were with spalls and incipient cracks which developed after the final impregnation and heat treatment. Larger and much better controlled equipment is available today and superior impregnation systems and techniques are known, but production of low permeability graphite using liquid impregnation as a final step is still difficult.

At the present time radiation damage studies show that isotropic or nearly isotropic graphites do not change dimensions as rapidly under neutron irradiation as do anisotropic grades. Isotropy is, therefore, desirable in graphite for molten-salt reactor use. Isotropy on the microscopic scale is obtainable only through the selection of proper starting materials. Bulk isotropy can be obtained even with anisometric particles by special forming techniques such as isostatic molding. There is not enough known to date about radiation damage mechanism and effects to rule out either technique for making isotropic graphite. It does appear, however, that needle-like particles are likely to lead to greater radiation damage, and that isometric particles or at least particles that are not highly oriented should be selected for best radiation resistance. Carbon materials that fall into this category include Gilsocarbon, air-blown and seeded petroleum cokes, fluid cokes, and carbon blacks. Most of the manufacturing technology applicable to oriented coke particles (such as in CGB) is translateable

6.4.4 Manufacturing Technology (Cont'd)

c - Graphite for Molten-Salt Breeder Reactors (Cont'd)

to isometric particles. Some problems are increased, however, because of the poorer thermal properties (increased thermal expansion-decreased thermal conductivity) of the isotropic graphite. Scale up to larger sizes is thus made more difficult because of the closer control necessary on pyrolysis and heat treating. The carbon industry has not yet produced this fine grained isotropic high density graphite in the sizes and shapes desired for a molten-salt breeder reactor.

Pyrolytically Sealed Graphite

It is desirable to have the graphite in the core region of the MSBR sealed to prevent the intrusion of ^{135}Xe gas and other fission product gases if the sealing can be accomplished and the economics are favorable. Current experimental work at ORNL suggests that graphite can be sealed with high density isotropic carbon deposited from propylene gas at 1250 C and that at least moderate doses of neutron irradiation can be received and still retain effectiveness of the seal. This work is still in progress but in very small scale (irradiation samples are 3/8" dia x 3/4" long thin walled cylinders).

Pyrolytic graphite has been a commercial product by several manufacturers for special applications such as rocket nozzle inserts and reentry hardware for about the past ten years. Most of the pyrolytic graphite produced commercially is high density (2.1-2.2 gm/cc) from high temperature deposition from methane. Problems associated with pyrolytic carbon processes include control of substrate temperature (uniformity) control of gas flows and concentrations,

6.4.4 Manufacturing Technology (Cont'd)

c - Graphite for Molten-Salt Breeder Reactors (Cont'd)

Pyrolytically Sealed Graphite (Cont'd)

dust, and change of structure with thickness of deposit. Many of the problems must be solved specifically for the geometry of the pieces involved. The 4" x 4" x 15' long hollow central core bars as presently conceived for the reference MSBR are most difficult shapes to pyrolytically coat to a uniform thickness, especially in the small diameter inner core region. Extensive development work will be required to determine whether an acceptable coating can be applied and to determine the general magnitude of the cost.

6.5 Hastelloy Alloy N

Standard Hastelloy Alloy N was developed at Oak Ridge National Laboratory during the Aircraft Nuclear Propulsion Program specifically as a container material for molten fluorides. Later, at the inception of the MSRE the properties of this alloy had been determined and were considered to be more than adequate for application in this reactor experiment. The following requirements were placed on the alloy as the material of construction:

1 - Ability to be melted and fabricated into complex shapes;

2 - Moderate strength and ductility at high temperatures;

3 - Stable properties at high temperatures;

4 - Corrosion resistance to molten uranium-bearing fluoride fuels;

5 - Corrosion resistance to coolant salts;

6 - Good oxidation resistance;

7 - Ability to be joined by welding.

6.5 Hastelloy Alloy N (Cont'd)

With experience gained through operation of the MSRE, it became apparent that radiation damage resistance is an equally important requirement of the structural material since exposure of standard Hastelloy Alloy N to the thermal neutron environment of this reactor resulted in deterioration of mechanical properties.

In addition, the application of the alloy in the electric generating system of future molten-salt power reactors will require compatibility of the alloy with steam. The requirements of the structural material outlined above are discussed in more detail relative to molten-salt reactor technology in the following sections of this report.

6.5.1 Composition

Standard Hastelloy Alloy N, whose composition is shown in Table 6.12 is a nickel-base alloy solution strengthened with molybdenum and with sufficient chromium to be oxidation resistant; however, the chemistry has been controlled to preclude aging embrittlement by the precipitation of $Ni_X Mo_Y$ intermetallic compounds. The carbon content has been limited to minimize fabrication problems, but is sufficient to promote the formation of carbides, M_6C and $M_{23}C_6$, which slightly enhance the strength of the material. Iron is included in the alloy to allow a wider selection of raw materials in the preparation of the alloy.

6.5.2 Melting and Casting

Conventional melting and casting practices for nickel and its alloys can be used to prepare standard Hastelloy Alloy N. These include air and vacuum induction, electric arc, consumable arc, and electroslag melting methods. The usual precautions must be taken to avoid gassy melts together with sulfur contamination. Elements

Table 6.12

Composition of Standard Hastelloy Alloy N

Element	Composition, Weight Percent
Nickel	Balance
Molybdenum	15-18
Chromium	6-8
Iron	5 max.
Carbon	0.04-0.08
Silicon	1 max.
Manganese	0.8 max.
Aluminum and Titanium	0.5 max.
Boron	0.01 max.
Phosphorus	0.015 max.
Sulfur	0.02 max.

6.5 Hastelloy Alloy N (Cont'd)

6.5.2 Melting and Casting (Cont'd)

such as manganese, silicon, and aluminum are added to deoxidize the metal.

The alloy has been cast in molds of water-cooled copper, graphite, rammed magnesia, and cast iron. Impellers and volutes for the fuel and coolant pumps of the MSRE were made from sand castings of the alloy. Chemistry requirements for the impellers and volutes did not deviate from the chemistry specification for wrought material. Radiographic quality levels of those castings were Class 1 (ASME Boiler and Pressure Vessel Code) in areas of high stress and Class 2 in other areas; however, considerable weld repair was required to obtain this quality.

6.5.3 Fabrication

Standard Hastelloy Alloy N has been produced on a commercial basis in a variety of shapes including plate, sheet, rod, wire, and welded and seamless tubing by conventional methods of hot and cold forming.

Hot forging of ingots can be carried out both on press- and hammer-type forges between 1850-2250°F. Hot-rolling is readily accomplished between 2100-2200°F using reductions of about 10 percent per pass. The optimum extrusion temperature range is 2150-2200°F for extrusion ratios of 4:1 to 12:1. Extrusion rate is one of the most critical variables in tube blank extrusion. It should be kept to about 1 in. of billet length per second in order to avoid hot cracking.

The ductility of standard Hastelloy Alloy N at room temperature allows cold-working operations such as rolling, swaging, tube reducing, and drawing to be performed successfully. The alloy work hardens rapidly and, therefore, requires frequent annealing in order to prevent the formation of splits and cracks.

6.5 Hastelloy Alloy N (Cont'd)

6.5.3 Fabrication (Cont'd)

A reduction in area on the order of 50 percent is possible between anneals.

The forming of standard Hastelloy Alloy N heads for the MSRE was performed by hot and cold methods. Heads 3 to 4 ft in diameter were successfully made by the hot-forming method using starting temperatures of 2000-2100°F. Cold-forming was used to fabricate heads as small as 9 in. in diameter by 1/2 in. thick and as large as 60 in. in diameter by 1-1/8 in. thick without the use of intermediate anneals.

The alloy can be fully annealed by holding at 2150 ± 25°F for approximately 1 hour per inch of thickness, or a minimum time of 10-15 minutes. The temperature used for stress-relieving is 1600 ± 25°F. Heat-treatment requirements for standard Hastelloy Alloy N in the MSRE called for the material to be annealed after any forming or working and to be stress-relieved after final fabrication.

Standard Hastelloy Alloy N can be machined in a manner similar to other nickel-base Hastelloy-type alloys. Conventional cemented carbide tools, cutting speeds of about 35 to 50 fpm and feeds of 0.015 in. or less yield satisfactory results. Depths of finishing cuts should be greater than 0.005 in. in order to machine below the work-hardened surface that occurs in this alloy.

6.5.4 Welding

Experience with standard Hastelloy Alloy N has shown that it exhibits relatively good weldability. MSRE, for example, contained hundreds of satisfactory welds in various section sizes. These welds were made by the inert-gas-shielded tungsten-arc process. Tests of some

6.5 Hastelloy Alloy N (Cont'd)

6.5.4 Welding (Cont'd)

of the early heats of the alloy indicated a susceptibility to weld-metal cracking when these materials were subjected to welding under restraint. In some cases this problem was associated with a high boron content of the heats, and in others to melting practice used to produce the alloy. Adjustment of alloy preparation procedure and incorporation of weldability testing of all heats of material purchased for the MSRE insured weldability of the material. At present, the gas tungsten-arc welding process is the only technique that has been used for the construction of reactors of this material. The MSRE experience has proven the applicability of this process. The weld filler metal used for joining Hastelloy Alloy N was of the same basic composition as the wrought product.

6.5.5 Oxidation Resistance

The oxidation resistance of nickel-molybdenum Hastelloy-type alloys depends on the service temperature, the temperature cycle, the molybdenum content, and the chromium content. The oxidation rate of the binary nickel-molybdenum alloy passes through a maximum for the alloy containing 15 percent Mo, and the scale formed by the oxidation is $NiMoO_4$ and NiO. Upon thermal cycling from above 1400°F to below 660°F, the $NiMoO_4$ undergoes a phase transformation which causes the protective scale on the oxidized metal to spall. Subsequent temperature cycles then result in an accelerated oxidation rate. Similarly, the oxidation rate of nickel-molybdenum alloys containing chromium passes through a maximum as the chromium content of the alloys is increased from 2 to 6 percent Cr. Alloys containing more than 6 percent Cr are insensitive to thermal cycling and to the molybdenum content because the oxide scale is predominantly stable Cr_2O_3. An abrupt

6.5 Hastelloy Alloy N (Cont'd)

6.5.5 Oxidation Resistance (Cont'd)

decrease (by a factor of about 40) in the oxidation rate at 1800°F is observed when the chromium content is increased from 5.9 percent to 6.2 percent.

The oxidation resistance of standard Hastelloy Alloy N is excellent, and continuous operation at temperatures up to 1800°F is feasible. Intermittent use at temperatures as high as 1900°F could be tolerated. For temperatures up to 1200°F, the oxidation rate is not measurable; it is essentially zero after 1000 hours of exposure in static air, as well as in nitrogen containing small quantities of air (the MSRE cell environment). It is estimated that oxidation of 0.001 to 0.002 in. would occur in 100,000 hours of operation at 1200°F. The effect of temperature on the oxidation rate of the alloy is shown in Figure 6.43.

6.5.6 Corrosion Resistance to Fuel Salts

Corrosion of metals in molten fluoride fuel salt mixtures occurs by oxidation of the metal components to their fluoride salts, which are readily dissolved by the molten fuel. This precludes any possibility of protection by passivation of the metal surface by corrosion products, and the extent of corrosion is then controlled by the thermodynamic driving force of the oxidation reaction. Oxidation reactions stem from three sources:

1 - Reactions involving impurities in the salt, for example:

$$2\ HF + Cr \longrightarrow CrF_2 + H_2$$

$$NiF_2 + Cr \longrightarrow CrF_2 + Ni$$

$$FeF_2 + Cr \longrightarrow CrF_2 + Fe$$

6.5 Hastelloy Alloy N (Cont'd)

6.5.6 Corrosion Resistance to Fuel Salts (Cont'd)

2 - Reactions involving impurities in or on the metal, for example:

$$2\ Fe_2O_3 + 3\ CrF_4 \longrightarrow 3\ CrO_2 + 4\ FeF_3$$

FeF_3 now reacts with Cr

3 - Reactions involving components in the salt, for example:

$$Cr + 2\ UF_4 \longrightarrow 2\ UF_3 + CrF_2$$

In the case of Hastelloy Alloy N, corrosion is manifested by the selective oxidation and removal of chromium. When it becomes depleted, subsurface voids can form in the depletion zone. Corrosion is time and temperature dependent. In practical applications, the major source of corrosion by fluoride mixtures is derived from trace impurities in the salt rather than the major salt components.

Extensive corrosion testing demonstrated excellent compatibility of standard Hastelloy Alloy N with fluoride salts. Data were generated in thermal convection and forced circulation loops.

In the first phase of the test program, the corrosion properties of various fluoride salt mixtures were compared in standard Hastelloy Alloy N thermal-convection loops which operated for 1000 hr. Specific salt mixtures, whose compositions are listed in Table 6.13, were selected to provide an evaluation of (1) the corrosion properties of beryllium-bearing fuels, and (2) the corrosion properties of beryllium-fluoride mixtures containing large quantities of thorium. The second phase of testing, which again used thermal-convection loops, involved more extensive investigations for longer time periods and two temperature levels, 1250 and 1350°F. The third phase of the testing

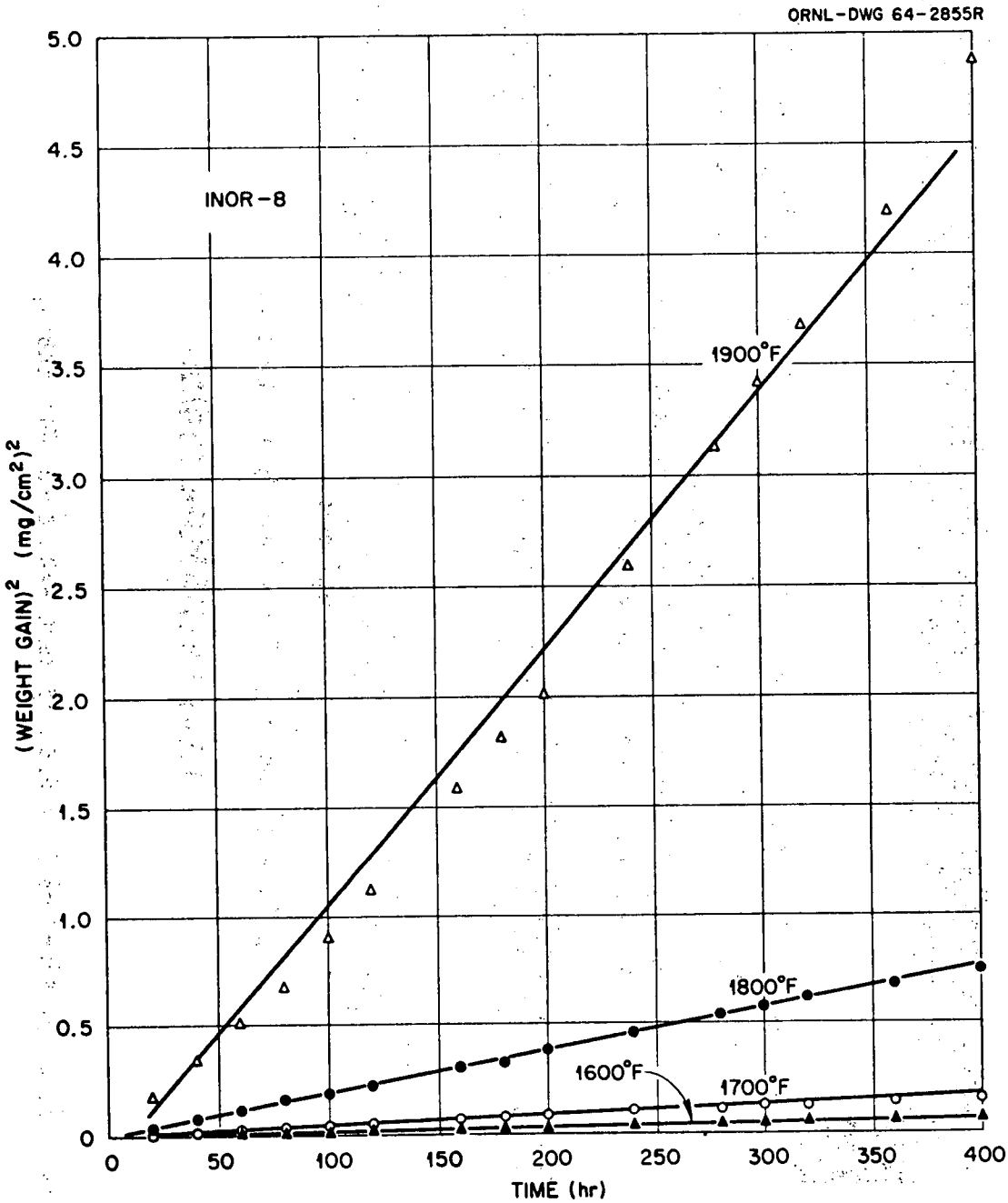

Fig. 6.43. Effect of Temperature on Oxidation of Standard Hastelloy alloy N.

R - 55178

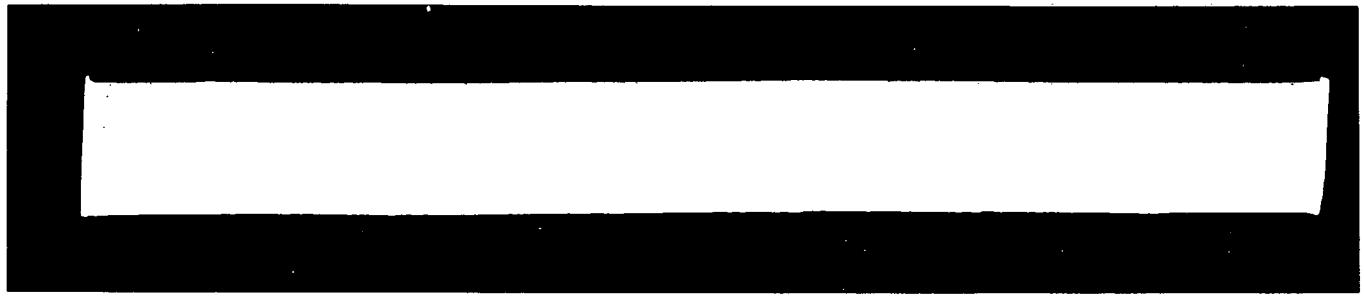

UNSTRESSED

Section of Tube Wall As-Cut From Heat Exchanger.
Corrosion-Cracking Barely Visible.

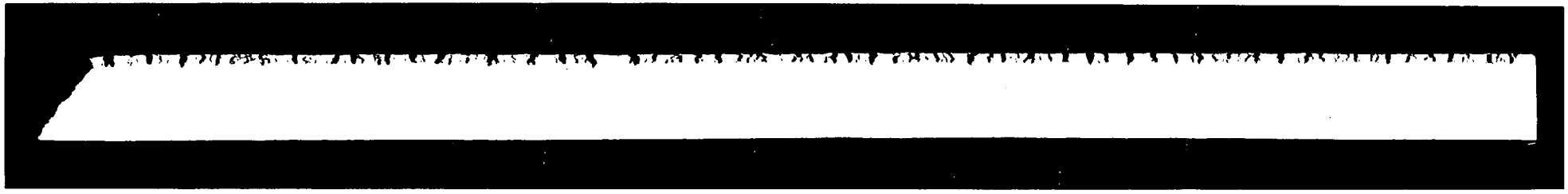

STRESSED

Section of Tube Wall after Testing in Tension.

HEAT EXCHANGER TUBING

Fig. 6.44 Cracking Found on Fuel Side of MSRE Heat Exchanger Tubing.

Table 6.13

Compositions of Molten-Salt Mixtures Tested for Corrosiveness in Standard HASTELLOY Alloy N Thermal-Convection Loops

Salt Mixture	Composition, mole %					
	NaF	LiF	ZrF_4	BeF_2	UF_4	ThF_4
122	57		42		1	
129	55.3		40.7		4	
123	53			46	1	
124	58			35		7
125	53			46	0.5	0.5
126		53		46	1	
127		58		35		7
128		71				29
130		62		37	1	
131		60		36	4	
133		71		16		13
134		62		36.5	0.5	1
135	53			45.5	0.5	1
136		70		10	20	
Bu-14 + 0.5 U		67		18.5	0.5	14

was conducted in forced-circulation loops at flow rates and temperature conditions simulating those of an operating reactor system. All of these loops operated with maximum fuel-salt temperatures of 1250-1500°F and with approximately 200°F temperature drops.

Essentially no attack or deposition was found with any of the fluorides in standard Hastelloy Alloy N loops in the Phase-I studies. The maximum attack found after 8760 hr in the Phase-II tests was limited surface roughening and pitting to a depth of 1/2 mil. Attack in most cases was accompanied by a thin surface layer. No deposit or other evidence of mass transfer was found in any of the cold legs.

In the third phase of the program, employing forced-circulation loops, tubular inserts in the heated sections of some of the loops provided information about the weight losses occurring during the tests. Salt samples taken from the pump bowls provided a semi-continuous indication of corrosion-product concentration in the circulating systems. A summary of the operating conditions and results of the metallographic examination of the forced-circulation loops are presented in Table 6.14. The operating times of these systems ranged from 6500-20,000 hr. Eight of the loops were operated for over 14,000 hr.

The corrosion rates of standard Hastelloy Alloy N in the pumped loops operated with maximum temperatures between 1300-1500°F indicated that corrosion reactions effectively go to completion in the first few thousand hours of loop operation. As shown in Table 6.15, weight losses in 10,000- and 15,000-hr tests in pumped loops containing $LiF-BeF_2-UF_4$ salts showed no measurable increase after the first 5000 hr of operation. Moreover, changes in

Table 6.14

Operating Conditions of Standard HASTELLOY Alloy N Forced-Circulation Loops and Results of Metallographic Examinations of Loop Materials

Loop Number	Duration Of Test (Hr)	Salt Mixture[a/]	Maximum Fluid-Metal Interface Temperature (°F)	ΔT (°F)	Reynolds Number	Flow Rate (gal/min.)	Results of Metallographic Examination
9354-1	14,563	126	1300	200	2000	2.5	Heavy surface roughening and pitting to 1-1/2 mils
9354-4	15,140	130	1300	200	3000	2.5	No attack
9354-5	14,503	130	1300	200	3000	2.5	No attack
MSRP-6	20,000	134	1300	200	2300	1.5	Pitted surface layer to 2 mils
MSRP-7	20,000	133	1300	200	3100	1.8	Pitted surface layer to 1 mil
MSRP-8	9,633	124	1300	200	4000	2.0	No attack
MSRP-9	9,687	134	1300	200	2300	1.8	No attack
MSRP-10	20,000	135	1300	200	3400	2.0	Pitted surface layer to 1/2 mil
MSRP-11	20,000	123	1300	200	3200	2.0	Pitted surface layer to 1 mil
MSRP-12	14,498	134	1300	200	2300	1.8	No attack
MSRP-13	8,085	136	1300	200	3900	2.0	Heavy surface roughening and pitting
MSRP-14	9,800	Bu-14 + 0.5 U	1300	200			Pitted surface layer to 1/2 mil
MSRP-15	10,200	Bu-14 + 0.5 U	1400	200			Pitted surface layer to 2/3 mil
MSRP-16	6,500	Bu-14 + 0.5 U	1500	200			Moderate subsurface void formation to 4 mils

a/ See Table 6.13

Table 6.15

Corrosion Rates of Inserts Located in the Hot Legs of Standard HASTELLOY Alloy N Forced-Circulation Loops as a Function of Operation Temperature

Loop Temperature Gradient: 200°F.
Flow Rate: Approximately 2.0 gal/min.
Reynolds Number: Approximately 3000

Loop Number	Salt Mixture[a/]	Insert Temperature[b/] (°F)	Time (Hr)	Weight Loss per Unit Area (mg/cm^2)	Equivalent Loss in Wall Thickness (microns)
9354-4	130	1300	5,000	1.8	2.0
			10,000	2.1	2.3
			15,140	1.8	2.0
MSRP-14	Bu-14	1300	2,200	0.7	0.8
			8,460	3.8	4.3
			10,570	5.1	5.8
MSRP-15	Bu-14	1400	8,770	11.2	12.7
			10,880	10.0[c/]	11.2
MSRP-16	Bu-14	1500	5,250	9.6	10.9
			7,240	9.0[c/]	9.1

a/ Salt Compositions:
130 $LiF-BeF_2-UF_4$ (62-37-1 mole %)
Bu-14 $LiF-BeF_2-ThF_4-UF_4$ (67-18.5-14-0.5 mole %).

b/ Same as maximum wall temperature.

c/ Average of two inserts.

concentrations of corrosion products in the circulating salt leveled off in the same time period. The metallographic appearance of the loop surfaces, however, was noticeably affected by the test temperature. At the highest test temperature (1500°F), standard Hastelloy Alloy N surfaces were depleted of chromium (as indicated by the appearance of shallow subsurface voids) to a maximum depth of 4 mils. At 1300-1400°F, the surfaces exhibited no evidence of attack or other metallographic changes during the first 5000 hr of operation. At still longer test times a thin continuous intermetallic layer was faintly discernible. Chemical analyses of exposed surfaces suggested that the layer was an intermetallic transformation product of the nickel-molybdenum system.

The corrosion data for standard Hastelloy Alloy N exposed in the forced-circulation loops indicated that corrosion reactions with fluoride salts at MSRE temperature (1200°F) would be essentially complete within the first 5000 hr of operation, and would not generally exceed 1 mil even after 20,000 hr. No significant increase in corrosion would occur unless the temperature increased to about 1500°F. However, unexpectedly, post-operation examination of MSRE revealed that all standard Hastelloy Alloy N surfaces exposed to fuel salt contained cracks 5 to 10 mils deep. An example of this cracking is shown in Figure 6.44. The depth of penetration did not appear to vary with location within the reactor. This phenomenon is currently attributed to corrosion caused by impurities such as fission products or by oxidizing conditions of the fuel salt. Fission products, while not entirely discounted, are believed less likely the cause. This conclusion is based on ORNL observation that similar cracking occurs in

6.5 Hastelloy Alloy N (Cont'd)

6.5.6 Corrosion Resistance to Fuel Salts (Cont'd)

specimens exposed to fuel salt contaminated with an impurity such as FeF_2.

The cracking observed in MSRE was quite likely caused by oxidizing conditions of the fuel salt. These conditions could have been caused by air and/or water vapor entering the system. During the lifetime of MSRE, the fuel salt was drained, the primary system flushed, and opened fourteen times. It is likely that each time some air entered the primary system. Even though the primary system was purged with helium prior to recharging it with fuel salt, oxygen or water vapor probably would have been absorbed by the graphite and subsequently driven into the fuel salt when the graphite returned to high temperature.

If oxidixing salt conditions are the cause of the cracking, it can be prevented in future molten-salt reactors. Commercial reactors will be exposed to atmospheric contamination much less frequently, and the chemical process plant should remove contaminants from the fuel salt and maintain the desired oxidation potential.

6.5.7 Corrosion Resistance to Coolant Salts

A sodium fluoroborate salt ($NaBF_4$ -8 mole percent NaF) has been identified as a potential coolant salt for molten-salt reactors. This salt is less expensive and has a lower melting point (725°F) than the LiF-BeF_2 salt used as the coolant in the MSRE. Corrosion behavior of standard Hastelloy Alloy N could be expected to be essentially the same as that toward the fuel salt, i.e., of the major constituents of the alloy, chromium is much more readily oxidized by fluoride salts than Fe, Ni, or Mo. Thus, attack is normally manifested by the selective removal of chromium. The rate-limiting step in chromium

6.5.7 Corrosion Resistance to Coolant Salts (Cont'd)

removal from standard Hastelloy Alloy N by fluoride salt corrosion is the solid-state diffusion of chromium in the alloy. Other oxidizing reactions may occur depending on the salt composition and impurity content. This occurs in fluoroborate salt systems when large amounts of H_2O and/or oxygen (> 500 ppm) are present. Water and oxygen result in the formation of strong oxidants such as HF.

Loop testing of standard Hastelloy Alloy N with the $NaBF_4$-8 mole percent NaF salt has been in progress for some time. Thermal convection loops containing removable specimens have operated in excess of three years and have shown a maximum corrosion rate of 0.7 mil/year at a temperature of 1120°F. Corrosion has generally been selective toward chromium, but there have been short periods when impurities have caused general attack of the alloy. The latter periods were caused by leaks in the valves of the loops. Although the overall corrosion rates in these loops were not excessive, the rates observed in the absence of leaks have been about an order of magnitude lower.

6.5.8 Corrosion Resistance to Steam

The compatibility of standard Hastelloy Alloy N with steam appears to be fairly good. Samples exposed to 1000°F - 3500 psi steam in the Bull Run Facility show small weight gain after 6000 hr with the loss of metal less than 0.25 mil/year, assuming uniform corrosion. A 2-1/4 Cr steel tested under the same conditions corrodes at a rate of about 1 mil/year. In 1100°F - 900 psi steam of the Bartow Plant of the Florida Power Corporation the corrosion rate of standard Hastelloy Alloy N is less than 0.5 mil/year after more than 13,000 hr exposure. These data are summarized in Figure 6.45.

6.5 Hastelloy Alloy N (Cont'd)

6.5.9 Mechanical Properties

Mechanical properties tests were performed on eight commercial-size heats of standard Hastelloy Alloy N and results showed the strength of the alloy to be greater than the austenitic stainless steels. Five of the heats were experimental ones and were used to establish design data for the alloy. Data from this study were reviewed by the ASME Boiler and Pressure Vessel Code Committee and Code approval was obtained under Case 1315 for Unfired Pressure Vessel construction and Case 1345 for Nuclear Vessel construction. The recognized allowable stresses are tabulated in Table 6.16. The remaining three heats, randomly selected from material used to fabricate MSRE components, were tested to evaluate the effects of large-scale production and improved quality requirements. The commercial heats used for MSRE construction exhibited strengths equal to or greater than the experimental heats.

Tensile tests were performed on the experimental heats and specifications were thereby extablished for the commercial heats. Figure 6.46 is a summary of the ultimate strengths from room temperature to 1800°F for both types of material. Similar data on the 0.2 percent offset yield strength are shown in Figure 6.47. The values for fracture ductility are presented in Figure 6.48. The strength and ductility values from both the longitudinal and transverse specimens are comparable, showing no anisotropy effects.

Creep-rupture tests were performed on sheet and rod speciments in both air and molten salts. Most of the testing was confined to the 1100 to 1300°F temperature range. A few tests, however, were conducted at temperatures up to 1700°F. Summary curves representing stress vs minimum creep rate for the MSRE heats of standard Hastelloy Alloy N are shown in Figure 6.49. The data for heat 5055 are

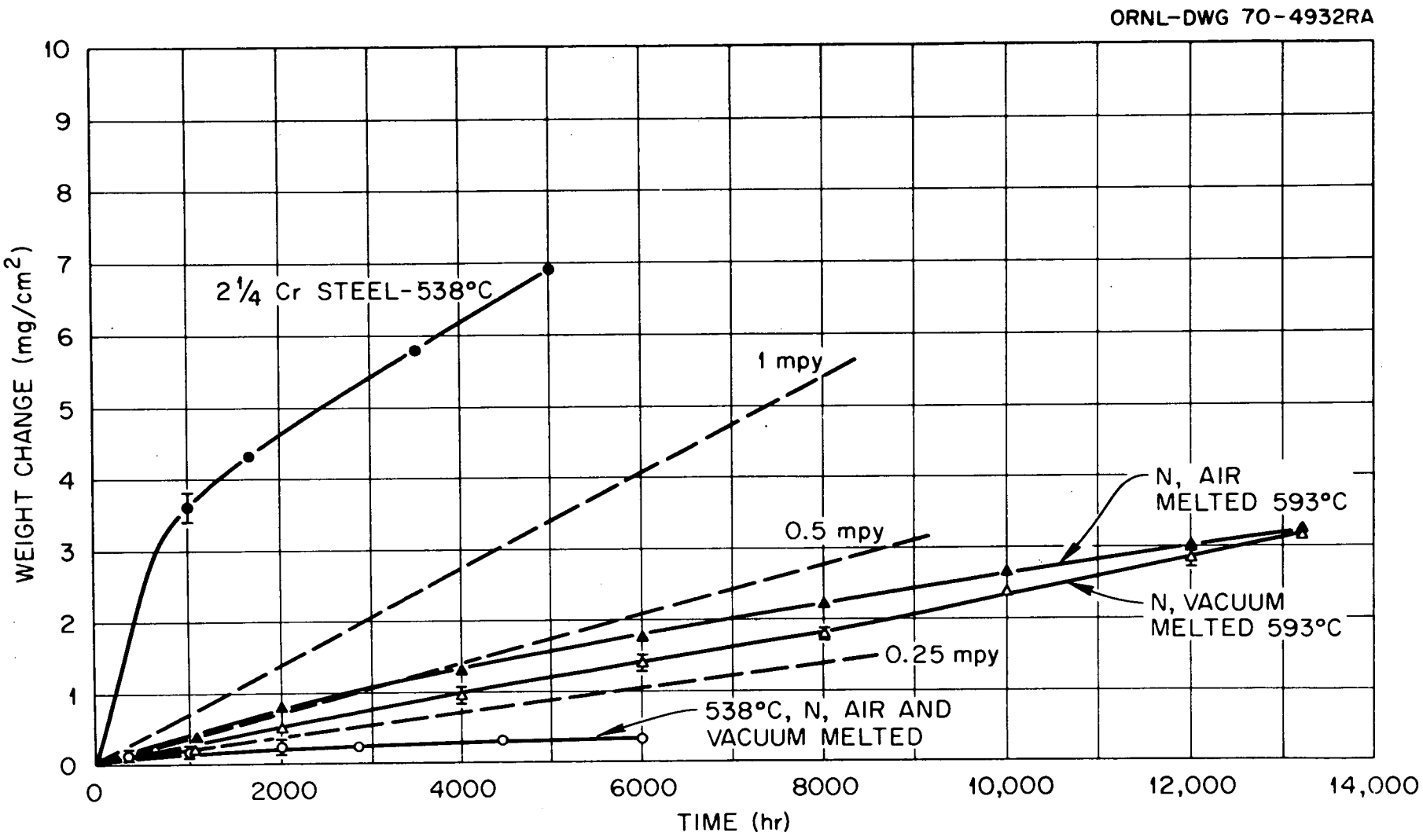

Fig. 6.45. Corrosion of Standard HASTELLOY alloy N in Steam.

Table 6.16

Maximum Allowable Stresses for Standard HASTELLOY Alloy N Reported by ASME Boiler and Pressure Vessel Code

Temperature (°F)	Maximum Allowable Stress, psi	
	Material Other than Bolting	Bolting
100	25,000	10,000
200	24,000	9,300
300	23,000	8,600
400	21,000	8,000
500	20,000	7,700
600	20,000	7,500
700	19,000	7,200
800	18,000	7,000
900	18,000	6,800
1000	17,000	6,600
1100	13,000	6,000
1200	6,000	6,000
1300	3,500	3,500

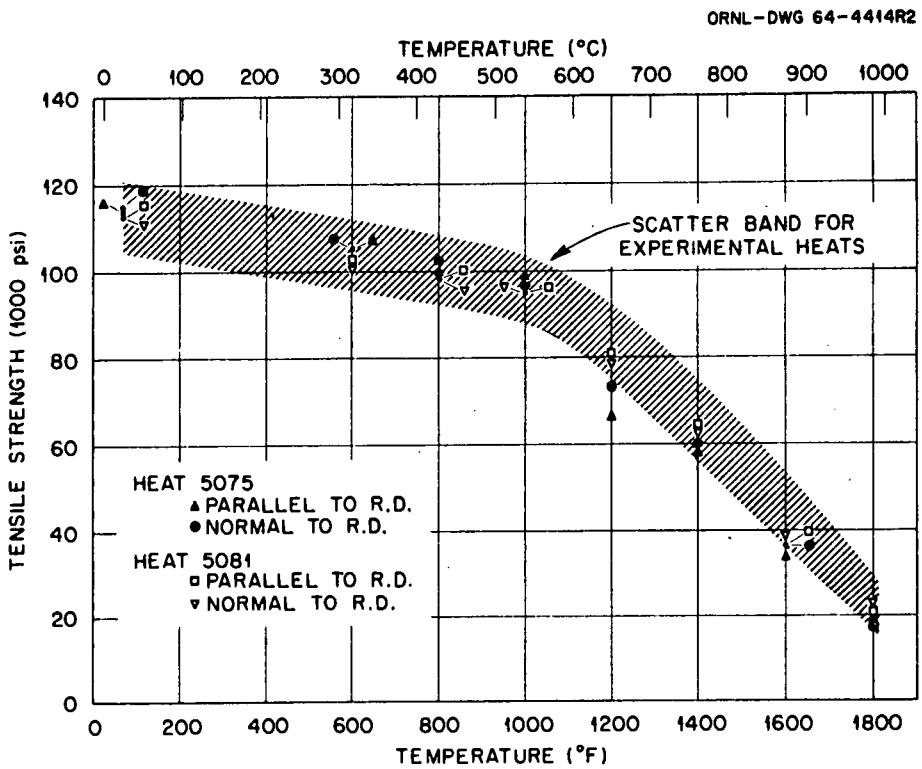

Fig. 6.46. Tensile Strength at Various Temperatures for Standard Hastelloy alloy N.

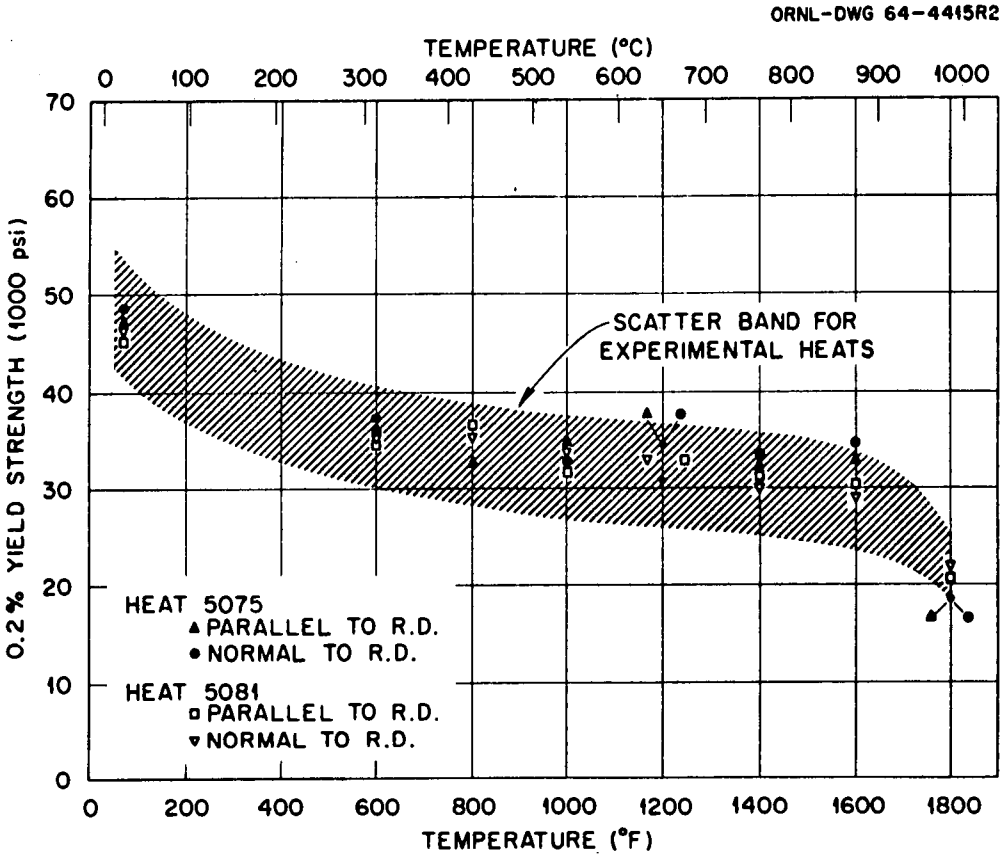

Fig. 6.47. Yield Strength Values for Standard Hastelloy alloy N.

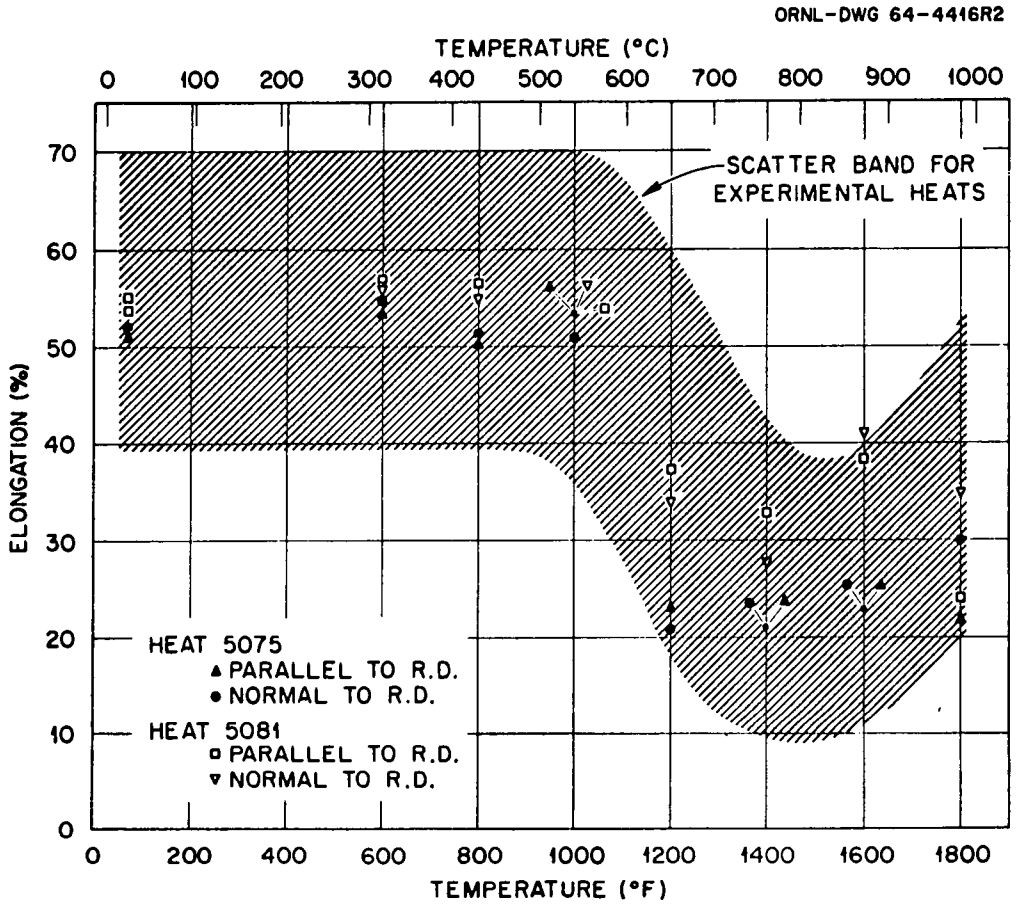

Fig. 6.48. Total Elongation Values for Standard Hastelloy alloy N.

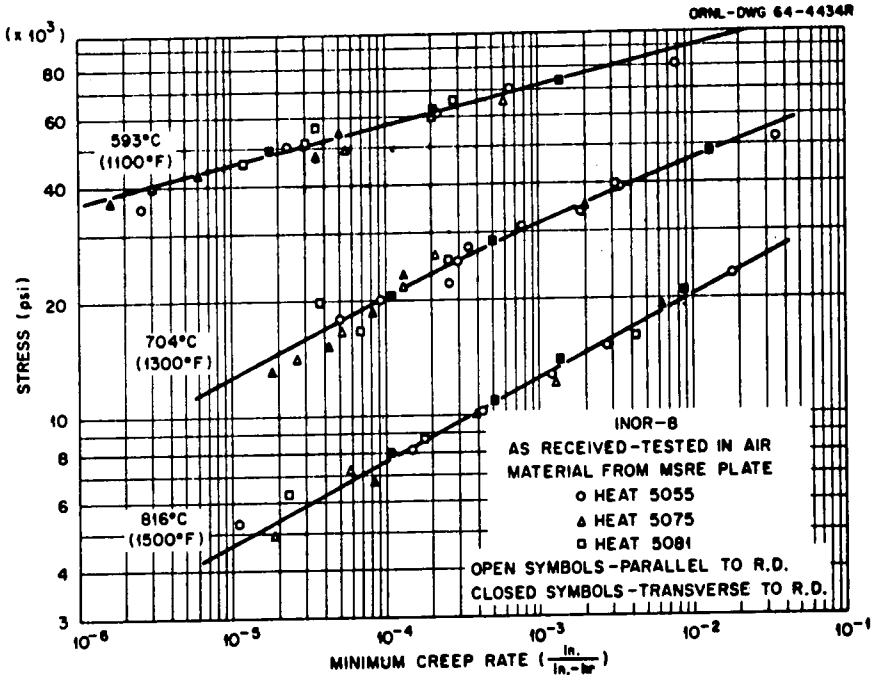

Fig. 6.49. Effect of Stress on Minimum Creep Rate of Standard Hastelloy, alloy N.

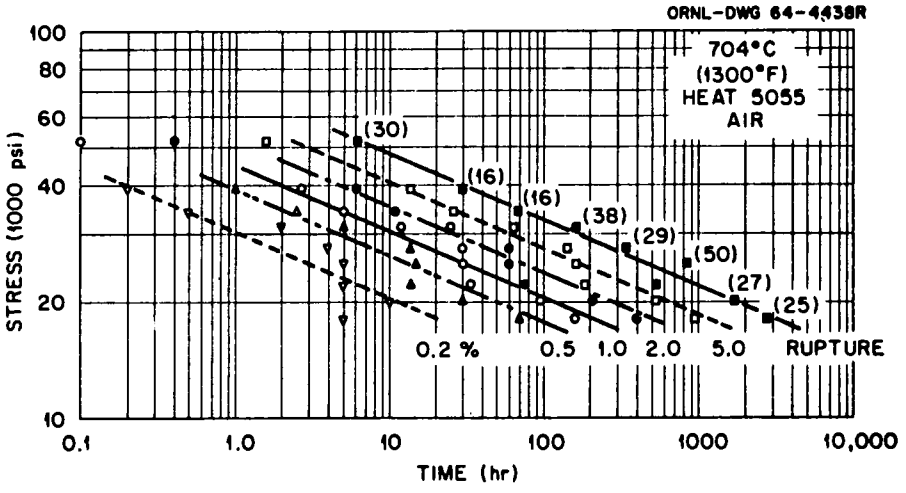

Fig. 6.50. Time to Reach Various Strains for a Given Stress. Numbers in parentheses indicate fracture ductilities. (Open symbols - specimens parallel to rolling direction, closed symbols - specimens perpendicular to rolling direction.)

6.5.9 Mechanical Properties (Cont'd)

plotted to show the time to various strains at 1300°F in Figure 6.50. The rupture life of the alloy plotted as a function of stress is shown in Figure 6.51. The creep properties in molten-salt environments were not significantly different from those obtained in air.

6.5.10 Irradiation Damage

Exposure of standard Hastelloy Alloy N to neutron irradiation causes very marked reduction in ductility of the material. Significant variables influencing the degree of embrittlement are neutron fluence, and post-irradiation deformation temperature and rate. A large effort has been made over the past several years investigating effects of these variables and results can be more or less typified by the data presented in Figures 6.52 and 6.53 obtained from MSRE surveillance specimens. The fracture strain is shown as a function of test temperature and neutron fluence at a constant strain rate of 0.05 in./in./min in Figure 6.52. Generally, the fracture strain is decreased with increasing fluence. At low fluence the ductility reduction at low test temperatures is restricted to room temperature and recovers at higher test temperatures, but at higher fluences the fracture strain is reduced over a wider temperature range. This embrittlement is attributed to carbide precipitation. The ductility reduction above 932°F is associated with the presence of helium (discussed below) and the increased tendency for intergranular fracture. The fracture strain at a given temperature above 932°F generally decreases with increasing thermal fluence.

The sensitivity of the fracture strain of standard Hastelloy Alloy N at 1200°F to thermal fluence (helium content) is illustrated in Figure 6.53 for three strain

rates. The two higher strain rates were obtained by tensile testing, and the fracture strain decreases with increasing helium content. At a strain rate of 0.1 percent/hr, the fracture strain drops abruptly with the presence of 1 ppm helium and then decreases gradually with increasing helium content.

The principal cause of irradiation damage in standard Hastelloy Alloy N has been traced to the helium generated in the alloy by the transmutation of ^{10}B according to the following thermal neutron reaction:

$$^{10}B + n \longrightarrow {}^{4}He + {}^{7}Li$$

An example of helium bubbles present in the irradiated alloy can be seen in Figure 6.54. This is a transmission electron photomicrograph and the helium bubbles, in this case, are visible as small white spots surrounding a large M_6C carbide particle.

Boron is an impurity in the alloy that comes from the refractories used in melting. Careful commercial practice makes it possible to produce alloys containing 1-5 ppm boron. Irradiation tests, however, show that the amount of helium required to cause embrittlement is so low that even alloys containing 0.1 ppm of boron are badly damaged in this respect. The strong influence of such a small quantity of boron is probably due to the segregation of boron at the grain boundaries, where helium production can have a profound effect on the fracture behavior. It has thus been concluded that the problem of irradiation induced embrittlement cannot be solved by reducing the boron level, but rather through modification of the alloy composition as described in section 6.5.11.

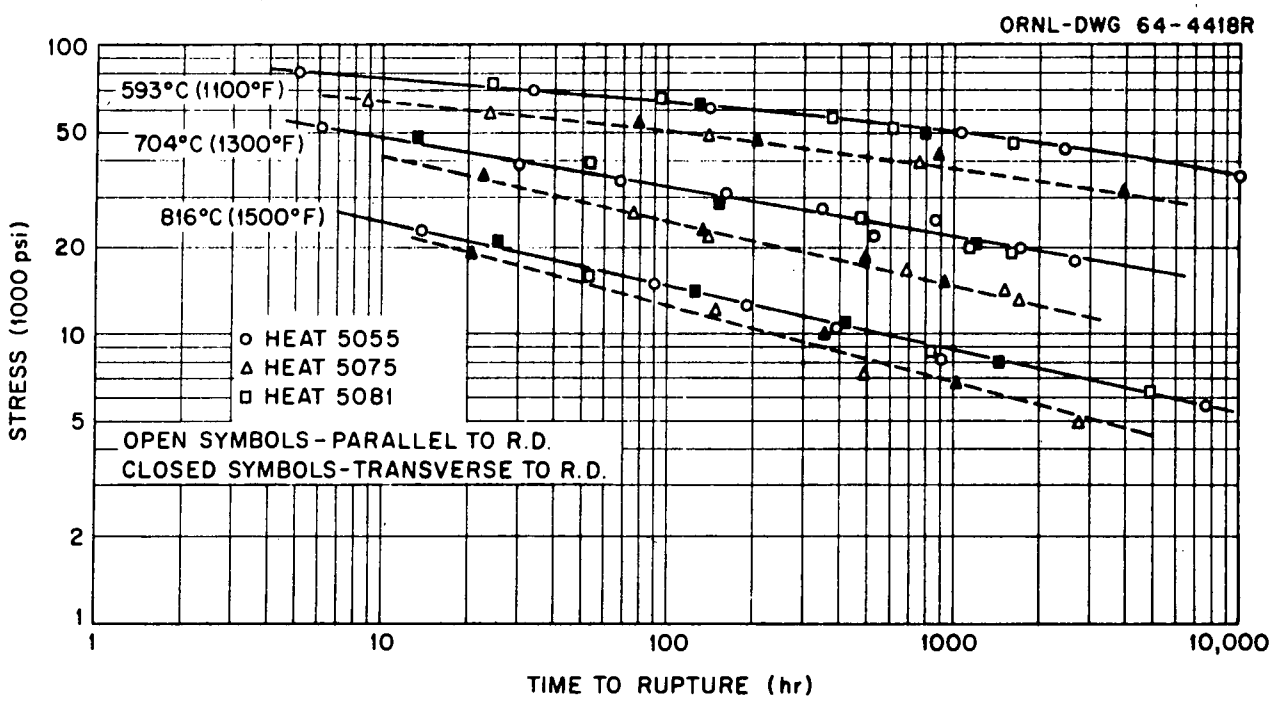

Fig. 6.51. Rupture Life of Standard Hastelloy alloy N at Given Stresses and Temperatures.

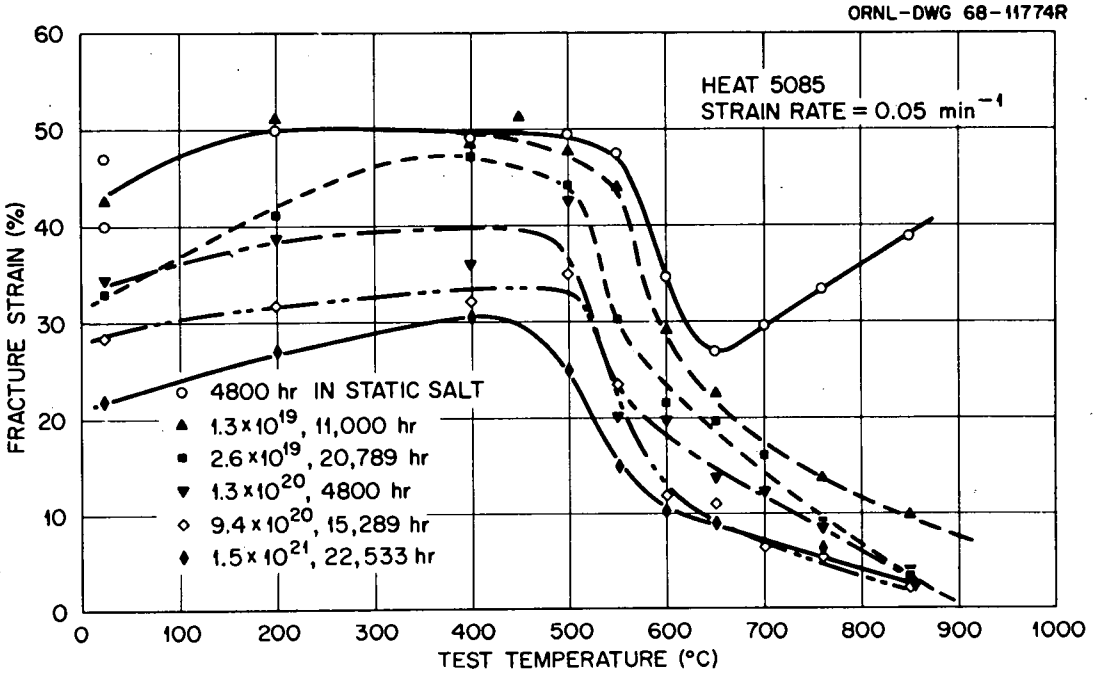

Fig. 6.52. Postirradiation Tensile Properties of MSRE Surveillance Samples.

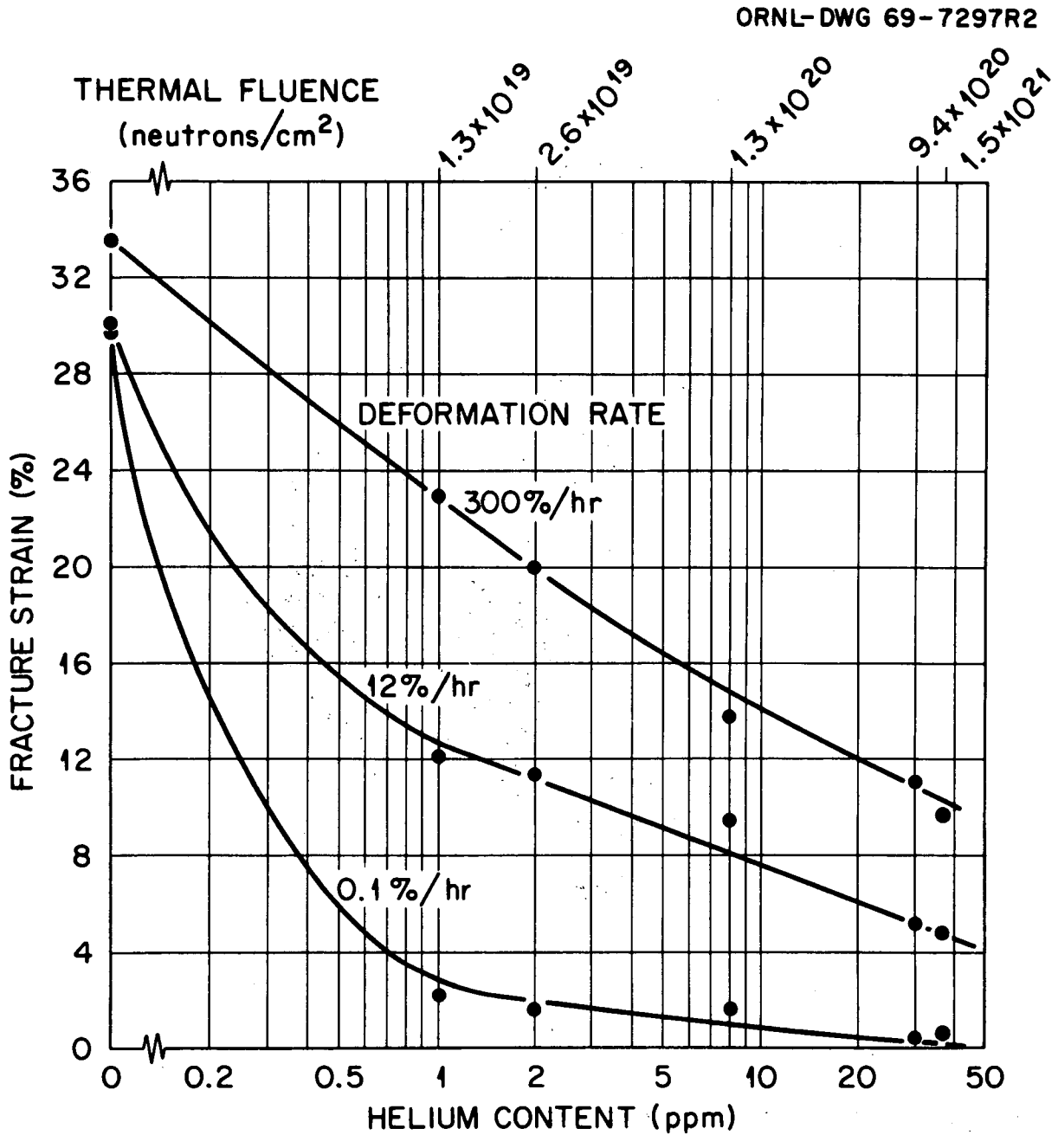

Fig. 6.53. Variation of the Fracture Strain with Calculated Helium Content and Strain Rate for Standard Hastelloy alloy N (Heat 5085) at 1200 degrees F.

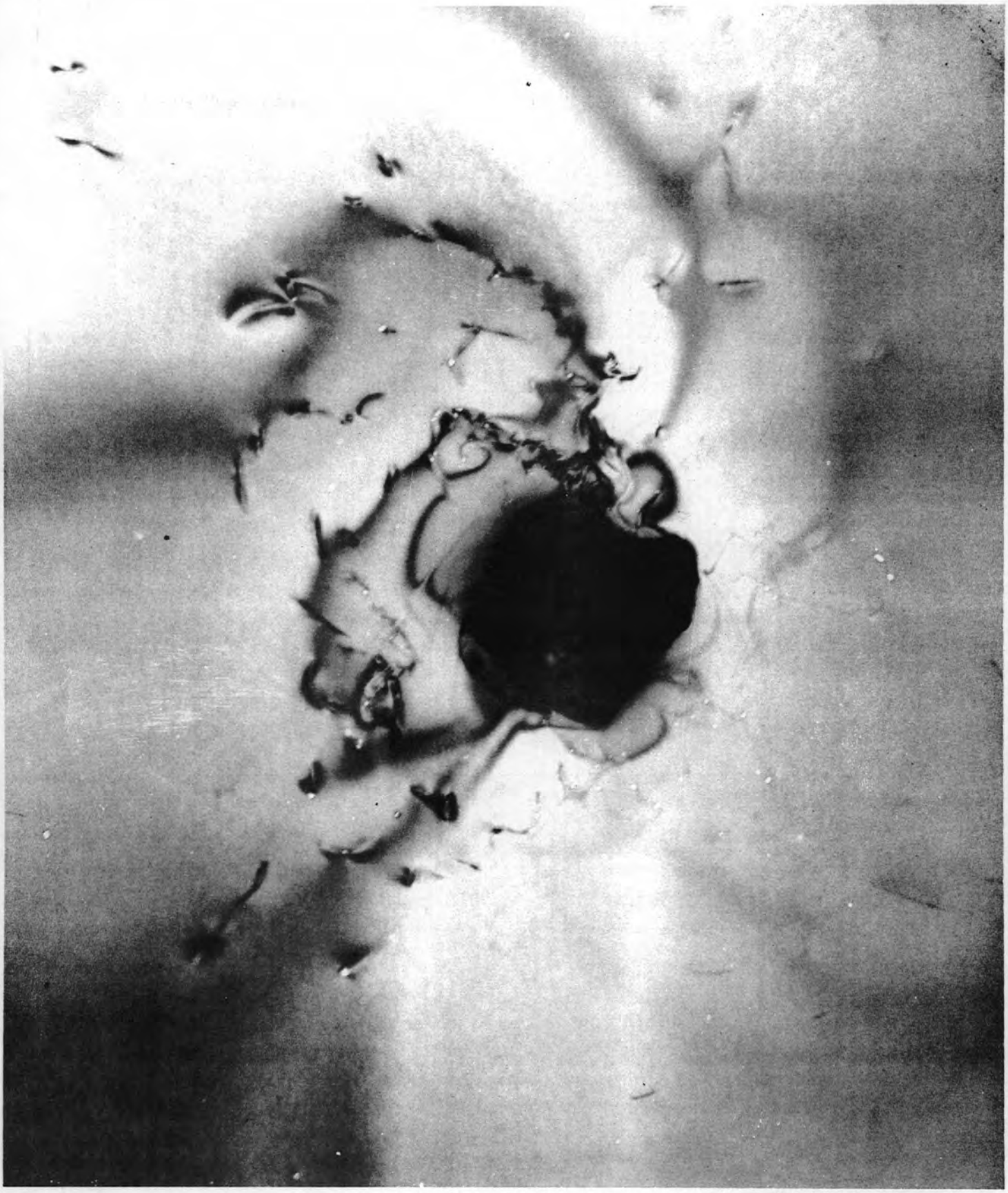

Fig. 6.54. Transmission Electron Photomicrograph of Standard Hastelloy alloy N (Heat 5085) Exposed to the MSRE Core for 15,289 hr at 1200° F. The thermal fluence was 9.4×10^{20} neutrons/cm^2, enough to transmute most of the ^{10}B in this material to helium.

6.5 Hastelloy Alloy N (Cont'd)

6.5.11 Modified Hastelloy Alloy N

Work is underway to develop a modified Hastelloy Alloy N composition with improved radiation damage resistance over that shown by the standard alloy. Although the chemistry of the modified alloy has not been finalized, progress points to a composition which will be included within the ranges tabulated in Table 6.17.

The rationale for alloy modification has been to effect alteration of the carbide morphology and form of very fine uniformly dispersed carbide structure. Thus, numerous sites would be provided for accumulation of the boron. It is, thereby, hoped that the generated helium will be distributed uniformly throughout the material, rather than accumulate in grain boundaries. Alteration of the carbide morphology has been accomplished by reducing the molybdenum content of the alloy to 12 percent and reducing the silicon content from 1 percent maximum to 0.1 percent maximum. With the addition of low concentrations of elements such as titanium, hafnium, and columbium, dispersions of very fine MC-type carbides have been achieved in the alloy as shown in Figure 6.55.

Several experimental modified Hastelloy Alloy N compositions listed in Table 6.18 were irradiated in the MSRE. The creep properties of these alloys are compared with those of standard Hastelloy Alloy N in Figure 6.56. The rupture lives of the irradiated, modified alloys are about equivalent to those of unirradiated standard Hastelloy Alloy N. The creep rates are lower for the modified alloys by as much as a factor of 3. Heats 67-502 (0.49 percent Ti) and 67-504 (0.50 percent Hf) have the lowest creep rates. Quite a range of fracture strains resulted with a minimum of about 0.5 percent for standard Hastelloy Alloy N and a minimum of about

Table 6.17

Chemical Composition of Standard and Modified Hastelloy Alloy N

Element	Concentration, Weight Percent[a/] Standard Alloy	Modified Alloy
Nickel	Balance	Balance
Molybdenum	15.0-18.0	11.0-13.0
Chromium	6.0-8.0	6.0-8.0
Iron	5.0	5.0
Carbon	0.04-0.08	0.04-0.08
Manganese	1.0	0.2
Silicon	1.0	0.1
Tungsten	0.5	0.1
Aluminum		0.1
Titanium	0.5	2.0
Copper	0.35	0.1
Cobalt	0.20	0.2
Phosphorus	0.015	0.015
Sulfur	0.020	0.015
Boron	0.010	0.0010
Others, total	0.50	-
Hafnium		1.0
Niobium		2.0

a/ Single values are maximum concentrations.

Fig. 6.55. Transmission Electron Photomicrograph of 0.7% Hafnium-Modified HASTELLOY alloy N.

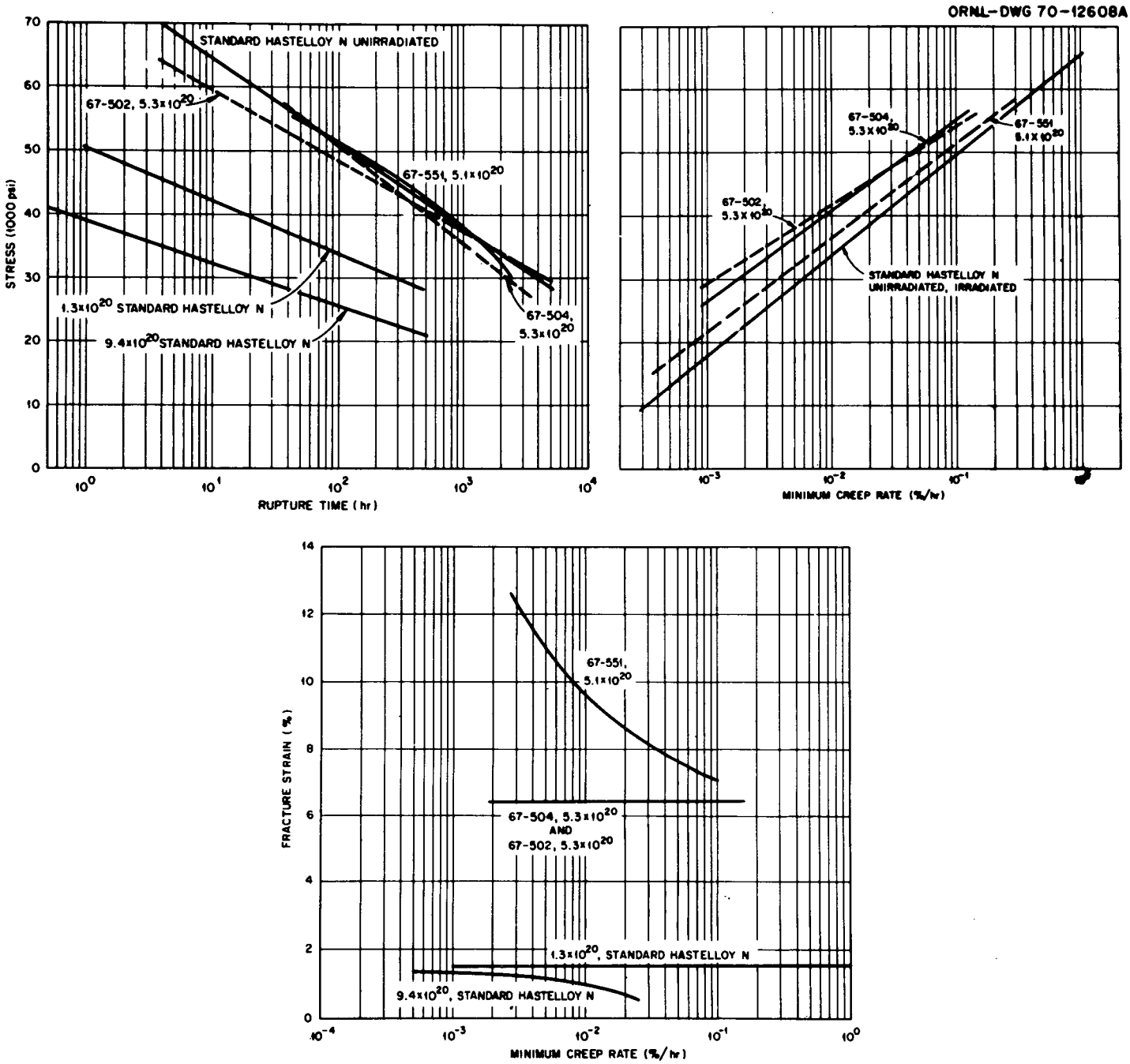

Fig. 6.56. Creep Properties at 1200° F of Several Modified HASTELLOY alloy N Compositions after Irradiation in the MSRE at 1200° F.

Table 6.18

Chemical Analysis of Modified Hastelloy Alloy N Compositions Irradiated in MSRE

Element	Analysis, Weight Percent		
	67-502	67-551	67-504
Cr	7.18	7.0	6.94
Fe	0.034	0.02	0.05
Mo	12.0	12.2	12.4
C	0.05	0.028	0.07
Si	0.015	0.02	0.01
Co	0.02	0.03	0.02
W	2.15	0.001	0.03
Mn	0.14	0.12	0.12
V	0.06	<0.001	0.01
P	0.001	0.0006	0.002
S	<0.002	<0.002	0.003
Al	0.02	<0.05	0.003
Ti	0.49	1.1	<0.02
Cu	0.04	0.01	0.03
O	0.0002	0.0004	<0.0001
N	<0.0001	0.0003	0.0003
Zr	<0.01	<0.01	0.01
Hf	<0.01		0.50
B	0.0001	0.0002	0.00003

6.5.11 Modified Hastelloy Alloy N (Cont'd)

7 percent for heat 67-551 (1.1 percent Ti). Heats 67-502 (0.49 percent Ti) and 67-504 (0.50 percent Hf) had fracture strains of 6.4 percent.

None of the modified alloys have shown any adverse corrosion behavior in the salt. Thus, it would appear that several alloys hold promise for use in future molten-salt reactors that operate at 1200°F. However, these new alloys are very sensitive to irradiation temperature and the proposed 1300°F operating temperature of a breeder is too high for these alloys. Nevertheless, present work offers encouragement that an alloy that is stable at 1300°F can be developed by adding larger amounts of titanium or combined amounts of titanium, columbium, and hafnium.

Since modified Hastelloy Alloy N is in the experimental stage, it is not commercially available. Once the chemistry of the alloy has been finalized, the next step in the development of the material would be to establish industrial scale practices. This would involve the preparation of commercial size heats of the alloy to work out melting and casting procedures, and fabrication processes. It would be very desirable to produce the complete range of mill products required for construction of a reactor, such as heavy plate, sheet, bar, wire, pipe, and tubing. Property determinations should be made on these products. Evaluation of several heats would be desirable for establishing reproducibility. Furthermore, data will be required for presentation of the modified alloy in a code case for its acceptance as a vessel material for nuclear applications. It is very probable that documentation of the radiation damage resistance will be necessary before the modified alloy can be accepted as a material of construction.

7.0 MSR NUCLEAR CHARACTERISTICS

7.1 Unique Features of MSR's

Because the fuel is not in solid form, its composition can be adjusted, within limits, during operation. Thus, it is not essential that the critical mass be known precisely in advance of start-up. Criticality will be approached by slowly dissolving UF_4 in the salt, and if critical mass predictions are somewhat in error, the consequences are not serious.

Similarly, if the fraction of neutron absorptions in ^{232}Th is found to be in error due to imprecise cross sections or the method of analysis, the error can be corrected by adjusting the ^{232}Th concentration.

Because MSR's have the flexibility of altering the fuel composition readily, they can be operated on U or Pu either as converters or breeders.

Critical assemblies for MSR's are not necessary for determination of critical mass. They are useful, however, for experimentally determining neutron spectra, for determining control rod worths, and temperature coefficients of reactivity.

7.2 Figures-of-Merit

The breeding ratios and fissile inventories for the reactor concepts described in Section 3.0 are based on an optimum conservation coefficient.

The conservation coefficient CC is defined by:

$$CC = (B-1)P^2$$

where B = breeding ratio (total number of fissile atoms produced per fissile atom destroyed - ^{233}U, ^{235}U, ^{239}Pu, and ^{241}Pu)

P = specific power (MWt/kg-fissile).

The significance of the conservation coefficient is as follows: Consider a growing economy based on a single concept of nuclear power (i.e., either MSBR's, LMFBR's, or GCFBR's). If the nuclear power industry is growing linearly, then the reactor concept having the largest conservation coefficient will require the least amount of uranium to be mined before the growth rate becomes self-sustaining via breeding. As implied by the mathematical definition above, it is desired to have a large breeding ratio together with a low fissile inventory to attain a large CC.

Other figures-of-merit are worthy of consideration. The doubling time is frequently used. A small doubling time, together with a large fissile inventory may not, however, make the most efficient use of uranium resources.

7.3 Calculational Models

7.3.1 Geometry

ORNL has developed a special purpose neutron diffusion code ROD (Reactor Optimum Design) for analysis of MSR's. This code will accommodate spherical (R) or cylindrical (RZ) geometry. The RZ calculation, however, is not rigorous in that it does not solve the 2D neutron diffusion equations. Instead it synthesizes RZ geometry by coupling a radial calculation of an infinite cylinder with an axial calculation of an infinite slab via a buckling iteration procedure.

Although ROD does not permit completely general 2D geometry, it can accommodate a wide variety of multi-region reactor configurations. Virtually all practical MSR geometries can be represented quite well, including radial and axial blankets and reflectors, inlet and outlet plena, and a cylindrical vessel with flat heads. Dished heads cannot be represented.

ORNL generally uses nine energy groups shown in Table 7.1. Four coupled thermal groups are used to accommodate the effects of thorium resonances upon the spectrum of low

Table 7.1

NEUTRON ENERGY GROUPS FOR
MULTI-GROUP DIFFUSION CALCULATIONS

Group	Energy Range, ev
1	$14.9 - 0.820 \times 10^6$
2	$8.2 - 0.318 \times 10^5$
3	$3.18 - 0.123 \times 10^4$
4	$1.23 - 0.0478 \times 10^3$
5	$4.78 - 0.186 \times 10^1$
6	1.86 - 0.768
7	0.768 - 0.180
8	0.180 - 0.060
9	0.060 - 0.00474

7.3.1 Geometry (Cont'd)

energy neutrons. The multi-group constants are generated by a 1D transport code, XSDRN. This code performs cylindricized cell calculations using a 123-group cross section library. The 123-group structure is then collapsed to nine groups. This calculation is done for each reactor zone (material mixture). Resonance integrals are calculated by the Nordheim treatment which requires a value for the probability that epithermal neutrons will escape from the fuel to the moderator region. This value is calculated for the cell geometry, determined by the graphite element configuration, by a Monte Carlo code, RAFFLE. If reflective boundary conditions are applied to the cell, the effect of neutrons born in one fuel lump and suffering their first collision in an adjacent fuel lump is accounted for rigorously. Dancoff correction factors are, therefore, zero.

The special feature in ROD which makes it especially useful for MSR analysis is its provision for computing the equilibrium salt (and graphite) composition. The equilibrium composition is required for predicting equilibrium nuclear performance.

7.3.2 Approach to Equilibrium

With start-up on ^{235}U or Pu and conversion to the Th-^{233}U cycle, high power density cores approach steady state nuclear performance after about four years of operation. Thus steady state performance does not differ significantly from the average over the plant life and steady state operation is an acceptable basis for accessing potential performance. Low power density cores equilibriate more slowly. Equilibrium nuclear performance occurs essentially when ^{233}U reaches its steady state concentration. Other heavy isotopes will continue to build up over the life of the plant but have little effect on the nuclear performance. All important parasitic absorbers equilibriate within a few months. Thus,

7.3.2 Approach to Equilibrium (Cont'd)

if an MSR were started up on its equilibrium fuel, steady state performance would be reached very early in plant life.

Steady state nuclear performance occurs when, for each isotope, the total production rate from all sources equals the total loss rate from all removal mechanisms. The source terms are:

1 - Feed (fresh and recycle)

2 - Nuclear transmutation

3 - Radioactive decay

The removal mechanisms are:

1 - Chemical removal (salt discard and chemical processing)

2 - Burnup

3 - Radioactive decay

It is instructive to consider these mechanisms as they pertain to the buildup and saturation of three important isotopes: ^{135}Xe, ^{233}Pa, and ^{233}U.

a - ^{135}Xe

The fission product ^{135}Xe is produced by direct fission yield and by decay of ^{135}I which, in turn, is produced by the decay of ^{135}Te. ^{135}Te quickly decays with a short half-life (11 sec) to ^{135}I. Hence, ^{135}Te will reach its equilibrium concentration very quickly. The equilibrium concentration of ^{135}Te will be such that its decay rate equals its production rate and only negligible amounts will be removed by burnup or chemical processing. ^{135}I (6.7 hr half-life), however, builds up to a much higher concentration because of its longer half-life. Although a small fraction of ^{135}I is removed by chemical processing, most of it decays in the fuel salt. Very little is destroyed by neutron capture.

7.3.2 Approach to Equilibrium (Cont'd)

a - ^{135}Xe (Cont'd)

Because of its large neutron absorption cross section, the effective lifetime of ^{135}Xe in the primary system would be controlled by burnup if it were not purged from the salt. In order for the xenon extraction system to dominate burnup as a removal mechanism, it must give rise to a removal time of about 50 sec. In this case the time required for the xenon to reach its equilibrium concentration in the salt would be controlled by the build-up rate of ^{135}I. Hence, the equilibrium ^{135}Xe concentration will be reached within several half-lives of ^{135}I, or roughly one day of steady power operation. More will be said later about xenon transients in Section 12.5.

The daughter product ^{135}Cs (2.3×10^6 yr half-life) is removed by chemical processing but also accumulates in the reactor graphite because of a small portion of the xenon which diffuses into the graphite and decays there. Although Cs alone does not significantly influence the neutron balance, it together with noble metals and other fission products build up to a level where they do make a small effect. Neutron absorptions in slowly saturating materials is accounted for by introducing a lumped absorber whose average value is based on the build-up rate on graphite and the useful graphite lifetime.

b - ^{233}Pa

^{233}Pa, having a half-life of 27.0 days, approaches its equilibrium inventory in the chemical plant after several months of operation. In the primary system, however, protactinium experiences a mean lifetime of only ten days; hence, its concentration in the fuel salt buildup to 88 percent of equilibrium in about one month.

7.3.2 Approach to Equilbrium (Cont'd)

c - ^{233}U

Consider the time required for conversion from the start-up fuel (^{235}U or Pu) to equilibrium operation with ^{233}U as the principle fuel. It is a reasonable approximation to assume ^{235}U or ^{239}Pu burns out and bred ^{233}U builds up exponentially. A 1000 MWe plant operating at 44 percent thermal efficiency produces about 2300 MWt. Assuming one gram of fissile burns per MWD, 2.3 kg/day of fissile are burned in this MSBR. If the reactor has a breeding ration near unity[1/], then approximately 2.3 kg/day of bred fuel are produced. This rate of burnup is related to an effective fissile decay constant λ_e and inventory I by, 2.3 kg/day = $\lambda_e I$.

Thus smaller cores have smaller inventories and larger values for λ_e. A moderately high power density core having a four-year graphite lifetime will have a fissile inventory of about 1500 kg. The equation above yields a value for λ_e of about 0.00187/day, or an atom half-life of about 1.5 years (at 0.8 plant factor). Approximately three half-lives or four years is required for the ^{233}U to reach 88 percent of its steady state concentration. A very low power density concept which requires no graphite replacement has an inventory of about 2300 kg and will approach equilibrium after about seven years of operation. The concept of a single fluid core with a separate blanket salt may have a fissile inventory of only 900 kg. This concept would equilibriate in less than three years.

1/ ORNL calculations show that both low and high power density cores operating on an equilibrium ^{232}Th-^{233}U cycle can have breeding ratios in the range of 1.05-1.07. Although the initial breeding ratio with start-up on ^{235}U or Pu may be as low as 0.8, it quickly builds up and exceeds unity within two years of operation.

7.3.2 Approach to Equilbrium (Cont'd)

c - ^{233}U (Cont'd)

The equilibrium concentration of ^{234}U and ^{236}Pu occurs much more slowly; but because they contribute very little in the neutron balance, equilibrium performance is essentially established when ^{233}U approaches equilibrium.

7.3.3 Calculation of Equilibrium Salt Composition

The nuclear characteristics of an MSR influence the equilibrium salt composition to the extent that the neutron flux and spectrum affects isotope transmutation and burnup rates. Conversely, the salt composition affects the nuclear performance. Thus, to determine the nuclear performance, it is necessary to perform a steady state composition calculation, a neutron diffusion calculation, and to iterate between these until they converge. When converged, the nuclear calculation will apply to the steady state salt composition and the steady state salt composition will be consistent with isotope production and burnup rates as determined by the neutron diffusion calculation. ROD was developed to perform this iteration procedure automatically. The iteration procedure is as follows:

1 - An initial guess of the salt composition and the salt fraction is specified. Similarly, the composition of graphite and Hastelloy N are also specified but these values are treated as constants.

2 - Isotope removal times (based on the salt throughput and isotopic removal efficiency) are specified to account for salt cleanup by the purge-gas and chemical processing systems.

3 - A nuclear diffusion calculation is performed to determine the critical fuel concentration and isotope transmutation rates.

7.3.3 Calculation of Equilibrium Salt Composition (Cont'd)

4 - An equilibrium composition calculation updates the salt composition by solving the steady state rate balance equations (one equation for each isotope). The fuel concentration is also adjusted to retain criticality and satisfy equilibrium requirements.

5 - This new salt composition is used in another neutron diffusion calculation to calculate improved transmutation and burnup rates.

This iteration procedure continues until convergence, i.e., isotope production rates calculated by the neutron diffusion code are consistent with the equilibrium criteria. The final diffusion calculation yields group fluxes and isotope reaction rates. ROD is capable of treating 50 isotopes explicitly. Each of these isotopes must satisfy the equilibrium convergence criteria. In addition, ROD will treat 200 isotopes of low importance. These isotopes, mostly fission products, are lumped into groups which behave similarly chemically and, therefore, have similar removal times. The relative concentrations of isotopes within a group is about constant so that group average production rates and group average neutron cross sections can be defined. Each group is then treated as one of the 50 isotopes receiving explicit treatment. Each of the individual isotopes assigned to a group is not required to equilibriate.

7.3.4 Comparison of ROD with CITATION

Because ROD synthesizes two dimensions by incorporating a buckling iteration technique which has no proven mathematical basis, it is necessary to establish the validity of ROD calculations by comparing ROD calculations with a true 2D calculation. Satisfactory agreement suggests that the buckling iteration technique in ROD is sufficient for MSR calculations. Table 7.2 presents a comparison of ROD with CITATION (2D

Table 7.2

Comparison of ROD and CITATION Calculations
of the Single-Fluid 1000-MWe MSBR Reference Design

	CITATION	ROD	Difference
Identification: CC58			
Breeding ratio (excluding processing loss)	1.0661	1.0647	-0.0014
Peak damage flux, 10^{14} neutrons cm^{-2} sec^{-1} (E > 50 kev)	3.42	3.20	-0.22
Peak power density, w/cm^3	69.1	65.2	-3.9
Neutron balance, absorptions			
^{232}Th	0.9904	0.9889	-0.0015
^{233}Pe	0.0017	0.0017	
^{233}U	0.9248	0.9248	
^{234}U	0.0811	0.0809	-0.0002
^{235}U	0.0752	0.0752	
^{236}U	0.0085	0.0085	
^{237}Np	0.0059	0.0059	
^{9}Be	0.0071	0.0071	
^{7}Li	0.0160	0.0160	
^{6}Li	0.0023	0.0023	
F	0.0206	0.0206	
Graphite	0.0517	0.0522	+0.0005
Fission products	0.0196	0.0196	
Delayed neutrons lost	0.0032	0.0032	
Leakage	0.0234	0.0244	+0.0010
Sum ($\eta\epsilon$)	2.2315	2.2316	+0.0001

Ref: ORNL 4449 - MSRP Semiannual Progress Report, August 31, 1969, sections by H. F. Bauman and W. R. Cobb.

7.3.4 Comparison of ROD with CITATION (Cont'd)

diffusion theory) for a 1000 MWe single fluid MSBR. Those results suggest that ROD underpredicts the peak fast neutron flux and the peak power density by about 6 percent. The neutron balances, however, are in remarkable agreement. Both calculations had a common basis in that they both used the equilibrium salt composition computed by ROD, the same neutron cross sections and nearly the same geometry. The difference in geometry is that CITATION incorporated the curved top and bottom heads whereas ROD treated the heads as if they were flat.

The agreement indicated in Table 7.2 is more than adequate. Thus, there is no reason to dispute the calculational model or methods used in ROD. The possibility remains, of course, that both calculations are in error due to a common error in the input data. This possibility can never be completely discredited until these calculated results are verified by independent calculations performed by other workers who compiled the input data from independent sources and use different codes. As yet, calculations having this level of independence have not been performed. The molten salt group has examined the ORNL calculations in detail, and it appears that the physics calculations are correct and adequate for predicting MSR nuclear performance.

Because of ROD's ability to calculate equilibrium salt compositions automatically, it has been the main computational tool for MSR analysis.

7.4 Comparison of MSRE Calculations with Experimental Data

Physics calculations[1/] for MSRE predicted a critical concentration of ^{235}U at zero power of 32.77 gm/l-salt at 1181°F. This is in excellent agreement with the book value, based on weighted amounts

1/ B. E. Prince, "Zero-Power Physics Experiments on the Molten Salt Reactor Experiment," USAEC Report ORNL-4233, Oak Ridge National Laboratory, February 1968.

7.4 Comparison of MSRE Calculations with Experimental Data (Cont'd)

of ^{235}U added to the salt, of 32.8 $\pm$ 0.3 gm/l and the analytical value, based on chemical analysis of the salt, of 32.4 $\pm$ 0.3 gm/l. No arbitrary normalization of the calculations was done.

Calculated and measured control rod worths agreed to within 10 percent and the concentration coefficient of reactivity for ^{235}U was within 5 percent.

The preceding results demonstrate excellent calculational capability for MSR's containing no fission products or other reactivity effects resulting from power production.

The observed and calculated temperature coefficient of reactivity agreed to within 20 percent. This result is entirely satisfactory since there are several uncertainties in the model and potential sources of error in the calculation.

The reactivity loss due to transport of delayed neutron precursors was not predicted well initially because of an oversimplified model. As a result of this discrepancy, the model was upgraded to account for delayed neutrons emitted in inlet and outlet plena. The more complete model produces much better agreement yielding 0.222 percent $\Delta k/k$ (stagnant salt with respect to full flow) compared with the observed value of 0.217 $\pm$ .004 percent $\Delta k/k$.

Reactor kinetics experiments using neutron noise analysis and cross correlation techniques with pseudo-random reactivity perturbations gave qualitative agreement with theory and indicated a high degree of stability.

In sum, these results demonstrate excellent capability for calculating MSRE-type reactors.

7.5 Comparison of MSRE and MSBR Calculations

MSBR calculations will differ in several ways from MSRE calculations.

7.5 Comparison of MSRE and MSBR Calculations (Cont'd)

7.5.1 Neutron Leakage

First, the larger core size of the MSBR means less neutron leakage. Since the purpose of the buckling iteration scheme used in ROD is to synthesize radial and axial neutron leakage, this approximation will be better for MSBR's than for MSRE simply because leakage is less important.

7.5.2 Effect of ^{232}Th

Unlike MSRE, MSBR's will contain ^{232}Th which absorbs more neutrons than any other isotope. Neutron flux depressions will occur in the flow channels, particularly in the energy range of the ^{232}Th resonances. To account for this strong self-shielding effect the calculational models described in Section 7.3 are used. The Nordheim method of evaluating resonance integrals, the application of multi-group transport theory to calculate cell-averaged cross sections, and four thermal groups permitting up-scattering in the neutron diffusion calculations is entirely adequate for MSBR calculations. Nevertheless, the presence of Th in the salt represents a significant departure from MSRE.

7.5.3 Fission Product Distribution

Fission product behavior was not important in MSRE because neutron economy was of little interest. The purpose of MSRE was to demonstrate the concept of a circulating fuel reactor and the compatibility of materials. A 1000 MWe MSBR will produce more fission products in a few days than MSRE produced in its entire life.

The behavior of fission products can influence the breeding gain of an MSBR substantially. Thus, it is important to be able to predict fission product behavior.

The concentration of fission products which stay in the salt can be predicted easily. Fission gases can enter the graphite and ^{135}Xe can absorb a significant fraction of the neutrons.

7.5.3 Fission Product Distribution (Cont'd)

The mass transfer coefficients and models used for predicting xenon transfer to the graphite are quite uncertain. It has been assumed by ORNL, however, that fission gas poisoning can be maintained at a value of 0.005 in the neutron balance (i.e., 0.005 neutron absorptions in fission gas, primarily ^{135}Xe, per neutron absorption in fissile isotopes. This amounts to a loss of 0.005 in breeding ratio). It is known that with no fission gas removal the poison fraction will be 0.05. With xenon stripping and/or graphite sealing it appears entirely reasonable that it can be reduced to about 0.005. This value has been assumed in the physics calculations presented in Table 7.2.

Noble metals and semi-noble metals are assumed to collect on all exposed surfaces, enter the chemical process plant, and enter the off-gas system. Their behavior is largely speculative. The uncertainty this introduces into the neutron balance, however, is not large. In the calculations presented in Table 7.2 it was assumed that 10 percent of the noble metals accumulate on core graphite. Based on a four-year graphite lifetime, the average loss in breeding ratio is 0.004.

7.6 Steady State Physics Characteristics

7.6.1 Neutron Balance for a Typical MSBR

Table 7.2 presents the neutron balance for a 1000 MWe single-fluid MSBR. It can be seen that graphite is the most significant parasitic neutron absorber. Following in importance is fluorine, fission products and ^{7}Li. A reduction in the graphite fraction (from 87 volume%) reduces the absorptions in graphite but increases absorptions in fluorine and lithium. It also hardens the neutron spectrum which, in turn, requires a greater concentration of fissile material. The overall effect of reducing the graphite fraction is a degradation of the conservation coefficient.

7.6.1 Neutron Balance for a Typical MSBR (Cont'd)

It is also apparent from Table 7.2 that ^{234}U absorbs a substantial fraction of the neutrons. ^{234}U is produced by neutron capture of ^{233}Pa and ^{233}U. In the MSBR spectrum 10.8 percent of the neutron absorptions in ^{233}U are captured. Thus, it is apparent from the neutron balance that most of the ^{234}U is produced by ^{233}U capture rather than ^{233}Pa capture. This is so because ^{233}Pa is removed from the salt by chemical processing. Without such processing the conversion ratio would be substantially less than unity. The magnitude of neutron losses to ^{234}U indicated in Table 7.2 is an intrinsic characteristic of the Th cycle in which ^{233}Pa is continuously removed from the salt and maintained at a low concentration.

Leakage accounts for substantial neutron losses in the single-fluid concept. A concept employing a single-fluid core surrounded by a separate fertile blanket salt would have much less neutron leakage because very few fissions would occur in the blanket. Elimination of neutron leakage could, in principle, increase the breeding ratio to about 1.08. By eliminating fuel from the blanket salt the fuel inventory can be greatly reduced and, hence, the doubling time decreased to as little as 12 years. Of course, the primary objection to this alternative is the requirement for keeping the core and blanket salts separate.

7.6.2 Effect of Chemical Processing

The neutron balance and, hence, nuclear performance is affected substantially by the rate and efficiency of chemical processing, the removal rate of ^{135}Xe, and neutron leakage. Figure 7.1 shows the effect of ^{233}Pa and rare earth removal times on chemical processing. It can be seen that the breeding ratio falls by about 0.06 from the curve for a three-day removal time to the curve for a 3000-day removal

7.6.2 Effect of Chemical Processing (Cont'd)

time. The curve for a three-day removal time is nearly identical to that for instantaneous removal because with a three-day removal time ^{233}Pa absorbs a negligible fraction of neutrons. The curve for a 3000-day removal time corresponds to essentially no removal because most of the ^{233}Pa atoms decay or absorb neutrons.

Figure 7.1 also shows the effect of rare earth removal rate on breeding ratio. It is likely that rare earths and ^{233}Pa will be extracted from the same salt stream. If the salt stream is sized for, say, a 10-day cycle time for ^{233}Pa, assuming that essentially all Pa is extracted from the stream then it is possible to extract rare earths also with a 10-day cycle. But because rare earths are not extracted as easily as Pa, only a portion will be removed from the stream. Thus the effective rare earth removal time will be greater than 10 days. It is reasonable, however, to achieve a rare earth removal in the range 25-50 days. Thus a breeding ratio over 1.05 appears feasible.

Without any chemical processing the reactor cannot operate as a breeder. Without chemical processing and with ^{235}U as feed, the conversion ratio will be 0.85-0.90. It will be somewhat higher with Pu feed.

7.6.3 Effect of Fission Gas Removal

To reduce neutron losses to ^{135}Xe to a level comparable to neutron losses to other parasitic absorbers (e.g., ^{237}Np, ^{238}Pa, and Sn) it is necessary to remove about 90 percent of the xenon from the salt. That is the removal rate must be about 90 percent of the production rate. This requirement seems attainable by introducing helium bubbles into the salt. These bubles absorb xenon and other volatiles. By continuously injecting fresh bubbles which survive about ten passes before removal, it appears that this target can be attained. In the 1000 MWe Reference Concept,ORNL estimates that ^{135}Xe

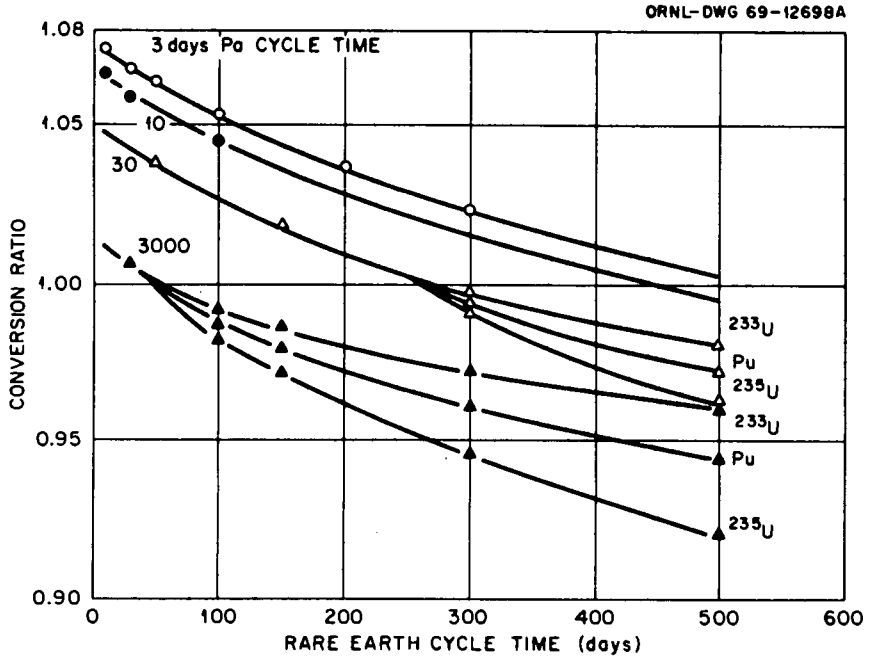

Fig. 7.1. Conversion ratio of a single-fluid MSBR as a function of processing cycle times and feed materials. The plutonium feed composition was assumed to be ^{239}Pu = 60%, ^{240}Pu = 24%, ^{241}Pu = 12%, and ^{242}Pu = 4%. Other parameters were held fixed at reference design values.)

7.6.3 Effect of Fission Gas Removal (Cont'd)

poisoning will amount to 0.005 in the neutron balance table (i.e., 0.005 absorptions in ^{135}Xe per absorption in fissile) with 90 percent removal. With no xenon removal the poison fraction would be 0.05 and virtually reduce the nuclear performance to a break-even converter.

7.6.4 Effect of Reactor Size

Neutron leakage is quite significant as indicated by the neutron balance in Table 7.2. If all leakage could be eliminated, the breeding gain would increase by about 0.02. Figure 7.2 and Table 7.3 show the effect of reactor size, i.e., leakage on nuclear performance. It is evident that below 1000 MWe the breeding gain decreases substantially. The blanketed concept mentioned above would obviously perform much better. Figure 7.2 shows that a 4000 MWe single-fluid reactor could have a breeding ratio over 1.08. In addition, it would have a lower specific inventory and a much shorter fuel doubling time.

7.7 Rationale for Choice of Design Parameters

The variable design parameters are:

a - ^{233}Th concentration in fuel salt

b - Graphite lifetime, determined by peak fast flux and, thus peak power density

c - Salt fraction of core and blanket regions

d - Region dimensions

Ideally each of these parameters would be chosen to maximize the desired figure-of-merit. Most, if not all, of ORNL's efforts have been oriented toward maximizing the conservation coefficient, CC.

7.7.1 Th Concentration

Figure 7.3 shows the effect of Th concentration on CC when all other parameters are optimized. It can be seen that the

Table 7.3

Performance of Single-Fluid MSBR's as a Function of Plant Size[a]

Reactor Power (MW(e))	500	1000	2000	4000
Core height, ft	9.44	11.0	17.44	23.0
Core diameter, ft	10.42	14.4	19.36	25.5
Salt specific volume, ft^3/MW(e)	1.75	1.68	1.62	1.55
Fuel specific inventory, kg/MW(e)	1.65	1.47	1.36	1.28
Peak power density, W/cm^3	62.2	65.2	66.1	65.9
Peak flux ($E > 50$ keV), 10^{14} neutrons cm^{-2} sec^{-1}	3.04	3.20	3.25	3.24
Core life, years at 0.8 plant factor	3.9	3.7	3.7	3.7
Leakage, neutrons per fissile absorption x 100	3.89	2.44	1.53	0.96
Breeding ratio	1.043	1.065	1.076	1.083
Annual fuel yield,[b] %/year	1.99	3.34	4.28	4.95
Conservation coefficient	8.0	15.1	21.0	25.9

a/ The thickness of core zone II, annulus, plenums, reflectors, and other parameters not otherwise indicated were held fixed at the reference design values indicated in Table 3.1.

b/ The plant factor is assumed to be 0.80.

ORNL-TM-4541 p.35

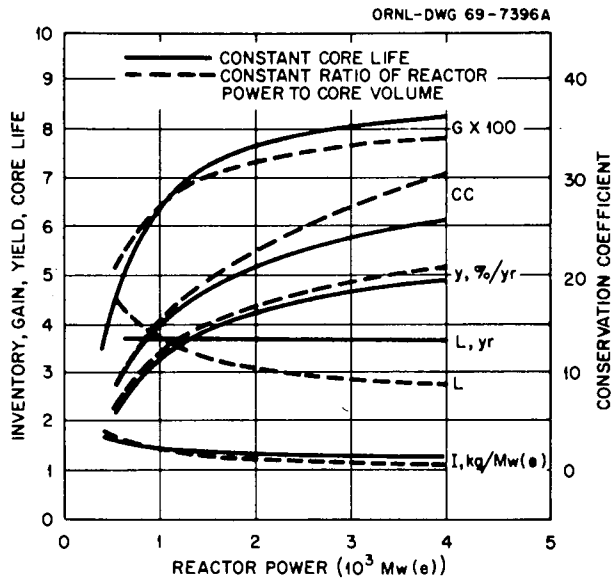

Fig. 7.2. Effect of Plant Size on MSBR Performance

ORNL-TM-4541 p.32

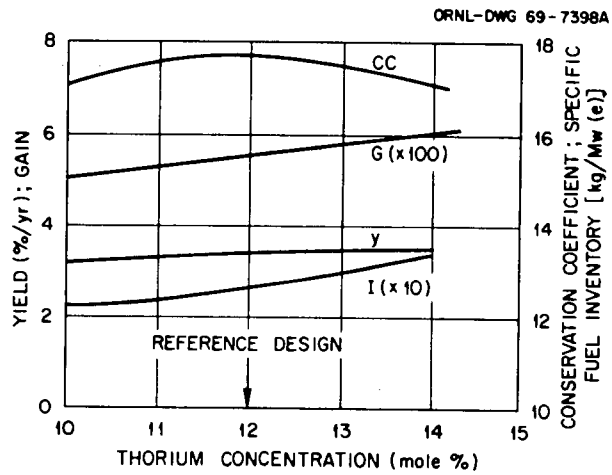

Fig. 7.3. Influence of thorium concentration on the performance of a single-fluid MSBR

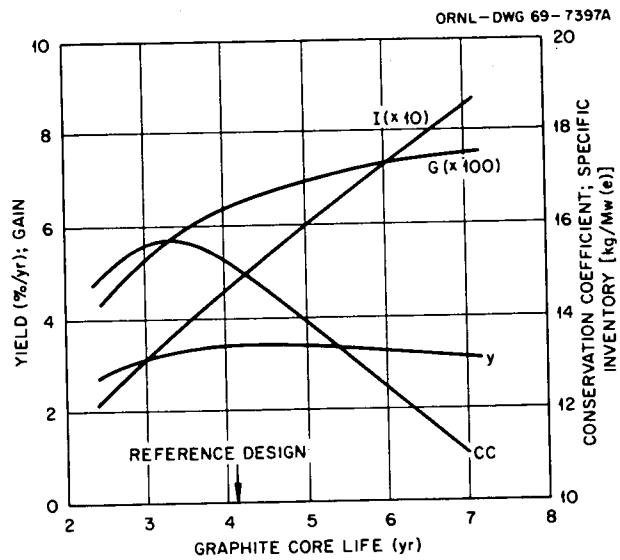

Fig. 7.4. Performance of a 1000 MWe MSBR as a function of core life (at 0.8 plant factor).

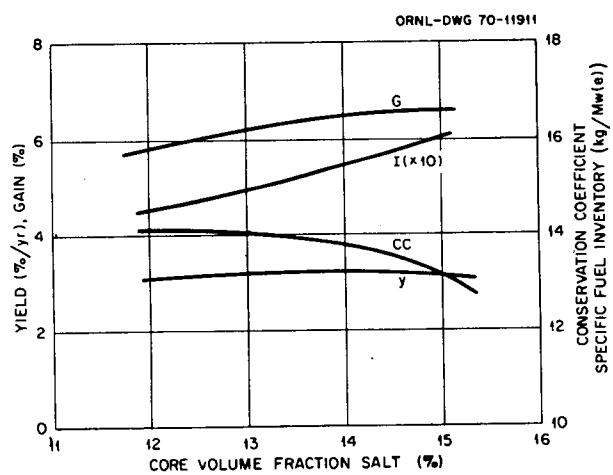

Fig. 7.5. Effect of core salt fraction on MSBR Performance. (Other parameters are held fixed at Reference Concept Values.)

7.7.1 Th Concentration (Cont'd)

optimum choice is about 12 mole percent. Although a greater concentration reduces neutron losses to parasitic absorbers, it requires a greater fissile inventory and, overall, a degradation in CC. Conversely, a smaller concentration permits a reduction in fissile inventory but this benefit is more than compensated by increased parasitic losses.

7.7.2 Graphite Lifetime

Figure 7.4 shows the effect of graphite lifetime, or more properly, peak power density for reactors producing a fixed amount of power. As suggested by the figure, small high power density cores will suffer high neutron leakage. Thus, the breeding gain is low and the CC is less than optimum. Very large low power density cores have low leakage but large fissile inventories. The optimum graphite lifetime appears to be about 3.3 years. In order for the graphite replacement interval to coincide with turbine-generator maintenance and to be periodic a four-year lifetime appears more attractive. It can be seen that CC has a broad optimum and 4.0 years is near the optimum.

7.7.3 Salt Fraction

Figure 7.5 shows the effect of salt fraction in the core region upon the CC. It can be seen that the CC decreases noticeably for salt fractions greater than 13 percent. Other calculations show that a broad optimum exists between 11-13 percent. It is not clear from the figure that 13 percent is the best choice. However, a smaller salt fraction would require smaller flow channels or larger graphite elements. Smaller flow channels would require a greater pressure drop across the core and thus a stronger vessel. Larger elements would run at a higher temperature and, thus, have a shorter life. It appears, therefore, that the largest flow channel which does not penalize performance is best.

7.7.3 Salt Fraction (Cont'd)

A similar set of calculations of various salt fractions in the blanket regions shows a broad optimum between 30-60 percent. A choice near the low end of this range seems preferable in order to avoid excessive quantities of ^{7}Li.

7.7.4 Region Dimensions

The dimensions of the core are set partly by the maximum permissible fast flux for a specified graphite temperature and lifetime. In addition, the power distribution and the fraction of power generation outside the core influence the core dimensions. The core and blanket dimensions are chosen for optimum CC subject to the constraints on total power and peak fast flux. The inlet and outlet plena, however, are chosen to provide adequate flow distributions with little regard to the CC. The reflector must be thick enough to reduce the heat load on the vessel (resulting primarily from gamma heating) to an acceptable level with adequate margin for uncertainties. Excessive reflector thickness causes the vessel to be unnecessarily large.

7.8 Uncertainties in Physics Calculations

Aside from the behavior of fission products, ^{135}Xe in particular, most of the uncertainty in physics calculations arises from uncertainties in ^{233}U data. Table 7.4 shows the results of an uncertainty analysis performed by Perry[1/]. Although this analysis was performed for a two-fluid concept which has since been abandoned, the results are applicable to any MSBR having a similar neutron balance. The neutron balance for the concept analyzed is very similar to that in Table 7.2.

The table shows the parameters varied, the magnitude of the variation, and the effect on breeding gain. It is clear that $^{233}\eta$

1/ A. M. Perry, "Influence of Neutron Data in the Design of Other Types of Power Reactors," ORNL-TM-2157, March 1968.

Table 7.4

Effect of Data Uncertainties on MSBR Performance

Nuclide	Quantity	Assigned Value	Assigned Uncertainty	δBR
^{233}U	η_o	2.293 (1)	0.010	0.008
	η/η_o	~1	0.5% (2)	0.009
	ν	2.50	0.01	0.003
	α	0.18	0.01 (3)	0.006
^{235}U	η_o		0.010	0.001
	η/η_o	~1	0.5%	0.001
	ν	2.43	0.01	-
	α	0.50	0.02	0.001
^{234}U	σ_a		10%	0.001
^{236}U	σ_a		15%	0.001
^{19}F	$\sigma(n, \alpha)$		30%	0.003
^{19}F	$\sigma(n, \gamma)$ resonance		30%	0.002
^{19}F	$\sigma(n, \gamma)$ thermal		7%	0.001
^{9}Be	$\sigma(n, \alpha)$		10%	0.001
^{9}Be	$\sigma(n, \gamma)$		10%	-
^{9}Be	$\sigma(n, 2n)$		15%	0.002
Li	σ_a		10%	0.003
C	σ_a		10%	0.004
FP	σ_a (thermal)		10%	-
FP	σ_a (resonance)		30%	0.003

$$\left[\sum_i (\delta\ BR)_i^2\right]^{\frac{1}{2}} = 0.016$$

Reference: A. M. Perry, ORNL-TM-2157

1) $\eta_o = \eta$ (2200 m/sec).
2) Spectrum averaged uncertainty for $E < 0.5$ ev.
3) Spectrum averaged uncertainty for $E > 0.5$ ev.

is, by far, the major contributor to the total uncertainty. Assuming each entry in the table is independent, each of the terms are combined quadratically. Together they yield an uncertainty in breeding ratio of 0.016. The first two entries alone combine to yield 0.012.

Table 7.4 contains all important nuclides except ^{232}Th. ^{232}Th can be omitted because any error in cross section can be compensated by adjusting its concentration.

Three general conclusions are possible:

1 - The major source of uncertainty is ^{233}U data. The overall uncertainty is substantial - 27 percent of the breeding gain if the breeding ratio is 1.06.

2 - Contributions by all light isotopes together give rise to an uncertainty in breeding gain of 0.0073, or about 12 percent.

3 - The success or failure of the MSBR does not depend on physics. There is ample margin in breeding gain to accommodate the worst credible outcome of these uncertainties without losing the capability to breed.

8.0 FLUORINATION IN MOLTEN SALTS

8.1 Summary

The uranium fluorination system, called the "Fluoride Volatility Process," has been researched at ORNL since 1954. Sufficient laboratory work was done to permit the successful operation of a batch pilot plant to recover uranium from the molten salt (NaF-ZrF_4-UF_4) used in the Aircraft Reactor Experiment. The advantages of this process when compared to conventional aqueous processing routes are: (a) the small volume of fission product waste; (b) the convenient form of the UF_6 product which is easily converted to UF_4 for fuel recycle; (c) the virtual elimination of processing criticality hazards; and (d) the high decontamination factors attainable for the UF_6 product. The main disadvantage for this process is the extremely corrosive nature of the fluorine-molten salt mixtures at these high processing temperatures.

A simplified process flow sheet for a continuous fluorination process is shown in Figure 8.1. The fluorination process is divided into four parts, the fluorination system, the UF_6 decontamination system, the cold trap system, and the purge-gas system. This fluorination system described is applicable to all three fluorination sections in the chemical processing system, although the fluorination of the waste salt stream will probably be done batchwise.

Fuel salt (1) from the reactor is contacted with recycled fluorine gas in reactor (B) at 1 000-1 110°F (550-600 C), where the uranium is converted to the volatile UF_6 (3) according to Equation (1). The lower limit to the operating temperature is 930°F (500 C), the melting point of the fuel salt. Up to 99 percent of the uranium is removed here. The UF_6 enters into a decontamination system consisting of pelletized sodium fluoride (NaF) beds operating at various temperatures.

The UF_6 decontamination system consists of three NaF beds, one on the adsorption cycle, one on the desorption cycle, and one being

8.1 Summary (Cont'd)

refilled with fresh, low-surface area NaF pellets. The adsorption cycle has two temperature zones, 750 and 250°F. As the UF_6 and fluorine gas pass through the 750°F zone, fission product fluorides are irreversibly adsorbed on the NaF. When this gas passes through the 250°F zone, the UF_6 is reversibly adsorbed on the NaF. The fluorine gas is sent to a surge drum for recycle to the fluorinator (B) after addition of fresh makeup fluorine (2).

At the end of the adsorption cycle, the bed is heated to 300°F to begin the UF_6 desorption cycle. Recycle fluorine gas is used to desorb the UF_6 from the NaF and carry it to the cold trap system. The cold trap system also has three units, one condensing the UF_6 out of the fluorine gas, one vaporizing the condensed UF_6 for recovery, and one on standby.

The cold trap condensing the UF_6 has two temperature zones, -40 and -80°F. Most of the UF_6 condenses in the -40°F zone. The -80°F zone serves as a backup for any UF_6 that may pass through the -40°F zone. The fluorine gas passes through to the purge drum for recycle. For recovery of the UF_6 from the cold trap system, the unit is heated to 160°F where the UF_6 vaporizes and passes on to the fuel salt reconstitution section.

Since the fluroine is recycled, a buildup of volatile fission products will occur in the gas phase; hence, a small portion of the gas is purged from the surge drum. In order to insure against escape of UF_6, the purged gas is passed through a high surface area NaF adsorption system at 220°F prior to being purged to a gas waste disposal system. When this adsorption bed contains a significant amount of UF_6, the bed temperature is increased to 300°F with fluorine gas flow to desorb the UF_6 and transport it to the cold trap system. During this period, the standby adsorption tower is used to remove the UF_6 from the purge-gas stream.

8.1.1 Fluorination System

Both batch and continuous runs have been made in the laboratory with resonable success. One can conclude that

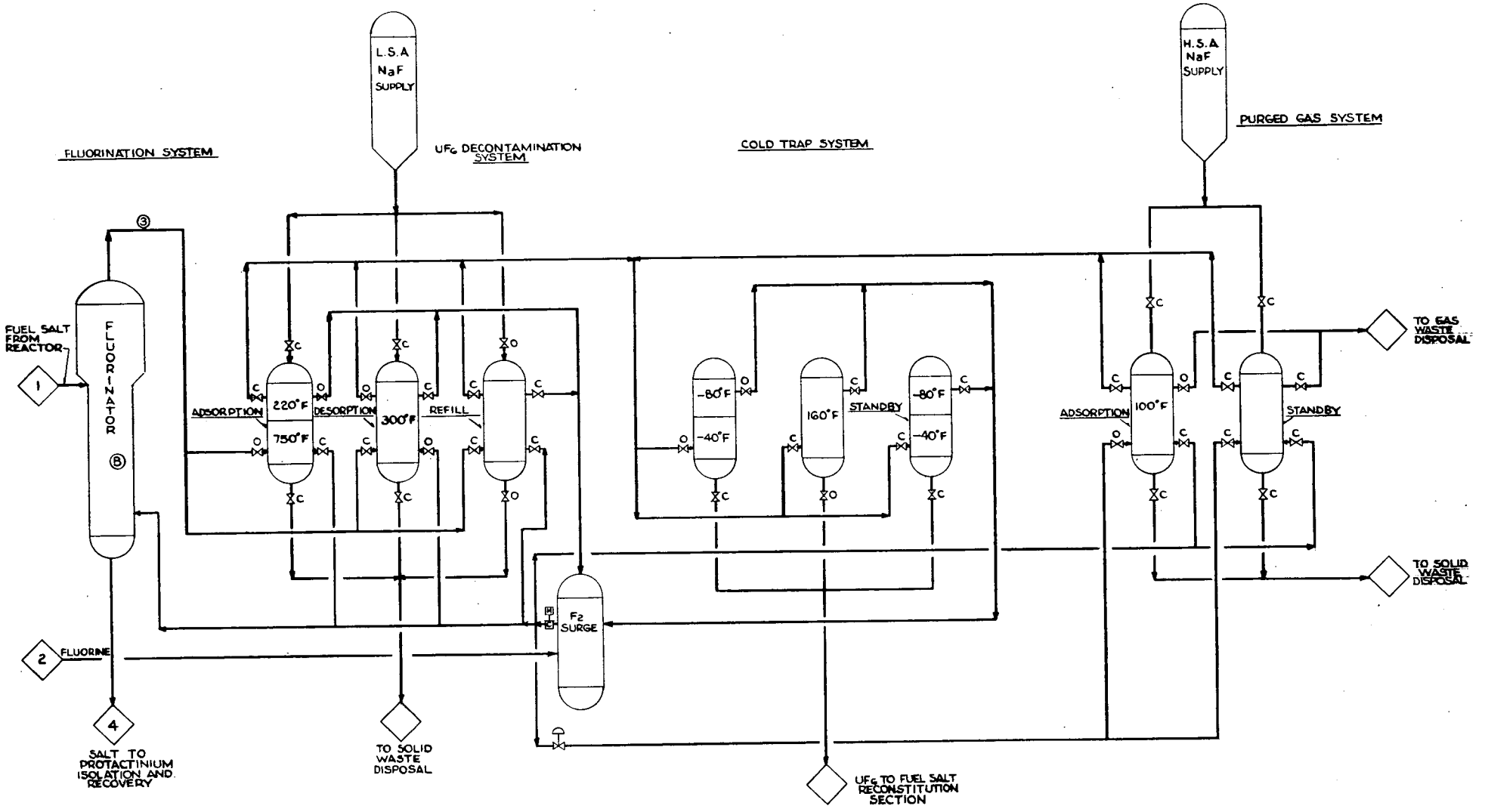

Fig. 8.1. Process Flow Sheet for Continuous Fluorination of Uranium in Molten Salt.

8.1.1 Fluorination System (Cont'd)

fluorination is technically feasible for recovering uranium from molten salts.

a - Reaction Mechanism

Interpretation of experimental results indicates the following reaction mechanism:

Dissolution of fluorine into the molten salt

$$F_{2(g)} \longrightarrow F_{2(salt)} \quad (1)$$

Conversion of UF_4 to UF_5 intermediate

$$UF_{4(salt)} + 1/2\ F_{2(salt)} \longrightarrow UF_{5(salt)} \quad (2)$$

Conversion of UF_5 intermediate to UF_6

$$UF_{5(salt)} + 1/2\ F_{2(salt)} \longrightarrow UF_{6(salt)} \quad (3)$$

Removal of UF_6 from salt

$$UF_{6(salt)} \longrightarrow UF_{6(g)} \quad (4)$$

Overall reaction

$$UF_{4(salt)} + F_{2(g)} \longrightarrow UF_{6(g)} \quad (5)$$

The dissolution of fluorine into the molten salt is probably the rate controlling step for the overall reaction. The existence of the UF_5 intermediate has been postulated from the experimental data. It is surmised that all the UF_4 will be converted to UF_5 before any significant UF_6 is formed if the fluorine is bubbled through a liquid bed height of 5 to 6 ft. At reaction temperatures of 1 000-1 110°F (550-600 C), the vapor pressure of the UF_6 is 680-850 atmospheres; therefore, the UF_6 will rapidly vaporize in the molten salt solution and pass into the fluorine gas phase.

Based on the per pass conversion of fluorine, the conversion of UF_4 to UF_5 is significantly faster than the

8.1.1 Fluorination System (Cont'd)

subsequent conversion to UF_6.

At the conditions used for fluorination, any plutonium fluoride formed as PuF_6 would not be expected to volatilize and exit the reactor with the fluorine gas stream. The ORNL experience indicates plutonium fluoride does not volatilize at these conditions.

b - Heat Generation

There are two sources of heat generation in the fluorination of uranium in molten salts, the heat of reaction and the fission product decay heat. The exothermic heat of reaction for Equation 5 is reported as 292,000 BTU/lb-mole at 1 022°F.

The fission product decay heat is dependent upon the elapsed time for the salt between the nuclear reactor and the fluorination reactor. In the reference design,[1/] this value is given as 191,500 BTU/hr-ft^3 salt.

c - Materials of Construction

Molten salt-fluorine mixtures are so corrosive at these temperatures that no known material of construction can contain these compounds. Where fluorine and molten salt are present, the equipment can be protected from corrosion by freezing a layer of salt on the vessel wall. This is accomplished by cooling the reactor wall. The heat necessary for maintaining molten salt adjacent to frozen salt is provided by the decay of fission products in the salt stream. The successful operation of a continuous fluorination system depends upon the heat balance that must be maintained in this reactor.

1/ ORNL-4541, June, 1971.

8.1.1 Fluorination System (Cont'd)

The area just above the frozen salt is very susceptible to corrosion. Great care must be exercised that the fluorine gas leaving the salt solution does not entrain any liquid. To do so may invite serious corrosion problems on the unprotected walls.

The protection of the fluorine inlet nozzle from corrosion is also a problem. A possible solution consists of introducing the fluorine through a short section of pipe which intersects the fluorinator at a 45° angle. This method of gas introduction appears feasible, but it will not produce small diameter gas bubbles that are desired in a mass-transfer limited reaction system.

In the absence of molten salt, the fluorine gas-bearing streams are contained satisfactorily by nickel or nickel-base alloys.

d - Volatile Fission Products

Some fluorides are volatile at the temperature used for fluorination of the molten salt. Table 8.1 lists the most probably volatile components of the molten salt stream along with their normal boiling points. Fewer volatile fission products will be encountered in the fluorination of uranium resulting from the decay of protactinium.

8.1.2 UF_6 Decontamination System

The NaF adsorption-desorption system for UF_6 decontamination has been operated successfully batchwise at the ORNL. The available information shows this system to be technically feasible and can operate on a continuous basis. Nickel or nickel-base alloys are satisfactory for this service.

a - Adsorption

The UF_6-fluorine-fission product stream passes through

Table 8.1

Volatile Fission Products From Molten Salt Fluorination

Compound	Boiling Point, °F, 1 Atm.
T_2	-423
Xe	-293
Kr	-243
CF_4	-198
TeF_6	-38
IF_7	+39
HF	67
TF	67
MoF_6	95
BrF_5	106
UF_6	130
PuF_6	144
CrF_5	243
SbF_5	300
NbF_5	443
RuF_5	518

8.1.2 UF_6 Decontamination System (Cont'd)

a two region adsorption bed containing low surface area NaF pellets: One region is maintained at a temperature of 750°F, the other at 220°F. The gaseous stream passes through the 750°F zone first where the fission product fluorides of niobium, ruthenium, and chromium are irreversibly adsorbed. At this temperature the UF_6 and other fission product fluorides are not adsorbed. Any PuF_6 is the gas stream, however, will adsorb on the NaF at this temperature. Also, any hydrogen and/or tritium fluorides present in the fluorine gas stream leaving the reactor will form an NaF · 2HF compound and will cause plugging in the system if temperatures are below 100°F.

The partially purified gas stream then passes through a low surface area NaF that is maintained at 220°F. At this temperature, the UF_6, neptunium, technetium, and part of the molybdenum fluoride will adsorb on the NaF. For the UF_6 the following occurs:

$$UF_{6(g)} + 2\ NaF_{(s)} \longrightarrow UF_6 \cdot 2\ NaF_{(s)} \qquad (6)$$

The iodine, bromine, tellurium, and part of the molybdenum fluorides will pass through the NaF bed and will be recycled with the fluorine gas. At 220°F, a small amount of UF_6 will also pass through the bed and be recycled with the fluorine gas.

Low surface area NaF (surface area of 0.07 m^2/g and void fraction of 0.28) is preferred to high surface area NaF (surface area of 1 m^2/g and a void fraction of 0.45) for the decontamination operation because of its higher capacity for UF_6. The maximum uranium loading was 0.56 lb UF_6/lb NaF for the low surface area variety versus 0.49 lb UF_6/lb NaF for the high surface area variety.

8.1.2 UF_6 Decontamination System (Cont'd)

There should be at least 2 volume percent fluorine in the gas stream to the adsorber to prevent the retention of uranium on the NaF due to the following reaction:

$$UF_{6(g)} + 2\ NaF_{(s)} \longrightarrow UF_5 \cdot NaF_{(s)} + 1/2\ F_{2(g)} \qquad (7)$$

The same precaution must be exercised for the UF_6 adsorption at 220°F. When the $UF_5 \cdot 2$ NaF product forms, it will not give up the uranium during the desorption cycle. Desorption of the UF_6 occurs by heating the NaF bed to 300°F and passing fluorine gas through the bed. The reverse of Reaction (6) occurs. Some fission product fluorides, e.g., molybdenum fluoride, also desorbs and passes on with the UF_6-fluorine stream.

The gas flow must contain at least 2 volume percent fluorine to prevent decomposition to the $UF_5 \cdot 2$ NaF complex as discussed above.

8.1.3 Cold Trap System

The UF_6 from desorption is collected in two cold traps connected in series. The primary trap is operated at -40°F, and the backup trap is operated at -80°F. The principal design consideration is heat transfer rate and minimum holdup of UF_6. A specially designed trap for minimum UF_6 holdup has been designed and operated successfully in the ORNL pilot plant. UF_6 removal is accomplished by heating the cold trap to 160°F to remove the UF_6 as a gas for further processing. Decontamination factors of 8.6×10^8 gross gamma activity and 1.2×10^9 gross beta activity have been experimentally achieved.

The fluorine gas stream from the cold trap contains some UF_6, molybdenum fluoride, and other components and is recycled to the system.

8.1.4 Purge-Gas System

A small amount of the recycle fluorine gas is purged to remove fission product fluorides that build up in the gas recycle. As a precaution, the exhaust gas is passed through a high surface area NaF adsorption bed held at ambient temperature to remove the last traces of UF_6 in the exhaust stream.

8.2 Processing of the Aircraft Reactor Experiment (ARE) Fuel[2/]

The highly enriched uranium used in the Aircraft Reactor Experiment was recovered in the Volatility Pilot Plant at Oak Ridge National Laboratory. This was the first time that a complete reactor charge was ever reprocessed by a nonaqueous technique.

8.2.1 Pilot Plant Description

The flow sheet used in these pilot plant studies is shown in Figure 8.2. The feed salt was a mixture of sodium fluoride, zirconium tetrafluoride, and uranium tetrafluoride with a melting point of 525 C. A fluorination batch consisted of about 50 liters of salt containing about 10 kg of uranium. Fluorine was bubbled through this salt at 15 to 20 standard liters/min, fluorinating the uranium tetrafluoride to uranium hexafluoride, which was volatile and left the fluorinator as a gas. More than 99 percent of the fission products remained in the salt. After fluorination was complete (2 to 3 hours), the waste salt was transferred to a waste can, allowed to freeze, and then buried.

During fluorination, gases leaving the fluorinator passed through a Complexible Radioactive Products Trap (the CRP Trap), which was a bed of sodium fluoride pellets held at 400 C. At this temperature, uranium hexafluoride passed through with the excess fluorine and the dry nitrogen, while some of the volatile fission products and corrosion

---

2/ Chem. Eng. Prog. Sym. Series, 56, No. 28, p. 57-61.

8.2.1 Pilot Plant Description (Cont'd)

products were retained. The gas leaving the CRP Trap entered the first adsorber, which was filled with sodium fluoride pellets at about 100 C. At this temperature all the uranium hexafluoride and most of the remaining fission products were adsorbed by the sodium fluoride. The unadsorbed gases go through a chemical trap at ambient temperature, which was another sodium fluoride bed. This trap served as a backstop to ensure that no uranium hexafluoride was lost. From it, the gas passed through a caustic scrubber tower to remove fluorine and then entered the off-gas system.

After fluorination and absorption were completed, the valving was changed to provide a flow directly from the fluorine supply through the two adsorbers in series, through the two cold traps in series, and through the chemical trap to the fluorine disposal and off-gas systems. The second adsorber was a duplicate of the first and was placed in the line for final decontamination of the uranium hexafluoride.

During the desorption step which followed, it was necessary to maintain a fluorine atmosphere to prevent partial reduction of uranium hexafluoride. The flow of gas to sweep the uranium hexafluoride from the adsorber was 8 standard liters/min of fluorine.

Desorption was accomplished by heating the sodium-uranium fluoride complex in the adsorbers to 400 C. When this temperature was attained, all the uranium hexafluoride was removed from the adsorbers and passed into the cold traps.

Most of the uranium hexafluoride condensed and froze in the -40 C cold trap; any uranium hexafluoride passing through this first cold trap froze in the -60 C cold trap. Again, the chemical trap serves as a safety factor.

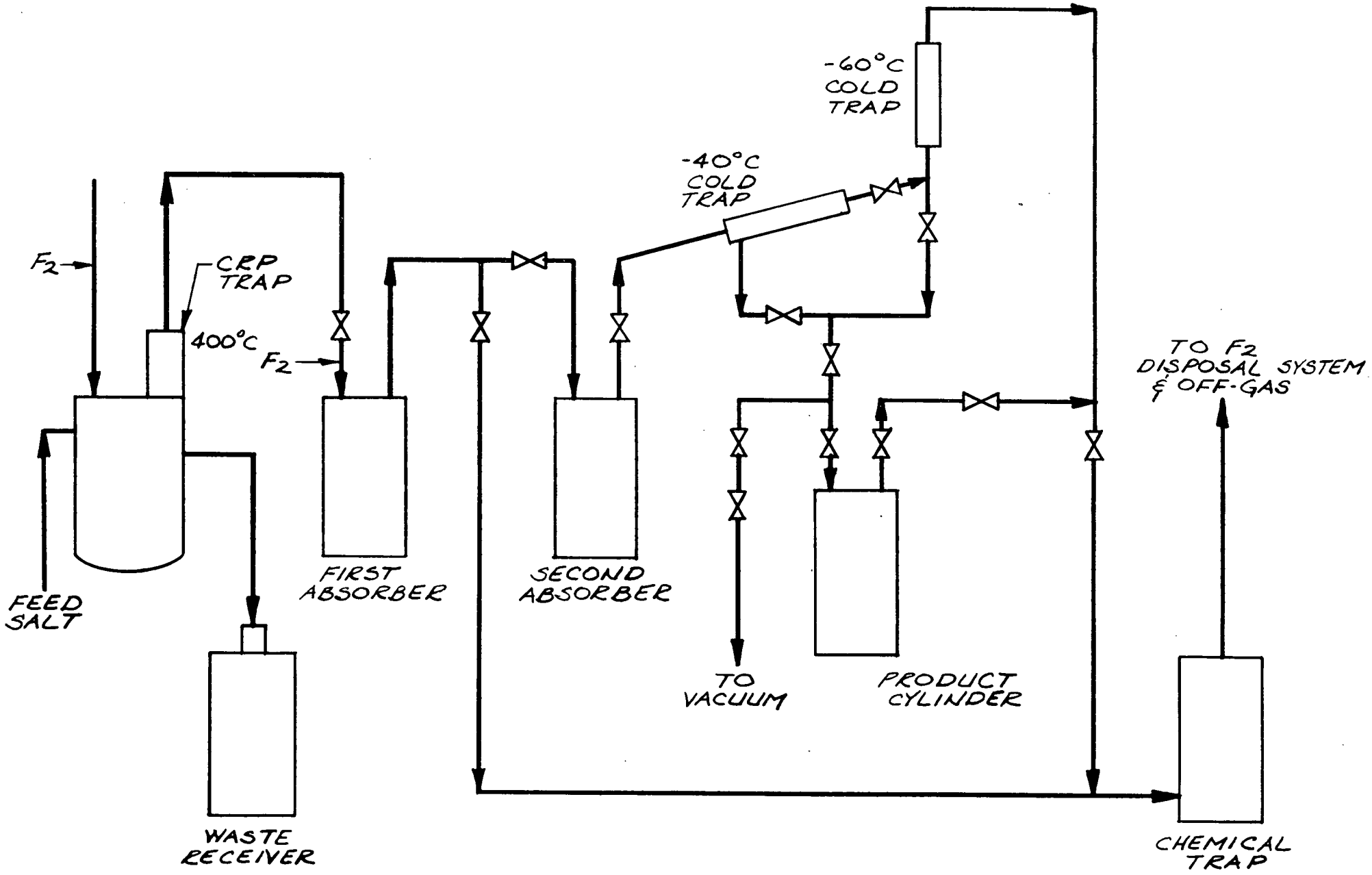

Fig. 8.2 Pilot Plant Flowsheet for ARE Fuel

8.2.1 Pilot Plant Description (Cont'd)

After desorption was complete, the cold trap and product cylinder system were isolated and evacuated. The entire system was then heated above 64 C, the triple point of uranium hexafluoride, thus liquefying the uranium hexafluoride in an atmosphere of uranium hexafluoride vapor. The liquid was drained to the product shipping cylinder, which was cooled to 0 C in order to effect a thermal transfer of most of the uranium hexafluoride vapor. At the completion of this thermal transfer, the product cylinder valves were closed and the cold traps were cooled to normal operating temperatures. Any uranium hexafluoride not transferred was frozen out in the cold traps and remained until the next run.

8.2.2 Processing

The ARE fuel was a fused salt consisting of 48 mole percent sodium fluoride, 49.5 mole percent zirconium fluoride, and 2.5 mole percent highly enriched uranium tetrafluoride. Since this fuel was low burnup, long-cooled material, it was suitable for the first Pilot Plant runs with irradiated feed. After only two runs, leaks developed which necessitated shutting down the plant. The fluorination data for these two runs are valid, but the material balance data are in error because of the leaks. After the system had been cleaned out, repaired, and modified slightly to reduce the possibility of leakage, the remainder of the ARE fuel was processed in four batches with no major difficulties.

After the ARE fuel was recovered, another series of runs was made to extend the development data. This series used an essentially nonirradiated salt similar to the ARE fuel; some of these runs were spiked with high-burnup salt to obtain further decontamination data, and this series will be referred to as "spiked" runs. During this series of nine runs, the only major difficulty was line plugging,

8.2.2 Processing (Cont'd)

which occurred when the concentration of nickel fluoride in the salt exceeded the solubility limit.

The salt used for the spiked runs has about twice the uranium content of the ARE fuel. Hence, for the first and third runs of this last series, the usual 50 liters of salt was charged, but fluorination was terminated when half the uranium had volatilized. The salt was kept molten, and fluorination was completed for the second and fourth runs.

Nickel fluoride is soluble in fused salt to the extent of less than 0.3 percent at 600 C and 1.1 percent at 700 C. The feed salt used had a high nickel content, and the nickel resulting from corrosion during the extended period of fluorination aggravated the situation. During the first four runs, fluorinator piping became plugged, and it was necessary to remove all high-melting point material from the fluorinator before processing could be continued. Subsequent runs were made by diluting the feed salt with an equal quantity of nickel-free barren salt, and no further difficulties were encountered.

a - Corrosion

Corrosion of the fluorinator was a serious problem, although the rate was not intolerable for pilot plant operation. Of the materials tested, L-nickel appeared to be the best for this application. Since the corrosion was worst with uranium present after the uranium tetrafluoride had been partially fluorinated, the walls of the L-nickel fluorinator were measured after the fourth spiked run. A sonic type of gauge, which measured total thickness but gave no indication of the amount of intergranular corrosion, was used. Total reduction in wall thickness during the six ARE runs and the first four spiked runs (903 hours at fluorination temperature) was 70 mils. Most of this occurred

8.2.2 Processing (Cont'd)

during the spiked runs. Maximum measured reduction during the remaining five runs (311 hours at fluorinating temperature) was only 2 mils.

b - Fluorination

Fluorination efficiency, in terms of both fluorine utilization and residual uranium, was slightly higher than had been predicted from laboratory data.

One of the criteria used was the consumption of fluorine before any uranium hexafluoride was evolved from the melt. In most of the pilot plant runs, this ranged from 0.7 to 1.1 moles of fluorine/mole of uranium tetrafluoride; however, in the first and third spiked runs, this was only 0.5 and 0.6, respectively. Since the uranium concentration in these last runs was about twice as high as in other runs, it appears that the initial fluorine requirement is primarily a function of the total amount of salt present and of the geometry of the system.

The second criterion was the total fluorine consumption before unreacted fluorine broke through the melt. Table 8.2 (in the columns headed F_2) shows this consumption prior to the breakthrough of unreacted fluorine in terms of the number of total moles of fluorine per mole of uranium initially present. At this point most of the uranium has been volatilized, and uranium recovery becomes increasingly more difficult. Even though the theoretical fluorine requirement is only 1 mole for each mole of uranium, in the ARE runs two to three times this quantity was necessary. In the spiked runs, fluorine consumption to this point ranged from 1.8 to 2.4 times theoretical if the first pair of runs were disregarded. In these first runs, excess fluorine was consumed in the excessive corrosion

Table 8.2

Fluorination Efficiency

	ARE RUNS				SPIKED RUNS			
	Moles F_2/Mole U		Residual U		Moles F_2/Mole U		Residual U	
Run	F_2	End	ppm	Grams	F_2	End	ppm	Grams
1	2.0	2.9	80	14	2.7	5.1	40	5
2	2.3	5.7	<3	1				
3	2.3	3.6	6	1	2.3	4.6	8	1
4	2.3	4.7	16	3				
5	2.6	3.5	5	1	2.4	3.4	<1	<1
6	2.8	5.7	5	1	1.8	2.8	3	<1
7					2.2	2.9	3	<1
8					2.3	3.3	8	1
9					2.2	3.1	1	<1

8.2.2 Processing (Cont'd)

mentioned earlier. It is not known whether the increased efficiency of fluorine utilization in the spiked runs was due to improvement in operating technique, a difference in the feed salt, a longer break-in period for the equipment, or a combination of these possibilities.

Essentially complete fluorination was demonstrated with reasonably low total fluorine consumption (e.g., spiked Runs 5 and 9). After the first ARE run, fluorination was carried beyond the point of economic justification primarily to establish worse conditions for decontamination than would be encountered in commercial practice.

c - Sodium Fluoride Adsorption

Retention of uranium on the sodium fluoride in the system must be kept to a minimum for economic reasons. The low retention in the CRP Trap (2 or 3 g a run) indicated this was possible. The high values (in some cases, up to 194 g) resulted from inadequate temperature control. However, even with some values excessively high, the total retained on all sodium fluoride in the system (Table 8.3) amounted to only 2 percent of the uranium processed in the ARE series and to less than 1 percent in the spiked series.

The retention on the two adsorbers is interesting in that these values are approximately the same as those previously obtained for single runs. In the case of the ARE, four runs were made with the same adsorber beds and nine spiked runs were made with a single filling of the absorbers. It seems that uranium retention in adsorbers is caused by impurities initially present in the sodium fluoride and is independent of the amount of uranium hexafluoride put through the bed.

Table 8.3

Sodium Fluoride Retention of Uranium Hexafluoride

Place Retained	UF_6 RETAINED, G of U: Are Runs 3 to 6	Spiked Runs 1 to 9
CRP Trap, Total	221	279
Range (a)	(3 to 194)	(2 to 189)
1st Absorber	28	14
2nd Absorber	16	4
Miscellaneous (b)	606	227
Total	871 (2.1% of Total U Processed)	524 (0.7% of Total U Processed)

(a) CRP trap was changed after every run in the ARE series, but sometimes after one or two runs in the spiked series; the value 189 in the spiked runs is the retention after two runs.

(b) The miscellaneous category includes all chemical traps and such items as purge of the system at the end of a series of runs. The amount involved is not large since a development unit should have greater "losses" to sodium fluoride than would a production unit.

8.2.2 Processing (Cont'd)

d - Material Balances

In the last four ARE runs, 98 percent of the uranium measured into the system was recovered as uranium hexafluoride in product shipping cylinders (Table 8.4). The 6 g remaining in the waste salt and the 871 g remaining by sodium fluoride are totals from Tables 8.2 and 8.3. The 200 g is the estimated amount held on walls of piping and vessels. The 0.7 percent more accounted for than was measured into the system is well within the limits of uncertainty.

In the nine spiked runs, more than 99 percent of the uranium measured into the system was recovered as uranium hexafluoride in product cylinders. Again, the 9 and the 524 g are totals from Tables 8.2 and 8.3. At the end of this series, the system was flushed with water to recover 320 g of uranium remaining on the walls of the piping and vessels. Here the amount accounted for was 0.3 percent more than was measured in.

e - Product Purity

The uranium hexafluoride product from the pilot plant was converted without difficulty to uranium tetrafluoride that was well within purity specifications. There was no detectable fission product activity in any product, and the gross β and gross γ of every product cylinder was equal to or less than what would be expected from the uranium alone. The product gross γ activities of 9 to 10 counts/(min) (mg of uranium) shows a gross γ decontamination factor of at least 10^4. Because of the low burnup and long decay of the fuel processed, the feed activities were low (Table 8.5). Feed with higher activities may give equally pure products; therefore, considerably higher decontamination factors may be possible. In laboratory studies a decontamination factor of at least 10^6 has been demonstrated, also

Table 8.4

Uranium Material Balance

	ARE Runs 3 to 6	Spiked Runs 1 to 9
Feed, g	40,638	72,331
UF_6 Product, g	39,830	71,761
% of Feed	(98.01)	(99.21)
Waste Salt, g	6	9
On NaF, g	871	524
Estimated Holdup, g	200	
Water Wash, g		320
Total, g	40,907	72,614

Table 8.5

Feed Salt Activities

	COUNTS/(MIN) (mg U)	
	ARE Runs	Spiked Runs
Gross γ	9×10^4	9.26×10^4
Gross β	2.5×10^5	4.14×10^5
Cs γ	-7×10^4	6.75×10^4
Nb γ	<80	2.00×10^4
Zr γ	<60	1.10×10^4
Ru γ	<140	<40
TRE β a/	1.6×10^5	3.41×10^5

a/ Total rare earth β activity.

8.2.2 Processing (Cont'd)

with product activities at background levels.

8.3 Laboratory Fluorination Tests[3/]

A series of small-scale fluorinations was carried out with a 48 mole percent LiF-52 mole percent BeF_2 eutectic mixture containing 0.8 mole percent UF_4. The eutectic salt composition was used to permit operation at lower temperatures. Fluorinations at 450, 500, and 550 C indicated that the rate of uranium removal increased with the temperature (Table 6). It was not determined whether the increased fluorination time apparently required for quantitative uranium recovery at the lower temperature was compensated for by a decreased corrosion rate.

Salt compositions of $LiF-BeF_2-ThF_4$(71-16-13 mole percent), containing 0.004 mole percent UF_4 and 0.014 mole percent UF_4, were fluorinated at 600 C for 90 min. Uranium concentrations in the salt of 0.0001 to 0.0002 weight percent were obtained and were the lowest uranium concentrations ever observed in laboratory fluorinations. Over 90 percent of the uranium was removed in 15 min.

8.4 Protactinium Fluoride Volatility Test

A salt of composition $LiF_4-BeF_2-ThF_4$ (71-16-13 mole percent) containing sufficient irradiated thorium to give a ^{233}Pa concentration of 5.5×10^{-9} g per gram of salt was fluorinated for 150 min at 600 C; no measurable decrease in protactinium activity in the salt was observed[3/].

Another experiment[4/] was made to investigate the possibility that a volatile fluoride might be formed. Natural protactinium ^{231}Pa was added to $LiF-BeF_2-ThF_4-UF_4$ (67-18.5-14-0.5 mole percent) to a

3/ ORNL-2626, October 31, 1968.

4/ ORNL-2973, April 30, 1960.

Table 8.6

Effect Of Fluorination Temperature On The Fluorination Of Uranium From $LiF-BeF_2$ (48-52 Mole %)*

Fluorination Time (hr)	Uranium in Salt (Wt %) After Treatment		
	At 450°C	At 500°C	At 550°C
0	3.39**	5.10	4.91
0.5	1.96	0.20	0.55
1.0	0.39	0.17	0.20
1.5	0.21	0.12	0.06
2.5	0.32	0.11	0.05

* No induction period before uranium evolution.

** 5 wt % added; some of the uranium probably precipitated as oxide.

8.4 Protactinium Fluoride Volatility Test (Cont'd)

concentration of 0.012 weight percent, and the salt was fluorinated for 2 hours at 650 C. No measureable amount of protactinium was removed from the salt, even though the uranium was removed.

8.5 Continuous Fluorination Tests

The continuous fluorinator consisted of a 1-inch diameter nickel tube.

Two runs were made with an $NaF-LiF-ZrF_4$ (37-26-37 mole percent) salt containing 1 weight percent UF_4 in one case and 0.2 weight percent in the other[5/]. For the first case, fluorination at 700 C with excess fluorine and with an average residence time for salt in the fluorinator of 40 min resulted in a uranium content in the effluent salt of 100 to 200 ppm, 1 to 2 percent of the original concentration. In the other experiment, with the temperature in the range 600 to 650 C, the uranium content of the overflow salt was 25 to 50 ppm, again 1 to 2 percent of the feed concentration. The nickel content in the salt increased throughout a run, never reaching a steady state. Corrosion rates based on nickel concentrations were about 1 mil/hour at 700 C and 0.1 to 0.2 mil/hr at 610 C.

Experimental studies of continuous fluorination of molten salt were also made in another 1-inch diameter nickel column with a salt depth of 48 inches[6/]. Tests in which 15 cm^3/min of molten salt ($NaF-LiF-ZrF_4$) containing 0.5 weight percent UF_4 was contacted countercurrently with 70 cm^3/min of F_2 (STP) at 600 C showed a 96 to 99.4 percent removal of uranium from the salt during a 1-hour period of continuous operation. Material balances were complicated by the corrosion of the nickel vessel. Complete removal of uranium from the salt with no corrosion would yield, for the above conditions, a UF_6 concentration of 17.6 mole percent in the off-gas. Observed concentrations ranged as high as 35 mole percent UF_6.

5/ ORNL-3122, February 28, 1961.

6/ ORNL-3936, February 28, 1966.

8.5 Continuous Fluorination Tests (Cont'd)

Another system[7/] built to study continuous fluorination consisted of a 1-inch diameter nickel fluorinator 72 inches long and auxiliary equipment (Figure 8.3) which allowed the countercurrent contact of a molten salt with F_2. Experiments could be carried out with molten-salt flow rates of 3 to 50 cm^3/min with fluorinator salt depths of 12 to 54 inches. The system was constructed of nickel with the exception of molten-salt transfer lines, which were Hastelloy N. The fluorinator off-gas passed through a 400 C NaF bed for removal of chromium fluorides, a 100 C NaF trap for removal of UF_6, and a soda-lime bed for F_2 disposal. Analyses for F_2, UF_6, and N_2 were made prior to the 100 C NaF bed with a gas chromatograph.

Experiments were done at 600 to 650 C using an NaF-LiF-ZrF_4 mixture (37-26-37 mole percent) containing 0.2 to 0.5 weight percent UF_4 and having a melting point of ~550 C. Salt feed rates of 5 to 21 cm^3/min and F_2 rates of 75 to 250 cm^3/min (STP) were used with molten-salt depths of 40 to 52 inches. Uranium removal during one pass through the fluorinator varied from 95 percent to 99.6 percent as determined from salt samples. Equipment operation was smooth, although several plugs developed in salt transfer lines and in the fluorinator off-gas.

During one run (CF-10), a molten-salt feed rate of 20.7 cm^3/min and an F_2 feed rate of 250 cm^3/min (STP) were maintained for a 2.5-hour period. The concentration of U in the feed salt was 0.32 weight percent, and the fluorinator was operated at 650 C with a salt depth of 48 inches. The U concentration in the salt discharged from the fluorinator during the last hour of operation was 0.0020 weight percent as determined from four salt samples taken at 15-min intervals. Based on inlet and exit U concentrations in the salt, 99.4 percent of the U, was removed by the fluorinator. The equipment operated smoothly during the run, salt and gas feed rates were constant, and the system appeared to have reached steady state during the last hour of operation.

7/ ORNL-4037, August 31, 1966.

8.5 Continuous Fluorination Tests (Cont'd)

Three additional experiments[8/] were made at 600 C using the NaF-LiF-ZrF_4 mixture containing 0.37 to 1.16 weight percent UF_4 and having a melting point of ~475 C. Salt feed rates of 9.8 to 30 cm^3/min and F_2 rates of 235 to 335 cm^3/min (STP) were used with molten-salt depths of 48 inches. Uranium removal during one pass through the fluorinator varied from 99.36 to 99.89 percent, as determined from salt samples.

During the best run, a molten-salt feed rate of 10.2 cm^3/min and an F_2 feed rate of 235 cm^3/min (STP) were maintained for a 2.5-hour period. At steady state, 99.89 percent of the uranium was removed by the fluorinator, as determined from inlet and exit concentrations of uranium in the salt. Later in the run, a molten-salt feed rate of 22.5 cm^3/min and an F_2 rate of 270 cm^3/min (STP) were maintained for a 2.5-hour period. With these conditions, the uranium removal at steady state was 99.62 percent. The uranium concentration in the feed salt was 1.16 weight percent, and fluorine utilizations were 15.6 and 30 percent, respectively. The equipment operated smoothly during the run, salt and gas feed rates were constant, and the system was operated at steady state for 2 hours at each of the above conditions.

8.6 Fluorine Disposal Experiments

Excess fluorine that is purged from the system must be disposed of or radioactivity may be released to the stack. The following describes the work done to date.

8.6.1 Charcoal[9/]

Seven runs were made in order to determine the characteristics of the charcoal-fluorine reaction and its possible use for a fluorine disposal system. An average of 5.89 g of

8/ ORNL-4119, February 28, 1967.

9/ ORNL-3282, February 28, 1962.

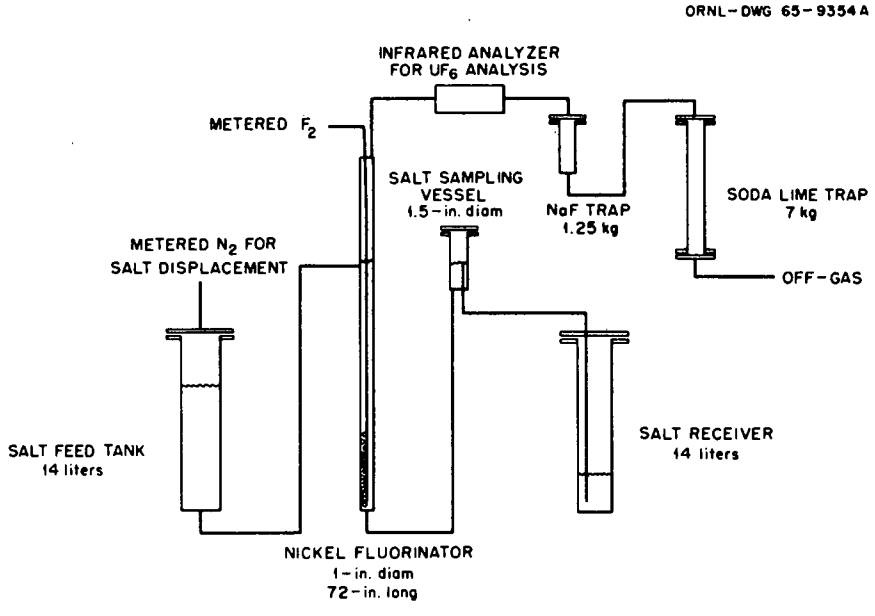

Fig. 8.3. Equipment for Removal of Uranium From Molten Salt by Continuous Fluorination.

8.6.1 Charcoal (Cont'd)

fluorine was successfully combined with 1.00 g of charcoal. The combustion reaction was nonexplosive and reached a steady-state temperature of ~450 C, independent of the fluorine flow rate between 1.00 and 2.25 standard liters per minute of 100 percent fluorine.

Mass spectrographic analysis of the off-gas at steady state indicated an average mole-percentage composition of 52.6 percent CF_4; 23.4 percent N_2; 12.2 percent CO_2; 5.6 percent COF_2; 2.1 percent C_3F_8; 1.3 percent of a mixture of C_4F_{10}, C_5F_{12}, C_6F_{14}, and higher homologues; Ar; and H_2, with F_2 always <0.01 percent.

Hydrogen fluoride, solids, and condensable liquids were trapped from the off-gas before the mass-spectrographic samples were taken. During the three longest runs, an average of 0.846 g HF was produced per gram of charcoal consumed, and ~0.01 g of solids was deposited in the off-gas line per gram of charcoal consumed, and ~0.1 g of liquid was trapped per gram of charcoal consumed. The solids, of a resinous nature, contained 29.3 weight percent carbon and 47.9 weight percent fluorine and melted over a range of 60 to 105 C but decomposed before a boiling temperature was reached. The liquid contained 54.0 weight percent HF, 43.0 percent H_2O, and a small amount of high-molecular weight fluorocarbons; the liquid had a density of ~1.25 g/cc.

Although the commercial charcoal used was not homogeneous, an average composition was 73.16 percent fixed carbon, 8.79 percent H_2O, 2.13 percent ash, and 15.92 percent volatile matter (all weight percentages). To reduce the HF, condensable liquids, and resinous solids entrained in the off-gas, two runs were made with charcoal preheated to 650 C. The amount of HF produced was reduced by a factor of 2; a negligible amount of liquid was noted, but enough solid was formed in the off- gas line to plug it.

8.6.1 Charcoal (Cont'd)

Studies using a thermogravometric balance indicated the greatest rate of weight loss occurred between 400 and 750 C. Heating the charcoal to 1 000 C removed almost all the volatile matter, water, and some of the mineral-ash components.

Fluorination and thermal stress caused the size of the charcoal pieces to change from an initial ~1.0 in^3 to an ash-charcoal residue with a size distribution of 77.9 percent >2 mesh, 6.6 percent between 2 and 4 mesh, 0.69 percent between 4 and 8 mesh, 1.23 percent between 8 and 25 mesh, 0.92 percent between 25 and 50 mesh, 1.31 percent between 50 and 100 mesh, and 0.84 percent <100 mesh.

8.6.2 SO_2 Process[10/]

The original concept for the processing facility involved reacting fluorine with sulfur dioxide gas at temperatures above 400°F to form sulfuryl fluoride, SO_2F_2, a relatively inert gas that could be discharged to the atmosphere. Later a heated bed of activated alumina was provided downstream of the SO_2-F_2 reactor to remove traces of fluorine during normal operation and to protect the charcoal traps in case of a malfunction of the reactor.

Four test runs were made on this system. Despite various modifications and improvements, in each run there was some temperature increase in the alumina bed, implying that some fluorine was reaching it. Later it was shown that decomposition of SO_2F_2 at temperatures above 800°F was probably the cause of the temperature rise in the later tests. Since it had not been possible to demonstrate complete reaction of the fluorine with the SO_2-F_2 scheme, the decision was made to adopt the alternative of reacting the fluorine with a caustic solution.

10/ ORNL-4344, August 31, 1968.

8.6.3 Caustic Process[10/]

The results of laboratory experiments and a brief test in the MSRE caustic scrubber tank showed that a solution of 2 M KOH + 0.33 M KI very efficiently removed fluorine from a helium-fluorine stream. An extended test of the fluorine disposal in the caustic solution was made. This test showed that a filter was needed downstream of the caustic scrubber to handle molybdenum oxides entrained in the off-gas. The oxides were produced in the caustic solution from corrosion-product MoF_6. A larger off-gas line to a high-area glass-fiber filter was then installed. Tests were then made to study features of the process that were important in operation of the MSRE facility. Observations were made on the amount of corrosion to be expected, the effect of helium dilution of the fluorine, the formation and character of precipitates, and the permissible fraction of solution capacity which should be used. Most of the work was carried out with 2 M KOH-0.33 M KI solution; later this was modified to include 0.2 M $K_2B_4O_7$ to provide neutron poisoning. The handling of mists and smoke in the outlet stream of the scrubber represented another problem area which was investigated in the laboratory.

a - KIO_3 Precipitate

The oxidizing power of F_2 leads, in addition to the evolution of O_2, to the formation of potassium iodate (KIO_3). Copious quantities of this material were found to precipitate at 80 percent saturation. At 50 percent saturation, its precipitation was only faintly noticeable. X-ray diffraction and chemical analyses were used to identify the material, which is produced in a rather pure form except for the presence of corrosion products.

b - Neutron Poisoning

Tests made at 0.16, 0.20, and 0.24 M $K_2B_4O_7$ in 2 M KOH-0.33 M KI solution indicated that the chemistry of the

8.6.3 Caustic Process (Cont'd)

system was only affected at the highest of these three concentrations (evidence of molecular I_2 production). This was in conformity with an initial test where 0.5 M $K_2B_4O_7$ had been found to cause the immediate release of free iodine. Since 0.2 M $K_2B_4O_7$ was equivalent to 8.75 g of boron per liter, this was considered adequate for poisoning of the scrub solution.

c - Mist

It was evident in all laboratory tests that a certain amount of mist was always generated. Efforts to identify the chemical components of the mist were not successful, since the material was extremely difficult to trap; however, analyses for fluoride and iodide were extremely low. It seemed probable that the mist was stabilized by the presence of I_2 or H_2O_2.

In an engineering test of the MSRE facility, an additional gas colloid problem was encountered. Corrosion of the hot processing vessel (containing no salt) with fluorine led to the production of MoF_6. Hydrolysis of this MoF_6 in the scrubber led to production of an aerosol of hydrated MoO_3 (based on chemical analyses and X-ray diffraction results) which deposited and plugged the off-gas line. Duplication of this MoO_3 aerosol production was verified in laboratory tests with scrub solution and F_2 containing MoF_6.

Laboratory tests with different filtration and trapping methods showed that only a high-efficiency fiber glass filter was effective in stopping the MoO_3 aerosol and, at the same time, the always present scrub mist.

8.7 Chromium Fluoride Trapping[6/]

Fluorides of chromium may be present in the fuel salt as a result of corrosion of the reactor and associated equipment. A potential problem associated with the recovery of the uranium as UF_6 is the

8.7 Chromium Fluoride Trapping (Cont'd)

presence of volatile fluorides of chromium (CrF_4 and CrF_5) in the fluorinator off-gas. These fluorides can contaminate the UF_6 product and render equipment inoperative by deposition in lines, valves, etc.

Experiments were carried out in which 1 liter/min of F_2 (STP) was sparged through a molten NaF-LiF-ZrF_4 mixture (37-26-37 mol percent) at 650 C which contained 0.5 to 4 weight percent CrF_3. The resulting off-gas containing fluorine and volatile fluorides of chromium then passed through beds of pelleted NaF at 400 C for removal of chromium fluorides. In some tests, a UF_6 flow of 100 cm^3/min was added to the F_2.

It was concluded that (1) fixed beds of NaF at 400 C are effective in removing fluorides of chromium from a gas stream which also contains UF_6 and F_2, (2) pelleted NaF having a surface area of 0.074 m^2/g and a void fraction of 0.277 is superior to material having a surface area of 1 m^2/g and a void fraction of 0.45 and has an effective capacity of about 20 g of chromium per 100 g of NaF, and (3) uranium losses to the 400 C NaF bed of less than 0.01 percent are achievable when working with a gas stream that contains 0.4 mole of CrF_5 per mole of UF_6 in F_2.

8.8 Frozen Wall Experiment[11/]

The experimental equipment consisted of a 5-inch diameter, 8-ft high column fabricated from Schedule 40 nickel pipe (Figure 8.4). An internal heat source consisting of three Calrod heaters contained in a 3/4-inch diameter Schedule 40 Inconel pipe is used to simulate a volume heat source in the molten salt. Two sets of internal thermocouples located near the center of each of two test sections indicated the radial temperature gradient, from which one could infer the location of the interface between molten and frozen salt. Each test section was independently cooled by air

11/ ORNL-4254, February 29, 1968.

8.8 Frozen Wall Experiment (Cont'd)

flowing through spirally wound 3/8-inch diameter nickel tubing. Additional Calrod heaters were wound on the external surface of the fluorinator to provide auxiliary heat during heatup and to provide control of temperatures at the ends of the column. A 63-34 mole percent $LiF-ZrF_4$ mixture, which has a liquidus of 595 C and a phase diagram similar to the $LiF-BeF_2$ system, was metered from the feed tank for periods as long as 5 hours, which allowed collection of data for a 1- to 2-hour period of steady state operation.

The principal objective of the experiments, demonstrating that a layer of frozen salt could be formed and maintained under approximate operating conditions, was achieved.

In general the frozen wall thickness and temperature profiles in the frozen salt were in good agreement with the values predicted by relations obtained by assuming purely radial heat flow from a volume heat source. Frozen wall thickness ranged from 0.3 to 0.8 inch. The effect of heat generation in the layer of frozen salt was not simulated in these experiments.

The thermal conductivity of the frozen salt was calculated for each run from the experimentally determined temperature gradient and the measured heat flux. The relative agreement of calculated values was taken to be indicative of consistency of the experimental data. Thermal conductivities calculated from the upper test section data were closely grouped around 0.75 BTU $hour^{-1}$ $foot^{-1}$ $(^{o}F)^{-1}$; however, values from the lower section were more widely scattered and were generally about 100 percent higher.

The heating-cooling system used on the column produced some variation in external wall temperature (and hence frozen wall thickness). In a typical run, the difference between salt liquidus and wall temperature ranged from 85 to 140 C.

Protection of the fluorine inlet nozzle from corrosion is an anticipated problem associated with operation of a frozen-wall fluorinator. A possible solution incorporated in the present system consists in introducing the fluorine through a short section of 3-inch

8.8 Frozen Wall Experiment (Cont'd)

diameter pipe which intersects the fluorinator at a 45° angle, as shown in Figure 8.4.

The inlet section would be protected from corrosion by a layer of frozen salt as in the fluorinator. Tests with the present system indicate satisfactory operation when the surfaces of the inlet section are covered by a layer of frozen salt produced by maintaining wall temperatures below the salt liquidus. Heat is supplied to this section in the present case as a result of turbulence in the molten salt caused by bubbles; in an actual case, heat would be generated in the salt as a result of fission product decay. This method of gas introduction appears to be feasible, although it will not produce small diameter gas bubbles.

8.9 Fluorination-Corrosion Study[11/]

The fluorination-corrosion tests were made with MSRE-type salt in a 1.87-inch ID Hastelloy N reactor. The uranium was volatilized out of the salt with an intermediate inert-gas sparging period to simulate changing of the NaF sorbent beds used for recovery of the UF_6. A gas flow rate of 146 ml/min (STP) was used in the 1.87-inch ID reactor.

Two tests were made, one at 450 C and one at 500 C, each with 340 g of $LiF-BeF_2-ZrF_4-UF_4$ (63-32-5-0.8 mole percent). Salt samples were taken during the runs at intervals (after He sparging) determined by the necessity of changing a 12-g NaF trap used for recovery of the UF_6. In each test, 50 percent F_2-50 percent He (146 ml/min) was used initially, followed by pure fluorine (146 ml/min) at the end of the run to ensure complete uranium recovery. In the test at 500 C, pure fluorine was used throughout. A trap containing 2 M KOH was employed to sorb unused fluorine and volatile chromium and molybdenum compounds that passed through the NaF trap.

As shown in Table 8.7, the UF_6 volatilization rate and the degree of fluorine utilization were higher at 500 C than at 450 C. The amount of chromium leached from the Hastelloy N reactor increased

Table 8.7
Uranium Volatilization And Corrosion Results In Fluorination Tests With MSRE Salt In Hastelloy N At Two Temperatures

Temperature (°C)	Fluorine Concentration (%)	Total Time (Hr)	Corrosion (mg In Salt)(a) Cr	Corrosion (mg In Salt)(a) Fe	Volatile Material U (%)	Volatile Material Cr (mg)	Fluorine Utilization Efficiency (%)
450	50	0.5	13	4	5.4		4.0
	50	2.0	42	35	14.2		2.1
	50	3.5	93	60	44.7		7.5
	50	5.0	118	73	68.0		5.6
	100	6.0	103	82	92.2		2.2
	100	8.0	143	152	100	2.4	0.7
	100	12.0	128	93		5.5	
	100	16.0	117	96		14.7	
500	50	1.0	75	49	18.5		7.6
	50	1.75	153	95	38.5		11.0
	50	2.25	194	122	55.1		13.8
	100	2.75	224	126	83.4		11.7
	100	6.75	150	139	100	15	1.8
	100	10.75	140	180		27	
500	100	0.75	74	17	28.7		7.1
	100	1.25	112	48	59.4		11.4
	100	1.58	139	48	90.7		17.6
	100	2.58	136	71	98.9		1.5
	100	6.58	125	71	100	9	0.1
	100	10.58	102	82		12	

(a) Corrected for initial values at zero time.

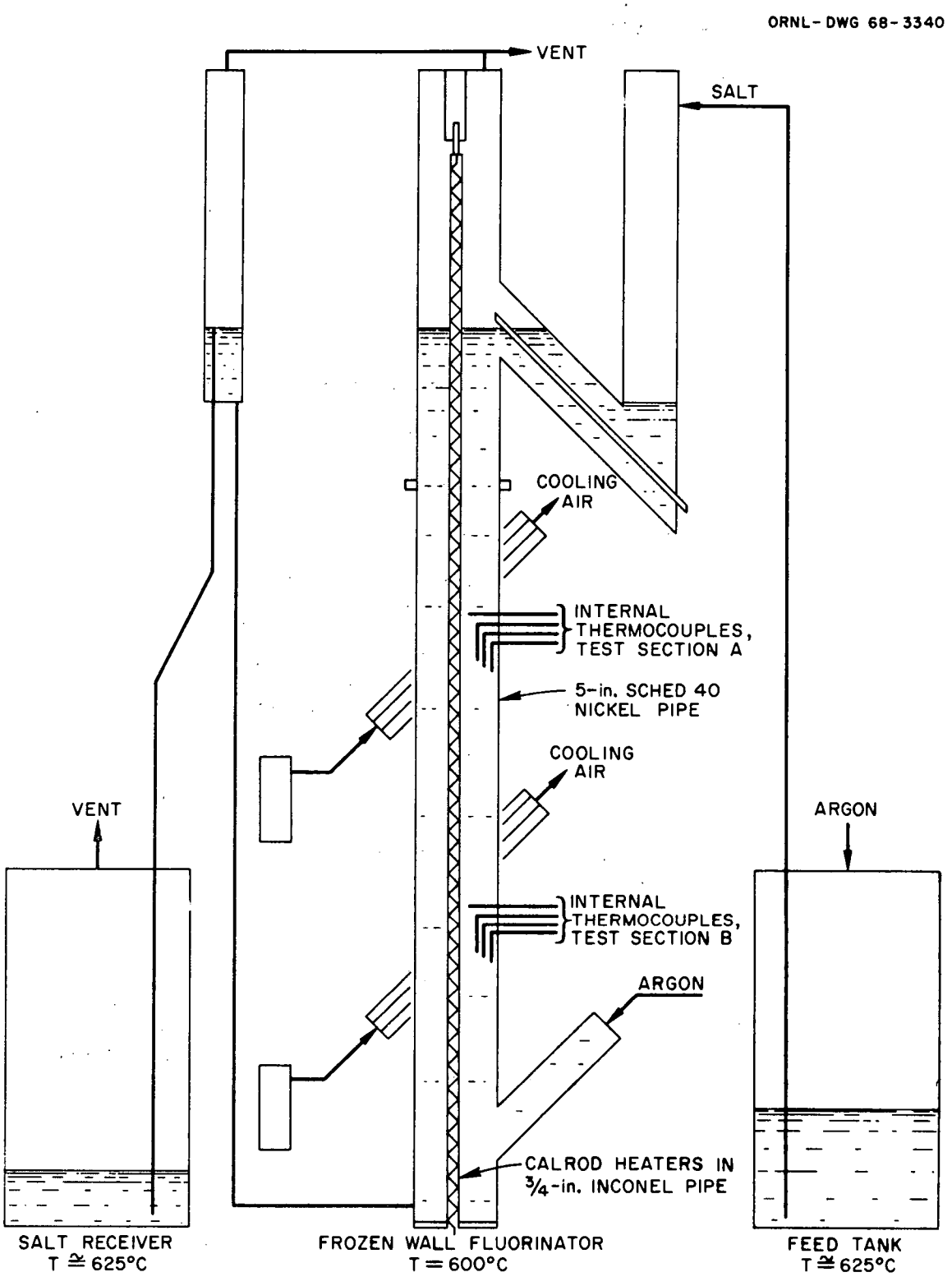

Fig. 8.4. Experimental Equipment for Studying Formation of Frozen Salt Layer for Corrosion Protection. Height of column, 8 ft; height of each test section, 1.75 ft.

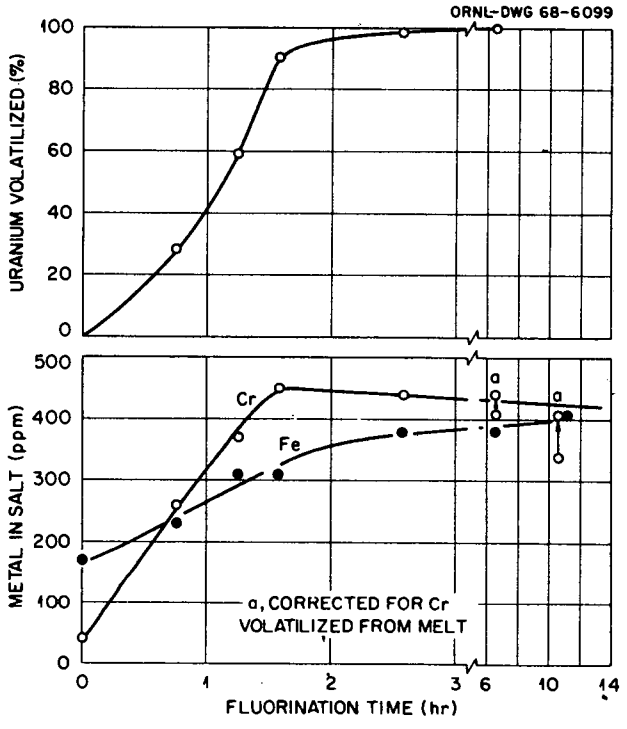

Fig. 8.5. Relationship Between Corrosion of Hastelloy N and UF_6 Volatilization in Fluorination of MSRE-Type Salt at 500°C.

8.9 Fluorination-Corrosion Study (Cont'd)

with temperature. The effect of temperature on the solubilization of iron and nickel from the reactor is not as clear (the dip tube, thermocouple well, and reactor bottom were made of Ni-200). Figure 8.5 shows the relation between chromium and iron leaching and uranium volatilization for the third run (with pure fluorine); corrosion appears to occur predominantly in the uranium volatilization period.

Various estimates of the corrosion rate were calculated from the chromium data using different time periods (Table 8.8). There was good agreement between the rate calculated from the period in which most of the chromium was leached and that over the period where most of the uranium was volatilized. The estimates for the complete runs are somewhat arbitrary because fluorination was continued after the uranium had been removed to observe chromium behavior.

Volatility of chromium and molybdenum was also observed in these runs. A chromium compound (probably CrF_5) appeared to volatilize only after most of the uranium had been removed from the salt (Table 8.7). This chromium compound was effectively trapped by NaF at 25 C, forming an orange complex compound. Molybdenum (probably as MoF_6) volatilized to a large extent throughout each run and, as expected from the dissociation pressure of $MoF_6 \cdot 2NaF$, was not completely recovered in the 25 C NaF trap. Most of it passed through to the KOH scrub solution.

The fluorine utilization efficiency figures (calculated from UF_6 output and fluorine input) suggest that the utilization was highest during the first 2 hours of fluorination.

8.10 Fission Product Behavior[11/]

Four fluorination tests were completed using specially prepared MSRE-type salt samples. The samples consisted of copper capsules each containing about 46 g of $LiF-BeF_2-ZrF_4-UF_4$ (65.4-29.4-5.0-0.2 mole percent). Each salt sample was melted out under an inert atmosphere into a suitable nickel fluorinating vessel and then was

Table 8.8

Estimates Of Rates Of Corrosion Of Hastelloy N In Fluorination Tests

Temperature (°C)	Fluorine Concentration (%)	Corrosion Rate (Mills/Hr) In Period Of		
		Maximum Rate of Cr Change	80-95% U Volatili-zation	Complete Run
450	50 and 100	0.19	0.12	0.05
500	50 and 100	0.58	0.45	0.12
500	100	0.50	0.49	0.07

8.10 Fission Product Behavior (Cont'd)

spiked with about 0.1 mc of ^{103}Ru, ^{95}Nb, ^{131}I, or ^{132}Te. Solutions of these tracers were first evaporated to dryness with the corresponding carrier (about 40 to 50 mg) onto 0.5-g quantities of LiF. Fluorination was carried out by heating the salt to 550 C in an inert atmosphere and then passing a mixture of 25 percent F_2-75 percent N_2 through the melt for 30 min followed by pure fluorine for an additional 30 min at 100 ml/min (STP). The product gas stream (containing F_2, UF_6, and volatile fission product activity) was passed through a 20-g NaF trap at 400 C to remove the fission products and then into a 10-g NaF trap at 25 C, where the UF_6 product was sorbed. An additional 5-g NaF trap was inserted downstream for determination of any uranium breakthrough.

Based on a makeup value of 1.185 weight percent uranium in each of the initial salt samples, the total uranium found in three tests corresponded to recoveries of 99.27, 100.22, and 97.65 percent. However, corresponding uranium losses in the tests, based on analyses of the traps and waste salt were respectively, 0.034, 0.059, and 0.076 weight percent, indicating actual recoveries greater than 99.9 percent (see Table 8.9).

Decontamination factors obtained for ^{103}Ru, ^{95}Nb, and ^{132}Te during the fluorination step have been greater than 10^5, and thus these nuclides apparently do not make a significant contribution to the overall activity level of the UF_6 product. The relative amounts volatilized from the salt during fluorination were, respectively, about 10^{-3}, 10, and greater than 99 percent, with corresponding material balances of about 95, 10, and 0.1 percent. Essentially all the ruthenium and niobium that was volatilized was trapped on the 400 C NaF trap; however, no appreciable sorption of tellurium was detected (Table 8.10). Attempts to achieve an adequate decontamination factor (greater than 10^3) for ^{131}I have been unsuccessful so far. In the first two tests, where the UF_6 sorption trap consisted of 10 g of NaF at 25 C, decontamination factors of 14 and 8 were obtained. In the third test, decreasing the amount of NaF to 5 g and increasing the sorption temperature to 100 C

Table 8.9

Uranium Recoveries And Losses During Fluorination From MSRE-Type Salt and Sorption on NaF

Run No.	Uranium Makeup Value (Wt %)	Uranium Recovery(a) (Wt %)	Uranium Losses (% Of Total Found) Trap No. 1(b)	Trap No. 2(c)	Waste Salt	Total
1	1.185	99.27	0.012	0.009	0.013	0.034
2	1.185	100.22	0.051	0.006	0.002	0.059
3	1.185	97.65	0.026	0.022	0.022	0.076

(a) Based on analysis of all traps and scrubber solutions.

(b) 400°C NaF trap.

(c) 25°C NaF backup trap.

Table 8.10

Behavior of ^{103}Ru, ^{95}Nb, and ^{132}Te During Fluorination of Uranium From MSRE-Type Salt at 550°C

Nuclide	Total Activity (Dis/Min)					Amount of Nuclides Volatilized (%)	UF_6 Product Decontamination Factor
	MSRE Salt (Initial)	400°C NaF Trap	NaF Backup Trap	Waste Salt	UF_6 Product Trap		
^{103}Ru	-2×10^8	$<10^3$	$<10^3$	1.9×10^8	$<10^3$	10^{-3}	$>10^5$
^{95}Nb	-2×10^8	3×10^7	$<10^3$	9×10^7	$<10^3$	10	$>10^5$
^{132}Te	-2×10^8	$<10^3$	$<10^3$	4.3×10^5	$<10^3$	>99	$>10^5$

8.10 Fission Product Behavior (Cont'd)

resulted in a higher, but still inadequate, decontamination factor of 35 (Table 8.11). In this test the measurement of the temperature of the sorption bed may have been highly in error.

8.11 Processing of MSRE Salt[12/]

The Molten Salt Reactor Experiment (MSRE) fuel contained 65 mole percent LiF_4, 30 mole percent BeF_2, 5 mole percent ZrF_4, and 0.9 mole percent $^{238-235}UF_4$. The reactor fuel had operated for slightly more than one equivalent full-power year or 72 400 Mwhr.

The MSRE Fuel Processing Facility was constructed in a small cell in the reactor building to recover the original uranium charge from the salt to permit the addition of the ^{233}U fuel charge for the second phase of reactor operation.

8.11.1 Pilot Plant Process Description

The process flow sheet is shown in Figure 8.6. The molten salt was forced from the drain tank under pressure, through a freeze valve in the drain tank cell, through a metallic filter (backflow) and another freeze valve in the processing cell to the fuel storage tank. The transfer was made at 1 000 to 1 100°F, a temperature that is well above the freezing point of the salt but not hot enough to reduce the strength of the metallic filter element below a safe limit. The transfer was made with the lowest possible pressure in order to minimize stress on the filter element as the gas blew through at the end of the transfer and also to minimize entrainment of salt or activity from the fuel storage tank.

The salt was then cooled to within 50°F of the liquidus temperature to minimize corrosion and fission product volatilization during fluorination. The sample line was purged

12/ ORNL-TM-2578, August, 1969.

Table 8.11

Behavior of ^{131}I During Fluorination of Uranium From FSRE-Type Salt at 550°C

Run No.	Total Activity (Dis/Min) MSRE Salt (Initial)	400°C NaF Trap	Backup Trap	KOH Scrub Trap	Waste Salt	UF_6 Trap	^{131}I Volatilized (%)	Decontamination Factor
1	2×10^8	$\sim 10^3$	1.3×10^6		$<10^3$	1.4×10^7	>99	14
2	2×10^8	1.8×10^4	5.3×10^6	2×10^7	2×10^4	2.5×10^7	>99	8
3	1×10^9	5.6×10^6	7.2×10^7		2.7×10^6	2.9×10^7	>99	35

8.11.1 Pilot Plant Process Description (Cont'd)

with helium to prevent condensation of UF_6 at the cold upper end. The salt was sparged with either pure fluorine or a fluorine-helium mixture at a relatively high flow rate (~40 liters/min) to convert the UF_4 to UF_5. Fluorine utilization was high during this period. When all the UF_4 had been converted to UF_5, UF_6 began to form and volatilize, as indicated by a temperature rise in the first absorber and by a rise on the inlet mass flowmeter. When this occurred, the fluorine flow was reduced to 15 or 25 liters/min to increase the absorber residence time for more efficient absorption and to increase the fluorine utilization.

The gas leaving the fuel storage tank consisted of UF_6, excess fluorine, helium, MoF_6 and some CrF_4 or CrF_5 from corrosion, IF_7, and the fluorides of some other fission products such as tellurium, niobium, ruthenium, and antimony. The gas passed through a 750°F sodium fluoride trap where the chromium fluoride and most of the volatilized fission products, except iodine and tellurium, were retained. A small fluorine flow was introduced upstream of this bed to ensure an excess of fluorine and to prevent any nonvolatile UF_6 from forming and remaining on the heated NaF in the event that the fluorine utilization was near 100 percent. Although the fluorine utilization was not high enough to require this additional fluorine stream, a small flow was maintained to prevent diffusion and condensation of UF_6 in the line.

The gas stream, which now consisted of UF_6, fluorine, helium, MoF_6, IF_7, TeF_6, and a trace of other fission products, left the shielded cell and passed through five NaF absorbers in a sealed cubicle in the operating area. These absorbers were heated to 200 to 250°F to increase the reaction rate and to minimize MoF_6 absorption. The UF_6 piping was heated to at least 140°F to prevent condensation of UF_6. As the UF_6 began to load on a given absorber and the temperature

ORNL-DWG 68-8994

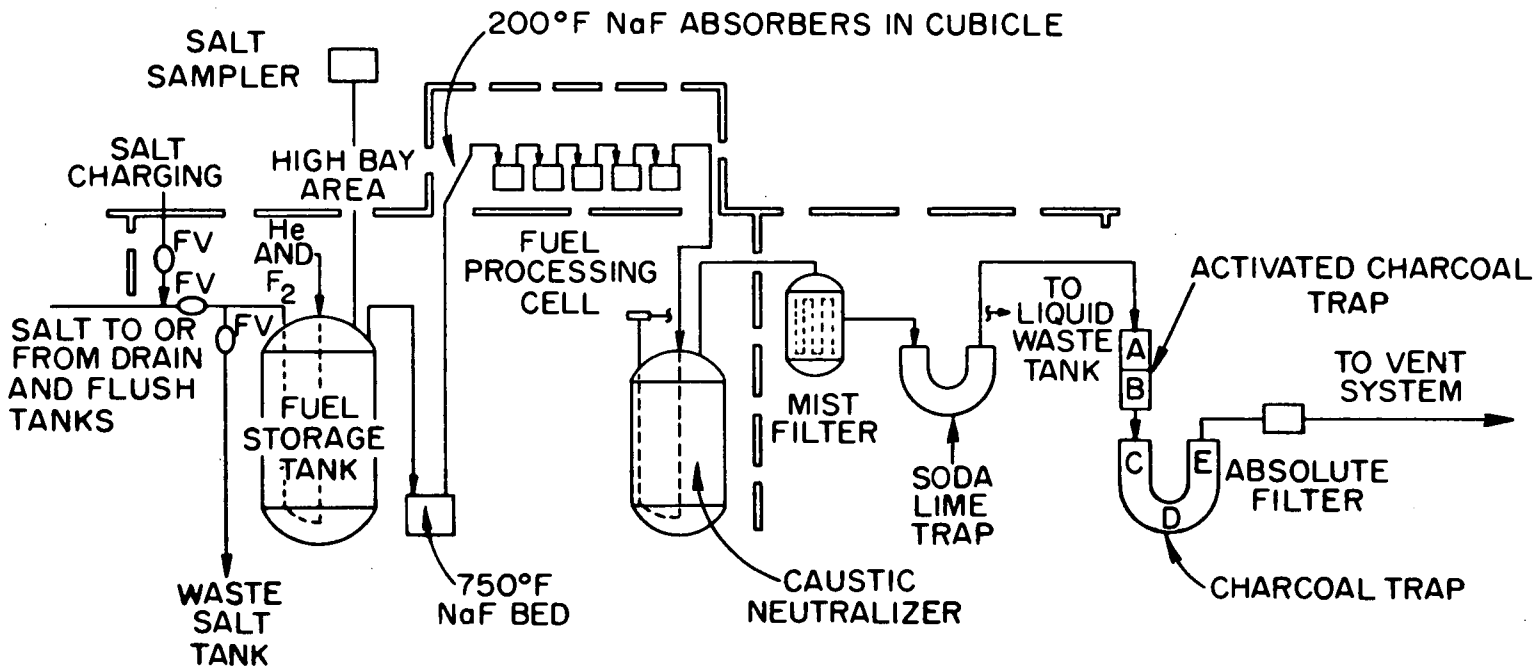

Fig. 8.6. MSRE Fuel Salt Processing System.

8.11.1 Pilot Plant Process Description (Cont'd)

started to rise, the cooling air was turned on that particular absorber to limit the temperature to a maximum of 350°F. High temperature reduced the uranium loading by promoting surface absorption and reducing penetration of the UF_6 to the inside of the pellets. The final absorber was operated below 250°F, where the partial pressure of UF_6 over the $UF_6 \cdot 2$ NaF complex allowed only a negligible amount of uranium to reach the caustic scrubber.

If the gas stream leaving the absorbers contained greater than 50 percent fluorine, it was diluted with helium before reaching the caustic scrubber. This allowed a smooth reaction in the scrubber without the production of a flame or pressure oscillations. The caustic scrubber was charged with 1,300 liters of 2 M KOH -- 0.33 M KI containing 0.2 M $K_2B_4O_7$, which was added as a soluble neutron poison. The reaction that occurred in the scrubber is:

$$6\ F_2 + 12\ KOH + KI \rightarrow 12\ KF + 6\ H_2O + 3/2\ O_2 + KIO_3 \qquad (8)$$

The scrubber solution was replaced before one-half of the KOH had been consumed, as determined by fluorine flow and calculated utilization, because dip tube corrosion was increased when the OH-concentration was less than 1 M. Besides fluorine, most of the molybdenum and iodine were removed in the scrubber.

A high-surface-area filter located downstream of the scrubber removed any particulate matter from the scrubber. During test runs, hydrated oxides of molybdenum collected at sharp bends in the line from the scrubber. A soda-lime trap (a mixture of sodium and calcium hydrates) provided a means for detecting fluorine and a means for removing traces of fluorine from the scrubber off-gas before it reached the charcoal absorbers. The trap was operated at room temperature, and the temperatures were monitored.

8.11.1 Pilot Plant Process Description (Cont'd)

Activated impregnated charcoal traps sorbed any iodine that was not removed in the caustic scrubber. The gas leaving the charcoal traps consisted of only helium and oxygen that was produced in the caustic scrubber; the oxygen amounted to about 25 percent of the fluorine flow to the scrubber. This gas flowed through a flame arrester and then through an absolute filter before being routed to the cell exhaust. It was monitored for gamma activity and iodine before being mixed with the rest of the building exhaust gas, which passed through additional filters and was finally discharged from a 100-ft tall stack.

When there was no longer any evidence of absorber heating, the fluorine flow was stopped and the salt was sampled and analyzed. The uranium concentration in the salt was expected to be less than 50 ppm at this time.

8.11.2 Equipment Description

a - Fuel Storage Tank/Fluorinator

The construction of the fuel storage tank, or fluorinator (see Figure 8.7), was similar to that of the reactor drain tanks, except that the fluorinator was 30 inches taller to provide about 38 percent freeboard above the normal liquid level. This extra height minimized salt carryover during gas sparging. The tank was suspended inside the heater and insulation assembly to minimize the weight cell tare weight. There was no provision for cooling since the heat loss limits the temperature to less than 200°F after 2 weeks' decay (Figure 8.8).

The fuel storage tank was heated by four sets of heaters, which provide 5.8 kw on the bottom, 11.6 kw on the lower sides, 5.8 kw on the upper sides, and 2 kw on the top. Each group of heaters was controlled by a separate powerstat. During the period in which UF_4 was converted to UF_5 (when the fluorine utilization was high), the

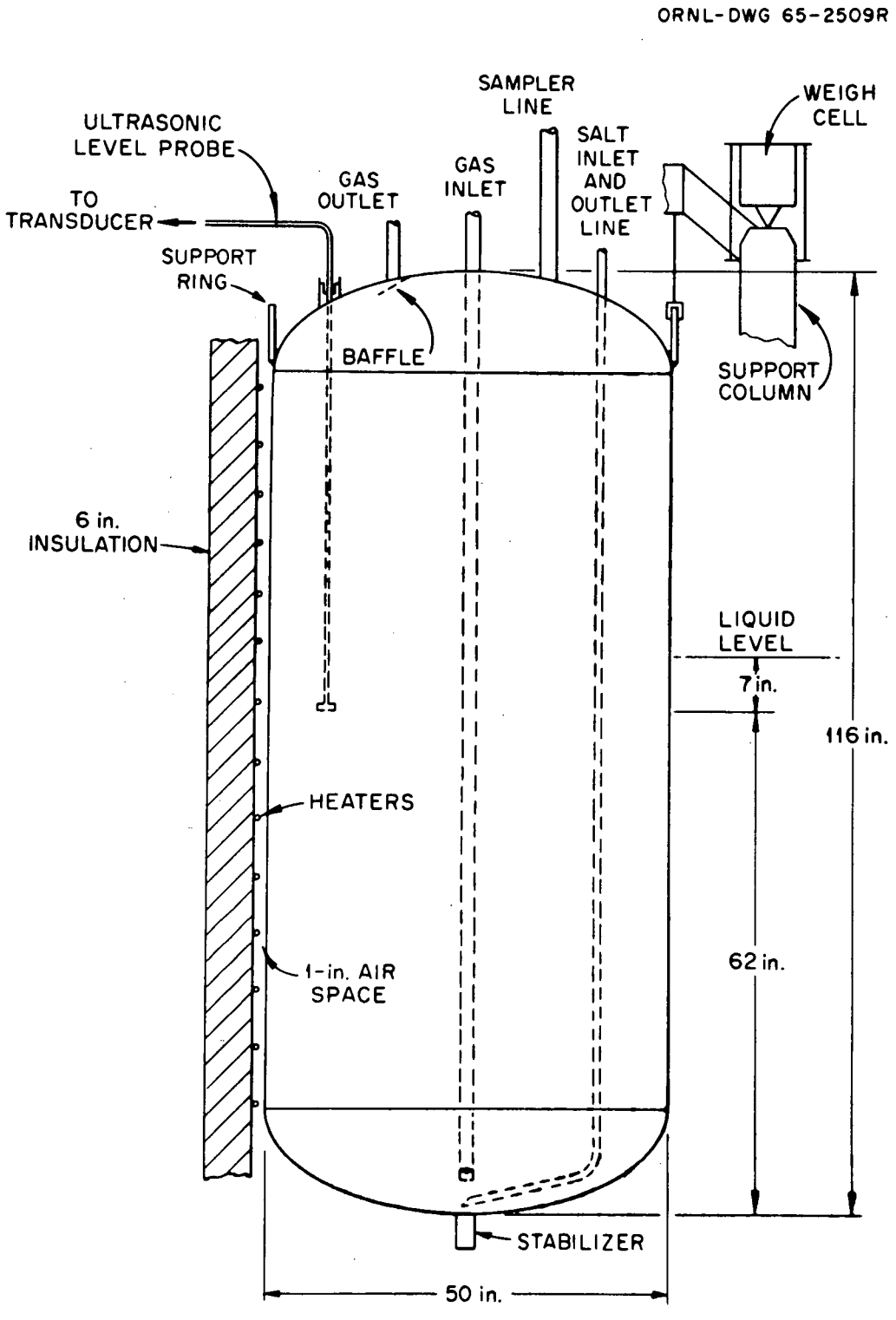

Fig. 8.7. Fuel Storage Tank.

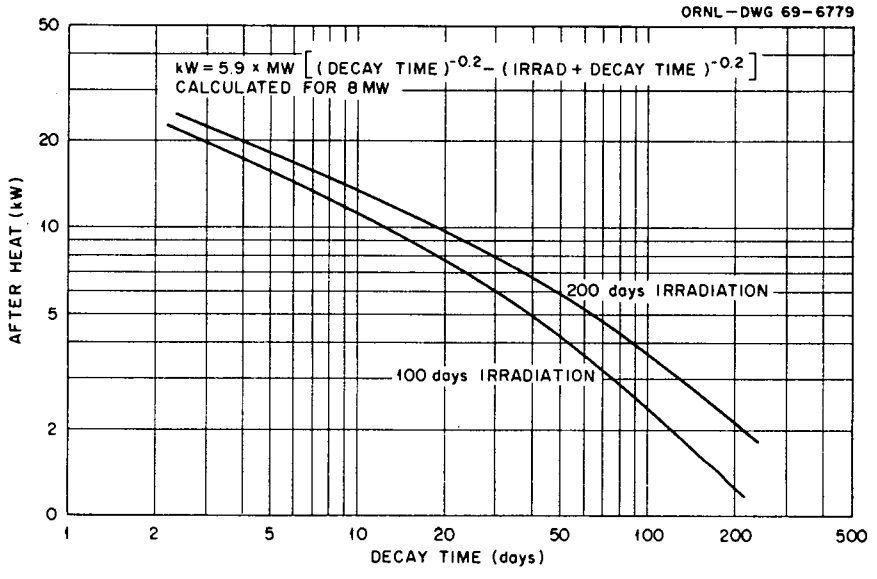

Fig. 8.8. MSRE After Heat.

8.11.2 Equipment Description (Cont'd)

a - Fuel Storage Tank/Fluorinator (Cont'd)

heat of reaction, plus the afterheat, provided sufficient heat to maintain the salt at 850°F. About 12 kw of electrical heat was required during the reduction operation at 1225°F.

The gas inlet line for the fuel storage tank had a normal submergence of 64 in., and the differential pressure between this line and the gas space provided an indication of liquid level. The tank was equipped with an ultrasonic probe to check the weigh cell calibration during the filling and emptying operations.

Several safety interlocks are provided on the fuel storage tank:

1 - The gas sparge line was automatically vented if the pressure in this line decreases to that of the gas space. This prevents accidental backup of molten salt in the cold gas inlet line.

2 - An automatic valve opened in the tank off-gas line if the tank pressure reaches 50 psig. An alarm sounded at 5 psig, which was a pressure higher than that normally found during operation.

3 - Fluorine flow to the tank was stopped if the helium purge flow down the sampler line stops. This minimized the amount of fluorine, UF_6, or radioactive gases which could diffuse into lines leaving the cell in the event that the helium supply was lost.

4 - The fluorine supply valve was designed so that it must be closed before the salt sampler valve can be opened.

b - NaF Trap

The NaF trap, shown in Figure 8.9 was operated at 750 to 800°F. In this temperature range, volatile

8.11.2 Equipment Description (Cont'd)

b - NaF Trap (Cont'd)

ruthenium, niobium, antimony, and chromium fluorides were absorbed, while uranium and molybdenum hexafluorides passed through. The slightly oversized line from the fuel storage tank was also heated to 750°F to prevent the absorption of uranium at the trap inlet. The trap had two sets of heaters that were separately controlled, 2.25 kw in the center pipe and 9 kw on the sides. There were three thermocouples located in wells at the inlet, center, and outlet of the trap, respectively, which were maintained at temperatures within 10°F of each other. With 4 in. of insulation, the heat loss was about 1270 w at 775°F.

To prevent the trap from plugging with volatilized chromium fluorides, it was designed to be replaceable. The piping associated with the trap was flanged, with provision for remote leak detection, and the heater and thermocouple leads were provided with disconnects. Because of the anticipated high radiation level, a defective trap would be disconnected and moved to an empty space within the cell instead of being removed from the cell. However, no increase in pressure drop was detected between the fuel storage tank and the absorber inlet. Chromium fluoride volatilization was expected as the uranium concentration in the salt decreased, but such volatilization was apparently almost insignificant until the concentration became as low as 20 ppm.

c - Caustic Scrubber

The caustic scrubber shown in Figure 8.10 was used for disposal of excess fluorine. The Monel spray ring distributor originally installed in the tank was replaced with two dip lines, each with three 3/8-in. holes, as shown in the figure. The dip lines had

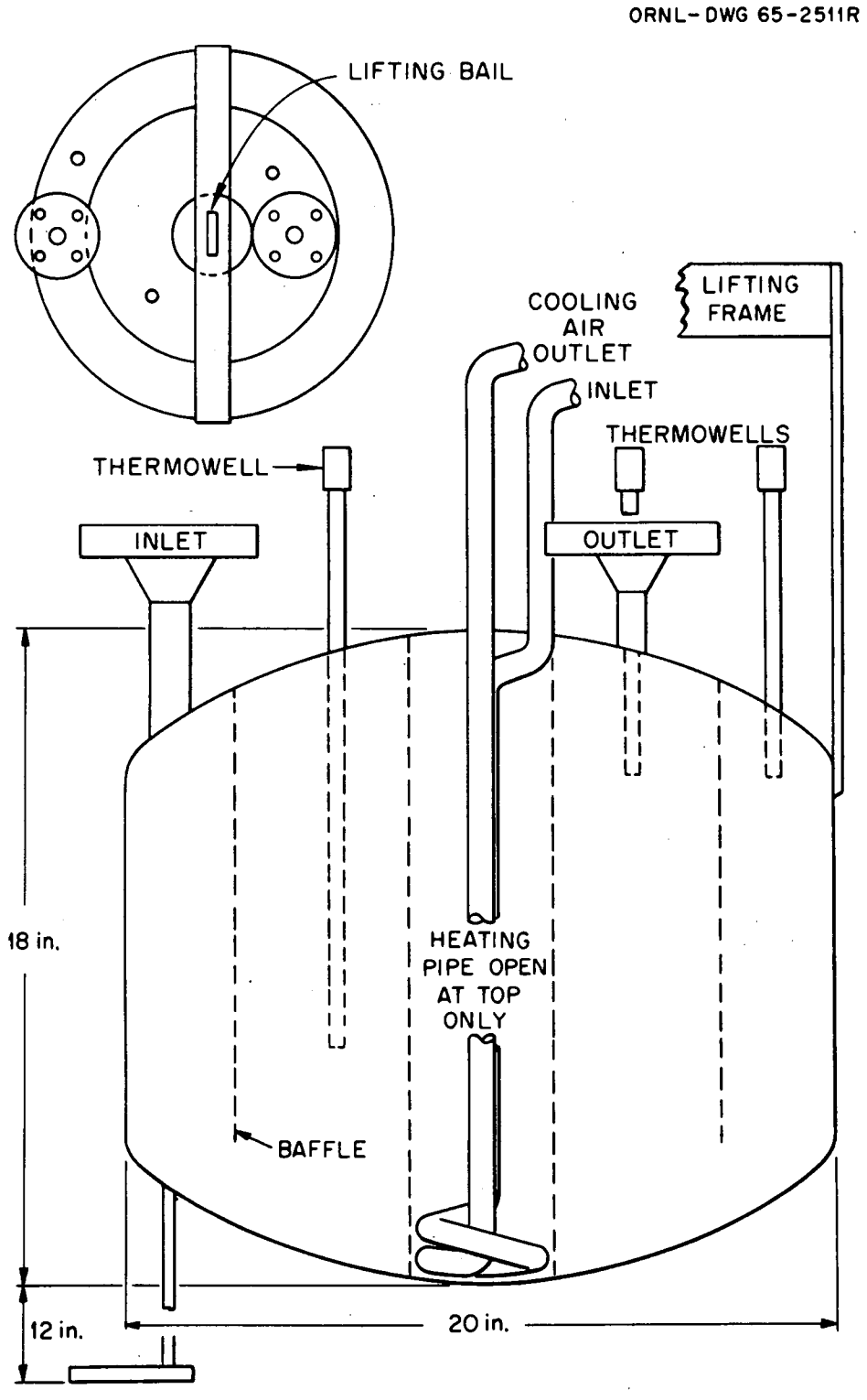

Fig. 8.9. Sodium Fluoride Trap

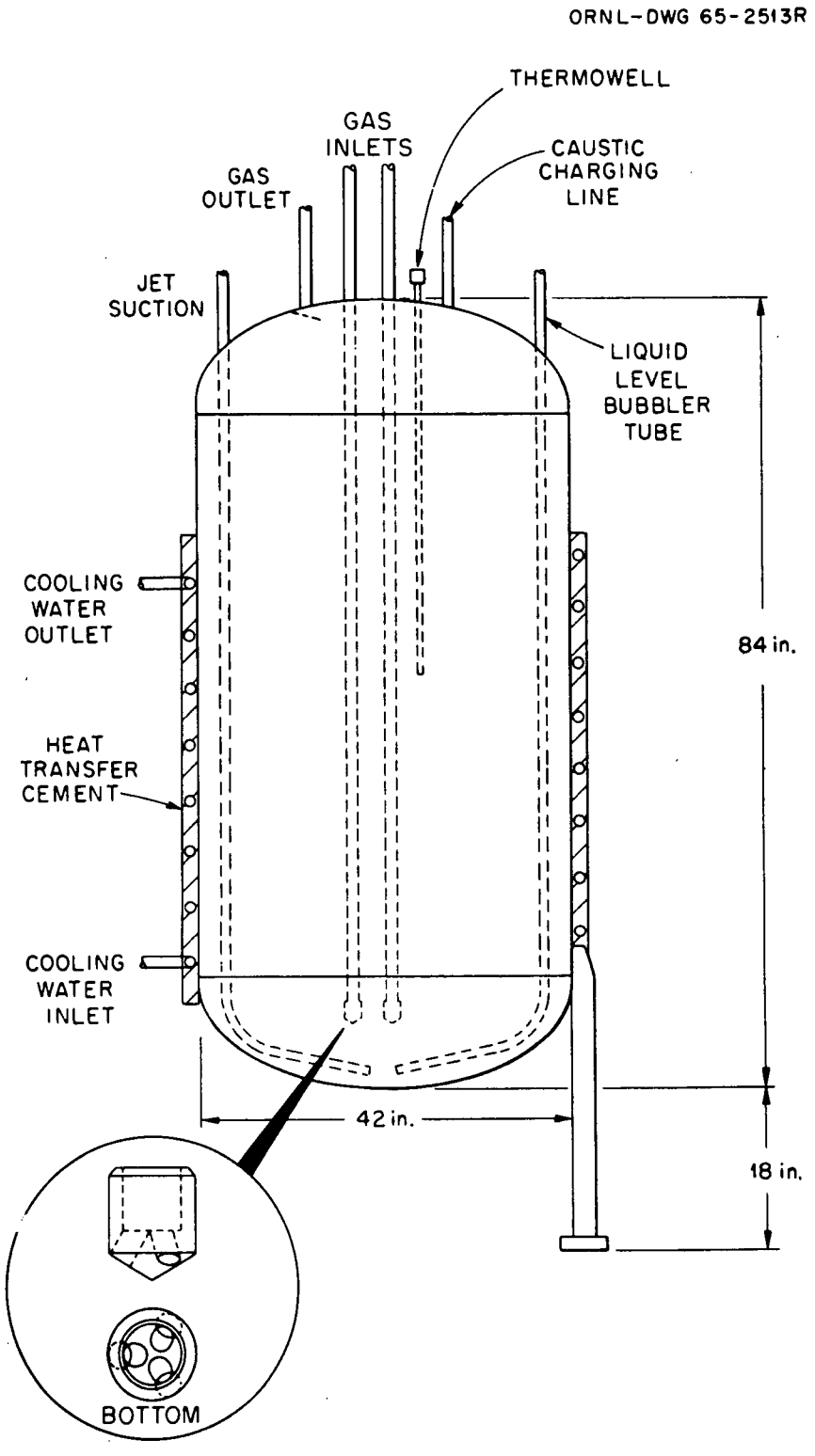

Fig. 8.10. Caustic Scrubber.

8.11.2 Equipment Description (Cont'd)

c - Caustic Scrubber (Cont'd)

shutoff valves with extension handles to permit alternating the lines when plugging occurs. The new dip lines were made of Inconel, which had a higher corrosion resistance (than Monel) to the KOH-KI-F_2 reaction. The scrubber and other internal piping were originally constructed of Inconel. The cooling water to the coil was not metered; however, only a fraction of the full flow was required to control the temperature during fluorination. On one occasion, in which the temperature was allowed to increase from less than 80°F to greater than 100°F, no decrease in plugging was noted.

The caustic scrubber was equipped with a contact microphone similar to the one used for the fuel storage tank. It was used intermittently as a check on the gas flow rate through the dip lines. During a 2-hour period in Run 6, unusually loud, rapid noises, accompanied by rapid but small pressure fluctuations in the line to the scrubber, were heard. Switching dip tubes restored the normal bubble flow sound.

d - Mist Filter

The mist filter was a high efficiency Fiberglas air filter consisting of fifty-five 9-1/2-in. diameter by 28-in. long bags hanging vertically in a 30-in. diameter by 4-ft high stainless steel vessel. The total filter area was about 50 ft^2. The filter, which was mounted in an opening in a horizontal support plate near the top of the vessel, was caulked to prevent bypassing. The tank was heated with steam coils that were wrapped around the tank to prevent condensation of the moisture that is carried over from the caustic scrubber. A thermowell installed in the gas space above the filter

8.11.2 Equipment Description (Cont'd)

d - Mist Filter (Cont'd)

was used to adjust the amount of insulation in order to prevent overheating and damage to the filter binder.

e - Soda-Lime Trap

The soda-lime trap, shown in Figure 8.11, was charged with SO_2 soda-lime, which is very effective for the removal of fluorine at room temperature. To prevent excessive pressure drop with a gas having a high fluorine content, the soda-lime was mixed with an equal volume of 4-to 8-mesh alumina, which has a very slow reaction rate at low temperatures. To prevent condensation of water vapor in the gas from the scrubber, the soda-lime trap was insulated and traced with low-temperature steam tubing.

Thermocouples were installed near the inlet and near the outlet. During the processing of the flush and fuel salts, no temperature rise was observed. Thus it appears that no unreacted fluorine escaped from the caustic scrubber.

f - Charcoal Traps

The charcoal traps shown in Figure 8.12 were considerably overdesigned to permit the handling of the large amount of iodine that was present in 30-day decayed MSRE fuel. The original trap (inlet) was initially charged with replaceable cannisters, each of which had a total bed depth of 1-1/2 inches. The final capacities and residence times are shown in Table 8.12.

The traps were steam-traced in the same manner as the soda-lime trap. Surface thermocouples (TE) are located at the inlet of the first trap and at the inlet and the outlet of the backup trap. Temperatures were maintained between 175 and 205°F during processing, and no additional heating was detected at any time.

ORNL-DWG 68-2730A

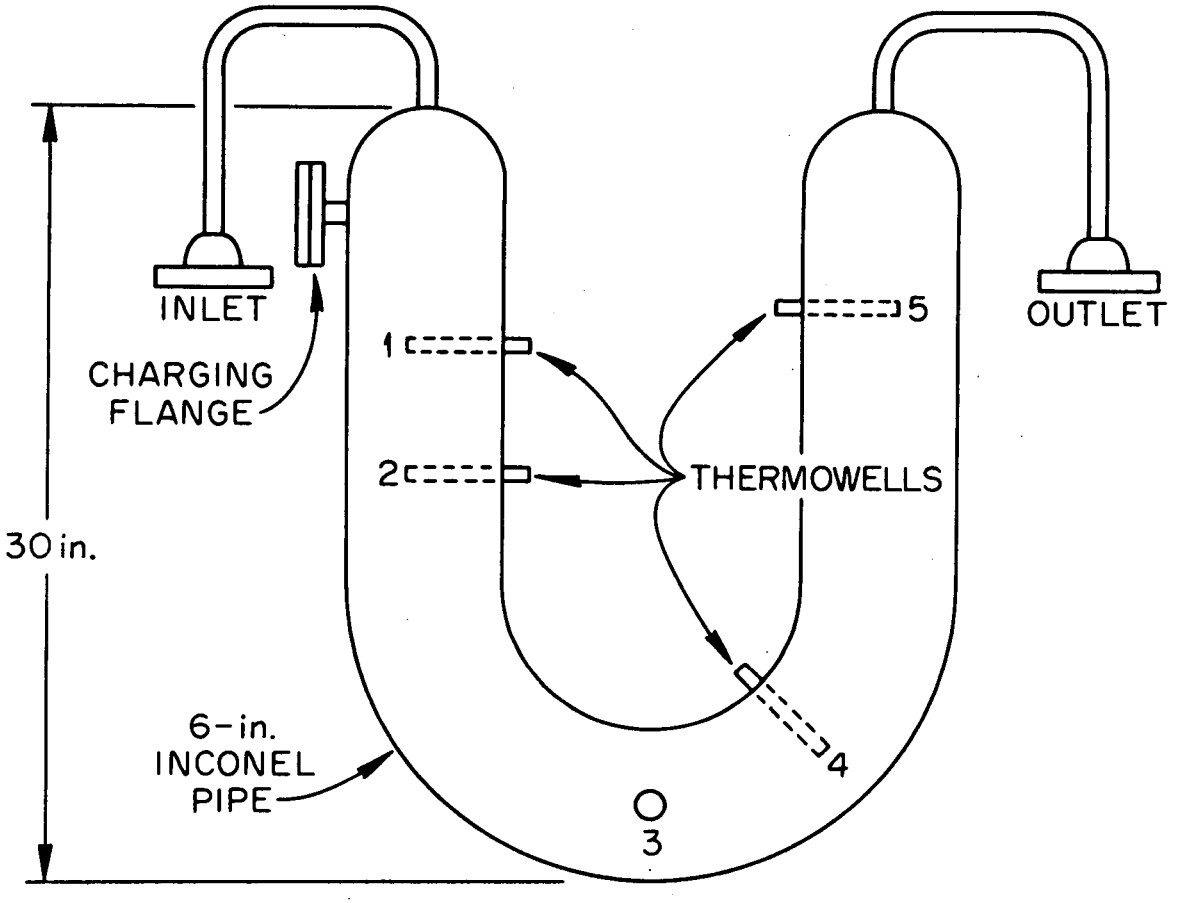

Fig. 8.11. Soda-Lime Trap

ORNL-DWG 68-13777

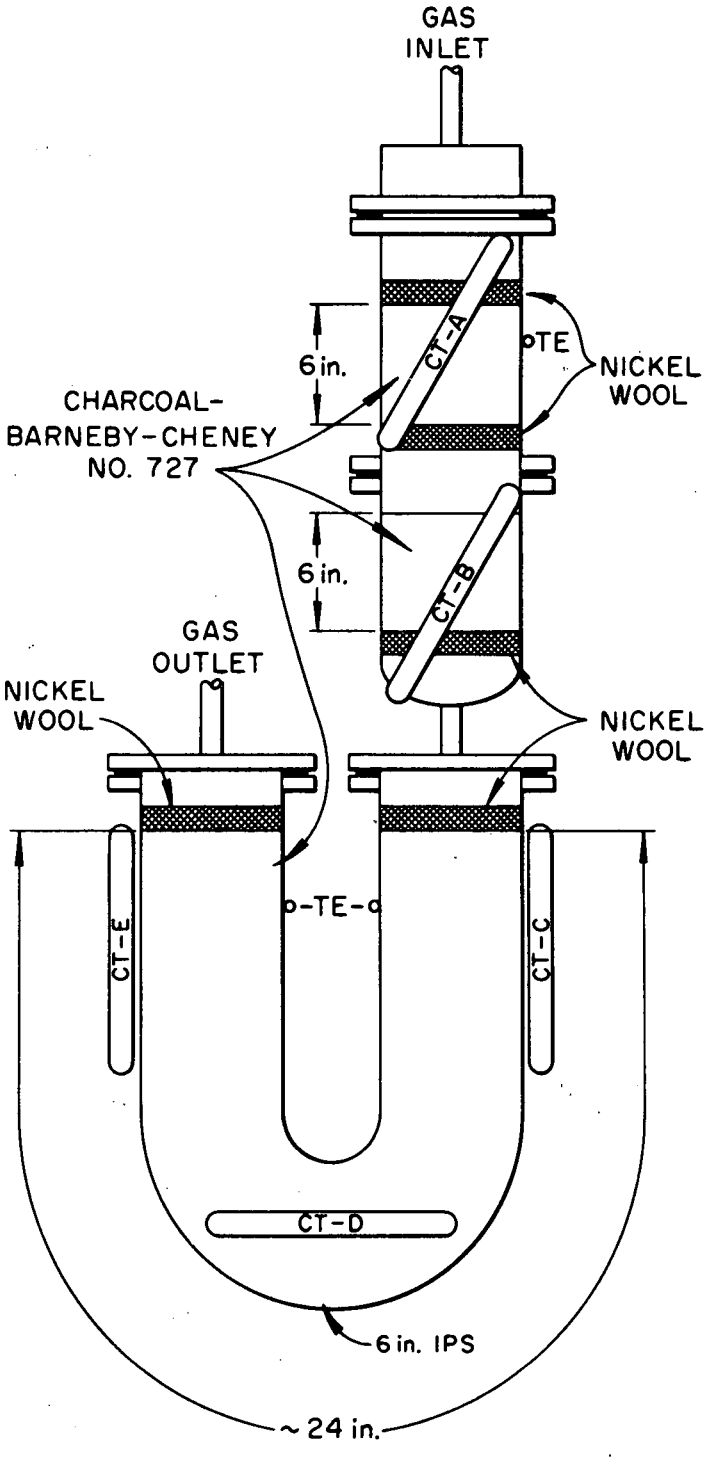

Fig. 8.12. Charcoal Traps

Table 8.12

Charcoal Traps

Trap	Diameter (In.)	Length (In.)	Volume (Liters)	Residence Time At Average Flow of 16 Std Liters/Min (See)
Inlet	6	12	5.84	22
Backup	6	22	3.17	12
Total		34	9.01	34

8.11.2 Equipment Description (Cont'd)

f - Charcoal Traps (Cont'd)

Four ion chambers, located at the inlet and the outlet of each trap, were used to detect the accumulation of iodine; however, because the fuel had been allowed to decay for such a lengthy period, none of the readings increased during processing. Five chambers (CT-A-E), as shown in Figure 8.12, were used during the fluorine reactor tests.

g - UF_6 Adsorbers

Five absorbers (Figure 8.13), connected in series, were located in a 9 ft 4 in. x 2 ft 4 in. x 2 ft 2 in. sealed cubicle located in the operating area above the processing cell. The cubicle was vented to the cell, where a blower provided additional negative pressure (below the -0.3 in. H_2O in the cell) when air was being used to cool the absorbers. This blower failed during fuel salt run 1. When loaded to within 1/2 in. of the top, each absorber held about 25 kg of NaF. The minimum cross-sectional area (outlet side) was 0.46 ft^2.

Each absorber was mounted in an insulated can with a removable insulated cover. An air cooling coil and an electric heater were positioned below each absorber. A separate thermocouple on the bottom plate of each heater indicated overheating or burnout of a heating element. Each heater was used to heat each absorber to about 200°F before the start of UF_6 absorption. When absorption began, the heat was turned off and air was turned on.

All absorber piping located upstream of the final absorber was heated and insulated to prevent condensation of UF_6. The absorbers were connected with removable jumpers having ring-joint flanges. The flanges were leak-tested before the absorber cubicle was sealed. Copper rings were used, and a torque wrench was employed to ensure that the pressure on the rings was uniform.

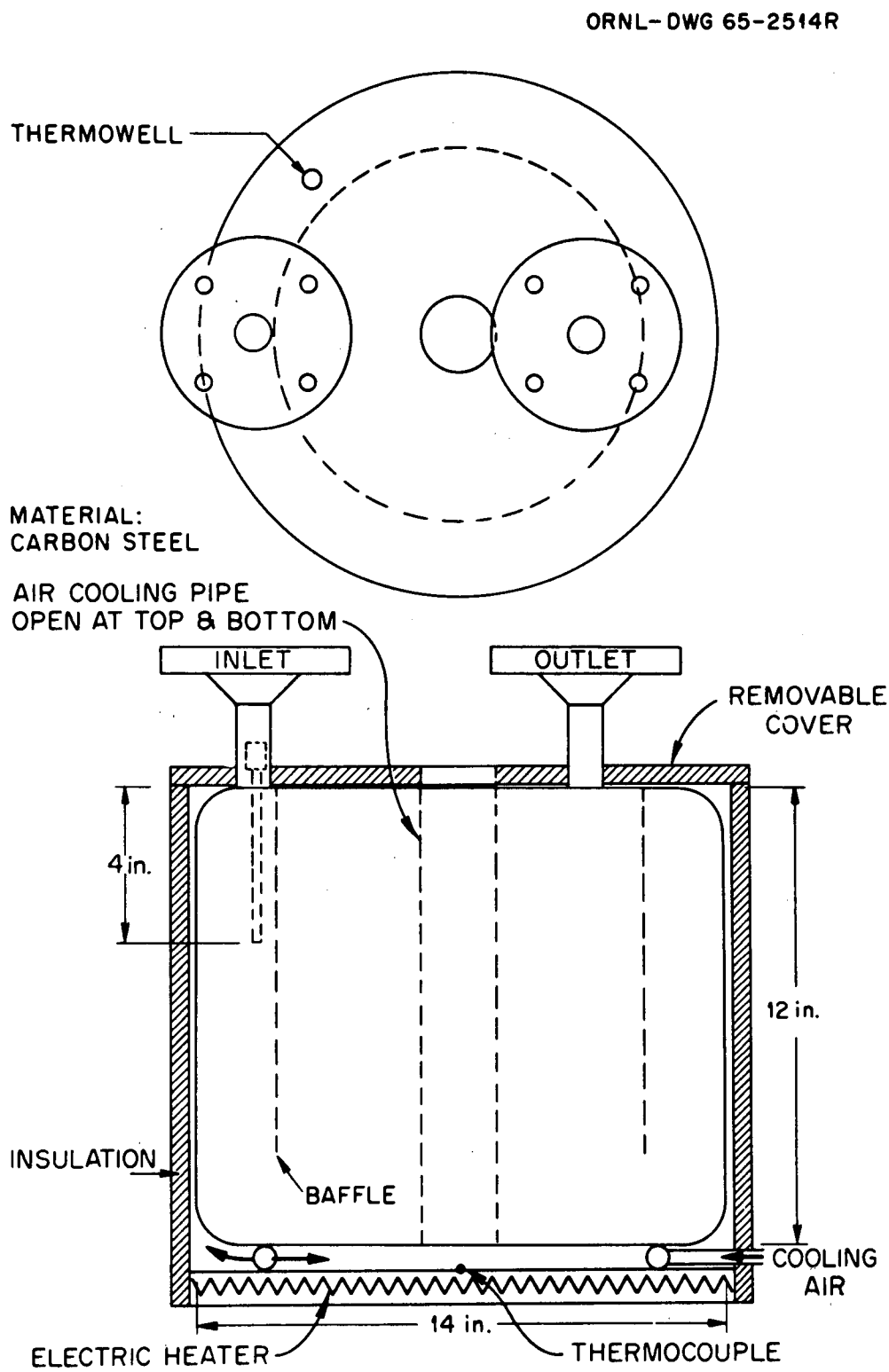

Fig. 8.13. UF_6 Absorbers

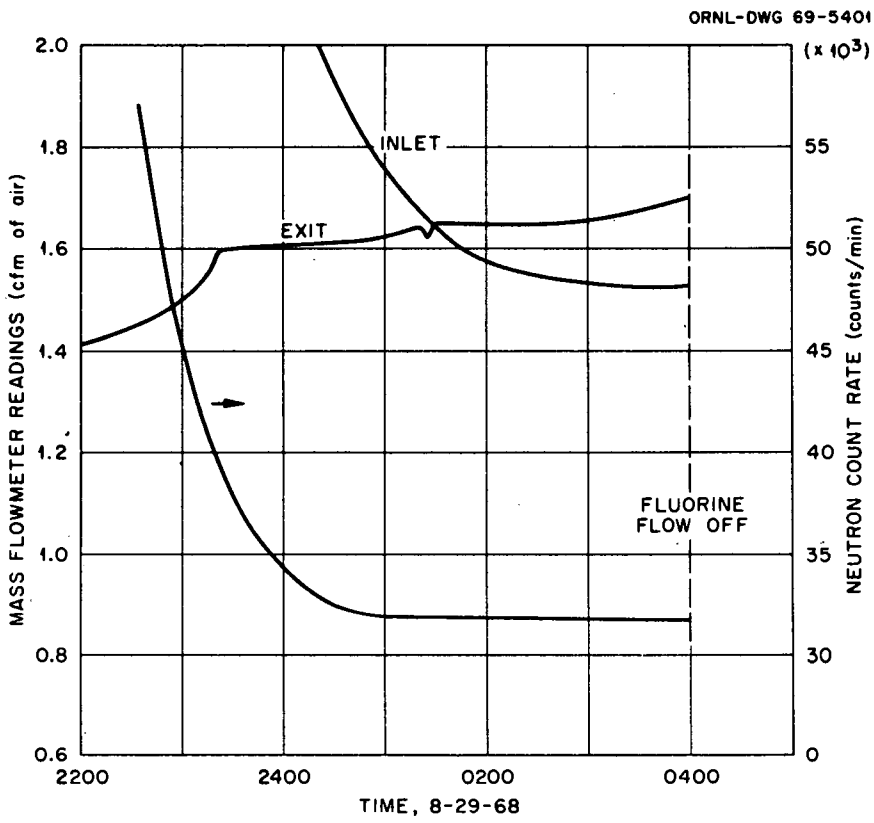

Fig. 8.14. Mass Flowmeter Readings at End of Run No. 6

8.11.3 Fluorination of Flush Salt

The flush salt picked up about 6-1/2 kg of uranium from the fuel salt during the seven flushes.

Fluorination was started by sparging with 25 std liters of fluorine per minute diluted with 20 std liters of helium per minute. An additional 15 std liters of helium per minute was used to purge the sample line. The reading on the inlet mass flowmeter rose rapidly and reached a maximum after 48 min of fluorine sparging. The peak reading corresponded to a fluorine utilization of about 15 percent. The readings of the thermocouples on the No. 1 and No. 2 absorbers rose but lagged the initial rise in the mass flowmeter reading by 20 to 30 min. The reading on the exit mass flowmeter rose as expected as the fluorine utilization decreased from its peak but attained a much higher reading than expected. When the reading for this meter went off-scale, the fluorine was bypassed around the salt to investigate the reason for this high reading. It was concluded that MoF_6 was the cause; therefore, fluorine sparging was resumed after 95 min. After a total of 5 hours of fluorine sparging, the fluorine supply was exhausted. Since the reading on the inlet flowmeter had almost become constant, the salt was sampled and had a uranium analysis of 24 ppm. Fluorine sparging was carried out for an additional 109 min. Analysis of a salt sample taken at this time indicated a uranium concentration of only 7 ppm (desired $<$ 10 ppm).

The absorbers were loaded with low-surface-area NaF for the flush salt processing and were heated to 200-250°F to increase the reaction rate. Since the amount of uranium in the flush salt was only about half the capacity of one absorber, very little uranium was expected to be deposited on the last four absorbers. However, almost 30 percent was collected on the second absorber and possible 3 percent on the third, although no temperature rise was detected on the last three absorbers. For the fuel salt runs, it was, therefore, decided to use only high-surface-area material in the final three absorbers to permit operation with only

8.11.3 Fluorination of Flush Salt (Cont'd)

one backup absorber. The temperature rise on the first absorber was only 39°F; thus cooling air was not required. Although some plugging of the caustic scrubber dip lines occurred, switching to the spare line for several minutes always cleared the line.

8.11.4 Fluorination of Fuel Salt

Salt was sparged for 30 min. at a flow rate of 20 std liters/min. The fluorine flow was then increased to 40 std liters/min for the conversion of UF_4 to UF_5. Fluorine utilization was very high (~70 percent) during this period. For almost 6 hours, the adsorber inlet and outlet meters read the same, indicating that no adsorbable compounds were volatilized. For the next 100 min, the readings on both meters rose (the inlet meter at the faster rate), but no adsorber heating was noted. This was interpreted to indicate MoF_6 (from Hastelloy-N by corrosion) volatilization and either decreasing fluorine utilization or incomplete adsorption of the MoF_6 on the NaF. After 7-1/2 hours, UF_6 adsorption was indicated by a temperature rise on the first absorber. Fluorine flow as decreased to increase fluorine utilization and adsorber residence time.

To ensure that essentially no uranium was lost to the caustic scrubber, a fifth absorber was used as a backup. The first run was terminated when uranium broke through to the third adsorber. Since no temperature rise was observed for the fourth adsorber during purging, the second run was continued until uranium broke through to the fourth adsorber. The third, fourth, and fifth runs were terminated after 60, 75, and 95 min, respectively, of loading on the fourth adsorber without any temperature rise being observed on the fifth adsorber. The sixth run completed the operation; no uranium was found on the fourth or fifth adsorber. Fluorine flow was stopped when the inlet mass flowmeter showed no further decrease for an hour (Figure 8.14). End point determination was somewhat difficult because of the almost

8.11.4 Fluorination of Fuel Salt (Cont'd)

continuous buildup of restrictions in the scrubber dip tubes, accompanied by an increase in system pressure and a decrease in fluorine flow. The increase in the reading of the exit meter at the end of the run was probably due to MoF_6 being desorbed since the reading was too high to be accounted for by helium and fluorine. The neutron counter near the fuel storage tank provided another sensitive indication of the end point. The neutron count rate fell rapidly during the last few hours of fluorination but had become constant by the time the fluorine flow was stopped.

After Run 6, analysis of a fuel salt sample indicated 26 ppm, or about 130 g, of uranium remaining in the salt. This was a very acceptable loss.

8.11.5 Fluorine Utilization

The efficiency of the fluorination reaction was measured by the percentage of the fluorine (after subtracting the fluorine consumed by corrosion) that was used in the reaction with the uranium. The fluorine consumed by corrosion was assumed to be constant at 2.5 std liters/min. Correction was also made for the inert gases present (assumed to be nitrogen) in the fluorine supply and the effect of the reduced gas density on the orifice flowmeter. Fluorine utilization is a function of melt temperature, fluorine flow rate, uranium concentration, and dip tube submergence. Laboratory tests had shown a decrease in utilization from 8.0 to 3.8 percent as the temperature was reduced from 930°F to 840°F. The higher utilization (average, 39 percent) during the fuel salt processing was probably due both to lower gas velocities by a factor of 5 and greater dip tube submergence (by a factor of 15) than used in laboratory tests. Utilization was very high before the start of UF_6 volatilization (average, 71 percent) and, after that, seemed to be relatively insensitive to uranium concentration until nearly all the uranium was volatilized

8.11.5 Fluorine Utilization (Cont'd)

(see Figures 8.15, 8.16 and 8.17). The highest average utilization during UF_6 volatilization occurred in the fifth run (see Table 8.13).

Until 90 min before the start of UF_6 volatilization, the readings of the adsorber inlet and outlet mass flowmeters were equal, indicating the absence of any adsorbable constituents in the gas stream. These flowmeters were used to calculate the fluorine utilization, as shown in Figure 8.18. The utilization decreased when the fluorine flow rate was increased and also when MoF_6 and UF_6 began to be vaporized. It is thus assumed that the fluorine utilization does not change, when the fluorine flow is steady, until volatilization begins. During the MoF_6 volatilization period (before UF_6 volatilization began), the utilization was calculated by difference, using the utilizations in the two previous periods and assuming that all the UF_4 was converted to UF_5 prior to uranium volatilization. The fluorine flow rates were adjusted for the fluorine that was consumed by corrosion. During the volatilization of UF_6, the fluorine utilization was calculated from the increase in absorber weights. The inlet mass flowmeter indicated a high utilization toward the end of each run because of the stratification of the dense UF_6 in the fuel-storage-tank gas space.

The fluorine flow rates calculated from the decrease in pressure in the fluorine trailers agree reasonably well with the results obtained with the orifice flowmeter except in Runs 2 and 5. In Run 2 a fluorine flow of 90 percent of the rate indicated by the flowmeter was used since this produces: (1) utilizations in reasonable agreement with those observed in the other runs, (2) an integrated UF_6 flow from the inlet meter that is in agreement with the absorber weight increase, and (3) a reasonable amount of MoF_6 leaving the absorbers as calculated from the outlet meter. In Run 5 a fluorine flow of 110 percent of the rate indicated by the flowmeter was used.

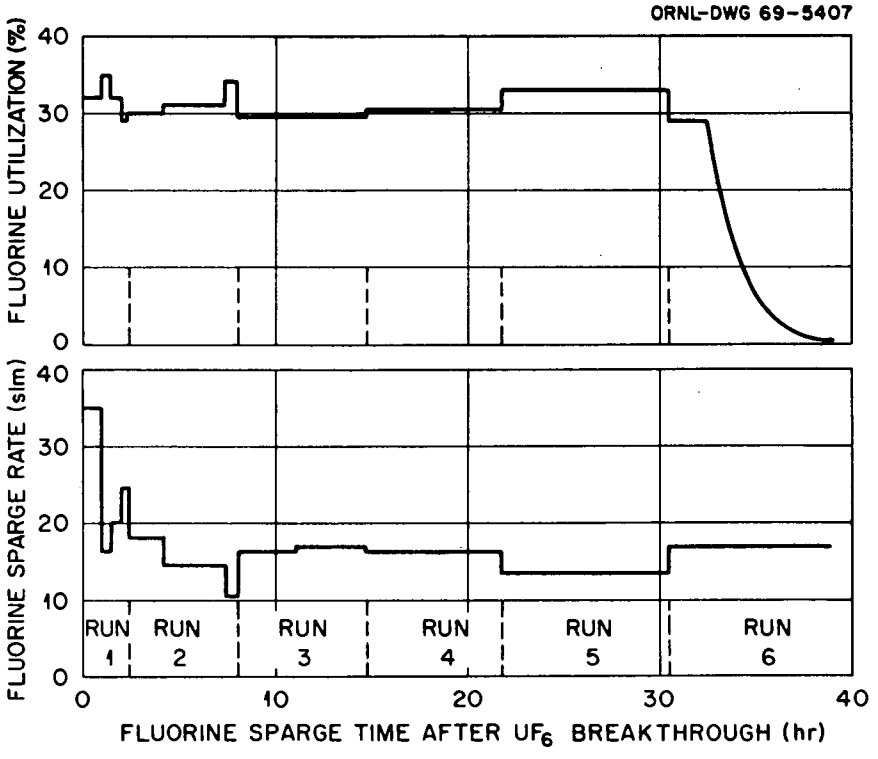

Fig. 8.15. Fluorine Flow Rate vrs Utilization.

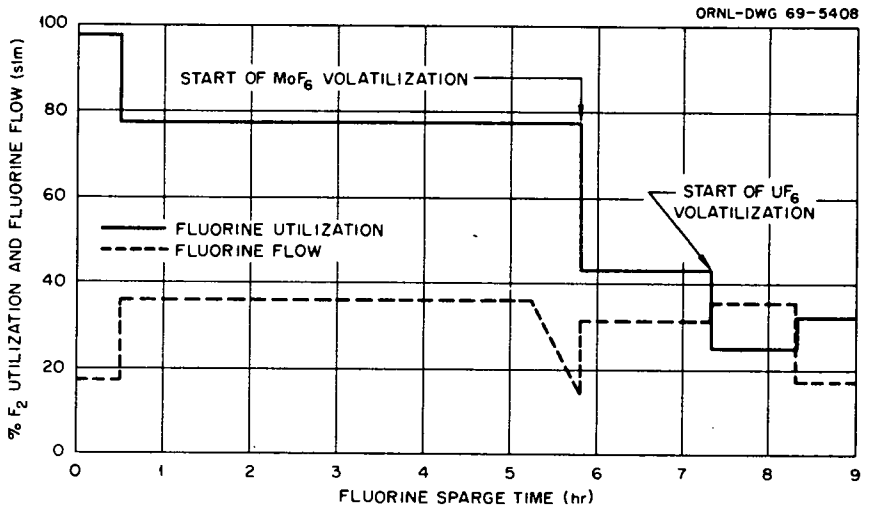

Fig. 8.16. Fluorine Utilization at the Start of Run 1.

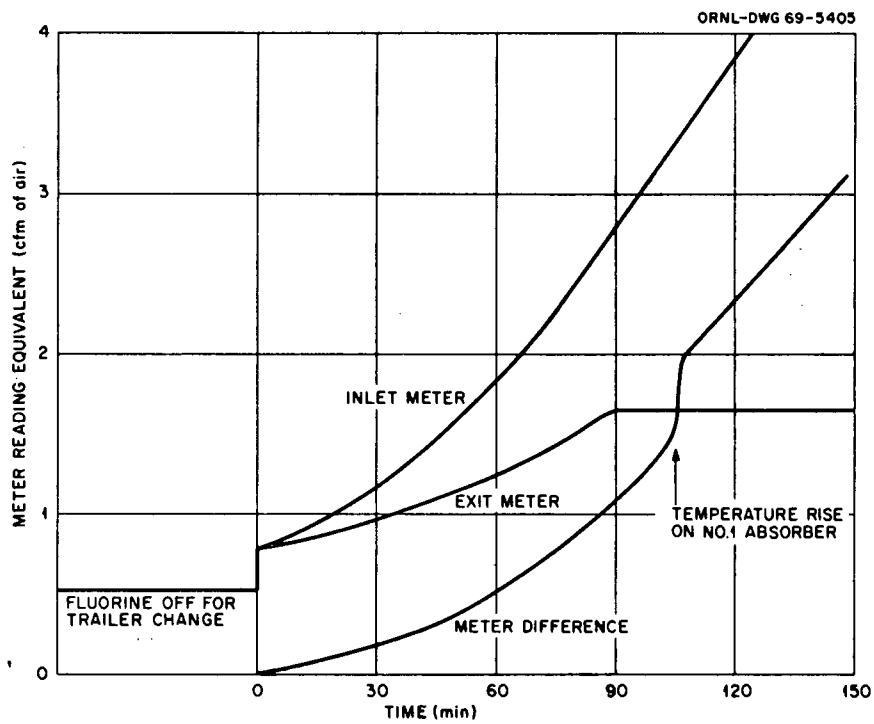

Fig. 8.17. Mass Flowmeter Readings Before Start of Volatilization of UF_6 From Fuel Salt.

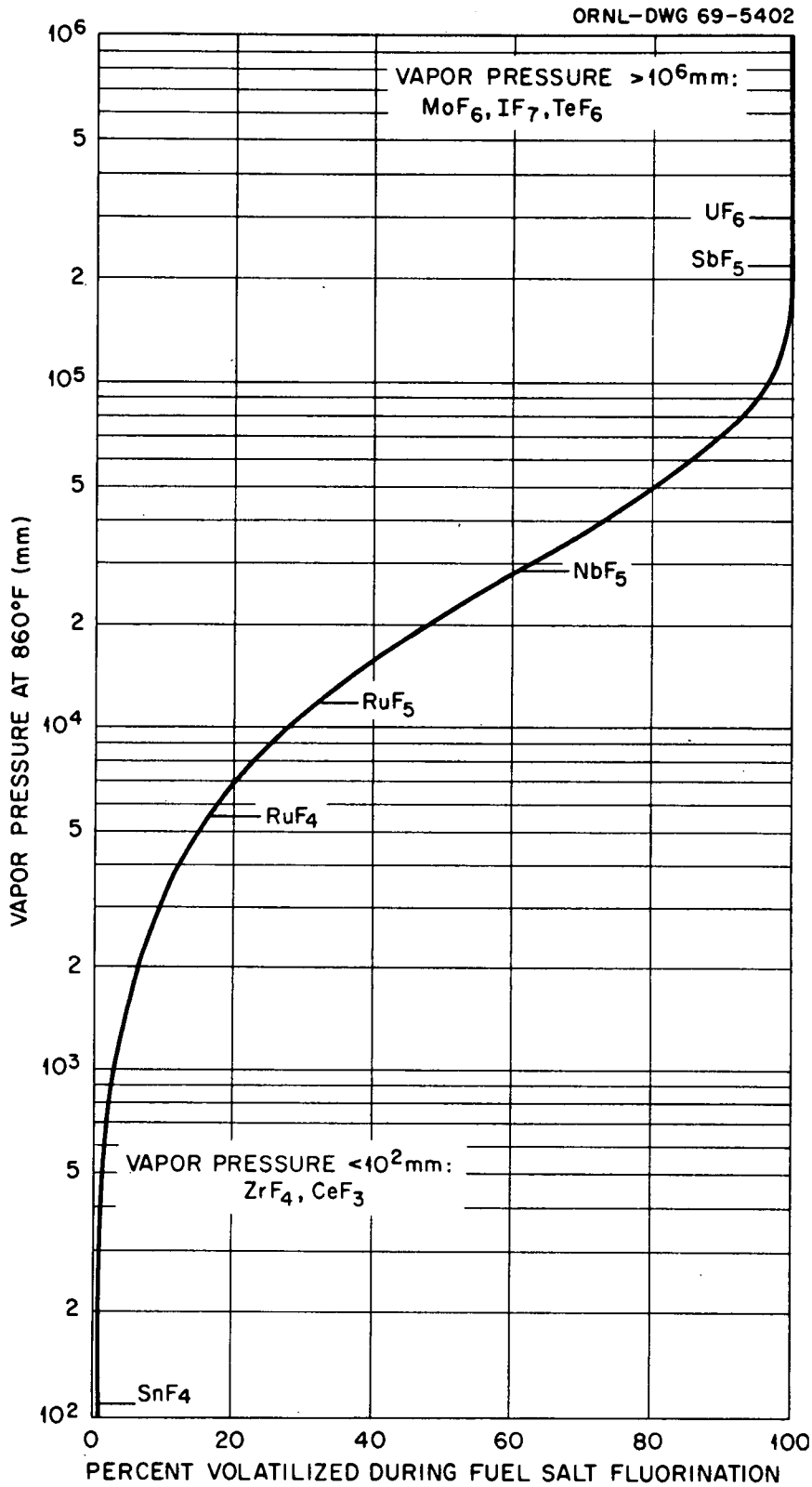

Fig. 8.18. Calculated Fission Product Volatilization During Fuel Salt Fluorination.

Table 8.13

Fluorine Utilization

	Corrected F_2 Flow (std liters/min)	Percentage F_2 Utilization
Flush salt	19.8	7.7
Fuel salt, overall	18.8	39
Run 1--Before MoF_6 volatilization	17.1	98
--Before MoF_6 volatilization	36.0	77
--During MoF_6 volatilization	31.5	43
--During UF_6 volatilization	26.2	32
Run 2--During UF_6 volatilization	15.3	31
Run 3--During UF_6 volatilization	16.7	29
Run 4--During UF_6 volatilization	16.2	31
Run 5--During UF_6 volatilization	13.5	33
Run 6--During UF_6 volatilization	16.9	13

Table 8.14

Corrosion During Fluorination

	Corrosion (mils/hr), Based On:				
	Mo	Ni	Fe	Cr	Average[a/]
Flush salt		0.10	0.2	0.15	0.11
Fuel salt	0.2	0.04	0.2	0.14	0.09

[a/] Weighted for concentration in Hastelloy-N.

8.11.6 Corrosion

One of the major problems encountered during processing was the corrosion of the fuel storage tank. Coupon testing in the Volatility Pilot Plant[13/] and at Battelle Memorial Institute[14/] had shown Hastelloy-N to be superior, as a material of construction, to nickel (mainly because of the absence of intergranular corrosion) and as resistant to corrosion as any of the other materials tested; however, the corrosion rate was still much higher than desired. The corrosion rates shown in Table 8.14 were calculated from the increase in Cr, Fe, and Ni contents of the salt and from the amount of MoF_6 volatilized (Figure 8.16).

The corrosion rates calculated during flush salt processing may be high since they include a 2-hour conditioning period at 1 125°F with fluorine. All other fluorine exposures were at 850 to 860°F. The corrosion rate, based on molybdenum, was calculated from the rise of the reading of the inlet mass flowmeter prior to the temperature rise in the first absorber (Figure 8.17). It is believed that this rise was due to the presence of MoF_6, which is more volatile than UF_6 and has almost as large a heat capacity. The corrosion due to molybdenum in the flush salt could not be calculated directly because of the short time interval (20 min) between the two indications. The equivalent time interval for the fuel salt was 90 min; thus the calculation in this case should be reasonably accurate. A 15-min time lag in the temperature response was assumed in the calculations. With the fuel salt there was a simultaneous, but smaller, rise on the exit flowmeter reading. This is believed to be caused mainly by the increasing amount of unreacted fluorine due to reduced utilization. The average exit meter reading agreed reasonably well with the calculated reading

---

13/ ORNL-2832, June 5, 1961.

14/ BMI-X-234, May 27, 1963.

8.11.6 Corrosion (Cont'd)

for 43 percent fluorine utilization (see Table 8.13). The higher corrosion rate, based on molybdenum, is probably due to surface leaching and rapid volatilization of the highly volatile MoF_6.

8.11.7 Molybdenum

During reactor operation, corrosion product and fission product molybdenum exists as finely divided metal. In this form, most of it leaves the salt, either in the gas stream or by deposition on the graphite and metal surfaces. During fluorination, the molybdenum in the Hastelloy-N fuel storage tank is attacked and converted to MoF_6. Molybdenum is the only major constituent of the fuel storage tank forming a highly volatile fluoride. (Chromium fluoride is not volatilized until essentially all of the UF_6 has been volatilized.) As seen in Table 8.15, MoF_6 is somewhat more volatile than UF_6. The molybdenum complex, $MoF_6 \cdot 3$ NaF, is much less stable than the uranium complex $UF_6 \cdot 3$ NaF.

Table 8.15

Comparison Between MoF_6 and UF_6

	UF_6	MoF_6
Boiling point at 760 mm, °F	147	95
Partial pressure over NaF at 200°F, mm	0.001	2

8.11.7 Molybdenum (Cont'd)

At the start of fuel salt fluorination, it is likely that nonvolatile MoF_3 is formed and is not converted to MoF_6 until most of the UF_4 is converted to UF_5. Because of the higher volatility of MoF_6, volatilization would be expected to begin before UF_6 begins to volatilize. This was verified by the increase in the reading on the absorber inlet mass flowmeter about 1-1/2 hours before an absorber temperature rise was noted (see Figure 8.18). During this period of MoF_6 volatilization, the reading on the absorber outlet meter indicated that no MoF_6 was present in the exit gas stream until near the start of UF_6 absorption.

After UF_6 began to volatilize, the absorber outlet mass flowmeter was used to calculate the amount of MoF_6 leaving the absorbers. The molybdenum in the absorber outlet stream was also calculated by two other methods: from the gas flow and the MoF_6 vapor pressure and by subtracting the amount of MoF_6 retained on the absorbers from the amount of MoF_6 produced by corrosion. A good correlation of the data, except in Run 6, was obtained, showing that the amount of absorbed MoF_6 increases as the amount of UF_6 passed through the NaF increases. The data, which are only approximations, are compared in Table 8.16. This table also shows the amount of molybdenum found in the caustic scrubber solutions. The reason for the excessive amount of MoF_6 leaving the absorbers in Run 6 is not clear. The amount of molybdenum that passed through the scrubber is not known. There was no accumulation of solids in the line from the scrubber as was experienced during the second scrubber test run; however, the mist filter was not examined.

From the random samples of NaF analyzed for molybdenum, the following observations were made concerning the absorption of MoF_6:

a - Absorption was higher on high-surface-area NaF than on low-surface-area NaF.

Table 8.16

Disposition Of Volatilized Molybdenum

	Molybdenum (g)					
			In Absorber Outlet Stream			
	Produced by Corrosion(a)	Absorbed on NaF(b)	Amount Produced Minus Amount Absorbed	From Flow and Vapor Pressure	From Mass Flowmeter	In Caustic Scrubber
Flush Salt	990	28	962	940	(c)	260
Fuel Salt						
Run 1	1,270	130	1,140	246	670	107
Run 2	739	210	519	427	364	72
Run 3	868	330	538	257	267	86
Run 4	914	375	539	132	870	24
Run 5	1,131	425	706	271	663	17
Run 6	1,114	112	1,002	399	3,120	67
Total Fuel	6,036	1,582	4,444	1,732	5,954	373
Total	7,026	1,610	5,406	2,672	(c)	633

(a) At a constant corrosion rate of 0.2 mils/hr.

(b) From a correlation of absorbed Mo vs UF_6 through NaF.

(c) Unable to calculate.

8.11.7 Molybdenum (Cont'd)

b - Absorption was higher on pellets than powder, probably because MoF_6 was trapped inside the pellets.

c - Absorption was higher on NaF that has been exposed to UF_6 and increases with the UF_6 concentration in the gas stream. Run 6 appears to be an exception in this respect.

8.11.8 Plutonium

Since the MSRE fuel salt contained 66 weight percent ^{238}U, a significant amount of ^{239}Pu was produced. At the time of reactor shutdown, the plutonium concentration in the fuel salt was calculated to be 112 ppm (560 g). Five salt samples withdrawn after fluorination, after reduction, and after return of the salt batch to the reactor drain tank showed an average concentration of 110 ppm. This confirms the expectation that plutonium would not be volatilized under the relatively mild conditions required for uranium volatilization.

8.11.9 Niobium

Figure 8.19 shows the amounts of fission product fluorides calculated to be volatilized during fluorination of the fuel salt. The iodine and tellurium fluorides pass through both NaF beds to the caustic scrubber and charcoal traps. Because of the five-month decay time, ^{99}Mo was not present in detectable amounts. Ruthenium, niobium, and antimony exist as metals during reactor operation and, as such, were continuously removed by deposition or by the off-gas stream. Since ruthenium was formed directly by fission and since radioactive antimony had no long-lived precursors, the amounts of these isotopes in the processed salt were small as compared with miobium, which grows in from nonvolatile ^{95}Zr.

Figure 8.19 shows the buildup of ^{95}Nb after reactor shutdown and the buildup after fluorination, assuming complete volatilization. Aslo shown is a comparison between the

8.11.9 Niobium (Cont'd)

amount of niobium found in salt samples taken before and after fluorination and the amount of niobium which should have been present from zirconium decay (Assuming no niobium present at sample time) when the sample was analyzed several months after processing. Since the sample prior to fluorination showed less niobium than would have grown in from zirconium decay, it is impossible to say whether there was any appreciable amount of niobium in the salt before fluorination. At least 60 percent of the grown-in niobium must have been lost during sample preparation (before analysis). This loss did not occur in the post-fluorination samples, as seen in Figure 8.19, when the salt was in an oxidized state. The close agreement between the calculated amount and the sample analysis probably indicates that there was very little niobium left in the salt after fluorination.

Figure 8.18 indicates that approximately 60 percent of the niobium in the fuel salt volatilized during fluorination. It is not known, however, how much niobium was present in the salt at that time. From the lack of heat generation in the NaF trap, the volatilized niobium is believed to constitute less than 10 percent of the 9×10^4 curies which would have grown in after reactor shutdown. (A temperature rise of $20^{\circ}F$ would have been observed from the heat generation from 9,000 curies of ^{95}Nb.) The temperature of the trap remained constant; that is, no heater adjustment was required throughout the six runs. Apparently, most of the niobium was removed from the salt by deposition in the drain tank or in backflowing through the salt filter during salt transfer. At the end of this transfer, the transfer gas blowthrough carried a small amount of metallic niobium to the absorber filter. Although this filter was decontaminated prior to fluorination, undoubtedly some of the niobium was deposited on the upstream piping. During fluorination, this niobium would be converted to volatile NbF_5 and collect on the UF_6 absorbers (any niobium upstream of the NaF trap should be absorbed on the trap).

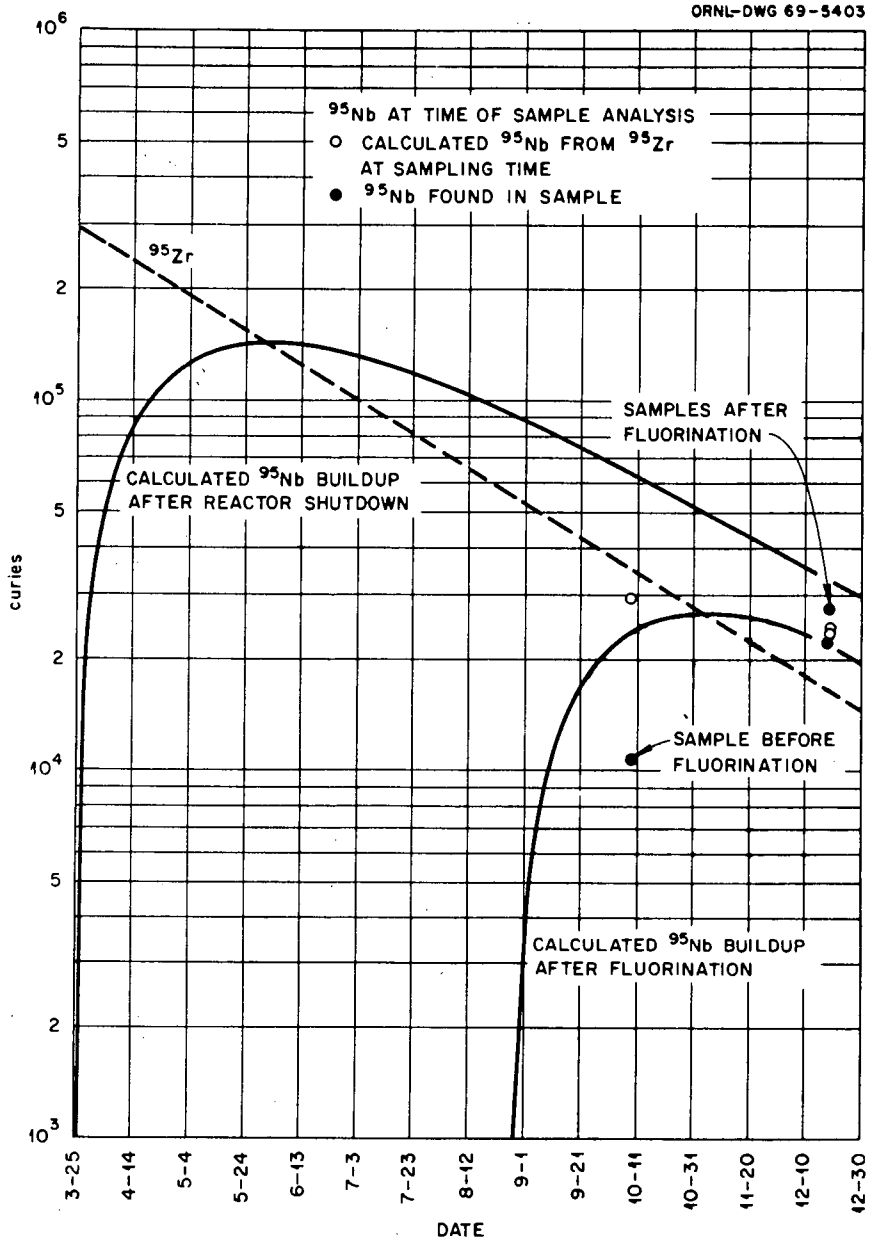

Fig. 8.19. Buildup of ^{95}Nb From ^{95}Zr Decay.

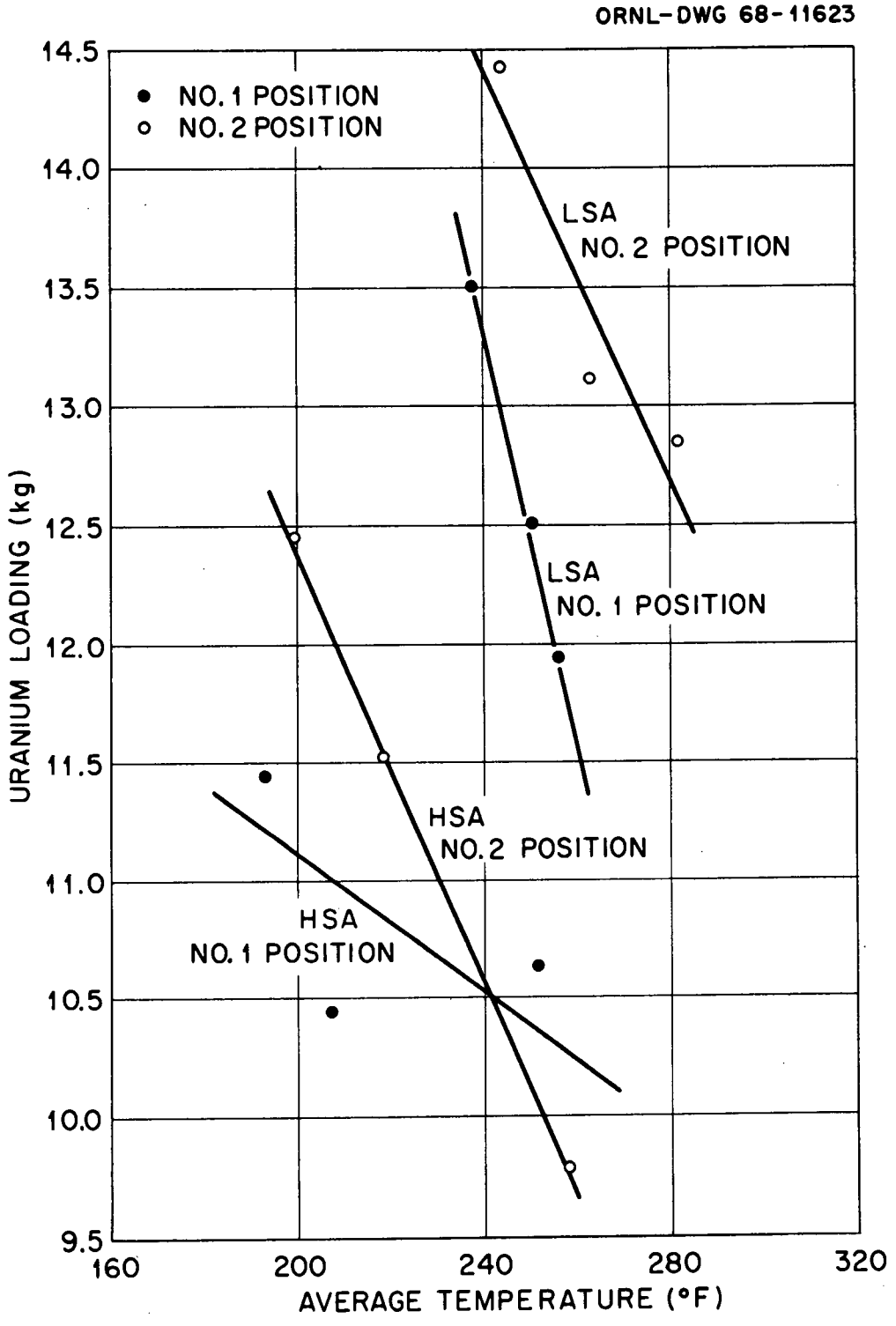

Fig. 8.20. Comparison of LSA and HSA NaF Loading.

8.11.10 Iodine and Tellurium

During fluorination, volatile IF_7 is formed and passes through both NaF beds. It is removed by the caustic scrubber by reaction with the KOH and by exchange with the KI. A total of 404 mc of ^{131}I was calculated to be in the fuel salt at the start of processing. Analysis of the caustic scrubber solutions showed that 288 mc was collected during Run 1 and 10 mc was collected during Run 2 for a 74 percent accountability. This is in reasonable agreement with the results of iodine analyses of fuel salt (during reactor operation), which showed about 65 percent of the calculated amount. The discrepancy between the calculated amount and the analyzed amount was caused by the loss of metallic ^{131}Te before decay. There was no indication that any iodine collected on the charcoal beds downstream of the scrubber.

Tellurium exists primarily in the metallic state during reactor operation and, as such, was removed from the salt by deposition and by the off-gas stream. Freeze-valve samples showed less than 1 percent remaining in the salt. Since ^{129}Te has no long-lived precursor, the activity will not grow back in after reactor shutdown. Any tellurium remaining in the salt will be converted to the volatile TeF_6 during fluorination. Because of the low MPC for ^{129m}Te (10^{-8} $\mu c/cc$), at least 94 percent of the remaining 1 percent would have to be removed from the gas stream before the stream is discharged from the stack. Tellurium hexafluoride was not absorbed on NaF at any temperature, and removal in the caustic scrubber was not very efficient. However, since analyses of the scrubber solutions showed tellurium to be below the limit of detection, it was probable that less than 1 percent was present in the salt at reactor shutdown. Any tellurium passing through the scrubber would have been removed by the activated alumina in the soda-lime trap.

8.11.11 Uranium Adsorption

Two types of NaF were used: a high-surface-area (HSA) material (1 m^2/g), prepared by heating $NaHF_2$ pellets, and a low-surface-area (LSA) material (0.063 m^2/g), prepared from NaF powder and water and sintered at 700 C. The LSA material was originally specified for the MSRE Fuel Processing Plant because of its higher capacity for both CrF_5 (on the 750°F NaF trap) and for UF_6. (This high capacity is due to the slower surface reaction and greater penetration to the inside of the pellets.) The low MoF_6 retention observed during the final fluorine disposal test suggested that the reaction rate with UF_6 might be too slow for complete uranium adsorption under the planned operating conditions. Subsequent laboratory tests (10) confirmed the much slower reaction rate with the LSA material. The absorbers were, therefore, heated to increase the reaction rate, and the LSA NaF was restricted to the No. 1 and No. 2 positions of the group of five absorbers.

A comparison of the results obtained with the two types of NaF is shown in Figure 8.20. Three absorbers loaded with each type of material were used in the first position, and three were used in the second position, during the six runs. In the first position, the NaF was exposed to a higher UF_6 concentration; this resulted in a lower loading than in the second position where the slower reaction rate permitted deeper penetration of the pellets. Except in one case, higher loadings were obtained at lower temperatures; in that particular case, the absorber had been used in a previous run where a small amount of uranium was absorbed.

In spite of the fact that the LSA NaF absorbers were operated at higher temperatures (to compensate for the slower reaction rate), the total loading was 13 to 14 percent higher. The maximum uranium loading obtained was 0.56 g per g of NaF as compared with 0.49 g per g of NaF for the HSA material. Both of these absorbers were in the second position.

8.11.11 Uranium Adsorption (Cont'd)

The three lowest loadings shown in Figure 8.20 for the LSA NaF contained from 11 to 18 percent HSA (added later to more fully charge the absorbers), which undoubtedly reduced the loading on thes absorbers.

The time required for a breakthrough of UF_6 from a given absorber to the subsequent absorber varies directly with the residence time of the gas stream in the absorber, as shown in Figure 8.21. The first absorber in Run 1 had an unusually short breakthrough time (25 sec), which was possibly caused by absorption of MoF_6 that had been volatilized before the start of UF_6 volatilization.

The conditions and loadings are summarized in Table 8.17. These loadings are high since no allowance was made for absorbed MoF_6.

8.11.12 Uranium Product Purity

The inlet of the first absorber in each run was analyzed for gross beta and gamma activity about 12 days after fluorination. The results are shown in Figure 8.22. The activity associated with uranium daughters at the same time is also shown. At the time of the analyses, the ^{235}U daughters had reached equilibrium, while the ^{238}U daughters had attained only about 30 percent of equilibrium. The only activities appreciably above background were the gamma activity in the first run and the gamma activity on the first absorber of the second run. (The activity in the feed salt before fluorination, counted at the same time, was 2.66×10^{13} gross gamma and 3.8×10^{13} gross beta counts per minute per gram of uranium.) The average gross beta and gamma decontamination factors (DF) for the six absorbers analyzed, after correction for uranium daughter activity, were 1.2×10^9 and 8.6×10^8, respectively.

Table 8.17

Summary of UF_6 Absorption Data

Run	Absorber	Type NaF	Aver. Temp. (°F)	Flow Through Absorber Minus N_2 He and Unreacted F_2: Corrected Flow Rate (Std Liters/Min)	Flow Through Absorber Minus N_2 He and Unreacted F_2: Superficial Gas Velocity (fps)	Average Gas Residence Time (Excluding UF_6 (Sec)	Uranium Absorbed(a) (kg)
Flush	1	LSA	244	20.0	0.038	18.3	4.65
	2	LSA	226	20.0	0.037	18.7	1.83
	3	LSA	210	20.0	0.036	19.2	0.15
Average			227	20.0	0.037	18.7	6.63
Fuel							
1	1	LSA	261	39.4	0.077	9.1	12.53
	2	HSA	258	28.5	0.055	12.6	9.80
	3	HSA	258	28.5	0.055	12.6	3.49
2	1	LSA	255	21.2	0.041	17.0	11.98
	2	LSA	282	17.9	0.036	19.3	12.86
	3	HSA	265	17.0	0.033	20.8	8.36
	4	HSA	253	17.0	0.033	21.2	0.61
3	1	HSA	252	18.7	0.036	19.3	10.66
	2	LSA	263	18.8	0.037	18.9	13.14
	3	HSA	258	18.8	0.037	19.1	11.91
	4	HSA	274	18.9	0.038	18.6	5.73
4	1	HSA	193	19.5	0.034	20.2	11.42
	2	HSA	218	19.5	0.036	19.5	11.55
	3	HSA	217	19.5	0.036	19.5	11.24
	4	HSA	220	19.5	0.036	19.4	9.83
5	1	LSA	238	16.0	0.030	23.0	13.51
	2	LSA	243	15.1	0.029	24.2	14.45
	3	HSA	188	15.1	0.026	26.3	12.37
	4	HSA	207	15.1	0.027	25.5	8.94
6	1	HSA	207	38.7	0.070	10.0	10.45
	2	HSA	200	38.7	0.069	10.1	12.47
	3	HSA	179	38.7	0.067	10.4	0.55
Aver			236	22.7	0.043	18.0	217.85

(a) These weights include absorbed MoF_6.

(b) Total Weights.

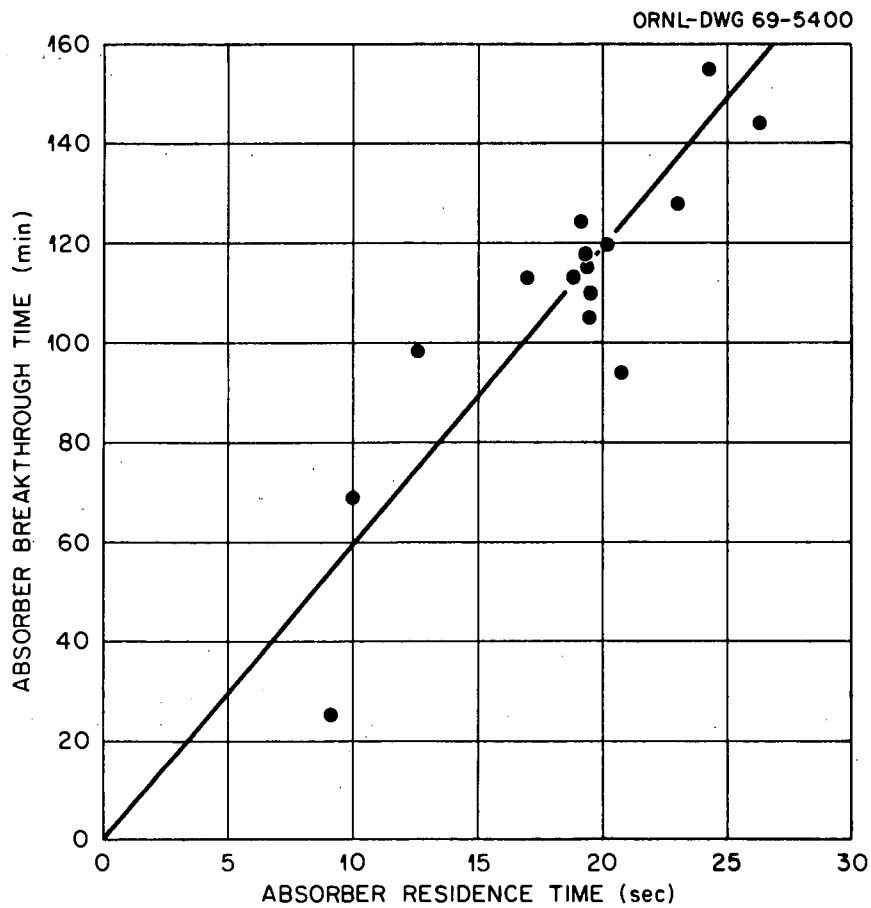

Fig. 8.21. Absorber Residence Time vrs UF_6 Breakthrough Time.

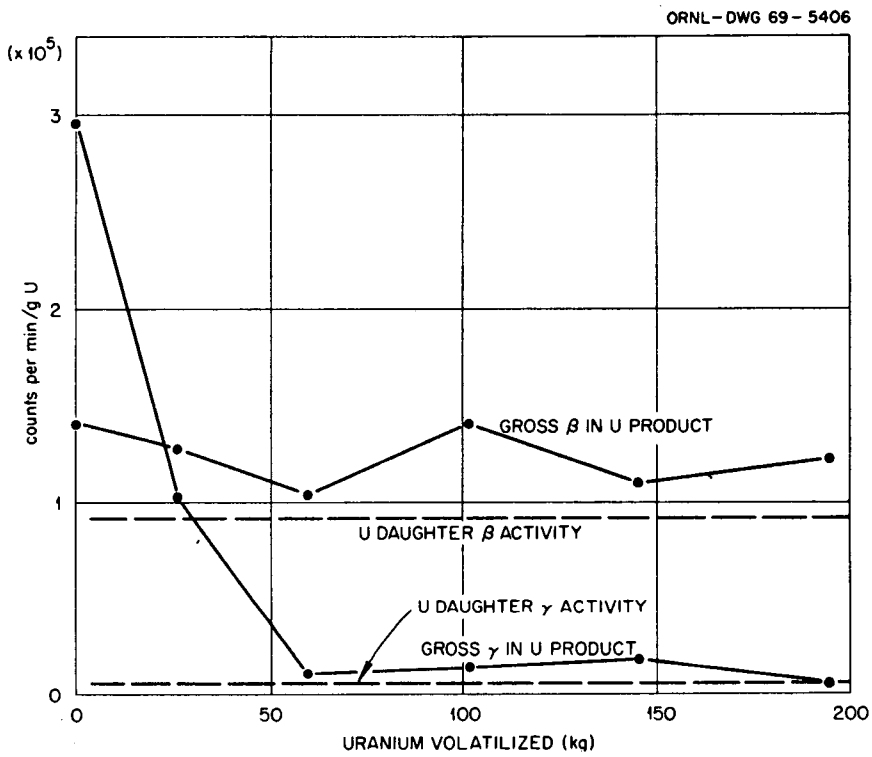

Fig. 8.22. Gross Activity in Uranium Product.

8.12 Fluorination-Valence State Study[10/]

MSRE salt fluorination tests were made in 1.87-inch ID reactors constructed of nickel 200. A gas flow rate of 146 ml/min (STP) was used. Sampling of the salt without interruption of the fluorination procedure was achieved by taking a quick-freeze sample with a 1/8-inch nickel rod inserted through a tee at the top of the reactor. The valence of uranium in the salt samples was calculated from separate determinations of the U(IV) and U(VI) concentration. The tests were made with 340 g of $LiF-BeF_2-ZrF_4-UF_4$ (63-32-5-0.8 mole percent); the salt depth was about 3 inches.

A test of 500 C with pure fluorine illustrated the relationship between the degree of uranium volatilization and the uranium valence in the salt (Figure 8.23). Some UF_6 was observed to evolve when the uranium valence in the salt was as low as 4.1. At 500 C there was an extensive evolution of UF_6 as the valence increased from 4 to 5. The valence continued to increase (from 5 toward 6) as the remaining part of the uranium volatilized. The fact that an intermediate stable species of U(V) was formed is indicated from the curve inflection; however, in this case the volatilization of UF_6 was too rapid for this intermediate equilibrium species U(V) to be clearly seen.

In another test at a lower temperature (450 C), the valence plot shows a definite inflection at about the value of five (Figure 8.24). In this test the fluorine flow was stopped and helium sparging was started after 1 hour to determine whether helium sparging or corrosion would lead to a rapid decrease of the uranium valence from 5 to 4. Such a decrease might be expected from one of the two following reactions:

$$2UF_5 \longrightarrow UF_6 + UF_4, \qquad (9)$$

$$2UF_5 + Ni \longrightarrow 2UF_4 + NiF_2. \qquad (10)$$

Surprisingly, in the 1.5-hour helium sparging period, there was no significant effect on the valence. When fluorine flow was resumed, the same rapid UF_6 evolution and valence increase occurred as in the test at 500 C. However, it was clear that the valence plot of

8.12 Fluorination-Valence State Study (Cont'd)

the 450 C data would have had a much larger inflection, even in the absence of a helium sparge period, than the plot of the 500 C data.

The main conclusions can be summarized as follows:

1 - The depth of salt in the MSRE fluorination reactor (5 to 6 ft) will probably result in the conversion of all of the uranium to the U(V) species before any significant UF_6 volatilization takes place. The results, however, do not lead to any conclusion about fluorine utilization. The latter might be more critically dependent on fluorination temperature than on the depth of salt.

2 - Interruption of the fluorination procedure in MSRE processing for the changing of NaF sorption beds (as they become loaded with UF_6) should not lead to any difficulty in resuming fluorine gas flow. Volatilization of UF_6 should resume almost immediately after such an interruption due to the stability of the U(V) species during the shutdown period. During this period, however, it would probably be best to avoid extensive sparging with helium in order to minimize the evolution of UF_6 by disproportionation reaction (9).

3 - The stability of the U(V) species is of particular interest to the corrosion picture. The dotted line in Figure 8.24 represents the rate of valence change expected if the corrosion reaction (10) should occur at a rate equivalent to 0.67 mil/hr. The fact that the valence did not decrease suggests that corrosion will not be a problem during the shutdown periods required for the changing of sorption beds. Possibly total corrosion during the processing of MSRE fuel will be less than expected if the wall of the reactor is in contact with salt containing only U(V); that is, corrosion should be high only in the central salt volume where UF_6 is "boiling out" as it is formed and where the valence of the uranium possibly becomes much greater than 5. The latter applies to the boundary salt layer surrounding the F_2-UF_6 gas that rises through the salt.

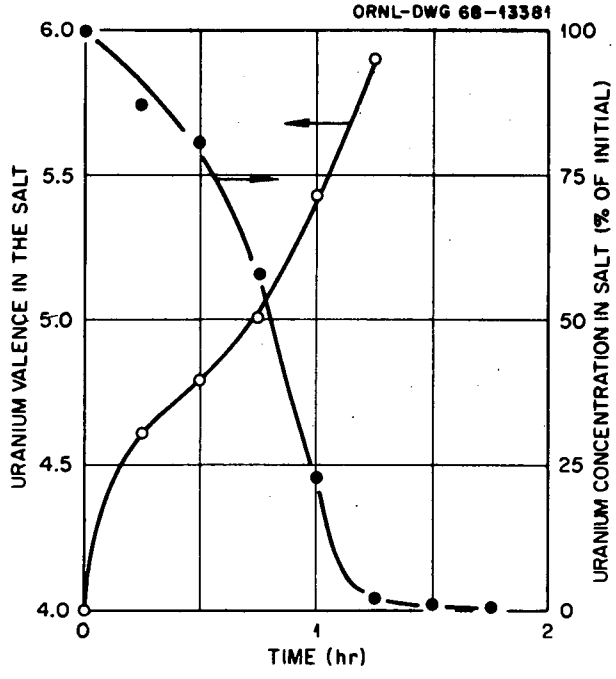

Fig. 8.23. Change of Uranium Valence in the Fluorination of MSRE-Type Salt at 500°C with Pure Fluorine.

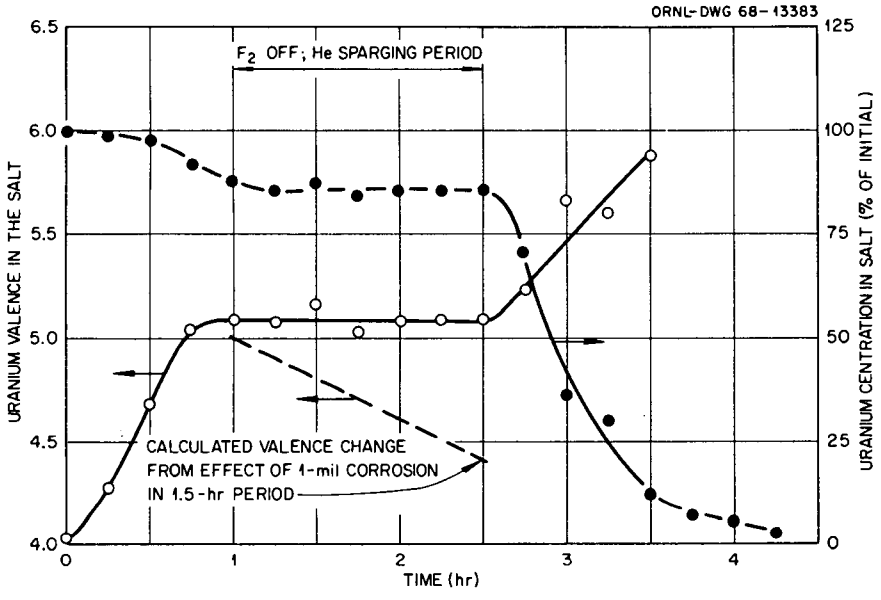

Fig. 8.24. Change of Uranium Valence in the Fluorination of MSRE-Type Salt at 450°C with Pure Fluorine: Stability of U(V) Species During He Sparging.

8.13 UF_6-NaF Adsorption Equilibria[10/]

Since the utilization of fluorine in the early part of the fluorination might be high, there was concern as to whether sufficient fluorine would be available to prevent disproportionation and uranium loss. Therefore, a study was undertaken to determine the validity of an equilibrium condition for the reaction

$$UF_5 \cdot NaF + 1/2\ F_2 \longrightarrow UF_6 + NaF \qquad (11)$$

at 400 C.

The various F_2-UF_6 mixtures used in the study were produced by equilibration in a nickel reservoir vessel (250-ml volume) containing about 100 g of UF_6 at 54 C (P_{UF_6} = 660 mm Hg) with the appropriate precalibrated mixtures of fluorine and nitrogen. (The temperature of the UF_6 reservoir was held constant to $\pm$0.5 C by means of a carefully controlled water bath.) By adjusting the initial F_2/N_2 ratio, mixtures with F_2 concentrations ranging from 11 to 0.3 volume percent at atmospheric pressure were obtained. Each mixture was allowed to pass through a 10-g bed of NaF (-12 + 20 mesh) at 400 C for 20 min. Unreacted UF_6 passing through the bed was recovered on a backup trap of NaF at 100 C.

In the first three of a series of six tests, the fluorine concentrations in the gas mixture were 11, 5.5, and 2.1 volume percent, respectively (see Table 8.18). Subsequent coulometric analyses of the beds for uranium yielded calculated values for equilibrium constants of 3.8×10^5, 3.3×10^5, and 4.2×10^5, respectively. The equilibrium value, K, was calculated by means of the equation

$$K = \frac{P_{UF_6}}{P_{F_2}^{\frac{1}{2}} N_{U(V)}}, \qquad (12)$$

in which $N_{U(V)}$ is the mole fraction of uranium present on the NaF; it was assumed that the activity of NaF was unity. The close correspondence of these values indicated that equilibrium conditions were obtained. In Run 5 the UF_6 reservoir temperature was raised

Table 8.18

Uranium Retention On NaF at 400°C

Run No.(a)	F_2 Concentration in Gas (Vol %)	U Concentration in NaF (ppm)	K $\times 10^5$
6	0	36,400	
5	0.3	840	1.3
3	2.1	89	4.2
2	5.5	71	3.3
1	11.0	39	3.8

(a) Results of run 4 invalid due to operational error.

8.13 UF_6-NaF Adsorption Equilibria (Cont'd)

to 55.5 C (P_{UF_6} = 720 mm) to eliminate the need for a low fluorine flow rate at low fluorine concentrations. In this test a fluorine concentration of 0.3 volume percent was achieved. The calculated equilibrium constant was 1.3×10^5, which was somewhat lower than those values obtained at higher F_2 concentrations. When UF_6 was passed through a similar 400 C NaF bed in a test with no fluorine present (Run 6), the amount retained as a result of disproportionation was 3.64 percent. Comparison of this value with the corresponding value of 0.084 percent obtained in a test where 0.3 volume percent F_2 was present in the stream demonstrates the necessity of having at least 0.3 volume percent F_2 present during the decontamination step of the process.

The results of the tests indicate that if fluorine utilization is nearly quantitative in the early part of the fluorination step, a supplemental fluorine supply through the sorption traps would be required.

8.14 Temperature Effect on UF_6 Adsorption[10/]

Some uncertainty existed with regard to the correct temperature and type of NaF to be used for recovering UF_6. This uncertainty arose partially from the results of one engineering test in the MSRE facility in which it was observed that MoF_6 had not attained equilibrium with sorption beds containing low-surface-area NaF at about 35 to 45 C.

Two grades of porous NaF are available. A low-surface-area product is prepared from NaF powder by pelletizing with water, drying, and finally fluorinating at 250 to 350 C. It is characterized by a surface area of 0.07 m^2/g and a void fraction of 0.28. A high-surface-area product is prepared by the decomposition of NaF·HF pellets at 200 to 400 C, followed by sintering at 400 to 700 C to obtain pellet strength. It is characterized by a surface area of about 1 m^2/g and a void fraction of 0.45.

A comparative study of UF_6 sorption at different temperatures was therefore undertaken with the two types of material. A series of

six tests with low-surface-area material in the range of 25 to 100 C clearly showed that temperature had a large effect. Two tests of high-surface-area material at 25 and 100 C gave practically identical results, showing that temperature is not important with this material.

The sorption tests were made by passing a mixture of 15 mole percent UF_6-85 mole percent F_2 through a 5-g test bed for 3 min. The sorption test trap was maintained at constant temperature in a water bath; a 5-g backup NaF trap was held at 100 C for the sorption of UF_6 passing through the test material. Both traps were quartz U-tubes (8.5 mm ID) specially designed for visibility so that the yellow $UF_6 \cdot 2NaF$ complex could be observed. The traps were filled with sieved material: -8 + 20 mesh for the low-surface-area NaF and -12 + 20 mesh for the high-surface-area material. The F_2-UF_6 gas mixture was prepared by passing F_2 through a UF_6 reservoir held at 24 C in a constant-temperature bath.

The sorption results were significantly better for the high-surface-area NaF than for the low-surface-area material (Table 8.19). Even at 80 and 100 C, the loss through the latter was an order of magnitude greater than that through the high-surface-area NaF. The quantitative data were confirmed by visual observations: the yellow sorption band in high-surface-area NaF was never more than 1 to 2 cm in length (even at 25 C), whereas the sorptive band with low-surface-area material at 100 C was 4 to 5 cm.

A semilogarithmic plot of the low-surface-area sorption data (Figure 8.25) was surprisingly linear through four points; this indicated that the process was possibly diffusion controlled (based on an apparent activation energy of only 4.6 kcal per mole of UF_6).

Table 8.19

UF_6 Sorption Tests With Low- and High-Surface Area NaF at Various Temperatures

Low-Surface-Area NaF

Temperature (°C)	U Loss (%)
25	61
46	37.2
55	22.2
67	1.0
80	0.087
100	0.063

High-Surface-Area NaF

25	0.0024
100	0.0079

8.15 Axial Mixing[15/]

Axial mixing is important in the design of tubular reactors such as the continuous fluorinator. Bautista and McNeese previously reported results obtained in studies of axial mixing in a 2-inch diameter open column using air and water. The experimental technique involved photometric measurement of the steady state concentration profile, in the column, of a tracer (cupric nitrate) that was fed continuously to the bottom of the column. Data have now been obtained on the effects of two physical properties, continuous-phase viscosity and surface tension, on the axial dispersion coefficient.

Molten salts of interest have a viscosity of about 30 centipoises, and the viscosity of the glycerol solution used in this study is 15 centipoises. The surface tension of molten salts of interest in 100 to 200 dynes/cm, while that of the butanol solutions varied between 37.8 dynes/cm and the value for water (72 dynes/cm).

The results of the study are summarized in Figure 8.26, which shows the despersion coefficient as a function of the air flow rate. The dashed line represents the earlier results of Bautista and McNeese, who found that the data fall into two regions. The first region, which covered low air flow rates, corresponded to conditions when individual bubbles formed at the orifice travel up the column without coalescence. The second region, which occurred at air flow rates above 30 cm^3/sec, corresponded to "slugging" flow.

Increasing the liquid viscosity to 15 centipoises (by adding glycerol) decreased the dispersion coefficient in the "bubble" (lower) region; however, the transition point between the regions was not changed. The coefficient increased more rapidly with air flow rate in the slugging region, at least up to the curve by Bautista and McNeese.

15/ ORNL-4449, August 31, 1969.

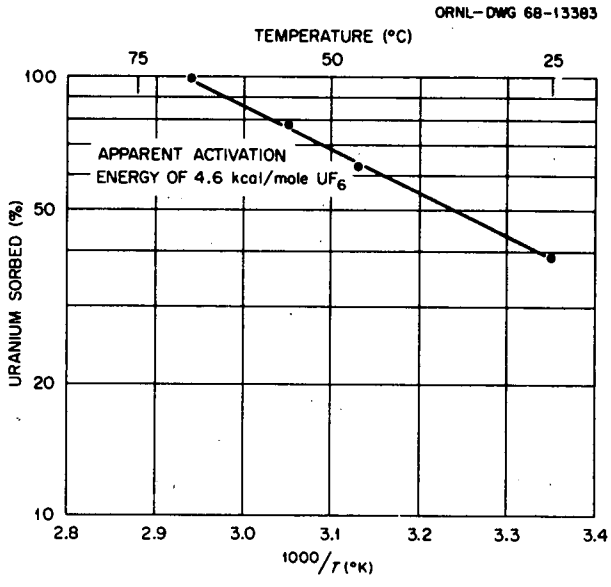

Fig. 8.25. Variation of Effectiveness of UF_6 Sorption on Low-Surface-Area NaF with Temperature.

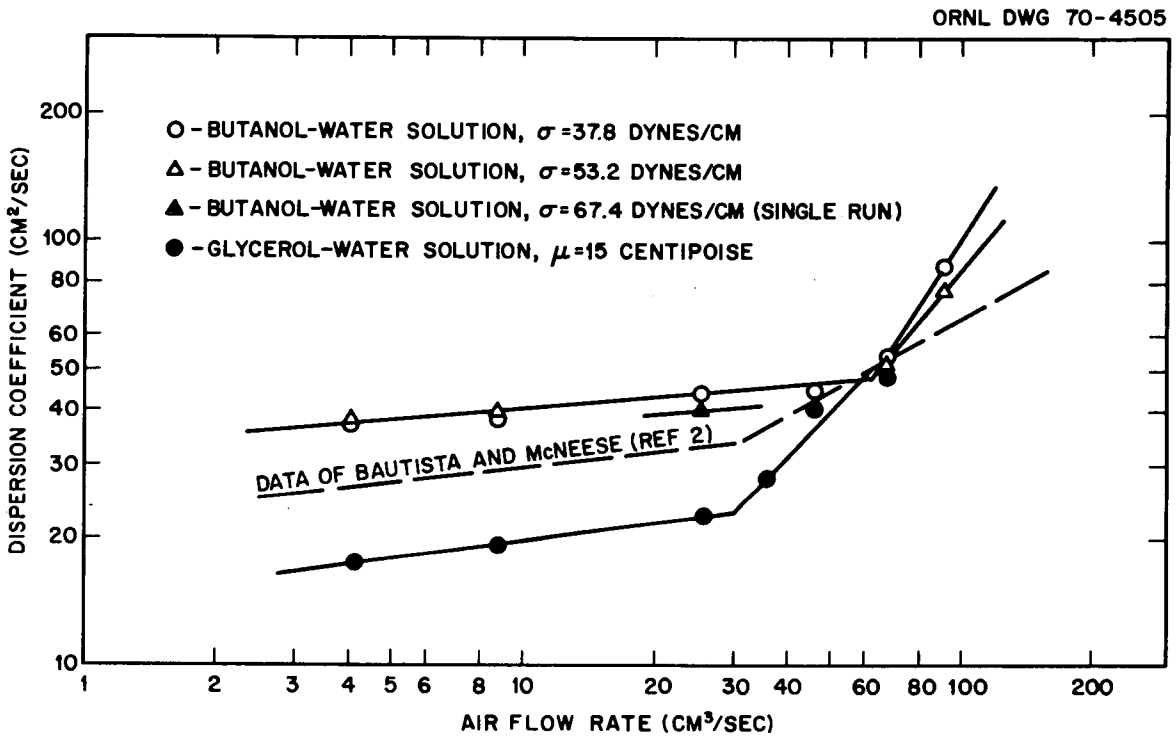

Fig. 8.26. Effect of Gas Flow Rate, Liquid-Phase Viscosity, and Surface Tension on Axial Dispersion Coefficient.

8.15 Axial Mixing (Cont'd)

Decreasing the surface tension increased the dispersion coefficient in the bubble region, although there is little difference between the data obtained from a solution having a surface tension of 37.8 dynes/cm and those obtained from a solution having a surface tension of 53.2 dynes/cm. The transition point occurred at a higher air flow rate and the bubble region curve intersected the slugging region curve of Bautista and McNeese. The dependence of the dispersion coefficient on air flow rate appears to be somewhat greater than that observed with air and water, but insufficient data are available to reach a definite conclusion on this point.

The data obtained indicate that higher viscosity and higher surface tension lead to lower dispersion coefficients, which is in the favorable direction for molten salt systems.

Additional data[16/] show the importance of column diameter and gas inlet diameter. The experimental technique, using air and water, consisted in measuring the concentration profile of a tracer along the length of the column. Results obtained with three gas inlet diameters (0.04, 0.06, and 0.085 inch ID) in a 2-inch ID, 6-ft long column are shown in Figure 8.27. The dispersion coefficient is independent of gas inlet diameter for the size range studied. Similar measurements in 1-1/2- and 3-inch diameter columns using inlet diameters ranging from 0.04 to 0.17 showed no effect of gas inlet diameter.

Figure 8.28 shows the effect of column diameter on dispersion coefficient for 1.5-, 2-, and 3-inch diameter columns. In the slugging region, the dispersion coefficient data from the three columns showed little difference for a given volumetric gas flow rate. These data, however, do not extend to high gas rates for all column diameters; therefore, extrapolation to larger gas flow rate values is questionable. In the bubble region, results from the 2-inch and 3-inch diameter columns are essentially the same. Results

16/ ORNL-4622, August 31, 1970.

8.15 Axial Mixing (Cont'd)

for the 1-1/2-inch column indicate significantly lower values for the dispersion coefficient and show a greater dependence on gas flow rate than has been observed for the larger columns.

8.16 Corrosion Rates In Continuous Fluorinators[17/]

Nickel is the preferred material of construction for fluorinators since it exhibits greater resistance to attack from gaseous fluorine than other materials. Its resistance to attack by fluorine results from a tightly adhering film of the NiF_2 corrosion product through which fluorine must diffuse to react with the metallic substrate. The rate of reaction with nickel is greatly reduced, although not to zero, once a protective NiF_2 film is formed on a nickel surface exposed to gaseous fluorine. The purpose of the frozen salt film in a continuous fluorinator is to prevent the protective NiF_2 film from being washed away by the molten salt. (No benefit is assumed for any added resistance to fluorine diffusion which may be offered by the frozen salt film.) However, it is likely that the protective NiF_2 film will be destroyed unintentionally several times during the operating life of a fluorinator, resulting in relatively high corrosion rates during the period required for the formation of a new NiF_2 film. Expected corrosion rates have been estimated, which result from periodic destruction of the NiF_2 film during operation of a continuous fluorinator.

Data for the corrosion of Ni-200 and Ni-201 exposed to gaseous fluorine at a pressure of 1 atm were collected from the literature and were used to calculate rate constants for the reaction between nickel and fluorine at 1 atm pressure in the temperature range 360 to 700 C, the reaction was assumed to follow a parabolic rate law. The reaction of high-purity nickel with fluorine initially follows a parabolic rate law from 300 to 600 C but that, after a certain exposure time, the reaction rate decreases and follows

17/ ORNL-4682, March 31, 1971.

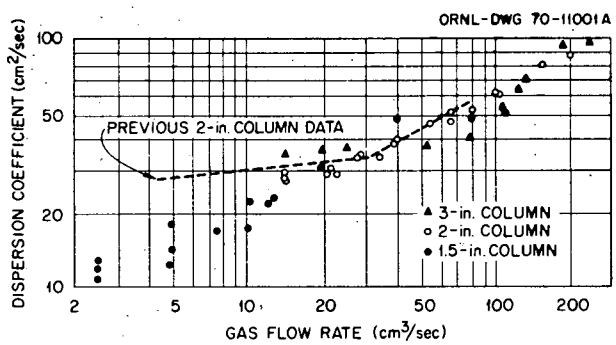

Fig. 8.27. Effect of Gas Flow Rate and Orifice Diameter on Axial Dispersion in a 2-In.-Diam. Open Column.

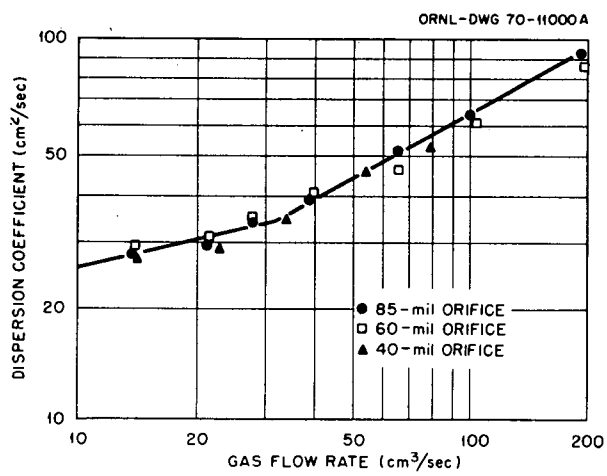

Fig. 8.28. Effect of Column Diameter on Dispersion Coefficient in an Open Column.

8.16 Corrosion Rates In Continuous Fluorinators (Cont'd)

a third- or higher-order rate law. Thus the assumption of a parabolic relation takes into account the time dependence of the reaction rate but should yield conservatively high estimates of the extent of corrosion.

The extent of corrosion of nickel in fluorine was assumed to be described by the equation.

$$d = k\sqrt{t}, \tag{13}$$

where

d = depth of nickel attacked by F_2 mils;

t = time of exposure of nickel metal to gaseous fluorine, measured from the time when no NiF_2 film exists;

k = parabolic rate constant, mils $hr^{-1/2}$

Rate constants were calculated for 41 measurements for which the exposure times ranged from 5 hr to 960 hr. Most of the exposure times were in the range of 30 to 150 hr. Fourteen measurements had been made to determine the rate of corrosion of Ni-201 in the temperature range 380 to 700 C; exposure times varied from 5 to 132 hr. The best least-squares representations of the data, which showed considerable scatter, are given below:

$$\text{In } k = 0.3773 - \frac{3691}{T} \text{ for Ni-200,} \tag{14}$$

$$\text{In } k = 4.3083 - \frac{7836}{T} \text{ for Ni-201,} \tag{15}$$

where k has units of mils $hr^{-1/2}$ and T has units of ^{o}K. The largest deviations of individual data points from these two equations were about an order of magnitude higher and an order of magnitude lower.

If n is the number of times per year that the NiF_2 film is destroyed, the extent of corrosion experienced each year (8760 hr) is given in mils by

$$D = nk\sqrt{\frac{8760}{n}} \tag{16}$$

and is the average corrosion rate per year. If the NiF_2 film

8.16 Corrosion Rates In Continuous Fluorinators (Cont'd)

were destroyed 52 times per year, the average corrosion rates at 450 C (the approximate wall temperature that will be used in a frozen-wall fluorinator) would be 2.9 mils/year for Ni-200 and 0.97 mil/year for Ni-201. If the film were destroyed 12 times annually, the average corrosion rates would be 1.4 mils/year and 0.47 mil/year for Ni-200 and Ni-201 respectively. According to these results, Ni-201 seems to be more resistant to corrosion than Ni-200; however, either material shows satisfactory corrosion resistance if the NiF_2 film is kept intact for periods having an average length as great as one week. It appears that the anticipated corrosion rate would be influenced much more strongly by the length of time that a protective NiF_2 film is absent in the presence of fluorine and molten salt than by the frequency of destruction of the NiF_2 film in the absence of fluorine.

9.0 REDUCTIVE EXTRACTION

9.1 Introduction

The principal objectives of fuel processing are the isolation of ^{233}Pa from regions of high neutron flux during its decay to ^{233}U and the removal of fission products from the system. It is also necessary to remove impurities from the reactor fuel salt which may arise from corrosion or maloperation of the reactor system. The fuel processing system is an integral part of the reactor system and is operated continuously.

The processing methods are based on reductive extraction, which involves the selective distribution of materials between salt and bismuth containing reducing agents such as thorium and lithium. The isolation of protactinium by reductive extraction is relatively straightforward since there are significant differences in chemical behavior between protactinium and the other components of the fuel salt (U, Th, Li, and Be), as is evidenced by the distribution ratios of these materials between fuel salt and bismuth containing a reductant. Extraction of the protactinium into bismuth requires the prior and complete removal of uranium from the fuel salt. Fluorination is used for removing most of the uranium from the fuel salt prior to protactinium isolation. The quantity of reductant required can be purchased economically.

The removal of the rare-earth fission products from the fuel salt is more difficult because the chemical behavior of the rare-earth fluorides is similar to that of thorium fluoride, which is a major component of the fuel salt.

The rare-earth-removal method exploits the relatively large differences in the extent to which rare earths and thorium distribute between bismuth containing a reductant and lithium chloride.

The following sections describe the system incorporating the fluorination-reductive-extraction process for protactinium isolation and the metal-transfer process for rare-earth removal.

9.1.1 Protactinium Isolation

The fluorination-reductive-extraction system for isolating protactinium is shown in Figure 9.1. The salt stream from the reactor first passes through a fluorinator, where 95-99 percent of the uranium is removed. The salt stream leaving the fluorinator is countercurrently contacted with a bismuth stream containing lithium and thorium in a multistage contactor in order to remove the uranium and protactinium from the salt. The bismuth stream leaving the column, which contains the extracted uranium and protactinium as well as lithium and thorium, is contacted with an $HF-H_2$ mixture in the presence of a molten-salt stream in order to remove these materials from the bismuth. The salt stream which flows through the hydrofluorinator also circulates through a fluorinator, where about 95 percent of the uranium is removed, and through a tank which contains most of the protactinium. Uranium produced in the tank by decay of protactinium is removed by the circulating salt stream. Reductant (lithium) is added to the bismuth stream leaving the hydrofluorinator, and the resulting stream is returned to the extraction column. The salt stream leaving the column is essentially free of uranium and protactinium and is processed for removal of rare earths before being returned to the reactor.

9.1.2 Rare-Earth Removal

Rare-earth and alkaline-earth fission products can be removed effectively from the fuel salt by the metal-transfer process. In this process, bismuth containing thorium and lithium is used to transport the rare-earth fission products from the reactor fuel salt to an acceptor salt. LiCl is the preferred acceptor salt.

Both thorium and rare earths transfer to the bismuth; however, because of favorable distribution coefficients, only a small fraction of the thorium transfers with the rare

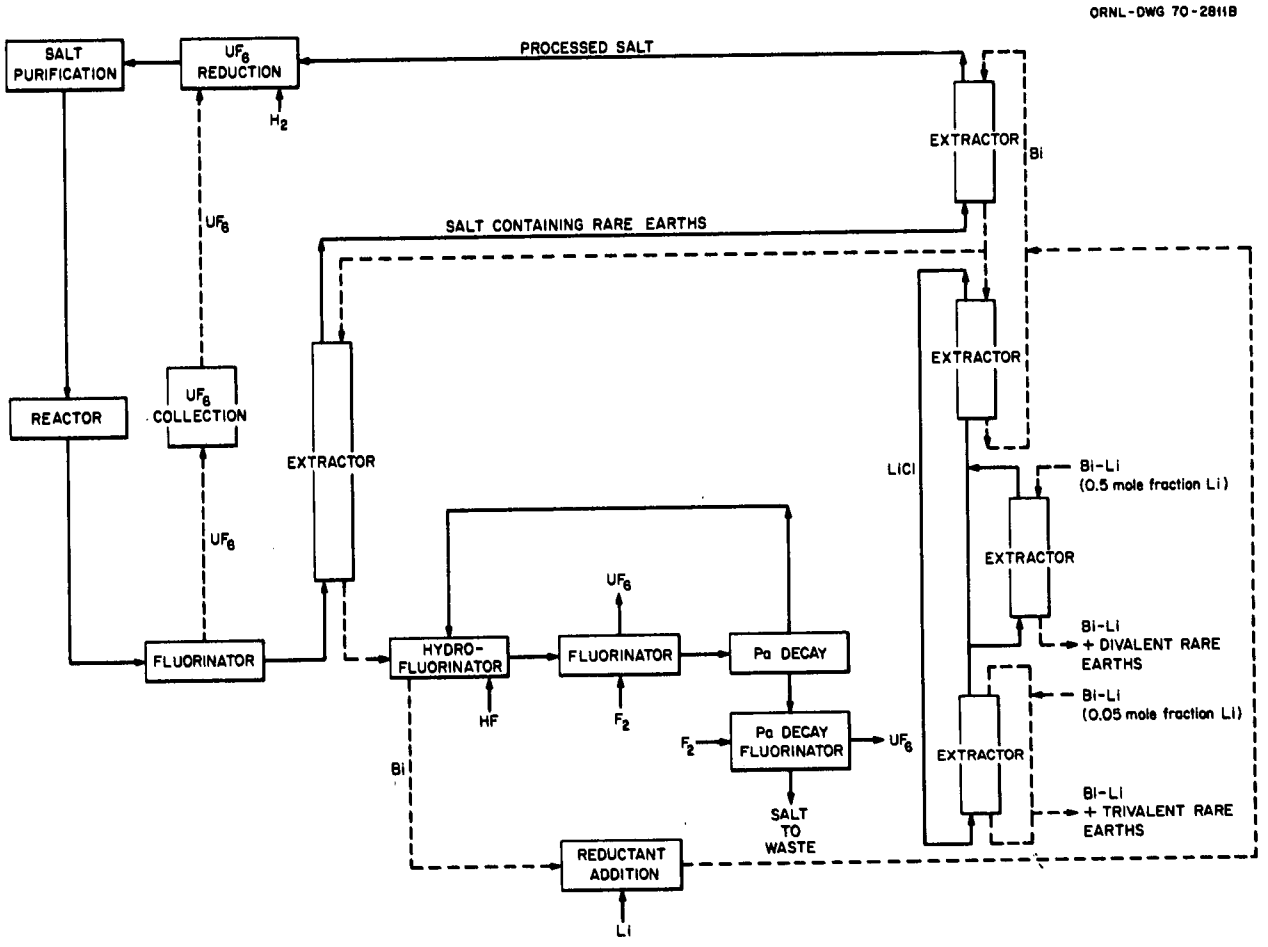

Fig. 9.1. Protactinium isolation with uranium removal by fluorination.

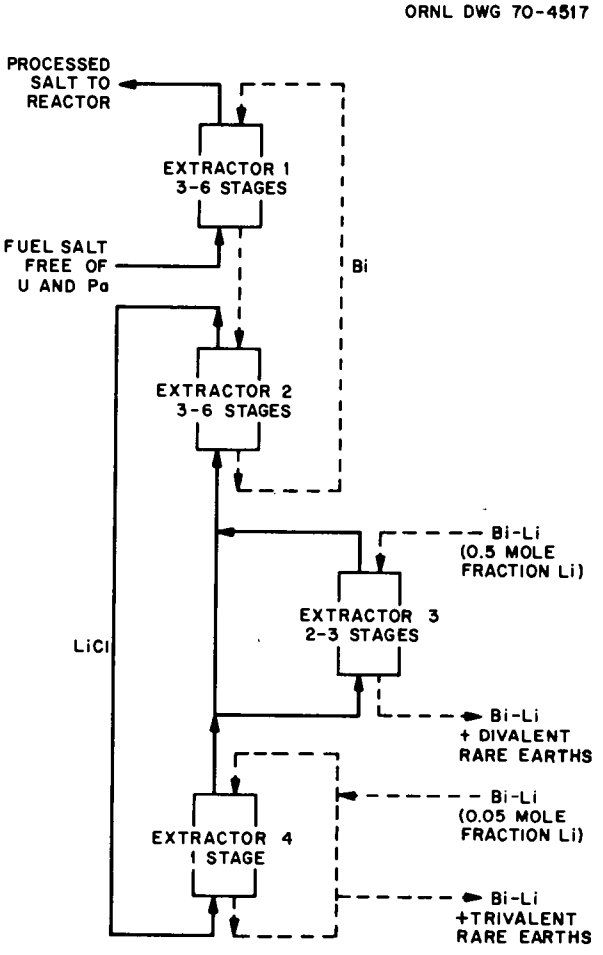

Fig. 9.2. Mass transfer process for removal of rare earths from a single-fluid MSBR.

9.1.2 Rare-Earth Removal (Cont'd)

earths from the bismuth to the LiCl. The effective thorium-rare-earth separation factors for the various rare earths range from about 10^4 to about 10^8. The final step of the process is removal of the rare earths from the LiCl by extraction with bismuth containing 0.05 to 0.50 mole fraction lithium.

The process flowsheet (Figure 9.2) includes four extractors that operate at about 640 C. Fuel salt from the protactinium isolation system, which is free of uranium and protactinium but contains the rare earths at the reactor concentration, is countercurrently contacted with bismuth containing approximately 0.002 mole fraction lithium and 0.0025 mole fraction thorium (90 percent of thorium solubility) in Extractor 1. Fractions of the rare earths transfer to the downflowing metal stream and are carried into Extractor 2. Here, the bismuth stream is contacted countercurrently with LiCl, and fractions of the rare earths and a trace of the thorium transfer to the LiCl. The resulting LiCl stream is routed to Extractor 4, where it is contacted with a bismuth solution having a lithium concentration of 0.5 mole fraction for removal of trivalent rare earths. About 2 percent of the LiCl leaving Extractor 4 is routed to Extractor 3, where it is contacted with a bismuth solution having a lithium concentration of 0.5 mole fraction for removal of divalent rare earths (samarium and europium) and the alkaline earths (barium and strontium). The LiCl from Extractors 3 and 4 (still containing some rare earths) is then returned to Extractor 2.

9.1.3 Data Presentation

For the reduction of a metal fluoride with lithium reductant dissolved in a metal

$$MF_n + nLi_{(m)} \longrightarrow M_{(m)} + nLiF \qquad (1)$$

the equilibrium distribution of component M between the molten fluoride salt and a liquid metal phase (bismuth) can be expressed as a distribution coefficient D_m defined as:

9.1.3 Data Presentation (Cont'd)

$$D_m = \frac{\text{mole fraction of component M in bismuth phase}}{\text{mole fraction of component M in salt phase}} \quad (2)$$

$$\log D_m = n \log X_{Li(m)} + \log K_M^* \quad (3)$$

where n = valence of component as its fluoride, MFn in the salt

$X_{Li(m)}$ = equilibrium lithium concentration in bismuth phase (atom fraction)

K_M^* = constant

A quantity K_Q can be defined as

$$K_Q = D_M X_{Li(m)}^{-n} \quad (4)$$

or as a difference in standard reduction potentials[1/]

$$E'_{o,M} - E'_{o,Li} = \Delta E'_o = \frac{RT}{nF} \ln D_M - \frac{RT}{F} \ln D_{Li} \quad (5)$$

From Equations (4) and (5)

$$\log K_Q = \frac{nF\Delta E'_o - n \log X_{LiF}}{2.303\ RT} \quad (6)$$

Alternatively

$$\log D_M = n \log C_{Li(m)} + \log K_M \quad (7)$$

where $C_{Li(m)}$ = atom percent lithium concentration in the metal phase

Or, it has been shown[2/] that

$$\log D_M = n \log D_{Li} + \log K'_M \quad (8)$$

For an equilibrium reaction

$$K_Q = \frac{X_M}{X_{MF}} \cdot \frac{X_{LiF}^n}{X_{Li}^n} = \frac{D_M}{D_{Li}^n} \quad (9)$$

where K_Q = equilibrium quotient.

1/ ORNL-4119, p. 150, February 28, 1967

2/ ORNL-4076, p. 34, December 31, 1966.

Table 9.1

Equilibrium Constants for Lithium Protactinium, Thorium, Uranium System 3/

Fuel Salt: $LiF-BeF_2-ThF_4$ (72-16-12 Mole %)

	Temperature (°C)	
	600	700
$\text{Log } D^4_{Li}/D_{Pa}$	-12.560 ± 0.498	-11.867 ± 0.338
$\text{Log } D^4_{Li}/D_{Th}$	-9.74 ± 0.292	-8.981 ± 0.399
$\text{Log } D_{Pa}/D_{Th}$	2.966 ± 0.348	2.859 ± 0.129
$\text{Log } D^3_{Li}/D_U$	-10.703 ± 0.700	-10.253 ± 0.460
$\Delta E_{o(Li-Th)}$	-0.422 ± 0.013	-0.434 ± 0.019
$\Delta E_{o(Li-Li)}$	-0.544 ± 0.022	-0.573 ± 0.016
$\Delta E_{o(Li-U)}$	-0.618 ± 0.040	-0.660 ± 0.030
$\Delta E_{o(Pa-U)}$	-0.072 ± 0.018	-0.087 ± 0.025

9.1.3 Data Presentation (Cont'd)

The temperature dependence of K_M^* was expressed as

$$\log K_M^* = A + \frac{B}{T} \tag{10}$$

where A and B = constants

T = temperature, ^oK.

The separation factor is defined as

$$\alpha_{A-B} = \frac{D_{M(A)}}{D_{M(B)}} \tag{11}$$

All subsequent data are reported in the above manner.

9.2 Protactinium Isolation and Rare-Earth Removal

9.2.1 Reductive Extraction of Uranium, Sodium, Europium, Lanthanum from Fuel Salts[3/]

Data obtained on the distribution of several solutes between two-fluid MSBR fuel salt, $LiF-BeF_2$ (66-34 mole percent), and lithium-bismuth solutions are given in Tables 9.2 and 9.3. In calculating values of Q and $\Delta E'_o$, n was assumed to be unity for lithium and sodium, 2 for europium, 3 for lanthanum, and 4 for uranium. Average $\Delta E'_o$ values (Table 9.2) are given at those temperatures where more than one distribution coefficient was obtained. The values obtained for lanthanum and europium are in reasonable agreement with those reported by Moulton and Shaffer[4/5/]. However, the value for uranium at 600 C (based on three data points, Table 9.3) is 0.14 v higher than the value reported by Moulton and Shaffer[4/]. The $\Delta E'_o$ values appear to be constant over the temperature range from 500 to 700 C. If $\Delta E'_o$ is constant, plots of log Q vs 1/T should be linear (see Eq. 6). Plots of the data for europium and lanthanum

3/ ORNL-4344, August 31, 1968.

4/ Moulton and Shaffer, unpublished results, December 14, 1967.

5/ ORNL-4119, pp. 155-56, February 28, 1967.

Table 9.2

ΔE_o Values for the Distribution of Various Solutes Between Different Fluoride Salts and Lithium-Bismuth Solutions

Salt Composition (Mole %)			Temperature	ΔE_o (ev)				
LiF	BeF_2	ThF_4	(^oC)	U	La	Eu	Na	Th
66	34	0	500			0.27		
66	34	0	600			0.32		
66	34	0	600		0.40	0.30		
66	34	0	600	0.54	0.45	0.32		0.36
66	34	0	600	0.68				
70	19	11	600	0.66		0.33		0.41
66	34	0	602			0.31		
66	34	0	605		0.44	0.27	0.20	
66	34	0	675	0.60	0.43			
66	34	0	700			0.30		
66	34	0	700			0.34		

Table 9.3

Effect of Temperature on Distribution of Europium and Lanthanum Between $LiF-BeF_2$ (66-36 Mole %) and Li-Bi Solutions

Temperature (°C)	$10^4/T_1$ (°K)	Li Concentration in Metal Phase C_{Li} (At. %)	D_{Eu}	D_{La}	D_U	Q Eu x 10^3	Q La x 10^8
500	12.94	4.02	14.3			8.83	
583	11.68	4.95	16.4			6.67	
583	11.68	3.46	17.1			14.3	
600	11.45	0.0133			1.74		
600	11.45	0.0232			5.41		
600	11.45	0.0313			53.6		
600	11.45					6.68	0.29
600	11.45					11.4	
600	11.45					11.4	2.16
602	11.43	2.56	5.41			8.26	
605	11.39	0.119		0.092			0.55
605	11.39	0.119		0.90			5.34
605	11.39	0.208		0.705			0.78
605	11.39	0.298		5.12			1.93
605	11.39	4.84	6.36			2.72	
608	11.35	0.85	0.82			11.3	
675	10.55	0.238		0.487	1,021		0.36
675	10.55	0.298		0.672	1,788		0.25
675	10.55	0.298		0.926			0.35
675	10.55	0.416		1.09			0.15
675	10.55	0.506		2.01			0.16
700	10.28	5.11	8.66			3.32	
700	10.28					7.64	
800	9.32					5.53	

9.2.1 Reductive Extraction of Uranium, Sodium, Europium, Lanthanum from Fuel Salts (Cont'd)

are shown in Figure 9.3; the lines were placed using average values of $\Delta E'_o$ of 0.43 and 0.30 for lanthanum and europium, respectively (Table 9.2). Although the data points are highly scattered, it does appear that Q decreases with increasing temperature. This dependence of Q on temperature shows that the rare earths are less easily extracted at the higher temperatures.

The data given in Tables 9.2 and 9.3 show that uranium can easily be removed from the fuel salt by reductive extraction. Furthermore, separation from the rare earths is very good; at 600 C the separation factors (D_U/D_{Ln}) are at least 1000. The data also show that once the uranium has been extracted, the rare earths can be removed from the salt by increasing the lithium concentration in the metal phase.

9.2.2 Reductive Extraction of Uranium, Thorium, and Europium from MSBR Fuel Salt[3/]

Two experiments involving equilibration of fuel salt with lithium-bismuth solutions at 600 C were completed at 600 C.

The distribution coefficients obtained are given in Table 9.4. Those for uranium can be represented by the relationship

$$\log D_U = 4 \log C_{Li} + 7.874, \qquad (12)$$

in which C_{Li} is the lithium concentration in the metal phase (at. percent). This equation was obtained by visually fitting what appeared to be the best line of slope 4 through the points in the lithium concentration range of 0.002 to 0.03 at. percent, where the analyses were the most accurate. These data are shown in Figure 9.4; the distribution coefficients obtained using $LiF-BeF_2$ (66-34 mole percent) as the salt phase are included for comparison.

Table 9.4

Distribution of Lithium, Uranium, Thorium, and Europium Between $LiF-BeF_2-ThF_4$ (70-19-11 Mole %) and Bismuth Solutions at 600°C

Experiment No.	Lithium Concentration in Metal Phase (At. %) C_{Li}	D_U	D_{Th}	D_{Eu}
72	0.000672	0.00021		
72	0.00119	0.00013		
2	0.00321	0.0638		
2	0.00579	0.0267		
72	0.00584	0.311		
2	0.00726	0.132		
2	0.00747	0.238		
72	0.00873	0.134		
2	0.00988	2.47		
72	0.00997	0.827		
2	0.0112	1.12		
72	0.0128	1.47		
72	0.0133	2.28		
72	0.0136	4.08		
72	0.0176	5.07		
2	0.0182	15.1		
72	0.0285	15.2		
72	0.0376	26.1		
2	0.0570	102	0.00131	0.0041
72	0.0623	129	0.00229	
72	0.0786	168	0.00327	
72	0.0816	155	0.00573	
72	0.0855		0.00802	
2	0.0939		0.00998	0.011
2	0.997	333	0.00712	0.014
72	0.114		0.0131	
2	0.175	759	0.0152	

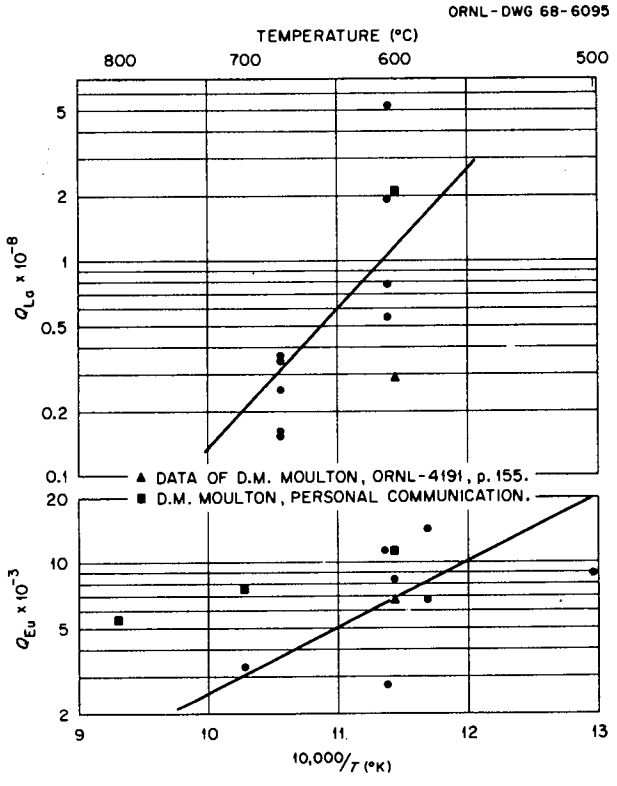

Fig. 9.3. Dependence of log Q on Temperature.

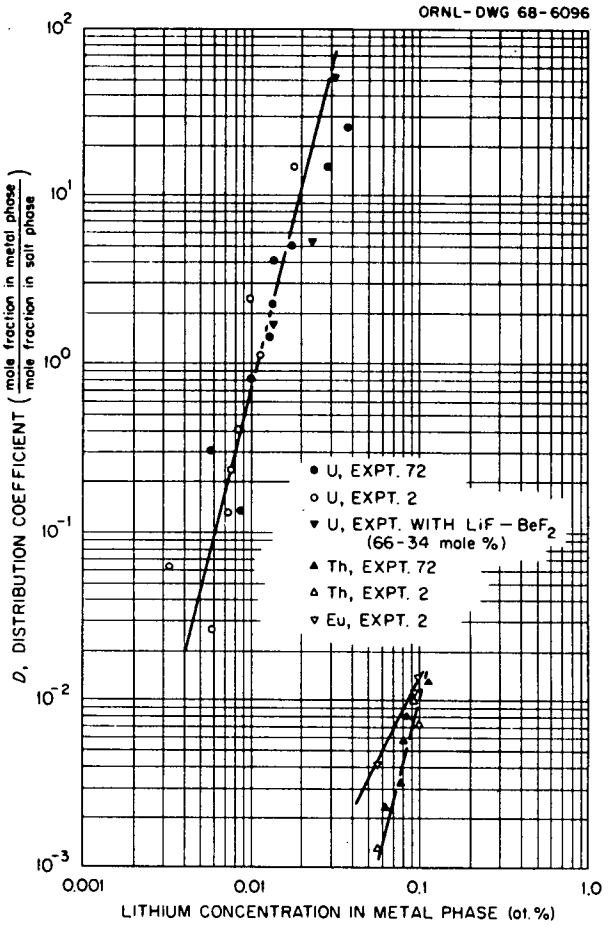

Fig. 9.4. Effect of Lithium Concentration in Metal Phase on the Distribution of Uranium, Thorium, and Europium Between $LiF-BeF_2-ThF_4$ (70-19-11 Mole %) and Bismuth at 600°C.

9.2.2 Reductive Extraction of Uranium, Thorium, and Europium from MSBR Fuel Salt (Cont'd)

The distribution coefficients for thorium (Table 9.4) can be represented by the equation

$$\log D_{Th} = 4 \log C_{Li} + 2.00, \qquad (13)$$

which was also obtained by a visual fit of the data (Figure 9.4). The line through the three points obtained for europium (Figure 9.4) was drawn with a slop of 2.

The data show that uranium can be easily extracted from single-fluid MSBR salt, leaving thorium and rare earths in the salt; the separation factors (D_U/D_{Th} and D_U/D_{Eu}) are at least 10^4.

9.2.3 Extraction of Thorium and Rare Earths Europium, Lanthanum, and Neodymium[3/]

For a given system, the highest possible distribution coefficients are obtained when the metal phase is saturated with thorium and, accordingly, will be denoted as D^{max}. At a given temperature, D_{Th}^{max} is simply the solubility of thorium in bismuth (atom fraction) divided by the ThF_4 concentration in the salt (mole fraction); thus the value of D_{Th}^{max} depends only on the ThF_4 concentration in the salt and provides a convenient reference point for the correlation of data. The separation factors determined at D_{Th}^{max} will be denoted by α^*, although it is emphasized that these are not necessarily the maximum separation factors attainable. If the valence of the other component is less than 4, the separation factor decreases as the thorium concentration in the metal phase increases, and α^* is actually the lowest value possible. If the valence of the other component is also 4, the separation factor is α^*, regardless of the thorium concentration in the metal phase.

Typical plots of log D_M vs log D_{Li} using data from experiments with two different salt compositions are shown in Figure 9.5. These plots illustrate: (1) the scatter in

9.2.3 Extraction of Thorium and Rare Earths Europium, Lanthanum, and Neodymium (Cont'd)

data points is typical of experiments of this type; (2) the fact that the data can be represented in this manner suggests that many of the assumptions made in the original thermodynamic treatment of the equilibria involved are reasonably valid (the slopes of the lines are 2,3, and 4 for Eu, La, and Th, respectively); (3) since the ThF_4 concentration in both salts was about 12 mole percent, the same value of 1.46×10^{-2} for D_{Th}^{max} was obtained in each experiment. However, since the corresponding values for D_{Li}^{max} were markedly different, it is obvious that the activity of the ThF_4 and/or the LiF changed with salt composition. It was suggested that these changes in activity might be related to differences in the "free fluoride" equivalence of the salts. Free fluoride equivalence (FF) is defined as

$$FF = LiF \text{ (mole percent)} - 2\ BeF_2 \text{ (mole percent)} - 3\ ThF_4 \text{ (mole percent)}. \quad (14)$$

This concept appears to have some validity in that the values for α^* for several rare earths increase with increasing free fluoride equivalence of the salt, both at 600 and 700°F (Table 9.5 and Figure 9.6). The data in Table 9.5 also suggest that temperature has very little effect on the values of α^*. More experiments of this type are needed to better define the relationship between the separation factor and the free fluoride equivalence of the salt.

9.2.4 Reductive Extraction of Uranium, Protactinium, and Thorium from Fuel Salts[3/]

Distribution coefficients for protactinium at 600 C using $LiF-BeF_2-ThF_4$ (69.2-19.4-11.4 mole percent) as the salt phase are shown in Figure 9.7. The slope of the line is 4, showing that the protactinium species in the salt phase

ORNL-4344
p 296

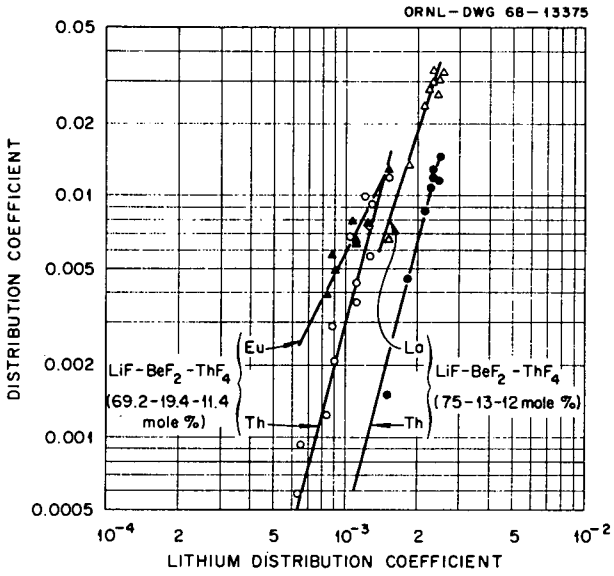

Fig. 9.5 Distribution of Thorium and Rare Earths Between $LiF-BeF_2-ThF_4$ Salts and Bismuth Solution of 600°C.

ORNL-4344
p 297

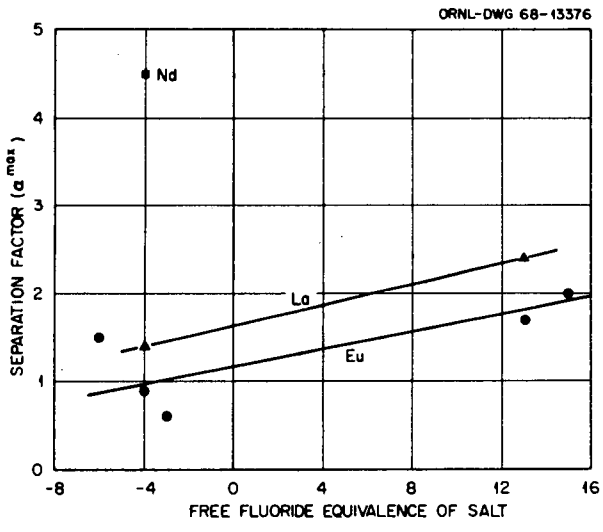

Fig. 9.6 Effect of Free Fluoride Equivalence of $LiF-BeF_2-ThF_4$ Salts on Rare-Earth-Thorium Separation Factors (α^{max}) at 600 C.

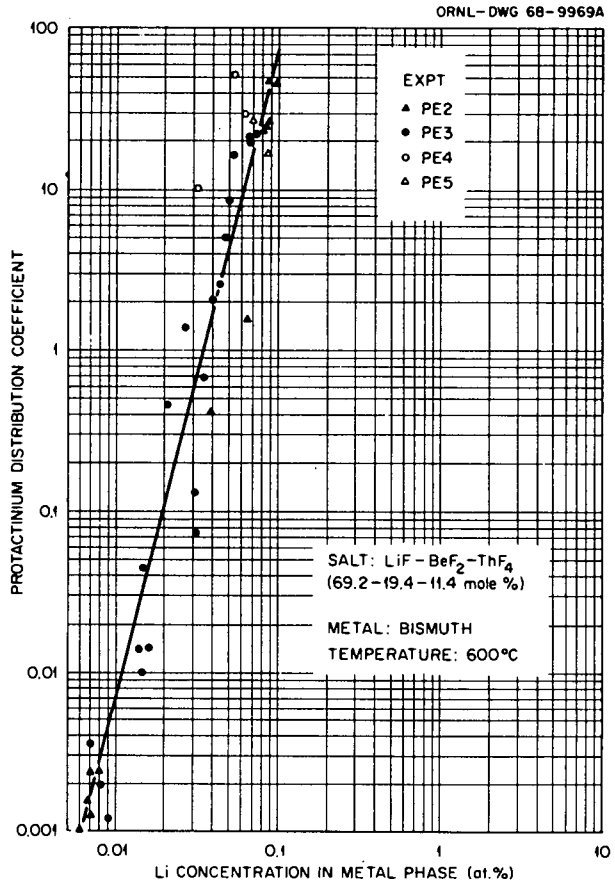

Fig. 9.7. Distribution of Protactinium Between LiF-BeF_2-ThF_4(69.2-19.4-11.4 mole %) and Li-Bi Solutions at 600°C.

Table 9.5

Distribution of Thorium, Rare Earths, and Lithium Between $LiF-BeF_2-ThF_4$ Salts and Thorium-Saturated Bismuth Solutions at 600 to 700°C

Salt Composition (Mole %)			Rare Earth	Free Fluoride Equivalence	Temperature (°C)	D^{max}			
LiF	BeF_2	ThF_4				Li	Th	Rare Earth	α*
73.0	2.0	25.0	Eu^{2+}	-6	600	0.00169	0.0065	0.01	1.5
			Eu^{2+}		650	0.0028	0.0115	0.0163	1.4
69.2	19.4	11.4	Eu^{2+}	-4	600	0.00149	0.0145	0.0130	0.9
			La^{3+}		600			0.0205	1.4
			Nd^{3+}		600			0.066	4.5
			La^{3+}		700	0.0046	0.040	0.060	1.5
68.0	25.0	7.0	Eu^{2+}	-3	600	0.00162	0.025	0.015	0.6
75.0	13.0	12.0	Eu^{2+}	13	600	0.00242	0.0147	0.026	1.7
			La^{3+}		600			0.035	2.4
			Eu^{2+}		700	0.00747	0.040	0.068	1.7
			La^{3+}		700			0.10	2.5
73.4	21.4	5.2	Eu^{2+}	15	600	0.0033	0.0349	0.0697	2.0

9.2.4 Reductive Extraction of Uranium, Protactinium, and Thorium from Fuel Salts (Cont'd)

was tetravalent. These data yield a value of 0.579 v for ΔE_o, the difference in half-cell reduction potentials as defined by Moulton[1/]. This value, when compared with previously reported[6/] values for uranium and thorium, confirms earlier indications that protactinium is readily separable from uranium and thorium. The separation factors obtained are

$$a_{U-Pa} = 100 \text{ and } a_{Pa-Th} = 4300.$$

Another experiment, UF_4 and PaF_4 present in the salt, $LiF-BeF_2-ThF_4$ (69.2-19.4-11.4 mole percent), were reduced by addition of crystal-bar thorium to the system. The amount of thorium added was sufficient to reduce all of the UF_4 and about 95 percent of the PaF_4. The resulting metal phase contained about 5,000 ppm U, 750 ppm Th, and 70 ppm Pa; the protactinium concentration in the salt was about 10 ppm. The system remained practically unchanged for 128 hours (Table 9.6). The results of this experiment provide proof that protactinium can be maintained in solution with bismuth in a molybdenum container and that good material balances can be maintained if oxidants are excluded from the system.

9.2.5 Reductive Extraction of Uranium, Protactinium, and Thorium from Fuel Salts—Further Studies[7/]

Measurements were made to determine equilibrium quotient for the extraction reaction

$$Pa^{4+}(F) + Th^{o}(Bi) \rightleftharpoons Pa^{o}(Bi) + Th^{4+}(F), \qquad (15)$$

$$Q_{Th}^{Pa} = \frac{X_{Pa^o}(Bi)/X_{Pa^{4+}}(F)}{X_{Th^o}(Bi)/X_{Th^{4+}}(F)}, \qquad (16)$$

6/ ORNL-4254, p. 243, February 29, 1968.

7/ ORNL-4396, February 28, 1969.

ORNL-4396
p 190

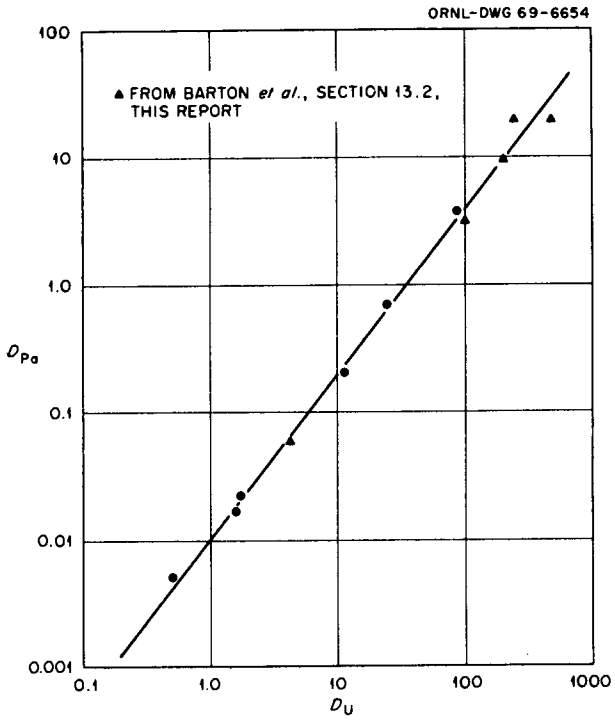

Fig. 9.8 Variation of Pa Distribution Coefficient with U Distribution Coefficient.

ORNL-4396
p 190

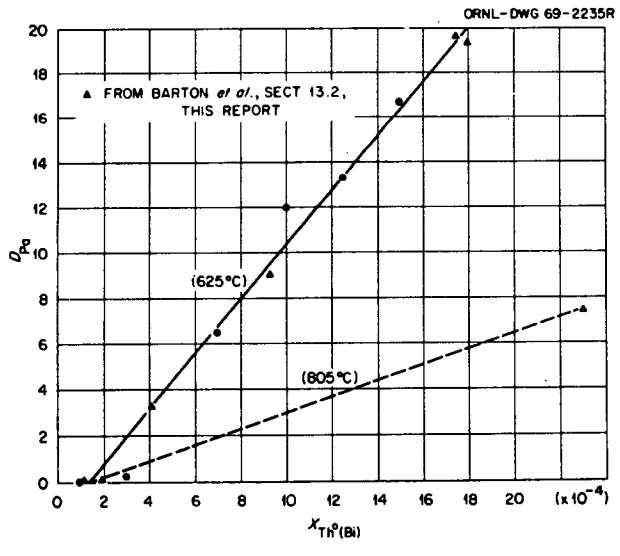

Fig. 9.9 Variation of Pa Distribution Coefficient with Mole Fraction of Thorium in the Bismuth Phase.

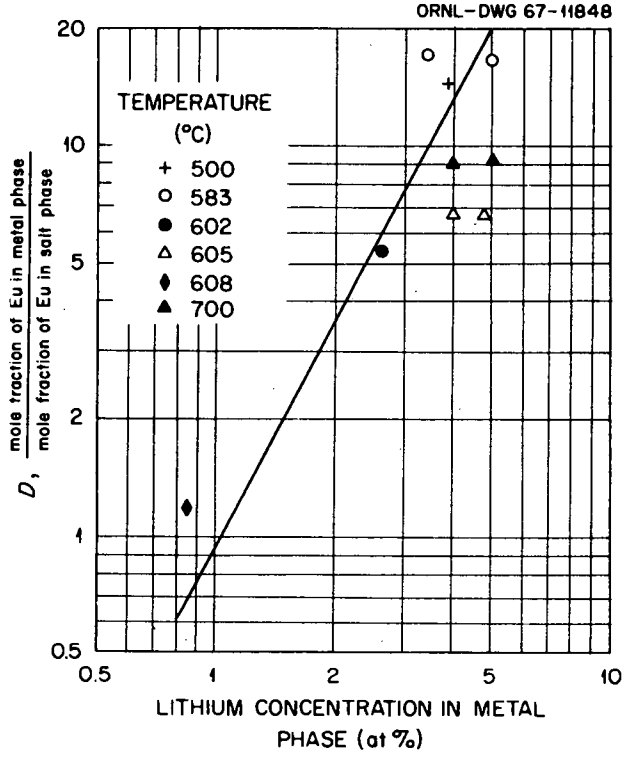

Fig. 9.10. Distribution of Europium Between LiF-BeF_2 (66-34 mole %) and Li-Bi Solutions. Data points, this study; solid line, data of Shaffer, Moulton, et al. (see Reactor Chem. Div. Ann. Progr. Rept. Dec. 31, 1966. ORNL-4076).

Table 9.6

Distribution of Thorium, Uranium, and Protactinium Between $LiF-BeF_2-ThF_4$ (69.2-19.4-11.4 Mole %) and Bismuth Solutions at 600°C

Total Equilibration Time (Hr)	Concentration in Metal Phase (wt ppm)			Li Concentration in Metal Phase (At. %)		
	Th	U	Pa	C_{Li}	D_{Th}	D_{Pa}
18	820	4,990	71.0	0.0896	0.00649	19.9
42	600	5,300	67.6	0.0717	0.00475	29.9
114	750	5,070	67.6	0.0568	0.00593	
128		5,200	72.3			

9.2.5 Reductive Extraction of Uranium, Protactinium, and Thorium from Fuel Salts—Further Studies (Cont'd)

and to determine also whether this quotient depends significantly on the concentration of Pa^o and/or U^o in the bismuth phase.

The correlation of D_{Pa} versus D_U, where $D_M = X_{M(Bi)}/X_{M(F)}$, in Figures 9.8 and 9.9 is excellent, giving the expected slope of 4/3, which confirms that protactinium is tetravalent and uranium is trivalent under these extraction conditions. This correlation further indicates that interactions of U^o and Pa^o do not occur in the bismuth phase at the concentration levels involved. From the results in Figures 9.8 and 9.9 we have:

$$Q_{Pa}^{U} = D_U^{4/3}/D_{Pa} = 121 \text{ (625 C)}$$

$$Q_{Th}^{Pa} = D_{Pa}/D_{Th} = 1450 \text{ (625 C)}$$

One result reported by Barton et al may be used to calculate

$$Q_{Th}^{Pa} = 414 \text{ (805 C)}$$

The two results are given within their uncertainty by

$$\log Q_{Th}^{Pa} = 2830/T \qquad (17)$$

This would indicate that ΔS for the extraction reaction 15 is zero, a result which could well be general for such reactions which involve ions of similar size and valence in the salt phase and metal of similar character in the bismuth phase. The value of Q_{Th}^{Pa} is unaffected by the presence of up to 7,000 ppm uranium in the bismuth phase.

9.2.6 Reductive Extraction of Europium from Fuel Salt[8/]

The values of D obtained in this study are given in Table 9.7 and are compared in Figure 9.10 with those obtained by

8/ ORNL-4191, p. 248, August 31, 1967.

Table 9.7

Distribution of Europium Between $LiF-BeF_2$ (66-34 Mole %) and Lithium-Bismuth Solutions

Experiment	Lithium Concentration in Metal Phase (Atom %) C_{Li}	Temperature (^{o}C)	Amount of Europium in Metal Phase (%)	D
CES75	0.85	608	52	1.2
CES66	2.6	602	81	5.4
CES66	3.4	583	93	17.1
JFL64	3.9	500	92	14.8
JFL64	4.0	605	84	6.7
JFL64	4.0	700	88	9.1
JFL64	4.8	605	84	6.7
CES66	5.0	583	93	16.8
JFL64	5.1	700	88	9.1

9.2.6 Reductive Extraction of Europium from Fuel Salt (Cont'd)

Shaffer, Moulton, et al[9/] at 600 C. Agreement between the two sets of data is reasonably good. It also appears that temperature has no marked effect on the equilibrium distribution of europium between the two phases.

An emission-spectrographic or a neutron-activation method was used to analyze for europium in both the salt and metal phases. The data reported are from experiments in which the eurpoium balance was 90 to 110 percent. Each sample of the metal phase was analyzed for lithium by both an emission spectrographic and a flame photometric method. In some instances, the values obtained were markedly different; this is readily apparent in the data obtained from experiment JFL64.

9.2.7 Reductive Extraction of Cerium by Thorium from Fuel Salt Mixtures[10/]

The experimental procedure was directed primarily toward the evaluation of pertinent equilibrium data according to Eq. (18). If the activity coefficients remain constant during each individual extraction experiment, then the concentrations of reaction constituents may be equated to a constant by the relation

$$K_Q = \frac{D^4_{Ce}}{D^3_{Th}}, \qquad (18)$$

Typical data obtained during one extraction experiment are illustrated in Figure 9.11 and demonstrate reasonable agreement with Eq. (18). Equilibrium quotients for similar extractions from the various salt mixtures studied are shown in Table 9.8. The relation of these equilibrium quotients at 600 C to the "free fluoride" model is illustrated in Figure 9.12. Although empirical, these results provide a

9/ ORNL-4076, December 31, 1966.

10/ ORNL-4344, p. 177, August 31, 1968.

ORNL-4344
p 177

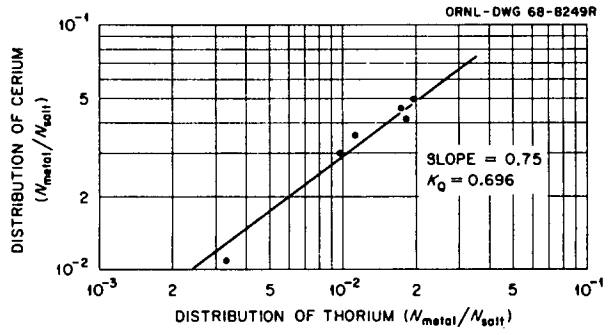

Fig. 9.11 Distribution of Thorium

ORNL-4344
p 178

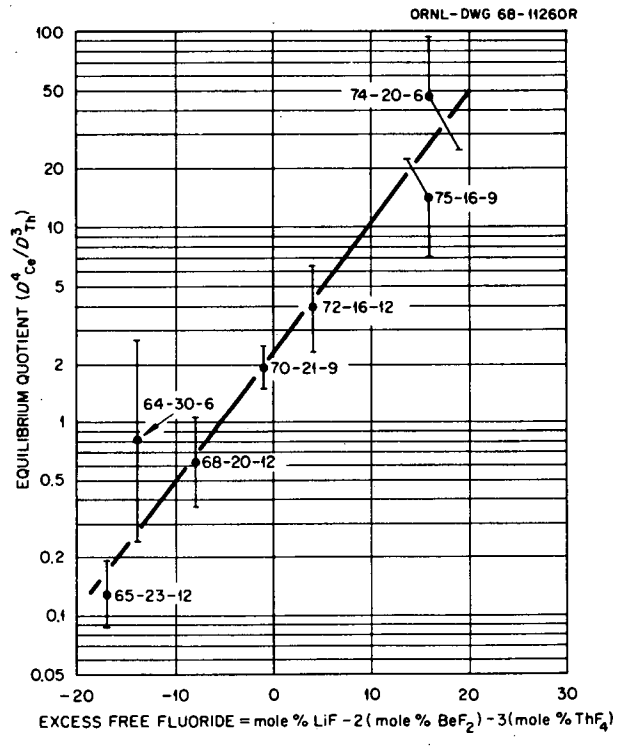

Fig. 9.12 Effect of Salt Composition on the Equilibrium Reduction of Cerium by Thorium from LiF-BeF_2-ThF_4 Mixtures into Bismuth at 600 C.

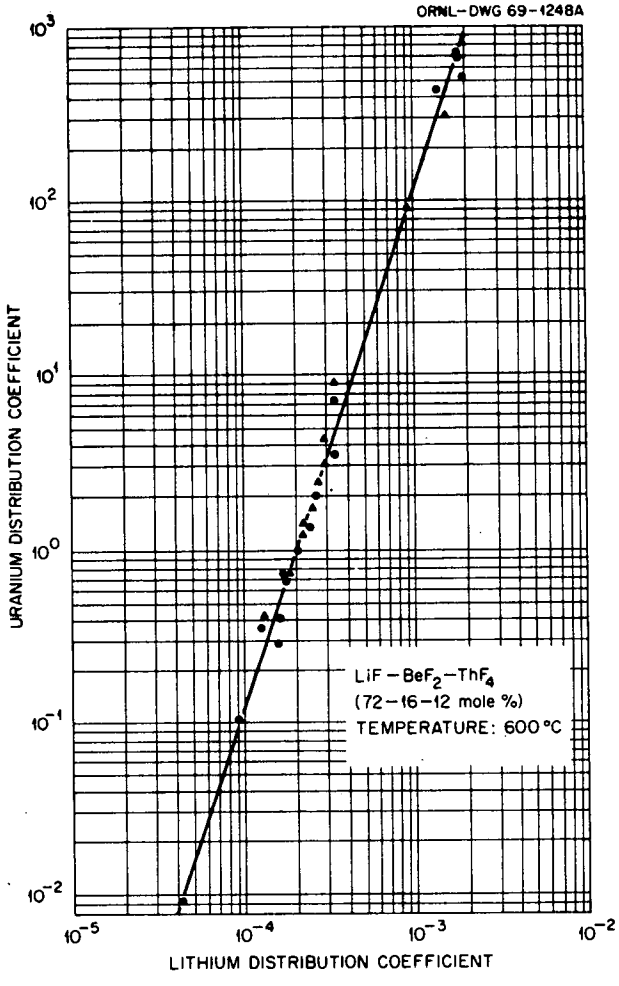

Fig. 9.13. Equilibrium Distribution of Uranium Between LiF-BeF_2-ThF_4 (72-16-12 Mole %) and Bismuth Solutions at 600°C.

Table 9.8

Equilibrium Quotients for the Reductive Extraction of Cerium By Thorium from $LiF-BeF_2-ThF_4$ Mixtures into Bismuth

Salt Composition (Mole %)			Free	T=	T=	T=	T=	T=	T=
LiF	BeF_2	ThF_4	Fluoride	500 C	550 C	600 C	700 C	750 C	800 C
72	16	12	+4			3.8	2.8		
65	23	12	-17	2.96		0.13	0.47		
64	30	6	-14	0.32		0.80	1.2		
70	21	9	-1	1.1		1.9	2.4		
68	20	12	-8	0.58		0.62	2.2		
75	16	9	+16	4.4	8.58	14.0	26.5	41.3	
78	16	6	+28				54.9	76.6	174.5
74	20	6	+16	3.9	10.6	46.7	34.6	46.0	

9.2.7 Reductive Extraction of Cerium by Thorium from Fuel Salt Mixtures (Cont'd)

reasonable basis for predicting rare-earth extraction behavior over the salt composition region of interest in the MSBR program.

Since the experimental data were not necessarily obtained up to the solubility limit of thorium in bismuth, the values calculated for the equilibrium quotients are useful in establishing limiting parameters of the extraction process. The solubility of thorium in bismuth is expressed by the equation[11/]

$$\log (\text{at. percent Th}) = 3.30 - 3410/T(^{o}K), \qquad (19)$$

Calculated values for limiting distribution coefficients and separation factors are presented in Table 9.9.

9.2.8 Reductive Extraction of Cerium, Neodymium, and Samarium from Fuel Salt Mixtures[12/]

Values for their distribution coefficients, D, and their separation factors, α, at 600 and 700 C when the bismuth was saturated with thorium are as follows:

Rare Earth	600 C		700 C	
	D_M	D_M/D_{Th}	D_M	D_M/D_{Th}
Cerium	0.077	3.67	0.157	2.64
Neodymium	0.051	2.43	0.142	2.68
Samarium	0.045	2.14	0.082	1.55

These separation factors are based on D_{Th} = 0.021 at 600 C and D_{Th} = 0.053 at 700 C.

The investigation of salt composition effects on the reductive extraction of cerium into bismuth was extended to two additional salt compositions[13/]. In the mixture LiF-BeF_2-ThF_4 (67-30-3 mole percent), the extraction of cerium

11/ Bryner, J. S., and M. B. Brodsky, Proc. Ind. Intern. Conf. At. Energy 7, 209 (1958)

12/ ORNL-4396, p. 191, February 28, 1969.

13/ ORNL-4344, p. 176, August 31, 1968.

Table 9.9

Calculated Values for the Distribution Coefficient of Cerium and its Separation from Thorium by Reductive Extraction from $LiF-BeF_2-ThF_4$ Mixtures into Bismuth

Salt Composition (Mole %)			D_{Ce} at T		$\alpha = D_{Ce}/D_{Th}$ at T	
LiF	BeF_2	ThF_4	T= 600 C	T= 700 C	T= 600 C	T= 700 C
72	16	12	0.077	0.14	3.67	2.64
65	23	12	0.033	0.10	1.57	1.89
64	30	6	0.088	0.20	2.10	1.89
70	21	9	0.081	0.17	2.89	2.43
68	20	12	0.049	0.13	2.33	2.45
75	16	9	0.133	0.31	4.75	4.43
78	16	6		0.51		4.81
74	20	6	0.243	0.45	5.79	4.25

Table 9.10

Separation for Uranium and Protactinium Between $LiF-BeF_2-ThF_4$ (72-16-12 Mole %) and Bi-Th Alloy

Experiment	Temperature (°C)	Average X_{Th}(Bi) x 10^3	α^U_{Th}	α^{Pa}_{Th}	α^U_{Pa}
Part 1	630	1.26	25,800	1680	15.4
Part 2A	630	1.67	25,300	1275	19.8
Part 2B	805	2.34	6,000	380	15.8

9.2.8 Reductive Extraction of Cerium, Neodymium, and Samarium from Fuel Salt Mixtures (Cont'd)

by thorium can be described by the equation

$$K_Q = D^4_{Ce}/D^3_{Th} = 8.2 \text{ at } 600 \text{ C}$$

At the limiting reduction potential of thorium saturation in bismuth, the distribution coefficient for cerium is about 0.26 and the separation factor is about 3.2 at 600 C. The equilibrium distribution of cerium between the salt solvent mixture, $LiF-BeF_2-ThF_4$ (76.8-6.2-17 mole percent), and bismuth yielded a value of about 5.3 for the equilibrium constant K_Q at 600 C. At thorium saturation in bismuth, the distribution coefficient for cerium is about 0.064 and its separation factor is about 4.4 at 600 C. The experimental results obtained for both of these salt mixtures are in fair agreement with the "free fluoride" model.

9.2.9 Separation Factors for Uranium, Protactinium, and Thorium from Fuel Salt Mixtures[12/]

An experiment was conducted (8-20-68) in which the salt $LiF-BeF_2-ThF_4-UF_4$ (72-16-12-0.25 mole percent) containing 100 ppm ^{231}Pa was equilibrated with Bi-Th alloy in a molybdenum container. The experiment was conducted in two parts. Initially (part 1) sufficient thorium was added to the bismuth to reduce all the UF_4 and PaF_4 to the metals and leave an excess of 1,700 ppm of thorium. This mixture was held at 630° for about seven days, during which time the only changes involved changing the sparge gas between argon and helium, flowing or static. The protactinium and uranium concentrations were essentially constant, regardless of the sparge gas or flow condition. The protactinium and uranium were then returned to the salt phase by oxidation with H_2-HF, and reduction was again effected (part 2), but this time with incremental thorium additions. With the melt temperature at 630 C (part 2A) additions

9.2.9 Separation Factors for Uranium, Protactinium, and Thorium from Fuel Salt Mixtures (Cont'd)

were continued until thorium solubility in bismuth at this temperature was exceeded. The temperature was then increased to 805 C and equilibrium reestablished (part 2B).

Separation factors calculated for this experiment are shown in Table 9.10.

The large separation factors in the table confirm that uranium, protactinium, and thorium can be effectively separated in a fuel processing plant using the reductive extraction method.

9.2.10 Extraction of Uranium, Protactinium, Zirconium, and Plutonium from Fuel Salts[14/]

The equilibrium distribution of uranium, zirconium, protactinium, and plutonium between several typical $LiF-BeF_2-ThF_4$ single-fluid MSBR fuel salts and liquid bismuth solutions has been measured. The behavior of these elements is of primary interest in the protactinium isolation portion of the reference reductive extraction flowsheet.

In most of the previous studies[15,16,17,18/], the valence of the uranium species in the salt phase during extraction was taken to be 4. Thermodynamic considerations[19/] using data for $LiF-BeF_2$ systems indicate that at 600 C the valence of the uranium should be very close to 3 when the lithium concentration in the bismuth phase is greater than about 2 wt ppm (0.006 at. percent). The results of recent

14/ ORNL-4396, p. 279, February 28, 1969.

15/ ORNL-4344, p. 292, August 31, 1968.

16/ ORNL-4272, p. 14, May 31, 1968.

17/ ORNL-4229, p. 41, December 31, 1967.

18/ ORNL-4254, p. 152, February 29, 1968.

19/ ORNL-TM-2486

9.2.10 Extraction of Uranium, Protactinium, Zirconium, and Plutonium from Fuel Salts (Cont'd)

experiments using refined analytical methods show that this is generally true for uranium in $LiF-BeF_2-ThF_4$ solutions at 600 C. This is illustrated by the plot of log D_U vs log D_{Li} shown in Figure 9.13; these data were obtained in two separate experiments at 600 C using $LiF-BeF_2-ThF_4$ (72-16-12 mole percent). The line has a slope of 3. Similar data were obtained in experiments with other salt compositions. Further evidence for the trivalency of uranium in the salt phase is provided by plots of log D_U vs either log D_{Zr} or log D_{Pa}. Uranium and zirconium data from two experiments at 600 C using $LiF-BeF_2-ThF_4$ (72-16-12 mole percent) are shown in Figure 9.14. The slope of this plot of log D_{Zr} vs log D_U is 1.33, as would be expected if the uranium existed as a trivalent species in the salt. More importantly, these data show that uranium and zirconium will behave almost identically in the proposed reductive extraction process. Special provision will have to be made to remove zirconium from the system at one point in the process.

The results of previous studies[15/] indicated that protactinium existed as a tetravalent species in the salt phase in a reductive extraction system. Additional experimentation has verified this conclusion. This is illustrated by the plots of log D_{Pa} vs log D_U and log D_{Th} shown in Figure 9.15. These data were obtained with $LiF-BeF_2-ThF_4$ (72-16-12 mole percent) at 600 C. The slope of the Pa-Th line is 1, as expected from two tetravalent species; the slope of the Pa-U plot is 1.33, which is consistent with the presence of tetravalent protactinium and trivalent in uranium in the salt phase. Plutonium was expected to be trivalent in these systems. This expectation was confirmed, as illustrated by the plots of log D_{Pa} and log D_{Th} vs log D_{Pu} shown in Figure 9.16; the slope of each line is 1.33.

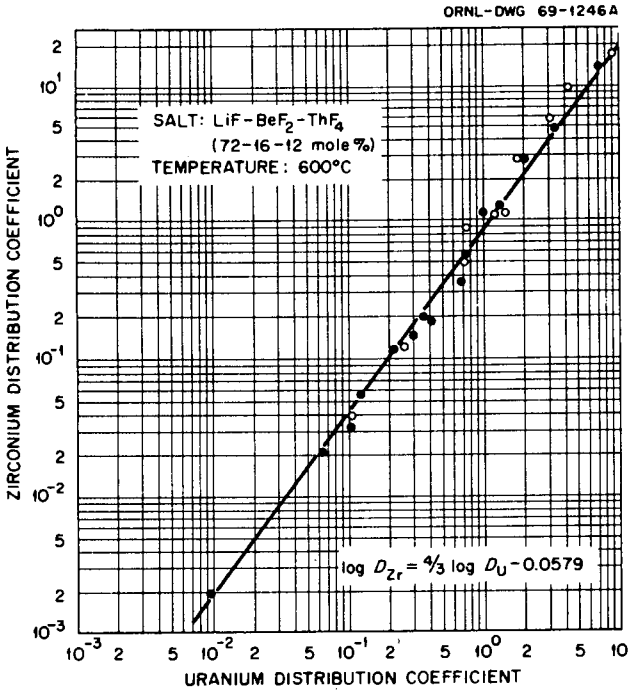

Fig. 9.14 Equilibrium Distribution of Uranium and Zirconium Between LiF-BeF_2-ThF_4 (72-16-12 Mole %) and Bismuth Solutions at 600 C.

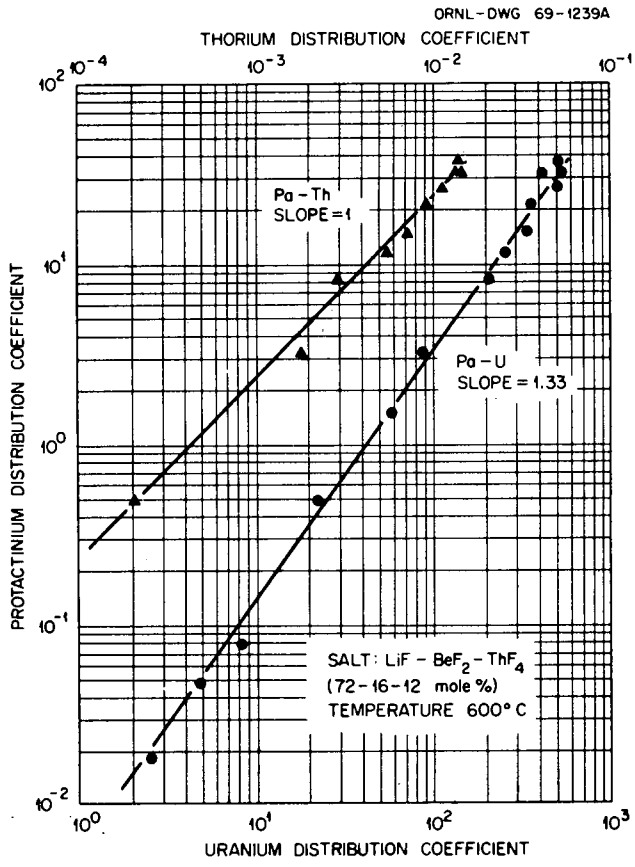

Fig. 9.15 Equilibrium Distribution of Protactinium, Thorium, and Uranium between LiF-BeF_2-ThF_4 (72-16-12 Mole %) and Bismuth Solutions at 600 C.

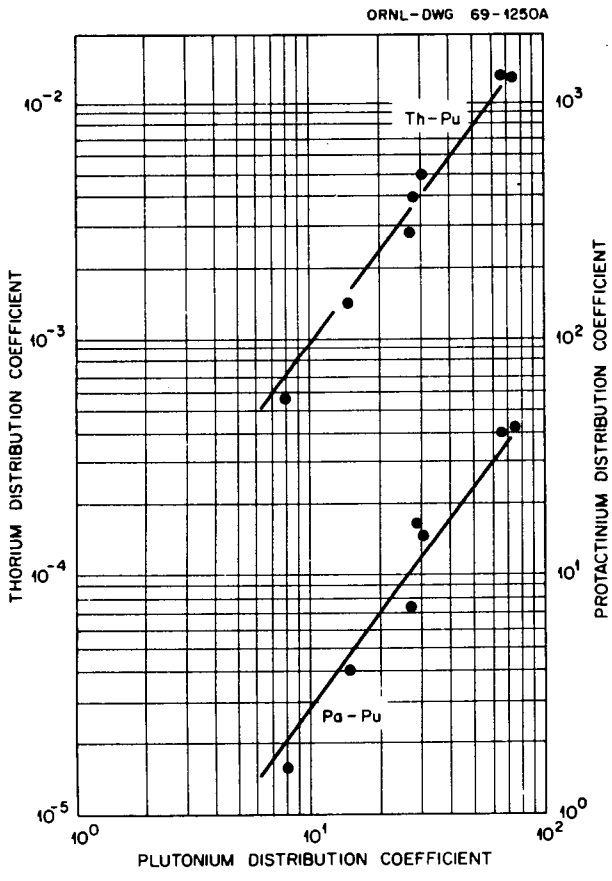

Fig. 9.16 Equilibrium Distribution of Thorium, Protactinium, and Plutonium Between LiF-BeF_2-ThF_4 (72-16-12 Mole %) and Bismuth Solutions at 600 C.

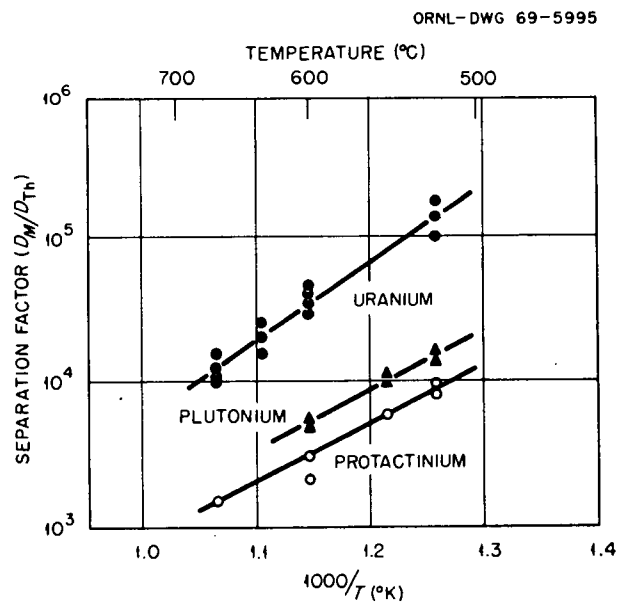

Fig. 9.17 Variation of Metal-Thorium Separation Factors with Temperature. Data obtained with LiF-BeF_2-ThF_4 (72-16-12 Mole %). Bismuth phase was saturated with Thorium at each temperature.

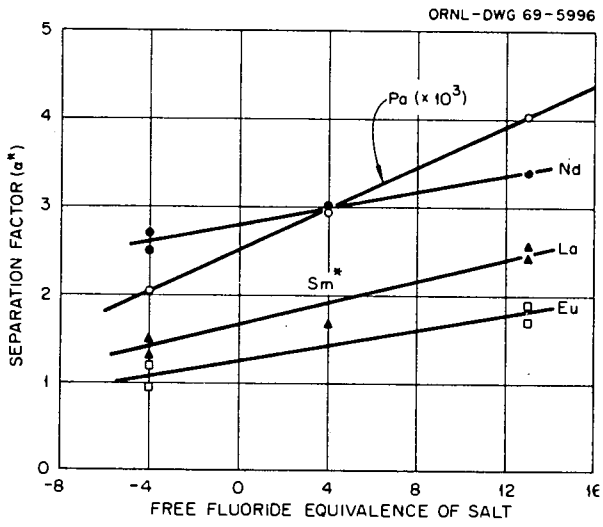

Fig. 9.18. Effect of "Free-Fluoride" Equivalence of LiF-BeF_2-ThF_4 Salts on Rare-Earth - Thorium and Protactinium-Thorium Separation Factors (α*) at 600°C. ThF_4 concentration in the salts, about 12 mole %).

9.2.10 Extraction of Uranium, Protactinium, Zirconium, and Plutonium from Fuel Salts (Cont'd)

Most of the distribution coefficient data obtained so far for uranium, protactinium, zirconium, plutonium, and thorium are compiled in Table 9.11. The data were not analyzed statistically; the equations were obtained by visually fitting what appeared to be the best line through the experimental data. Close inspection of the equations reveals that the distribution coefficients very as the composition of the salt is changed. The difference in Pa-Th behavior is most noticeable; for example, with the salts containing about 12 mole percent ThF_4, the Pa-Th separation factor increased from about 2100 to 4400 as the "free fluoride" equivalence of the salt increased from -4 to +13. "Free fluoride" equivalence (FF) is defined by Equation 14. The fact that the Pa-Th separation factors obtained with $LiBeF_2$ (66-34 mole percent) and $LiF-ThF_4$ (73-27 mole percent) do not correlate with those obtained with salts containing about 12 mole percent ThF_4 emphasizes that the "free fluoride" model is far from ideal. The U-Pu separation factor was about 10 in the two systems in which plutonium was present. Both the U-Pa and Pu-Pa separation factors are variable since the valences of the species are different. When the bismuth phase was saturated with thorium (D_{Th} = 0.0145 for salts in which the ThF_4 concentration is 12 mole percent), the U-Pa separation factor was about 15 to 20 regardless of the salt composition. These data show that, for MSBR fuel salts containing about 12 mole percent ThF_4, separation of uranium from protactinium should be relatively easy, expecially if the reductant concentration in the metal phase is kept low. The Pu-Pa separation is not so easy, but separation factors greater than 10 can probably be achieved by maintaining a very low reductant concentration in the metal phase.

In several experiments, distribution coefficients for the various components were determined as a function of temperature under conditions where the metal phase was saturated

Table 9.11

Equilibrium Distribution of Uranium, Protactinium, Plutonium, Thorium, and Zirconium Between $LiF-BeF_2-ThF_4$ Salts and Bismuth Solutions

Salt Composition (Mole %) LiF	BeF_2	ThF_4	"Free Fluoride" Equivalence	Temperature (C)	Equilibrium Expression	Pa-Th Separation Factor D_{Pa}/D_{Th}
69.2	19.4	11.4	-4	600	$\log D_{Th} = 4 \log C_{Li} + 2.077$	2,100
					$\log D_{Pa} = 4 \log C_{Li} + 5.398$	
					$\log D_{U} = 3 \log C_{Li} + 5.817$	
					$\log D_{Pu} = 3 \log C_{Li} + 4.796$	
66.0	34.0	0	0	600	$\log D_{Th} = 4 \log C_{Li} + 2.453$	3,700
					$\log D_{Pa} = 4 \log C_{Li} + 6.026$	
					$\log D_{U} = 3 \log C_{Li} + 5.971$	
72.0	16.0	12.0	4	600	$\log D_{Th} = 4 \log C_{Li} + 1.653$	3,000
					$\log D_{Pa} = 4 \log C_{Li} + 5.144$	
					$\log D_{U} = 3 \log C_{Li} + 5.484$	
					$\log D_{Pu} = 3 \text{ Log} C_{Li} + 4.518$	
					$\log D_{Zf} = 4 \log C_{Li} + 7.254$	
75.0	13.0	12.0	13	600	$\log D_{Th} = 4 \log C_{Li} + 1.152$	4,400
					$\log D_{Pa} = 4 \log C_{Li} + 4.798$	
					$\log D_{U} = 3 \log C_{Li} + 5.231$	
73.0	0	27.0	-8	650	$\log D_{Th} = 4 \log C_{Li} + 0.849$	2,360
					$\log D_{Pa} = 4 \log C_{Li} + 4.222$	
					$\log D_{U} = 3 \log C_{Li} + 4.655 \ (D_U > 1)$	

9.2.10 Extraction of Uranium, Protactinium, Zirconium, and Plutonium from Fuel Salts (Cont'd)

with thorium. The effect of temperature on the metal-thorium separation factors obtained with $LiF-BeF_2-ThF_4$ (72-16-12 mole percent) is shown in Figure 9.17. As seen, these separation factors increase regularly with decreasing temperature.

9.2.11 Extraction of Rare Earths Europium, Lanthanum, Neodymium, and Samarium from Fuel Salts[7/]

Distribution coefficients for thorium and several rare earths were measured at 600 to 700 C using a variety of $LiF-BeF_2-ThF_4$ solutions in which the ThF_4 concentration was about 12 mole percent. The highest distribution coefficients for the respective components in the system are attained when the metal phase is saturated with thorium. This condition provides a convenient reference point for the correlation of the data. Distribution coefficients obtained when the metal phase is saturated with thorium are designated at D^{max}, and the rare-earth-thorium separation factors (D_{RE}/D_{Th}) determined at D_{Th}^{max} are denoted by α^*. The data obtained are given in Table 9.12. As illustrated in Figure 9.18 the data correlate well with the caluclated "free fluoride" equivalence of the salt.

The rare-earth-thorium separation factors generally were in the range of 1 to 3.5 over the range of conditions investigated. Increasing the temperature from 600 to 700 C usually produced a small decrease in the separation factor; this is consistent with the earlier observation that temperature had very little effect on α^*.

It is interesting to note that the average values of D_{Th}^{max} obtained at 600 and 700 C correspond to thorium concentrations in the bismuth of about 1850 and 5600 wt ppm, respectively. These values are in excellent agreement with those obtained by direct measurement of the solubility of thorium in bismuth.

Table 9.12

Distribution of Thorium, Rare Earths, and Lithium Between $LiF-BeF_2-ThF_4$ Salts and Thorium-Saturated Bismuth Solutions at 600 and 700 C

Salt Composition (Mole %) LiF	BeF_2	ThF_4	"Free Fluoride" Equivalence	Temperature (C)	Rare Earth	D^{max} Li	Th	Rare Earth	α*
						x 10^{-3}	x 10^{-2}	x 10^{-2}	
69.2	19.4	11.4	-4	600	Eu^{2+}	1.45	1.35	1.3	0.96
					Eu^{2+}	1.59	1.30	1.5	1.2
					La^{3+}	1.61	1.51	2.0	1.3
					La^{3+}	1.49	1.44	2.1	1.5
					Nd^{3+}	1.65	1.53	4.2	2.7
					Nd^{3+}	1.62	1.49	3.8	2.5
				700	La^{3+}	4.60	4.0	6.0	1.5
					Nd^{3+}	4.23	4.94	13.9	2.8
72.0	16.0	12.0	+4	600	La^{3+}	1.88	1.45	2.3	1.6
					Sm(a)	1.88	1.54	3.2	2.1
					Nd^{3+}	2.16	1.40	4.2	3.0
				700	Sm(a)	5.02	4.55	9.7	2.1
					Nd^{3+}	5.29	4.41	8.6	1.9
75.0	13.0	12.0	+13	600	Eu^{2+}	2.28	1.49	2.8	1.9
					Eu^{2+}	2.33	1.50	2.6	1.7
					La^{3+}	2.43	1.40	3.5	2.5
					La^{3+}	2.40	1.36	3.3	2.4
					Nd^{3+}	2.40	1.50	5.6	3.7
				700	Eu^{2+}	6.19	3.92	6.7	1.7
					La^{3+}	6.48	4.35	7.6	1.8
					Nd^{3+}	6.95	4.11	14.0	3.4

(a) The average valence of Sm in this experiment was 2.7, indicating that both Sm^{2+} and Sm^{3+} were present in the salt.

9.2.11 Extraction of Rare Earths Europium, Lanthanum, Neodymium, and Samarium from Fuel Salts (Cont'd)

Although the rare-earth-thorium separation factors increased slightly with increasing "free fluoride" equivalence of the salt, no significant enhancement of the separation factors over those obtained with the reference carrier salt, $LiF-BeF_2-ThF_4$ (72-16-12 mole percent) appears to be possible by changing the salt composition.

9.2.12 Reductive Extraction of Transuranium Elements Neptunium, Plutonium, Americium, Curium, and Californium from Fuel Salts[20/]

Data for several transuranium elements were obtained with $LiF-BeF_2-ThF_4$ (72-16-12 mole percent) at 600 C. The distribution coefficients obtained for neptunium are shown in Figure 9.19, and those for plutonium, americium, curium, and californium are shown in Figure 9.20. The distribution coefficients can be reproduced from the equations given in Table 9.13. Within experimental error, each species was trivalent in the salt phase. The data obtained for neptunium show that its extractability is between that of uranium and plutonium. The uranium-neptunium and neptunium-plutonium separation factors are each about 3. As seen in Figure 9.20, plutonium, americium, and californium are nearly inseparable, whereas the plutonium- curium separation factor is about 10. These results indicate that curium would probably coextract with protactinium in the process.

9.2.13 Rare-Earth Separation of Promethium, Europium, Lanthanum, Samarium, and Thorium from Fuel Salts[21/]

Distribution coefficients for thorium and several rare earths were measured with $LiF-BeF_2-ThF_4$ (72-16-12 mole percent). Additional measurements include those for promethium and europium.

The average promethium distribution coefficient from the

20/ ORNL-4449, p. 215, August 31, 1969.

21/ ORNL-4449, p. 217, August 31, 1969.

Table 9.13

Expressions for the Distribution Coefficients for Several Transuranium Elements Using $LiF-BeF_2-ThF_4$ (72-16-12 Mole %) and Liquid Bismuth at 600 C

Element	Equilibrium Expression
Np	$\log D_{Np} = 3 \log D_{Li} + 10.514$
Pu	$\log D_{Pu} = 3 \log D_{Li} + 9.979$
Am	$\log D_{Am} = 3 \log D_{Li} + 9.865$
Cm	$\log D_{Cm} = 3 \log D_{Li} + 9.090$
Cf	$\log D_{Cf} = 3 \log D_{Li} + 9.952$

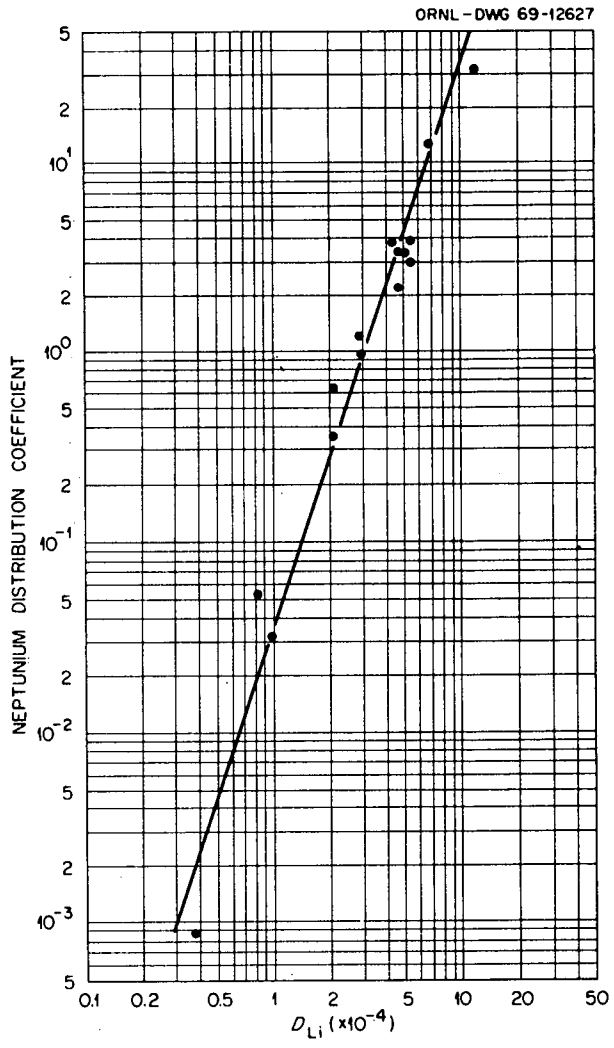

Fig. 9.19 Equilibrium Distribution of Neptunium Between LiF-BeF_2-ThF_4 (72-16-12 Mole %) and Bismuth Solutions at 600 C.

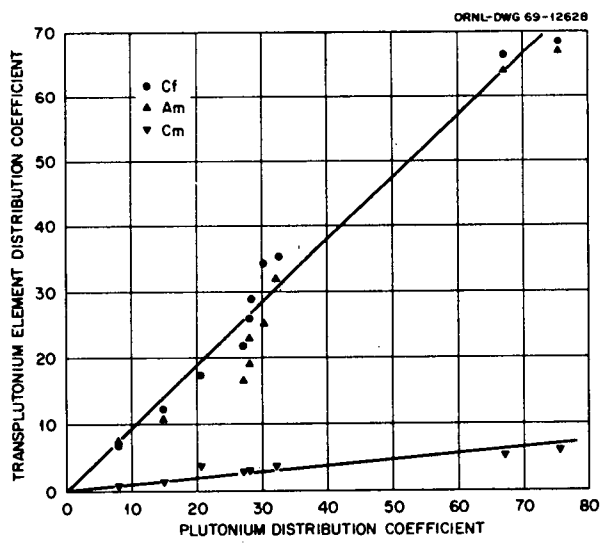

Fig. 9.20 Distribution Coefficients for Transuranium Elements Obtained at 600 C with LiF-BeF_2-ThF_4 (72-16-12 Mole %) and Bismuth.

ORNL-4449
p 217

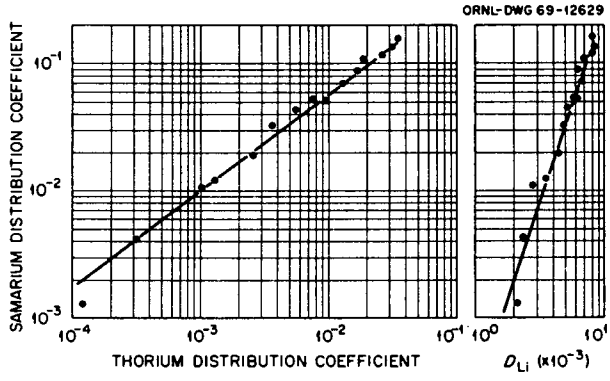

Fig. 9.21 Equilibrium Distribution of Thorium and Samarium Between LiF-BeF_2-ThF_4 (80.5-6.1-13.4 Mole %) and Bismuth Solutions at 700 C.

ORNL-4548
p 178

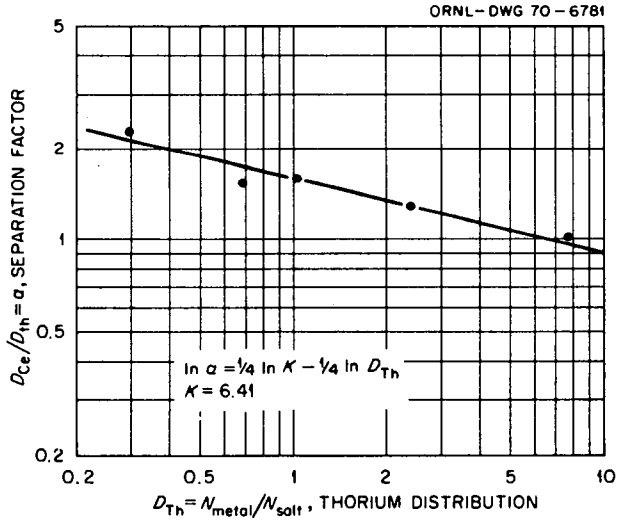

Fig. 9.22 Effect of Thorium Distribution on the Separation of Cerium from Thorium During Reductive Extraction from LiF-BeF_2 (66-34 Mole %) into Bismuth at 600 C.

9.2.13 Rare-Earth Separation of Promethium, Europium, Lanthanum, Samarium, and Thorium from Fuel Salts (Cont'd)

four pairs of samples was 0.025 ± 0.003, yielding a promethium-thorium separation factor of 1.7 ± 0.3.

The distribution coefficients obtained for europium at 600 C using $LiF-BeF_2-ThF_4$ (72-16-12 mole percent) can be expressed as $\log D_{Eu} = 2 \log D_{Li} + 3.74$. These results, along with those obtained for thorium, showed that the europium-thorium separation factor was about 1.1 at 600 C when the bismuth phase was saturated with thorium. At thorium saturation of the bismuth phase, the separation factor decreased from about 1.6 to about 0.9 as the temperature was increased from 525 to 750 C.

The effect of temperature on the lanthanum-thorium and samarium-thorium separation factors was determined in separate experiments with $LiF-BeF_2-ThF_4$ (72-16-12 mole percent). In each experiment, about four pairs of samples were taken at each of several temperatures between 525 and 750 C; the bismuth phase was saturated with thorium in each case. Average values for the respective distribution coefficients and separation factors are given in Table 9.14. The samarium-thorium separation factor was about 2 regardless of the temperature, whereas the lanthanum-thorium separation factor decreased from about 2 to 1.5 as the temperature was increased from 525 to 750 C. Despite the scatter in the data, these results (and those for europium given above) clearly show that temperature has no marked effect on the rare-earth-thorium separation factors.

The extractability of samarium and thorium from such a salt, $LiF-BeF_2-ThF_4$ (80.5-6.1-13.4 mole percent), which has a "free fluoride" equivalence of +28, was determined at 700 C. The distribution coefficients obtained in this experiment are shown in Figure 9.21. The slope of the line representing the plot of $\log D_{Li}$ vs $\log D_{Sm}$ is 3, whereas that for the plot of $\log D_{Sm}$ vs $\log D_{Th}$ is 3/4.

Table 9.14

Effect of Temperature on Rare-Earth-Thorium Separation Factors Obtained with $LiF-BeF_2-ThF_4$ (72-16-12 Mole %)

Temperature (C)	Rare Earth	Thorium Concentration in Bismuth ppm	D_{RE}	D_{Th}	Separation Factor
525	La	843	0.0125	0.00633	1.97
	Sm	785	0.0115	0.00589	1.95
560	La	1,290	0.0206	0.00968	2.13
	Sm	1,210	0.0189	0.00908	2.08
600	La	2,082	0.0251	0.0156	1.60
	Sm	2,080	0.033	0.0156	2.11
650	La	3,830	0.0448	0.0287	1.56
	Sm	3,788	0.0562	0.0284	1.98
700	Sm	6,022	0.0962	0.0452	2.13
750	La	10,230	0.113	0.0768	1.47
	Sm	8,772	0.113	0.0658	1.72

9.2.13 Rare-Earth Separation of Promethium, Europium, Lanthanum, Samarium, and Thorium from Fuel Salts (Cont'd)

These results show that the samarium species in the salt phase was primarily trivalent. When the bismuth phase was saturated with thorium ($D_{Th} \sim 0.035$), the samarium distributution coefficient was about 0.14, corresponding to a separation factor of 4. This separation factor is only about twice as high as that obtained at 700 C with $LiF-BeF_2-ThF_4$ (72-16-12 mole percent).

9.2.14 Extraction of Cerium and Thorium from Fuel Salt Mixtures[22/]

The extraction of cerium at low and varying thorium concentrations in the salt phase has been studied. The purpose of this experiment was to provide data relating to the thermodynamic activity of ThF_4 in the salt phase.

The distributions at equilibrium of cerium and thorium between the two liquid phases are related to the similar distribution of lithium by the equations

$$CeF_3 + 3Li^o_{Bi} \rightleftharpoons Ce^o_{Bi} + 3LiF \qquad (20)$$

and

$$ThF_4 + 4Li^o_{Bi} \rightleftharpoons Th^o_{Bi} + 4LiF. \qquad (21)$$

The value for the equilibrium quotient for the reduction of cerium by lithium (eq. 20) was 3.26×10^9. The corresponding value for the reduction of thorium by lithium (Eq. 21) was 2.59×10^{12}. The separation of cerium from thorium ($\alpha = D_{Ce}/D_{Th}$) was evaluated by the equation

$$\ln \alpha = 1/4 \ln K - 1/4 \ln D_{Th}, \qquad (22)$$

as shown in Figure 9.22. The equilibrium quotient for the reduction of cerium by thorium was 6.41

22/ORNL-4548, p. 178, February 28, 1970.

9.2.15 Extraction of Barium and Thorium from Fuel Salts[23,24]

Recently, distribution coefficients were determined for barium at 600 to 690 C using $LiF-BeF_2-ThF_4$ (72-16-12 mole percent) as the salt phase and at 600 and 640 C using $LiF-BeF_2$ (66-34 mole percent) as the salt phase. The data at each temperature could be expressed as

$$\log D_{Ba} = 2 \log X_{Li} + \log K^*. \qquad (23)$$

The values obtained for log K* are given in Table 9.15. The distribution coefficients measured for barium are very nearly the same as those obtained for europium; thus the behavior of these two elements in the reductive extraction process will be nearly identical.

9.2.16 Thorium, Lithium Distribution from Fuel Salts in the Presence of Nickel[25]

The thorium and nickel solubility data are plotted in Figure 9.23, together with the derived line (with theoretical slope): $X_{Th} \times X_{Ni} = 2.3 \times 10^{-6}$, where X is the mole fraction in bismuth. If permissiveness on the scatter of data is granted, there is a reasonable fit to the theoretical slope. The solubility product constant obtained is a factor of four greater than that reported[26] for 600 C (6.2×10^{-7}) and is consistent with expectations for the higher temperature.

The thorium and lithium data for the same samples are plotted in Figure 9.24, together with the derived line (with theoretical slope):

$$\frac{X_{Th}}{X_{Li}^4} = 4.7 \times 10^7$$

23/ ORNL-4548, February 28, 1970.

24/ ORNL, February 1970 Monthly Report.

25/ ORNL, September 1970 Monthly Report.

26/ ORNL-4396, p. 287, February 28, 1969.

Table 9.15

Distribution Data for Barium

Salt	Temp. (C)	Log K^*_{Ba}
$LiF-BeF_2$ (66-34)	600	4.021
$LiF-BeF_2-ThF_4$ (72-16-12)	600	4.049
$LiF-BeF_2$ (66-34)	640	3.728
$LiF-BeF_2-ThF_4$ (72-16-12)	645	3.678
$LiF-BeF_2-ThF_4$ (72-16-12)	690	3.530

9.2.16 Thorium, Lithium Distribution from Fuel Salts in the Presence of Nickel (Cont'd)

where X is the mole fraction in bismuth. The corresponding log 10 distribution equation for this fluoride salt is

$$\log D_{Th} = 4 \log D_{Li} + 8.022.$$

The thorium and lithium distributions for this fluoride salt have been previously reported[27/] for 600 and 700 C. Simple interpolation of this earlier data was made using the derived equation:

$$\log (D_{Th}/(D_{Li})^4) = 8987 \ (1/T^oK) - 1.4844.$$

The resulting estimated $\log_{10}$ distribution equation for 650 C is

$$\log D_{Th} = 4 \log D_{Li} + 8.251$$

Considering the scatter of the present data and the inaccuracy of simple interpolation of log K, there is remarkably close agreement of these distributions at 650 C. Within the limitations mentioned, the present data show that the distribution of soluble thorium is unaffected by the presence of $ThNiBi_x$ in the bismuth phase.

9.2.17 Extraction of Sodium from Fuel Salts[28/]

Current design for an MSBR utilizes sodium fluoroborate for the intermediate heat transfer fluid. Any leakage into the primary fuel system would contaminate the fuel with NaF and BF_3. The boron trifluoride would probably be removed by gas stripping, but the sodium fluoride would remain in the fuel mixture. This experiment was performed to evaluate the effect of sodium on the reductive extraction fuel reprocessing system and to measure its distribution between fluoride salt and bismuth.

27/ ORNL-4396, p. 284, February 28, 1969.

28/ ORNL monthly report, April, 1970.

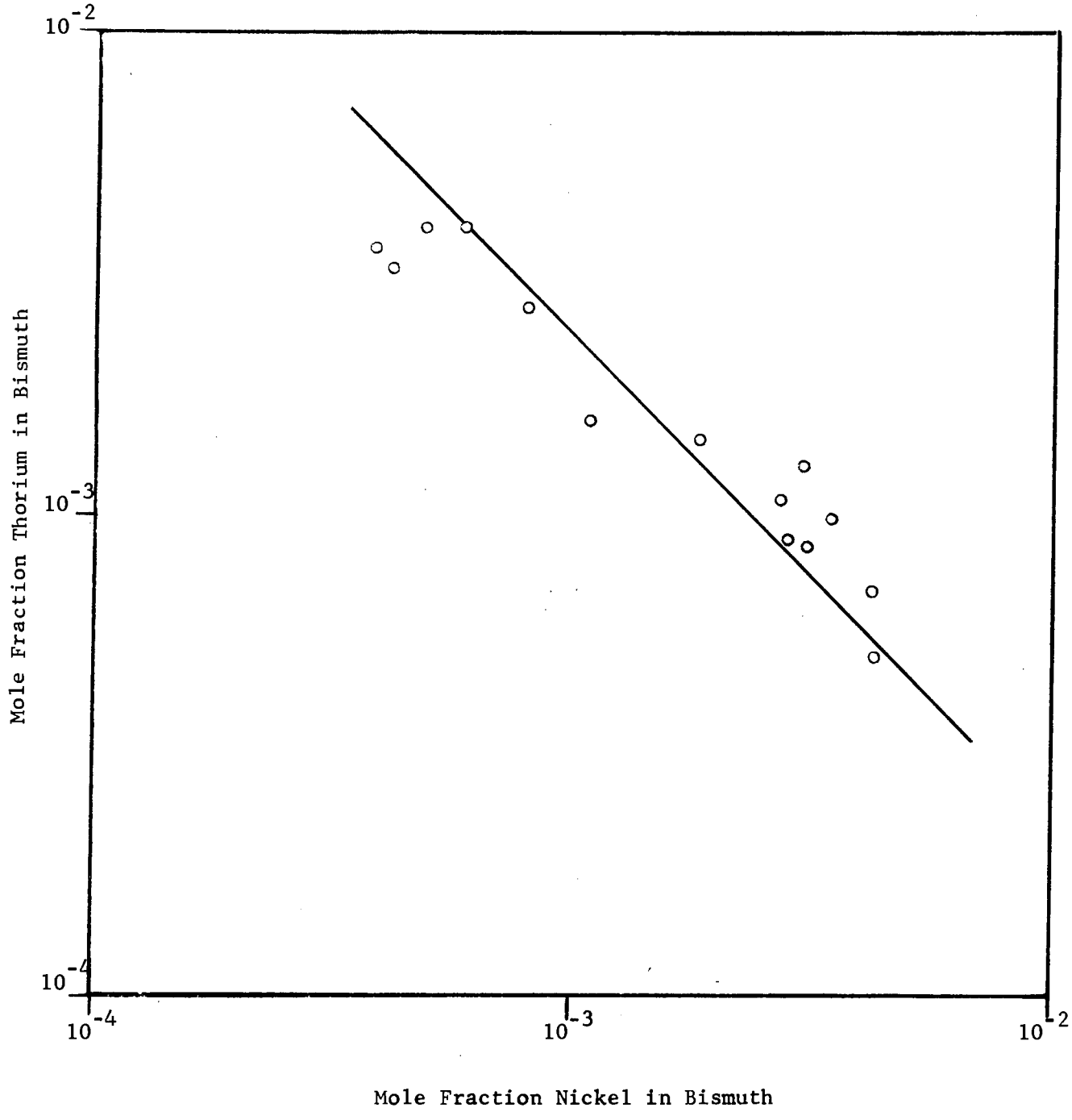

Fig. 9.23 $LiF-BeF_2-ThF_4$ (72-16-12 mole %) and Bismuth at 650°C, Five Experiments at Nickel and Thorium Saturation

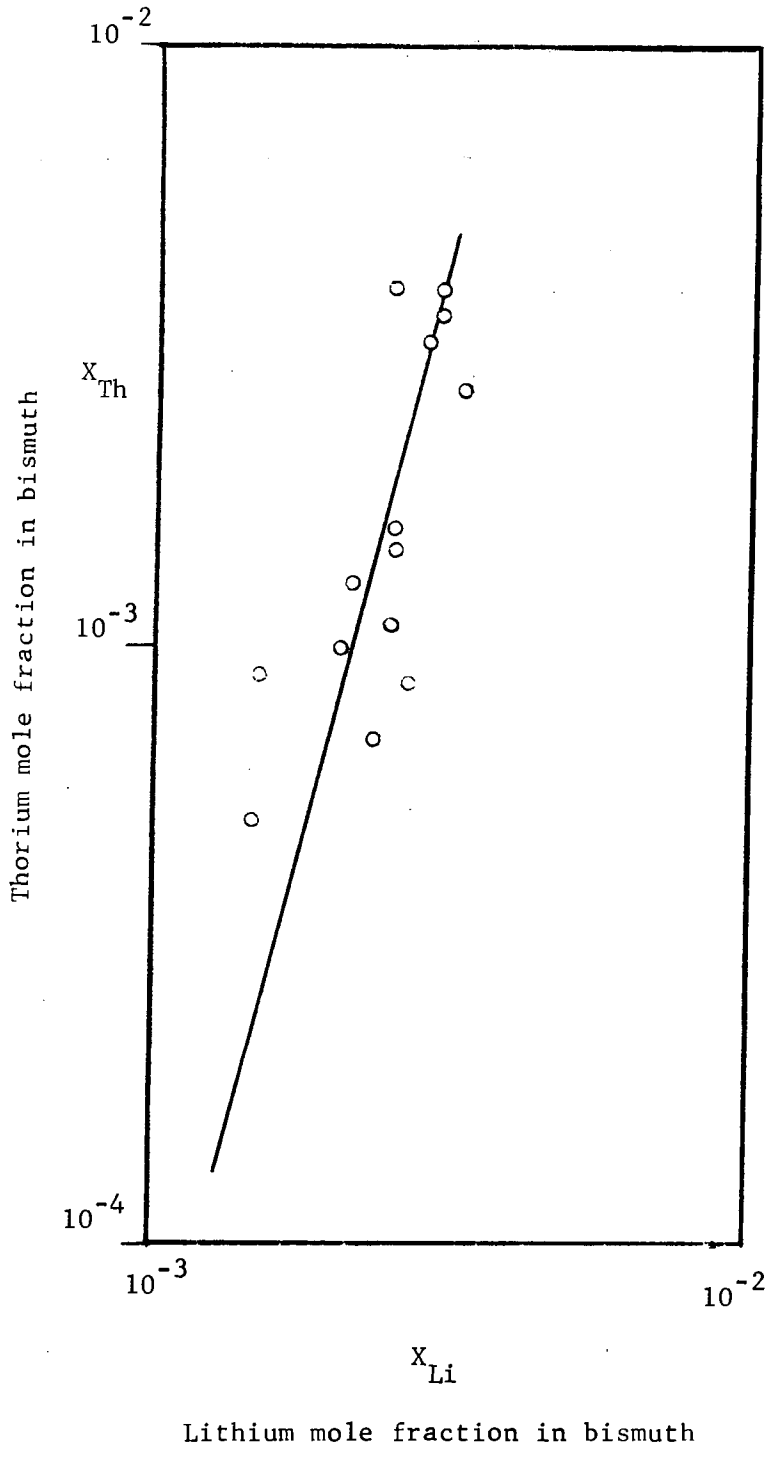

Fig. 9.24 $LiF-BeF_2-ThF_4$ (72-16-12 mole %) and Bismuth at 650°C, Five Experiments at Nickel and Thorium Saturation

9.2.17 Extraction of Sodium from Fuel Salts (Cont'd)

The distribution coefficients obtained for sodium were:

$$\log D_{Na} = \log X_{Li} + 1.186$$

The separation factor obtained for sodium was:

$$D_{Na}/D_{Li} = 10.9.$$

9.2.18 Extraction of Strontium from Fuel Salts[28/]

The distribution of the alkaline earth fission product strontium in the reductive extraction process was investigated.

The distribution coefficients obtained for strontium were:

$$\text{Log } D_{Sr} = 2 \log X_{Li} + 2.093$$

The separation factor obtained for strontium was:

$$D_{Sr}/D_{Li} = 0.296.$$

The equilibrium quotient obtained was:

$$K_Q = D_{Sr}/(D_{Li})^2 = 65.$$

9.2.19 Extraction of Rubidium from Fuel Salts[25/]

The fluoride salt consisted of $LiF\text{-}BeF_2\text{-}ThF_4$ (72-16-12 mole percent) to which RbCl (labeled with several millicuries of Rb-86) was added to make 1.476×10^{-2} mole percent. The salt was treated in a nickel preparation vessel at 650 C according to standard hydrofluorination procedures, followed by hydrogen sparging, and 3058 grams were transferred at 650 C to the extraction vessel under flowing argon.

The rubidium distributions obtained are plotted in Figure 9.25, together with the derived line (with theoretical slope):

$$\log D_{Rb} = \log X_{Li} + 1.077$$

The equilibrium quotient was $(D_{Rb}/D_{Li}) = 8.623$.

9.2.20 Extraction of Cesium from Fuel Salts[29/]

The fluoride salt consisted of $LiF-BeF_2-ThF_4$ (72-16-12 mole percent) to which CsF (labeled with several millicuries of Cs-137) was added to make 0.95×10^{-2} mole percent. The salt was treated in a nickel preparation vessel at 650 C according to standard hydrofluorination procedures, followed by hydrogen sparging.

The equilibrium quotient obtained in this experiment was

$$(D_{Cs}/D_{Li}) = 15.05 \pm 0.81,$$

the mean of 15 samples at the 0.95 conf. level. This quotient is 25 percent greater than that for sodium and is 90 percent greater than that for potassium in the fluoride/bismuth equilibrium extractions. The distribution equation for this composition of salt was

$$\log D_{Cs} = \log X_{Li} + 1.320$$

9.3 Metal Transfer Process

When solutions of lithium in bismuth are used to remove rare-earth fission products from an MSBR fuel salt, thorium will be extracted in about the same proportion. However, the rare earths can then be oxidized from the bismuth into a chloride without disturbing the thorium. The separation is possible because of the relative instability of thorium chloride.

9.3.1 Distribution of Cerium, Strontium, and Europium[30/]

The behavior of cerium, europium, and strontium in the bismuth-lithium chloride system was examined. The cerium-lithium ratios are shown in Figure 9.26. Excluding the values indicated by open circles, for which the lithium numbers are out of line

---

29/ ORNL monthly report, December, 1970-June, 1971.

30/ ORNL-4548, p. 171, February 28, 1970.

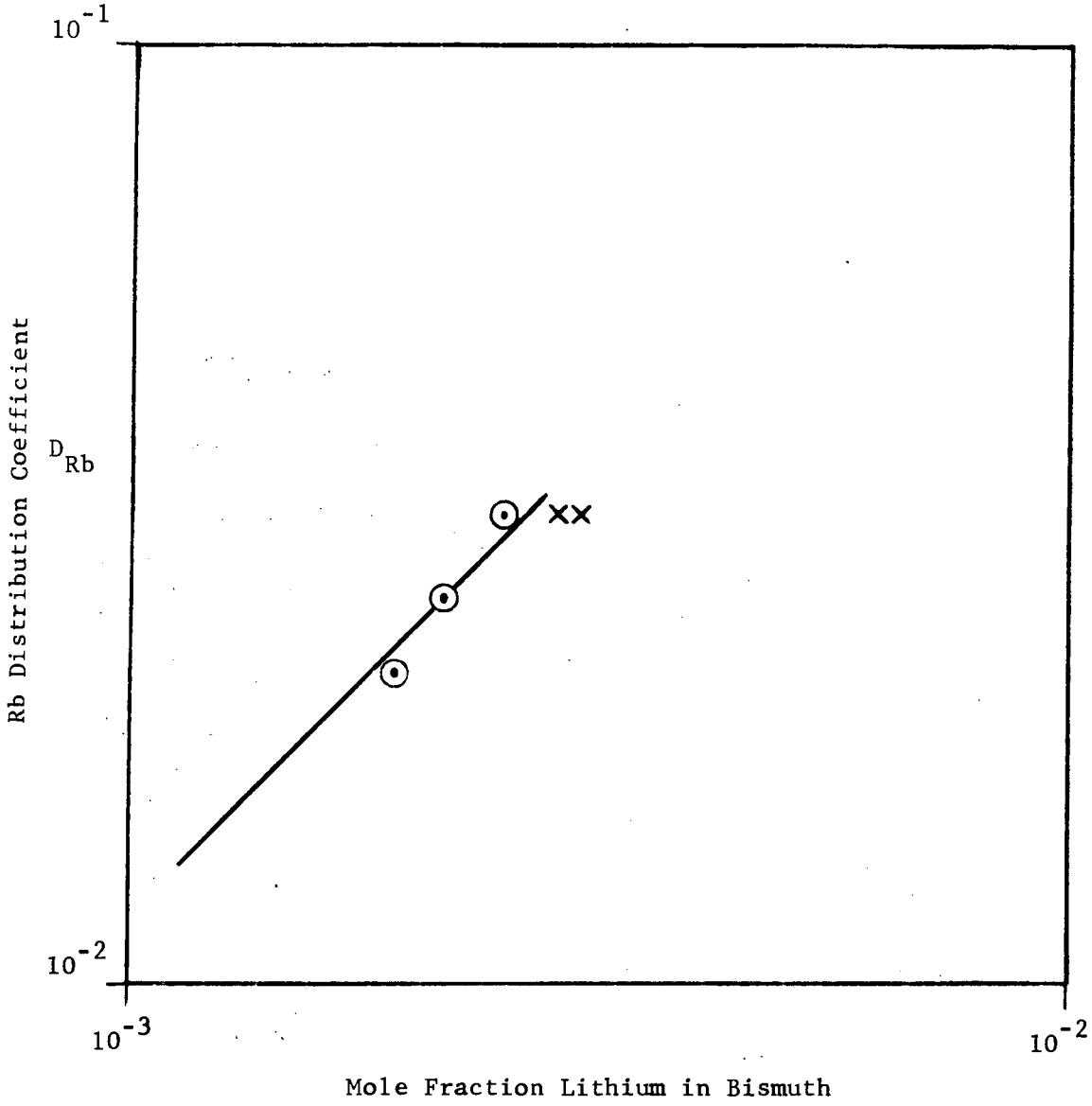

Fig. 9.25. Distribution of Rubidium Between $LiF-BeF_2-ThF_4$ (72-16-12 mole %) and Bismuth, 650°C

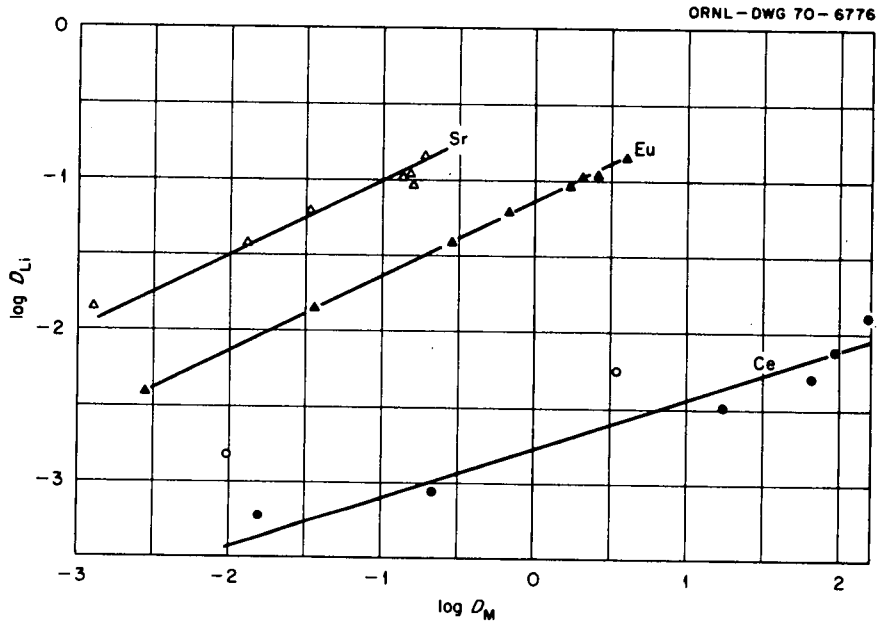

Fig. 9.26. The Distribution of Ce, Eu, and Sr Between LiCl and Bi at 650°C as a Function of D_2.

9.3.1 Distribution of Cerium, Strontium, and Europium (Cont'd)

$$\log (D_{Ce}/D_{Li}^3) = 8.312 \pm 0.384$$

The thorium distributions could not be found accurately because the salt concentration was too low. Strontium and europium distributions are also shown in Figure 9.26. Again the thorium values were unusable. The distribution coefficients (D_M/D_{Li}^2) are given by

$$\log K_{Eu} = 2.284 \pm 0.025$$

and

$$\log K_{Sr} = 1.024 \pm 0.141$$

From these experiments, it is obvious that all three of these fission products will distribute strongly into lithium chloride, leaving the thorium behind.

9.3.2 Extraction of Cesium from LiCl into Bismuth[31/]

Experimental determination of the distribution of cesium and lithium between bismuth and lithium chloride when lithium metal is added for reductive extraction was made. Knowledge of the behavior of fission product cesium in this stage of the metal transfer process is important not only to confirm that cesium is easily extracted from bismuth into lithium chloride, but also to determine the concentration of lithium which would be required for the back extraction of bismuth in the final contactor.

The distribution coefficients obtained for cesium were:

$$\log D_{Cs} = \log X_{Li} - 1.503$$

The data are plotted in Figure 9.27 and are shown with the derived theoretical line with slope of 1. The point at 0.0054 mole fraction lithium was not used in positioning the line since the counting rate of that bismuth sample

31/ ORNL-4548, February 28, 1970.

9.3.2 Extraction of Cesium from LiCl into Bismuth (Cont'd)

was only 21 counts min^{-1} g^{-1}. For comparison, contamination with 100 μg of salt would elevate the counting rate by 50 counts/min. In several cases one of the pellets of a sample pair exhibited a higher counting rate by about 50 counts/min and was not included in the results shown. The equilibrium quotient obtained was:

$$D_{Cs}/D_{Li} = 0.031$$

9.3.3 Distribution Data for Uranium, Protactinium, Thorium and Various Rare Earths in Metal Transfer Systems[32/]

Some of the distribution coefficient data obtained in these studies are shown in Figures 9.28 and 9.29. Data obtained for uranium, neodymium, and europium when LiCl was used as the salt phase are presented (Figure 9.28) as plots of log D vs log X_{Li}. The slopes of the lines indicate that n is 3, 3, and 2 for uranium, neodymium, and europium, respectively. Plots of log D_{Pa} vs log D_{Th} and of log D_U vs log D_{Th} using data obtained with LiCl at 640 C are shown in Figure 9.29. Since uranium was trivalent, the slopes of the respective lines show that both thorium and protactinium were tetravalent in the salt under the experimental conditions employed. Valued of log K* obtained thus far using a variety of salts are compiles in Table 9.16. These results show that, from a chemical viewpoint, LiCl and LiBr will be equally good as acceptor salts and that the distribution behavior of most of the elements will be rather insensitive to temperature changes.

Inspection of the data in Table 9.16 reveals that the presence of fluoride in either LiCl or LiBr causes a change in distribution behavior, particularly that of thorium. This is illustrated by the data obtained for thorium and lanthanum in LiCl-LiF and LiBr-LiF solutions at 640 and 600 C, respectively (Figure 9.30). These data indicate that the thorium-lanthanum separation factor will be decreased if the acceptor salt

32/ ORNL-4548, p. 290, February 28, 1970

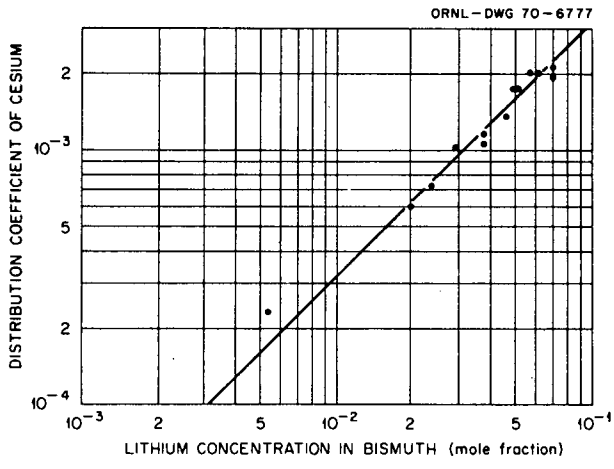

Fig. 9.27. Distribution Coefficients of Cesium in LiCl and Bismuth Solutions at 650°C.

ORNL DWG 70-4501

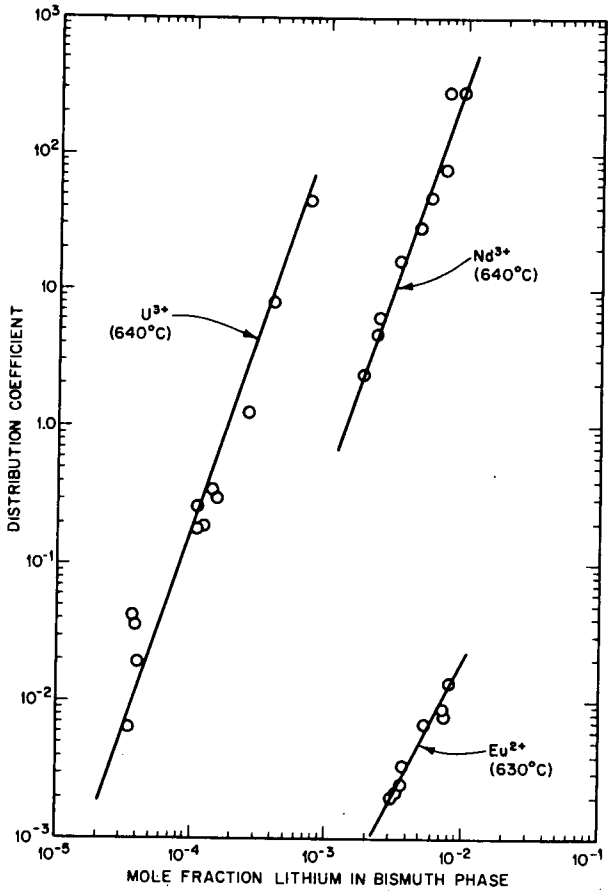

Fig. 9.28 Equilibrium Distribution of Uranium, Neodymium, and Europium Between Molten LiCl and Liquid Bismuth Solutions.

ORNL DWG 70-4502

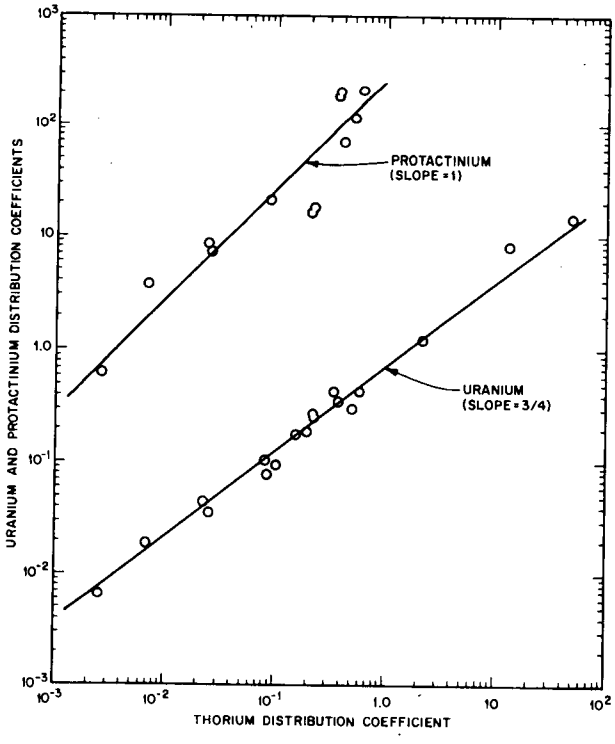

Fig. 9.29 Distribution Coefficients for Thorium, Uranium, and Protactinium Obtained with Molten LiCl and Liquid Bismuth Solutions at 640 C.

ORNL DWG 70-4503

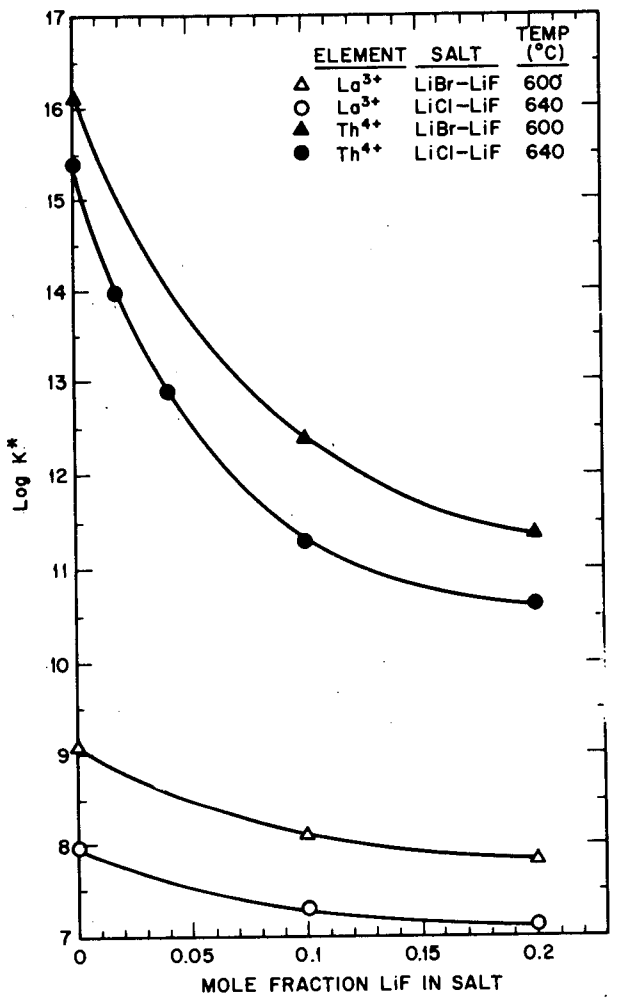

Fig. 9.30. Values of log λ* Obtained for Lanthanum and Thorium Using LiBr-LiF and LiCl-LiF as the Salt Phase.

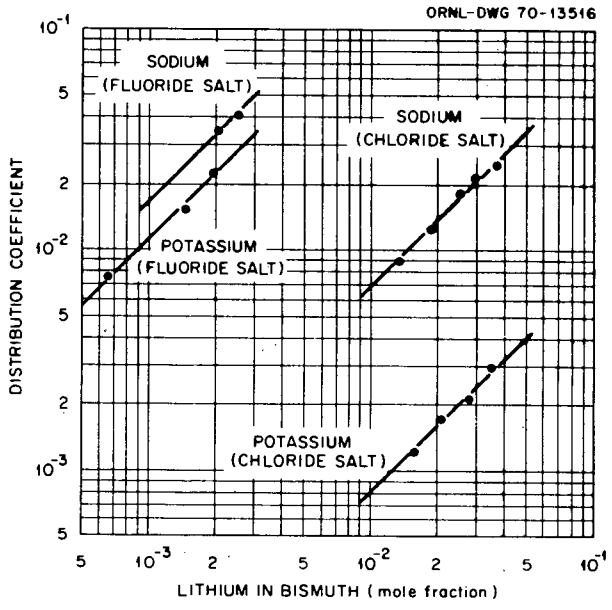

Fig. 9.31. Reductive Extraction into Bismuth, 650°C.

Table 9.16

Values of Log K*Derived from Distribution Coefficient Data

$$\text{Log } D = n \text{ Log } X_{Li} + \text{Log } K^*$$

Temperature (C)	Salt	Element	Log K*
630	LiCl	Eu^{2+}	2.301
640	LiCl	Ba^{2+}	1.702
		La^{3+}	7.973
		Nd^{3+}	8.633
		Sm^{2+}	2.886
		Th^{4+}	15.358
		Pa^{4+}	17.838
		U^{3+}	11.278
640	LiCl-LiF (98.1-1.9 Mole %)	Th^{4+}	13.974
640	LiCl-LiF (96-4 Mole %)	Th^{4}	12.90
		Pa^{4+}	14.7
		U^{3+}	10.80
640	LiCl-LiF (90-10 Mole %)	La^{3+}	7.288
		Th^{4+}	11.309
600	LiCl-LiF (80-20 Mole %)	La^{3+}	7.235
		Nd^{3+}	7.644
		Th^{4+}	10.964
640	LiCl-LiF (80-20 Mole %)	La^{3+}	7.124
		Th^{4+}	10.629
700	LiCl-LiF (80-20 Mole %)	Nd^{3+}	6.732
		Th^{4+}	9.602
575	LiBr	Ba^{2+}	1.497
600	LiBr	Ba^{2+}	1.443
		La^{3+}	9.079
		Nd^{3+}	8.919
		Th^{4+}	16.16
640	LiBr	La^{3+}	8.266
		Nd^{3+}	8.834
650	LiBr	Ba^{2+}	1.358
700	LiBr	Ba^{2+}	1.316
		Nd^{3+}	8.430
600	LiBr-LiF (90-10 Mole %)	La^{3+}	8.158
		Th^{4+}	12.380
600	LiBr-LiF (80-20 Mole %)	La^{3+}	7.840
		Th^{4+}	11.373

9.3.3 Distribution Data for Uranium, Protactinium, Thorium, and Various Rare Earths in Metal Transfer Systems (Cont'd)

becomes contaminated with fluoride fuel salt.

9.3.4 Distribution of Sodium and Potassium in Metal Transfer Salts[33/]

The distributions of sodium and potassium for both the fluoride/bismuth and chloride/bismuth extractions have been measured at 650 C.

The results obtained are shown in Figure 9.31 together with the derived theoretical lines. In the fluoride/bismuth experiments

$$\log D_{Na} = \log X_{Li} + 1.225 \text{ and}$$

$$\log D_K = \log X_{Li} + 1.045, \ \log (D_{Na}/D_{Li}) = 1.080,$$

$$\text{and } \log (D_K/D_{Li}) = 0.899.$$

The separation factors, D_M/D_{Li}, for sodium and potassium from 72-16-12 fluoride were 30 percent to 70 percent smaller than the separation factors for trivalent rare earths. In the chloride/bismuth experiments

$$\log D_{Na} = \log X_{Li} - 0.164 \text{ and}$$

$$\log D_K = \log X_{Li} - 1.099; \ \log (D_{Na}/D_{Li}) = -0.168,$$

$$\text{and } \log (D_K/D_{Li}) = -1.104.$$

9.3.5 Measurement of Distribution Coefficients in Molten Salt-Metal Systems[34/]

Most of the values of n and $\log K_M^*$ obtained using various salt phases are given in Table 9.17. The original data, as plots of $\log D_M$ vs $\log N_{Li}$, obtained at 700 C for plutonium, curium, and californium with LiCl as the salt

33/ ORNL-4622, p. 107, August 31, 1970.

34/ ORNL-4682, p. 10, March 31, 1971.

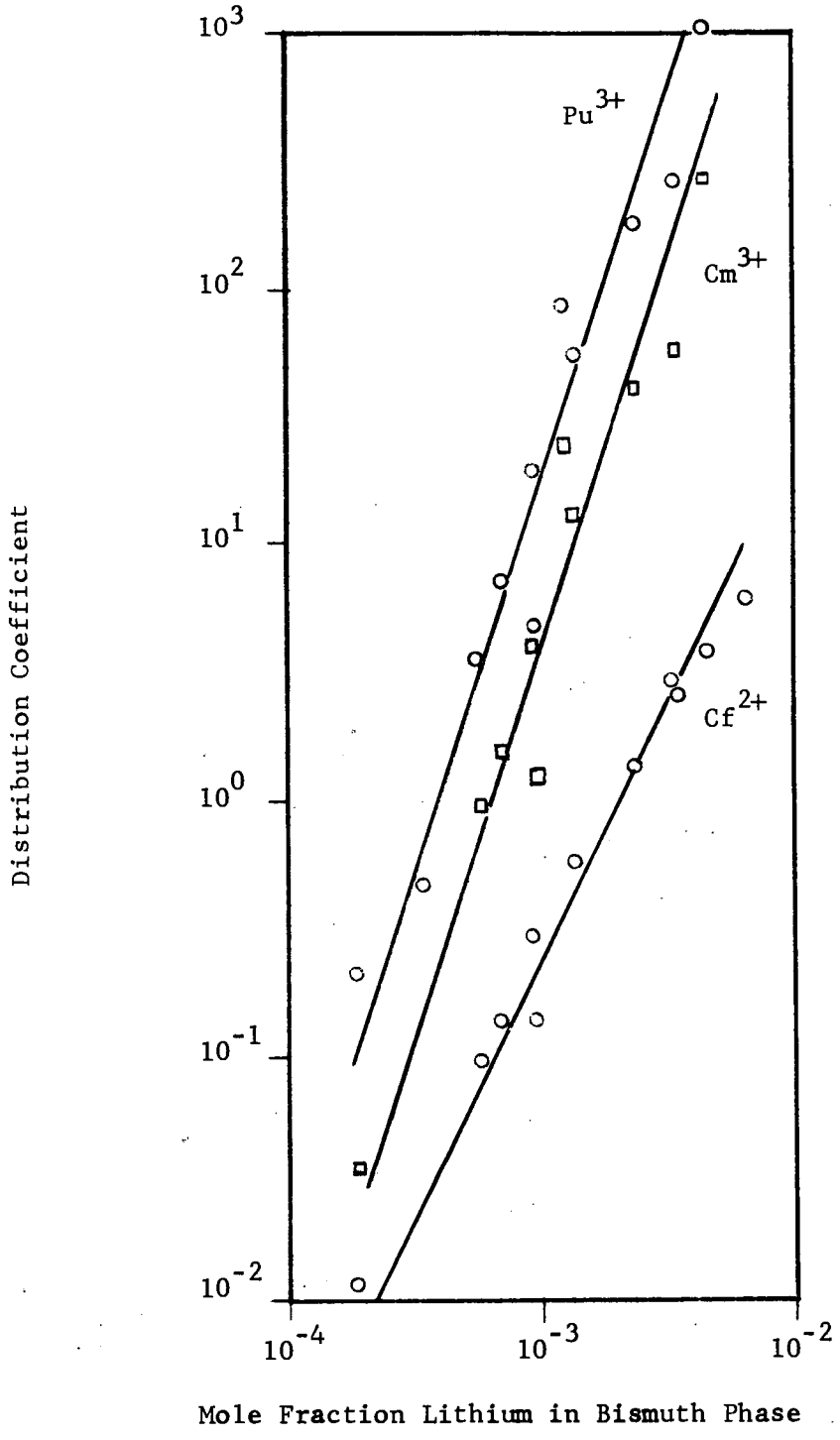

Fig. 9.32 Equilibrium Distribution of Plutonium, Curium, and Californium Between Molten LiCl and Liquid Bismuth Solutions at 700°C

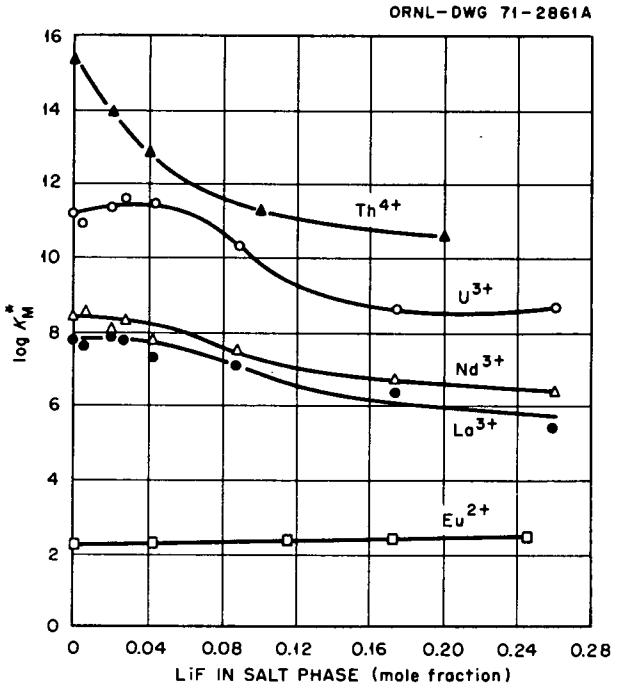

Fig. 9.33. Variation of log K_M* with salt composition. Salt phase was an LiCl-LiF solution; data obtained at 640°C except for europium, which was obtained at 650°C.

Table 9.17

Values of n and Log K_M^* Obtained in Measurements of the Equilibrium Distribution of Several Solutes Between Bismuth Solutions and Molten Lithium Halide Salts

Element	Composition of Salt Phase (Mole %) LiCl	LiF	LiBr	Temperature (C)	n	Log K_M^*
La	100	0	0	640	3	7.796 ± 0.4
Nd					3	8.374 ± 0.4
U					3	11.197 ± 0.4
Np					3	10.33 ± 0.1
Pu					3	10.126 ± 0.1
Am					3	10.16 ± 0.2
Cm					3	9.406 ± 0.1
Cf					2	5.38 ± 0.2
Th	0	0	100	640	4	14.8 ± 0.7
Pa					4	15.7 ± 0.8
U					3	10.6 ± 0.5
La	99.5	0.5	0	640	3	7.607 ± 0.4
Nd					3	8.568 ± 0.4
U					3	10.954 ± 0.4
La	98.0	1.99	0	640	3	7.878 ± 0.4
Nd					3	8.064 ± 0.4
U					3	11.329 ± 0.4
La	97.4	2.65	0	640	3	7.789 ± 0.4
Nd					3	8.310 ± 0.4
U					3	11.624 ± 0.4
La	95.7	4.33	0	640	3	7.372 ± 0.4
Nd					3	7.805 ± 0.4
U					3	11.480 ± 0.4
La	91.2	8.82	0	640	3	7.182 ± 0.4
Nd					3	7.521 ± 0.4
U					3	10.340 ± 0.4
La	82.6	17.41	0	640	3	6.458 ± 0.4
Nd					3	6.739 ± 0.4
U					3	8.604 ± 0.4
La	73.9	26.07	0	640	3	5.494 ± 0.4
Nd					3	6.354 ± 0.4
U					3	8.758 ± 0.4
U	100	0	0	675	3	10.11 ± 0.3
La	100	0	0	700	3	7.185 ± 0.1
Nd					3	7.831 ± 0.1
Sm					2	2.756 ± 0.1
Eu					2	2.133 ± 0.1
Th					4	13.772 ± 0.1
Pa					4	15.8 ± 0.4
U					3	10.192 ± 0.1
Np					3	10.369 ± 0.1
Pu					3	10.223 ± 0.1
Cm					3	9.589 ± 0.1
Cf					2	5.43 ± 0.2

9.3.5 Measurement of Distribution Coefficients in Molten Salt-Metal Systems (Cont'd)

phase are shown in Figure 9.32. Generally, the values of n obtained (Table 9.17) were those expected; an exception was californium, which existed primarily in the 2+ oxidation state at 640 C and was almost totally divalent at 700 C (Figure 9.32). These results confirm our earlier evidence for the existence of Cf(II) under the experimental conditions employed.

The data given in Table 9.17 when used in conjunction with previous data, allowed one to determine the temperature dependence of log K_M^* for several elements. With each element for which sufficient data were obtained, the relationship

$$\log K_M^* = A + B/T(^oK)$$

was obeyed. Values of A and B for several elements, obtained with either LiCl of LiBr as the salt phase, are given in Table 9.18. These data confirm earlier indications that the distribution behavior of the di- and trivalent elements is rather insensitive to temperature changes and that the distribution coefficients for a given element at a given temperature are about the same with LiCl and LiBr. On the other hand, the available data indicate that the values of log K_M^* for tetravalent elements such as thorium and protactinium are more strongly dependent on temperature than the values for the di- and trivalent elements.

The effect of LiF concentration on log K_M^* for several elements is shown graphically in Figure 9.33. The values of log K_M^* for lanthanum, neodymium, and uranium are those given in Table 9.17; the data for thorium and europium were reported previously. As seen in Figure 9.33, the values of log K_M^* for the di- and trivalent species did not vary markedly when the LiF concentration was in the

Table 9.18

Temperature Dependence of Log K_M^* for Several Elements

Log $K_M^* = A + B/T$ (°K)

Temperature Range 625 to 750 C

Salt	Element	A	B	Standard Deviation of Log K_M^*
LiCl	Ba^{2+}	-0.6907	2,189	0.02
	La^{3+}	-2.6585	9,697	0.1
	Nd^{3+}	-3.3568	10,900	0.08
	Sm^{2+}	0.7518	1,950	0.05
	Eu^{2+}	-0.1584	2,250	0.05
LiBr	Ba^{2+}	-0.0733	1,333	0.02
	Nd^{3+}	4.4046	4,297	0.1

9.3.5 Measurement of Distribution Coefficients in Molten Salt-Metal Systems (Cont'd)

range of 0 to about 4 mole percent. However, the value of K_{Th}^* decreased by about 2 orders of magnitude as the LiF concentration was increased from 0 to 4 mole percent. These data indicate that contamination of the LiCl acceptor salt with fluoride fuel salt in amounts that are equivalent to 4 mole percent LiF or less will not affect the extent to which the rare earths are removed in the metal transfer process. The presence of fluoride in the acceptor salt would, however, cause a decrease in the thorium-rare-earth decontamination factor.

Previously, values of log K_{Pm}^* were presented that were obtained in an experiment at 640°C involving several LiCl-LiF solutions as the salt phase and also estimated the neodymium-promethium separation factor (D_{Nd}/D_{Pm}) to be 3 ± 2. The LiF concentration in the solutions ranged from about 2 to 18 mole percent. Inspection of the gamma spectra of samples taken in this experiment revealed that a significant amount of ^{147}Nd was present along with the promethium. Analysis of these spectra showed the neodymium-promethium separation factor to be independent of the LiF concentration in the salt and yielded an average separation factor of 8.3 ± 1.8. Assuming that this separation factor is also valid with LiCl as the salt phase, we estimate

$$\log K_{Pm}^* = 7.66 \pm 0.4$$

at 640°C. This estimate indicates that promethium would behave much like lanthanum in the metal transfer process.

9.3.6 Extraction of Cesium from Lithium Chloride[35/]

The distribution coefficients obtained for cesium were:

$$\log D_{Cs} = \log X_{Li} - 1.503$$

35/ ORNL monthly report, February, 1970.

9.3.6 Extraction of Cesium from Lithium Chloride (Cont'd)

The data are plotted in Figure 9.34 and are shown with the derived theoretical line with slope of one. The point at 0.0054 mole fraction lithium was not used in positioning the line since the counting rate of that 1 gram bismuth pellet was only 21 cpm. For comparison, contamination of a pellet with 100 micrograms of salt would elevate the counting rate by 50 cpm. The most likely cause of bias in these data would be salt contamination of a bismuth pellet. In several cases one of the pellets of a sample pair exhibited a higher counting rate by about 50 cpm and was not included in the results shown.

9.3.7 Distribution of Barium, Lanthanum, Neodymium, and Thorium in Lithium Bromide[35]

Data were obtained on the equilibrium distribution of barium, lanthanum, neodymium, and thorium between liquid bismuth solutions and molten LiBr. The distribution coefficients at each temperature could be expressed as

$$\log D = n \log X_{Li} + \log K^*$$

The values of log K* obtained with LiBr as the salt phase are as follows:

Element	Temp (°C)	log K*
Ba^{2+}	575	1.497
Ba^{2+}	600	1.443
La^{3+}	600	9.079
Nd^{3+}	600	8.919
Th^{4+}	600	16.16
Nd^{3+}	640	8.834
Ba^{2+}	650	1.359
Ba^{2+}	700	1.316
Nd^{3+}	700	8.430

9.3.7 Distribution of Barium, Lanthanum, Neodymium, and Thorium in Lithium Bromide (Cont'd)

These data are in accord with those obtained earlier in showing that temperature has little effect on log K*. The distribution coefficients determined with LiBr are about the same as those obtained with LiCl, indicating again that either of these salts could serve as the acceptor in a metal-transfer process.

9.3.8 Extraction of Europium and Strontium from Lithium Chloride[28/]

The distribution of europium and strontium fission products between bismuth and lithium chloride at 650 C was studied.

The thorium content of the salt was too low to give reliable data, but the other metals came out quite well. The calculated equilibrium constants are

$$\log D_{Eu}/D_{Li}^2 = 2.284 \pm .025$$

$$\log D_{Sr}/D_{Li}^2 = 1.024 \pm .141$$

9.3.9 Extraction of Protactinium from Lithium Chloride[36/]

Experiments involving protactinium were conducted at both 640 and 700 C. The species in the salt phase appeared to be tetravalent in each case. Data from these two experiments yielded the expression

$$\log K_{Pa}^* = -15 + 29970/T(^{o}K).$$

9.3.10 Distribution of Transuranium Elements in Lithium Chloride[37/]

The distribution of selected transuranium elements between molten LiCl and bismuth solutions were determined at 640 C. Although this experiment was terminated prematurely due to the rupture of the molybdenum crucible, enough data were obtained to define the relative behavior of the elements involved. Analysis of the data showed that, under the

36/ ORNL monthly report, May, 1970.

37/ ORNL monthly report, August, 1970.

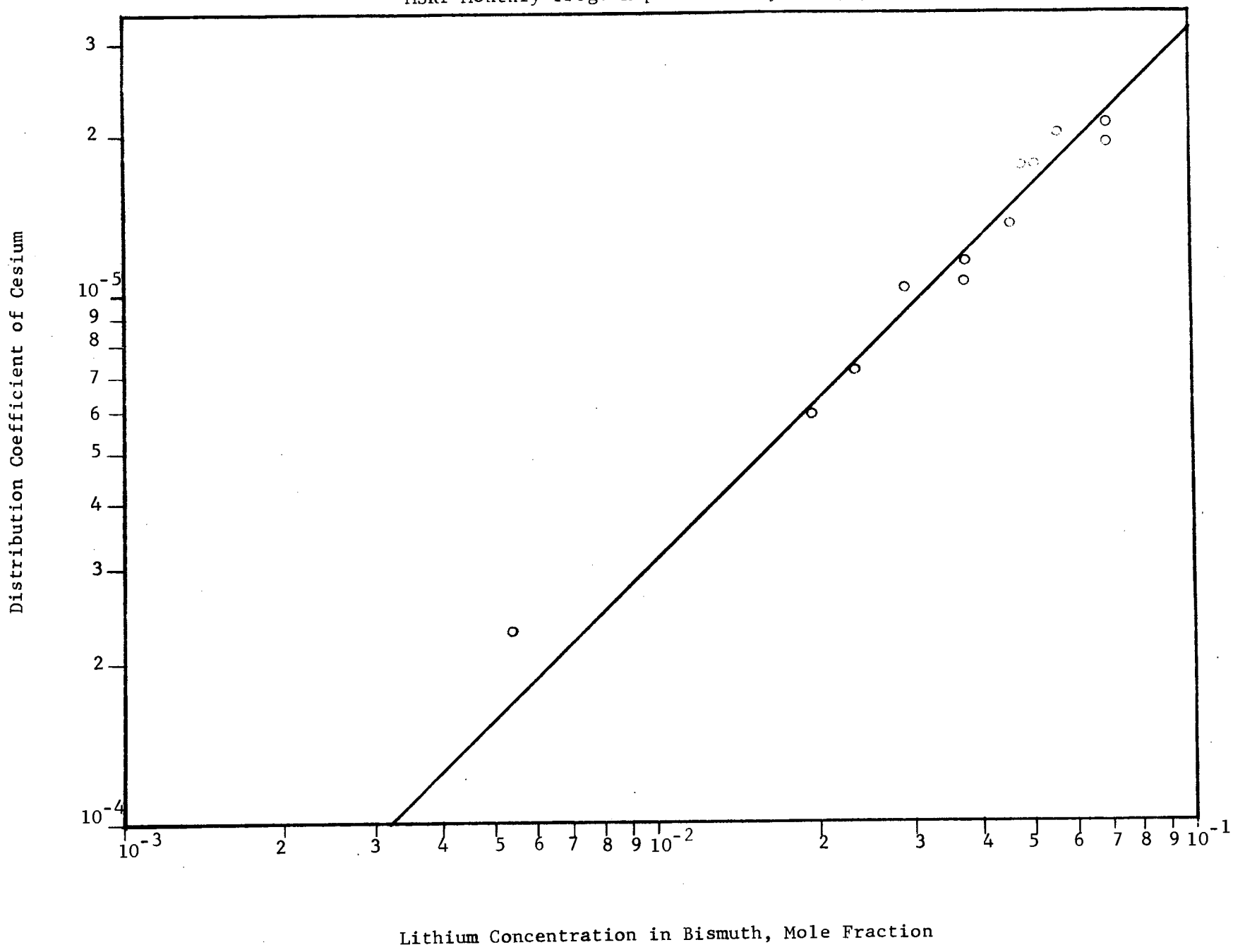

Fig. 9.34. Distribution Coefficient for Cesium in LiCl and Bi Solutions at 650°C

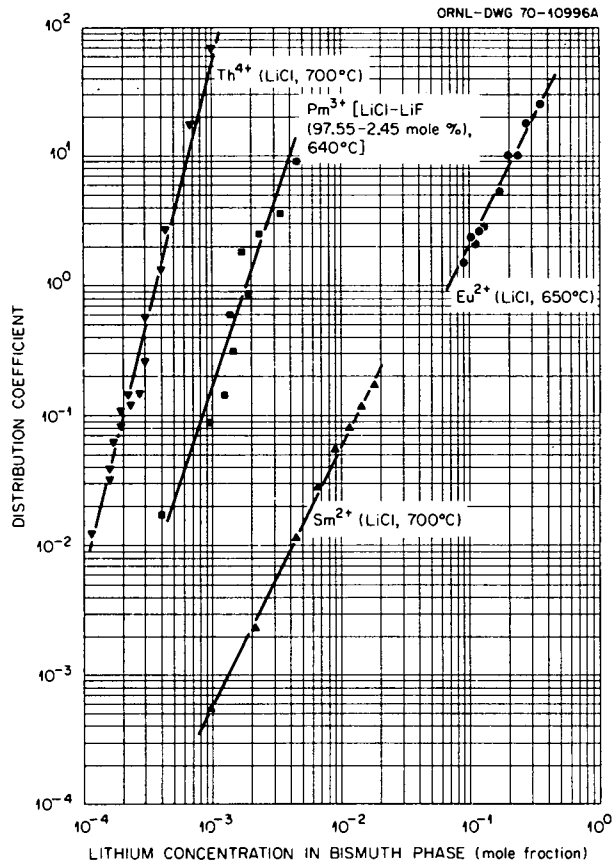

Fig. 9.35 Distribution Coefficient Isotherms Obtained for Several Elements with Various Salt Phases.

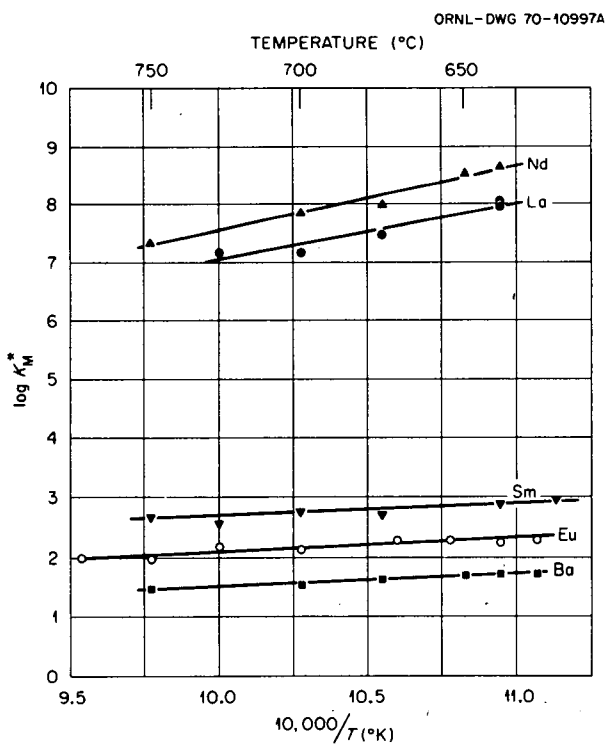

Fig. 9.36 Effect of Temperature on the Values of log K_M^* Obtained for Several Elements Using LiCl as the Salt Phase.

9.3.10 Distribution of Transuranium Elements in Lithium Chloride (Cont'd)

experimental conditions employed (mole fraction of lithium in the bismuth phase between 0.0016 and 0.0023), plutonium, neptunium, americium, and curium existed primarily as trivalent species in the salt phase and that californium was almost entirely divalent in the salt. The formation of divalent californium was not surprising; however, based on earlier data obtained with $LiF-BeF_2$ (66.7-33.3 mole percent) as the salt phase at 600 C, we would have expected the americium to be divalent in the salt phase. As seen from the approximate values of log K* given in Table 9.19, the ease of extraction of the transuranium elements from LiCl decreases with increasing atomic number of the element.

9.3.11 Distribution of Europium in Lithium Chloride[37/]

In the metal-transfer process being developed for the removal of rare earths from MSBR fuel salt, liquid Li-Bi alloys having high lithium concentrations are used to strip the rare earths from the LiCl or LiBr acceptor salt. Trivalent rare earths such as lanthanum, neodymium, and promethium (along with the thorium present in the acceptor salt) would be stripped into liquid Li-Bi (5-95 atom percent), whereas the divalent rare earths such as europium and samarium (along with some other fission products such as barium and strontium) would be stripped into liquid Li-Bi (about 40-60 atom percent). In the analysis of the flowsheet, it was assumed that values of log K* obtained with bismuth solutions having low lithium concentration were also valid when the lithium concentration in the bismuth phase was 5 atom percent or higher. This assumption appears to be valid, based on the results of an experiment involving the extraction of 650 C of europium from LiCl into lithium-bismuth solutions having lithium concentrations of 10 to 35 atom percent. The europium

Table 9.19

Equilibrium Distribution of Uranium and some Transuranium Elements Between Molten LiCl and Bismuth Solutions at 640 C

$$\text{Log } D = n \text{ Log } X_{Li} + \text{Log } K^*$$

(X_{Li} Varied from 0.0016 to 0.0023)

Element	n	Log K^*
U	3	11.278
Np	3	10.50
Pu	3	10.33
Am	3	10.16
Cm	3	9.49
Cf	2	5.38

9.3.11 Distribution of Europium in Lithium Chloride (Cont'd)

distribution coefficients (D_{Eu}) obtained in this experiment could be expressed by the usual relationship:

$$\log D_{Eu} = 2 \log X_{Li} + \log K^*_{Eu}$$

The data yielded $\log K^*_{Eu} = 2.325$, which is in good agreement with the value of about 2.28 obtained in earlier studies in which the lithium concentration in the bismuth phase was less than 1 atom percent. At one point in this experiment, the europium concentration in the metal phase was about 3,000 wt ppm when the lithium concentration was about 35 atom percent.

9.3.12 Distribution of Europium in Lithium Chloride-Fluoride Salts[25/]

We have initiated a series of experiments to determine the distribution behavior of selected solutes using LiCl-LiF as the salt phase. In the first experiment, distribution coefficients were obtained for europium at 650 C, using several LiCl-LiF solutions. Average values of $\log K^*_{Eu} = \log D_{Eu} - 2 \log X_{Li}$, in which X_{Li} is the mole fraction of lithium in the bismuth phase are given in Table 9.20. The estimated uncertainty in each value of $\log K^*_{Eu}$ is $\pm$ 0.08. As seen, $\log K^*_{Eu}$ increased only slightly with increasing LiF concentration in the salt phase. These results are in agreement with those obtained previously and indicate that fluoride contamination of the LiCl acceptor salt in the metal-transfer process will not markedly affect the removal of such divalent species as europium, samarium, and barium.

9.3.13 Extraction of Uranium from Lithium Chloride[38/]

The uranium distribution coefficients (D_U) obtained with LiCl at 675 C could be expressed by the usual relationship:

38/ ORNL monthly report, October, 1970.

Table 9.20

Values of Log K^*_{Eu} Obtained at 650 C with LiCl-LiF Solutions as the Salt Phase

LiF Concentration in Solution (Mole %)	Log K^*_{Eu}
0	2.279
2.01	2.322
4.06	2.401
6.64	2.378
10.67	2.513
15.93	2.446

9.3.13 Extraction of Uranium from Lithium Chloride (Cont'd)

$\log D_U = 3 \log X_{Li} + \log K_U^*$. The data yielded $\log K_U^* = 10.11 \pm 0.3$, which is somewhat lower than the value of about 10.6 expected from our previous measurements at 640 and 700 C.

9.3.14 Distribution Coefficients in Metal Transfer Systems[39/]

Additional distribution coefficients obtained, using LiCl, LiBr, LiCl-LiF, and LiBr-LiF as the salt phases, are summarized in Table9.21 and several isotherms are shown in Figure 9.35. In general, the uncertainty in $\log K_M^*$ was 0.06 or less; exceptions are noted in Table 9.21. Plots of $\log K_M^*$ vs 1/T, using data obtained with several elements, were found to be linear over the temperature range of about 625 to 750 C (Figure 9.36) thus for each element the temperature dependence of $\log K_M^*$ could be expressed as $\log K_M^* = A + B/T$. Values of A and B for several elements, obtained with either LiCl or LiBr as the salt phase, are given in Table 9.22. These data confirm earlier indications that the distribution behavior of most elements is rather insensitive to temperature changes and that the distribution coefficients for a given element at a given temperature are about the same with LiCl and LiBr. A detailed analysis of the effect of temperature on the metal transfer process has not yet been made.

An experiment was performed to determine qualitatively the behavior of zirconium in the metal transfer process. The zirconium distribution coefficients calculated from chemical analyses of the samples were scattered between 10 and 230; the average value was 85 when the mole fraction of lithium in the bismuth phase was 4.5×10^{-4} (15 wt ppm). This distribution coefficient is about the same as that obtained with $LiF-BeF_2-ThF_4$ (72-16-12 mole percent) at the

39/ ORNL-4622, p. 204, August 31, 1970.

Table 9.21

Values of Log K_M^* Obtained from Distribution Coefficient Isotherms: $\text{Log } D_M = n \text{ Log } X_{Li} + \text{Log } K_M^*$

Salt	Temperature (C)	Element	Log K_M^*
LiBr	640	Th^{4+}	14.8 (±0.7)
		Pa^{4+}	15.7 (±0.8)
		U^{3+}	10.6 (±0.5)
LiCl-LiF (97.55-2.45 Mole %)	640	Pm^{3+}	8.22
LiCl	650	Eu^{2+}	2.325
LiCl	700	La^{3+}	7.185
		Nd^{3+}	7.831
		Sm^{2+}	2.756
		Eu^{2+}	2.133
		Th^{4+}	13.772
		Pa^{4+}	15.8 (±0.4)
		U^{3+}	10.192

same lithium concentration in the bismuth phase. Consequently, if zirconium has not been removed from the salt with either the protactinium or uranium, it will be extracted along with the rare earths in the metal transfer process.

The main feature of the metal transfer process is the selective transport of rare earths from a fluoride fuel salt into an LiCl or LiBr acceptor salt. The rare earths would be stripped from the acceptor salt by extraction into lithium-bismuth solutions having lithium concentrations of 5 at. percent or higher. More specifically, the trivalent rare earths (and the small amount of thorium that would also be present in the acceptor salt) would be extracted into liquid lithium-bismuth (5-95 at. percent), and the divalent rare earths (europium and samarium) would be extracted into liquid lithium-bismuth (about 40-60 at. percent). If was assumed that the values of log K_M^* obtained with bismuth solutions of low lithium concentration were also valid when the lithium concentration in the bismuth phase was 5 at. percent or higher. This assumption appears to be warranted, based on the results of the experiment at 650 C in which europium was extracted from LiCl into lithium-bismuth solutions having lithium concentrations of 10 to 35 at. percent (Table 9.21, Figure 9.35). The value of log K_{Eu}^* obtained in this experiment (2.325) is in good agreement with the value of 2.28 expected from the correlation (Table 9.22) of the europium distribution coefficients obtained previously. In the earlier experiments the lithium concentration in the bismuth phase was always lower than about 1 at. percent.

The distribution behavior of several solutes, using LiCl-LiF and LiBr-LiF solutions as the salt phase, is being studied to determine the effect of fluoride on the metal transfer process in the event that the acceptor salt

Table 9.22

Temperature Dependence of Log K_M^* for Several Elements

$\text{Log } K_M^* = A + B/T \ (^oK)$

Temperature Range 625 to 750 C

Salt	Element	A	B	Standard Deviation of Log K_M^*
LiCl	Ba^{2+}	-0.6907	2,189	0.02
	La^{3+}	-2.6585	9,697	0.1
	Nd^{3+}	-3.3568	10,900	0.08
	Sm^{2+}	0.7518	1,950	0.05
	Eu^{2+}	-0.1584	2,250	0.05
LiCl-LiF (97.55-2.45 Mole%)	Pm^{3+}	-1.2356	8,536	0.33
LiBr	Ba^{2+}	-0.0733	1,333	0.02
	Nd^{3+}	4.046	4,297	0.1

9.3.14 Distribution Coefficients in Metal Transfer Systems (Cont'd)

becomes contaminated with fluoride fuel salt. It was shown previously that the presence of fluoride in either LiCl or LiBr caused a change in the distribution behavior of lanthanum and thorium, particularly thorium. Data for promethium and europium, using LiCl-LiF solutions as the salt phase, were obtained (Table 9.23). At 640 C the values of log K^*_{Pm} decreased systematically as the LiF concentration in the salt phase increased. This behavior is similar to that found previously for lanthanum and shows that the thorium-promethium separation factor will also be decreased if the acceptor salt becomes contaminated with fuel salt. No value for log K^*_{Pm} was obtained with pure LiCl as the salt phase; however, the estimated value of 8.4 indicates that the behavior of promethium is similar to that of neodymium. The estimated neodymium-promethium separation factor at 640 C with pure LiCl as the salt phase is 3 ± 2. Furthermore, this separation factor is not expected to change significantly with temperature because the values of log K^*_{Pm} obtained with LiCl-LiF (97.55-2.45 mole percent) had about the same temperature dependence as the values of log K^*_{La} and log K^*_{Nd} obtained with LiCl as the salt phase; that is, the values of B were of the same magnitude (Table 9.22).

As shown in Table 9.23, the values for log K^*_{Eu} at 650 C showed a slight increase when LiF was present in the salt phase. The magnitude of the change is such that contamination of the acceptor salt with fluoride would not markedly affect the behavior of europium in the metal transfer process.

9.3.15 Engineering Metal Transfer Experiments[40/]

Two engineering experiments (MTE-1 and -2 for the study

40/ ORNL-4682, p. 24, March 31, 1971.

Table 9.23

Effect of LiF Concentration on Values of Log K_M^* Obtained for Promethium and Europium, Using LiCl-LiF Solutions as the Salt Phase

Element	Temperature (C)	LiF Concentration in Salt (Mole %)	Log K_M^*
Pm^{3+}	640	0	8.4
		2.45	8.22
		6.59	7.22
		10.22	6.86
		17.56	6.14
Eu^{2+}	650	0	2.279
		4.39	2.265
		11.5	2.398
		17.3	2.381
		24.6	2.374

9.3.15 Engineering Metal Transfer Experiments (Cont'd)

of the metal transfer process for removing rare earths from single-fluid MSBR fuel salt were completed. The main objectives of these experiments were (1) demonstration of the selective removal of rare earths from fluoride salt containing thorium fluoride, (2) collection of the rare earths in a lithium-bismuth solution, and (3) verification of previous distribution coefficient data. All of these objectives were accomplished. Both experiments were performed in the 6-in-diameter carbon-steel vessel shown schematically in Figure 9.37. The vessel had two compartments that were interconnected at the bottom by a pool of bismuth saturated with thorium. One compartment contained fluoride salt (72-16-12 mole percent $LiF-BeF_2-ThF_4$) to which tracer quantities of ^{147}Nd and sufficient LaF_3 to produce a concentration of 0.3 mole percent had been added. The other compartment contained LiCl, as well as a cup containing a lithium-bismuth solution. During operation, LiCl was circulated through the lithium-bismuth cup at the rate of about 25 cm^3/min. The concentration of reductant (35 at. percent lithium) in the lithium-bismuth was sufficiently high that, at equilibrium, essentially all of the neodymium and lanthanum would have been extracted from the LiCl that was circulated through the lithium-bismuth cup.

The quantities of materials used in the two experiments are given in Table 9.24. The LiCl was purified prior to use by contact with bismuth saturated with thorium at 650 C. Both the carbon-steel vessel and the bismuth were treated with hydrogen at 650 C to remove oxides. The argon used as cover gas for the experiment was purified by passage through a bed of uranium turnings at 600 C and a bed of molecular sieves. The experiment and operating conditions used for the two experiments were similar with the follow-in exceptions:

Table 9.24

Materials Used In Metal Transfer Experiments MTE-1 and 2

	Run No.	Volume (cm^3)	Moles (g)
Fluoride Salt ($LiF-BeF_2-ThF_4-LaF_3$, 72-15.7-12-0.3 Mole % plus ^{147}Nd Tracer)	MTE-1	709	36.6
	MTE-2	789	40.7
Bismuth Saturated with Thorium	MTE-1	797	36.8
	MTE-2	799	36.9
LiCl	MTE-1	1,042	36.6
	MTE-2	1,042	36.6
Li-Bi (35 at % Li)	MTE-1	192	11.1
	MTE-2	164	9.5

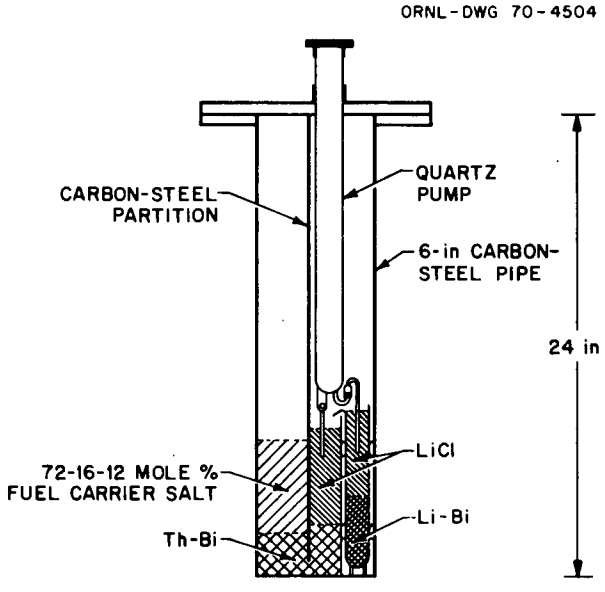

Fig. 9.37. Carbon-steel vessel for use in the metal transfer experiments.

ORNL-4676
p 250

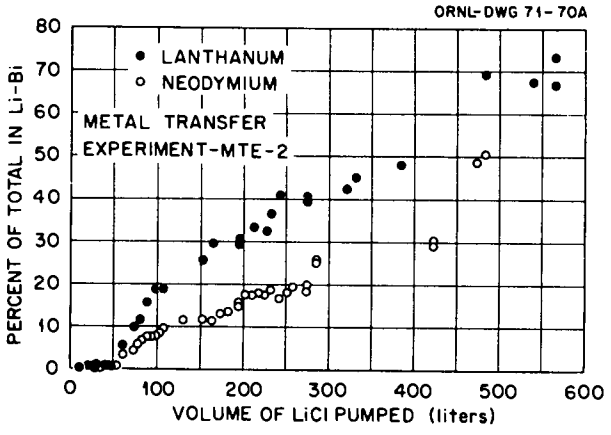

Fig. 9.38 Rate of accumulation of lanthanum and neodymium in the lithium-bismuth solution.

ORNL-4676
p 250

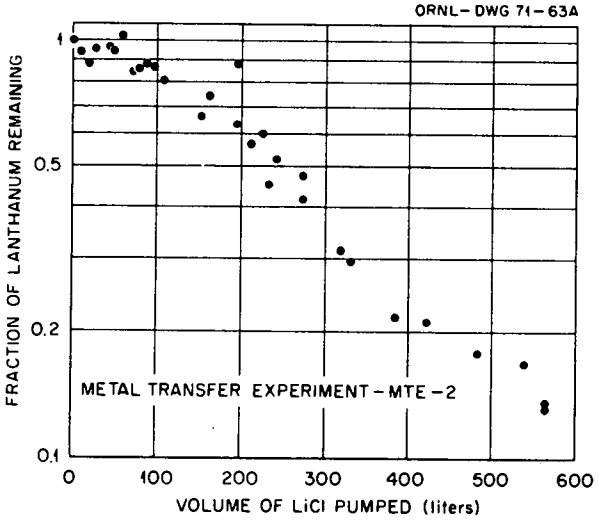

Fig. 9.39 Rate of removal of lanthanum from the fluoride salt.

ORNL-4676
p 258

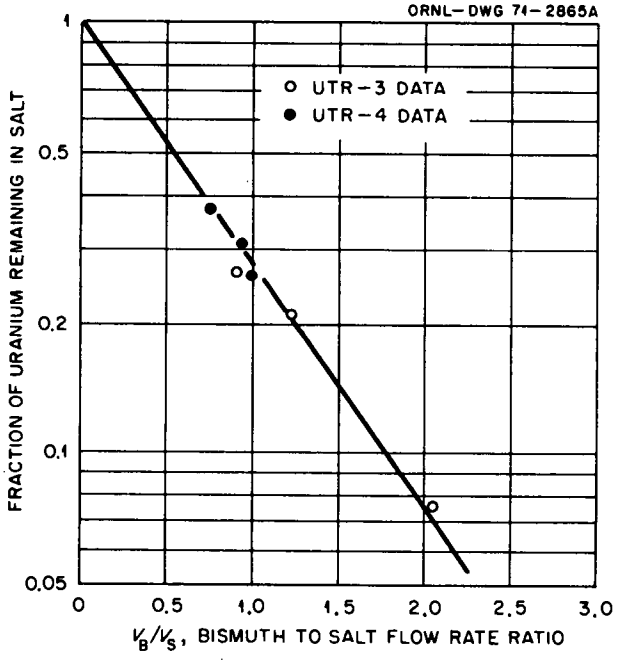

Fig. 9.40 Mass Transfer of uranium from $LiFBeF_2$-ThF_4 (72-16-12 Mole %) to bismuth containing reductant at 600 C in an 0.82-in.-diam, 24-in.-long packed column.

9.3.15 Engineering Metal Transfer Experiments (Cont'd)

1 - A quartz pump having sapphire check valves was used to circulate the LiCl in experiment MTE-1, whereas a carbon-steel pump having molten bismuth check valves was used in MTE-2;

2 - Simple sparge tubes were used in MTE-L to promote contact between the salt and bismuth phases, while in run MTE-2 gas-lift sparge tubes were used to disperse the metal into the salt phase;

3 - The quantity of ^{147}Nd tracer added to the fluoride salt was increased in MTE-2 to 7 mCi (from the 2 mCi used in MTE-1) to facilitate the detection of the tracer;

4 - The operating temperature was about 660 C in MTE-1 and about 650 C in MTE-2.

In the first experiment (MTE-1), the LiCl was pumped through the lithium-bismuth container for 3 hours at a flow rate of 25 cm^3/min. Pumping was then stopped, and the system was allowed to approach equilibrium during a 4-hr period. At this point, filtered samples of the salt and metal phases were taken. During the pumping and equilibration periods, the bismuth-thorium phase was forced to flow back and forth between the fluoride and chloride compartments at a rate equivalent to 10 percent of the metal volume every 7 minutes in order to promote mixing in the bismuth-thorium phase. The duration of the experiment was one week, during which the LiCl pump was operated 50.5 hours. The distribution coefficients for lanthanum and neodymium between the fluoride salt and the thorium-saturated bismuth were relatively constant throughout the run; the respective averages, 0.044 and 0.073, were in good agreement with expected values. The distribution coefficients for lanthanum and neodymium between the LiCl and the thorium-saturated bismuth were higher than anticipated during the first part of the run but approached the expected values near the end of the run.

Approximately 50 percent of the lanthanum and 25 percent of the neodymium (after correcting for ^{147}Nd decay) originally

Table 9.25

Variation of Beryllium, Thorium, and Fluoride Concentrations in the LiCl After Addition of 1 Vol % Fuel Carrier Salt

Time After Addition (Hr)	Pumping Time (Hr)	Fluoride (Wt %)	Beryllium (ppm)	Thorium (ppm)
0	0	0.98[a]	490[a]	9,480[a]
19.8	0	1.49	490	7,200
45.4	0	1.08	500	1,100
69.7	0	1.81	320	
93	0	2.03	490	644
115.9	5.9	2.34	470	
163.9	20.3	1.07	120	1,400
188.8	27.4	0.91		350
188.8	27.4	1.7 [b]	135[b]	171[b]

(a) Calculated values based on the amount of fluoride salt added.

(b) Salt taken from vessel after experiment was concluded.

9.3.15 Engineering Metal Transfer Experiments (Cont'd)

present in the fluoride salt were removed during the run; however, the lanthanum and neodymium did not collect in the lithium-bismuth as expected. After the run was completed, most of the lanthanum and neodymium that had been removed from the fluoride salt was found in a 1/8-in. thick layer of black material located at the interface between the LiCl and the bismuth-thorium. The composition of the material (wt percent) was 3.6 percent La, 7.7 percent Th, 12.0 percent Li, 59.1 percent Cl, 4.4 percent O, 0.95 percent Si, 0.54 percent Fe, and about 12 percent Bi. It is believed that oxides introduced into the system from the quartz pump or from moisture and air introduced when the system was opened for maintenance before the run may account for the accumulation of the rare earths in the black material.

In the second experiment (MTE-2), quartz was eliminated from the system by the use of a carbon-steel pump, and contact between the salt and metal phases was improved by the use of gas-lift sparge tubes. During this experiment, the neodymium and lanthanum originally added to the fluoride salt transferred to the lithium-bismuth solution as expected. The experiment was operated for about three months before it was shut down for disassembly and inspection. During this time, the pump was operated 441 hours, and 702 liters of LiCl was circulated through the lithium-bismuth container. The sequence of operations carried out consisted of pumping the LiCl through the lithium-bismuth container for 3 hours at a flow rate of 25 cm^3/min, then stopping the pumping, and allowing a period of 4 hours for the system to approach equilibrium before filtered samples of the salt and metal phases were taken. This sequence was repeated three shifts per day during the first week and two shifts per day during the second week of operation. For the remainder of the three-month period,

9.3.15 Engineering Metal Transfer Experiments (Cont'd)

the pump was operated during the entire day shift and the system was allowed to approach equilibrium at night and on weekends.

The rate of accumulation of rare earths in this solution is shown in Figure 9.38. There was essentially no accumulation of lanthanum or neodymium in the solution until operation of a gas-lift sparge tube was initiated (after about 50 liters of LiCl had been circulated through the lithium-bismuth compartment). After 400 liters of LiCl had been circulated (about two-thirds through the run), about 50 percent of the lanthanum and 30 percent of the neodymium originally in the fluoride salt was found to be in the lithium-bismuth solution. During this time, 70 to 100 percent of the lanthanum and neodymium initially charged to the system could be accounted for by filtered samples taken of each phase, indicating that most of the rare earths remained in solution. During the last one-third of the run, the rare earths continued to accumulate in the lithium-bismuth solution, but the rate of accumulation could not be determined accurately because a leak developed in the lithium-bismuth cup, allowing about 30 percent of the solution to flow into the area between the cup and holder. The extent of removal of lanthanum from the fluoride salt is shown in Figure 9.39, which indicates that more than 85 percent of the lanthanum had been removed at the end of the experiment; about 50 percent of the neodymium was also removed. Approximately 10 to 20 percent of the rare earths were removed from the LiCl as it was circulated through the lithium-bismuth compartment. There was no measurable accumulation of thorium (<10 ppm) in the lithium-bismuth solution during the experiment, thus demonstrating that the rare earths can be deposited in this solution without significant amounts of thorium also being deposited. The thorium-lanthanum decontamination factor was about 10^5. The distribution coefficients for lanthanum and

9.3.15 Engineering Metal Transfer Experiments (Cont'd)

neodymium remained relatively constant during the experiment. The average values of the distribution coefficients for lanthanum (0.05) and neodymium (0.06) between the fluoride salt and the bismuth-thorium solutions are in good agreement with expected values. The average values of the distribution coefficients between the LiCl and the bismuth-thorium solution were somewhat higher than expected for lanthanum (3.1) and near the expected value for neodymium (4.8). During the run, the lithium concentration in the lithium-bismuth solution decreased from 35 to 13 at. percent. Only a small fraction of this decrease was due to the reaction of lithium with rare-earth chlorides; the principal reason for the decrease has not yet been determined. The bismuth-thorium phase remained saturated with thorium throughout the run indicating that there was no excessive loss of thorium from the bismuth phase during the experiment.

Eight days before the end of the experiment, 1 vol percent fluoride salt was added to the LiCl compartment to simulate entrainment of fluoride salt in the bismuth. Concentrations of beryllium, thorium, and fluoride in the LiCl were determined periodically after the addition of fuel carrier salt to the LiCl near the end of the experiment, as shown in Table 9.25. During the 93-hour period in which the LiCl was not circulated through the lithium-bismuth container, the beryllium concentration remained constant at the initial value of 490 ppm and the thorium concentration decreased, as expected, from the initial value of 9 480 ppm to a value of 644 ppm. When circulation of the LiCl was resumed, the beryllium concentration in the LiCl began to decrease; after 27 hours of operation, a concentration of 135 ppm was observed. The thorium concentration in the LiCl at this time was 171 ppm.

9.4 Reductive Extraction Engineering Studies

9.4.1 Uranium Mass Transfer Studies[41/]

Experimental work in the flow-through reductive extraction facility was continued.

In preparation for the first mass transfer run (UTR-1), a sufficient quantity of $LiF-UF_4$ eutectic mixture was added to the salt feed tank to produce a uranium concentration of 0.0003 mole fraction, and thorium metal was added to the bismuth in the treatment vessel. Hydrodynamically, run UTR-1 was successful. A uniform flow rate of each phase was maintained at 105 ml/min (~62 percent of flooding) for 90 minutes; during this period, seven sets of simultaneous samples (salt out, bismuth out) were taken from the flowing-stream samplers. The flow rates were then increased to 129 ml/min (~76 percent of flooding) for 50 minutes. Surprisingly, however, analyses of flowing bismuth samples showed that only a small fraction (<0.5 percent) of the uranium was extracted from the salt phase. Subsequent investigation revealed that a cube of thorium metal had blocked the charging port in the treatment vessel and that there was essentially no reductant in the bismuth phase during the experiment.

Thorium metal was added directly to the bismuth feed tank in preparation for the next mass transfer run. Dissolution of the thorium was slow, requiring a total of about 300 hours (including 120 hours at 650 C). Operating conditions and results for run UTR-2 are summarized in Table 9.26. About 95 percent of the uranium was extracted into the bismuth phase, which initially contained a 140 percent stoichiometric excess of reductant. Conditions for the experiment were chosen such that a relatively large fraction of the uranium would be extracted, although these

---

41/ ORNL-4682, p. 20, March 31, 1971.

Table 9.26

Data Obtained From Uranium Mass Transfer Experiments in an 0.82-In.-ID by 24-In.-High Column at 600 C

	Uranium Concentration in Salt (ppm)								
	Salt Feed X_i	Salt Effluent X_o	Maximum Equilibrium Value, X* (a)	Salt Flow Rate (cm^3/min)	Bismuth Flow Rate (cm^3/min)	Metal-to-Salt Flow Rate Ratio	Fraction of Flooding	Fraction of U Extracted from Salt	Fraction of U Remaining in Salt
UTR-2	808	40	~0.8	52	247	4.75	0.77	~0.95	0.05
UTR-3	2,100	159	3.6	100	205	2.05	0.87	0.92	0.076
		445	9.4	160	195	1.22	1.04	0.79	0.212
		561	10.3	220	200	0.91	1.23	0.73	0.267
UTR-4	1,680	524	9.7	149	140	0.94	0.85	0.69	0.312
		439	7.2	118	117	1.0	0.69	0.74	0.261
		626	9.7	210	157	0.75	1.07	0.63	0.373

(a) Calculated as the concentration that would be in equilibrium with the observed concentrations of reductant (lithium) and uranium in the bismuth effluent.

9.4.1 Uranium Mass Transfer Studies (Cont'd)

conditions are not optimum for the determination of mass transfer performance. This experiment was important in that it was the first successful demonstration of the reductive extraction of uranium into bismuth in a flowing system.

Prior to run UTR-3, 122.5 g of thorium metal was added to the treatment vessel, which contained about 10 percent of the salt (1.5 liters) and most of the bismuth (~17 liters) present in the system. The thorium dissolved in the bismuth at a very low rate (~0.3 percent/hr.) which was nearly equivalent to the rate observed in the bismuth feed tank prior to run UTR-2. In order to improve the contact between thorium and the bismuth, an additional 119 g of thorium (contained in a 1-in diameter perforated steel basket) was suspended in the bismuth. The resulting dissolution rate was about ten times the earlier rate; about 85 percent of the thorium dissolved in a 22-hour period. Samples of the bismuth phase showed a range of thorium concentrations and suggested the existence of a concentration gradient in the bismuth pool. The final thorium concentration in the bismuth is believed to have been 1 200 ppm. The thorium-bismuth solution and the salt were then transferred to the feed tanks. The solubility of thorium in the bismuth at the feed tank temperature (540 C) is about 900 ppm. The final uranium concentration in the salt feed tank was 2 100 ppm.

During run UTR-3, bismuth was fed to an 0.82-in. ID by 24-in. high extraction column at the rate of about 200 cm^3/min, and salt was fed to the column at the rates of 100, 160, and 220 cm^3/min. Under the first combination of operating conditions, five sets of samples were taken of the salt and bismuth streams leaving the column; however, only one set of samples was taken under each of the other combinations of conditions, after a salt volume equivalent

to three column volumes had passed through the column. As shown in Table 9.26, the fraction of the uranium extracted from the salt decreased from 0.92 to 0.73 as the salt flow rate was increased.

The thorium dissolution rate in the treatment vessel prior to run UTR-4 was about the same as that observed prior to run UTR-3. Some nonuniformity in thorium concentration was observed in the bismuth. The final thorium concentration in the bismuth feed tank was about 1 100 ppm, and the uranium concentration in the salt feed tank was 1 680 ppm. During run UTR-4, the system was operated at three sets of salt and bismuth flow rates. Eleven pairs of samples were taken from the salt and bismuth streams leaving the column. The fraction of extracted uranium ranged from 63 to 74 percent, as shown in Table 9.26 and Figure 9.40.

The uranium extraction data from runs UTR-3 and -4 can be correlated in terms of the height of an overall transfer unit based on the salt phase (HTU) if several assumptions are made. The chief assumption is that the rate at which uranium transfers to the bismuth phase will be controlled by the diffusive resistance in the salt film when the extraction factor is high and when the salt film is composed largely of nontransferring ions. In runs UTR-3 and -4, a small amount of uranium was added to the salt after it had been equilibrated with the bismuth phase; no significant transfer of lithium and thorium occurred in the column. In this case, the overall transfer coefficient based on the salt phase is equal to the individual salt film transfer coefficient. By definition, the HTU and the number of overall transfer units based on the salt phase (NTU) developed in the column are related as

$$H = HTU \cdot NTU, \qquad (23)$$

where H is column length. If it is assumed that uranium is the major component transferring from the salt and that the controlling resistance to transfer is in the salt phase, HTU can be written as

$$HTU = \frac{V_s}{ka} \tag{24}$$

where V_s is the superficial velocity of the salt in the column and ka is the product of the overall mass transfer coefficient based on the salt phase and the interfacial area between the salt and bismuth phases per unit column volume. It has been previously observed that the dispersed-phase holdup is approximately proportional to the flow rate of the dispersed phase except at conditions near flooding. We would, therefore, expect the interfacial area between the salt and the bismuth phases to be proportional to the bismuth flow rate, so that

$$ka = k' V_{Bi} \tag{25}$$

where k' is a constant and V_{Bi} is the superficial velocity of the bismuth in the column. The number of overall transfer units, based on the salt phase, developed in the column is defined as

$$NTU = \int_{X_i}^{X_o} \frac{dX}{X^* - X} \tag{26}$$

where

X = uranium concentration in the bulk salt,

X^* = uranium concentration in the salt in equilibrium with the bulk bismuth phase,

X_i = uranium concentration in the salt fed to the column,

X_o = uranium concentration in the salt leaving the column.

As shown in Table 9.26, the value of X^* at the bottom of the column is much smaller than the value of X_o; thus one would expect that $X^* \ll X$ throughout the column. In this

case, Eq. 26 would become

$$NTU = -\ln\frac{X_o}{X_i} \tag{27}$$

Combining Eqs. 23, 24, 25, and 27 and rearranging yields the relation

$$\ln\frac{X_o}{X_i} = -k'H\frac{V_{Bi}}{V_s} \tag{28}$$

which states that a semilogarithmic plot of the fraction of the uranium remaining in the salt vs the bismuth-to-salt flow rate ratio should yield a straight line having a slope of -k'H. This line would pass through an ordinal value of 1.0 at a bismuth-to-salt flow rate ratio of zero.

As shown in Figure 9.40, the data from runs UTR-3 and -4 are well represented by Eq. 28. For these data, the constant k' has the value of 0.0529 in^{-1}. The product of the overall transfer coefficient, based on the salt phase, and the interfacial area is given by the relation

$$ka = 0.0529V_{Bi}, \tag{29}$$

where ka is the overall rate constant based on the salt phase, sec^{-1}, and V_{Bi} is the superficial velocity of the bismuth in the column, in/sec. Values for the overall rate constant for the present data range from 0.012 to 0.021 sec^{-1} and compare favorably with a preliminary value of 0.0076 sec^{-1} measured[31] for the transfer of uranium from a 96.2-3.6-0.2 wt percent Cd-Mg-U solution to a molten salt (50-30-20 mole percent $MgCl_2$-NaCl-KCl) at temperatures ranging from 560 to 610 C.

The HTU values for the data from runs UTR-3 and -4 are given by the expression

$$HTU = \frac{18.9}{V_{Bi}/V_s}, \tag{30}$$

9.4.1 Uranium Mass Transfer Studies (Cont'd)

where HTU is the height of the overall transfer unit based on the salt phase, in, and V_{Bi}/V_s is the bismuth-to-salt flow rate ratio. The HTU values range from 0.77 ft at a flow rate ratio of 2.05 to 2.1 ft at a flow rate ratio of 0.75.

In order to measure mass transfer rates in the column under more closely controlled conditions and under conditions where the controlling resistance is not necessarily in the salt phase, preparations were begun for experiments in which the rate of exchange of zirconium isotopes will be measured between salt and bismuth phases otherwise at equilibrium. Residual reductant was removed from the treatment vessel by hydrofluorinating the salt and bismuth for 20 hours with 70-30 mole percent H_2-HF. Following the usual H_2 sparge for reduction of iron fluoride, the two phases were transferred to the feed tanks. A hydrodynamic experiment (UTR-5) was then carried out (1) to remove from the system any bismuth having a high thorium concentration and (2) to test the sampling and analysis techniques under conditions where no mass transfer should occur. Surprisingly, the reported uranium concentrations of salt samples removed from the column effluent varied by ±35 percent from the average value, which was in excellent agreement with the indicated uranium concentrations of the salt feed and catch tanks.

9.4.2 Flooding and Pressure Drop Studies in Packed Columns

The proposed method for removing protactinium and fission products from a single-fluid molten-salt breeder reactor (or from the blanket salt of two-fluid reactors) involves reductive extraction using liquid bismuth containing lithium and thorium reductants. Equipment is needed to efficiently contact streams of salt and bismuth. The properties of these fluids are very different from those

9.4.2 Flooding and Pressure Drop Studies in Packed Columns (Cont'd)

of aqueous and organic fluids with which most experience with liquid-liquid extraction equipment has been obtained. For instance, the difference between the densities of the salt and metal phases will be between 5.5 and 7.5 g/ml, while aqueous-organic systems have differences between 0.05 and 0.2 g/ml. Similarly, the interfacial tension between bismuth and molten salt could be as much as a factor of 10 greater than that usually seen in aqueous-organic systems.

Since the correlations used to design liquid-liquid extraction systems are based upon conditions far removed from those of current interest, experimental data from systems similar to the molten-salt-bismuth system are needed. Because experiments with bismuth and molten salt are difficult, a mercury-water system will be used initially to provide the hydrodynamic data necessary to allow intelligent selection of contactor types to test with the process fluids. This simulated system will provide quantitative data on flooding rates, pressure drop, holdup, and backmixing, as well as qualitative information on flow patterns and drop size.

The experiments in this study are carried out in a 1-in. ID, 2-ft long glass column. Mercury is circulated between the column and a hold tank by a diaphragm pump containing tantalum check values. Distilled water is circulated through the column by a small centrifugal pump. Ball valves are located at each end of the 1-in. column and allow flow to and from the column to be stopped instantly for holdup measurements. Each end of the column also contains a section of 2-in. pipe. These sections, which are partially packed with the packing material of interest, allow lower velocities for coalescence, as well as provide space for the inlet and outlet lines.

9.4.2 Flooding and Pressure Drop Studies in Packed Columns (Cont'd)

Pressure drop and holdup data for a 2-ft length of the 1-in. column packed with 1/4-in. Raschig rings are shown in Figures 9.41 and 9.42. These results are similar to all the data obtained with other packing materials. Pressure drop and holdup for larger packing sizes (where the mercury is well dispersed) may be related by the semiempirical equations

$$\frac{\Delta P}{L} = K_1 V_s X + k_2 \left(\frac{C}{1 - X} \right) X$$

and

$$V_s = \frac{g}{g_c} \frac{\Delta \rho}{k_1} - \frac{1}{k_1} \frac{\Delta P}{L} - k_3 D,$$

where

ΔP = pressure drop due to flow (e.g., total pressure drop across the column less the static head),

L = length of column,

V_s = superficial slip velocity,

X = holdup,

C, D = continuous- and dispersed-phase superficial velocities,

$\Delta \rho$ = density difference,

k_1, k_2, k_3 = constants.

Thus with three constants (k_1, k_2, and k_3) the hydrodynamic aspects (holdup, pressure drop, and, by implication, flooding rates) of a dispersed-flow column can be related. Unfortunately, only two of the four packing materials tested gave dispersed flow, and to adequately evaluate any relationship between the hydrodynamic variables will require data from more packing materials.

Measurements of pressure drop and dispersed-phase holdup were carried out with a 2-in. ID column packed with 1/2-in. Raschig rings. The holdup data were similar to those

ORNL-4396
p 296

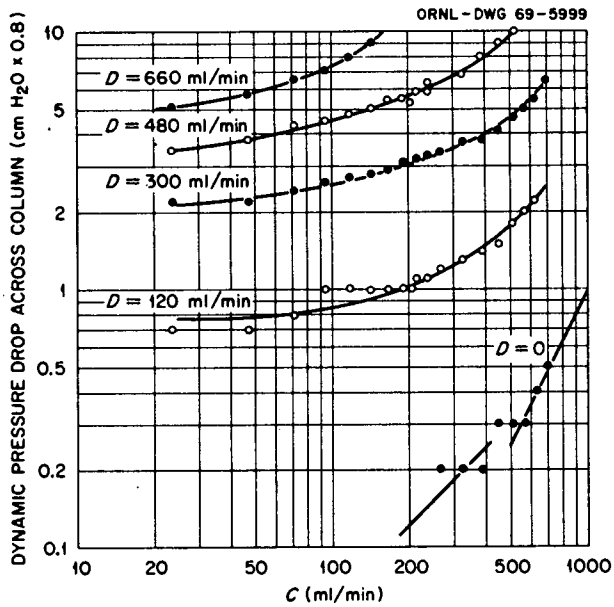

Fig. 9.41 Pressure Drop Across the 1-in. Mercury-Water Column Packed with ¼-in. Raschig Rings.

ORNL-4396
p 296

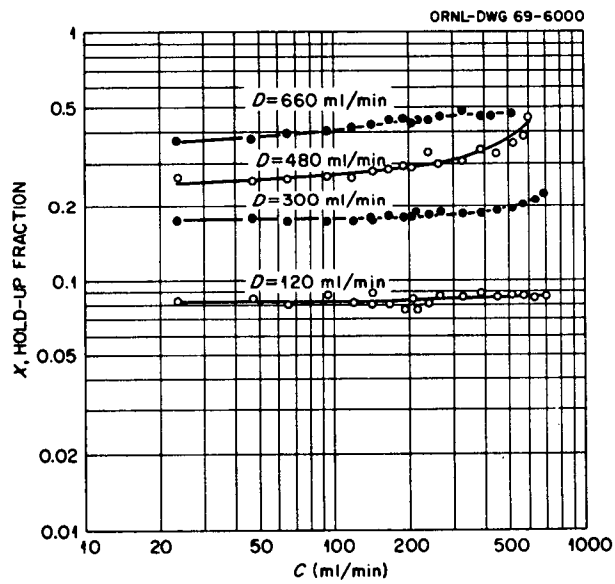

Fig. 9.42 Dispersed Phase Holdup in the 1-in. Mercury-Water Column Packed with ¼-in. Raschig Rings.

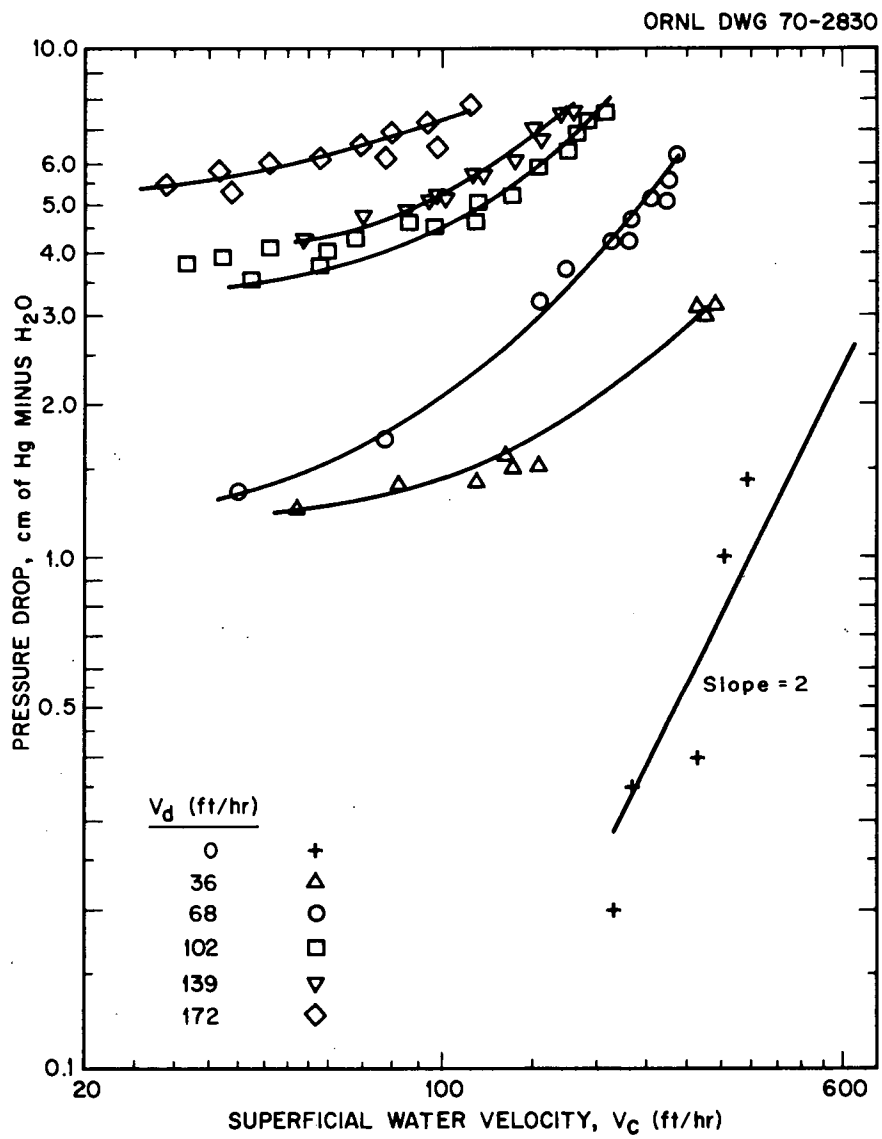

Fig. 9.43. Pressure Drop vs Superficial Water Velocity in a 2-in. Column Packed with 3/8-in. Raschig Rings

obtained previously with smaller packing materials; the results can be correlated by the assumption of a constant superficial slip velocity, V_s, defined as

$$V_s = \frac{V_c}{1 - X} + \frac{V_d}{X}, \tag{32}$$

where V_c and V_d are superficial velocities of the continuous and dispersed phases, respectively, and X is the fraction of the column void fraction occupied by the dispersed phase. Fifty-nine holdup measurements were made with the 1/2-in. Raschig ring packing. The calculated superficial slip velocity was 1531 ± 249 ft/hr.

The superficial slip velocities for packings studied previously were also calculated, and standard deviations of 10 to 15 percent (estimated to be the experimental error in the holdup data) were observed. The data for 1/4-in Raschig rings and solid cylinders in 1- and 2-in. ID columns suggest that the superficial slip velocity is also expected to be dependent on packing size and that although the slip velocity for 3/8-in. Raschig rings (i.e., 819 ft/hr) is approximately equal to that for 1/4-in. Raschig rings, the slip velocity for 1/2-in. Raschig rings (1531 ft/hr) is considerably higher than that for smaller packing.

The observation that the dispersed-phase holdup data can be correlated on the basis of a constant superficial slip velocity is especially important, since this suggests a method for correlating flooding data. At flooding it is assumed that the following conditions obtain:

$$\frac{\partial V_d}{\partial X} = \frac{\partial V_c}{\partial X} = 0. \tag{33}$$

If the superficial slip velocity remains constant up to flooding, combining Eqs (1) and (2) yields the relation:

$$(V_{c,\,flood})^{1/2} + (V_{d,\,flood})^{1/2} = V_s^{1/2}, \tag{34}$$

where $V_{c,flood}$ and $V_{d,flood}$ are the continuous- and dispersed-phase superficial velocities at flooding. Thus a plot of $(V_{c,flood})^{1/2}$ vs $(V_{d,flood})^{1/2}$ should produce a straight line having a slope of -1. This has been observed in the literature, and our previous flooding data with 1/4-in. and 3/8-in. Raschig rings and 1/4-in. solid cylinders are well represented by this correlation. It was not possible to flood the column packed with 1/2-in. Raschig rings because of insufficient capacities in the mercury and water pumping systems, although the column appeared to be approaching flooding at the highest flow rates used. Hence it was not possible to verify experimentally that the slip velocity, as caluclated from holdup measurements, is equal to the value that would be determined from flooding data.

To date, our attempts to correlate pressure drop data have not been successful. The pressure drop behavior is especially complex at low water flow rates, where the pressure drop observed with water flow is actually lower than observed with no water flow. Since this is contrary to our expectations, we are continuing to study the phenomenon.

We have attempted to extend the correlations developed for the mercury-water system in order to obtain relations that are applicable to molten-salt-bismuth systems. The physical properties of the fluids were not varied in these studies, and there are significant differences in properties between the mercury-water system and molten-salt-bismuth systems. The most important ones were considered to be the viscosity of the continuous phase and the difference in densities of the phases. The slip velocity is assumed to be directly proportional to the difference in the densities of the phases. The correction for changes in interfacial tension is believed to be small since the interfacial tension for the mercury-water system is approximately

equal to that for a molten-salt-bismuth system. The interaction of the dispersed phase with the continuous phase is expected to be inertail in nature, and the continuous-phase viscosity should have only a slight effect.

On the basis of these considerations and the data discussed earlier, the superficial slip velocity for a given packing size was assumed to be proportional to both the packing void fraction and the difference in densities of the phases. The resulting relation for the flooding rates in a salt-bismuth system is then

$$(V_{c,flood})^{1/2} + (V_{d,flood})^{1/2} = \left[V_{s,Hg-H_2O} \left(\frac{\Delta\rho}{\Delta\rho_{Hg-H_2O}} \right) \left(\frac{\varepsilon}{\varepsilon_{ref}} \right) \right]^{1/2} \qquad (35)$$

where

$V_{c,flood}$ = continuous-phase superficial velocity at flooding,

$V_{d,flood}$ = dispersed-phase superficial velocity at flooding,

$V_{s,Hg-H_2O}$ = superficial slip velocity for the mercury-water system with the type of packing to be used,

$\Delta\rho$ = difference in densities of the phases,

$\Delta\rho_{Hg-H_2O}$ = difference in densities of mercury and water,

ε = packing void fraction,

ε_{ref} = void fraction of packing for which $V_{s,Hg-H_2O}$ was determined.

Values of $V_{s,Hg-H_2O}$ and associated values of ε_{ref} are given below for the packing sizes studied to date.

Superficial Slip Velocities for Several Packing Sizes and Associated Packing Void Fraction Values

Packing Size (in)	Superficial Slip Velocity (ft/hr)	Reference Packing Void Fraction
1/4	315	0.314
3/8	819	0.684
1/2	1531	0.71

A study of pressure drop, holdup, and flooding rates in a 2-in. ID packed column was made by a group of MIT Practice School students[43/]. Mercury and water were used to simulate bismuth and molten salt.

Two different packing materials were studied: 1/4-in. solid cylindrical packing (which had previously been tested in the 1-in. column) and 3/8-in. Raschig rings. The 1/4-in. packing was tested in order that data from the 1-in. and 2-in. columns could be compared. The agreement between the two sets of data is excellent. Most of the minor differences can be attributed to the small difference in the void fractions of the two columns. Because of wall effects, 1/4-in. material packs more densely (i.e., has a lower void fraction) in 2-in. than in 1-in. columns.

The results for 3/8-in. Raschig rings are shown in Figures 9.43 and 9.45. The pressure drop and holdup curves are similar to those observed earlier with 1/4-in. packing. The flooding curve shown in Figure 9.45 is surprisingly close to that observed previously with 1/4-in. Raschig rings. It appears that the flooding data for 1/4-in. solid packing and for 1/4- and 3/8-in. Raschig rings can be represented by a single curve if the superficial velocities are divided by the void fraction, as shown in Figure 9.45

43/ ORNL-4548, p. 302, February 28, 1970.

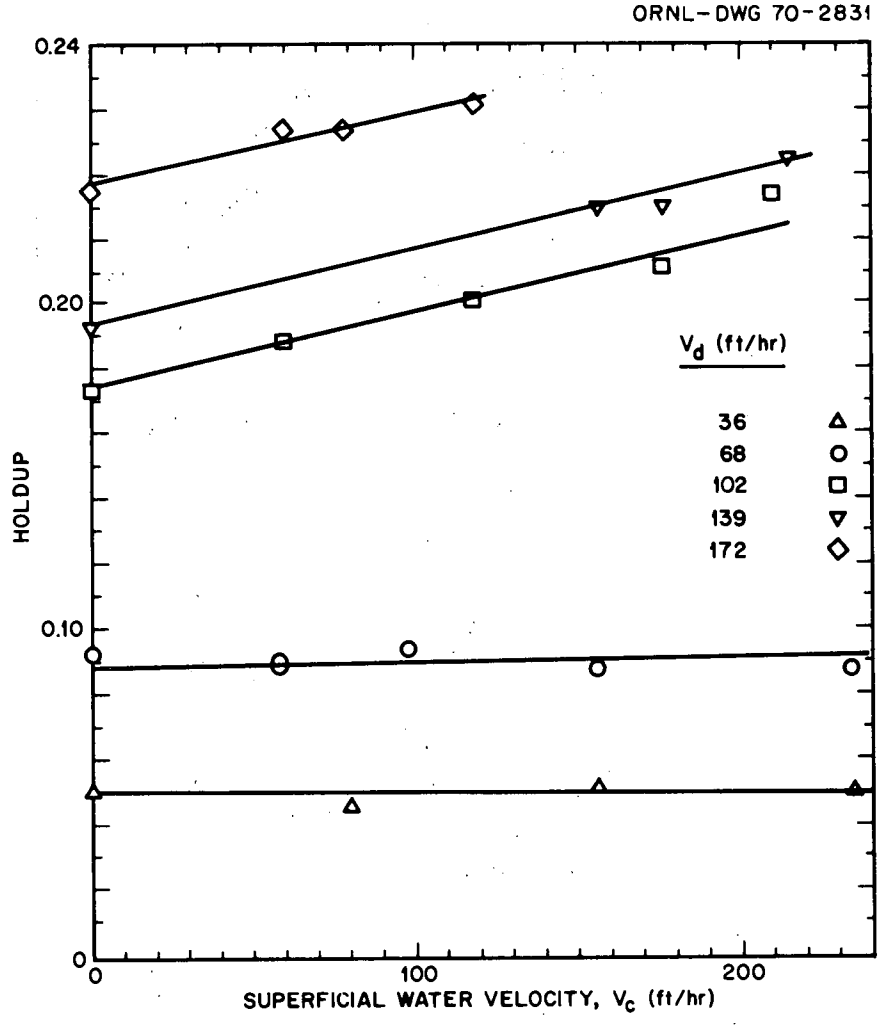

Fig. 9.44. Holdup vs Superficial Water Velocity in a 2-in. Column Packed With 3/8-in. Raschig Rings

ORNL-4548
p 304

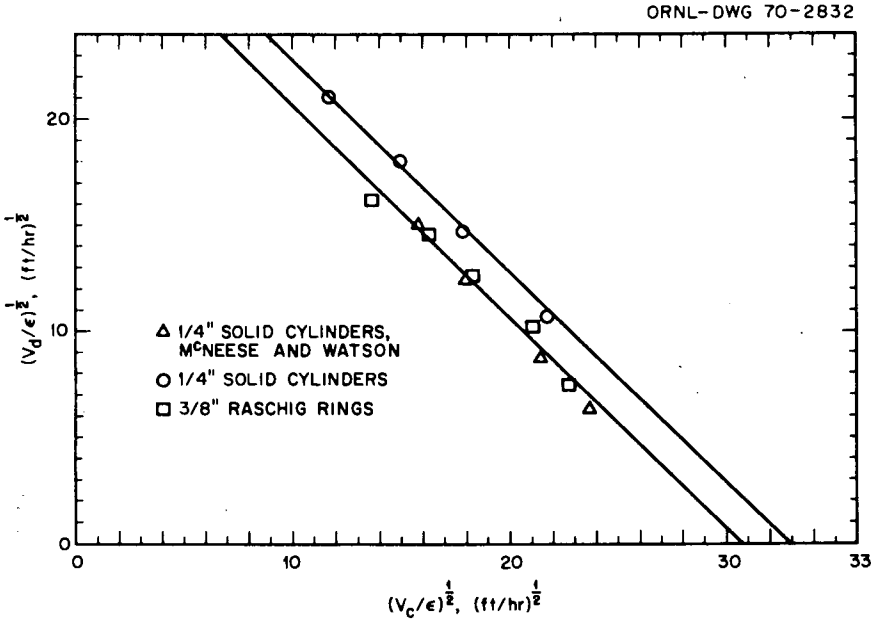

Fig. 9.45 Flooding Lines for 1/4-in. Solid Cylinders and 3/8-in. Raschig Rings.

ORNL-4676
p 259

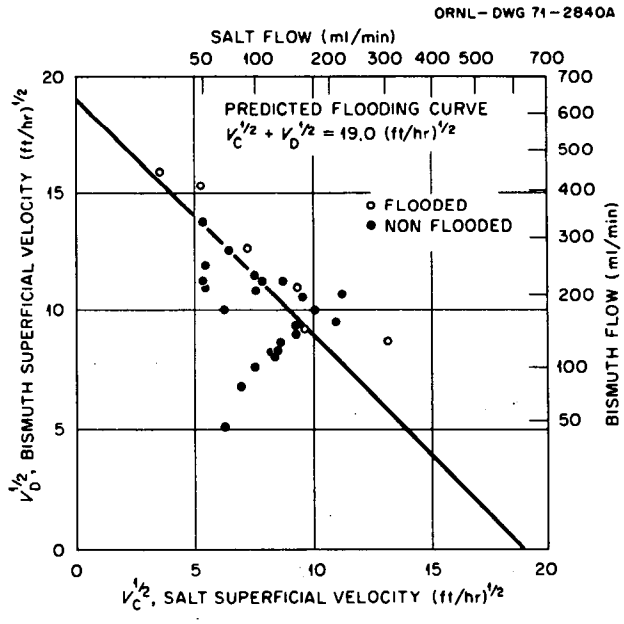

Fig. 9.46 Flooding Data for the Bismuth-Salt System Compared with the Flooding Curve Predicted from Data for a Mercury-Water System. Column, 0.824 in. ID, packed with 1/4-in. Raschig rings, ϵ = 0.84; temperature, 600 C; molten salt, $LiF-BeF_2-ThF_4$ (72-16-12 mole %).

and as indicated in Eq. 31. The resulting curve is linear and has a slope of approximately -1 when the square roots of the phase velocities are plotted against each other. These conditions correspond to a constant slip velocity at flooding. Thus the flooding conditions for these three packing materials, using mercury and water, can be approximated by a single equation,

$$V_c^{1/2} + V_d^{1/2} = 31\varepsilon^{1/2}, \tag{31}$$

where V_c and V_d are the continuous- and dispersed-phase superficial velocities, respectively, expressed in feet per hour, and ε is the void fraction. This expression indictates that the flooding rate does not depend upon the packing size; however, it is believed that the flooding rate will increase with packing sizes larger than 3/8 inch.

The model that had been proposed to relate pressure drop, holdup, and flooding rates from the 1-in. column data predicted flooding rates reasonably well for the 1/4-in. packing. There appears to be some difference between the slopes of the estimated and measured flooding curves, but the estimated curve is still reasonably close to the data. With the 3/8-in. packing, however, the predicted flooding curve was significantly higher than the experimental curve.

Three hydrodynamic experiments in which bismuth and molten salt were countercurrently contacted were made with the new column. The resulting flooding data are compared in Figure 9.46 with values predicted from a flooding correlation developed from studies with a mercury-water system. The agreement between the measured and predicted values is good in that points obtained under nonflooded conditions lie below the predicted flooding curve and points obtained under flooding conditions lie above or close to the flooding curve. This is particularly important because it indicates that simulated systems, such as the mercury-water system, can be used to develop correlations applicable to

9.4.2 Flooding and Pressure Drop Studies in Packed Columns (Cont'd)

bismuth-molten-salt systems. Such correlations aid in the planning and analysis of experiments using molten salt and bismuth and facilitate development of the technology required for designing and operating salt-metal systems.

The final hydrodynamic experiment was carried out to measure pressure drop through the column when only salt was flowing through it. Since only a small pressure drop was expected, it was necessary that the bismuth-salt interface at the bottom of the column be depressed below the salt inlet. This was accomplished by routing the argon off-gas flow through a mercury seal to pressurize the top of the column, the salt overflow sampler, and the salt receiver. Observed pressure drops through the column were 2, 2.5, and 5 in H_2O at salt flow rates of 68, 127, and 224 ml/min, respectively; values predicted by the Ergun equation for these flow rates were 0.5, 1, and 2 in H_2O, respectively.

During the flooding runs, salt flow rates of 50 to 400 cm^3/min were used with argon or hydrogen flow rates of up to 7.5 or 30 liters/min respectively; the temperature was 700 C in each case[44/]. The pressure drop across the column increased linearly with increases in gas flow rate, as shown in Figure 9.47, which summarizes the best data from the ten runs. The salt flow rate was found to have only a minor effect on pressure drop.

Data showing the dependence of slip velocity on continuous-phase viscosity were obtained by an MIT Practice School group. A 2-in. diameter, 24-in. long column packed with 3/8-in Teflon Raschig rings, which were not wet by either phase, was used in the study. The experimental system was modified so that water or water-glycerin solutions could

44/ ORNL-4682, p. 22, March 31, 1971.

ORNL-4622
p 224

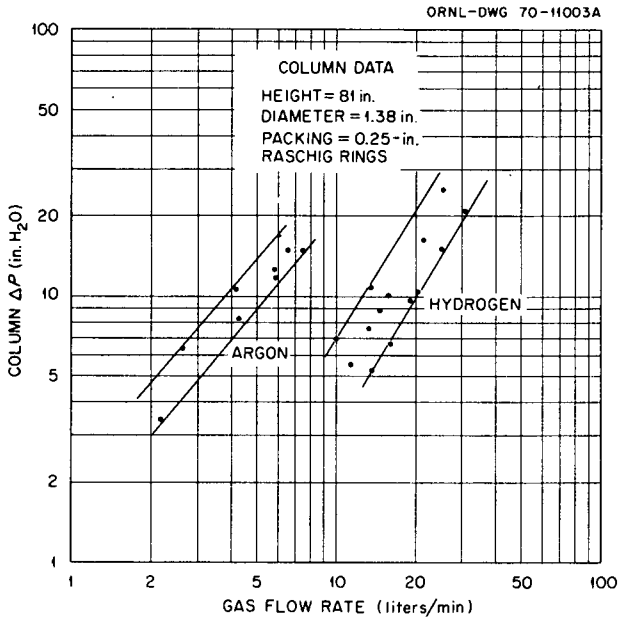

Fig. 9.47 Column pressure drop during counter-current flow of molten salt (66-34 mole % $LiF-BeF_2$) and either argon or hydrogen.

ORNL-4676
p 261

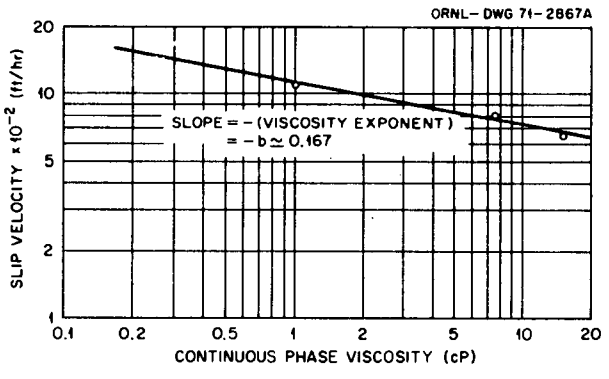

Fig. 9.48 Variation of slip velocity with continuous-phase viscosity in a 2-in-diam column packed with 3/8-in. Raschig rings.

ORNL-DWG 70-4506A

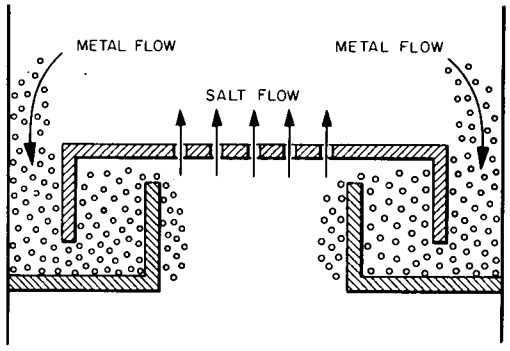

Fig. 9.49 Schematic Diagram of an Axial Mixing Preventer.

ORNL-4548
p 305

ORNL DWG 70-4507

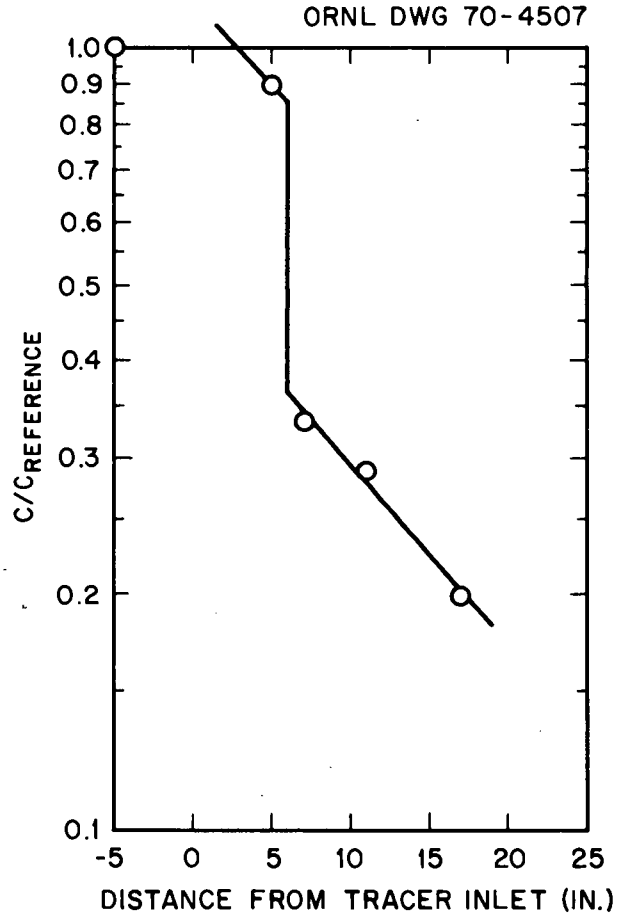

Fig. 9.50 Concentration Profile Using a Backflow Preventer with a Single 3/8-in. Sieve Opening. Mercury flow rate, 400 ml/min; water flow rate, 115 ml/min.

be recirculated through the column at constant temperature by installation of a heat exchanger and an aqueous-phase surge tank. Data were obtained with glycerin solutions having viscosities of 7.5 and 15 cP, as well as with water (which has a viscosity of 1 cP), since repacking a column can alter the slip velocity by as much as 10 percent.

The results obtained were similar to those observed previously for mercury and water. The dispersed-phase holdup could be correlated in terms of a constant slip velocity for the three cases involving nonwetted packing. The relative standard deviations for the slip velocities were about ± 10 percent; no dependence on the flow rate of either phase was noted. The variation of slip velocity with continuous-phase viscosity is shown in Figure 9.48, which indicates that the slip velocity is proportional to the -0.167 power of the continuous-phase viscosity. As expected, the dependence is not large. However, neglect of this effect was significant in the earlier extrapolation from a water-mercury system to a salt-bismuth system since the continuous-phase viscosity changed by a factor of 12.

After the dependence of slip velocity on the continuous-phase viscosity was known, it was possible to reevaluate the dependence of slip velocity on the difference in the densities of the two phases by using the two data points afforded by the mercury-water and the salt-bismuth data. If it is assumed that the dependence of slip velocity on the difference in densities is a power-type dependence, a power of 0.5 is calculated. This result is interesting in that it is the same as the dependence of drop terminal velocity on the difference in densities in the inertial region, where the drag coefficient is essentially constant. The final relation of predicting the variation of slip velocity with packing void fraction, the difference in the densities of the phases, and the continuous-phase viscosity is, then,

9.4.2 Flooding and Pressure Drop Studies in Packed Columns (Cont'd)

$$V_s = V_s\ (Hg\text{-}H_2O) \left(\frac{\varepsilon}{\varepsilon_{ref}}\right) \left(\frac{\mu}{\mu_{H_2O}}\right)^{-0.167} \times \left(\frac{\Delta\rho}{\Delta\rho_{Hg\text{-}H_2O}}\right)^{0.5} \qquad (36)$$

where

V_s = slip velocity,

$V_s(Hg\text{-}H_2O)$ = slip velocity for mercury-water for the packing size considered,

ε = packing void fraction,

ε_{ref} = void fraction for packing for which $V_s(Hg\text{-}H_2O)$ was determined,

μ = viscosity of continuous phase,

μ_{H_2O} = viscosity of water at 20 C,

$\Delta\rho$ = difference in the densities of the phases,

$\Delta\rho_{Hg\text{-}H_2O}$ = difference in the densities of mercury and water for 20 C.

Slip velocity values calculated from Eq. 36 can then be used for determining the throughputs at flooding and the dispersed-phase holdup.

9.5 Axial Mixing in Columns

9.5.1 Packed Columns[45/]

Calculations of predicted reductive extraction column performance indicated that prohibitively long columns would be required because of the axial backmixing in systems requiring high volumetric flow ratios (metal to salt). A rare earth removal system that exploits the small distribution coefficient of the rare earths between the fuel carrier salt and a reducing bismuth phase is a system of this type.

45/ ORNL-4548, p. 304, February 28, 1970.

9.5.1 Packed Columns (Cont'd)

Column modifications which will decrease the effect of axial mixing and thus improve column performance were studied. The proposed modifications involve placing devices at several points along the column to reduce or prevent axial mixing across the column at these points. If the devices are separated by a distance equivalent to one theoretical extraction stage when no backmixing occurs between the stages, the efficiency of the column (height of the column with perfect devices divided by the height of the column with imperfect devices) in the rare-earth system when the flow ratio is 100:1 would be greater than 75 percent if less than 15 percent of the salt flowing through a particular segment is recycled or backmixed to the segment below. These conditions do not appear difficult to achieve and will result in satisfactory column heights (probably less than 3 ft/stage).

The type of device under investigation is illustrated in Figure 9.49. The metal flows down the annular section of the upper piece into what is effectively an inverted bubble cap. As the metal flows over the weir in the lower piece, it forms a seal that forces the salt to pass upward through a sieve plat in the center of the column. The sieve plate is a restriction which can be designed in such a manner that the salt velocity through the openings will be reasonably high when a low salt flow rate is employed. Thus one would expect relatively little back-diffusion of salt through the openings in the sieve plate.

Two designs of "backflow preventers" were tested to date, using mercury and water to simulate bismuth and molten salt. The column was packed with 3/8-in. diameter Raschig rings, and at least one backflow preventer was inserted near the middle of the column. The countercurrent flow of mercury and water was established, and a tracer solution

9.5.1 Packed Columns (Cont'd)

(cupric nitrate) was injected near the top of the column at a constant rate. The solution in the column was analyzed for the tracer at several points down the column on both sides of the backflow preventers. If the logarithm of the tracer concentration is plotted as a function of distance down the column, a discontinuity is observed at the preventor location, as illustrated in Figure 9.50. The ratio of the concentrations at the discontinuity is then a measure of the fraction of solution back-diffusing through the preventer.

The fraction or percentage of backflow through a preventer appears to be principally a function of the water velocity through the sieve opening and of the diameter of the sieve openings. No dependence of backmixing on mercury rate was evident; however, the relatively few changes in mercury rate and the usual data scatter make this conclusion tentative. It is expected that a significant dependence on metal flow rate would be observed if the metal flow rate were increased to the point that complete coalescence was not obtained in the metal downcomer.

Data obtained with the backflow preventers are presented in Figure 9.51. Although there is considerable scatter in the data through which the lines were drawn, the lines are believed to be representative. The first back flow preventer contained a 1/2-in. deep bubble cap and a 1/8-in. thick sieve plate containing four 3/32-in. diameter holes. One can see that the extent of backmixing decreases as the water flow rate increases and that backmixing of less than 15 percent can be expected (water flow rate greater than 90 ml/min or 22 ml/min per hole). The openings were then drilled out to a diameter of 1/4 in., and the top curve shown in Figure 9.51 was obtained. Again one can see the decrease in backmixing as the water flow rate increases.

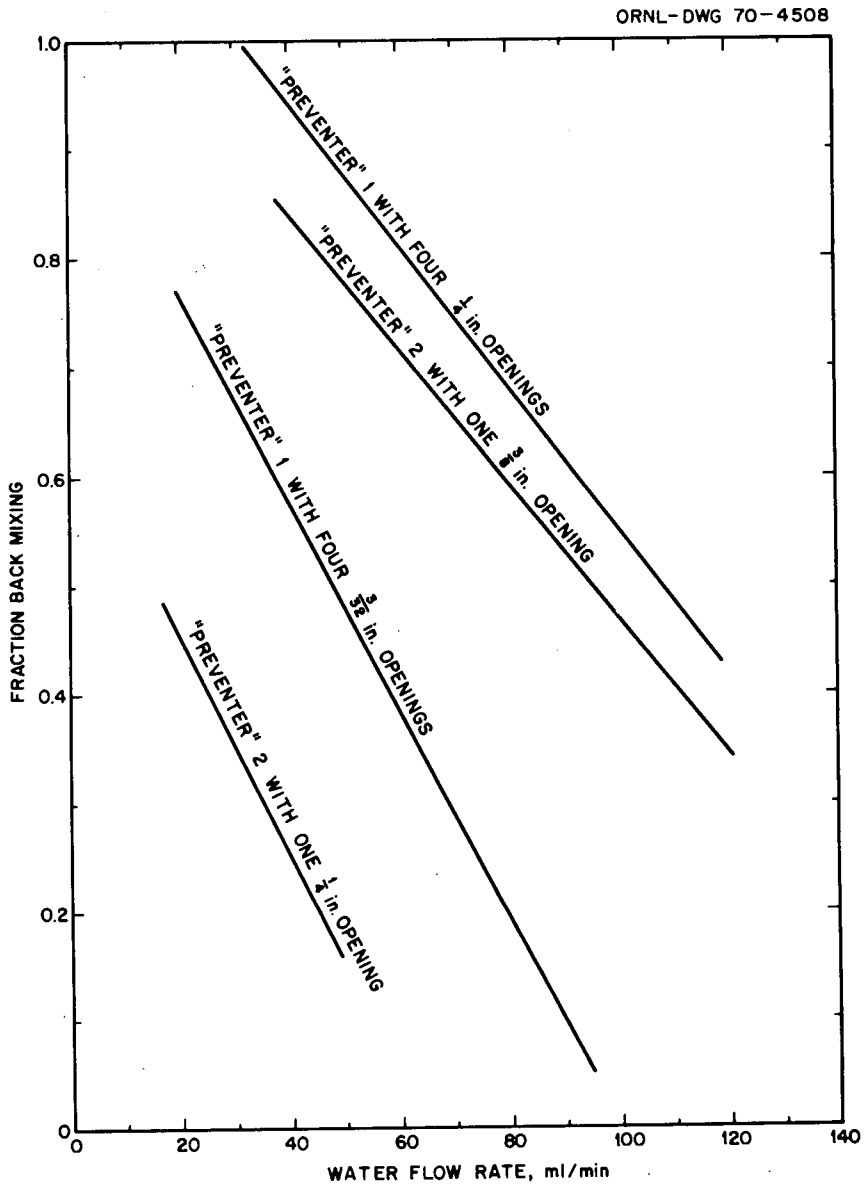

Fig. 9.51. Summary of Backflow Preventer Results

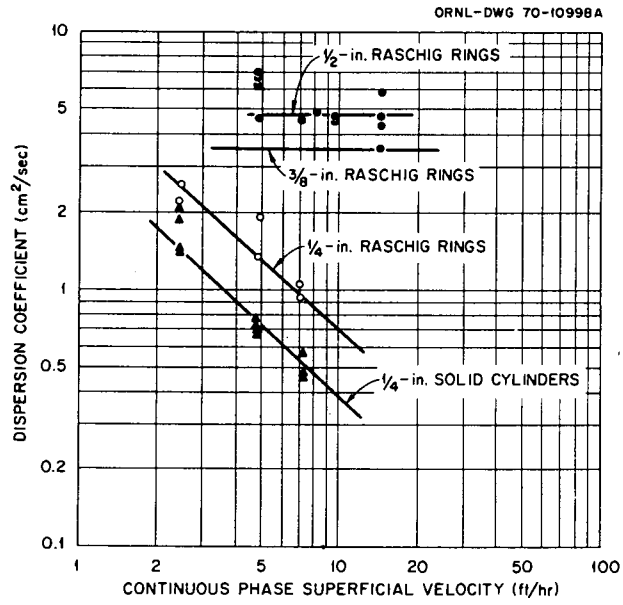

Fig. 9.52. Axial Dispersion Coefficients in Packed Columns during Countercurrent Flow of Mercury and Water.

9.5.1 Packed Columns (Cont'd)

Backmixing did not reach an acceptably low level in any of these experiments; however, an extrapolation of the curve predicts that backmixing would become less than 15 percent at water rates between 150 and 200 ml/min (approximately 50 ml/min per hole). A second preventer, which had a 2-in. deep bubble cap and only a single 1/16-in. diameter opening in the orifice, was tested; however, no backmixing could be detected at the lowest measureable water rate (23.5 ml/min). The diameter of the opening was increased to 1/8 in., but again no backmixing was detected. When the diameter of the opening was increased to 1/4 in., the results shown in Figure 9.51 were obtained. For this preventer, backmixing was less than 15 percent when the water flow rate was greater than 50 ml/min. (This value agrees with the results estimated by extrapolating results from the preventer with four 1/4-in. holes.) The diameter of the sieve opening was then further increased to 3/8 in., and the results shown in Figure 9.51 were obtained. Backmixing was increased considerably by this change in diameter; however, at sufficiently high water flow rates, backmixing can be reduced to any desired percentage.

The only undesirable feature of these backmixing preventers (other than their complexity relative to simple packed columns) is their reduction of the column capacity or flooding rate. The devices just discussed were operated at metal flow rates as high as 94 ft/hr (column superficial velocity), which is approximately 15 percent of the flooding rate for a column packed with 3/8-in. Raschig rings. At the lower metal rates an accumulation of uncoalesced and coalesced mercury was noted above the backflow preventer, but as the metal throughput was increased, it appeared that back-transfer of water through the preventer occurred. It is expected that the design can be improved in order to allow higher metal flow rates.

9.5.1 Packed Columns (Cont'd)

These experiments have demonstrated that devices can be designed to reduce backmixing to an acceptable level. Although the acceptable level has been defined to be about 15 percent, one could achieve even lower values if desired. The principal design parameters are the diameter of the sieve opening and the salt flow rate per hole. Although openings 3/8 in. in diameter or greater could be used, the required water or salt velocity increases very sharply as the hole size increases. At present, 1/4-in. diameter openings appear to be a good choice and will be effective with a flow rate as low as 50 ml/min per hole. The devices are relatively simple; however, the column capacity is decreased. A greater column capacity may be achieved with larger diameter columns in cases where larger bubble caps can be employed.

Figure 9.52 provides a comparison of the data obtained during this reporting period for 1/4-in. Raschig rings, 1/4-in. solid cylinders, and 1/2-in. Raschig rings with the previous results for 3/8-in. Raschig rings.

In each case the axial dispersion coefficient was independent of the dispersed-phase (mercury) flow rate. Dispersion coefficients for 3/8- and 1/2-in. packing were also independent of the continuous-phase (water) flow rate; their values were 3.5 and 4.8 cm^2/sec, respectively. Data for the 1/4-in. packing indicate that the dispersion coefficient is inversely proportional to the continuous-phase flow rate. Differences between the dispersion coefficients for the two 1/4-in. packing materials are probably related to the difference in the packing void fractions of the materials. The data appear to portray two types of behavior, one for 1/4-in. packing and one for larger packing.

Axial dispersion coefficient data obtained during countercurrent flow of liquids having low densities and small

9.5.1 Packed Columns (Cont'd)

differences in densities in columns packed with materials that are wet by the liquids are reported in the literature. Data of Vermeulen, Moon, Hennico, and Miyauchi[46/] suggest that, for conditions corresponding to the present studies, the dispersion coefficient should be proportional to the quantity

$$\varepsilon_d^{1/2} \frac{V_d}{(V_c)^{1/2}},$$

where

ε = packing void fraction,

d = packing diameter,

V_d = superficial velocity of the dispersed phase,

V_c = superficial velocity of the continuous phase.

The data obtained in the present study are not in agreement with the predicted dependence on flow rates. However, it should be noted that the conditions of the present study are significantly different from those for which the reported correlation was developed. Lack of agreement is not surprising, since similar differences in behavior have been observed previously between the mercury-water system and aqueous-organic systems.

a - Estimation of Axial Backmixing in Both Phases in Countercurrent Contactors

An approximate equation that predicts the effects of axial backmixing in one phase on the performance of a countercurrent contactor. This equation was useful in estimating the column heights required in the protactinium and rare-earth removal system. A similar empirical equation has been developed to predict column

46/ Chem. Eng. Prog. 62, 95 (1966).

9.5.1 Packed Columns (Cont'd)

a - Estimation of Axial Backmixing in Both Phases in Countercurrent Contactors (Cont'd)

performance when backmixing occurs in both phases. The proposed equation is:

$$\eta \approx 1 - \frac{1}{N_{Pex} + 1 - F + 1/NTU} - \frac{F}{N_{Pey} - 1 + F + 1/NTU} \tag{37}$$

where

η = the length of the column without backmixing divided by the length of the column with backmixing,

N_{Pex} = Peclet number in phase x = $U_x(HTU_p)/E_x$,

N_{Pey} = Peclet number in phase y = $U_y(HTU_p)/E_y$,

HTU_p = height of a transfer unit with phase flow,

U_x = superficial velocity of the reference phase,

E = axial diffusion coefficient,

F = extraction factor = mU_x/U_y,

m = distribution coefficient,

NTU = number of transfer units required to achieve a given separation if the phases are in plug flow.

This equation predicts efficiencies to within approximately 0.07 (i.e., the difference between the estimated and the calculated efficiency will be less than 0.07) when

$NTU \geq 2$,

$\eta \geq 0.2$,

$N_{Pex} \geq F - \frac{1}{NTU}$,

and

$N_{Pey} \geq 1.5$.

9.5.2 Open Columns[47,48]

A study of axial mixing in a 2-in. diameter open column during the countercurrent flow of air and glycerol or butanol solutions was completed at the MIT Practice School.

Molten salts of interest have a viscosity of about 30 centipoises; water (used in previous studies) has a viscosity of approximately 1 centipoise; and the viscosity of the glycerol solution used in this study is 15 centipoises. The surface tension of molten salts of interest is 100 to 200 dynes/cm, while that of the butanol solutions varied between 37.8 dynes/cm and the value for water (72 dynes/cm).

The results of the study are summarized in Figure 9.53, which shows the dispersion coefficient as a function of the air flow rate. The dashed line represents the earlier results of Bautista and McNeese, who found that the data fall into two regions. The first region, which covers low air flow rates, corresponds to conditions when individual bubbles formed at the orifice travel up the column without coalescence. The second region, which occurs at air flow rates above 30 cm^3/sec, corresponds to "slugging" flow.

Increasing the liquid viscosity to 15 centipoises (by adding glycerol) decreased the dispersion coefficient in the "bubble" (lower) region; however, the transition point between the regions was not changed. The coefficient increased more rapidly with air flow rate in the slugging region, at least up to the curve by Bautista and McNeese.

Decreasing the surface tension increased the dispersion coefficient in the bubble region, although there is little difference between the data obtained from a solution having a surface tension of 37.8 dynes/cm and those obtained from

---

47/ ORNL-4548, p. 307, February 28, 1970.

48/ ORNL-4682, p. 31, March 31, 1971.

9.5.2 Open Columns (Cont'd)

a solution having a surface tension of 53.2 dynes/cm. The transition point occurred at a higher air flow rate, and the bubble region curve intersected the slugging region curve of Bautista and McNeese. The dependence of the dispersion coefficient on air flow rate appears to be somewhat greater than that observed with air and water, but insufficient data are available to reach a definite conclusion on this point.

This study was especially useful since it represented the first systematic attempt to vary physical properties in a bubble column. The data obtained indicate that higher viscosity and higher surface tension lead to lower dispersion coefficients,which is in the favorable direction for molten-salt systems. However, the variation of physical properties did not cover a wide range of conditions; also, when liquid mixtures are used, there is always a possibility that one component will concentrate at the interface and result in properties in this region which do not correspond to conditions in the bulk liquid.

Additional data showing the importance of column diameter and gas inlet diameter have been obtained in a study at the MIT Practice School using air-water system. The experimental technique consisted in measuring the concentration profile of a tracer along the length of the column. Results obtained with three gas inlet diameters (0.04, 0.06, and 0.085 in. ID) in a 2-in ID, 6-ft long column are shown in Figure 9.54. The dispersion coefficient is seen to be independent of gas inlet diameter for the size range studied. We have also made similar measurements in 1-1/2- and 3-in. diameter columns using inlet diameters ranging from 0.04 to 0.17 inch. No effect of gas inlet diameter was found.

It is not surprising that the dispersion coefficient is

ORNL-4548
p 308

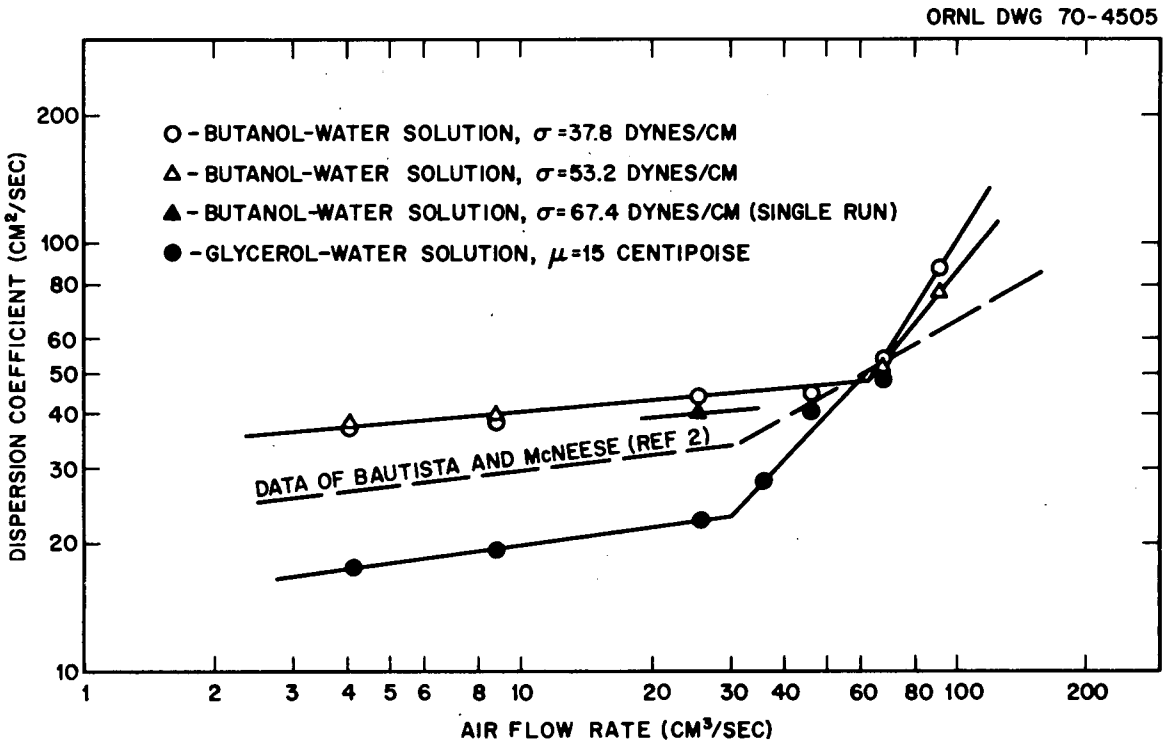

Fig. 9.53 Effect of Gas Flow Rate, Liquid-Phase Viscosity, and Surface Tension on Axial Dispersion Coefficient.

ORNL-4622
p 216

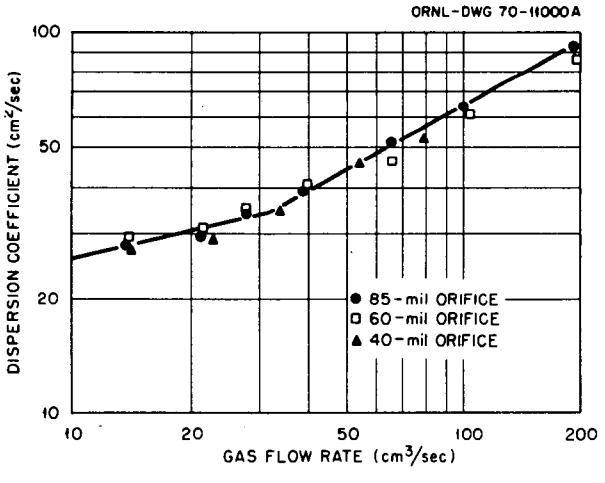

Fig. 9.54 Effect of Gas Flow Rate and Orifice Diameter on Axial Dispersion in a 2-in.-diam Open Column.

ORNL-4122
p 217

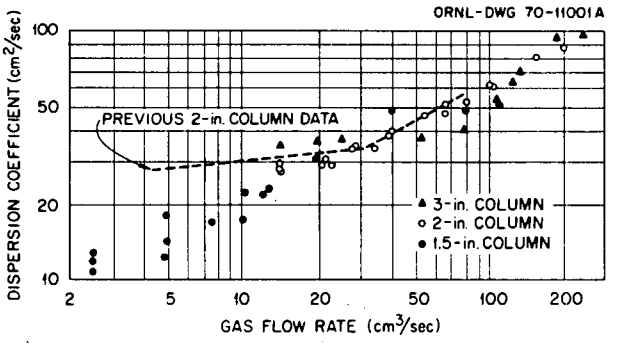

Fig. 9.55 Effect of Column Diameter on Dispersion Coefficient in an Open Column.

ORNL-4676
p 266

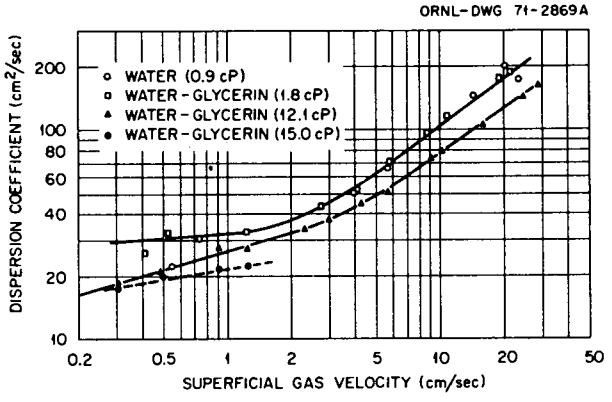

Fig. 9.56 Variation of dispersion coefficient with superficial gas velocity and column diameter in open bubble columns.

ORNL-4344
p 297

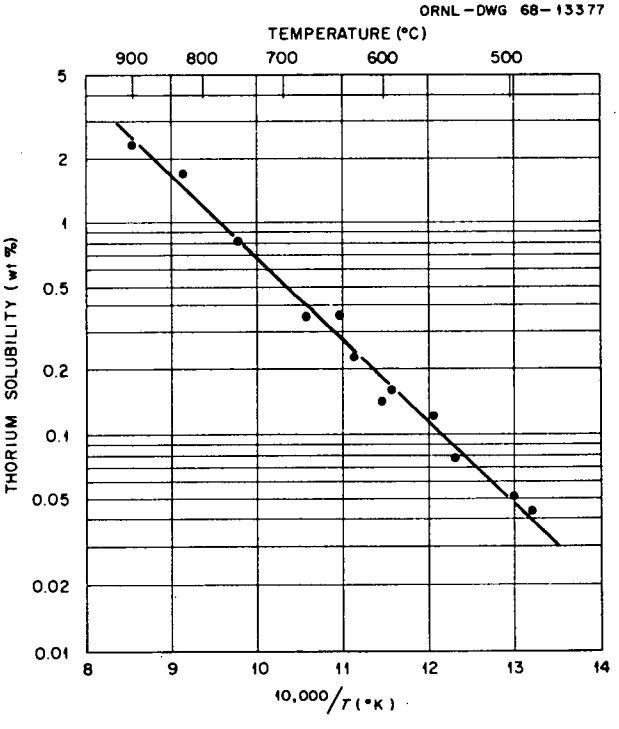

Fig. 9.57 Solubility of Thorium in Bismuth At Various Temperatures.

ORNL-4396
p 287

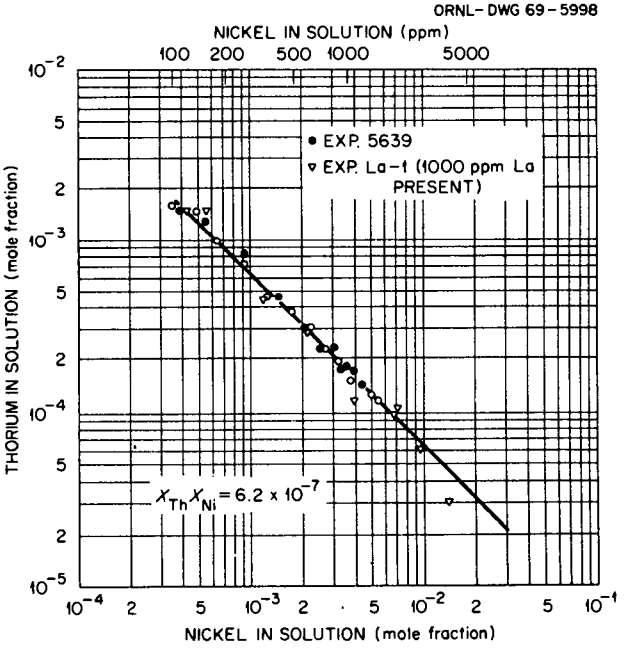

Fig. 9.58 Mutual Solubility of Thorium and Nickel in Bismuth at 600 C.

9.5.2 Open Columns (Cont'd)

independent of gas inlet diameter in the slugging region (high gas flow rates), since a great deal of bubble coalescence occurs and the final bubble population may be essentially independent of the gas inlet diameter. However, in the bubbly region (low gas flow rates), little coalescence occurs, and gas inlet diameter would appear to be more important. It has been postulated that chain bubbling occurs at low gas rates (i.e., that gas bubbles are not formed consecutively). In this case the bubble diameter would not be highly dependent on the gas inlet diameter.

Even with different bubble diameters, one would not expect large differences in bubble rise velocities, and possibly the changes in dispersion coefficients would be small. Davies and Taylor report that the bubble rise velocity is proportional to the 1/6 power of the bubble volume. Thus, even for conditions resulting in the release of single bubbles (i.e., where bubble volume is proportional to the cube root of the inlet diameter), one would find little variation in rise velocities with changes in inlet diameter, and hence little variation in dispersion coefficient.

Figure 9.55 shows the effect of column diameter on dispersion coefficient for 1.5-, 2-, and 3-in. diameter columns. In the slugging region the dispersion coefficient data from the three columns showed little difference for a given volumetric gas flow rate. These data, however, do not extend to high gas rates for all column diameters; therefore, extrapolation to larger gas flow rate values is questionable. In the bubbly region, results from the 2-in. and 3-in. diameter columns are essentially the same. Results for the 1-1/2-in. column indicate significantly lower values for the dispersion coefficient and show a greater dependence on gas flow rate than has been observed for the larger columns.

9.5.2 Open Columns (Cont'd)

Continuous fluorinators are envisioned as open columns through which fluorine is bubbled countercurrent to a flow of molten salt. Efforts were directed toward developing an improved experimental technique, which was then used to study the variation of dispersion coefficient with changes in column diameter, gas inlet design, and liquid physical properties. The experimental technique is a transient one that involves injecting a small quantity of KCl solution at the top of the column and observing the rate of buildup of tracer at the bottom of the column. The KCl concentration is measured with a small conductivity probe. Earlier studies, which used a steady-state technique, demonstrated that the axial dispersion coefficient is not dependent on the superficial velocity of the liquid in the range of interest; hence, the transient studies were carried out with no flow of liquid through the column. This was particularly useful for studying the effect of the physical properties of the liquid since relatively small volumes of solution were required.

The variation of dispersion coefficient with column diameter and superficial gas velocity is shown in Figure 9.56 for column diameters ranging from 1 to 6 in. and superficial gas velocities ranging from 0.25 to 64 cm/sec. The effect of changes in the viscosity of the liquid in the range 0.9 to 15 cP was determined with water-glycerin solutions. Viscosity had little effect in 3- and 6-in. diameter columns; however, increasing the viscosity from 1.0 to 15 cP reduced the dispersion coefficient in 1.5- and 2-in. diameter columns by as much as 20 percent. Since the diameter of continuous fluorinators will be 6 in. or larger, the viscosity of the liquid will not affect the dispersion coefficient. The effect of surface tension was studied using butanol and isopropanol solutions; the dispersion coefficient was found to decrease as the surface tension

9.5.2 Open Columns (Cont'd)

was decreased. The number and size of the gas inlets were found to be important only for gas superficial velocities below the slugging region.

9.6 Solubilities in Reductive Extraction

9.6.1 Thorium in Bismuth[3/]

The results of a prior study indicated that the solubility of thorium in liquid bismuth at 600 C was about 3000 wt ppm. Since the thorium concentrations obtained at D_{Th}^{max} in reductive extraction experiments were only about 2000 wt ppm, direct measurements of the solubility were made to determine whether the literature value was high or whether some other component, for example, lithium, present in the reductive extraction systems was depressing the thorium solubility. Measurements were made in the temperature range 482 to 817 C. The system was contained in a mild-steel crucible under an argon atmosphere. Sufficient crystal-bar thorium was used to ensure saturation at temperatures as high as 950 C. Samples of the saturated liquid were removed for analysis using a variety of stainless steel vacuum-type filters.

A plot of log S vs 1/T, presenting average solubility values at several temperatures, is shown in Figure 9.57. The line through the points is

$$\log S \text{ (wt ppm)} = -3850/T + 7.677 \qquad (38)$$

These solubility data are in excellent agreement with the values indicated by reductive extraction experiments at 600 to 700 C, suggesting that the presence of lithium, uranium, rare earths, and other elements in low concentration have no marked effect on the thorium solubility.

9.6.2 Protactinium and Thorium in Bismuth[37/]

The feasibility of the proposed protactinium recovery process has been subjected to question because it had not

9.6.2 Protactinium and Thorium in Bismuth (Cont'd)

been demonstrated that protactinium was sufficiently soluble in bismuth, U-Bi, and Th-Bi solutions for process application. A calculation of the concentration profiles expected in a reductive extraction contactor indicated that the solubility of protactinium in bismuth had to be at least as high as that of throium and that protactinium had to be soluble to about 1000 wt ppm when the concentrations of uranium or thorium in the bismuth were about 1000 wt ppm if the desired process conditions were to be attained.

Experiment PE7 was conducted in an attempt to demonstrate that the desired process conditions could be met.

Subsequent analyses of samples of the metal phase (Table 9.27, samples 2 and 3) yielded protactinium concentrations as high as 2078 wt ppm. Since raising or lowering the temperature by 50° produced no significant change in the protactinium concentration in the bismuth (Table 9.27, samples 4, 5 and 7), it was concluded that the solubility of protactinium in bismuth is at least 2050 wt ppm at 550 C. When the temperature was lowered to 500 C, the protactinium concentration in the bismuth decreased to about 1200 wt ppm (Table 9.27, sample 6), with a corresponding decrease in protactinium material balance. Assuming that the solubility at 500 C is about 1200 wt ppm and that the apparent heat of solution is about the same as that of thorium, the solubility of protactinium in bismuth at 600 C is estimated to be about 4500 wt ppm.

These results show that one objective of experiment PE7, the demonstration of the mutual solubility of protactinium and thorium at the 1000-ppm level, was not met. Since thorium and lithium were present in amounts much less than originally thought, the reported number of 1200 ppm is probably very close to the true solubility of protactinium in bismuth at 500 C. Furthermore, the original conclusion that the solubility of protactinium in bismuth is high enough for process application is still valid.

Table 9.27

Results of Experiment Pe7, Demonstrating the High Solubility of Protactinium and Uranium in Bismuth

Sample	Temperature (C)	Total Time (Days)	Concentration in Metal Phase (Wt ppm)		
			Pa	Th[a]	U
1[b]	600	0.16	1,124		
2	600	3.0	1,874		
3	600	5.0	2,078	60	
4	650	5.1	2,078	60	
5	560	6.0	2,078		
6	500	7.0	1,199	40	
7	550	7.3	2,059	60	
8[c]	600	9.0	668	17	1,090

(a) These thorium concentrations were calculated from the measured protactinium distribution coefficient and the Pa-Th separation factor determined in a separate experiment with $LiF-BeF_2$ (66-34 mole %).

(b) A small amount of thorium was added to the metal phase after this sample was taken.

(c) A small amount of UF_4 was added before this sample was taken.

9.6.2 Protactinium and Thorium in Bismuth (Cont'd)

Toward the end of experiment PE7, sufficient UF_4 was added to the system to effect oxidation of some of the protactinium from the metal phase. Under the equilibrium condition established, the metal phase contained about 668 ppm Pa and 1090 ppm U, with corresponding uranium and protactinium material balances of nearly 100 percent. Thus the mutual solubility of uranium and protactinium in bismuth appears to be high.

9.6.3 Effect of Nickel on Thorium in Bismuth[49/]

Data obtained show that the thorium solubility at 600 C (about 2000 wt ppm) is not affected by the presence of uranium and zirconium at concentrations of 2000 ppm, either singly or in combination. Similar results were obtained with uranium, plutonium, and thorium; solutions containing about 2000 ppm thorium and at least 2000 ppm uranium and plutonium have been produced. Lithium and lanthanum, in concentrations up to about 1000 ppm, had no detectable effect on the thorium solubility. Nickel was the only element encountered in this work that had a marked effect.

The effect of nickel on the solubility of thorium in bismuth at 600 C was investigated in two experiments. The results are shown in Figure 9.58. The solid circles were obtained in experiment 5639 by back titration with crystal-bar thorium. The data from these experiments can be expressed as a mole fraction solubility product,

$$K_{xp} = X_{Th}X_{Ni} = 6.2 \times 10^{-7} \qquad (39)$$

over the range of concentrations investigated. This is the type of behavior expected if the Th/Ni atom ratio in the solid phase were 1. This appeared to be the case; by material balance calculations, the Th/Ni atom ratio in the

49/ ORNL-4396, p. 287, February 28, 1969.

9.6.3 Effect of Nickel on Thorium in Bismuth (Cont'd)

solid phase was 0.90 to 0.99 throughout each experiment. No attempt was made to isolate and identify the solid phase. It could be ThNi (which would not be inconsistent with the reported Th-Ni phase diagram), or it could be a ternary bismuthide, $ThNiBi_x$. The data indicate that a bismuth solution saturated with thorium at 600 C could accomodate up to about 100 ppm nickel before precipitation of a thorium- and nickel-containing solid would occur. It was also of interest to note that the lanthanum concentration in the liquid phase remained unchanged, even when the nickel concentration was 5000 ppm.

9.6.4 Bismuth in Fuel Salt[50/]

During the chemical processing of MSBR fuel by either the reductive extraction or the metal transfer process, the fuel salt will be contacted with liquid bismuth before it is returned to the reactor. Since nickel-base alloys are corroded by bismuth, the presence of bismuth in the salt could cause serious damage to a reactor vessel constructed of Hastelloy N. Therefore a means for ensuring that the fuel salt being returned to the reactor is free of bismuth must be devised. Attempts have been made to measure the solubility of bismuth in $LiF-BeF_2-ThF_4$ (72-16-12 mole percent).

About 125 g of salt and 5 g of bismuth were heated to 700 C in a mild steel container under an atmosphere of purified argon. Filtered samples of the salt were taken periodically and were analyzed for bismuth by both a polarographic and a spectroscopic method. After 75 days at 700 C, the system was cooled to 600 C, where it was held for an additional 35 days. Although the analytical data obtained in this experiment are erratic and inconsistent(Table 9.29),it is obvious that the solubility of

50/ ORNL-4548, p. 292, February 28, 1970.

Table 9.29

Analytical Results Obtained in Experiment to Determine the Solubility of Bismuth in $LiF-BeF_2-ThF_4$ (72-16-12 Mole %)

Temperature (C)	Time at Temperature (Days)	Sample	Bismuth Analysis of Salt (ppm) Polarographic Method	Spectrographic Method
700	8	1	10	9.2
		2		4.3
	15	3	4.5	0.6
		4		0.55
	40	5	5.0	
		6		0.5
	56	7	2.0	2.8
		8	2.0	2.0
	75	9	<1	1.9
		10	1.5	1.5
600	14	11	1.5	2.9
		12	7.0	4.4
	35	13	0.2	
		14	0.56	

9.6.4 Bismuth in Fuel Salt (Cont'd)

bismuth in the salt was low (<5 ppm) under the conditions used. The cause of the disparity between the two analytical methods is not known and must be found before meaningful data can be obtained.

9.6.5 Neodymium in Lithium-Bismuth-Thorium Solutions[51/]

In the first experiment the solubility of neodymium in liquid lithium-bismuth (~38-62 at. percent) was measured over the temperature range 475 to 700 C. The experiment was initiated by heating bismuth, neodymium, and lithium (about 186, 10, and 4 g, respectively) in a molybdenum crucible under argon to 475 C and maintaining the system at this temperature for 24 hours before sampling the liquid phase. The temperature of the system was then increased progressively to 700 C; after reaching 700 C the temperature of the system was lowered incrementally to 475 C. At least 4 hours was allowed at each temperature for the attainment of equilibrium before a filtered sample of the liquid phase was removed for analysis. Flame photometric analyses of the samples indicated a variation in lithium concentration between about 1.9 and 2.2 wt percent during the experiment; the average lithium concentration was 2.0 wt percent, which corresponds to 38 at. percent in the liquid phase. The results of neutron activation analyses of the samples for neodymium are shown in Figure 9.59 as a plot of $\log_{10}S$ (wt percent neodymium) vs 1/T (^{o}K). The absence of a hysteretic effect in this plot indicates that equilibrium was attained at each temperature. The solubility data can be expressed as

$$\log_{10}S \text{ (wt ppm neodymium)} = 6.257 - 1809/T \ (^{o}K).$$

As seen in Figure 9.59, these values are considerably higher than the reported solubility of neodymium in pure bismuth.

51/ ORNL-4622, p. 207 August 31, 1970.

9.6.5 Neodymium in Lithium-Bismuth-Thorium Solutions (Cont'd)

Following the determination of neodymium solubilities, about 1 g of thorium was added to the system. Analyses of filtered samples showed that at 650 C the solubility of thorium in liquid Li-Bi-Nd (38.0-61.1-0.9 at. percent) was less than 15 wt ppm. For comparison, the solubility of thorium in liquid bismuth at 650 C is about 3500 wt ppm.

9.6.6 Thorium and Neodymium in Lithium-Bismuth Solutions[52/]

Solubilities of thorium and neodymium in several lithium-bismuth solutions were measured. The results are summarized in Tables 9.30 and 9.31 and are shown graphically in Figures 9.60 and 9.61. At each temperature below 750 C, the thorium solubility in lithium-bismuth solutions increased by about a factor of 3 as the lithium concentration in the solution increased from 0 to about 40 at. percent. Similarly, the neodymium solubility increased regularly as the lithium concentration increased from 0 to 25 at. percent. However, when the lithium concentration was increased from 25 to 38 at. percent at 640 C, the neodymium solubility decreased to about the same value that was obtained with pure bismuth as the solvent (Figure 9.61). We are redetermining the neodymium solubilities in Li-Bi (40-60 at. percent) to confirm this behavior.

A series of experiments was conducted in an attempt to measure the mutual solubilities of thorium and neodymium at 640 C in lithium-bismuth solutions having lithium concentrations ranging from 0 to 20 at. percent. The mutual solubility limit was approached by making incremental additions of neodymium to the thorium-saturated liquid lithium-bismuth solution. The data obtained in this series of experiments were somewhat scattered, due primarily to the difficulty in analyzing for thorium at a relatively low concentration (less than 0.35 wt percent) in the presence of neodymium at a high concentration (up to about 2 wt percent). However, the following general conclusions

52/ ORNL-4682, p. 15, March 31, 1971.

ORNL-4622
p 207

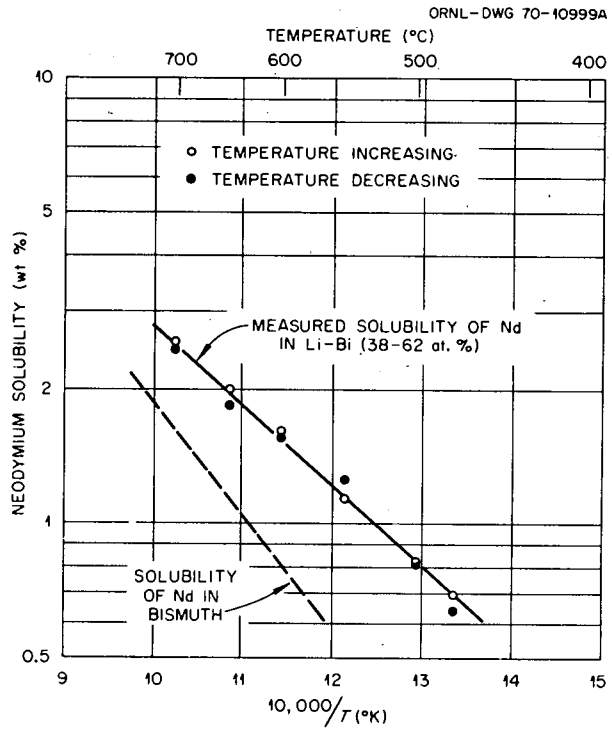

Fig. 9.59 Solubility of Neodymium in Lithium-Bismuth (38-62 at. %).

ORNL-4676
p 245

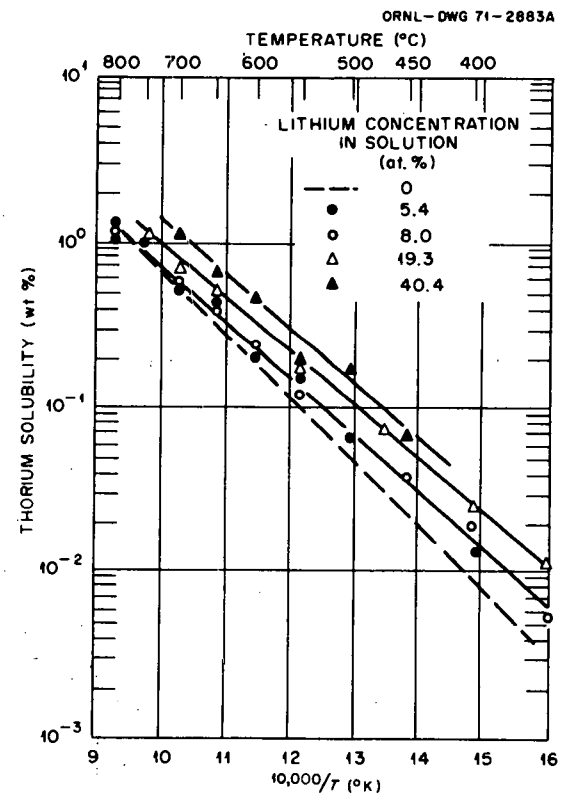

Fig. 9.60 Thorium solubility in lithium-bismuth solutions. Data for 0 at.% lithium taken from ref. 26.

ORNL-4676
p 245

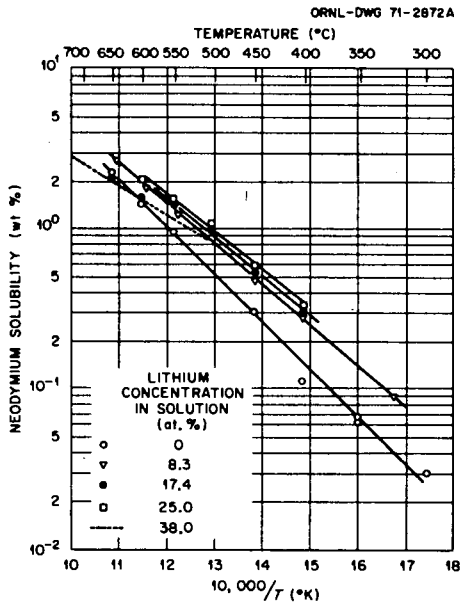

Fig. 9.61 Solubility of neodymium in lithium-bismuth solutions. The solubility of neodymium in lithium-bismuth (38-62- at.%) was taken from ref. 11. The solubility of neodymium in bismuth (lithium = 0 at.%) should be considered preliminary.

ORNL-4548
p 174

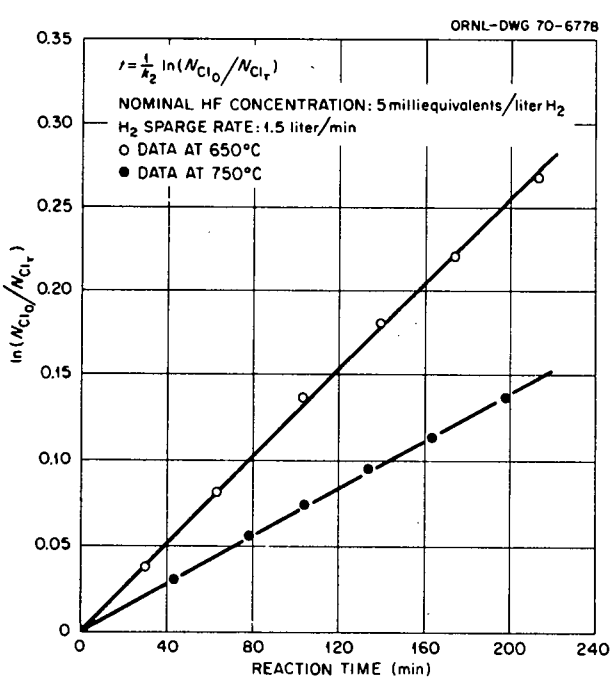

Fig. 9.62 Relative Rate of Removal of Chloride from Lif-Bef$_2$-ThF$_4$ (72-16-12 Mole %) by HF-H$_2$ Sparge at 650 and 750 C.

ORNL-4548
p 174

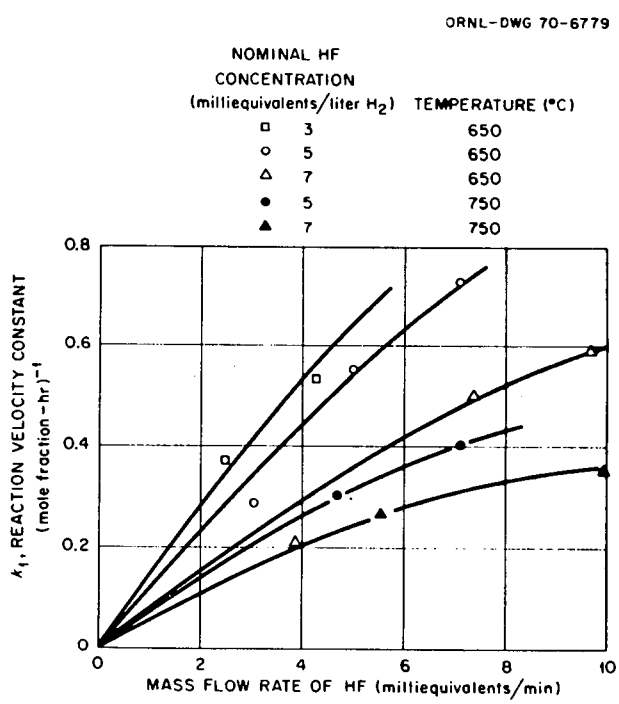

Fig. 9.63 Effect of Gas Sparge Conditions on the Removal of Chloride from LiF-BeF$_2$-ThF$_4$ (72-16-12 Mole %) by Reaction with HF at 650 and 750 C.

Table 9.30

Solubility of Thorium in Liquid Lithium-Bismuth Solutions

Li Concentration in Solution (At. %)	Temperature Range (C)	Thorium Solubility, Log S_{Th} (Wt ppm) = A + B/T(°K)	
		A	B
0	350 - 800	7.708	-3,852
5.4	350 - 800	7.073	-3,205
8.0	350 - 800	7.073	-3,205
19.3	400 - 750	7.133	-3,164
40.4	450 - 750	7.473	-3,333

Table 9.31

Solubility of Neodymium in Liquid Lithium-Bismuth Solutions

Li Concentration in Solution (At. %)	Temperature Range (C)	Neodymium Solubility, Log S_{Nd} (Wt ppm) = A + B/T(°K)	
		A	B
0	500 - 700	6.68	-2,200
8.32	400 - 700	7.19	-2,531
17.4	450 - 700	7.11	-2,435
25.0	450 - 700	7.07	-2,379
38	475 - 700	6.26	-1,809

9.6.6 Thorium and Neodymium in Lithium-Bismuth Solutions (Cont'd)

can be drawn from the data: (1) Neodymium, in concentrations below about 1 wt percent, appeared to have no effect on the thorium solubility (about 0.35 wt percent) in lithium-bismuth solutions at 640 C; as the neodymium concentration was increased from 1 to about 2 wt percent (saturation), the thorium concentration decreased almost linearly from about 0.35 to about 0.1 wt percent. (2) The effect appeared to be reversible. Additions of thorium to lithium-bismuth solutions saturated with neodymium caused a decrease in the neodymium concentration to about 1 wt percent as the thorium concentration increased to about 0.35 wt percent.

The above results indicate that the mutual solubility of thorium and rare earths should be much higher than required in the solution, Li-Bi (5-95 at. percent), proposed for stripping of the trivalent rare earths (La,Pm,Nd) from the LiCl acceptor salt.

9.6.7 Lithium and Bismuth in Lithium Chloride[24/]

Argonne National Laboratory has reported that equilibration of molten LiCl-LiF (75-25 mole percent) with liquid Li-Bi alloys resulted in a significant solubilization of both bismuth and lithium in the salt phase. For example, with Li-Bi (50-50 at. percent) as the metal phase, the bismuth and lithium solubilities in the salt phase were about 150 and 20 wt ppm, respectively, at 650 C.

In initial experiments, molten LiCl is being equilibrated with liquid Li-Bi (32-68 at.percent) and with solid Li_3Bi. At present preliminary data indicate that the bismuth concentration in the salt in equilibrium with the liquid Li-Bi solution is 300 to 400 wt ppm in the temperature range 650-750 C. The corresponding lithium concentrations have not yet been accurately determined, and no data are available from the system involving solid Li_3Bi.

9.7 Removal of Chloride from Fuel Salt[53/]

In MSBR fuel reprocessing technology, lithium chloride is employed for the back extraction of rare earths from bismuth to effect their separation from thorium. This close coupling of molten LiCl to the reactor system could possibly result in the contamination of the fluoride fuel mixture with chloride ion. Although this event would probably not affect the physical and chemical properties of the fluoride mixture, chloride concentrations as low as 20 ppm (1 percent of N_{UF4}) would have a significant effect on the neutron economy of the breeder reactor. Therefore an experimental program has been conducted to examine the feasibility of an HF-H_2 sparge treatment for removing chloride from a simulated MSBR fuel solvent mixture and to provide a basis for perliminary engineering design of a process system. Specifically, equilibrium quotients and velocity constants were determined for the reaction

$$Cl^- + HF \rightleftharpoons F^- + HCl \qquad (40)$$

as functions of temperature, HF concentrations in H_2, and gas sparge rates.

The reaction vessel was constructed from a 16-in. length of 4-in. IPS nickel pipe with welded end closures of 1/4-in. nickel plate. Penetrations through the top plate provided for insertion of a 1/4-in. gas sparge tube and a thermowell, for gas exhaust, and for withdrawal of salt samples. Approximately 2.7 kg of LiF-BeF_2-ThF_4 (72-16-12 mole percent), which had been previously purified, was contained in a 3-3/4-in. diameter nickel liner within the reaction vessel. The gas sparge tube extended to within 1/2 in. of the bottom, so that a gas bubble path of about 5 in. in the salt was created; no other provisions for salt agitation were made. Chloride concentrations of about 1 wt percent, introduced at NaCl, were maintained for analytical expediency.

Samples of the salt phase were withdrawn for chloride analyses at the beginning and end of each reaction period. Acid gas concentrations in the influent and effluent streams were determined

53/ ORNL-4548, p. 173, February 28, 1970.

periodically by titration with standard caustic solutions referenced to the flow of hydrogen and reaction time. Aliquots of the gas effluent titration solutions were submitted to the Analytical Chemistry Division for chloride analyses. Intermittent concentrations of chloride in the salt phase were determined by graphical integration of data from these gas-phase analyses. Seventeen reaction periods of 4 hours each were conducted at 650 and 750 C, at gas sparge rates of 0.5, 1, and 1.5 liters/min of H_2 (STP), and at nominal HF influent concentrations of 3, 5, and 7 meq of HF per liter of H_2. Operation of the experimental assembly was terminated at this point because of corrosion of the top plate of the reaction vessel.

Reaction Velocity Constants — The reaction noted by Eq. (1) would be expected to follow the second-order rate expression

$$-\frac{dN_{Cl}}{dt} = k_1 N_{Cl} N_{HF}, \tag{41}$$

where N is the respective mole fraction of chloride ion and HF. However, for a gas sparge experiment where the HF concentration in the gas influent is maintained constant, the reaction rate can more simply be defined by the first-order expression

$$-\frac{dN_{Cl}}{dt} = k_2 N_{Cl}. \tag{42}$$

Each experiment where reaction rate data could be obtained showed very good agreement with the integrated form of this equation. Typical results are shown in Figure 9.62. The dependence of k_2 on HF concentration for these pseudo-first-order reaction conditions becomes

$$k_2 = k_1 N_{HF}. \tag{43}$$

The dependence of the reaction rate on gas flow rate is related to stripping efficiency and mass flow rate of HF, and in these experiments to the relative agitation of the melt. Values for k_1 (Eq. 43) for data obtained at 650 and 750 C are plotted vs the mass flow rate of HF and related to nominal HF concentrations in Figure 9.63.

9.7 Removal of Chloride from Fuel Salt (Cont'd)

Equilibrium Quotients — Although these experiments were not conducted under ideal equilibrium conditions, calculations of equilibrium quotients for each experimental point showed that steady-state conditions between the gas and liquid phases did prevail. These values, based on the equation

$$K_Q = \frac{P_{HCl} N_{F^-}}{P_{HF} N_{Cl^-}}, \tag{44}$$

were derived from analyses of the gas effluent and from the chloride content of the melt, hypothetically calculated as the cation mole fraction of NaCl. An average value of K_Q obtained for each experiment. These apparent equilibrium constants should approach true equilibrium conditions as the gas residence time in the salt phase becomes infinite (zero flow rate). However, values for K_Q obtained at 650 C varied from about 6 to 10 and did not show a satisfactory correlation with gas sparge rates. Values for K_Q at 750 C were constant at about 4.4 ± 0.5.

9.8 Removal of Fluoride from Molten Lithium Chloride[54/]

During operation of the MSBR fuel reprocessing plant by the reductive extraction process, rare earths will be back-extracted from molten bismuth into molten lithium chloride. This process step provides, as its primary feature, for the separation of rare earths from thorium. If the fluoride fuel is entrained or has finite solubility in the molten bismuth stream, contamination of the molten LiCl system will occur. In this event thorium will be more readily extracted into the chloride phase, and the corresponding separation of rare earths from thorium will become less effective. Thus a process for stripping fluoride ion from molten chlorides may be required for the satisfactory operation of the fuel reprocessing plant. This experimental program examined in the reaction

$$BCl_3(g) + 3LiF(d) \rightleftharpoons 3LiC(l) + BF_3(g) \tag{45}$$

for possible application to MSBR fuel reprocessing technology.

54/ ORNL-4622, p. 106, August 31, 1970.

9.8 Removal of Fluoride from Molten Lithium Chloride (Cont'd)

The experimental procedure was similar to that used for studying the removal of chloride ion from a simulated MSBR fuel solvent. Boron trichloride admixed with hydrogen was bubbled through molten LiCl at 650 C to which known amounts of LiF had been added. Samples of the gas influent and effluent streams were periodically collected in water and analyzed by titration with standard caustic solution. Filtered samples of the molten salt were also withdrawn at intervals during the reaction period and analyzed for fluoride ion.

The results from four of eight experiments conducted thus far are shown in Figure 9.64; they demonstrate the effectiveness of this method for removing fluoride ion from molten LiCl. Initial concentrations of 5000 to 10,000 ppm by weight fluoride were rapidly diminished to low values within the 4-hr reaction periods at low BCl_3 concentration (0.8 millimole per liter of H_2) in the sparge gas stream.

After establishing that essentially complete fluoride removal from LiCl (<40 ppm) could be achieved, the purpose of subsequent experiments was to determine relative reaction velocity constants and equilibrium quotients. However, experimental conditions imposed thus far have been inadequate for these determinations. As shown by Figure 9.65, the reaction of fluoride ion with BCl_3 has been essentially quantitative even at these low concentrations. Thus the rate of chemical reaction has been controlled by the rate at which BCl_3 was admitted to the system. Values calculated for the equilibrium relation given by

$$K = \frac{N_{BF_3}}{N_{BCl_3}} \cdot \frac{1}{N_{F^-}^3}, \qquad (46)$$

where estimates of the BCl_3 concentration over the melt could be made, showed a continuous increase as the fluoride ion concentration in the melt deminished and approached a value of 10^{14} as a limit.

The high rate of chemical recombination observed by these experiments and the effectiveness of fluoride removal are very favorable

ORNL-4622
p 106

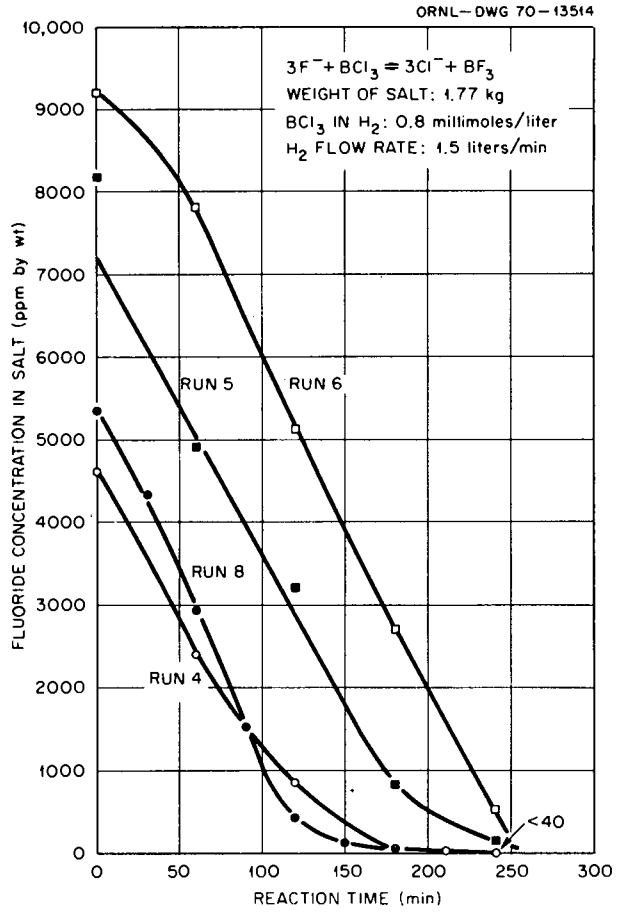

Fig. 9.64 Removal of Fluoride from Molten LiCl by Reaction with BCl_3 at 650 C.

ORNL-4622
p 107

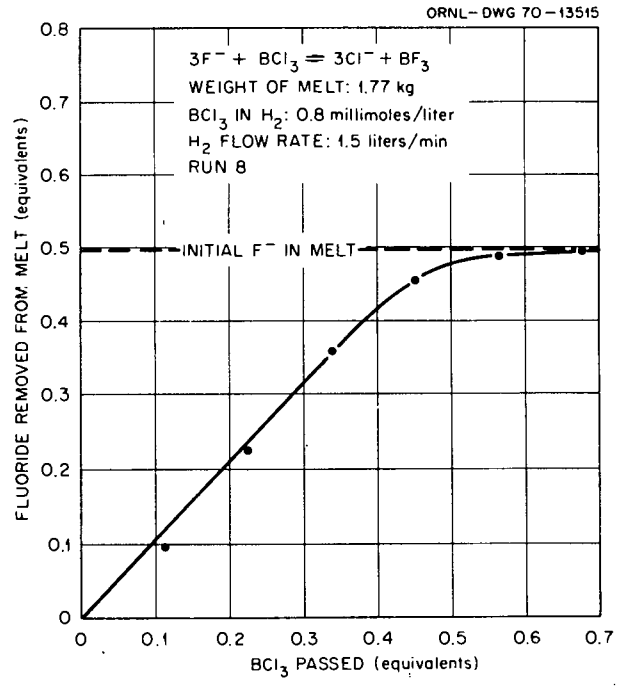

Fig. 9.65 Material Balance on Removal of Fluoride from LiCl by Reaction with BCl_3 at 650 C.

9.8 Removal of Fluoride from Molten Lithium Chloride (Cont'd)

attributes of this proposed chemical process. In addition chemical analyses of salt samples have indicated that measureable corrosion of the nickel reaction vessel by BCl_3 has not occurred. Chemical analyses also indicated that the boron content of the melt, used repetitively, increased to about 200 ppm during initial experiments and has remained essentially constant at that value during the later experiments. However, a spectrochemical method has failed to detect boron concentrations above an analytical limit of 50 ppm. Although the differences in the analytical methods have not been resolved, the presence of this small boron concentration in the salt is not a serious deterrent for the process. Elemental boron is not wet by bismuth even at temperatures of 1500 to 1600 C. Its transport to the fluoride fuel should then be limited to a salt entrainment condition and should be a negligible process consideration.

9.9 Iron Fluoride Reduction[55,56/]

The iron concentration in the fuel salt was increased to about 400 ppm by the addition of iron fluoride prior to making 11 reduction runs. Data from these runs are given in Table 9.32. Although column operation was erratic, reasonable values were obtained for the mass transfer coefficients. These coefficients are about twice those obtained by the MIT Practice School group in 1968 using a 3.375 in. ID column. The last nine runs were made with $LiF-BeF_2-ThF_4$ (72.0-14.4-13.6 mole percent). After the first three runs, the iron analyses became erratic, probably because some of the reduced iron particles passed through the sampler filter or because the samples had been contaminated with iron during sample preparation.

55/ ORNL monthly report, November, 1970

56/ ORNL-4682, p. 37, March 31, 1971.

Table 9.32

Data from Iron Fluoride Reduction Runs
Column Temperature, 700 C

Run No.	Date	Gas Flow Rate (Std Liters/Min) H_2	Gas Flow Rate (Std Liters/Min) Ar	Salt Flow Rate (cm^3/Min)	Analyses of Filtered Samples (ppm Iron) Feed	Analyses of Filtered Samples (ppm Iron) Product	Percent of Batch Contacted	Mass Transfer Coefficient,(b) K_1 (Ft/Hr)
1	7-27	20		100	425	307	71.4	0.018
2	7-28	13.5		100	307	228	72.9	0.016
3	10-22	16.6		100	220	158	75.3	0.015
4	11- 3	14.6		210	158	373	84.7	
5	11- 4	18.2		161	373	137	68.8	
6	11- 5	4.5	4.5	106	137	110	81.8	0.011
7	11- 6	3.9	3.9	142	110	70	81.8	0.030
8	11- 9	24.0		103	70	75	86.5	
9A	11-13	4.5	4.5	93	75	55(c)	79.4(d)	0.012
9B	11-13	3.5	3.5	136				
10	11-17	14.1		105	69(e)	77(c)	81.8	
11	11-19	3.1	4.5	117	207	339 104(c)	81.2	

(a) The first two runs used $LiF-BeF_2$ (66-34); the remaining runs used $LiF-Be_2-ThF_4$.

(b) Based on outside surface of Raschig rings only since salt is considered to be nonwetting; K_1 is 78 percent of these values if entire area of the Raschig rings is used as the basis.

(c) Average of flowing-stream samples; no batch samples were taken after the run.

(d) A value of 100 percent is used in calculating K_1 since samples are of flowing-stream type.

(e) Calculated from flowing-stream samples from previous runs.

10.0 OFF-GAS SYSTEM TECHNOLOGY

The purpose of the off-gas system is to extract fission gases from the fuel salt and dispose of them safely. It is convenient to discuss the off-gas system in two parts: The purge system, which separates fission gases from the primary system; and the cleanup system, which removes fission gas from purge gas (helium or argon).

The off-gas system performs the following functions:

1 - It reduced the concentration of ^{135}Xe in the fuel salt (and, indirectly, the concentration in graphite) to a level sufficiently low that xenon poisoning is not the dominant parasitic fission product.

2 - It continually removes other contaminants (e.g., long-lived isotopes, hydrocarbons, corrosion products, etc.) so that they do not continue to build up throughout the life of the plant.

3 - It greatly reduces the activity of moderate or long-lived fission gases in the fuel salt.

10.1 Purge Gas System

To effect efficient fission gas transfer from the fuel salt to the purge gas it is necessary to provide a large surface area where the fuel salt and purge gas make contact. Two ways of attaining this surface area have been proposed:

1 - Continuous injection and extraction of purge gas bubbles into the salt.

2 - Continuous salt spraying into small droplets in a spray chamber.

10.1.1 Bubble Injection and Extraction

This method, proposed by ORNL, involves injecting bubbles into a side stream of fuel salt taken from the discharge side of the pump.

10.1.1 Bubble Injection and Extraction (Cont'd)

Small xenon laden bubbles, previously injected into the salt stream, are removed from the salt by a bubble separator. Downstream of the bubble separator fresh bubbles are injected into the salt side stream which returns to the suction side of the pump.

The bubble separator might be a set of swirl vanes which cause rotational motion and drive the bubbles into a central vortex. An alternate form of bubble separator might be a spray chamber discussed below.

Recent experiments reported at the Semiannual Information Meeting [1/] indicate that bubbles passing through a pump will be broken up into fairly small sizes, about 0.001-0.002 in. diameter. Thus, a special device to generate small bubbles does not appear necessary. Conversely, the problem of getting bubbles out of the salt, while maintaining an acceptably low void fraction in the salt, may be a problem. The question of what is an acceptable bubble fraction is not yet answered definitively. It has arbitrarily been limited to about 1 percent in the core, but there is no compelling reason why it could not be 2 or 3 percent. It is known, however, that bubbles have a small, positive reactivity worth (with respect to fuel salt). The larger the normal void fraction, the greater the potential for a reactivity accident. However, the magnitude of reactivity insertion via this mechanism is small, and this does not appear to be a serious consideration. The breeding performance will diminish somewhat by the higher void fraction but not seriously. The void fraction in the salt is a

1/ Presentation by C. H. Gabbard, ORNL April 20, 1971.

10.1.1 Bubble Injection and Extraction (Cont'd)

function of purge-gas throughput and bubble stripping efficiency (i.e., the rate at which salt is stripped of bubbles).

Consider the mechanism for xenon removal and the xenon distribution in an MSR. The amount of xenon poisoning is proportional to the amount of xenon in bubbles, salt, and graphite:

$$f_B C_B + f_S C_S + f_G C_G$$

f_i = volume fractions

C_i = xenon concentrations

Analyses indicate that even for sealed graphite most of the xenon poisoning is due to xenon in graphite. The $f_S C_S$ term is next in significance and the $f_B C_B$ term is smallest by a wide margin. The production rate of xenon at steady state is proportional to reactor power, but because it is produced from decay of ^{135}I (6.7 hour half-life) it is produced uniformly throughout the salt. The rate of transfer to gas bubbles is given by

$$R = Ah\ (C_S - kC_B)$$

R = transfer rate

A = bubble surface area

h = mass transfer coefficient

k = solubility constant

A similar equation describes transfer to graphite. To maintain a low xenon poison fraction, about 90 percent of the xenon produced must transfer to bubbles. Most of the balance transfers to graphite. The xenon concentration in bubbles C_B can be controlled by the throughput of purge gas which can easily be made large enough that

10.1.1 Bubble Injection and Extraction (Cont'd)

$kC_B << C_S$. Hence C_S is controlled primarily by A and h, but also by some transfer to graphite. The mass transfer coefficient h is dependent upon the diffusivity of ^{135}Xe in the salt and the turbulence of the salt. Although turbulence accelerates xenon transfer to bubbles it also accelerates transfer to graphite. It is not clear if turbulence greatly affects the relative distribution. The total surface area A, however, is controlled by the purge gas throughput and the bubble size.

Based on an assumed mass transfer coefficient of 2 ft/hr and a helium gas stream of 9 scfm broken into 0.02 in. diameter bubbles, ORNL analyses indicate that with partially sealed graphite a poison fraction of 0.5 percent can be attained. If the bubbles are broken into 0.002 in. diameter bubbles by the pump, the xenon transfer area will be increased by a factor of ten. Diffusion theory of xenon in salt predicts that h will be ten times larger for these smaller bubbles. This indicates the transfer rate R to bubbles will increase somewhat, and the concentration C_S will decrease dramatically. Assuming the smaller bubbles can be removed from the salt, it seems reasonable that C_S would be reduced enough to eliminate the need for sealing the graphite. Analysis suggests that if C_S is reduced by a factor of 5 from the reference case, the graphite seal is unnecessary.

Consider the problem of removing bubbles from the salt. If a side stream of salt was sprayed into droplets 0.002-0.01 in. in diameter, it seems that most bubbles will escape. Droplets this size can easily be made with pressure nozzles using the pressure drop available across the primary pumps. Bubble removal via the swirl vanes still appears attractive, however, and ORNL has had

10.1.1 Bubble Injection and Extraction (Cont'd)

some success in removing 0.001-0.005 in. diameter bubbles from glycerin-water mixtures [2/].

10.1.2 Spray Chambers

The second method for transferring xenon from the salt to the gas stream was to provide a large surface area simply by spraying the salt into small droplets. In order to get efficient xenon transfer within a reasonable contact time (1-5 seconds), it is necessary that the droplets be very small - 100-200 microns. Generation of droplets this small consume a substantial amount of power and for this reason this method appears less attractive than the bubble method. It is a feasible alternative, however, if the bubble separator fails.

10.2 Purge-Gas Cleanup System

Regardless of the method for transferring fission gas to the purge gas a system for cleaning the purge gas is required. It must serve three functions:

1 - Maintain sufficiently low ^{135}Xe back pressure in the gas returned to the salt.

2 - Remove other contaminants such as water vapor, hydrocarbons, volatile fluorides, and any other material which could be detrimental to the reactor.

3 - Provide a small stream of very clean gas for special uses where direct access by personnel is required.

10.2.1 ^{135}Xe Back Pressure

During normal steady state operation the ^{135}Xe back pressure kC_B/C_S in bubbles surviving ten passes around the primary loop is about 1 percent (for 9 scfm and

2/ Charles Gabbard, ORNL, Private communication.

10.2.1 ^{135}Xe Back Pressure (Cont'd)

90 percent ^{135}Xe removal). Hence the back pressure is not significantly limiting the rate of xenon transfer to bubbles. This contaminated purge-gas stream can be cleansed as follows:

1 - It can flow into a tank for cooling and holdup to allow sufficient decay of ^{135}Xe.

2 - It can flow directly into a cleanup system which physically separates fission gases from the purge gas by charcoal sorption.

3 - It can flow into a holdup tank and then into a cleanup system.

In each of these three cases the purge gas is recycled back into the salt.

10.2.2 Holdup Tank

The first case assumes there is a reservoir of gas into which the stream empties. The reservoir then supplies the stream returning to the salt. Assuming approximately 90 percent of the ^{135}Xe produced enters the holdup tank, it is clear that some xenon will be carried back into the primary system, and the concentration of ^{135}Xe in the tank will buildup to a level at which its decay rate equals its net transfer rate to bubbles. This condition of equilibrium defines the concentration of ^{135}Xe in the tank and in the purge gas returning to the fuel salt. Analysis shows that a gas volume of about 6500 ft^3 is large enough that the equilibirum concentration of ^{135}Xe in the return stream is low enough to give a poison fraction of about 0.5 percent. Thus, it is possible to achieve sufficient cleanup of ^{135}Xe simply by dilution and decay.

10.2.2 Holdup Tank (Cont'd)

The activity of these fission gases will build up until the decay for each isotope equals its production rate. For an MSR producing 2250 MWt, the total equilibrium fission gas activity amounts to about 8×10^8 curies. Thus, for safety reasons it may be desirable to avoid one large, high temperature tank containing fission gases, and instead, dispose of them via charcoal sorption. It appears, however, that such tanks could be made sufficiently reliable.

10.2.3 Charcoal Sorption

ORNL proposed a system which consists of about 27 miles of piping filled with charcoal and submerged in water pools. A contaminated gas stream (11 scfm) enters at 1000-1300°F and is cooled by boiling water. Further down the pipes the temperature drops to where the charcoal becomes effective as an absorber. Based on the principle of dynamic adsorption, this system reduces the ^{135}Xe concentration in the outlet gas to about 3 percent of that at the inlet. This is equivalent to 48 hours of decay. 9 scfm are compressed and recycled into the salt. 2 scfm receive further purification for use in the primary pump purge glands. The 9 scfm stream returns to the salt stream having a ^{135}Xe back pressure of about 0.03 percent. Since the back pressure of the bubbles as they emerge from the salt is about 1 percent, and since those emerging are representative of the average, it follows that the average back pressure of bubbles in the salt is about 1 percent. Analysis shows, however, that the ^{135}Xe concentration in the return stream could be much greater - by at least a factor of ten - without increasing the average back pressure significantly or appreciably reducing the efficiency of xenon removal. Furthermore, the average back pressure in the bubbles

10.2.3 Charcoal Sorption (Cont'd)

could be increased well above 1 percent without significantly reducing the rate of xenon transfer to bubbles or increasing the poison fraction appreciably.

ORNL has proposed that the drain tank provide a two hour gas holdup for cooling before the contaminated purge gas enters the cleanup system. The equilibrium activity of fission gases in this tank is about 3×10^8 curies. The heat load due to decay of fission gases is reported to be about 9 MW. About 50 percent of the noble metals produced are assumed to be carried by the gas stream. The heat load due to decay of noble metals is also about 9 MW for a total normal drain tank heat load of about 18 MW. In this system the heat load in the charcoal beds due to decay of fission gases and their daughters is about 2 MWt. If the two hour holdup tank were bypassed, a total heat load of about 20 MWt would appear in the off-gas system. Of course, the 11 scfm gas stream could be cooled by passing it through a heat exchanger before entering the charcoal beds, but because the heat production is by radioactive decay, most of the heat will be produced in the charcoal. Thus, the heat production in charcoal will be large. This heat load will be a major consideration in the design of such an off-gas system because a low charcoal temperature is essential. The lower the temperature the better the sorption and the less graphite and piping required.

10.3 Removal of Other Contaminants

It must be assumed that other undesirable contaminants will appear in the gas stream. Tritium, noble metals, corrosion products, volatile fluorides, and perhaps hydrocarbons, will be present. It is desired that all the tritium enter the off-gas system, but it is not clear that it will. For design

10.3 Removal of Other Contaminants (Cont'd)

purposes, it is reasonable to assume that all tritium will enter the off-gas system.

There may be many ways to remove the aforementioned contaminants. Most will be sorbed by the charcoal. Tritium, however, may require special provisions. One way, proposed by ORNL, is to oxidize it by passing the gas stream over a hot (1500 F) CuO bed. Tritiated water can be sorbed by refrigerated charcoal. It is quite possible that it will be retained by the charcoal without any special provisions.

10.4 Provisions for a Clean Gas Stream

A high degree of cleanup can be attained by passing a portion of the gas stream emerging from the ^{135}Xe decay bed into another charcoal bed. This gas stream is essentially free of activity from fission gases having half-lives less than that of ^{135}Xe (9.2 hours). The activity in the gas stream is due mostly to decay of ^{131m}Xe (12 day half-life). This is removed by passing it into another charcoal holdup bed. ORNL chose a 90-day holdup bed which is equivalent to 7.5 half-lives. The gas stream emerging from this system contains primarily ^{85}Kr (10 year half-life) and tritium (12 year half-life) unless it too is removed. This gas stream has a very low activity and is used to bath penetrations in the primary system (pump and control rod seals, etc.) to prevent back flow of fission gases.

11.0 FUEL SALT DRAIN TANK TECHNOLOGY

The primary function of the drain tank is to provide a safe place to store the salt in any conceivable situation. The drain tank must satisfy certain performance criteria for each mode of operation. The modes of operation are as follows:

Normal, full power operation
Normal, scheduled shutdown
Abnormal, unscheduled shutdown

Obviously, its geometry and materials of construction must be such that subcriticality is guaranteed. During normal plant operation the drain tank must always be near operating temperature, and its cooling system must be ready to take up the full heat load if the salt should be dumped suddenly.

During normal shutdown it will contain the fuel salt and dissipate its decay heat. This situation differs from the abnormal shutdown in that normally the salt remains in the primary system for 10-14 days after shutdown and the heat load is then only about 2MW compared with about 50MW immediately after shutdown. The reason for the 10-14 day cooling interval is not to reduce the heat load on the drain tank cooling system; instead, it is to allow fission products that remain on graphite and Hastelloy N surfaces to decay sufficiently before the cooling capability of the salt is removed. For this reason it is important to avoid draining the salt immediately after power production.

Abnormal, unscheduled shutdown must have a very low probability of occurrence. Hypothetical, but credible circumstances resulting in a sudden drain are as follows:

1 - Loss of ability to remove the decay heat from the primary system. This could result from loss of all pumping power in the primary system and/or secondary system and/or loss of a heat sink. This could occur if all electric power were lost.

2 - Rupture of the primary system.

3 - Freeze valve failure.

11.0 FUEL SALT DRAIN TANK TECHNOLOGY (Cont'd)

Although the probability of a sudden drain can be made acceptably low as far as plant availability is concerned, uncooled fuel salt can conceivably be a threat to public safety. Thus, the drain tank cooling system must be able to accommodate the decay heat load within minutes after shutdown.

11.1 Design Criteria

The following design criteria follow from the principle objective of providing a safe place for storing the fuel salt under any conceivable circumstance:

1 - Subcriticality must be assured.

2 - The system must have a very low probability of unsafe failure such as loss of adequate cooling capability, leakage, or salt-coolant mixing if chemical reactions resulting in U precipitation occur.

3 - Contamination of the fuel salt must be highly unlikely.

4 - It must remain in readiness during normal operation.

5 - The cooling system must have a peak capacity of about 50 MW and the ability to pick up the heat load automatically if the salt should be dumped.

6 - It should have capability to return salt to the primary system.

7 - It must be instrumented adequately so that its availability is evident during normal operation, and its operation can be monitored when in use.

11.2 Design Philosophy

11.2.1 Subcriticality

This can easily be assured by keeping light isotopes out of the vicinity of the drain tank.

11.2.2 Probability of Unsafe Failure

Following are credible, unsafe failures which the drain tank system might suffer:

11.2.2 Probability of Unsafe Failure (Cont'd)

1 - The cooling capability might be lost.

2 - The drain tank itself might leak and, thereby, cause loss of control of the fuel salt.

3 - The cooling medium might leak into the fuel salt and cause a chemical reaction leading to precipitation of uranium.

Cooling capability can be assured sufficiently by employing:

a - many independent cooling circuits having excess capacity so that several individual loops can fail without jeopardizing adequate cooling capability, and

b - natural, rather than forced, circulation to avoid reliance upon machinery and power sources.

To guarantee against leakage of the drain tank itself, it can be placed within another tank. This makes periodic inspection impossible but offers a way of cooling the inner vessel.

To reduce the probability of fuel salt contamination and/or U precipitation via coolant leakage, two approaches exist:

a - An inert coolant can be used, or

b - cooling tubes having double barriers can be used.

NaK or Na are attractive coolants except for their ability to react with UF_4 and cause precipitation of UF_3. These coolants would require double barriers. Sodium fluoroborate and many other salts contain NaF which is difficult to remove from fuel salt, but does not cause precipitation. Inert gas and $^7LiF\text{-}BeF_2$ salts have been considered. Natural circulating gas systems have the disadvantage of requiring excessive heat transfer areas to accommodate the maximum credible heat load of 50 MW.

11.2.3 Contamination Prevention

At least two approaches are available:

1 - The coolant can be made compatible with the fuel salt so that a leak is of no consequence. This requires that the coolant be a $^7LiF\text{-}BeF_2$ or $^7LiF\text{-}BeF_2\text{-}ThF_4$ salt. Unfortunately, these salts have the disadvantages of being expensive, viscous, and having a high melting temperature. Otherwise it would be an ideal coolant.

2 - A double barrier can separate the fuel salt from the coolant. This requires that bayonet tubes be placed inside thimbles. Heat transfer will occur primarily by radiation across the gap. Since radiant heat transfer varies as T^4, radiation tends to keep temperatures within a narrow range in spite of wide variations in heat load. The disadvantage is that heat transfer is poor and a large number of bayonet tubes are required (about 1000) to accommodate 50 MW.

3 - Two drain tanks can be used together in a complimentary way. One could be used for normal drain (for which the fuel salt has had time to cool). This one requires a relatively small cooling capacity ($\sim$2 MWt) which can be accommodated by forced or natural convection of a gas (He or A) through bayonet tubes. This one will have a high utilization. The other drain tank must be available for emergency use. Thus, it must have a cooling capacity of 50 MW and, therefore, a liquid coolant - probably sodium fluoroborate. Because it will have a very low utilization, a single barrier may be acceptable. Since this tank has a high cooling capability, it can conveniently be used to hold up fission gases prior to entering the off-gas system.

11.2.4 State of Readiness

To assure that the drain tank is available, i.e., the cooling system is functioning properly, drain lines are open, and the system is leak tight, it is proposed to keep it in service continually. By keeping a flow of salt and/or fission product gases into the drain tank, it is clear that the lines are open. This salt flow also supplies a heat load to keep the coolant flowing (if it flows by natural convection) and produces temperature rises and flow rates which can be monitored. Finally, leakage can readily be detected by measurement of gaseous activity in the cell atmosphere.

11.2.5 Cooling Capacity

Although the peak heat load is about 50 MW, the normal heat load may be much lower - probably about 18 MW from fission gas and noble metal decay. Hence, the cooling system must have a sufficiently wide operating range. Furthermore, it should be able to follow the heat load as it changes to maintain temperature within an acceptable range. As previously mentioned, heat transfer by radiation accomplishes this automatically.

11.2.6 Salt Transfer

If a flow of salt is used to verify operation of the drain tank, it must be continually transferred back into the primary system, probably into the pump bowl. The elevation differential from the bottom of the drain tank to the pump suction will probably be at least 50 ft. This produces a static pressure of about 80 psi. The most promising way of returning salt is by jet pumps driven by the primary pump discharge. With jet pumps the maximum salt flow rate is limited to about 100 gpm. This limit is based on a practical limit to the physical size the jet pump can be. The size depends on the desired pumping capacity, the back pressure, and the volume of salt required to keep the pumps submerged.

11.2.6 Salt Transfer (Cont'd)

In principle, salt can be transferred by gas pressure. The problems with this approach are:

a - the tank is large and hot and sufficient strength would be hard to achieve with an adequate margin for safety.

b - The tank contains several hundred million curies of fission gases and it is undesirable to pressurize this gas.

11.2.7 Instrumentation

As yet instrumentation of the drain tank system has received little consideration. It is imperative, of course, that temperatures be monitored and circulation be maintained to prevent hot-spots. Measurement of temperatures and flow rates of the cooling fluid outside the drain tank cell are certainly possible and will verify operation of the system. This may be all the instrumentation required other than that for radiation measurements.

11.3 Choice of Coolants

Tables 11.1, 11.2 and 11.3 present a comparison of possible coolants. Although NaK is most attractive from the standpoint of its wide temperature range, it will cause precipitation of UF_3 if it should mix with the fuel salt. Thus, it would require a double barrier. Sodium fluoroborate ($NaBF_4$-NaF) does not cause precipitation because the sodium is already combined with fluorine. Although its liquidus is high, its viscosity is low and, thus, it may be suitable in a natural convection cooling loop. ^7LiF-BeF_2 salts are very expensive primarily because of ^7Li enrichment. These salts also have high viscosities and liquidus temperatures. Hitec (KNO_3-$NaNO_2$-$NaNO_3$) has very attractive properties but would cause precipitation of UO_2 if it leaked into the fuel salt.

Table 11.1 Qualitative Comparison of Fuel-Salt Drain Tank Coolants

Coolant	General ability to transfer heat at temperatures and rates required for an MSBR system	Ease of circulating required volumes	Ease and reliability of retention in closed system	Compatibility if mixed with fuel salt	Compatibility if spilled in cell	Cost of coolant	Cost and complexity of components and equipment	Radiation and thermal stability	Ease of instrumenting and controlling	Corrosion	Conclusions
Water and steam	Excellent as coolant; poor for adding heat	Excellent	Good; pressure can get high	Poor	Poor; generates high pressure and some $H_2 + O_2$ gas	Very low	Low	Good	Good; protect against freezing and high steam pressure	Requires Inconel or stainless steel and special treatment	Suitable for cooling, possibly best
Liquid metals, NaK and Na	Good for cooling or heating	Good	Excellent; low pressure, low corrosion	Poor	Good if N_2 in cell; poor if air	Low	Medium to high	Excellent	Excellent; protect against freezing	Stainless steel or possibly carbon steel	Excellent for heating or cooling in absence of air
Fused salts, fluorides, carbonates, and nitrate-nitrites	Good for cooling or heating	Good	Excellent; low pressure, low corrosion	Excellent to good	Excellent; protect against toxic vapors	Low to high	Medium to high	Excellent to good	Good; protect against freezing	Requires stainless steels or Hastelloy N	Excellent for heating or cooling
Organics, diphenyls and polyphenyls	Good for cooling; poor for heating	Excellent	Good; pressure can get high	Poor	Poor; generates high-pressure, flamable, and toxic vapor	Low	Medium; requires purification system	Fair; tends to decompose above 700°F	Good; protect against freezing and high pressure	Carbon steels	Fair
Gases, CO_2, N_2, and argon	Poor for heating or cooling	Poor	Good; pressure is high	Excellent	Good to excellent, depending on ratio of volume of pressurized gas to volume of cell or provisions for pressure relief	Low	Medium to high; large high-pressure systems	Excellent	Excellent	Carbon steels	Fair

Table 11.2

Properties of Possible Fused-Salt Coolants for Drain Tank System

	$NaBF_4$-NaF Eutectic	^7LiF-BeF_2 Peritectic	KNO_3-$NaNO_2$-$NaNO_3$ Eutectic
Composition, mole %	92-8	66-34	53-40-7
Viscosity, lb/ft-hr			
At 900°F	4.1	40.4	3.1
At 1150°F	2.6	18.7	2.5
Liquidus temperature, °F	725	856	288
Density, lb/ft^3			
At 900°F	119.4	125.5	108.0
At 1150°F	112.9	121.9	103.0
Specific heat, Btu/lb-°F	0.36	0.57	0.37
Thermal conductivity, Btu/hr-ft-°F	0.27	0.58	0.33

ORNL-4541 p. 93.

Table 11.3

Evaluation of Salt-Type Coolants and Water-Steam for Primary Drain Tank Cooling System

Coolant	Desirable Features	Undesirable Features
$NaBF_4$-NaF	a - Inexpensive (~ \$70/ft^3) b - High melting point means reduced thermal shock on drain tank. c - Relatively low viscosity.	a - Reactor must be shut down if coolant gets into fuel salt and the fuel must be processed. b - High melting point makes freezing in stack more likely. c - Hastelloy N would be required in coolant circuit.
^7LiF-BeF_2	a - No processing of fuel salt is required in event of leak. b - Least thermal shock on drain system. c - Extensive experience with this coolant in MSRE d - Hastelloy N may not be required in coolant circuit. e - No volume change in freezing.	a - Very expensive (~\$1500/ft^3). b - High melting point. c - High viscosity.
KNO_3-$NaNO_2$-$NaNO_3$	a - Inexpensive b - Carbon steel can be used up to 850°F. Stainless steel for higher temps. c - Low melting point.	a - Of doubtful stability at high temperatures and in radiation field. b - Salt processing on leak may be required.
Water-Steam	a - Has least danger of freezing. b - Lowest cost. c - Used in MSRE drain tank. d - Relatively easy to get natural circulation.	a - Requires double barrier tubes (e.g., bayonet). b - Relatively large number of tubes required.

ORNL-4541 p. 93.

12.0 INSTRUMENTATION, CONTROL, AND PROTECTIVE SYSTEMS

12.1 Philosophy

The function of the control system is to make the plant perform as desired under all modes of normal operation and shutdown. The protective system, on the other hand, should automatically initiate safety action to

a - protect the public
b - protect the plant personnel
c - protect the plant

under all credible accident conditions.

The control and safety systems should be independent of each other as much as practical to reduce the possibility of a single failure negating both systems. Both systems should be able to be tested during normal plant operation without compromising plant safety or availability. Both systems ideally should be fail-safe in that any instrumentation failure should automatically signal for safety action. To achieve adequate plant availability and safety, both systems should have sufficient redundancy of instrumentation channels arranged in logic systems which prevent unnecessary safety action.

The set points for initiation of safety action should be based on the following:

a - Consequences of exceeding set points
b - Consequences of an unscheduled shutdown
c - Reliability of the safety system itself
d - System kinetic response

The set points should be realistic in that they afford a comfortable safety margin and, yet, not so conservative that they initiate safety action unnecessarily.

If the control system is automated, it too, will have set points based on similar considerations. They will, of course, precede the set points of the safety system.

12.2 Steam Temperature and Flow Control

As proposed by ORNL, course steam temperature control will probably be achieved by varying the coolant salt flow rate. This method satisfies two objectives: Load transients can be accommodated by virtue of the stored energy in the coolant salt; and, load transients can be prevented from freezing coolant salt in the steam generator. Fine control can be accomplished by attemperation, also proposed by ORNL. Feedwater at a supercritical pressure can be injected into the superheated steam to maintain the desired temperature to within about one degree Fahrenheit.

Since the outlet steam temperature will be nearly constant, the steam flow must be proportional to power demand. Steam flow control can be regulated by the feedwater pumps driven by a position servo and a load demand signal.

12.3 Secondary System Flow Control

Flow control will be achieved by variable speed pumps. The steam temperature sensor would probably generate an error signal which drives a velocity servo which sets the coolant pump speed. This method of control will automatically seek a coolant flow rate which, at steady state, nulls the error in steam temperature.

12.4 Primary System Power Control

Because the reactor has negative temperature coefficient of reactivity, the reactor power will automatically follow the power demand. To affect a more prompt reactor response and to maintain positive control over temperatures in the primary and secondary system, it is better not to rely on such inherent mechanisms but rather to use control rods. Of course, the reactivity coefficients ultimately force the reactor power to match the load regardless of control rod motion, hence, the effect of control rods is to govern the time response of the system and to control the primary system temperatures. Several methods of reactivity control are possible. Since the

12.4 Primary System Power Control (Cont'd)

heat capacity of the primary and secondary systems can be used to accommodate load transients, it is desirable that the reactor power overshoot load changes somewhat to restore the stored energy to its desired level.

One method of reactivity control is to compare the power demand signal (used to set the feedwater pump speed) with the reactor power as indicated by neutron detectors. The error signal can then drive a velocity servo which adjusts the control rod position. This method of control will force the control rod to null the error signal. Although this method of control accelerates the reactor power response to load changes, it does not provide direct control over primary system temperatures.

One way to obtain direct temperature control is for the power demand signal to define the desired reactor outlet salt temperature and compare it with the observed temperature. The error signal could then control a velocity servo which drives the control rods. In this system the control rod attempts to hold the outlet temperature at the level commensurate with the power demand and, during a transient, it adds or decreases reactivity to accelerate the reactor response. The reactivity from temperature feedback will stabilize the reactor at the desired power level and, at that time, will cancel the reactivity insertion by the control rods. This method of control may require that the outlet salt temperature demand signal or the secondary pump be artificially programmed such that the fuel salt temperature in the cold leg does not fall too much when the load is increased.

Another method of control has the feature that it automatically attempts to hold constant the cold leg salt temperature while using only linear control components. The power demand signal defines a desired reactor outlet temperature. The difference between this and the actual reactor inlet temperature defines a modified power demand. This value is compared with the reactor power as indicated by a neutron detector and the error signal controls the velocity servo which drives the control

12.4 Primary System Power Control (Cont'd)

rods. This system is, therefore, sensitive to the cold leg salt temperature, and if it were to drop as a result of increased load, the modified power demand would be greater than the actual demand. Thus, the control rods would insert a greater amount of reactivity than in the previous case and cause the reactor system to respond faster. The overall effect is to prevent the cold leg temperature from falling as much by causing the reactor to respond more quickly. This method was originally proposed by ORNL[1/].

12.5 Short Term Reactivity Control

Short term reactivity control will probably be accomplished by graphite control rods which displace fuel salt. The reactivity worth of graphite with respect to fuel salt is positive but not large and, substantial uncertainty exists in calculations performed as of this writing. Since the reactivity required to override isothermal temperature coefficients is small (on the order of a dollar), the amount of excess reactivity required is small relative to other reactor concepts. Two dollars of excess reactivity in control rods is probably sufficient. Although the number and configuration of control rods is uncertain at this time, it appears that adequate excess reactivity can be attained with a reasonable number of nonpoison control rods.

A few poison safety rods will provide adequate shutdown margin. Safety rods may also be used as control rods for fast power reduction following loss of load. Fast power reduction may be necessary to avoid excessive outlet temperatures and thermal shock. As discussed below, long term reactivity control can be accomplished by adjusting the fuel salt composition. The safety rods must, therefore, be able to override all possible reactivity additions via this mechanism. Of course, they must be designed for fast reactivity withdrawal without the possibility

1/ ORNL-4541, pages 121-123, Sections by W H Sides, Jr.

12.5 Short Term Reactivity Control (Cont'd)

of fast reactivity insertion. These requirements are generally less stringent than those applied to water reactors and are clearly within present technology.

12.6 Long Term Reactivity Control

ORNL has proposed that long term reactivity adjustments be made by fuel salt composition adjustments. This, in principle, could be accomplished by fuel addition or removal by the processing plant.

The reactor operation and control should not depend on the availability of the processing plant, however. The processing plant is likely to be down frequently for routine maintenance or repair during which power production should not be interrupted Furthermore, it is desirable that the reactor be able to operate, albeit as a converter, in spite of prolonged outage of the process plant.

Thus, for high plant availability, alternate means for modifying fuel salt composition should be available apart from the processing plant. Another reason for alternate means of fuel concentration control is to provide fuel addition and removal rates faster than can be provided by the process plant. ^{135}Xe poisoning transients are too fast for the process plant (assuming a 1 gpm process stream) and too large for control rods. Utilities may want the flexibility of being able to start up anytime during the xenon transient. This could easily be accomplished by maintaining a supply of UF_4-LiF ready for dissolving in the fuel salt and a reservoir of depleted fuel salt available for salt dilution as the xenon burns out.

The maximum quantity of UF_4 required, and its insertion rate, is determined for start-up capability following a scram. It is assumed that salt continues to circulate and helium bubbles are continuously injected and removed following the scram.

12.7 Xenon Transients

Immediately after the scram, the xenon production via direct

12.7 Xenon Transients (Cont'd)

fission yield ceases. The production of ^{135}Xe via ^{135}I decay, which is 83 percent of the total during operation, continues. Thus, after shutdown the production rate of ^{135}Xe immediately drops to 83 percent of its previous value and decreases exponentially as the iodine decays. Because of continual mixing of the salt, the xenon production rate (per cc of salt) is spatially uniform throughout the salt. Thus, the xenon flux on the graphite surfaces throughout the core is uniform.

Prior to shutdown there was a steady state spatial distribution of xenon in the graphite. But since xenon burnup is proportional to neutron flux, the xenon concentration in the graphite at core center is a minimum and increases toward the edges. (In the reflector regions, the neutron flux during operation is relatively low and the xenon concentration in the graphite is such that its decay rate equals its influx rate.)

After shutdown xenon burnup in the core graphite ceases but the diffusion of xenon into the graphite continues. This gives rise to a transient very similar to that experienced by fixed fuel reactors. Because of continuous purging, however, the peak is much smaller than in water reactors. Nevertheless, the poison fraction is expected to rise from an initial value of 0.5 percent in the Reference Design to a peak of about 1.7 percent. This increase corresponds to a reactivity loss of approximately 0.5 percent $\Delta k/k$. This value is probably twice as large as the worth of all control rods. To override the xenon peak, fuel must be added in the amount of about 1 percent (14.7 kg fissile). The maximum rate of xenon build-up is only 0.34 percent poison fraction per hour and requires fuel addition at the initial rate of about 4 kg/hr. Capability to introduce fuel in the amount and rate indicated would provide complete flexibility to override xenon at any time during the transient.

If the reactor were started and operated at full power at the xenon peak, the poison would burn out at a rate which would

12.7 Xenon Transients (Cont'd)

require dilution of the salt at an initial rate of about 9 ft^3/hr. In all, a total dilution of about 1 percent or 17 ft^3 is required. Alternately, the poison safety rods might be used until the process plant, which is designed for steady state operation, catches up. Salt enrichment and dilution systems could be programmed to take automatic action for xenon override following any power transient.

There are other potential perturbations which could require larger amounts of fuel addition or dilution. The purge-gas system could fail resulting in the xenon poison fraction increasing from 0.5 percent to about 4.8 percent. To override this effect about 50 kg fissile must be added (3.5 percent of fissile inventory). A similar quantity of fissile would be required if the process plant were down for an extended period. Since the reactor would not operate as a breeder in this mode of operation, additional fuel would be required continuously. Assuming a conversion ratio of 0.8, less than 0.5 kg fissile/day would be required for full power operation.

MSBR's can easily be made to have flexibility of operation without depending on the process plant, purge-gas system, off-gas system, or high worth control elements. The values presented above are based on the ORNL Reference Concept. They are reasonable estimates for a wide range of concepts.

12.8 Measurements

Two potential problems exist in measuring neutron flux: First, making neutron detectors which will function reliably at high temperatures; second, having a sufficiently large neutron flux outside the vessel for start-up channels.

Quite possibly, it will be permissible simply to monitor delayed neutrons emitted at the vessel outlet nozzles. As a last resort, thimbles into the reflector could house neutron sensors for start-up channels. Sensors inside thimbles would have to

12.8 Measurements (Cont'd)

be cooled, probably by inert gas and be withdrawn during normal power operation.

Temperature measurements would be made from thermocouples welded to the Hastelloy N piping, or possibly in wells in the inlet and outlet piping. Thermocouples would be located throughout all systems in the plant. No problems of temperature measurement are foreseen except, of course, if in-core temperature measurements should be required. It does not appear that in-core measurements will be required.

Flow rate measurements may not be possible. In view of the success of MSRE in which flow rate was inferred from pump speed measurements, direct flow rate measurements may not be necessary. Possibly relative flow rates can be deduced by measuring delayed neutron emissions at various points around the primary loops. Relative intensities at various points would be related to salt transient time between points of measurement.

In conclusion, adequate instrumentation, control, and protective systems for MSBR's can probably be designed within existing technology.

13.0 RADWASTE

Little consideration has been given to the disposal of radwaste. Since MSBR's have little or no potential for explosive accidents, it seems reasonable that radwaste could be stored on-site for perhaps the life of the plant. Shipment for off-site disposal should always be available as an option.

The primary radwastes are discarded fuel salt, exposed graphite, and some long-lived fission product gases released when the refrigerated charcoal beds are regenerated. The following sections speculate what might be done with these wastes.

13.1 Fuel Salt

Since the chemical process plant is capable of removing uranium by fluorination, discarded salt will be stripped of uranium and protactinium on site. Many other constituents are of potential value (^{7}Li, Be, and Th) and could be recycled. It is known that LiF and BeF_2 can be recovered by distillation. BeF_2 can be recycled directly. LiF must be reduced to Li metal for use in the reductive extraction bismuth loops. It is speculated that ThF_4 can also be recovered by distillation. At present, it is not known if the cost of recycling these elements represents a savings relative to purchasing fresh material. Recycling these elements has the systematic effect of greatly reducing the bulk and disposal cost of radwaste. However, until economic processes for recovery are found, it is prudent to assume that discarded salt is of no value, and the plant owner must bear the disposal cost.

The following sections discuss the factors, as now known, which influence the rate of salt discard, cooling requirements during interim storage, and ultimate burial.

13.1.1 Rate of Salt Discard

The rate of salt discard is determined by two considerations:

1 - In an MSBR in which the chemical processing system effectively removes or concentrates fission and corrosion products, the salt discard rate is determined by the rate at which lithium is added to the bismuth streams.

2 - If the chemical processing system does not remove or concentrate all fission or corrosion products sufficiently, concentrations of those products must be limited by dilution, i.e., fresh salt addition and contaminated salt discard.

Thus, the discard rate depends upon the feed rate into the chemical process plant and the effectiveness of the chemical process.

In the ORNL Reference Concept the discard rate is controlled by the lithium feed rate and amounts to about 0.4 ft^3/day. To reduce the loss of ^{233}U and for economic processing, salt will be accumulated in batches, stored for decay of ^{233}Pu, fluorinated for recovery of ^{233}U, and finally discarded. Based on the half-line of ^{233}Pa, the minimum sized batch would probably be about 50 ft^3. Based on a policy of annual disposal, the batch volume would be about 150 ft^3. Thus, the range 50-150 ft^3 seems reasonable.

13.1.2 Heat Production in Discard Salt

In the Reference Concept the batch size is 92 ft^3 and is based on a 220 day accumulation. The decay heat of this quantity will amount to about 0.7 Mw. It will require cooling for many years. For this reason it appears that the most attractive approach to salt disposal is to ship it off-site for burial.

13.1.3 Salt Disposal

Disposal does not appear to be a serious problem. Since it freezes at 930°F, it could be put into

containers for burial in a salt mine. The containers must be designed such that the metal and salt remain at a satisfactory temperature. Alternately, the salt could be diluted to achieve a satisfactory power density and temperature distribution. One consideration is the possible evolution of free fluorine from radiolytic decompsition.

Fluorine pressures could become quite high (several atmospheres) unless the container is designed properly. Evolution of fluorine can be prevented by maintaining the salt temperature above 200°F. By designing the containers so that heat transfer to the salt (NaCl) bed occurs by radiation, the container and internal temperatures will remain within a narrow range over a wide range of heat production, due to the fact that radiant heat transfer varies as T^4. Furthermore, heat transfer by radiation cannot deteriorate due to fouling of surfaces. It can only improve. Radiation is, therefore, very reliable and attractive for long-term, maintenance-free heat transfer.

The salt may require dilution to limit the heat production rates or to provide space for free fluorine. It is speculated that this might be done by mixing it with spent graphite. The graphite might be in the form of small chips or in large chunks. It would enhance the thermal conductivity of the mixture and, therefore, provide a more uniform temperature distribution. In the Reference Concept, the graphite disposal rate is 600 ft^3/yr compared with 150 ft^3/yr of discarded salt. Some or all of it could be used for salt dilution if desired.

13.2 Graphite

Most of the radiation associated with the graphite is on the

surface. By remotely machining about 20 mils off the graphite surfaces the bulk of the radiation could be confined to a relatively small volume. The radiation level of the graphite elements could be reduced by about two orders of magnitude. The relatively small volume of surface material would contain essentially all the noble metals and most of the tritium. The radiation of the bulk would be due primarily to decay of ^{89}Sr (50.8 day half-life) which diffuses into the graphite as ^{89}Kr. After about one year the ^{89}Sr will have decayed to about one percent of its initial activity. At that time the heat production in the graphite bulk would amount to about 20 watts.

After decontaminating the surface (via scrubbing and/or machining) the bulk would probably be placed in a furnace to drive out the remaining fission gases - primarily ^{85}Kr. The elements might then be bagged and stored for decay of ^{89}Sr or possibly shipped directly to the burial grounds. The elements probably will not be burned because that would result in release to the atmosphere of the remaining radioactive isotopes including tritium.

13.3 Effluent from Charcoal Bed Regeneration

These effluents can be caught in numerous ways, one of which is a liquid nitrogen trap. The principle contaminants will be ^{85}Kr and tritium. These isotopes can easily be separated from nitrogen, stored in bottles and ultimately buried. Disposal of these effluents is entirely within present technology.

14.0 TRITIUM PROBLEM

Estimated tritium production in MSBR's is much greater than in a light water reactor of the same electrical output. ORNL estimated the production rate to be about 2420 curies per day in the Reference Design. About half the tritium production results from ther thermal neutron reaction $^{6}Li\ (n,\alpha)^{3}H$ and nearly as much from the fast neutron reaction $^{7}Li\ (n,\alpha\text{-}n)^{3}H$ with about 1.3 percent from ternary fission and a small contribution from $^{19}F\ (n,\alpha\ ^{17}O)^{3}H$. The tritium problem is aggravated in the MSBR because at the operating temperatures, elemental hydrogen tends to dissolve in most metals and hence, to diffuse through the metal walls of heat exchanger and steam generator tubes, as well as the vessel and piping. Of major concern is the amount of tritium which diffuses through the IHX and steam generator tubes into the steam-water system, since the problem of subsequent isolation of tritium from a large volume of water is well nigh insuperable.

Preliminary ORNL calculations indicate that for the Reference Concept roughly 13 percent of the tritium generated in the fuel salt would be removed in the off-gas systems as either T_2 or TF, roughly 18 percent would diffuse through the vessel walls and piping to the primary and secondary system containment cells and about 69 percent would reach the steam-water system. These results are generally applicable to any MSBR concept in which the carrier salt is a mixture of LiF and BeF_2 and having a secondary salt which couples the primary system to the steam system. This analysis did not take into account some important phenomena; namely:

a - The effect of hydrocarbons gettering the tritium and thereby preventing it from dissolving into the hastelloy.

b - The effect of graphite, as discussed below.

c - The effect of graphite powder deposited on all interior surfaces.

Although many of the constants used in the calculation (diffusivities, solubilities, etc.) are poorly known, the calculations appear to be sound. Individual constants can be changed substantially without affecting the nature of the problem.

14.1 Consequences of Tritium Release

The ideal solution to the tritium problem would be to minimize tritium production by changing the fuel salt composition to eliminate most of the lithium and beryllium content. Such an approach would virtually destroy any breeding potential of the reactor but might still lead to a reactor system capable of producing electricity economically.

There is good reason to believe that any tritium released to the off-gas systems and to the containment cells would be isolated by various means either for indefinite storage or possibly for useful purposes.

There appears to be no acceptable method of disposing of tritium once it reaches the steam-water system. Even though it could be released in the cooling water discharge without exceeding concentrations permitted by current standards for liquid effluent releases, there are strong pressures to minimize such releases and a large MSBR industry could lead to an intolerable accumulation of tritium in the hydrosphere. The alternative of retaining the tritium in the steam-water system is equally unacceptable. In the first place, it is not practical to build and maintain a system of adequate leak tightness. Secondly, even if leak tightness could be assured, tritium accumulations in the water of the Reference Design would be at a rate of about 0.7 million curies per year and the risk of system rupture or blowing of relief valves would be intolerable.

14.2 Measurements of Tritium Releases from MSRE

Shortly before operation of MSRE was terminated, attempts were made to measure tritium concentrations at various points to determine the disposition of tritium. The results of the measurements were somewhat inconclusive and certain inconsistencies were not recognized before the reactor was shut down. ORNL claims that calculations of tritium distribution made for MSRE conditions are in reasonable agreement with measured values. One observation which does not appear to be fully explained is that considerable

14.2 Measurements of Tritium Releases from MSRE (Cont'd)

amounts of tritium were being released from MSRE nearly three weeks after the reactor was shut down and drained. Calculations indicate a half-life for tritium in the MSRE fuel system of about 12 days compared to about a 12 minute half-life for the calculated MSRE Reference Design fuel salt. ORNL attributes the tritium holdup in MSRE to hydrocarbons deposited in the off-gas system as a result of inadvertent introduction of pump oil. However, there are questions regarding the behavior of the off-gas tritium content with heated CuO. In all probability there is some holdup of tritium in the MSRE in or on the graphite and in the metal walls as well as in oil decomposition products and similar holdup can be expected for MSBR. However, such holdup would be expected to reach steady state values during extended reactor operation and to have no important effect on tritium distribution.

Recent data obtained from the examination of MSRE data indicate that about 15 percent of the tritium ever produced in MSRE remains on the surface of the core graphite. It was also found on the inside surface of the Hastelloy N. It is speculated that hydrocarbons in the graphite and from oil leaks into the salt combined with tritium through hydrogen exchange and thereby put it into a chemical form less likely to escape. This is encouraging evidence suggesting that inert, hydrocarbons exposed to the fuel and coolant salt may solve the problem.

14.3 Possible Solutions to the Tritium Problem

In principle the amount of tritium reaching the steam-water can be reduced by:

1 - Reducing rate of tritium production in primary salt.

2 - Impeding transport from fuel salt to coolant salt and/or from coolant salt to steam.

14.3 Possible Solutions to the Tritium Problem (Cont'd)

3 - Enhancing transfer from fuel salt and/or coolant salt to off-gas systems in competition with transport to the steam-water system. While enhancing the transfer of tritium to the containment cells (relative to that to the steam-water system) would be acceptable, about the only practical way it could be accomplished would be to increase the tritium concentration in the salt which would result in a comparable increase in tritium transport to the steam-water system in any case except those covered in 2 above.

The following are some of the possible approaches which can be considered for solving the tritium problem. There is reason to believe that some combination will prove effective.

1 - Reduce or eliminate lithium and/or beryllium content of the fuel salt. With 99.995 percent enriched ^{7}Li in the MSBR Reference Design, ^{6}Li and ^{7}Li contribute nearly equal quantities of tritium. Neutron captures in Be produce ^{6}Li at essentially the same rate it is consumed. Hence, reduction of both Li and Be would be helpful. Suitable salts with acceptable melting points, uranium and thorium solubility and other properties might be found (e.g., using such fluorides as NaF and AlF_3) but at a severe sacrifice in breeding ratio.

2 - Improve fuel salt purge efficiency.

a - Increase interface area between fuel salt and gas, possibly through use of salt sprays rather than gas bubbles.

b - Increase gas purge rate.

c - Increase the UF_4 to UF_3 ratio above 10^3 to favor the formation of TF rather than T_2, thus enhancing tritium removal to the fuel off-gas. The amount by which the ratio can be increased is limited by the higher risk of corrosion but MSRE experience indicates lower corrosion

rates than expected even when the fuel salt was more oxidizing than planned.

d - Trap tritium in the off-gas system to minimize back diffusion through the salt film. This may be accomplished by sorption, chemical reaction or isotopic exchange. Suggested agents are oxides, getters such as Zr or hydrides such as ZrH_4 or hydrocarbons. Since a major fraction of the tritium may reach the off-gas as TF, the search for suitable agents should consider agents which will trap HF. Although cold-trapping would be useful, it would be advantageous to use an agent with a high affinity for tritium at elevated temperatures and preferably one which could be regenerated periodically by heat cycling.

3 - Add hydrogen to the fuel salt, either as molecular hydrogen or a compound (e.g., CH_4, $O\bar{H}$). ORNL has made calculations of the effect of adding hydrogen to the fuel salt. If one assumes that isotopic exchange (as well as chemical reactions) takes place rapidly at MSBR operating temperatures and that small isotopic effects on physical and chemical properties are negligible, the T/H ratio is identical for all chemical species. Hence the relative distribution of tritium to the various flow paths would be identical to that for hydrogen. Adding hydrogen increases the concentration of HF by the reaction.

$$\tfrac{1}{2}H_2 + F^- \rightleftharpoons HF + e$$

but since equilibrium is established when $C_{HF} = k\sqrt{C_{H2}}$, it is apparent that increasing the concentration of H_2 will decrease the concentration ratio of HF to H_2. Consequently, modest additions of H_2 (i.e., H/T ratios of 10^2 to 10^4) have a deleterious effect in that they tend to reduce the fraction of the tritium reaching the off-gas as TF and to increase the fraction reaching the steam-water system. Because

14.3 Possible Solutions to the Tritium Problem (Cont'd)

diffusion rates of H_2 through metals vary as $\sqrt{C_{H2}}$, whereas the diffusion rate through salt or gas varies as C_{H2}, a very high H_2 addition rate (H/T ratio $>10^6$ for the reference MSBR) would be effective in decreasing the fraction of tritium reaching the steam-water system to a tolerable level. The quantity of H_2 to be isolated from the off-gas system for storage is increased enormously. ORNL has even suggested that isotopic separation of tritium from hydrogen might be considered to ameliorate the waste problem or concentrate tritium for possible use. It may also be noted that the ORNL calculation apparently assumes that H_2 like T_2 is born in the fuel salt. Since this is obviously not possible, the H/T ratio in the off-gas is likely to be orders of magnitude higher than considered.

Addition of a hydrogen compound, such as CH_4, to the fuel salt might be more effective than adding molecular hydrogen, but the problems would be similar. This case has not been analyzed. Modest additions of H_2O or LiOH (to remove tritium as TOH in the off-gas) might be beneficial but is likely to cause corrosion problems or to precipitate BeO.

4 - Improve the coolant salt purge efficiency by any of the methods suggested for the fuel salt purge. Since the coolant salt contains no uranium, adjustment of the UF_4/UF_3 ratio is not applicable, but an equivalent oxidizing agent might be considered.

5 - Addition of hydrogen or its compounds to the coolant salt, Any addition of hydrogen to the fuel salt results in a comparable increase in coolant salt hydrogen content. In fact, since the diffusivity of H atoms through metal probably is greater than diffusivity of T atoms by the inverse square root of the atomic masses, the H/T ratio in the coolant salt is likely to be higher than that in the fuel salt. Similarly, any addition of molecular hydrogen to the coolant salt would be reflected in the fuel salt. It is doubtful that direct addition of molecular hydrogen to the coolant salt would be practiced.

14.3 Possible Solutions to the Tritium Problem (Cont'd)

ORNL has suggested that moderate amounts of H_2O could be added to (and continuously purged from) the coolant salt without seriously affecting the corrosion properties. In fact there is some question whether measures taken to remove H_2O and oxides from fluoborate coolant salt have been completely effective, so that the coolant salt may have a natural affinity for tritium. It is very likely, however, that the presence of small amounts of H_2O in fluoborate salt would result in hydrolysis and the formation of relatively stable hydro or hydroxy fluorides (e.g., HBF_4, $NaBF_3OH$ or $Na_2B(OH)_2F_3$) so that tritium might be trapped in the coolant salt in a form not readily purged. In such a case, the free tritium concentration would eventually build up to a steady state level approaching its equilibrium concentration. Consideration has also been given to use of ZrH_4 in the coolant salt loop.

6 - Coatings on heat exchanger and steam generator tubes. It is known that certain metals, such as tantalum and tungsten do not dissolve hydrogen. A thin coating of such metals on the tubes would be effective in reducing tritium transport, but it is questionable whether the cost could be justified or whether coatings with adequate integrity could be applied. There is also evidence that thin glassy coatings on metals can reduce the transport of hydrogen. The prospects of producing and maintaining an adequate glass coating at reasonable cost are small. Oxide coatings can have a similar effect. There is a prospect that with proper choice of tube material a self-healing oxide coating would form on the steam side of the steam generator tubes which, possibly with other measures, would reduce tritium transport to the steam to an acceptable level. Of course, fluoride salts are effective fluxing agents which would remove such coatings from the salt side of steam generators and heat exchangers.

14.3 Possible Solutions to the Tritium Problem (Cont'd)

7 - An additional loop between the coolant salt loop and the steam-water system. Consideration has been given to gas and such low melting salts as nitrate-nitrite mixtures (e.g., Hitec) for this purpose. The simplest embodiment of this concept would be double wall tubes in the steam generator and superheater with a (vented) gas gap. Nitrate-nitrite mixtures, which have been commonly used for high temperature heat transfer fluids, have instability and corrosion properties in the temperature range desired for MSBR. Because of their low melting point, they might alleviate some problems in preventing coolant freezing. It might be that a suitable composition salt could be found for this application. ORNL has given brief consideration to a concept in which a "fourth loop" would be used only for the steam generators and not for the superheaters or reheaters. This approach, in itself, would have little advantage because the surface area in the superheaters and reheaters of the MSBR exceeds that in the steam generators and the higher salt and metal temperatures in these regions enhance tritium diffusion. ORNL calculations for the reference MSBR indicate that only about 42 percent of the tritium reaching the steam water system arrives via the steam generator tubes. The balance transfers through the reheater tubes. It is to be expected that a nitrate salt would be strongly oxidizing and hence an effective trap for tritium. However, the ORNL scheme also proposes substitution of 2LiF BeF_2 for the sodium fluoroborate coolant salt since the former is expected to have a higher tolerance for H_2O.

8 - Substitution of gas coolant for sodium fluoroborate. Use of He gas as the secondary coolant for an MSBR would permit removal of tritium and minimize transport to the steam-water system. Several alternatives are possible:

14.3 Possible Solutions to the Tritium Problem (Cont'd)

a - Simple gas coolant with cleanup (by getters, traps, etc.) to remove tritium.

b - Addition of water vapor with an associated cleanup.

c - Fluidized bed, with cleanup for tritium removal. The principal advantage of the fluidized bed technique is to enhance heat transfer, possibly with reduced salt side tube surface area and hence less tritium migration.

15.0 MOLTEN SALT REACTOR SAFETY

15.1 Summary

At the present state of development of molten-salt reactor technology most of the safety technology is general, and even a preliminary safety analysis of an MSBR has not been performed. There is, however, a considerable background of technology bearing on MSR safety, and there are many fundamental facts that affect MSR safety which are distinctly different from solid fueled reactors[1/]. Most reactors can probably be made adequately safe by conservative design features and redundant engineering safeguards which, however, add to the cost of power. In this regard, molten-salt reactors have some inherent features that may result in cost savings relative to other systems:

1 - The primary and secondary systems contain very low pressure.

2 - The hot leg fuel salt temperature during normal operation is more than 1000°F below the boiling point.

3 - All but the very short-lived (<1 min. half-life) fission gases are removed from the fuel salt and isolated from the reactor system.

4 - Iodine and strontium form stable, nonvolatile fluoride compounds in the fuel salt.

5 - Salts do not react rapidly with air or water.

6 - Very little excess reactivity is required because of the homogeneous nature of the salt (i.e., no local fuel depletion). The fissile concentration is controlled via chemical processing (for breeders) or fuel addition (for converters).

1/ Rosenthal, et al, Nuclear Applications and Technology, Volume 8, February 1970.

15.1 Summary (Cont'd)

7 - The salt has a prompt negative temperature coefficient due to thermal expansion. Calculations show that this feature quickly terminates prompt power excursions resulting from any credible reactivity insertion. The prompt excursion is terminated before any phase changes or chemical reactions become possible. With delayed control action the entire excursion can be terminated without release of mechanical energy.

8 - MSR's have inherent dynamic stability.

Those features which give rise to the preceding safety advantageous characteristics also give rise to some disadvantageous characteristics:

1 - Instead of fission product activity being contained within and divided among many fuel elements, it is dispersed throughout four systems:

a - Primary system
b - Chemical process plant
c - Off-gas system
d - Fuel salt drain system

Each of these systems must have adequate safeguards and containment to assure against radiation release. It appears, however, that this requirement can be satisfied.

2 - Decay heat is produced long after shutdown wherever fission products accumulate. They will accumulate in the salt, on all surfaces exposed to fuel salt, in the drain tank, off-gas system, and chemical process plant. Thus, provisions for cooling must be available under all conceivable situations.

Preliminary evaluation of conceptual designs suggests that the safety characteristics of molten-salt reactors will be a net asset, but a thorough evaluation of fairly detailed designs will be required before the economic and practical importance of this can be assessed.

15.2 Safety Analysis by Systems

The most applicable background of overall safety technology for MSBR's is contained in TM-1858[2/] prepared in 1967 by ORNL. The system studied was the two-fluid breeder, but most of the safety considerations are pertinent to all molten-salt reactors. Other safety analyses dealing primarily with the molten-salt reactor experiment were prepared by ORNL and summaries are available[3/] [4/].

The studies and investigations associated with MSBR safety are summarized in terms of general and detailed studies which need to be done in order to evaluate MSBR safety. The favorable safety characteristics of MSBR systems arise from the low excess reactivity available to the reactor, the prompt negative temperature coefficient of reactivity, the low system pressures, the low level of fission gases and fission products retained within the reactor, the mobility of fluid fuel, and the ease of drainage of fuel from the reactor. At the same time, there are a number of possible incidents and safety aspects which need detailed investigation; these aspects are related to the specific plant design and involve both mechanical and nuclear design features. Plant systems which have a major influence on MSBR safety are the reactor system proper, the steam system, the fuel reprocessing system, the coolant systems, and the off-gas system.

The safety analysis requires delineation of possible incidents, their probability of occurrence, their consequences, and their prevention. Types of accidents which can take place include those due to reactivity additions. Reactor kinetic behavior

---

2/ Safety Program for Molten-Salt Breeder Reactors, ORNL-TM-1858, Paul R. Kasten.

3/ MSRE Design & Operation Report, Part V - Reactor Safety Analysis, ORNL-TM-732, August 1964, S. E. Beall et al.

4/ MSRE Design & Operation Report, Part VA - Safety Analysis of Operation, ORNL-TM-211, February 1968, P. N. Haubenreich et al.

15.2 Safety Analysis by Systems (Cont'd)

is influenced by reactivity coefficients and kinetics parameter values. Reactivity coefficients which must be considered include those associated with temperature, voids, pressure, fuel concentration, and graphite concentration. The function and design of control and safety rods must be fully investigated; these studies will determine the number, reactivity worth, placement, and response requirement of control rods. Possible reactor incidents must be evaluated as to their probability and their consequences.

Under normal operating conditions the MSBR could be load-following and self-controlling because of the negative temperature coefficient of reactivity associated with the fuel salt. The temperature coefficient also protects against excessively high reactor temperatures and pressures in case of reactivity incidents.

Start-up accidents also result in little energy release due to the large inherent neutron source strength even in clean fuel salt (nearly 10^7 n/sec due to the (α, n) reaction). The source will be much larger in salt containing fission products.

Reactivity additions and their safety implications which must be considered in detail involve the following: Changes in fluid-flow conditions; changes in fissile concentration in the salt; abrupt changes in fission product concentrations; control rod motion; the effect of pressure increases on reactivity (i.e., on void fraction and graphite penetration); and the effects of graphite behavior.

The integrity of plant containment under all incident conditions (nuclear and non-nuclear) should be evaluated for all credible possibilities; these include events such as mixing of coolant salt with water or steam; fuel or coolant salt spills and the associated thermal, chemical, corrosion, and criticality effects; temperature changes due to afterheat generation; container damage due to high temperature and/or corrosion; criticality in regions outside the core; flow blockage within the fuel or coolant streams,

15.2 Safety Analysis by Systems (Cont'd)

and flow blockage in the off-gas system. The consequences of such incidents must be determined in all cases. The following sections are taken almost entirely from Kasten's[2/] 1967 report.

15.2.1 Reactor System

The reactor system includes the core, the primary and secondary salt loops, the circulation pumps and the heat transfer components. There are several barriers to protect against the escape of radioactivity. The first is the primary reactor piping and equipment, the second is a containment vessel, and a third is the reactor building proper. All penetrations are equipped with sealing devices. Ordinarily, the activity of the coolant salt will be due to ^{16}N (7.1 sec. half-life) formed from the (n,α) reaction on fluorine, and ^{24}Na (15 hr. half-life) formed by the (n,α) reaction on ^{23}Na. In each case the neutron source for activation is the delayed neutron emission in the primary heat exchanger.

The low operating pressure of the reactor (about 75 psi design pressure) coupled with the 1000°F temperature interval between operating temperature and vaporization of the salt plus the high heat capacity of the salt-graphite system provides a safeguard against violent energy release from a nuclear excursion.

The design pressure for the reactor system cell is expected to be about 45 psi or less, depending on the amount of water available to convert to steam, the amount of energy available, and the cell volume. If necessary, pressure suppression systems could be provided with water storage tanks for condensation of vapors. It is doubtful

15.2.1 Reactor System (Cont'd)

if pressure suppression systems will be necessary except, perhaps, for the steam generator cell. Noncondensable gases would be contained and disposed of by passage through the off-gas system. Studies made for the MSRE suggest that corrosion of the steel liners and tanks by the HF will not be a serious problem.

The fuel drain tanks maintain subcritical storage of the fuel and also remove decay heat. Redundant cooling circuits will undoubtedly be provided. The coolant drain tank is similar to the fuel drain tank except no cooling is required. An inert cover gas system is provided to protect the molten salt from oxygen and moisture at all times. In order to keep stresses within equipment low, normal heating and cooling of the reactor will be done slowly at rates of 100°F/hr or less, applying temperature differences less than 100°F. However, the reactor system should withstand several severe thermal shocks (such as a rapid fuel salt temperature rise of about 400°F) without breaching.

The homogeneous and fluid nature of molten-salt fuels permits ready transport of material from one component or system to another.

From the viewpoint of safety, it is important that the fissile fuel remain homogeneously distributed in the carrier salt. This has been demonstrated repeatedly under both nonirradiation and irradiation conditions; in addition chemical stability of the fuel salts improves with increasing temperature, a favorable relation. Also the fuel salt expands with increasing temperature effectively leading to expulsion of fuel from the core region and leading to a negative temperature coefficient of reactivity. Because of the ease of fuel addition and removal, very little excess reactivity is provided within the reactor during normal operating conditions.

15.2.1 Reactor System (Cont'd)

Fission gases are continuously removed from the reactor core on a very short cycle time by salt spray or bubble removal systems with inert gas (argon or helium). Fuel processing takes place on about a 10-30 day cycle (for the fuel salt), so that the fission product content of the reactor system is always relatively low.

Drainage of the fuel salt plus flushing the system with carrier salt should remove a large fraction of the fission products from the circulating fuel system since the fuel salt does not wet the container material or the moderator.

15.2.2 Steam System

The steam system could influence reactor behavior. For example, rupture of the supercritical boiler-superheaters could lead to high pressure in the secondary coolant system, which in turn, could lead to rupture of the primary heat exchanger if proper safeguards are not employed. With proper design such a train of events would have little influence on the reactivity of the reactor core.

Molten salts doe not undergo a violent chemical reaction with water, but U and Be will be oxidized to UO_2 and BeO which precipitate. High temperature steam is produced when water contacts molten salt. In order to provide for steam producing accidents or for leakage of high-pressure steam into the coolant salt cells, a vapor-suppression system is used to provide pressure relief, and maintain pressures below the containment design pressure. Automatic block valves are provided in the steam lines to reduce the likelihood of draining the water in the steam system into these cells in the event of a rupture.

To protect against high pressures in the case of failure of a superheater tube in the heat exchanger, rupture discs are provided on the shell side of the superheaters and reheaters for venting the coolant system into the vapor

15.2.2 Steam System (Cont'd)

condensing system. These rupture discs protect against overpressure in the coolant salt circuit and thus protect the reactor system, which is separated from the coolant salt by the tube walls of the primary heat exchanger.

15.2.3 Fuel Reprocessing System

Another plant system of importance in the fuel reprocessing system, since it is integrated with the reactor plant and operates "on line." This operation could introduce reactivity changes into the reactor system. On the positive side of the safety considerations is the very small flow rate to the process plant. Thus, the rate at which the salt composition can be modified is low enough that no rapid reactivity additions to the reactor are possible.

The processing plant will use hydrogen and fluorine gases in the treatment of the salts. Care must be taken in utilizing these gases because of the hazards associated with obtaining explosive mixtures of hydrogen and fluorine.

The processing plant can utilize the same off-gas disposal system as the reactor system. This combined use should not introduce operating hazards. The integrity of the cooling systems needed for cooling of processing equipment must be assured, both during continuous processing and during storage.

Criticality must be considered, such that recovery of fissionable material constitutes no hazard. However, due to the relatively small quantities of fissile fuel held up in the processing plant and the homogeneous character of the materials handled, no difficulty is anticipated.

15.2.4 Off-Gas System

Xenon and krypton as well as tritium are stripped from the fuel salt in the reactor circulating system with

15.2.4 Off-Gas System (Cont'd)

helium. This gas, along with the gases generated, are treated in the off-gas system.

The molten salt system differs from other reactors in that essentially all the fission gases enter the off-gas system, whereas in solid-fueled reactors most of the fission gas remains inside the fuel elements. Thus, the MSR off-gas system will contain many times more activity and decay heat than that for solid fuel reactors.

The off-gas system must be designed to contain the radioactive gases safely and to provide reliable cooling of these gases. Also, while the vapor pressure of molten salts is very low, MSRE experience indicates that some particulate matter can be carried into the off-gas stream. Cold trapping or filtering must be provided in the off-gas lines for removing particulate. Any oil leakage and associated decomposition products entering the off-gas system must be accommodated without line plugging as occurred in MSRE. Particulate traps and good temperature control of the off-gas system appears to present no serious problem.

15.3 Operating Reactor Safety Aspects

In operating a power reactor there always exists the possibility that reactivity can be inadvertently added to the system, leading to a system disturbance. If this disturbance is very small, no ill effects result. Increasing the degree of disturbance can lead to conditions which affect reactor operation (operating safety) and eventually to conditions which affect the safety of the general public (ultimate safety). In this section the MSBR operations are discussed from the viewpoint of items which need to be evaluated from a safety standpoint such as reactivity coefficients, control rod function, possible reactivity events that could cause reactivity additions to the reactor, and the stability requirements of the reactor power plant. In general,

15.3 Operating Reactor Safety Aspects (Cont'd)

the specific situations which need to be evaluated are dependent upon the design and operational features of the system.

15.3.1 Reactivity Coefficients and Kinetics Parameters

A number of reactivity coefficients are associated with an MSBR system. These include those associated with temperature, voids, pressure, fuel concentration, graphite concentration, xenon concentration, fuel burnup, and fuel flow rate. From the viewpoint of reactor safety, the most important coefficients appear to be the temperature coefficients of reactivity for the fuel salt, the graphite moderator, and the fuel concentration coefficient of reactivity. There are special circumstances where others are also of importance. All of these need to be determined specifically.

Molten-salt reactors have, in general, a relatively large negative fuel temperature coefficient of reactivity, due to the expulsion of fuel from the core region with increasing temperature. The value for MSBR systems will be in the range of $-1 \times 10^{-5} \Delta k_e/^oF$ to $-5 \times 10^{-5} \Delta k_e/^oF$, the value being a function of design and operating conditions. This coefficient gives inherent control and safety to molten-salt systems, since any increase in power level tends to decrease the reactivity and thus decrease the power level. Since MSBR's will normally operate with only low values of excess reactivity available, the temperature coefficient appears sufficient for controlling the reactor without excessive temperature variations. This inherent control feature permits use of control rod mechanisms which have relatively slow action.

Increasing the prompt temperature coefficient of reactivity generally improves the safety and stability margins of reactor operations, provided that the reactivity

is added by means other than the temperature coefficient. However, the temperature coefficient itself can add reactivity by means of "cold slug" type occurrences. Such an occurrence in an MSBR would be normally associated with an increase of fluid flow rate; however, increasing the flow rate tends to decrease reactivity due to the associated increased loss in delayed neutrons. The effective value for the delayed neutron fraction in ^{233}U-fueled reactors is about 0.003 in fixed fuel systems; in MSBR systems, the effective value for beta during fuel circulation would be about 0.001.

Reactivity coefficients need to be determined in order to properly evaluate the safety of MSBR systems. Primary values appear to be the temperature coefficients associated with the fuel and with the graphite; the void coefficients associated with the fuel; concentration coefficients associated with the fissile and fertile salts in the core; reactivity coefficients associated with loss of fuel flow; effective delayed neutron fraction as a function of flow and power conditions; and the reactivity effects associated with graphite shrinkage, graphite breakup, and fuel soakup by graphite.

The reactivity coefficients need to be consistent with the kinetics model used in the safety evaluations, and time- and space-dependent criticality effects need to be included in such studies. These time- and space-dependent effects should include consideration of the different heating and flow rates within the reactor, afterheat generation, and the change in the effective delayed neutron fraction during a power pulse. Other parameters needed in the kinetics analysis include the prompt neutron lifetime and xenon poisoning effects.

15.3.2 Control-Rod Function

One or more control rods are provided in the MSBR in order to provide flexibility in reactor operations, and to control reactivity additions such that fuel temperatures and associated temperatures do not become excessive. As mentioned in Section 15.3.1, inherent control is provided through the negative temperature coefficient of reactivity, which provides prompt protection against reactivity additions. At the same time, if reactivity additions take place over a long-time interval, the total reactivity added may lead to undesirably high fuel temperatures if only the temperature coefficient is utilized (however, such temperatures may be permissible for relatively short times - order of hours). Installation of control rods which are slow acting (response time of about one sec) appears sufficient for controlling maximum fuel temperatures, and would permit reactivity control independent of fuel temperature. Control rods provide an easy means of controlling reactor power at low power levels where the temperature coefficient is a poor operational control.

The required reactivity worth of control rods is a function of shim and shutdown margin requirements, and needs to be investigated in detail. Control rod worth as a function of fuel concentration, power conditions, and reactor design should be studied.

In general, the control rods of the MSBR need not be used for shim requirements (e.g., change in steady state Xe level, or fuel temperature); rather, associated reactivity changes can be made by adjusting the fuel concentration. Reactor shutdown can be obtained by insertion of a control rod, or by stopping a fuel pump which leads to fuel drainage from the core region.

15.3.2 Control Rod Function (Cont'd)

It does not appear that control rods need to control large amounts of reactivity (probably less than 1/2 percent in reactivity) or to have fast response times (response times of about a second are probably sufficient). However, detailed studies need to be performed relative to specific requirements as a function of core design. The results obtained will be used to determine general considerations concerning control rods and MSBR safety.

15.3.3 Reactor Incidents

Items to be considered here concern physical events which influence system reactivity, as well as some which do not influence reactivity per se. Operational safety, or the ability to continue reactor operation after abnormal events, is involved, as well as ultimate safety where containment of gross radioactivity and public safety are the important concerns. These defintions are illustrated below.

Reactor plant incidents can also occur without the reactor itself being involved. For example, if mechanical failures occur which permit water or supercritical steam to contact secondary coolant salt within the cell containing the steam generators, high pressures could occur in the cell and lead to rupture of this containment. Release of steam containing particles of radioactive coolant salt could involve personnel hazard and ultimate safety.

The design of an MSBR plant must consider both operational and ultimate safety aspects; the resulting reactor plant must have operational safety assured under nearly all credible circumstances, and ultimate safety assured under all credible circumstances. Items which need to

15.3.3 Reactor Incidents (Cont'd)

be considered in such safety design studies are discussed below and are separated into those which involve reactivity additions to the reactor proper, those associated with mechanical and physical integrity, and items not covered in either of the above categories. In nearly all cases, these events require malfunction of equipment or reactor operation as indicated below.

15.3.4 Reactivity Additions

The protective devices available to the MSBR are similar to those in the MSRE. "Prompt" protection is afforded by the negative temperature coefficient of reactivity and "delayed" protection is provided by the control rods and also by drainage of fuel salt from the core region. Since all reactivity changes involve rates of addition rather than reactivity steps, an important factor in protection is the minimum neutron source strength which can exist in the core. The MSBR fuel contains an inherent neutron source of nearly 10^7 n/sec due to the α, n reactions resulting from the alpha decay of ^{233}U and ^{234}U in the fuel salt. An additional neutron source exists from the γ, n reaction resulting from the decay of fission products within the fuel salt; the photoneutron source is greater than 10^7 n/sec for about four months after reactor shutdown following a month's operation at power. Thus a strong internal neutron source is always present; if reactivity is added at low rates, multiplication of this source results in a significant increase in reactor power before large amounts of reactivity can be added to the system, which in turn permits the temperature coefficient to become effective after relatively small gross reactivity additions.

15.3.4 Reactivity Additions (Cont'd)

a - Net Fuel Addition to Core

Failure of the tubing in the boiler-superheater could allow the high-pressure steam to enter the coolant-salt system. To protect against a buildup of pressure in the coolant system, rupture discs are provided in the steam generator and reheaters, and also could be provided on the shell sides of the fuel and blanket heat exchangers. If these rupture discs fail to operate, or fail to operate quickly enough it is conceivable that a buildup of pressure in the coolant system could cause failure of the primary fuel heat exchanger. The likely means of failure would be rupture of the shell or collapse of the tubes, neither event transmitting the pressure increase to the fuel fluid. However, if there were localized weakness in a fuel-heat-exchanger tube, due to a defect in manufacture, fretting corrosion, etc., failure of a tube could occur leading to a buildup of pressure in the fuel system.

If steam does contact coolant salt, no exothermal reactions of any consequence are involved. Mixing of steam with coolant salt would oxidize the coolant salt, but no safety hazard would be introduced because of this action. However, the corrosiveness of the mixture to the container material needs determination. There are no fission products in the coolant salt, and the induced activity present would decay (the primary activity is associated with Na^{24} and N^{16}, having half-lives of about 15 hr and 7 sec, respectively). Cleanup of the system and repair or replacement of damaged equipment appears possible.

The coolant salt is compatible with the fuel salt, so leakage of coolant salt into the reactor system does not involve safety; any such leakage would reduce

15.3.4 Reactivity Additions (Cont'd)

a - Net Fuel Addition to Core (Cont'd)

reactivity. The BF_3 added to the reactor fuel could be readily removed by heating the salt, with the BF_3 removed as a gas.

Contacting fuel salt with steam would oxidize the uranium, but probably would not cause any problems other than those associated with subsequent cleanup of the fuel. However, possible reactivity effects due to fuel precipitation need to be studied specifically.

At this time it appears reasonable that engineered safeguards, such as installing rupture discs within the heat exchangers of the coolant system, and providing strengthened primary system heat exchanger tubes can either protect against such an accident, or keep the amount of fuel salt added to the core region small enough that ultimate safety is not involved. However, detailed studies are needed to examine this situation.

b - Reactivity Changes Due to Graphite Behavior

Shrinkage of graphite during radiation exposure can effectively influence fuel concentrations; however, the associated reactivity changes should take place at rates such that they can be readily compensated by adding or removing fuel through normal operations.

Graphite is compatible with molten salt, but fuel penetration into the graphite could take place with time. Here again, the time element involved would make such events insignificant from a safety viewpoint. If, on the other hand, a pressure rise took place in the core which caused the fuel to penetrate and fill voids in the graphite, perhaps a significant

15.3.4 Reactivity Additions (Cont'd)

b - Reactivity Changes Due to Graphite Behavior (Cont'd)

reactivity addition could be obtained. The actual addition is dependent upon the physical properties of the graphite employed. If the pressure rise occurs because of a previous reactivity addition, the pressure buildup itself would expel fuel salt from the core and tend to decrease reactivity.

Fuel-salt penetration in graphite appears to present little problem during normal operation, but may present difficulties during emergency shutdowns which require fuel-salt drainage. Fuel remaining in the graphite would generate decay heat which could lead to undesirably high temperatures (temperature distributions and levels influence thermal stresses and creep rates, which can affect the mechanical integrity of the graphite).

c - Reactivity Changes Associated With Changes in Flow Conditions

In a circulating-fuel reactor, an appreciable fraction of the delayed neutrons can be emitted external to the core under normal flow conditions. Increasing flow thus tends to lower the contribution of delayed neutrons to the fission chain and also decreases the average neutron lifetime of the reactor. While lowering the delayed neutron fraction (beta) is normally considered detrimental to safety, this is in the context of systems having instrument control. Lowering the value of beta in a system having inherent control under the condition that reactivity additions take place at relatively low rates does not significantly decrease the ultimate safety of the system. Also, the effective value of beta increases during a rise in power, a favorable condition.

15.3.4 Reactivity Additions (Cont'd)

c - Reactivity Changes Associated With Changes in Flow Conditions (Cont'd)

Since delayed neutrons are "lost" because of fuel circulation, stoppage of flow due to pump power failure would tend to add reactivity to the system. However, in the MSBR the reactivity addition would only be about 0.002. The fuel temperature rise due to afterheat during drainage of the core may be the most significant variable, and needs detailed study. Also, time delays in fuel drainage from the core following pump stoppage needs to be investigated experimentally, and the results interpreted relative to reactor safety.

Another reactivity incident possible with systems having a negative temperature coefficient of reactivity is that of the "cold slug" accident. Such an accident could occur by starting the fuel-circulating pump at a time when the fuel external to the core has been cooled well below that of the fuel in the core. The cooler fuel would add reactivity when it entered the core; this addition could exceed the reactivity decrease due to the "loss" of delayed neutrons associated with fluid transport. By going critical only with the pump on, making use of the control rod for this purpose, would avoid the "cold slug" incident. The seriousness of the cold slug incident and the control mechanisms needed under various circumstances need investigation.

d - Changes in Fuel Concentration

The reactor would initially be "filled" by adding fissile material to the carrier salt while the latter was circulating. If, however, following criticality and drainage of fuel salt from the reactor core, the

15.3.4 Reactivity Additions (Cont'd)

d - Changes in Fuel Concentration (Cont'd)

fissile concentration in the drained fuel salt were increased inadvertently, refilling the core could result in a supercritical reactor. Such an event is highly unlikely, since fuel would not be added in large amounts to the drained system; also, partial freezing of the fuel salt does not appear to lead to significant increases of fissile concentration in the fluid portion of the fuel. Specific cases need to be evaluated, however.

The rate of return of fuel from the processing plant is low, and it will be difficult to add reactivity at a high rate through the processing lines because of the limited rate at which fuel can be added. A more likely way to increase fuel concentration above the normal value would be to fill the core with fuel having a temperature lower than the critical temperature. A reactivity added by this means would correspond to a low-rate addition and should cause no difficulty.

If fuel were to accumulate outside the core region, and inadvertently return to the core, reactivity could be added rapidly to the reactor. Since the fuel is homogeneous and chemically stable, this event does not appear to be likely; also, any such possibility would be indicated by a previous reactivity loss. Nonetheless, the consequences of uranium precipitation or accumulation outside the core and its subsequent addition to the core region requires general evaluation. Such studies will help determine operating procedures consistent with reactor safety.

While none of the above events appears to constitute an operational or ultimate safety hazard, all should be considered in detail.

15.3.4 Reactivity Additions (Cont'd)

e - Reactivity Addition by Control Rod Movement

The presence of a control rod permits reactivity addition to the reactor by rod movement. Normally the reactor would be critical with the control rod completely inserted, but there could be conditions where criticality is achieved with the rod partially or completely removed. The amount and rate of reactivity addition associated with control rod movement under these conditions would be limited by the control rod worth (which will probably be under $0.005 \Delta k_e$) and the rate of insertion (which will be limited to a low value). As with the MSRE, no difficulty is foreseen, particularly if rod insertion does not continue after the power level reaches an initial peak value as a result of rod movement.

f - Reactivity Addition Due to Positive Pressure Coefficient

The MSBR design specifies use of helium to remove xenon from the circulating fuel. As a result of this operation, some gas will undoubtedly circulate through the MSBR core, resulting in a positive pressure coefficient of reactivity. The importance of this coefficient on safety is a function of the gas content of the core, which in turn is related to the ease of stripping xenon from the fuel salt and the efficiency of the gas separator used to remove sparge gas before it enters the core region. An increase in pressure would decrease the fraction gas in the core and increase reactivity. Experience with the MSRE indicates that the above is not a serious problem, but it needs to be evaluated specifically for the MSBR.

15.3.5 Mechanical and Physical Integrity - Containment

This subject is related to the reactivity additions discussed above. Here, the discussion is concerned with containment relative to events which do not necessarily require or result in reactivity additions to the reactor system. Some of the questions which arise are: What are the consequences of having water and salt in a cell if these materials accidentally make contact? What are the cooling conditions required if there is mixing of salt and water? What are the consequences of fuel-salt leakage or diffusion into the coolant-salt system? How practicable is it to maintain low leakage from a containment cell at the temperatures involved (leakage of no more than 1 percent of the containment volume per day)? What are the consequences of a major spill of fuel salt within the reactor cell?

The containment of the reactor plant has to be assured even though there is rupture of, or leakage from, the primary and secondary salt systems. Rupture and/or leakage may result from overheating, overstressing, corrosion, or other unexpected material failures. The severity of the containment problem will depend on the amount of salt spillage, the rate at which water mixes with hot salt, and the amount of water added to the cell. Consequences of a spill accident are heat generation, pressure buildup, and release of fission products into the cell, and these will need to be evaluated for specific cases. Problems associated with a major spill of fuel salt within the reactor cell must be considered in the detailed design of MSBR systems and must also be studied experimentally. If water is present, corrosion of steel by HF must be considered. The effects of local thermal expansion or energy deposition due to hot salt spillage needs evaluation. Provision should also be made that oil

15.3.5 Mechanical and Physical Integrity - Containment (Cont'd)

from the pump lubrication system does not contact hot components, although if this does occur, there normally would not be sufficient oxygen to support combustion in the cell atmosphere of inert gas (nitrogen). In order to assure containment, knowledge of the very long-term creep behavior of materials under plant operating conditions is needed. Information is also needed on the conditions required to produce "steam explosions" upon mixing of salt and water; similar information is needed for the mixing of oil and salt.

The containment of fission products should be assured, and release of these through the off-gas system must not constitute a safety hazard. This involves the amount of volatile material which is to be released and the amount of fission products carried in very small, mist-like salt particles. In any case, the release of material through the off-gas system should be controlled so that exposure of individuals is not excessive. This can be accomplished by filtration and retention systems as required. Beryllium and fluorine hazards, as well as radioactive iodine, must be considered relative to permissible release rates during normal operation as well as following a severe incident. The release of fission products upon mixing of fuel salt and water, or of salt and oil also needs determination.

In designing the reactor system containment, consideration must be given to the possibility of earthquakes. The effect of such an event on reactor containment is, of course, dependent upon its severity, which in turn is a function of local conditions. The possibility of flooding and associated consequences is also dependent upon local conditions.

15.3.5 Mechanical and Physical Integrity - Containment (Cont'd)

The most likely method of rupturing the secondary containment is through sabotage, missile damage, acts of nature, or excessive pressure. The generation of missiles in the reactor cell is not likely, since the reactor pressure is low. Missile damage and high pressures are more likely in the coolant cell and steam plant, and, although massive concrete shielding is provided, such events need further investigation. The containment cells will be protected by vapor-suppression systems, which should prevent the pressure from exceeding the containment design figure (~45 psig for present MSBR design) in case of buildup of steam pressure. In designing the vapor-suppression systems, it is necessary to consider the amount of salt and water that can come together and/or the leakage of high-pressure steam into the containment volume. Valves are located in the steam lines which can be closed to prevent draining all the steam system into the coolant cell. The reservoir of condensing water should be adequate to keep the cell pressure below the design containment pressure. Also, the supercritical steam systems contain relatively small amounts of water in comparison with subcritical systems.

15.3.6 Miscellaneous Incidents

Included here are possible incidents which are not covered in the above sections. These involve vessel criticality, heat removal, and heat addition conditions.

Studies are needed relative to the possibility of attaining supercritical conditions in fuel drain tanks and in vessels of the processing plant, along with consequences of such occurrences. Also, criticality conditions might occur as a result of fuel spills. In general, tanks which hold fuel should store it indefinitely in a subcritical condition. Accumulation of spilled fuel salt should be in regions which cannot attain criticality.

15.3.6 Miscellaneous Incidents (Cont'd)

The afterheat conditions which can exist within the reactor plant particularly need to be studied in detail, and cooling and heating provided and assured as needed. The temperatures occurring in the core following fuel drainage need to be evaluated as a function of fuel retention by the graphite. The influence of air contact on fuel salt needs study for conditions associated with core maintenance operations. The effects of salt freezing and melting in various parts of the primary and secondary salt circuits require evaluation, with equipment designed to minimize undesirable effects (e.g., rupture of equipment).

The consequences of flow blockage with the reactor system require investigation. A partial blockage could lead to salt boiling and temperature gradients which may affect the mechanical integrity of the moderator elements. Flow blockage may also lead to inability to remove all the fuel salt from the core, which may lead to afterheat problems and/or maintenance difficulties.

16.0 MAINTENANCE AND REPAIR

The successful maintenance and repair of MSRE only partially demonstrates the technical feasibility of maintaining and repairing an MSBR. The equipment size and radioactivity level expected in MSBR's will be much greater than presently experienced. Thus, maintenance and repair methods and procedures must be taken into account during the plant design.

The ORNL philosophy toward repair is to first protect against failure by good quality control and thorough inspections and, second, to remove and replace failed components. Failed components would be transferred to a hot cell for inspection and repair if feasible.

As for MSRE, MSBR systems will probably be arranged so that all components of contaminated systems are accessible from the cell top. All supports, electrical instrumentation and its connections, pipe connections, etc., are accessible and visible from the top through a maintenance shield.

To provide accessibility to all contaminated systems it is necessary for the biological shielding to be built in removable segments. Each segment will be interchangeable with a portable maintenance shield. This maintenance shield affords adequate shielding soon after the reactor is shut down. It will contain windows and ports through which long handled tools and power equipment can be manipulated. It will also contain provisions for manipulators, hoists, electrical power outlets, etc.

The hoists used for removing the biological shield segments and inserting the maintenance shield must be designed for fail-safe operation because the high bay area will be inaccessible during the shield replacement procedure. Thus, the probability of removing a section of biological shielding and not being able to insert the maintenance shield or replace the biological shield must be very small. This criterion is not new to the nuclear industry and satisfactory equipment, methods, and procedures are well within present technology.

There are two major methods of maintenance which are of importance to the technical feasibility of MSBR's: Semidirect and remote maintenance.

16.1 Semidirect

All of the equipment in the process plant and the off-gas system will become highly contaminated. ORNL indicates these activity levels may be ten times greater than experienced in MSRE. Nevertheless, MSRE experience is directly applicable to these systems. Since the components in these systems are small, replacement using the semi-direct methods demonstrated at MSRE appears entirely feasible. The larger radiation levels simply require appropriate changes in shielding design.

16.2 Remote

Any form of maintenance or repair of the primary system is well beyond any experience. The radiation levels, decay heat removal, and component size are far greater than experienced heretofore. Hence, thorough consideration of all conceivable maintenance and repair must be factored into the design.

In the ORNL Reference Design it was assumed that many permanent items designed to last for the plant life would require no maintenance. The reactor vessel, pump vessels, heat exchange shells, drain tank, thermal shielding and insulation, and primary piping, were among those items. No provisions for their maintenance or replacement were made in the design. Pump rotors, heat exchange tube bundles, bubble injectors and removers, etc., and the graphite core assembly require detailed replacement procedures. Of these, graphite replacement received, by far, the most consideration.

16.3 Graphite Replacement

In principle the core graphite can be replaced as a unit or in individual assemblies. Replacement as a unit has the potential advantages that less time is consumed and the downtime may be shorter. Because the transfer time is quite short, less than a few hours, the graphite can be without cooling during this interval.

16.3 Graphite Replacement (Cont'd)

By comparison, transfer of smaller, easily handled assemblies will take longer but require much simpler, more reliable, and less expensive equipment. To replace many assemblies the vessel will be open for perhaps two weeks during which it will be only partially loaded, special provision must be made for cooling.

The procedures for changing core graphite have been delineated somewhat for the ORNL Reference Concept. These procedures are generally applicable to any MSR in which the core graphite is replaced as a unit.

16.3.1 Unit Core Replacement

In the Reference Concept the reactor will be shut down about ten days prior to core removal.

After 10 days the heat production rate due to fission gases inside the graphite and noble metals on the graphite surface was estimated by ORNL to be about 0.2 MWt. This estimate is based on analyses of fission gas diffusion into graphite, 10 percent of the noble metals produced sticking to the graphite, and equilibrium operation prior to shutdown. This heat production rate in drained, uncooled graphite will give rise to a temperature rise rate of about $5^{o}F/hr$. Hence, it appears that the removal process can take many hours and not require a cooling system. ORNL estimated the radiation level outside the cask containing the graphite assembly to be ~1000 R/hr and the level at the outside wall of the reactor building to be less than 100 mR/hr.

A maintenance containment vessel is permanently installed over the reactor cell for the purpose of containing air-borne contaminants. It accomplishes this by providing an adjustable, cylindrical sleeve which meshes with the cask and forms a seal. It also contains high capacity fans which discharge into the off-gas system to assure inward movement of air.

16.3.1 Unit Core Replacement (Cont'd)

The cask is an integral part of a polar crane which transports the core to the interim storage cell. The cask contains four lifting hoists which lift the graphite matrix together with the top and bottom heads into the cask. It also has a two-leaf gate valve which seals the bottom of the cask.

The procedure proposed by ORNL for graphite replacement in the Reference Concept is as follows:

1 - The top of the maintenance containment vessel is removed to expose the reactor shield plugs.

2 - The control rod drive mechanism is disconnected at the top side of the shield plug and drawn into the cask, sealed, and stored. This involves direct and semi-remote operations.

3 - The control rod opening is closed with a blind flange, a remote operation.

4 - The top shield plug is then removed and the head hold-down bolts removed.

5 - The auxiliary hoist is engaged to the lower shield plug and hoist is initiated to assure clearance.

6 - The maintenance crew vacates the high bay area.

7 - The lower shield plug is removed and the maintenance shield is positioned in its place.

8 - Working through the maintenance shield with semi-remote methods, lifting rod ports are opened and the eight lifting rods are engaged with a dish which supports the replaceable graphite.

9 - The crew again vacates the area, and the maintenance shield is set aside.

10 - The core cask is centered over the reactor and sealed to the maintenance vessel.

16.3.1 Unit Core Replacement (Cont'd)

11 - The four cask hoists are connected to the lifting rods and the entire assembly - the bottom dish and reflector, the core assembly, together with the top head - is lifted into the cask.

12 - The cask bottom is closed and the seal with the maintenance containment released.

13 - The spent graphite is then centered over the spent core storage cell. The cask is sealed to the storage cell.

14 - The cask is opened and the assembly lowered into the cell where cooling is restored.

15 - The shield plug is placed over the spent core and the maintenance shield placed over the reactor vessel.

16 - After the cask is decontaminated, the work crew can return to the high bay area.

17 - The vessel could be inspected optically and ultrasonically.

18 - Again the high bay area is vacated and the maintenance shield removed.

19 - A new core assembly previously placed into the cask, is positioned over the vessel and sealed to the maintenance closure.

20 - The new assembly is lowered into the vessel. The 2 in. annulus provides clearance and no rotational orientation is required.

21 - The cask is removed and the maintenance shield replaced over the vessel.

22 - The maintenance crew returns, disengages the lifting rods, and reseals the lifting rod ports.

16.3.1 Unit Core Replacement (Cont'd)

23 - The area is again vacated, the maintenance shield removed and the lower shield plug inserted.

24 - The crew returns to replace the bolts to the top head flange.

25 - The top shield plug is replaced.

26 - Control rod drives reinstalled.

27 - The system is then leak tested and prepared for operation.

Much of this procedure can be made fail-safe in that backup procedures can be initiated to make the high bay area accessible. As long as it can be made accessible, personnel can enter and fix machinery so that the replacement procedure can resume. In a few steps, however, it appears that a single failure could paralize the operation, perhaps for a prolonged period. Beginning with step 10 when the cask is first positioned over the vessel, until step 16 when the cask is decontaminated, any failure which stops the operation would be very serious. If the initial radiation level were 1000 R/hr when the assembly was lifted into the cask, ten days after shutdown it would be about 160 R/hr 100 days later and about 50 R/hr 1000 days later. Thus, it appears that the plant could be out of operation for a long time. The consequences would not be nearly so serious if the failure occurred after step 14 when the assembly is lowered into the spent core cell.

To circumvent these potential problems the graphite could be handled in smaller assemblies.

16.3.2 Assembly Replacement

This approach would probably require the same procedure down to step 7. With the work shield in place, the top head would be unbolted and removed. If the vessel is

16.3.2 Assembly Replacement (Cont'd)

bottom supported and the top unobstructed, it could be slid to the side while remaining below the top deck. The primary pumps would have to be positioned so the head could pass between the shafts. Graphite assemblies could be replaced by either of two ways:

1 - They could be lifted into a cask above the work shield, moved aside, and discharged into a cell. A fresh assembly probably handled by an uncontaminated cask might then be inserted in the vacancy.

2 - They could be lifted clear of the vessel wall, but kept below the work shield, moved to the side of the vessel, then lowered through a penetration in the floor of the reactor cell into a storage cell.

Throughout either of these procedures the spent graphite must be cooled. Probably a gas steam driven by circulators in the off-gas system will provide sufficient cooling. If not, a special cooling system could be designed. The empty assembly positions would probably be closed to avoid starving the remaining graphite.

Regardless of method of replacement, the graphite handling equipment should be designed so it can be serviced efficiently. Moving parts should be accessible for replacement and provisions for installing shadow shielding, should it be needed, should be available.

16.4 Component Replacement

Replacement of a heat exchange bundle or a pump impeller will require a special cask with provisions for removing the decay heat. Because the heat capacity of the tube bundle or impeller is vastly smaller than the graphite, its rate of temperature rise in the absence of cooling will be much greater than the graphite core. Procedures for removal of the biological shield plugs and placement of a work shield would be similar to those for

16.4 Component Replacement (Cont'd)

the core. Semiremote methods would be required to cut welds or loosen bolts. The work shield would be removed, a cask positioned over the component. It would then be withdrawn and deposited remotely. Detailed procedures would have to be prepared as a part of the plant design.

16.5 Decontamination

MSRE experience indicates that particulate contamination can be almost entirely confined to equipment cells. Tools are bagged and later decontaminated. Particulate contamination has been successfully removed by high-pressure water jets alone or with the aid of detergents. Inhibited acids have been used successfully.

17.0 ACKNOWLEDGEMENTS

As always in such circumstances, it is impossible to acknowledge all of those whose encouragement and support made this study possible. However, it is a step in the right direction to express appreciation to the following:

Houston Lighting & Power Company

P H Robinson - Chairman
Carl B Sherman - President
K K Kreamer - Senior Vice President
John M McReynolds - Vice President
G W Oprea - Manager, Energy Control and Nuclear Program

Kansas Gas and Electric Company

Gordon Evans - Chairman
E S Hall - Vice President
Norman Pinkstaff - Coordinating Director

Middle South Services, Inc.

Gerald Andrus - Chairman
Floyd W Lewis - President, Middle South Utilities and formerly President, Louisiana Power & Light Company
Reeves E Ritchie - President, Arkansas Power & Light Company
R Baxter Wilson - Chairman, Mississippi Power & Light Company
Lionell Cucullu - Former President New Orleans Public Services Company, Inc.
William M Brewer, Jr - Vice President, Middle South Services
Dr Knox Broom - Manager, Nuclear Activities

Minnesota Power & Light Company

Jack F Rowe - Executive Vice President

Northeast Utilities Service Company

Marlowe G Moses - Senior Vice President
S Hale Lull - Vice President, Electric Systems Development
G R Parkos - Reactor Engineer

Texas Utilities

C A Tatum, Jr - President
L J Blaize - Vice President
L S Turner, Jr - President, Dallas Power & Light Company
Perry G Brittain - Vice President, Engineering and Purchasing, Dallas Power & Light Company
Burl B Hulsey, Jr - President, Texas Electric Service Company
E D Scarth - Vice President, Engineering, Texas Electric Service Company
Howard Drew - Director Research, Texas Electric Service Company

Texas Power & Light Company

T L Auston, Jr - President
George W Beams - Senior Vice President
John B Robuck - Vice President, Engineering

Union Electric Company

Earl K Dille - Executive Vice President
Burret Carother - Senior Vice President
Dr Gerald E Dreifke - Manager, Research and Development

Babcock & Wilcox Company

W H Rowand - Vice President
Dr P H Reinker - Vice President, Nuclear Power Generation
R A Webb - Manager, New Products and Services

Borg-Warner Corporation

John P Adams - President and General Manager, Byron Jackson Pump Division

Cabot Corporation

William D Manly - Vice President, Engineered Products Group
John D Leslie - General Manager, Stellite Division

Continental Oil Company

Howard W Blauvelt - President, CONOCO Chemicals
Dr M L Sharrah - Vice President and General Manager, Research and Development Department

Ebasco Services, Inc.

L F C Reichle - Vice President, Nuclear Department

Union Carbide Corporation

Dr John A Swartout - Vice President

We wish to express our appreciation to Dr Glenn T Seaborg, Chairman U S Atomic Energy Commission and AEC Commissioners Dr C E Larson and Wilfrid E Johnson, who attended the meeting at the commission offices at which the program of the Molten Salt Group was described, and who gave their encouragement.

We acknowledge the great cooperation of the members of the Molten Salt Program Staff at Oak Ridge National Laboratory in making available technical information and engaging in many discussions with the Group and express special thanks to Dr A M Weinberg, Director, Oak Ridge National Laboratory and Murray Rosenthal, Program Director, Molten Salt Reactor Program.